Exploring naphthalimide derivatives as sensitisers for genosensors

Huda Alsaeedi

A thesis submitted for Degree of Doctor of Philosophy

School of Chemistry

Cardiff University

September 2021

DECLARATION

To special people in my life.

Acknowledgements

At the beginning, I would like to express my gratitude to my supervisor Dr. Niek Buurma for giving me this opportunity to work on this research and to be part of his group. It is a pleasure to work with you.

I also thank Dr Seham Alterary from King Saud University, my co-supervisor for the first two years of my Ph.D., for her time and effort when I was part of the external joint supervision program (EJSP) between the two universities.

My thanks extend to all people I came across at Cardiff University, especially Haleema Otaif, Eman Al-Wattar, Ohud Alturki, Fatimah AlDawood, Emily Judd-Cooper and Liam McGrath for their friendship and nice company; I really appreciate all the moments that I spent with you. I thank my lab mates with whom I was happy to work, especially Jai Noah Maxwell who worked with me on some of the syntheses. I also thank Josh Rainbow, from the University of Bath, who is working on a parallel project developing genosensors for a stimulating and enlightening discussion.

My thanks also go to George Summers, Caru Shanahan and Siân Moseley from the PGR office for their kind words and support. I also thank Robin Hicks, Simon Waller and Tom Williams for the mass spectrometry data and Dr. Benson Kariuki for obtaining the crystallographic data. I don’t want to forget to thank the nice store staff, especially Jamie Cross.

Also, I thank my friends at KSU, especially Dr. Abeer Bin Beagan, Dr. Fatemah Alasmari and Dr. Saliha Aljbary, Dr. Ali Alsalme, Dr. Rais Khan and Mr. Jaber Alkabi for their support, no words can express my appreciation.

Most importantly, my sincere gratitude is to my beloved mother and dear departed father who supported me and encouraged me to be the person that I am, who believe in me and inspire me in many ways.

Finally, I thank Saudi Arabia's Ministry of Education for the scholarship and funding my Ph.D. studies.

list of contents

Summary

This thesis is divided into five chapters.

The first chapter describes the structure of DNA and discusses the ways that small molecules can bind with DNA and the driving forces for each mode of binding. Furthermore, the chapter describes how these small molecules that bind with DNA can be applied as sensitizers to detect DNA. Lastly, I briefly describe several techniques that can be used to detect ligand-DNA binding, including electrochemical techniques that can be applied in biosensors and other biophysical techniques such as UV-visible titration, isothermal titration calorimetry (ITC), electron paramagnetic resonance (EPR).

In chapter 2, a series of ferrocene-naphthalimide conjugates **2.12a-f** and **2.13a,c,e** were successfully synthesized and characterized using NMR spectroscopy and mass spectrometry. In these compounds, the naphthalimide scaffold is linked with a ferrocene moiety via a terminal diamine linker. Several solubilizing groups were introduced on C4 in the naphthalimide scaffold to produce compounds **2.12a-f** and **2.13a,c,f**. These solubilizing groups (1°-amine, 2°-amine and thiol group) have different effects on the solubility of the obtained ferrocene-naphthalimide conjugates. Moreover, the solubilizing groups affect the DNA-binding affinities for these compounds which have been studied using UV-visible titrations. Although most synthesised ferrocene-naphthalimide conjugates can be considered weak binders, **2.12f** and **2.13c** bind strongly with DNA with binding affinities of 3.8×10^5 and 1.01×10^5 M^{-1}, respectively. Generally, using linkers with different length to connect the naphthalimide scaffold and ferrocene moieties did not play a significant role in terms of binding with DNA except for one case when morpholine was used as a solubilizing group. In this case changing the length of the linker between the ferrocene and the naphthalimide has a remarkable effect on improving the binding affinity where the compound with a short linker **2.13c** exhibits stronger binding affinity than the compound with the longer ether-based linker.

In chapter 3, a series of bisnaphthalimide derivatives has been synthesized where two naphthalimide units were connected via several different linkers, including aliphatic, aromatic, and ether-containing linkers. Several solubilizing groups, viz. 1°-amine, 2°-amine and thiol groups, were introduced to both C4 positions in the resulting bisnaphthalimide scaffolds. The solubility for these compounds has been tested in MOPS buffer with solubilities typically in the range of 10^{-6} M^{-1} ~10^{-5} M^{-1} except in case of using thioglycolic acid as a solubilizing group where the solubility is higher and in the range of ~ $x10^{-4}$ M. DNA-binding affinities were investigated using UV-visible titrations. According to the DNA-binding affinities, most of the tested bisnaphthalimides such as **3.9e** and **3.12d** can be considered good DNA binders with binding affinities of 6.13×10^4 and 1.24×10^4 M^{-1}, respectively. On the other hand, compound **3.10b** is the most promising compound among this series as it binds relatively strongly

with DNA with binding affinity of 3.95 x10^5 M^{-1}. Unsurprisingly, bisnaphthalimides connected with thioglycolic acid do not bind with DNA due to the negatively charged carboxylates when the carboxylic acids get deprotonated in solution and electrostatically prevent bisnaphthalimide from binding with negatively charged DNA.

In chapter 4, a series of fused-ring-extended 1,8-naphthalimide derivatives were successfully synthesized. The synthesis involves synthesizing and separating two isomers of a building block for potential intercalators. Several solubilizing groups were introduced in C4 of the naphthalene ring. The DNA-binding properties for these compounds were studied using UV-visible titrations. It is found that this class of compounds binds strongly with DNA, however the titration curves show unusual behavior where we had to analyse the data in a slightly different way to obtain apparent DNA-binding affinities K_{app}. In general, there is no difference between these isomers in terms of binding with DNA. The binding properties for two isomers has remarkably improved when we used different groups (1°-amin, 2°-amine, thiol group) compared to bromo-substituted isomers. Compound **4.16a**, with ethanolamine as the solubilizing group, is the most promising compound among this series with an apparent DNA-binding affinity K_{app} of 8.45×10^4 M^{-1}. Using 2-mercaptoethanol **4.16d** and **4.17d** on the other hand show the lowest DNA-binding affinities (~10^3 M^{-1}). We note, however, that these binding affinities are apparent binding affinities and therefore likely underestimate the actual affinities of these compounds for DNA.

In chapter 5, a series of mono- and bisnaphthalimide-TEMPO conjugates has been successfully synthesized. The TEMPO moiety was connected to the naphthalimide scaffold using an amide-coupling reaction between 4-amino TEMPO and a carboxylic acid group connected to the naphthalimide unit. The solubility of the synthesized mono- and bisnaphthalimide TEMPO conjugates has been tested in MOPS buffer. Understandably, bisnaphthalimide derivatives were not sufficiently soluble but the mononaphthalimide-TEMPO conjugates are partially soluble. DNA-binding properties for the synthesized mononaphthalimide derivatives were studied using UV-visible titrations. Based on the binding affinities, this class of compound binds moderately with DNA. Among this series of compound, **5.12e** which contains two TEMPO moieties, binds with DNA better than the other compounds while **5.12b** that involves morpholine as solubilizing group binds with DNA with lower affinity.

Abbreviations and Symbols

A	Absorbance
A549 cells	Adenocarcinomic human alveolar basal epithelial cells
a.u.	Arbitrary unit
°C	Degrees Celsius
^{13}C	Carbon-13
cm^{-1}	Wavenumbers
d	Doublet
DMF	Dimethylformamide
DMSO	Dimethyl sulfoxide
DMSO-d_6	Deuterated dimethyl sulfoxide
DNA	Deoxyribonucleic acid
dsDNA	double-stranded deoxyribonucleic acid
ESI	Electrospray Ionisation
FSDNA	Fish sperm deoxyribonucleic acid
g	Grams
h	Hours
^{1}H	Proton (Hydrogen-1)
HeLa	Henrietta Lacks
Hz	Hertz
ICT	Internal Charge Transfer
J	coupling constant
K	Binding constant
KB cells	Subline of the ubiquitous KERATIN-forming tumor cell line HeLa.
m	Multiplet

MCF-7	Michigan Cancer Foundation-7
MGBs	Minor-groove binders
MIS	multiple independent binding sites
MOPS	3-(N-morpholino) propanesulfonic acid
m.p.	Melting point
m/z	Mass to charge ratio
NMR	Nuclear Magnetic Resonance
q	Quartet
quin	Quintet
s	Singlet
Sec	Seconds
SG	Solubilizing group
SGC-7901	Human gastric cancer cell line
ssDNA	Single-stranded deoxyribonucleic acid
t	Triplet
TLC	Thin Layer Chromatography
UV-Visible	Ultraviolet-Visible
v/v%	Volume/Volume
λ_{max}	Maximum wavelength

Chapter 1. DNA Binders

1. Introduction

1.1 Overview of DNA

Nucleic acids, viz. DNA and RNA, are essential biomacromolecules in cells. DNA was discovered in 1869 by Swiss physiological chemist Friedrich Miescher. Miescher noticed a slightly acidic substance in the nuclei of human white blood cells and coined it as 'nuclein' and from the 'nuclein' he separated proteins and nucleic acid components. This is considered the first successful isolation of deoxyribonucleic acid (DNA).[1] Widespread interest in nucleic acids started in 1940-1950s after Oswald Avery and his colleagues demonstrated that genes are made of DNA and that DNA is the genetic information carrier.[2] Later, the three-dimensional structure model of DNA was presented by James Watson and Francis Crick[3] on the basis of x-ray crystallographic work by Franklin and Wilkins to confirm the structure.[4] For this exemplary work, Watson, Crick, and Wilkins were awarded the Nobel prize in 1962.[4] Unfortunately, Franklin was not included in the award, even though her work was integral.[4]

1.1.1 Structure and function of the DNA

Deoxyribonucleic acid 'DNA' is a biomacromolecule that stores the genetic instructions that distinguish all known living organisms.[1, 5] DNA is made up of two anti-parallel chains of nucleotides (polynucleotides). Each nucleotide consisted of three components, 1) a nitrogenous base, or nucleobase (adenine, guanine, cytosine, and thymine), 2) a pentose sugar (deoxyribose) and 3) phosphate groups. These nucleotides are connected to each other covalently by 3', 5' phosphodiester bonds (Figure 1.1).[1, 6, 7] The sequence of the bases in the polynucleotides determines the information encoded for the organism,[8] with each set of three bases forming a codon which is translated into an amino acid during protein synthesis.

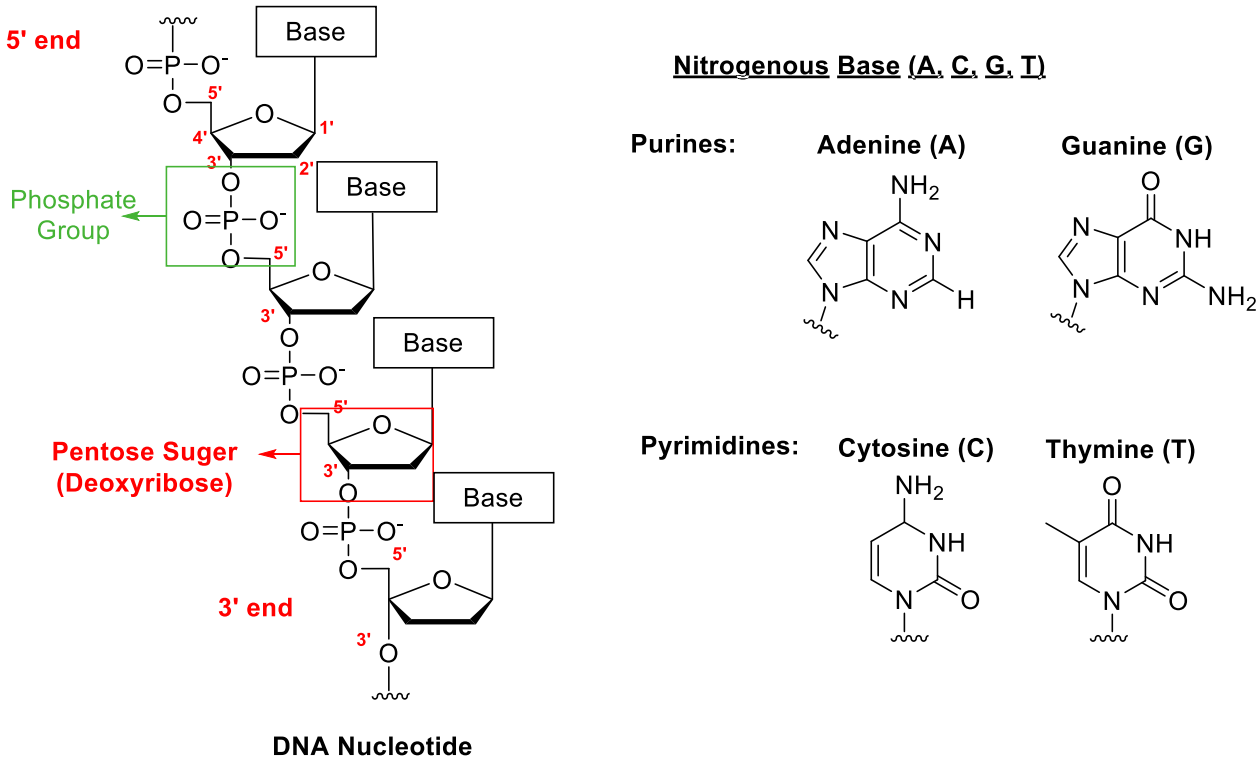

Figure 1.1 The molecular structure of DNA

Two anti-parallel DNA strands (polynucleotides) are held together by hydrogen bonding between the bases, forming so-called basepairs, and stacking between the consecutive basepairs.[1, 9] Each basepair has a structure that allows a specific number of hydrogen bonds to form due to the existence of electron-accepting and donating sites. Double hydrogen bonding occurs between A and T, whereas G and C have triple hydrogen bonding (Figure 1.2).[1] The arrangement of the base pairs causes the major and minor grooves to be formed in the double helix. [10]

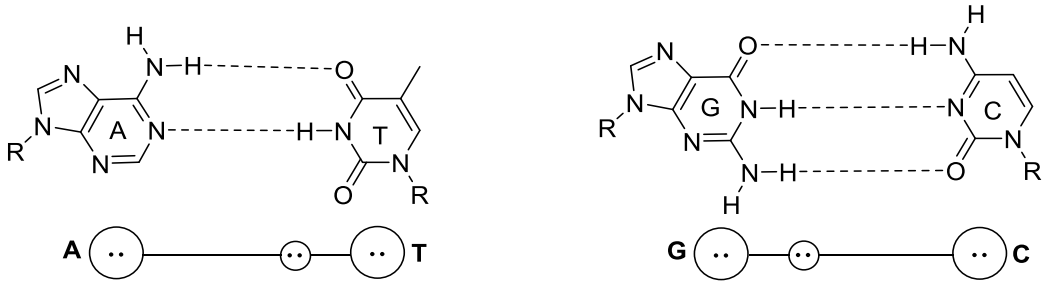

Figure 1.2 DNA complementary base pairs

In the helical structure, the region where the phosphate ester backbones are closer to each other is called a minor groove, and the region where the backbones are further apart is known as the major groove of duplex DNA (Figure 1.3).

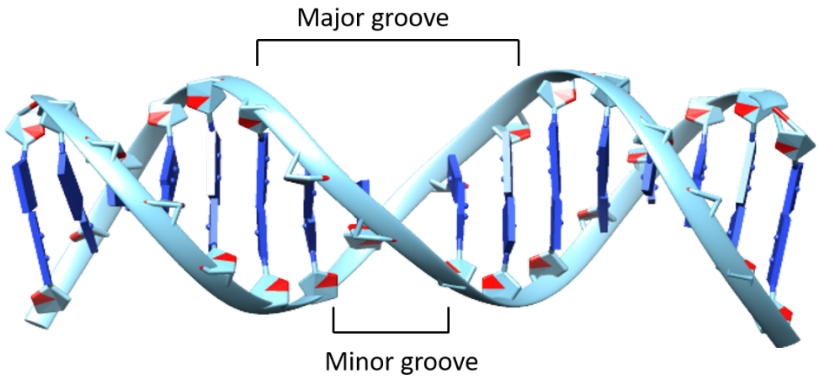

Figure 1.3 Major and minor grooves of DNA

There are many double-helical forms possible. However, DNA possesses three principal forms, viz. A, B, and Z forms.[7] These forms vary from one another in numerous ways like helical sense, pitch, groove width, base orientation, and sugar pucker (Table 1.1).[6, 8, 11]

Table 1.1 The differences in the A-, B- and Z-form DNA [8]

	A-form	B-form	Z-form
helix sense	right-handed	right-handed	left-handed
base pairs/turn	11	10.4	12
pitch per turn of Helix	25.3 Å	35.4 Å	45.6 Å
glycosyl bond	*anti*	*anti*	alternating *anti* and *syn*
sugar pucker	C3'-*endo*	C2'-*endo*	C:C2'-*endo*, G:C3'-*end*
major groove	narrow and very deep	wide and quite deep	flat
minor groove	very broad and shallow	narrow and quite deep	very narrow and deep

The three different forms of DNA are shown in Figure 1.4

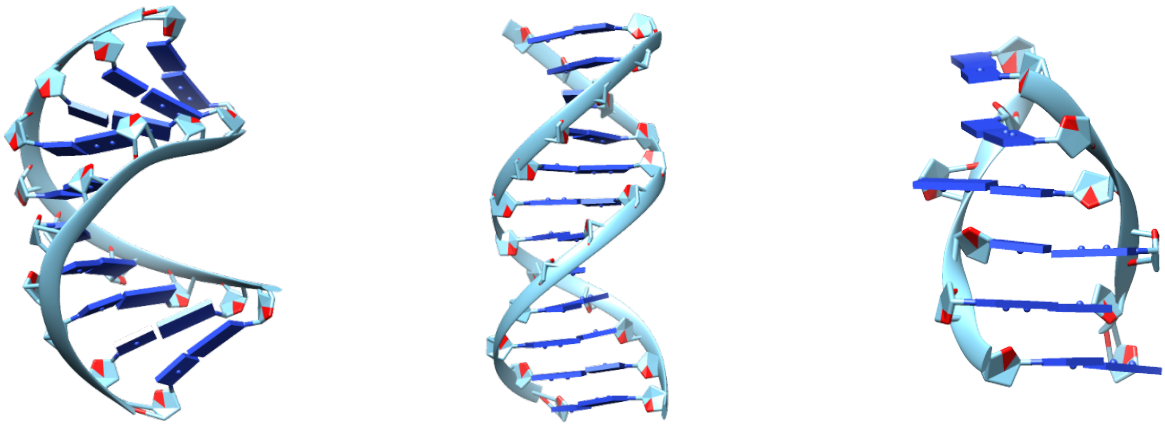

A-form DNA (PDB ID: 440D) B- form DNA (PDB ID: 425D) Z- form DNA (PDB ID: 1M6R)

Figure 1.4 The different forms of DNA

Understanding the structures of DNA was the foundation to develop an understanding of the connection between genetics and the everyday workings of the cell. Genetic information can get from the DNA into protein through transcription of the DNA into RNA first. Then, translation of the RNA leads to formation of a protein. However, this process cannot be reversed which means proteins do not change genetics, at least not directly. This conclusion has come to be known as the "Central Dogma" (Figure 1.5).[3]

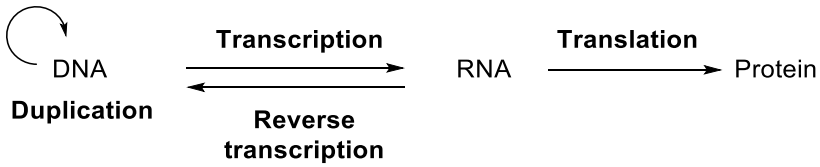

Figure 1.5 Central Dogma

Several organic and inorganic small molecules can bind with DNA forming DNA-ligand complexes with significant changes in torsion and conformation of the DNA.[8] These structural modifications can lead to the interruption of DNA replication, transcription, and DNA repair processes. Therefore, DNA binders are often used as chemotherapeutic agents.[12] Understanding how these small molecules bind with DNA is very important

information that helps to design not only DNA interacting molecules for chemotherapeutic purpose but also can be used for different applications such as biosensors for detection of DNA.

1.2 DNA Binders

In the field of molecular recognition, small molecules that interact with DNA (DNA binders) emerged as a field of interest for many researchers working on hereditary diseases. The molecules referred to as ligands bind to DNA to form DNA-ligand complexes.[13, 14] The ligands can bind irreversibly or reversibly with DNA and the stability of these DNA-ligand complexes is defined by the types of bonding present between the two.[7, 8, 15]

Irreversible interactions are due to covalent bonding between the ligand and the DNA. A prime example of this class is cis-platin (an anti-cancer drug), which binds to the DNA guanine nitrogen via covalent bonding to form stable complexes that stall transcription and cause cell death (Figure 1.6).[6, 8, 10, 16, 17]

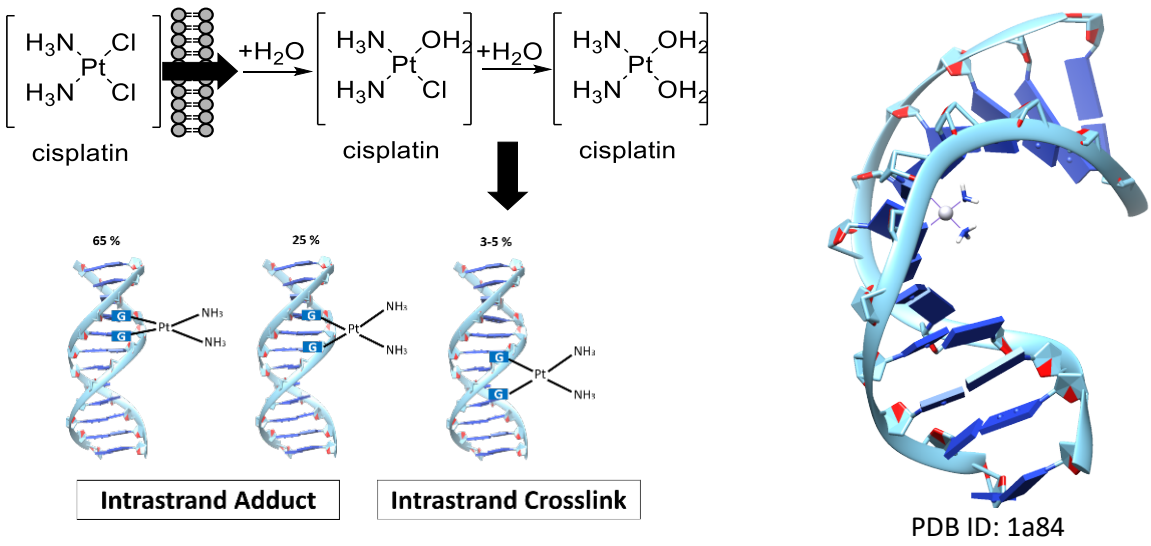

Figure 1.6 Cisplatin forms covalent bonds with DNA [16]

Reversible interactions between a ligand and DNA occur primarily via groove binding (major/minor groove) and intercalation.[15, 18] This interaction is stabilized by several forces such as hydrogen bonds between hydrogen bond donor/acceptor groups on the ligand/drug and complementary hydrogen bonding groups on the DNA strands (in particular on the bases, A, T, G, C). Hydrogen bonding is the most recognized force that stabilizes the binding, especially in groove binders where the hydrogen bonds are located at the minor/major grooves and give rise to

sequence selectivity. In addition, hydrophobic interactions, typically between aromatic surfaces and the relatively hydrophobic walls of the minor groove play an important role. Van der Waals interactions are another force that is known to be present in ligand/drug- DNA (or biomolecules) interactions, especially in case of intercalators.[15, 18] In addition, since DNA structure is negatively charged due to the presence of phosphate groups, cationic compounds electrostatically interact non-specifically with DNA backbone.[8]

1.2.1 DNA groove binding (GBs)

As the name suggests, groove binders bind in the minor or major groove of DNA. Since the major groove is wide, it allows larger ligands/molecules such as proteins to bind predominantly through recognition of hydrogen bond donating and accepting sites.[7, 8] Minor-groove binders (MGBs), on the contrary are generally small, flexible and elongated, positively charged molecules. Thus, minor-groove binders interact with negatively charged phosphate of the DNA electrostatically. Additionally, these molecules interact with the minor groove's hydrophobic walls and through hydrogen bonding at the bottom of the minor groove. From the chemical structure perspective, MGBs need to have a crescent-shape to facilitate the binding in the minor groove.[18] MGBs are often located in regions rich in A-T base pairs since there are more opportunities to form hydrogen bonds between MGBs and the AT region (N3, adenine) and (O2, thymine) compared to GC region (Figure 1.7). Also, A-T regions have less steric hindrance compared to G-C regions where the extra amino group in the guanine base sticks out into the minor groove.[8, 18]

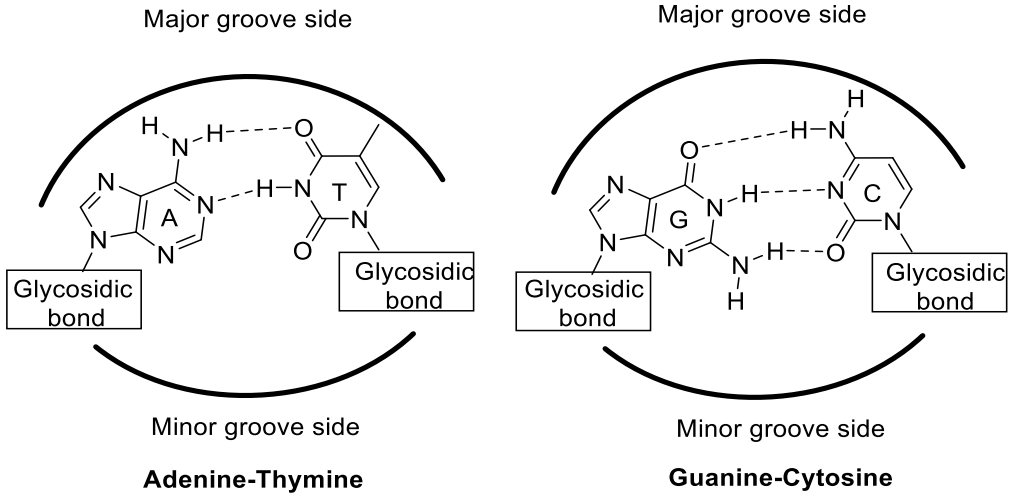

Figure 1.7 H-bond donor and acceptor characteristic for all base pairs in the minor and major groove of DNA [6]

MGBs bind with little conformational change to the DNA; thus, these interactions result in no changes to the DNA length. Therefore, no significant changes appear in viscosity and this observation is considered an indication that a compound is a groove binder.[8, 18]

Numerous compounds, whether synthesized or naturally isolated, are documented and recognized as MGBs. For instance, distamycin A[6, 14] and netropsin[6] (naturally isolated) are representative examples of polypyrroles and the polyamides class. These two compounds were the first two known MGBs and have a specific crescent concave shape that fits in the convex minor groove of the DNA, thus also termed as "shape-selective binders" (Scheme 1.1).[6]

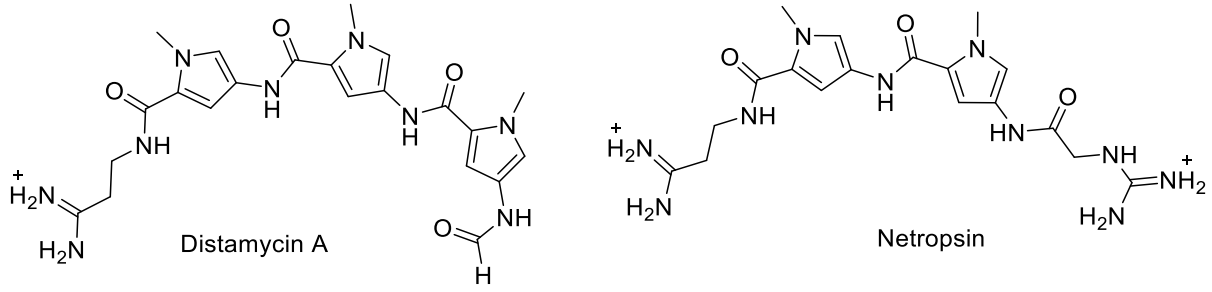

Scheme 1.1

Distamycin and netropsin present a significant specificity for A-T sequences (Figure 1.9). The conformation of netropsin changes to allow the compound to follow the minor groove curvature. The positive charge electrostatically interacts with the negatively charged phosphate groups.[6]

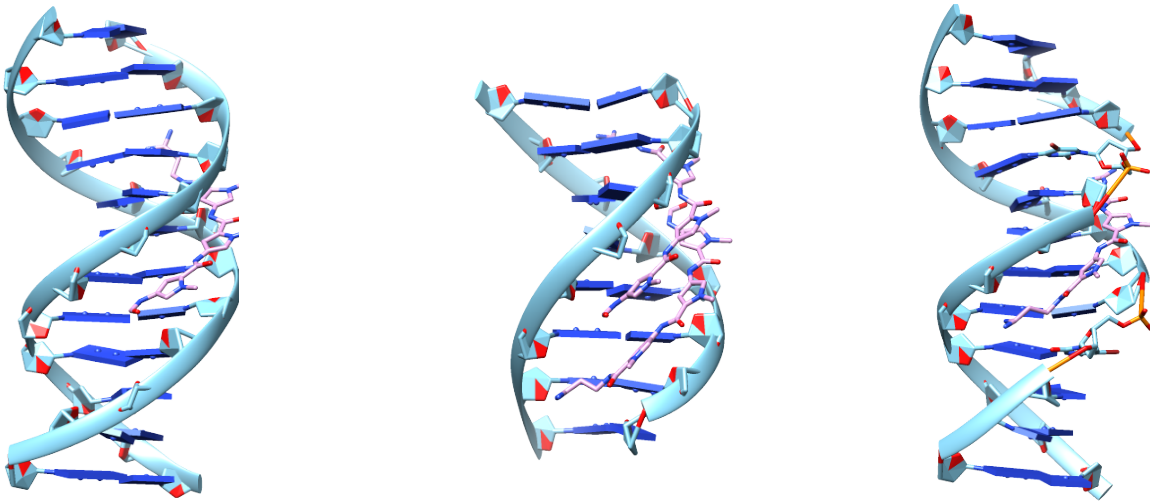

Distamycin A in 1:1 (PDB ID: 2DND) Distamycin A in 2:1 (PDB ID: 378d) Netropsin (PDB ID: 6bna)

Figure 1.8 The groove binding modes of distamycin and netropsin with DNA duplexes

In addition, Van der Waals interactions occur between the N-methyl pyrrole (Py) rings and the deoxyribose sugars. The binder-DNA complex is further stabilized via the hydrogen bonds between hydrogen atoms (N-H) on distamycin A and netropsin and sites on the A-T rich sequences. Therefore, these binders recognize the minor groove. Figure 1.9 shows the binding diagram with the hydrogen bond acceptors on N3, C2=O of A and T bases of the DNA.[6]

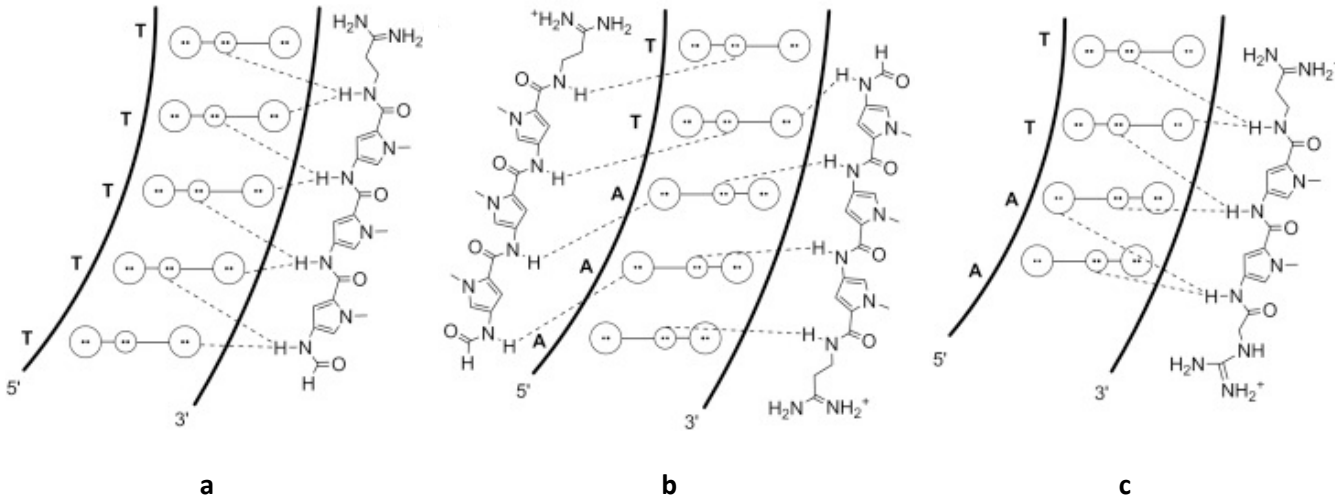

a **b** **c**

Figure 1.9 The hydrogen bond diagram between a) distamycin A in 1:1, b) distamycin A in 2:1 and c) netropsin DNA duplexe

Another class of compounds explored as MGBs is bisbenzimidazoles. Key representatives of this class are Hoechst 33258 and 33342 (Scheme 1.2). X-ray crystallography ascertained the binding mode of Hoechst 33258, and NMR exhibited minor groove binding at the A-T sequences.[6]

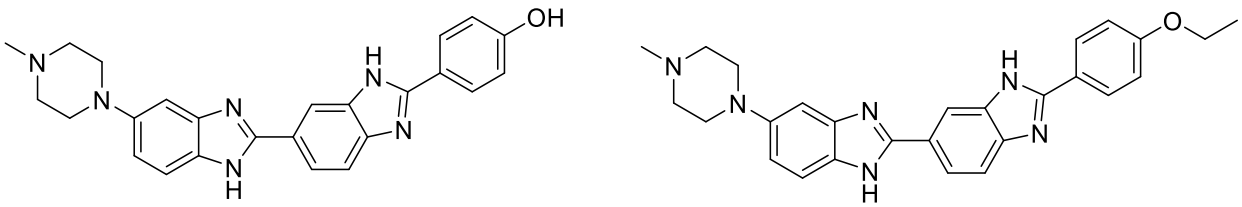

Hoechst 33258 Hoechst 33342

Scheme 1.2

Figure 1.10 shows that the binding between DNA and Hoechst 33258 is stabilized via bifurcated H-bonds between a protonated nitrogen on each benzimidazole in Hoechst 33258 and adenine (N3) and thymine (O3) from the DNA.[6]

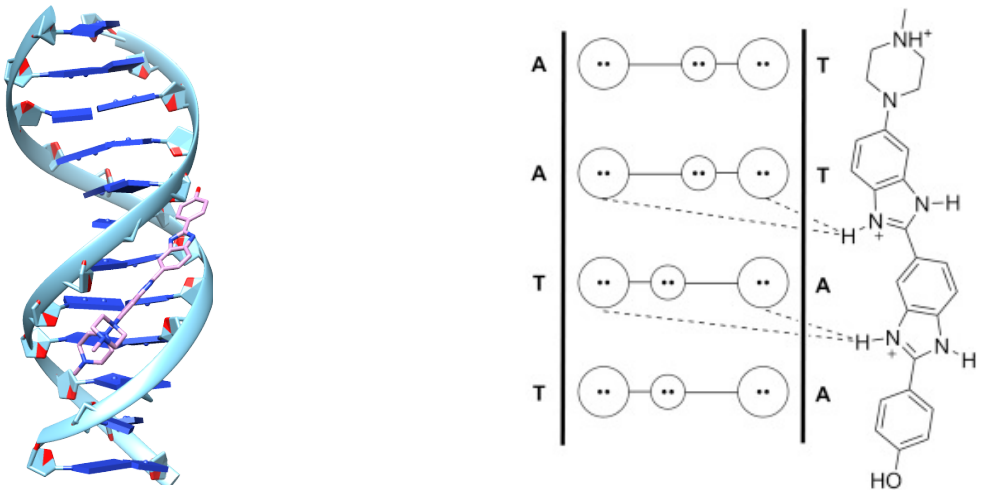

Hoescht 33258 (PDB ID: 8bna)

Figure 1.10 The groove binding modes of Hoechst 33258 (left), hydrogen bond diagram between Hoechst 33258 and DNA duplex [6] (right)

The challenging concept in synthesizing MGBs is to synthesise compounds that can recognize a specific sequence of base pairs of DNA. Several novel hairpin polyamides have been designed and synthesized to recognize several consecutive basepairs.[19-21] For instance, novel oligoamide ImPyPy (Figure 1.11) has been designed in order to recognize a sequence of three consecutive basepairs 5'-(G,C)(A,$T)_2$-3'. However, it was found that this compound recognizes the following five base pair sequence 5'-(W)G(W)C(W)-3' (W=A or T).[19]

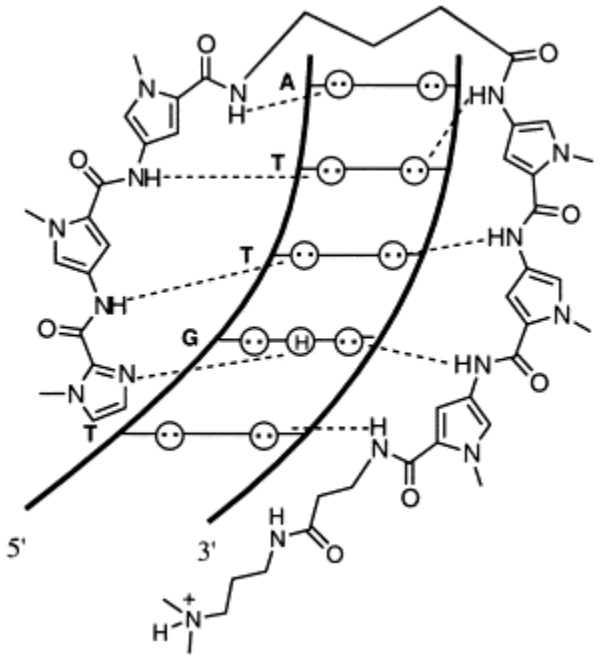

Figure 1.11 Hydrogen-bonding model of oligoamide ImPyPy

1.2.2 Intercalation

In 1961, Lerman introduced the concept of intercalation (non-covalent interaction). This DNA binding mode occurs when molecules possess planarity and slide in between the base pairs (Figure 1.12).[12, 22] Generally, DNA intercalators are flat aromatic systems with a strong binding ability resulting from inserting between two neighboring base pairs leading to stacking interactions.[13, 15, 23] The ligand-DNA complex maintains stability via π-π stacking and Van der Waals interactions between the aromatic system, in addition to electrostatic and hydrophobic interaction.[8, 22]

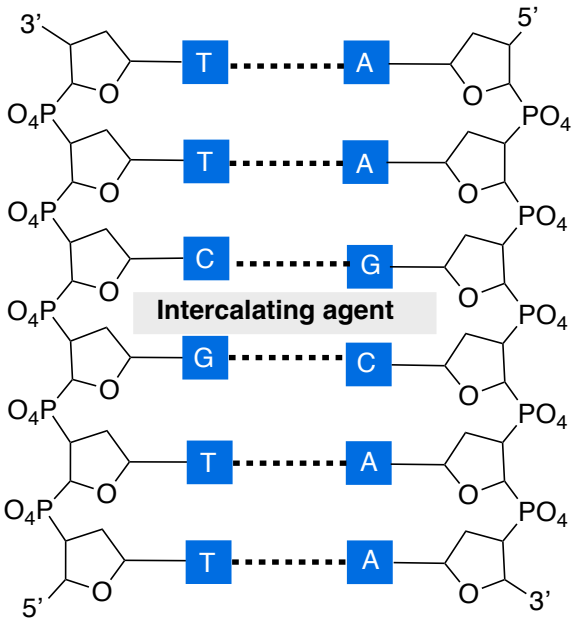

Figure 1.12 Interaction of a mono-intercalator between the basepairs of DNA

Intercalation requires changes in the torsional angles of the sugar-phosphate backbone of the DNA to allow two consecutive base pairs to move apart so that the aromatic compound can intercalate. This leads to unwinding, bending, etc., of the helical structure of the DNA. The rotation of torsional bonds creates the intercalation site by separating the base pairs, thus lengthening, and unwinding the double helix.[15, 22] This binding mode can be detected by hydrodynamic methods such as viscosity and sedimentation measurements.[22]

In theory, DNA intercalators can bind and insert between any two base pairs in a DNA double helix regardless of the presence of other intercalators between the neighboring base pairs. Consequently, all spaces between base-pairs might be assumed to be possible binding sites for a non-specific intercalator. However, once a compound intercalates between two base pairs it will change the conformation for the adjacent sites. That will reduce the chance for any molecule to bind in these neighboring binding sites. This principle is called the neighbour exclusion principle.[24]

Several fused aromatic scaffolds are verified as intercalators such as phenanthridines, phenanthrolines, acridines, anthraquinones, naphthalimides, naphthalene diimides (Scheme 1.3).[8, 12, 22]

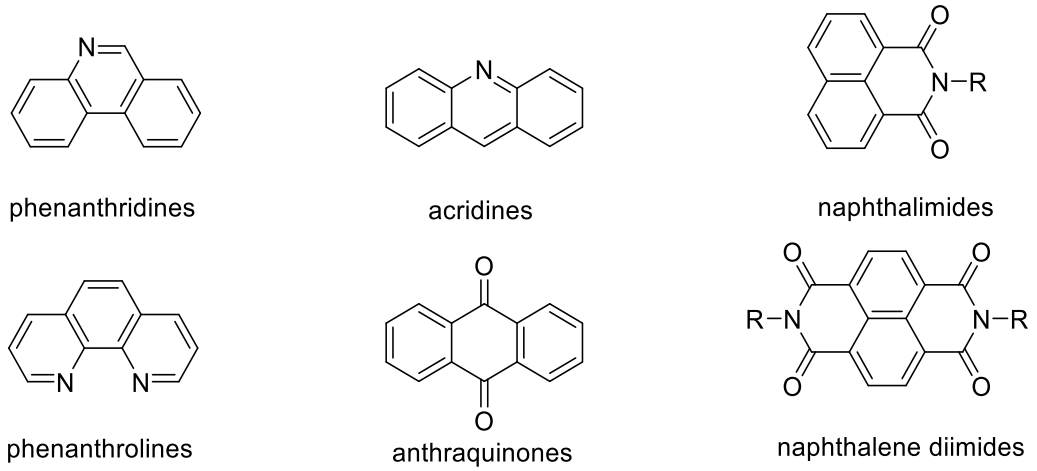

Scheme 1.3

Ever since the introduction of the intercalation concept, enormous efforts have been made towards the design and synthesis of mono- and bis-intercalators for various applications.[22]

1.2.2.1 Mono-intercalators

DNA intercalators have emerged from numerous classes of compounds and have been explored as potential anti-cancer drugs.[8, 22, 23, 25, 26]

Anthracycline is amongst one of the widely explored families of compounds commonly used in cancer chemotherapy. Representative compounds for this class are daunomycin and doxorubicin (Figure 1.13).[10, 27, 28]

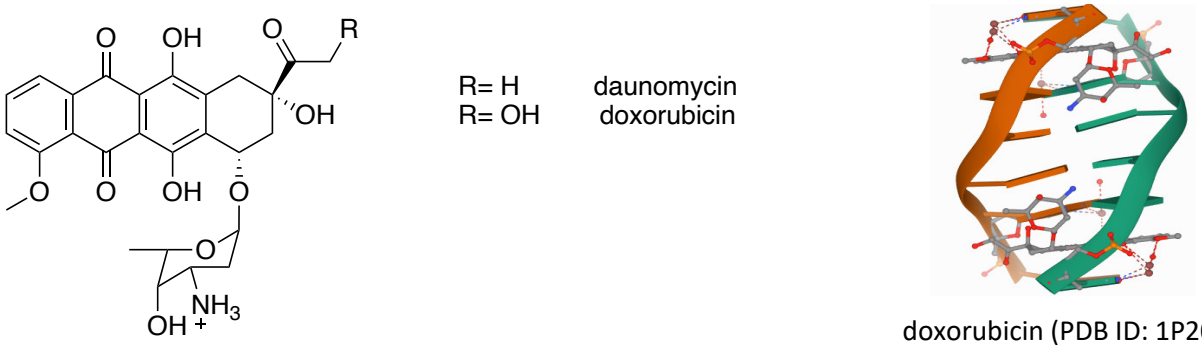

Figure 1.13 The chemical structure of daunomycin and doxorubicin (left), intercalation modes of doxorubicin (right)

The defining chemical structure of this class is an amino-sugar motif. This amino group gets protonated and plays an important role in the binding process by facilitating the electrostatic interaction between amino sugar and phosphate groups of the DNA. This electrostatic interaction forces the molecule to interact with the DNA groove, making the planar aromatic rings slides in between the G-C base pairs (intercalates) of the DNA double helix.

In 1956, Peacocke & Skerrett studied the binding properties of proflavine, from the acridine class, with DNA. The result of their study indicates two types of binding, one is a weak external binding mode, and the other one is strong. These two types of interaction were further studied by Lerman in 1961.[24, 29, 30] Lerman proposed that the strong binding is due to the insertion of proflavine between two base pairs and for the first time the term intercalation was used (Figure 1.14).[29] Although proflavine exhibited anticancer activity, it has not been used clinically due to non-selective binding to DNA.

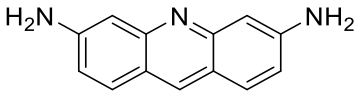

proflavin

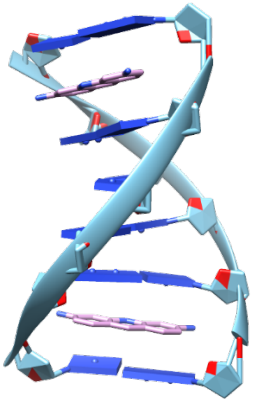

(PDB ID: 3ft6)

Figure 1.14 The chemical structure of proflavine (left), intercalation modes of proflavine (right)

In addition, there are a numerous other flat aromatic compounds that have been used as intercalators such as ethidium bromide and amsacrine (Scheme 1.4).[22, 29, 31]

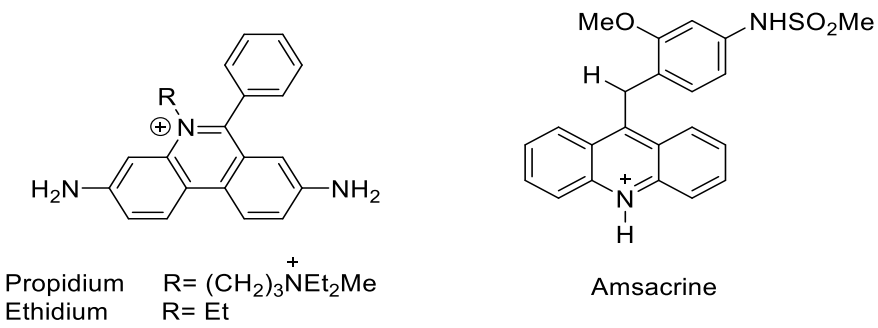

Scheme 1.4

1.2.2.2 Bis-intercalators

A strategy adopted by researchers to increase affinity for DNA is linking two monointercalators together. This dimerization of two monointercalators with varying linkers was a successful approach to design new anti-cancer compounds (Figure 1.15).[26] The length and rigidity of these linkers affect the ability of the two intercalator units to insert and stack between the base pairs.[12, 26, 32] Bisintercalators exhibit higher binding affinity towards DNA[33] because of the entropic favorability of multivalency that facilitates binding of the second intercalator after binding of the first intercalating group. This effect is sometimes described as slowing down the dissociation rate, thus increasing the affinity and as a result enhancing the anti-cancer activity.[25, 26, 34, 35] Moreover, the linkers can also play a role in enhancement of the binding affinity and selectivity by interacting with the DNA through the groove or with the phosphate groups.[26]

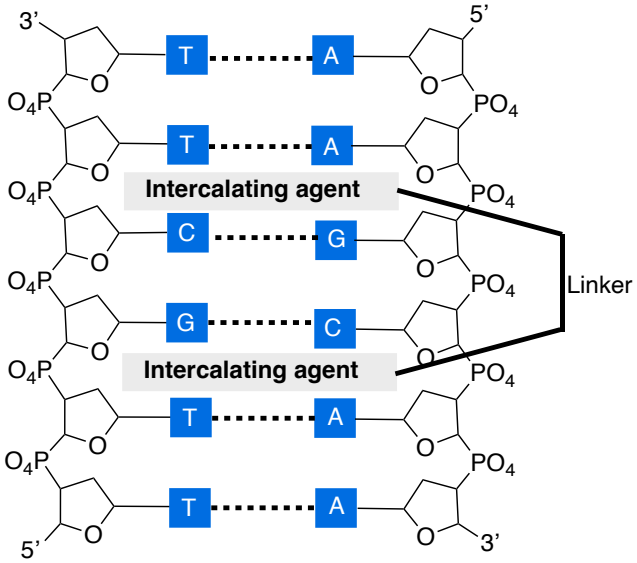

Figure 1.15 Interaction between a bis-intercalator and DNA

In 1986, Singh, Pattabiraman, Langridge, and Kollman studied for the first time the binding stability of triostin-A (a bis-intercalator) with the DNA sequence $d(CGTACG)_2$ via molecular dynamics simulation. This study showed that this particular bisintercalator caused a distortion of the DNA into a Hoogsteen form. In this Hoogsteen form, the bis-intercalator interacts with the neighboring A–T base pairs through Van der Waals interactions between the side chain of the drug and the adenine backbone which is helped by the reduced minor groove width in the Hoogsteen form of DNA.[32]

Another example of bisintercalators is ditercalinium (Scheme 1.5) where two units of 7H-pyridocarbazole are linked together with a rigid linker.[29, 36] The rigidity of the linker directed the intercalation toward G-C sites and the linker places itself in the major groove. As mentioned above, according to the neighbour exclusion principle the intercalation in the adjacent site is unpreferable due to the conformational changes which cause decreases in the free energy for the second unit intercalating at the adjacent sites. In addition, electrostatic and steric effects also play a role to decrease the chance of the intercalation at the adjacent site, which reinforces the neighbour exclusion principle.[29]

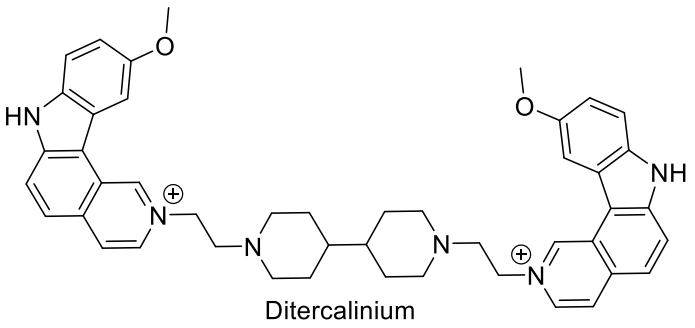

Ditercalinium

Scheme 1.5

Several well-known intercalators such as daunomycin, proflavin[37], ethidium bromide[38], thiazole orange, and oxazole orange were also dimerised using linkers such as spermine or spermidine to form the corresponding bis-intercalators. The chemical structure of bis-daunorubicin and the 3D-structure of DNA-bis-daunorubicin complex are shown in Figure 1.16.

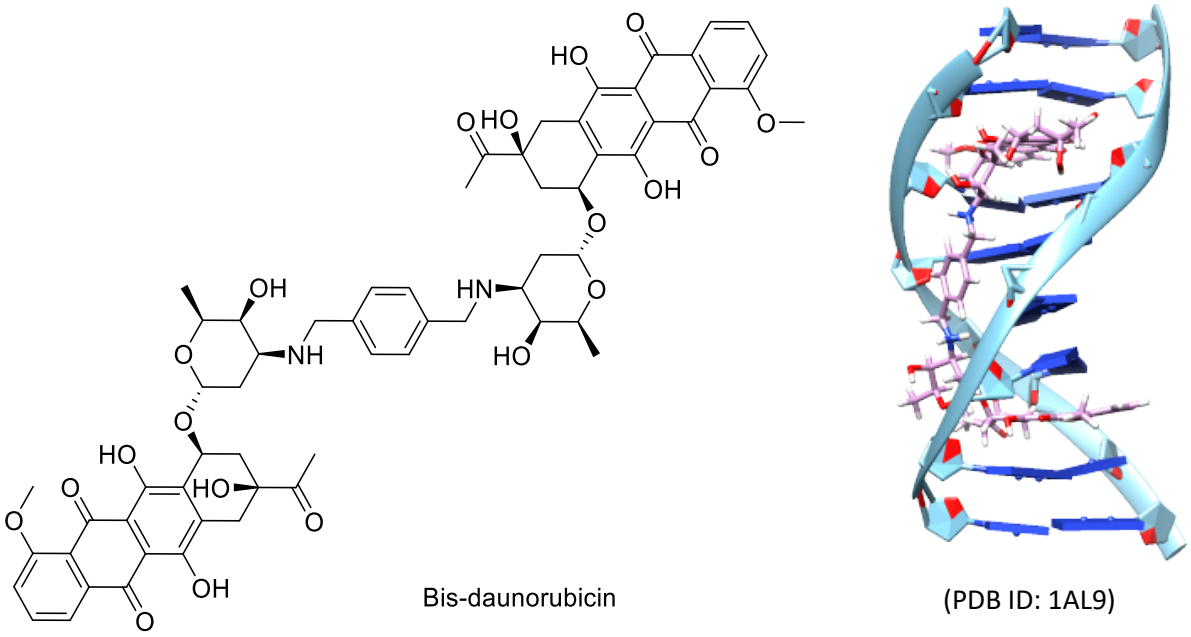

Figure 1.16 The chemical structure of bis-daunorubicin (left), intercalation modes of bis-daunorubicin (right)

1.2.2.3 Threading polyintercalators

Several intercalator units can be joined together via a linker to form threading intercalators or threading polyintercalators. This is an exciting class of intercalators that involve insertion of the intercalator units between the base pairs associated with a long linker lying alternatingly in the major or minor grooves of the DNA.[13] The benefit of this design of intercalators is the slow dissociation from the DNA helix due to the extensive molecular rearrangements needed from both binder and DNA to unbind. Also, interaction between several units of intercalator and DNA offers better opportunities for sequence recognition.[39] Moreover, threading intercalators form stable complexes with dsDNA in contrast to ssDNA that show no or little stability. Thus, this type of intercalator can be used to differentiate between ssDNA and dsDNA.[40]

To be able to synthesise threading polyintercalators, the intercalator unit needs to have two functional groups to link the intercalator units together. Naphthalene diimide, (NDI, Scheme 1.3), is a well-known intercalating unit that fits these criteria and is extensively used to synthesise bis- and polyintercalators.[41-43] These intercalator units are connected via peptides and aliphatic linkers (Scheme 1.6) with an impressive dissociation half-life of 16 days.[13, 44]

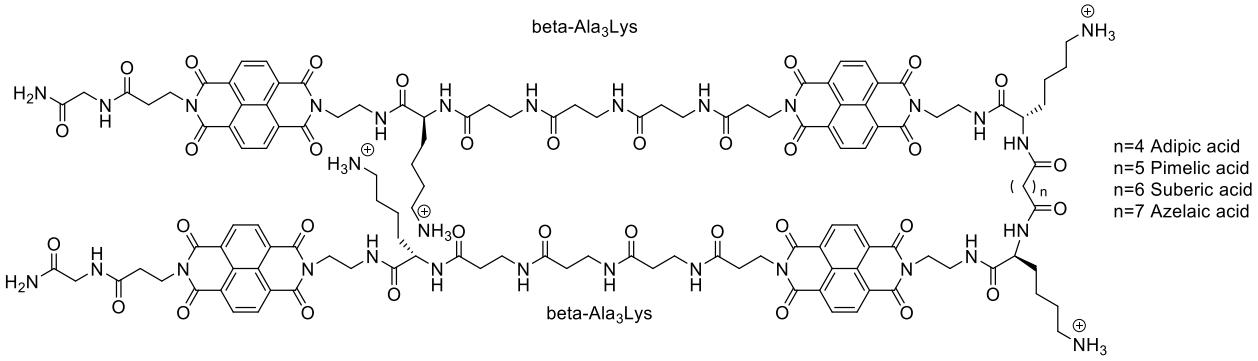

Scheme 1.6

The 3D-stucture of the resulting DNA-ligand complex is shown in Figure 1.17.

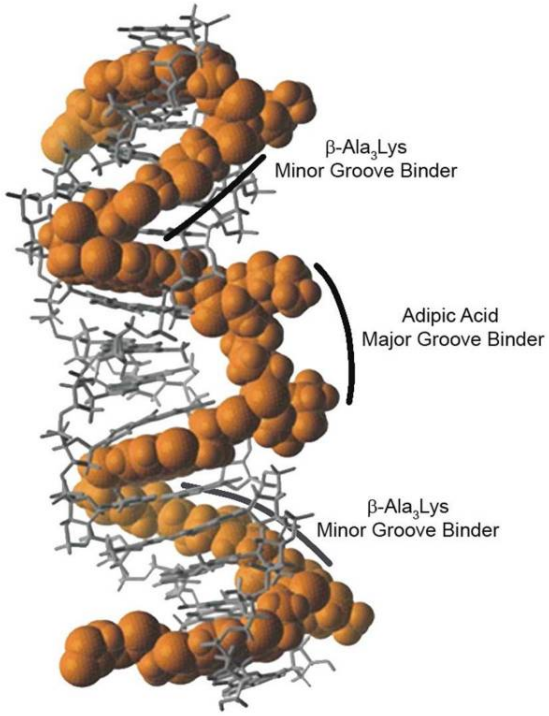

Figure 1.17 The intercalation modes of poly-naphthalene diimide [44]

In addition to naphthalene diimide, NDI, 1,5-disubstituted anthraquinone derivatives have also been used to synthesise a threading intercalator. One unit of anthraquinone derivative was used with two acridine moieties to synthesise a tris-intercalator (Scheme 1.7).[42]

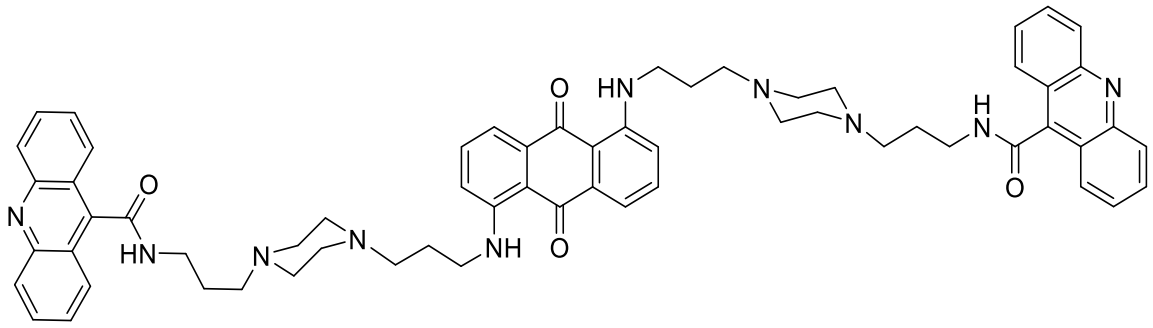

Scheme 1.7

In this case two possible binding mechanisms are proposed. The first one involves intercalation of all three units where the terminal intercalator slides into the DNA and goes out at the other side allowing the middle intercalator to intercalate (Figure 1.18 from I to II). Then the two terminal intercalators can intercalate (II to III). This binding mechanism was called the penetrating mode for tris-intercalation. The second mechanism involves the two terminal intercalators binding only (Figure 1.18 III).[42]

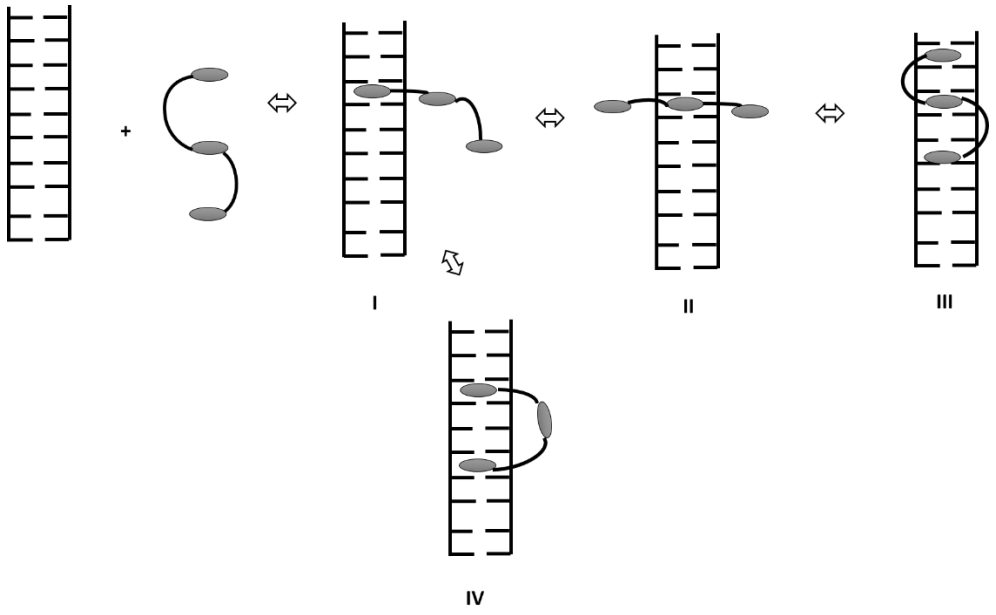

Figure 1.18 Schematic representation of proposed binding mechanisms

The UV-vis spectroscopy study indicates that the three intercalating units of the tris-intercalator bind to DNA according to the penetrating mechanism.[42]

1.3 DNA sensing

The detection of biochemical species such as nucleic acids and proteins is known as biosensing and a system achieving this detection as a biosensor. The application of biosensors varies from healthcare [45] to clinical diagnosis [46, 47] and environmental sciences.[45] A biosensor consists of a biotransducer linked with a bioreceptor that acts as a sensing element. Potential sensing elements include polysaccharides, DNA, RNA, enzyme, antibody, living cell. The sensing element recognizes a specific target analyte, and the transducer turns the recognition phenomenon/event into a measurable physical parameter or electronic signal.[48-50] Biosensors using a bioreceptor such as DNA or RNA are called genosensors, specifically a DNA sensor or an RNA sensor. DNA quantitative detection is beneficial for various applications such as tumor screening, molecular diagnosis, forensic identifications, food safety, and environmental monitoring. In 1956, Prof. Leland C. Clark was the first to develop a biosensor, viz. an enzyme electrode to measure glucose. Since then, modifications are going on to promote sensitivity, selectivity, and specificity of the sensors.

Designing DNA sensors mainly focuses on detecting DNA hybridization processes. The construction of these sensors typically starts with immobilizing a layer of single-stranded DNA (ssDNA) as a capture strand on a transducer's surface. In case the analyte contains the complementary DNA strand, often called the target strand, then DNA hybridization will occur to form the DNA double helix (Figure. 1.19).[50]

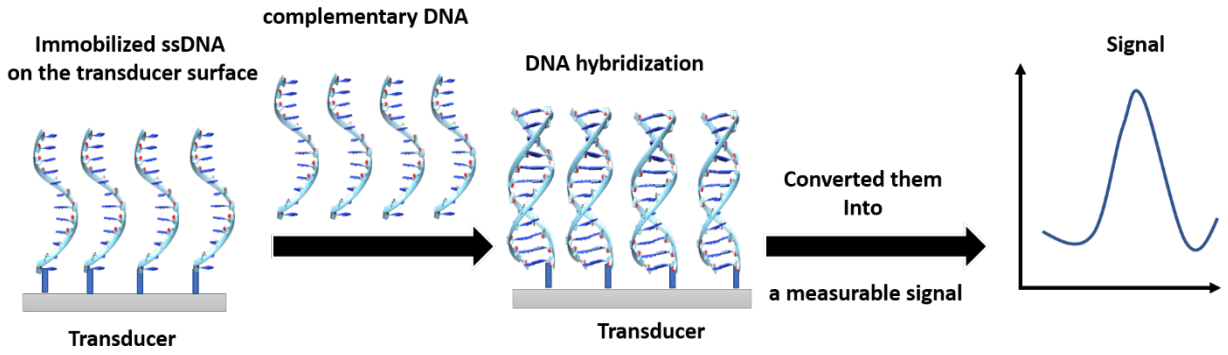

Figure 1.19 General design of DNA biosensor [50]

This hybridization can be measured and quantified as signals by transducers. In transducers, the electrochemical transducer has gained significant attention due to its simplicity and direct conversion of DNA hybridization into an electrical signal.

Sensitisers are one of the important parts of sensors that allow genosensors to detect the hybridisation events via spectroscopic or electrochemical methods. These sensitisers bind with the DNA in one of two ways. It can bind with the target DNA covalently in a sample preparation step and in this case, the sensor is described as “labelled” sensor. In the second way, sensitisers can bind with the DNA non-covalently and in this case the sensor is called a “label-free” sensor. Figure 1.20 shows the different ways of implementing the sensitizer in labeled and label-free sensors. In the labeled sensor the covalent labelling links the target strands and the sensitiser, while the label-free uses external sensitisers that can detect hybridisation by binding to dsDNA.[51]

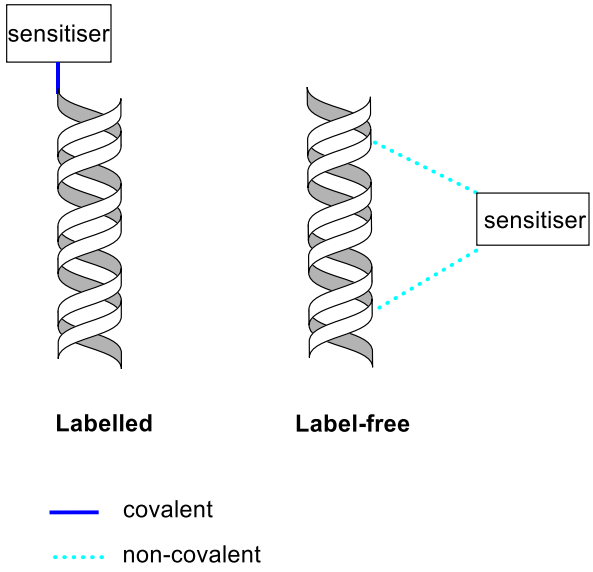

Figure 1.20 Labeled and label-free sensor

In term of simplicity, label-free sensing is a straightforward approach where the sensitizer is added in a separate step to recognize the hybridised DNA and bind non-covalently with the duplex.[51]

There are several factors that need to be considered in designing DNA sensitisers such as solubility, shape, size, and charges. For instance, synthesizing cationic compounds is highly desirable for many reasons. First, cationic compounds will electrostatically interact with the anionic phosphate backbone of DNA which increases the thermodynamic favourability of the binding. Secondly, binding studies require water-soluble compounds,

therefore binders with functionalities such as amines which bear charges at physiological pH is recommended to improve the solubility. However, the drawback of having positive charge on the DNA binders is the risk of significant non-specific binding between the binder and the DNA. Also, binding between cationic ligand with anionic phosphate group at DNA can form neutral DNA-ligand complex which could cause precipitation.[51]

1.4 Immobilization techniques for microarray detection

Microarrays or DNA chips are key tools for high-throughput analysis of biomolecules. The microarray's success depends on the good accessibility and functionality of the probes immobilized on the surface, density, and reproducibility. Different DNA immobilization techniques are used for DNA microarray production. The short oligonucleotides are DNA probes that can hybridize with specific target sequences. Thus, the immobilization step for the DNA probes is crucial to construct the microarrays. Immobilization means molecules attach to a surface, which obviously reduces or loses mobility. The process by which DNA strands are immobilized determines the microarray's property. Physicochemical properties of surface and probe determine the immobilization choice. The microarrays can be developed by making probes base-by-base or pre-synthesized and then spotted on the support.

Several techniques of immobilization have been developed. They are mainly based on three crucial mechanisms, physical adsorption, covalent immobilization, and streptavidin-biotin immobilization (Figure 1.21).

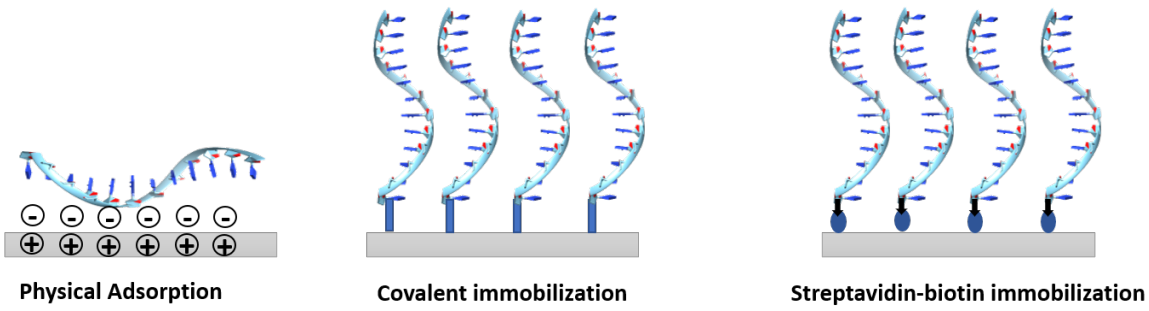

Figure 1.21 Immobilization techniques

1.5 Detection techniques in biosensors

1.5.1 Electrochemical techniques

In addition to using spectroscopic and thermodynamic parameters to study the binding properties and detect the hybridisation events, electrochemical techniques such as voltametric methods can be used. Due to simplicity and affordable instrumentation, the most common electrochemical techniques used to detect binding involve voltametric methods such as cyclic voltammetry (CV), differential pulse voltammetry (DPV) and Linear Sweep Voltammetry (LSV).

Cheng Fang *et al*. [52] have presented an interesting example aimed to use a redox probe (ferrocene carboxylic acid) to detect the hybridisation events using cyclic voltammetry. The first step in designing this sensor is immobilization of peptide nucleic acid (PNA) as a capture strand on a gold elecrode. PNA doesn't contain negatively charged phosphate groups, so it is neutral. Once the hybridisation events occur and the PNA-DNA duplex is formed, phosphate groups will be present in the hybrid duplex which allow (Zr^{+4}) to bind with the duplex and subsequently ferrocene carboxylic acid will bind electrostatically to Zr^{+4} (Figure 1.22).[52]

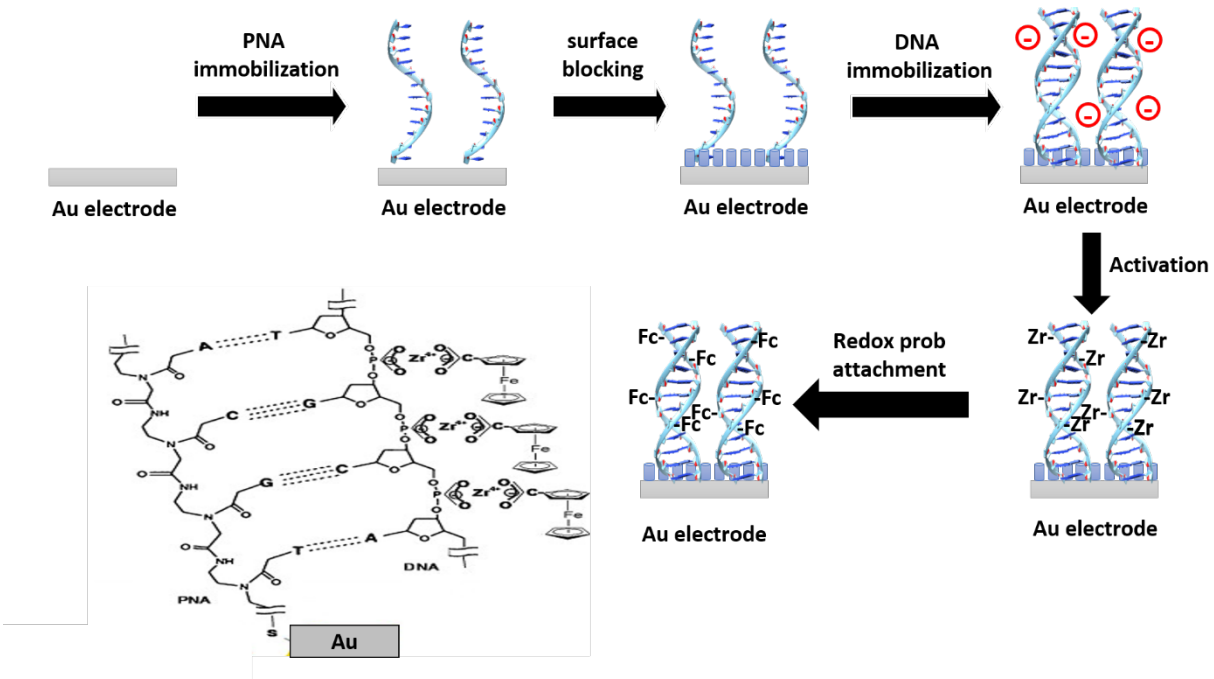

Figure 1.22 Schematic drawing of the modification on the gold electrode surface [52]

Similarly, in 2020, Wang *et al*. have used an approach to design a DNA sensor using a spin label compound (TEMPO-COOH) along with $ZrOCl_2.8H_2O$ (Zr^{+4}) and DPV as a detection technique. After the hybridization occurs, Zr^{+4} was used to bind with the negatively PNA-DNA duplex and subsequently TEMPO-COO^- binds with the duplex through Zr^{+4} (Figure 1.23).[53]

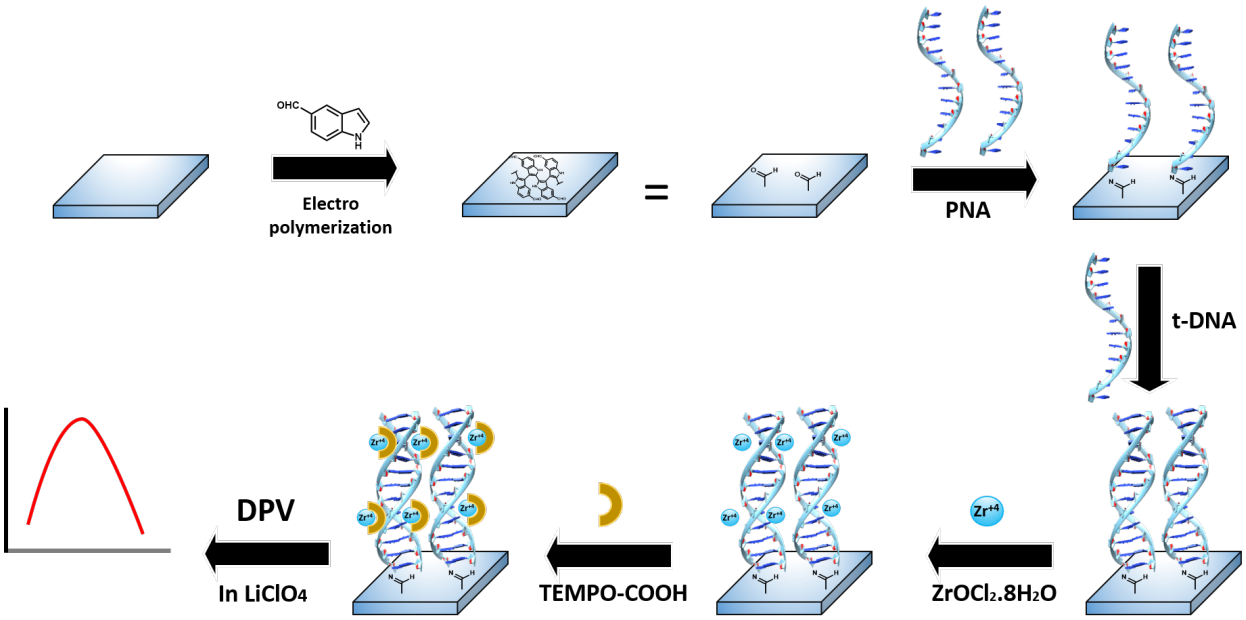

Figure 1.23 Schematic representation of proposed strategy for nucleic acids detection [53]

1.6 Biophysical techniques

For DNA binders to be appropriately investigated, thermodynamic parameters associated with binding need to be determined.[54] Several techniques can be used to measure and calculate these parameters such as ultraviolet-visible spectroscopy, isothermal titration calorimetry, and electron paramagnetic resonance (EPR).

1.6.1 Colourimetry (UV-Vis Titration)

Ultraviolet-visible spectroscopy (UV-Vis) is a cost-effective and simple technique to investigate the binding properties of DNA binders. It can be used to record the changes in the absorbance during the titration of DNA binder (ligand) with the DNA. Examining the shift of the absorbance either decreasing or increasing (hypochromic/ hyperchromic shift) or the shift of a band to a different wavelength (hypsochromic 'blue'/ bathochromic 'red'

shift) throughout the titration can be used to calculate the stoichiometry and the binding affinity (Figure 1.24).[55, 56]

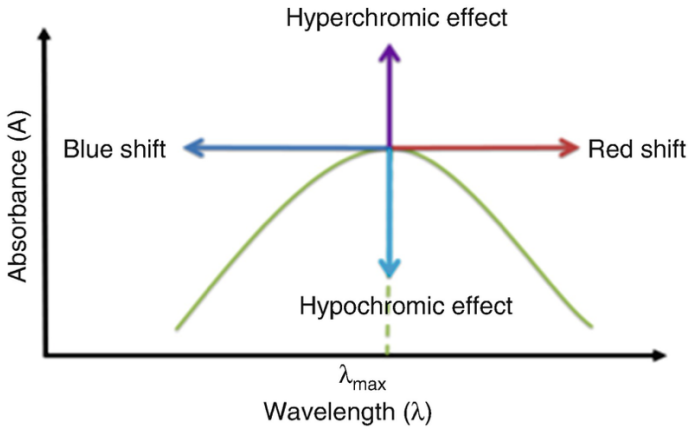

Figure 1.24 Absorption and intensity shift

The titration involves titrating a stock solution of DNA into a solution of binder. It is worth to mention that free binder absorption and DNA-bound binder absorption are usually different. Therefore, during the titration, the interaction with the DNA often results in hypochromism and bathochromism shifts.[55]

Furthermore, it is important to note that during the titration two factors can cause changes in the absorbance. The first one is the binding event, where the binder moves from a state where it is free in the solution to a state where it is bound to the DNA. The second factor is far less interesting, it is the dilution factor since the volume during the titration is increasing so the binder concentration and hence the absorbance will decrease.

In preparation of UV-vis titrations, the DNA binders need to be sufficiently soluble in buffered aqueous solution. Using different solvents is not an option since we need to preserve DNA from damage. However, it has been reported that duplex DNA sustains its stability in water-DMSO mixtures up to 10-vol% DMSO. Therefore, this mixture can be used to prepare the binder solutions assuming that the binders dissolve in DMSO.[57]

Analyzing the obtained data by plotting absorbance as a function of concentration of both ligand and DNA can provide access to the affinity constant (K_a) for the binder, and the size of the binding sites in base pairs (n). In its simplest form, K_a is an equilibrium constant for the interaction of the ligand with DNA binding sites.[54]

$$M + L \leftrightharpoons ML$$

$$\boldsymbol{K_a = [L]_b / [L]_f\,[ab]_f}$$

K_a	affinity constant	$[L]_f$	concentration of free ligand
$[L]_b$	concentration of bound ligand	$[bs]_f$	concentration of free binding sites

There are several models that can be used to analyze the data and calculate the binding constant K_a and binding site size *n*. The simplest model works under the assumption that the ligand binds to a single type of binding site. Therefore, the stoichiometry is presumed to be one. This model could work in case of protein-ligand interaction if the protein has just one binding site. However, this model cannot be used to study DNA-ligand interaction where the DNA is a polymeric molecule with many possible sites for the ligand to bind to.

Therefore, more complex models can be used to analyze UV-visible titration data for DNA. The multiple independent binding sites model (MIS) is the model that we decided to use. This model works under the assumption that all binding sites in DNA are equivalent and independent and therefore not affected by neighboring sites.[58] The drawback of this model is that DNA binding sites are not equal, and ligand bound to DNA has an influence on binding of another ligand. Also, the binding affinity is not the same for each binding site. This means that the model oversimplifies the processes involved. Nevertheless, it provides useful insight into binding affinity.

Other models such as the McGhee-von Hippel model[59] and those developed by Per Lincoln[60] consider cooperativity that is neglected by the MIS model. The cooperativity could be positive cooperativity, where the binding favorability increases in sequential binding events of interactions, and vice versa for negative cooperativity. In addition to cooperativity, these models include other factors such as inter-site influences and non-specific binding. Although the McGhee-von Hippel model takes into account most relevant factors, it assumes that all binding sites have the same basic binding affinity which is not realistic for heterogeneous DNA and therefore the interpretation of data using this model is misleading. It is worth to mention that Lincoln's models allow for investigations of more complex systems in which equilibria exist between different competing ligands.[59] This model is probably the best current model for studying interactions of small molecules and complexes with DNA, but its application required more data than typically obtained in exploratory studies.

1.6.2 Electron paramagnetic resonance (EPR) of DNA-binding compounds

Electron paramagnetic resonance spectroscopy (EPR) also known electron spin resonance spectroscopy (ESR) is a unique technique to study compounds with unpaired electrons such as free radicals or paramagnetic metal ions.[61-63] The principle that EPR works on is similar to NMR spectroscopy which involves applying a magnetic field to electron spins rather than to nuclear spins to create a population difference between spin-states to generate signals.[63] The energy difference (DE) between the high energy and low energy state of the electron can be measured using the following equation.

$$\Delta E = h\nu = g\beta B_o$$

Where h is Planck's constant, n is electromagnetic radiation frequency, g is the Lande splitting factor, b is the Bohr magneton of the electron and B_0 is the magnetic field in Tesla (T).[64, 65] The presence of free radicals cause large perturbations in the relaxation of nuclear spins, which makes structural determinations of paramagnetic compounds using NMR very difficult by causing signals to become very broad.[66]

EPR is a highly sensitive technique compared to NMR, it only requires μM concentrations in contrast to mM concentrations in case of NMR.[62, 63, 65] However, most compounds have at least one NMR-active nucleus that can be detected using NMR, whereas EPR applications are limited to compounds with open-shell systems.[62] Like NMR spectroscopy, EPR can be used for structural determination since the produced signals are sensitive to coupling and chemical environment such polarity, size, conformational changes and presence of other paramagnetic centers.[64] Consequently, EPR spectroscopy can be a very valuable technique in several fields such as radical chemistry,[67, 68] and biochemistry.[69-72]

Although EPR spectroscopy has not been used in biosensors, it was used in biochemistry studies including as spin labels or spin probes to monitor physical, biophysical, or biochemical properties of biomacromolecules.[73] The difference between spin labels and spin probes is like the difference between fluorescent labels and fluorescent probes. The paramagnetic moieties can be introduced covalently or non-covalently to form spin labels and spin probes, respectively.[64] Spin labeling can be used to study the interaction between oligo- and polynucleotides and labelled intercalators such as acridines and groove binder such as oxazolopyridocarbazole.[72, 74] That means it can be used to detect the formation of double-stranded DNA, i.e. hybridization.[71]

Nitroxide radicals (Scheme 1.8) are one of the most well-known classes of compounds extensively used as a spin labels and spin probes. This class consists of five- or six-membered heterocyclic rings with bulky neighboring methyl groups in close proximity to the unpaired electron, preventing it from reacting with other species, thus forming a persistent radical species.[75]

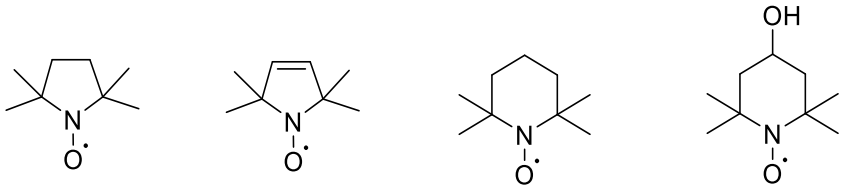

Scheme 1.8

TEMPO (2,2,6,6-tetramethylpiperidine-1-oxyl) is the most commonly used compound in this class. It has been utilized as a spin probe by linking TEMPO with RNA in various positions including the nucleobases, the ribose sugar, and the phosphate backbone (Scheme 1.9).[75] Generally, it has been reported that there are a distinguishable differences in EPR spectrum between unhybridised ssDNA and the dsDNA form in which the spin-labeled DNA fragment is involved in hybridization.[70]

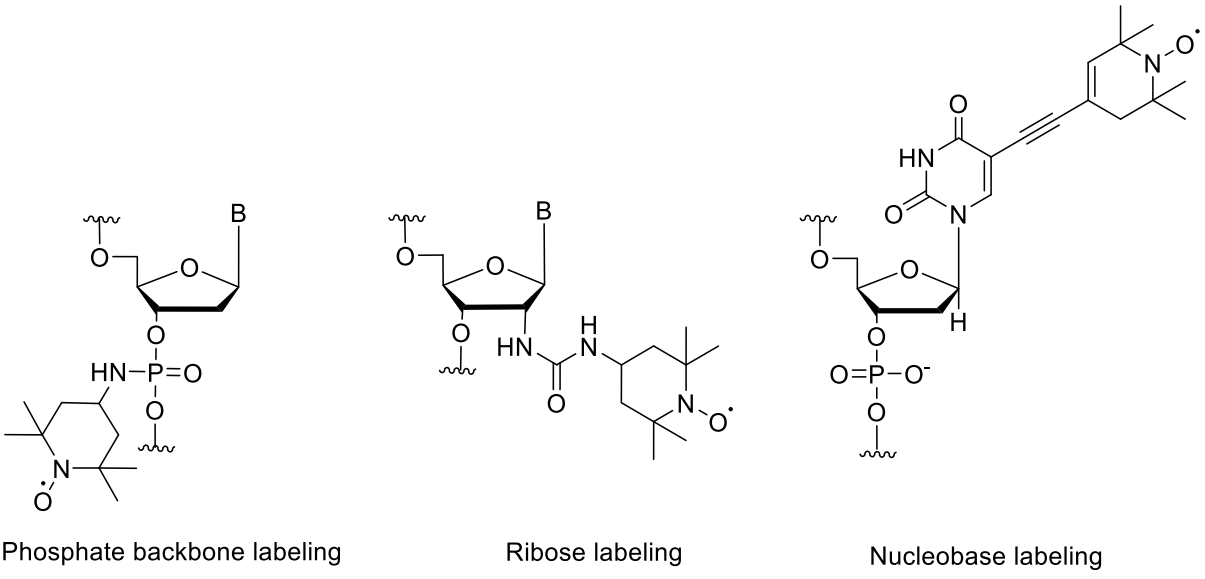

Scheme 1.9

In addition to connecting a nitroxide moiety to the biomacromolecules, nitroxides were also utilized to synthesise nitroxide-containing intercalators and groove binders. For instance, Belmont *et al*.[74] synthesized two labeled-acridine derivatives involving a nitroxyl radical. The binding affinity of these compounds were determined using two techniques, fluorescence spectroscopy and electron paramagnetic resonance. This study shows that binding affinities calculated using EPR spectroscopy are very similar to those calculated using fluorescence spectroscopy

(compound I, K_{fluo}=3x10^4 M^{-1}, K_{EPR}=2x10^4 M^{-1}, compound II, K_{fluo}=1.5x10^5 M^{-1}, K_{EPR}=2x10^5 M^{-1}). It also shows the differences in signal between free and bound species (Figure 1.25).

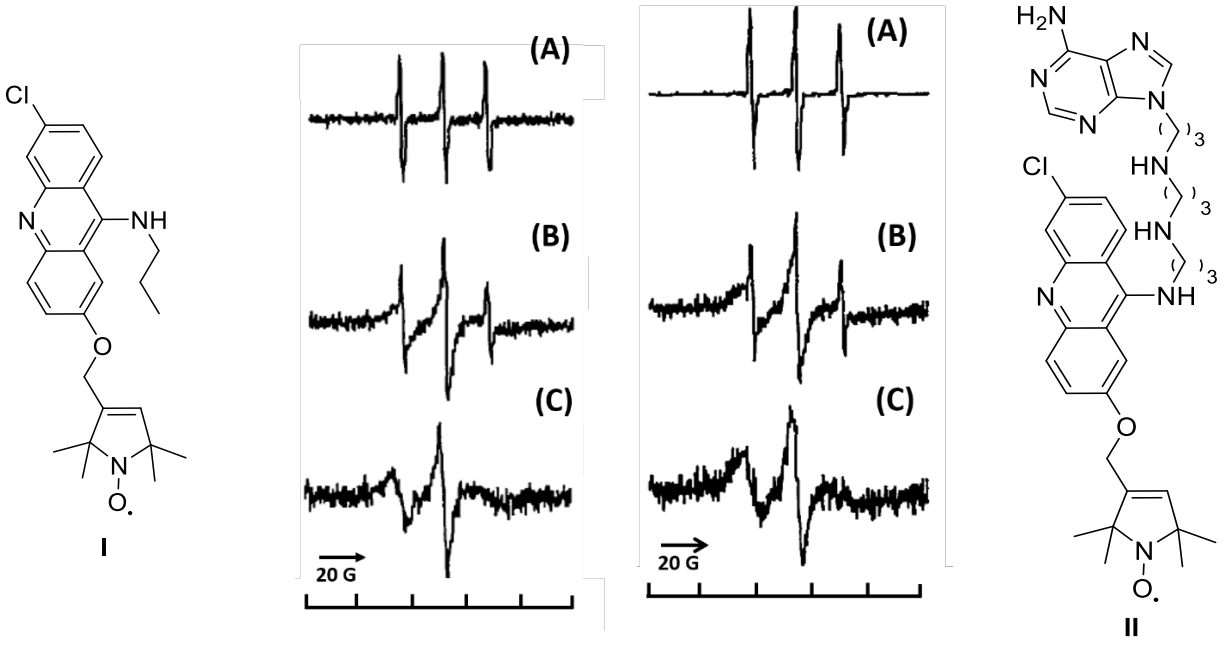

Figure 1.25 EPR spectra of the labelled acridine derivatives (I and II) in the absence (A) and presence of DNA (B) and difference spectrum (C).

EPR linewidths can be used to calculate rotational correlation time (τc), which is effectively the tumbling rate of a molecule. Upon binding, the τc of the acridine derivatives decrease, causing broadening of the EPR signal. The spectra for free and bound acridine derivatives can then be used to generate difference spectra, and allow τc to be calculated.[74]

1.7 Project Aims

This thesis aims to synthesise several functional naphthalimide derivatives and evaluate their DNA-binding properties.

Chapter 2 involves synthesizing ferrocene-naphthalimide conjugates (Scheme 1.14) where the naphthalimide skeleton is connected to a ferrocene moiety via two linkers. Introducing the ferrocene moiety to the target

compounds allowing us to study their DNA binding properties via electrochemical techniques in the future. However, the main scope for this thesis is to study the DNA binding properties for the synthesized compounds via UV-visible titrations. For exploring this class of compound several functionalize naphthalimide core were synthesized to enhance the solubility and study their effect of DNA binding affinities.

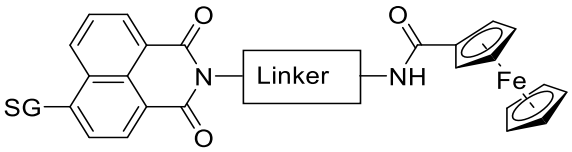

Scheme 1.10

Chapter 3 involves synthesizing several bisnaphthalimide derivatives where two units of naphthalimide are connected via several aliphatic and aromatic linkers (Scheme 1.5). Also, the naphthalimide scaffolds were functionalized using several solubilizing groups (1°-amine, 2°-amine, thiol group). This approach aims to improve the DNA-binding affinities by increases the possibility for the compound to intercalate with DNA via two units of intercalators. the solubilizing groups on the other hand were introduced for two reasons. The first, is to enhance the solubility of the synthesized hydrophobic bisnaphthalimides. Secondly, these solubilizing groups affect the spectroscopic properties of the naphthalimide chromophore and also play a role in the ability for these compounds to bind with DNA which will be studied using UV-visible titrations.

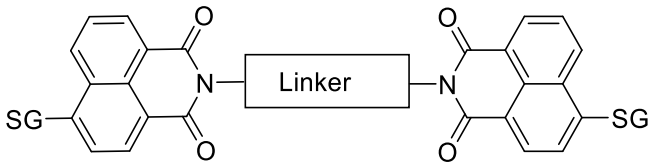

Scheme 1.11

Chapter 4 involves increasing the aromatic surface in comparison with naphthalimide, which several studies have shown is a successful approach to improve the DNA-binding properties. Therefore, two series of fused-ring-extended 1,8-naphthalimide derivatives (Scheme 1.16) were proposed. This proposed scheme involves synthesizing and separating two isomers with different solubilizing groups. Investigating the DNA-binding affinities

for these series of compounds will show whether the binding properties for these isomers are the same and to explore the effect of the different solubilizing groups in the DNA binding affinities

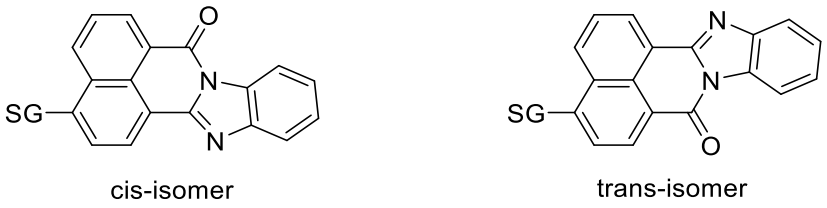

Scheme 1.12

Chapter 5 aims to expand the opportunities to investigate the DNA-binding affinities using a different technique. We propose to connect mono- and bisnaphthalimide scaffolds with a TEMPO moiety (Scheme 1.17) using an amide-dorming coupling reaction. This approach allows us to study DNA binding properties for these compounds using EPR in the future. However, the scope of this project is to investigate the binding properties using UV-visible titrations.

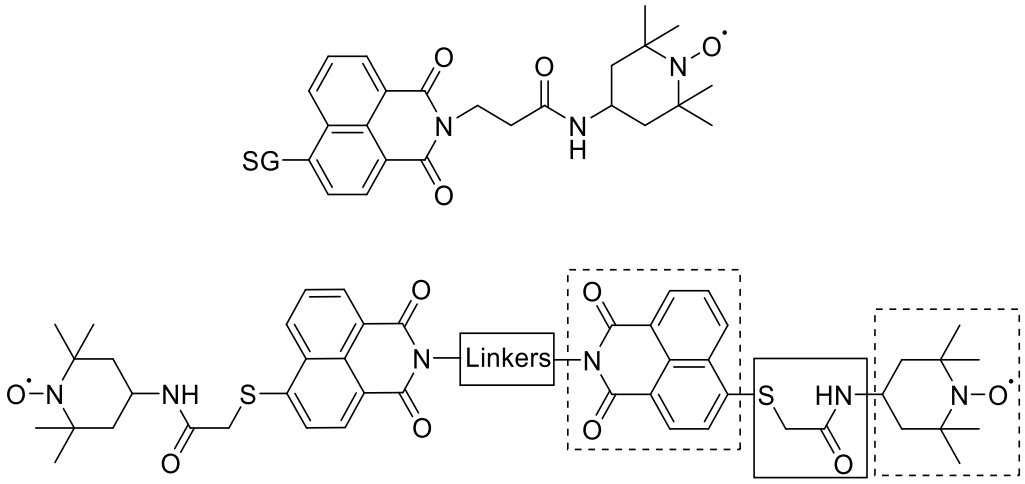

Scheme 1.13

References

1. Pray, L. In *Discovery of DNA Structure and Function: Watson and Crick*, 2013.

2. Cobb, M., Oswald Avery, DNA, and the transformation of biology. *Current Biology* **2014,** *24* (2), R55-R60.

3. van Holde, K. E.; Zlatanova, J., Chapter 9 - The Central Dogma. In *The Evolution of Molecular Biology*, van Holde, K. E.; Zlatanova, J., Eds. Academic Press: 2018; pp 87-94.

4. Portin, P., The birth and development of the DNA theory of inheritance: sixty years since the discovery of the structure of DNA. *Journal of Genetics* **2014,** *93* (1), 293-302.

5. Conti, A. A., "A hundred years since the birth of Rosalind Elsie Franklin, a brilliant and gifted scientist". *Internal and Emergency Medicine* **2021,** *16* (2), 531-532.

6. Withers, J. M.; Padroni, G.; Pauff, S. M.; Clark, A. W.; Mackay, S. P.; Burley, G. A., 5.07 - DNA Minor Groove Binders as Therapeutic Agents. In *Comprehensive Supramolecular Chemistry II*, Atwood, J. L., Ed. Elsevier: Oxford, 2017; pp 149-178.

7. Hamilton, P. L.; Arya, D. P., Natural product DNA major groove binders. *Natural Product Reports* **2012,** *29* (2), 134-143.

8. Bhaduri, S.; Ranjan, N.; Arya, D. P., An overview of recent advances in duplex DNA recognition by small molecules. *Beilstein J Org Chem* **2018,** *14*, 1051-1086.

9. Kaushik, M.; Kaushik, S.; Roy, K.; Singh, A.; Mahendru, S.; Kumar, M.; Chaudhary, S.; Ahmed, S.; Kukreti, S., A bouquet of DNA structures: Emerging diversity. *Biochem Biophys Rep* **2016,** *5*, 388-395.

10. Khan, G. S.; Shah, A.; Zia ur, R.; Barker, D., Chemistry of DNA minor groove binding agents. *Journal of Photochemistry and Photobiology B: Biology* **2012,** *115*, 105-118.

11. Chang, Y.-M.; Chen, C. K. M.; Hou, M.-H., Conformational Changes in DNA upon Ligand Binding Monitored by Circular Dichroism. *International Journal of Molecular Sciences* **2012,** *13* (3).

12. Brana, M. F.; Cacho, M.; Gradillas, A.; Pascual-Teresa, B. d.; Ramos, A., Intercalators as Anticancer Drugs. *Current Pharmaceutical Design* **2001,** *7* (17), 1745-1780.

13. Smith, A. R.; Ikkanda, B. A.; Holman, G. G.; Iverson, B. L., Subtle recognition of 14-base pair DNA sequences via threading polyintercalation. *Biochemistry* **2012,** *51* (22), 4445-52.

14. Cai, X.; Gray, P. J.; Von Hoff, D. D., DNA minor groove binders: Back in the groove. *Cancer Treatment Reviews* **2009,** *35* (5), 437-450.

15. Katarina, M.; Maro, B.; Mirela Baus, L.; Ljubica, G.-O., Antineoplastic DNA-Binding Compounds: Intercalating and Minor Groove Binding Drugs. *Archives of Industrial Hygiene and Toxicology* **2013,** *64* (4), 593-602.

16. Rocha, C. R. R.; Silva, M. M.; Quinet, A.; Cabral-Neto, J. B.; Menck, C. F. M., DNA repair pathways and cisplatin resistance: an intimate relationship. *Clinics* **2018,** *73* (suppl 1).

17. E, R., Insights into the Relative DNA Binding Affinity and Preferred Binding Mode of Homologous Compounds Using Isothermal Titration Calorimetry (ITC). In *Applications of Calorimetry in a Wide Context - Differential Scanning Calorimetry, Isothermal Titration Calorimetry and Microcalorimetry*, 2013.

18. Palchaudhuri, R.; Hergenrother, P. J., DNA as a target for anticancer compounds: methods to determine the mode of binding and the mechanism of action. *Current Opinion in Biotechnology* **2007,** *18* (6), 497-503.

19. Dervan, P. B., Molecular recognition of DNA by small molecules. *Bioorg Med Chem* **2001,** *9* (9), 2215-35.

20. Herman, D. M.; Baird, E. E.; Dervan, P. B., Stereochemical Control of the DNA Binding Affinity, Sequence Specificity, and Orientation Preference of Chiral Hairpin Polyamides in the Minor Groove. *Journal of the American Chemical Society* **1998,** *120* (7), 1382-1391.

21. Wurtz, N. R.; Dervan, P. B., Sequence specific alkylation of DNA by hairpin pyrrole–imidazole polyamide conjugates. *Chemistry & Biology* **2000,** *7* (3), 153-161.

22. Nial, J. W.; Craig, R. B.; Collins, J. G.; Sharon, K.; Janice, R. A.-W., DNA Intercalators in Cancer Therapy: Organic and Inorganic Drugs and Their Spectroscopic Tools of Analysis. *Mini-Reviews in Medicinal Chemistry* **2007,** *7* (6), 627-648.

23. Marverti, G.; Cusumano, M.; Ligabue, A.; Di Pietro, M. L.; Vainiglia, P. A.; Ferrari, A.; Bergomi, M.; Moruzzi, M. S.; Frassineti, C., Studies on the anti-proliferative effects of novel DNA-intercalating bipyridyl–thiourea–Pt(II) complexes against cisplatin-sensitive and -resistant human ovarian cancer cells. *Journal of Inorganic Biochemistry* **2008,** *102* (4), 699-712.

24. Karimi Goftar, M.; Moradi Kor, N.; Moradi Kor, Z., DNA Intercalators and Using Them as Anticancer Drugs. *International Journal of Advanced Biological and Biomedical Research* **2014,** *2* (3), 811-822.

25. Yang, P.; Yang, Q.; Qian, X., Novel DNA bis-intercalators of isoquinolino[4,5-bc]acridines: design, synthesis and evaluation of cytotoxic activity. *Tetrahedron* **2005,** *61* (50), 11895-11901.

26. Zhao, J.; Li, W.; Ma, R.; Chen, S.; Ren, S.; Jiang, T., Design, synthesis and DNA interaction study of new potential DNA bis-intercalators based on glucuronic acid. *Int J Mol Sci* **2013,** *14* (8), 16851-65.

27. Trieb, M.; Rauch, C.; Wellenzohn, B.; Wibowo, F.; Loerting, T.; Mayer, E.; Liedl, K. R., Shi, Coleman et al. 2009. *Journal of Biomolecular Structure and Dynamics* **2004,** *21* (5), 713-724.

28. Shi, W.; Coleman, R. S.; Lowary, T. L., Synthesis and DNA-binding affinity studies of glycosylated intercalators designed as functional mimics of the anthracycline antibiotics. *Organic & Biomolecular Chemistry* **2009,** *7* (18), 3709-3722.

29. Wilson, W. D., 7.12 - DNA Intercalators. In *Comprehensive Natural Products Chemistry*, Barton, S. D.; Nakanishi, K.; Meth-Cohn, O., Eds. Pergamon: Oxford, 1999; pp 427-476.

30. Luzzati, V.; Masson, F.; Lerman, L. S., Interaction of DNA and proflavine: A small-angle X-ray scattering study. *Journal of Molecular Biology* **1961,** *3* (5), 634-639.

31. Antonini, I., DNA-binding antitumor agents: from pyrimido[5,6,1-de]acridines to other intriguing classes of acridine derivatives. *Curr Med Chem* **2002,** *9* (18), 1701-16.

32. Mukherjee, A.; Sasikala, W. D., Chapter One - Drug–DNA Intercalation: From Discovery to the Molecular Mechanism. In *Advances in Protein Chemistry and Structural Biology*, Karabencheva-Christova, T., Ed. Academic Press: 2013; Vol. 92, pp 1-62.

33. Wakelin, L. P. G., Polyfunctional DNA intercalating agents. *Medicinal Research Reviews* **1986,** *6* (3), 275-340.

34. Huang, Y.; Song, Y.; Huang, M.; Fan, Y.-R.; Tian, D.-N.; Zhao, Q.-P.; Yang, X.-B.; Zhang, W.-N., Synthesis, DNA binding, and cytotoxicity activity of bis-naphalenyl compounds with different diamine linkers. *Research on Chemical Intermediates* **2016,** *42* (10), 7329-7344.

35. Rescifina, A.; Zagni, C.; Varrica, M. G.; Pistara, V.; Corsaro, A., Recent advances in small organic molecules as DNA intercalating agents: synthesis, activity, and modeling. *Eur J Med Chem* **2014,** *74*, 95-115.

36. Dupont, J.; Schwaller, M.-A.; Dodin, G., Ditercalinium, a Nucleic Acid Binder, Inhits the Respiratory Chain of Isolated Mammalian Mitochondria. *Cancer Research* **1990,** *50* (24), 7966.

37. Lorente, A.; Vázquez, Y. G.; Fernández, M. J.; Ferrández, A., Bisacridines with aromatic linking chains. Synthesis, DNA interaction, and antitumor activity. *Bioorg Med Chem* **2004,** *12* (16), 4307-12.

38. Jain, N.; Francis, S.; Friedman, S. H., Inhibition of therapeutically important polymerases with high affinity bis-intercalators. *Bioorganic & Medicinal Chemistry Letters* **2012,** *22* (14), 4844-4848.

39. Lee, J.; Guelev, V.; Sorey, S.; Hoffman, D. W.; Iverson, B. L., NMR Structural Analysis of a Modular Threading Tetraintercalator Bound to DNA. *Journal of the American Chemical Society* **2004,** *126* (43), 14036-14042.

40. Takenaka, S.; Yamashita, K.; Takagi, M.; Uto, Y.; Kondo, H., DNA Sensing on a DNA Probe-Modified Electrode Using Ferrocenylnaphthalene Diimide as the Electrochemically Active Ligand. *Analytical Chemistry* **2000,** *72* (6), 1334-1341.

41. Guelev, V.; Lee, J.; Ward, J.; Sorey, S.; Hoffman, D. W.; Iverson, B. L., Peptide bis-intercalator binds DNA via threading mode with sequence specific contacts in the major groove. *Chemistry & Biology* **2001,** *8* (5), 415-425.

42. Takagi, M.; Yokoyama, H.; Takenaka, S.; Yokoyama, M.; Kondo, H., Poly-intercalators Carrying Threading Intercalator Moieties as Novel DNA Targeting Ligands. *Journal of inclusion phenomena and molecular recognition in chemistry* **1998,** *32* (2), 375-383.

43. Holman, G.; Zewail-Foote, M.; Rhoden Smith, A.; Johnson, K.; Iverson, B., A Sequence-Specific Threading Tetraintercalator with an Extremely Slow Dissociation Rate Constant. *Nat Chem* **2011,** *3*, 875-81.

44. Rhoden Smith, A.; Iverson, B. L., Threading polyintercalators with extremely slow dissociation rates and extended DNA binding sites. *J Am Chem Soc* **2013,** *135* (34), 12783-9.

45. Vinoth, S.; Shalini Devi, K. S.; Pandikumar, A., A comprehensive review on graphitic carbon nitride based electrochemical and biosensors for environmental and healthcare applications. *TrAC Trends in Analytical Chemistry* **2021,** *140*, 116274.

46. Abolhasan, R.; Mehdizadeh, A.; Rashidi, M. R.; Aghebati-Maleki, L.; Yousefi, M., Application of hairpin DNA-based biosensors with various signal amplification strategies in clinical diagnosis. *Biosensors and Bioelectronics* **2019,** *129*, 164-174.

47. Gaiji, H.; Jolly, P.; Ustuner, S.; Goggins, S.; Abderrabba, M.; Frost, C. G.; Estrela, P., A Peptide Nucleic Acid (PNA)-DNA Ferrocenyl Intercalator for Electrochemical Sensing. *Electroanalysis* **2017,** *29* (3), 917-922.

48. Sun, W.; Qin, P.; Gao, H.; Li, G.; Jiao, K., Electrochemical DNA biosensor based on chitosan/nano-V2O5/MWCNTs composite film modified carbon ionic liquid electrode and its application to the LAMP product of Yersinia enterocolitica gene sequence. *Biosensors and Bioelectronics* **2010,** *25* (6), 1264-1270.

49. Wang, K.; Lei, Y.; Zhong, G.-X.; Zheng, Y.-J.; Sun, Z.-L.; Peng, H.-P.; Chen, W.; Liu, A.-L.; Chen, Y.-Z.; Lin, X.-H., Dual-probe electrochemical DNA biosensor based on the "Y" junction structure and restriction endonuclease assisted cyclic enzymatic amplification for detection of double-strand DNA of PML/RARα related fusion gene. *Biosensors and Bioelectronics* **2015,** *71*, 463-469.

50. Rashid, J. I. A.; Yusof, N. A., The strategies of DNA immobilization and hybridization detection mechanism in the construction of electrochemical DNA sensor: A review. *Sensing and Bio-Sensing Research* **2017,** *16*, 19-31.

51. Buurma, N. J., π-Conjugated DNA Binders. In *DNA in Supramolecular Chemistry and Nanotechnology*, 2014; pp 22-37.

52. Fang, C.; Ji, H.; Karen, W. Y.; Rafei, S. R. M., Electrochemical detection of oligonucleotide by attaching redox probes onto its backbone. *Biosensors and Bioelectronics* **2011,** *26* (5), 2670-2674.

53. Wang, C.; Liu, J.; Kong, J.; Zhang, X., Nitronyl nitroxide monoradical TEMPO as new electrochemical label for ultrasensitive detection of nucleic acids. *Analytica Chimica Acta* **2020,** *1136*, 19-24.

54. Bereznyak, E.; Gladkovskaya, N.; Dukhopelnykov, E.; Gerus, A.; Lantushenko, A.; Evstigneev, M., Thermal analysis of ligand-DNA interaction: determination of binding parameters. *Biophysics* **2015,** *2*, 423-440.

55. Sirajuddin, M.; Ali, S.; Badshah, A., Drug–DNA interactions and their study by UV–Visible, fluorescence spectroscopies and cyclic voltametry. *Journal of Photochemistry and Photobiology B: Biology* **2013,** *124*, 1-19.

56. Luo, Y.-L.; Baathulaa, K.; Kannekanti, V. K.; Zhou, C.-H.; Cai, G.-X., Novel benzimidazole derived naphthalimide triazoles: synthesis, antimicrobial activity and interactions with calf thymus DNA. *Science China Chemistry* **2015,** *58* (3), 483-494.

57. Escara, J. F.; Hutton, J. R., Thermal stability and renaturation of DNA in dimethyl sulfoxide solutions: Acceleration of the renaturation rate. *Biopolymers* **1980,** *19*.

58. Hahn, L.; Buurma, N. J.; Gade, L. H., A Water-Soluble Tetraazaperopyrene Dye as Strong G-Quadruplex DNA Binder. *Chemistry – A European Journal* **2016,** *22* (18), 6314-6322.

59. Lincoln, P., A generalized McGhee–von Hippel method for the cooperative binding of different competing ligands to an infinite one-dimensional lattice. *Chemical Physics Letters* **1998,** *288* (5), 647-656.

60. Mårtensson, A. K. F.; Lincoln, P., Competitive DNA binding of Ru(bpy)(2)dppz(2+) enantiomers studied with isothermal titration calorimetry (ITC) using a direct and general binding isotherm algorithm. *Phys Chem Chem Phys* **2018,** *20* (12), 7920-7930.

61. Karunakaran, C.; Balamurugan, M., Chapter Four - Electron Paramagnetic Resonance Spectroscopy. In *Spin Resonance Spectroscopy*, Karunakaran, C., Ed. Elsevier: 2018; pp 169-228.

62. Hagen, W. R., Chapter 4 - EPR spectroscopy. In *Practical Approaches to Biological Inorganic Chemistry (Second Edition)*, Crichton, R. R.; Louro, R. O., Eds. Elsevier: 2020; pp 121-154.

63. Roessler, M. M.; Salvadori, E., Principles and applications of EPR spectroscopy in the chemical sciences. *Chemical Society Reviews* **2018,** *47* (8), 2534-2553.

64. Melanson, M.; Sood, A.; Török, F.; Török, M., Introduction to spin label electron paramagnetic resonance spectroscopy of proteins. *Biochem Mol Biol Educ* **2013,** *41* (3), 156-162.

65. Sahu, I. D.; Lorigan, G. A., Electron Spin Resonance Spectroscopy | Spin Labeling and Spin Trapping. In *Encyclopedia of Analytical Science (Third Edition)*, Worsfold, P.; Poole, C.; Townshend, A.; Miró, M., Eds. Academic Press: Oxford, 2019; pp 315-327.

66. Satterlee, J. D., Fundamental Concepts of NMR in Paramagnetic Systems. Part II: Relaxation Effects. *Concepts in Magnetic Resonance* **1990,** *2* (3), 119-129.

67. Schubert, E.; Hett, T.; Schiemann, O.; NejatyJahromy, Y., EPR studies on the kinetics of the α-hydroxyethyl radical generated by Fenton-like chemistry. *Journal of Magnetic Resonance* **2016,** *265*, 10-15.

68. Takahashi, H.; Hirano, H.; Nomura, K.; Hagiwara, K.; Kawai, A., Rate constant measurements for radical addition reactions with C60 by means of time-resolved EPR and spin-echo detected pulsed EPR spectroscopy. *Chemical Physics Letters* **2021,** *763*, 138205.

69. Torricella, F.; Pierro, A.; Mileo, E.; Belle, V.; Bonucci, A., Nitroxide spin labels and EPR spectroscopy: A powerful association for protein dynamics studies. *Biochimica et Biophysica Acta (BBA) - Proteins and Proteomics* **2021,** *1869* (7), 140653.

70. Bannwarth, W.; Schmidt, D., Oligonucleotides containing spin-labeled 2'-deoxycytidine and 5-methyl-2'-deoxycytidine as probes for structural motifs of DNA. *Bioorganic & Medicinal Chemistry Letters* **1994,** *4* (8), 977-980.

71. Gannett, P. M.; Darian, E.; Powell, J.; Johnson, E. M., 2nd; Mundoma, C.; Greenbaum, N. L.; Ramsey, C. M.; Dalal, N. S.; Budil, D. E., Probing triplex formation by EPR spectroscopy using a newly synthesized spin label for oligonucleotides. *Nucleic Acids Res* **2002,** *30* (23), 5328-5337.

72. Keyes, R. S.; Bobst, E. V.; Cao, Y. Y.; Bobst, A. M., Overall and internal dynamics of DNA as monitored by five-atom-tethered spin labels. *Biophysical Journal* **1997,** *72* (1), 282-290.

73. Arroyo, C. M., Spin Trapping and Spin Labelling Studied Using EPR Spectroscopy. In *Encyclopedia of Spectroscopy and Spectrometry (Third Edition)*, Lindon, J. C.; Tranter, G. E.; Koppenaal, D. W., Eds. Academic Press: Oxford, 2017; pp 209-217.

74. Belmont, P.; Chapelle, C.; Demeunynck, M.; Michon, J.; Michon, P.; Lhomme, J., Introduction of a nitroxide group on position 2 of 9-phenoxyacridine: Easy access to spin labelled DNA-binding conjugates. *Bioorganic & Medicinal Chemistry Letters* **1998,** *8* (6), 669-674.

75. Esquiaqui, J. M.; Sherman, E. M.; Ye, J.-D.; Fanucci, G. E., Chapter Thirteen - Site-Directed Spin-Labeling Strategies and Electron Paramagnetic Resonance Spectroscopy for Large Riboswitches. In *Methods in Enzymology*, Burke-Aguero, D. H., Ed. Academic Press: 2014; Vol. 549, pp 287-311.

Chapter 2 Mono-naphthalimide derivatives as DNA-intercalators

Abstract

A series of ferrocene-naphthalimide conjugates **2.12a-f** and **2.13a,c,e** were successfully synthesized and characterized using NMR spectroscopy and mass spectrometry. In these compounds, the naphthalimide scaffold is linked with a ferrocene moiety via a terminal diamine linker. Several solubilizing groups were introduced on C4 in the naphthalimide scaffold to produce compounds **2.12a-f** and **2.13a,c,f**. These solubilizing groups (1°-amine, 2°-amine and thiol group) have different effects on the solubility of the obtained ferrocene-naphthalimide conjugates. Moreover, the solubilizing groups affect the DNA binding affinities for these compounds which have been studied using UV-visible titrations. Although most synthesised ferrocene-naphthalimide conjugates can be considered weak binders, **2.12f** and **2.13c** bind strongly with DNA with binding affinities of 3.8×10^5 and 1.01×10^5 M^{-1}, respectively. Generally, using linkers with different length to connect the naphthalimide scaffold and ferrocene moieties did not play a significant role in terms of binding with DNA except for one case when morpholine was used as a solubilizing group. In this case changing the length of the linker between the ferrocene and the naphthalimide has a remarkable effect on improving the binding affinity where the compound with a short linker **2.13c** exhibits stronger binding affinity than the compound with the longer ether-based linker.

2.1 Introduction

2.1.1 Naphthalimides

Naphthalimides are a well-known class of compounds with a variety of applications. Chemically, 1,8-naphthalimide derivatives are flat aromatic systems that can synthesized by the condensation of the corresponding 1,8-naphthalic anhydride and various primary amines (Scheme 2.1). This reaction can easily produce a large class of naphthalimide derivatives.[1-4]

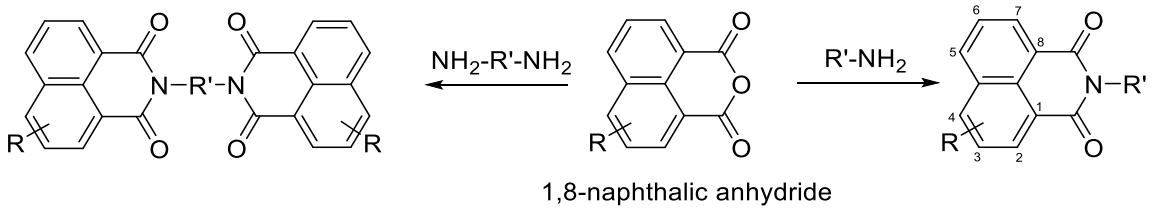

Scheme 2.1

In terms of synthesis protocols, using one equivalent of 1,8-naphthalic anhydride with one equivalent of primary amine leads to synthesis mono-naphthalimide derivatives. Using two equivalents of 1,8-naphthalic anhydride with terminal diamines produces linked bis-naphthalimides derivatives.[5-7]

Additionally, introducing different substituents to the naphthalimide skeleton creates numerous naphthalimide derivatives with different properties that widen the spectrum for several applications. Often, the introduction of such substituents is achieved through an S_NAr reaction (Scheme 2.2).

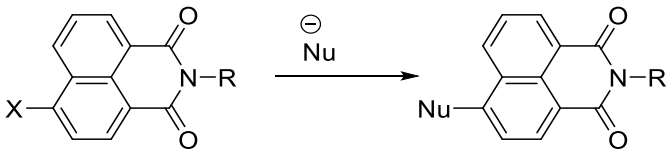

Scheme 2.2

This introduction of different functional groups can have a great impact on the electronic properties, with a consequent influence on the chemical, photochemical and spectroscopic properties.[5] For example, several functionalized 1,8-naphthalimide compounds show intramolecular charge transfer (ICT) and subsequently exhibit

a large bathochromic shift (red-shift) in both absorption and emission spectra. [8-10] Using different donating groups can cause changes in fluorescence properties.[10] Some substituents even allow intramolecular quenching of naphthalimide fluorescence.

As a result of all these properties, naphthalimides are recognized in different applications such as fluorescent markers in biology [11], fluorescent probes [12], cell imaging [13, 14], and fluorescent sensors[15, 16].

2.1.2 Naphthalimide derivatives in medicinal chemistry

In medicinal chemistry, numerous researchers have devoted and directed their work to discover and develop new compounds as safe drugs for cancer chemotherapy. Some of these drugs work via binding with the DNA as a groove binder or intercalator (See Chapter 1). Naphthalamide is one of the classes of compounds that are known to intercalate with DNA and several compounds in this class exhibit high anticancer activity.[1, 17]

In 1970, a first generation of mononaphthalimides was synthesized and tested against HeLa and KB cells in culture by Braňa and co-workers.[18] For example, amonafide **2.1** [19] and mitonafide **2.2** [20] (Scheme 2.3) are in this group of compounds; both **2.1** and **2.2** have a short linker chain from the naphthalimido ring leading to a tertiary amino group that may be protonated under physiological conditions.[21]

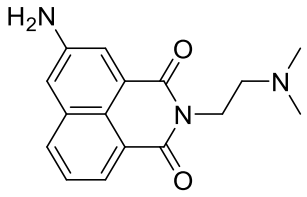

Amonafide **2.1**

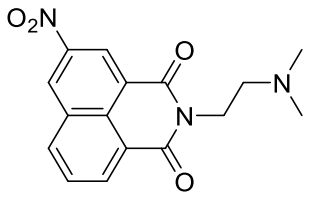

mitonafide **2.2**

Scheme 2.3

Subsequently, numerous naphthalimide derivatives were synthesized with variation in both the side chain and the ring substituents.[18] Some of these compounds have been tested in clinical trials for their anticancer activities.[20, 22-24] The studies show that amonafide **2.1** demonstrated potent anticancer activity against solid tumors.[19] However, due to unexpected central neurotoxicity, hematotoxicity and limited efficiency, the further application of amonafide in the clinical trial was limited.[2, 25, 26]

M.J. Waring *et al*. [27] studied the binding mode for amonafide **2.1** and mitonafide **2.2** and showed that the binding between these compounds and DNA causes an increase in the viscosity of sonicated rod-like DNA fragments. It was also shown that each bound drug molecule led to an increase in calculated length of of the DNA fragments of 2.2-2.5 Å. This information confirmed that these compounds bind to double-stranded DNA by intercalation.[27]

Efforts to improve selectivity, efficiency, and safety of these compounds, through development of a broad variety of novel naphthalimide derivatives (see, e.g., Scheme 2.4) have been reviewed.[20, 28, 29]

Lijuan Xie *et al.* [30] have synthesized a series of amonafide dervatives **2.3a-h** were the NH_2 group in amonafide was modified using several aliphatic and heterocycle groups (Scheme 2.4). The binding affinities for these compounds with ct-DNA were investigated using UV-visible titrations.

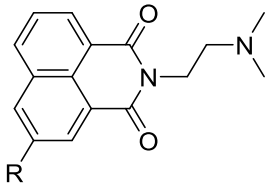

2.3a: R= $NH(CH_2)_2N(CH_3)_2$
2.3b: R= $NH(CH_2)_3N(CH_3)_2$
2.3c: R= $NH(CH_2)_3CH_3$
2.3d: R= $NHCH_2$-thiophene
2.3e: R= $N(CH_2)_5$
2.3f: R= $N(CH_2CH_2)_2O$
2.3g: R= $N(CH_2CH_2)_2S$
2.3h: R= $N(CH_2CH_2)_2NCH_3$

Scheme 2.4

The binding affinities of **2.3a,b,h** for DNA equal 1.85×10^5, 1.75×10^5, 2.48×10^5 M^{-1}, respectively and all compounds exhibit (marginally) better binding with ct-DNA compared to amonafide (1.05×10^5 M^{-1}). These 3 compounds all introduce a new $N(CH_3)_2$ group in the molecule, so it is likely that the increased affinity is the result of increased electrostatic interactions of the positively charges protonated form of these binders. The rest of the compounds exhibited weaker binding with ct-DNA in comparison with amonafide.[30]

Pattan Sirajuddin Nayab *et al.* [31] have synthesized a series of naphthalimide-based schiff bases (**2.4a-c**) with several substitutions on the benzene ring (Scheme 2.5). The binding proprieties for these compounds with ct-DNA were studied using UV-visable titrations.

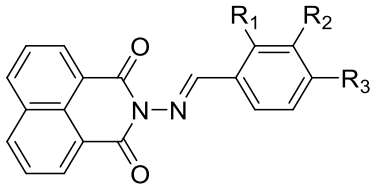

	R_1	R_2	R_3
2.4a	OH	OCH_3	H
2.4b	H	OC_2H_5	OH
2.4c	H	OCH_3	OCH_3

Scheme 2.5

Compound **2.4b** shows higher binding affinity in comparison with the other compounds. According to the authors, the docking study for these compounds were carried out using Auto Dock 4.0 and the results show that the binding energies for these compounds are between −8.20 to −8.69 kcal / mol, these negative values recommends that these compounds are binding to ct-DNA.

Jie Kang *et al*.[32] have synthesized several naphthalimide-metronidazole dervatives **2.5a-g** (Scheme 2.6) and the antibacterial activities for these compounds against gram-positive and gram-negative bacteria have been investigated.

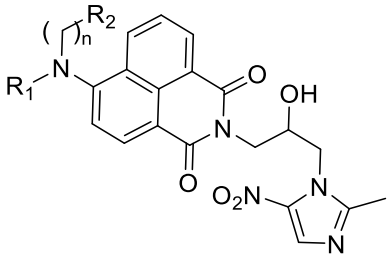

	R_1	R_2	n		R_1	R_2	n
2.5a	H	H	1	**2.5e**	H	H	12
2.5b	H	H	2	**2.5f**	H	OH	2
2.5c	H	H	3	**2.5g**	$-CH_2CH_3$	H	2
2.5d	H	H	4				

Scheme 2.6

Interestingly, **2.5b**, where ethylamine is linked to C4 of naphthalimide core, is the most promising compound among this series; it exhibits good antimicrobial activities against the tested bacteria. Therefore, the interactions of **2.5b** with calf thymus DNA were investigated using competition experiments with neutral red (NR). NR is a standard dye that is known to intercalate with DNA to form a NR-DNA complex. The absorption spectra of supramolecular interactions of **2.5b** with ct-DNA, using NR as a standard intercalator, show that **2.5b** intercalates with DNA.

2.1.3 Use of 1,8-naphthalimides as fluorescent probes and in sensors

Several 1,8-naphthalimides derivatives were used as fluorescent probes or in sensors due to the variation in their fluorescence upon interaction with analytes.[33] These compounds are extensively used to detect different species such as metal ions[34, 35], H^+ ion [36], and biological molecules such as enzymes. Therefore, 1,8-napthalimides could play a significant role in fields such as environment monitoring and some examples are summarized here.

Subhendu Sekhar Bag *et al.*[37] have synthesized two naphthalimide dervatives, viz. **2.6a-b**, with propargyl ends with either a donor or an acceptor substituent (Scheme 2.7). The UV–visible and fluorescence photophysical properties for these compounds have been investigated.

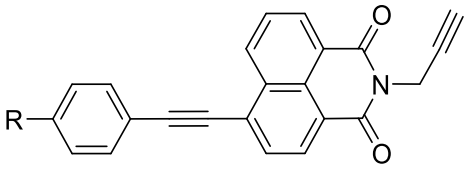

2.6a: R= -$N(CH_3)_2$
2.6b: R= -CN

Scheme 2.7

Compound **2.6a** shows an absorbance band assigned to ICT from the dimethylaminophenyl via the alkyne to the naphthalimide moiety. The fluorescene for this compound exhibits highly solvatochromic properties, where in hexane it shows fluorescene at λ_{max} = 474 nm whereas the λ_{max} = 611 nm in $CHCl_3$. In addition, the quantum yields show that the compound is fluorescent in apolar aprotic solvents but that the fluorescence is quenched in polar protic solvents, probably due to hydrogen bonding of the dye with water. The authors have shown that this differential quenching to the compound is translated into switch-on fluorescence when the compond interacts with DNA. [37]

In 2021, Zhenda Xie *et al*. [36] have synthesized a novel 1,8-naphthaimide derivative **2.7** that works as dual-analyte sensitive fluorescent probe (Scheme 2.8). This compound has two different recognition sites, one site is to detect pH in environmental and biological samples, and the other one is to target and detect the presence of Pd^0 in these samples. This compound responds to pH, with blue emission at 485 nm due to protonation of nitrogen of the morpholine group, and with yellow emission at 545 nm through irreversible loss of an allylcarbamate group in case the samples contain Pd^0.[36]

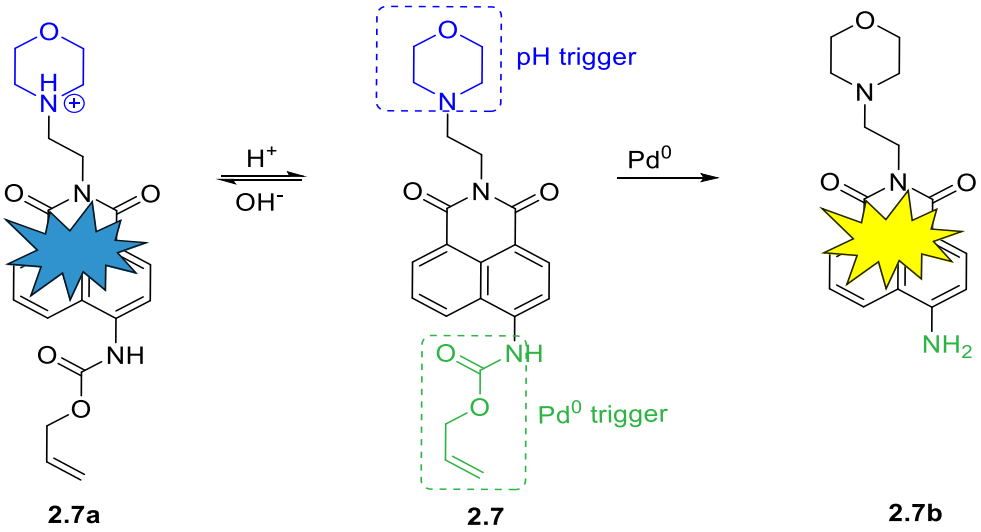

2.7a **2.7** **2.7b**

Scheme 2.8

In the same year, Anjong Florence Tikum *et al.*[38] have synthesized 1,8-naphthalimide derivative **2.8a** to detect CO in aqueous solution and living cells (Scheme 2.9). The authors found that the fluorescence of naphthalimide linked with ethylenediamine **2.8a** is quenched when coordinated to Pd(II). compound **2.8** regains its fluorescence if the sample contains CO, due to weak coordination between ethylenediamine and Pd(II) resulting in CO removing Pd from the complex.[38]

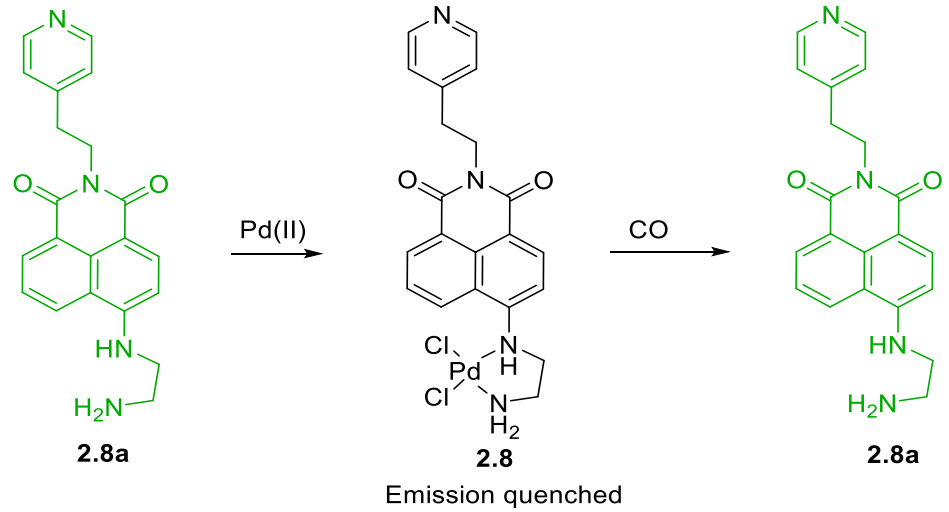

2.8a **2.8** **2.8a**

Emission quenched

Scheme 2.9

2.1.4 Ferrocene-appended naphthalimide sensitizers for genosensors

There are several ways to modify naphthalimide scaffolds. One of them is introducing other moieties that could change the naphthalimide's properties. Ferrocene (Fc) is an interesting well-known organometallic compound that can be oxidized reversibly and can therefore be used to add redox properties to naphthalimide derivatives. Although it has been reported that ferrocene works effectively as fluorescence quencher for naphthalimide,[39] ferrocene is also considered an excellent electrochemical signal transmitter. It is frequently used as a signal marker to detect RNA and DNA.[40, 41]

As stated in Chapter 1, a frequently used design for genosensors involves DNA (or PNA) capture strands imobilised on an electrode. Any hybridization events indicate that the sample contains the complementary target DNA strand. If a (hybrid) duplex is formed, the sensitizer will intercalate with the DNA*DNA or PNA*DNA duplex and produce a signal.[42]

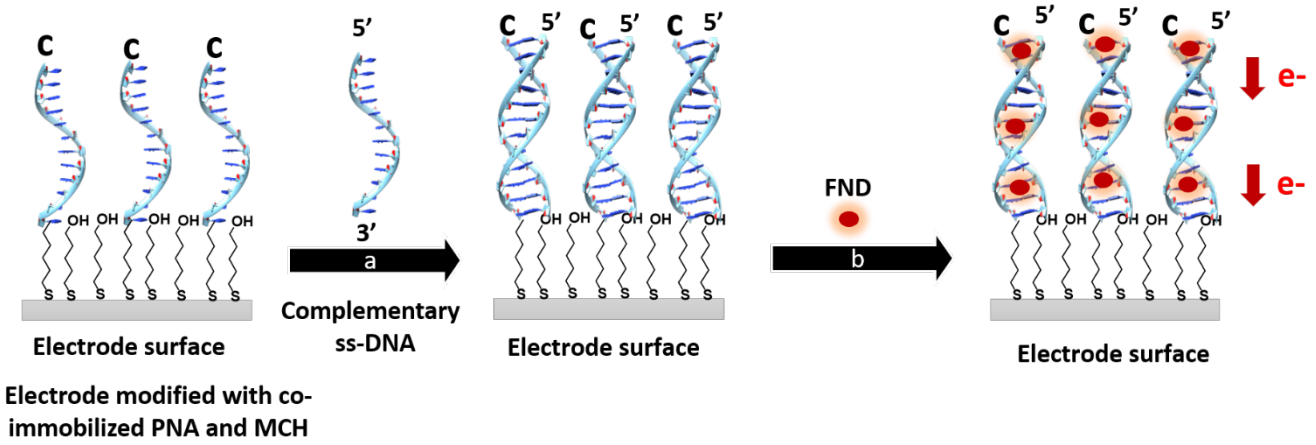

Figure 2.1 Schematic illustration of the FND based biosensor for investigation of PNA-DNA hybridization [42]

Shigeori Takenaka *et al.*[43] have synthesized naphthalene diimide linked with a ferrocene moiety (**2.9e**, Scheme 2.10). They successfully used this compound to detect the DNA hybridization event using single-stranded DNA capture strands immobilized on electrodes. The breakthrough here is the ability of this compound to differentiate between ssDNA and dsDNA.[43]

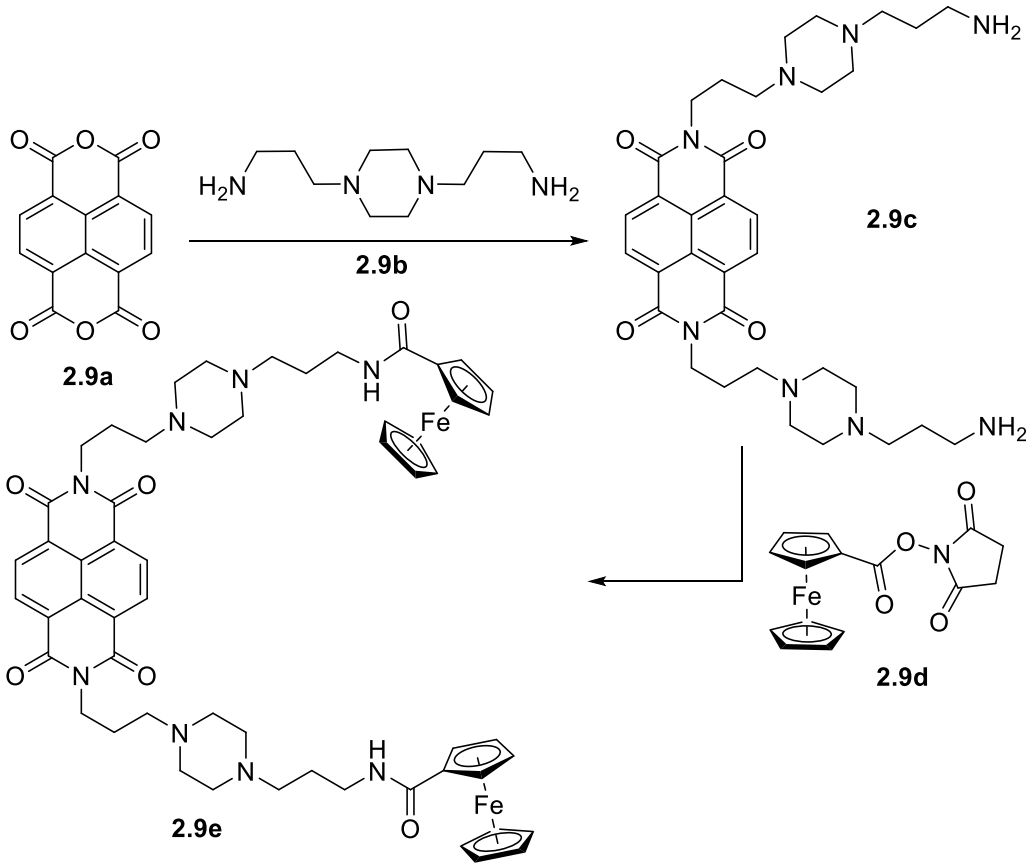

Scheme 2.10

Houda Gaiji *et al*.[42] have similarly synthesized naphthalene diimide linked with a ferrocene moiety via 2,2-(ethylenedioxy)bisethylamine as a linker (Scheme 2.11). This compound was also used as a sensitizer to recognize the hybridization events between a PNA capture strand immobilized on a gold electrode and a DNA target strand (figure 2.1).[42]

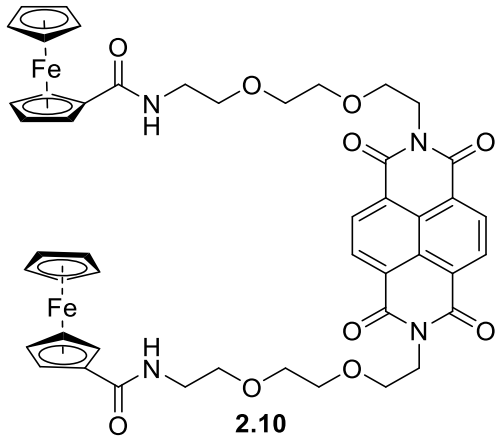

Scheme 2.11

2.1.5 Aims

Compound **2.10** in Scheme 2.13 is an interesting example that inspired us to use a similar approach to synthesise ferrocene-linked naphthalimide derivatives using different solubilizing groups at C4 in the naphthalimide unit. One of the aims of this chapter is therefore to synthesise a series of naphthalimide derivatives joined with a ferrocene moiety. The designed compounds contain two variable factors that could have an impact on the solubility and binding proprieties (Scheme 2.12).

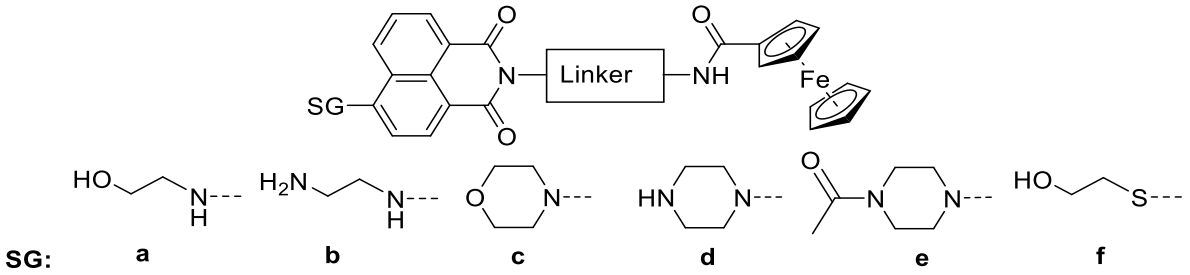

Scheme 2.12

The first factor is the length of the linker between the naphthalimide moiety and the ferrocene moiety. Two linkers with different chain lengths and properties were proposed. The second factor are the substituents in C-4 of the naphthalimide unit, indicated with SG (Solubilising Group) in Scheme 2.12.

The other aim of this chapter is to study the binding properties for the synthesized target compounds using UV-visible titrations.

2.2 Result and discussion

2.2.1 Docking studies for the proposed naphthalimide-ferrocene conjugates

Several naphthalimide derivatives involving a linked ferrocene moiety **2.12 a-f** were proposed. In all compounds, one unit of naphthalimide is connected to a ferrocene moiety via 2,2-(ethylenedioxy)bisethyl as a linker but with different solubilizing groups (SG) on the naphthalimide (Scheme 2.13).

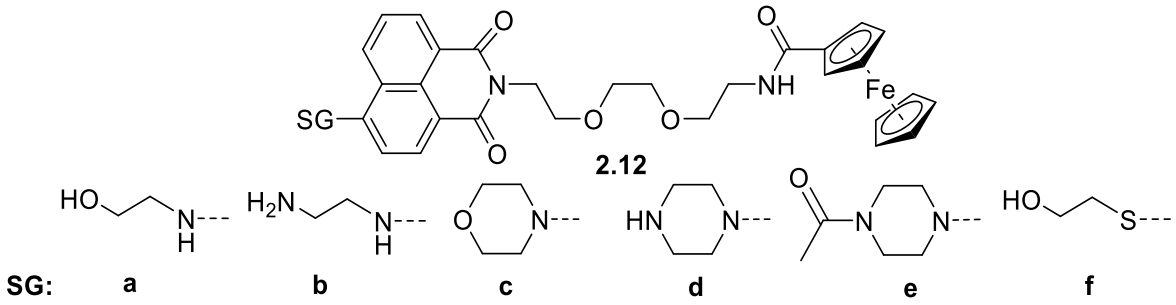

Scheme 2.13 proposed ferrocene- naphthalimide conjugates

One of the ways that can be used to explore whether a compound could bind with DNA through intercalation or through groove binding is a docking study. In its simplest form, a docking study takes DNA as a rigid structure and tests several binding modes for the compound. The binding modes are then ranked, based on the calculated binding affinities. These values are not necessarily directly related to the real values (here this is the case because the software we use has been optimized for docking small molecules into protein structures, rather than into nucleic acid structures), and they are used only to compare between each conformation.

The docking study for the proposed ferrocene-naphthalimide conjugates was carried out using AutoDock Vina [44] against a DNA structure with a pre-formed intercalation gap[45]. The top 10 binding modes are generated and ranked by the binding affinity. Only the top three binding modes for each compound are presented in Figure 2.2.

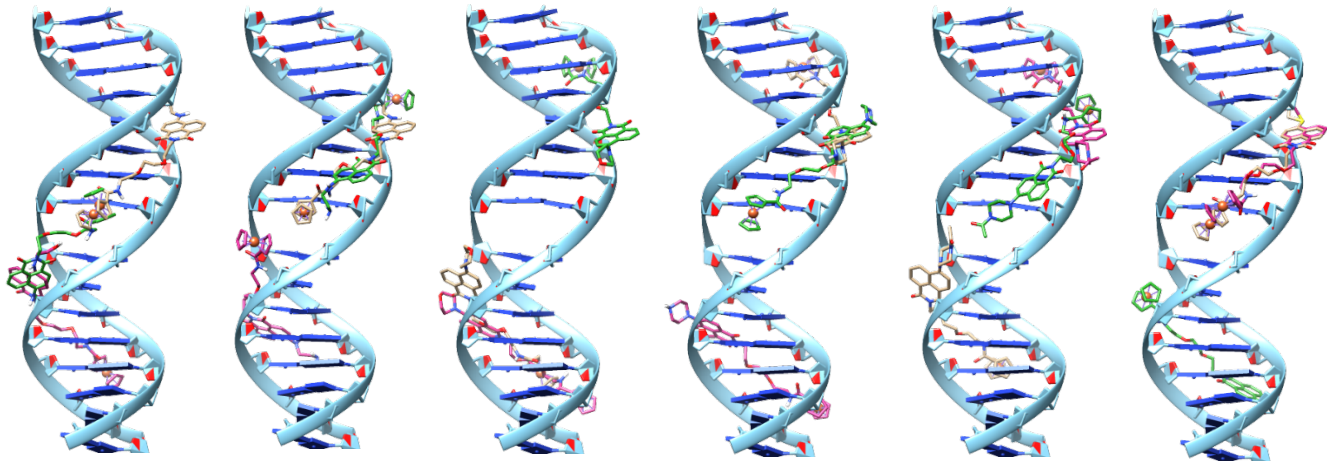

2.12a **2.12b** **2.12c** **2.12d** **2.12e** **2.12f**

Figure 2.2 Top 3 binding modes for proposed compounds (2.12 a-f) with open d(ATCGAGACGTCTCGAT)$_2$.

Unexpectedly, although the proposed ferrocene-naphthalimide derivatives contain an intercalating unit, the docking studies suggest that these compounds interact with DNA as groove binders. Table 2.1 illustrates the binding affinity for the top three binding modes and the type of binding for each compound (**2.12a-f**).

Table 2.1 The binding affinity for the top three binding mode of compounds (2.12a-f) using AutoDock Vina

		2.12a	2.12b	2.12c	2.12d	2.12e	2.12f
The binding affinity (kcal/mol)[b]	1st binding mode[a]	-8.6 (GB)	-8.3 (GB)	-9.5 (GB)	-9.1 (GB)	-9.4 (GB)	-8.7 (GB)
	2nd binding mode	-8.5 (GB)	-8.2 (GB)	-9.2 (GB)	-9.0 (GB)	-9.0 (GB)	-8.2 (GB)
	3rd binding mode	-8.5 (GB)	-8.2 (GB)	-9.1 (GB)	-8.9 (GB)	-8.9 (GB)	-8.2 (GB)

(I): intercalator, (GB): groove binder

a) The ranking of the binding modes is as produced by Vina

b) Binding affinities are only reported to 0.1 kcal mol^{-1} by Vina.

In addition to compounds **2.12a-f** in Scheme 2.15, similar naphthalimide-ferrocene conjugates are proposed using a shorter aliphatic linker, viz. 1,3-diamino propane (Scheme 2.14).

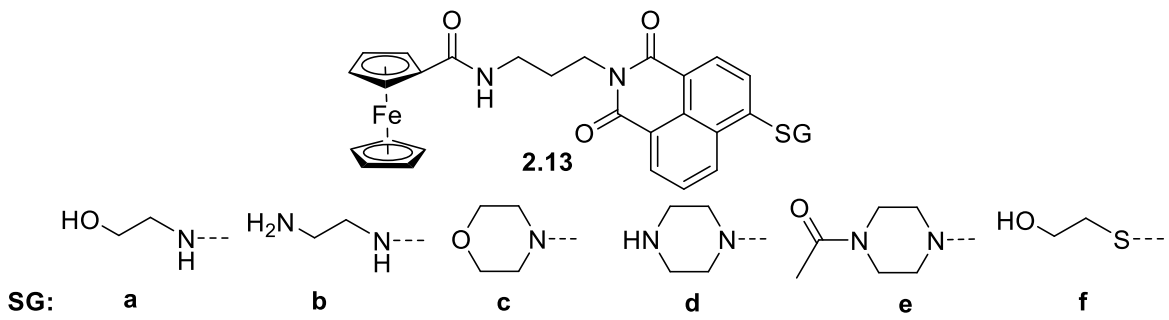

Scheme 2.14

The docking studies for the proposed ferrocene-naphthalimide conjugates **2.13a-f** were carried out, again generating the top 10 binding modes ranked by the binding affinity. The top three binding modes for each compound are presented in Figure 2.3.

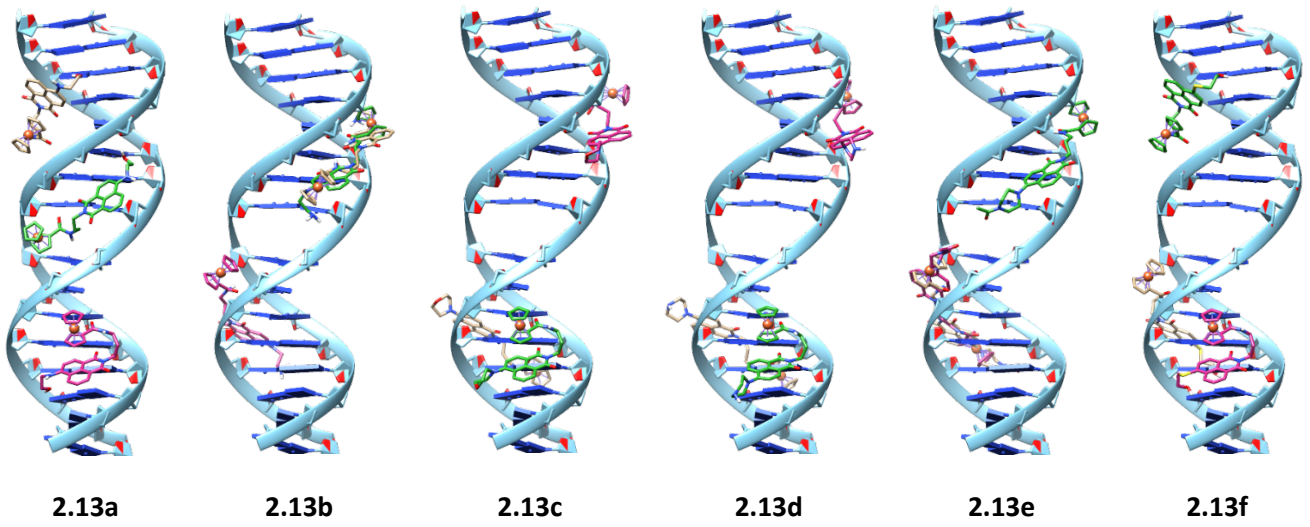

Figure 2.3 Top 3 binding mode for proposed compounds (2.13a-f) with open d(ATCGAGACGTCTCGAT)$_2$

This docking study also suggest that these proposed compound bind with DNA as groove binders. Table 2.2 illustrates the binding affinities for the top three binding modes and the type of binding for each compound **2.13a-f**.

Table 2.2 The binding affinity for the top three binding mode of compounds (2.13a-f)using AutoDock Vina

		2.13a	2.13b	2.13c	2.13d	2.13e	2.13f
The binding affinity (kcal/mol)[b]	**1st binding mode[a]**	-7.0 (GB)	-8.5 (GB)	-8.9 (GB)	-9.3 (GB)	-10.2 (GB)	-9.0 (GB)
	2nd binding mode	-7.0 (GB)	-8.3 (GB)	-8.8 (GB)	-9.2 (GB)	-10.1 (GB)	-8.9 (GB)
	3rd binding mode	-6.9 (GB)	-8.3 (GB)	-8.8 (GB)	-9.1 (GB)	-10.0 (GB)	-8.9 (GB)

(I): intercalator, (GB): groove binder

a) The ranking of the binding modes is as produced by Vina

b) Binding affinities are only reported to 0.1 kcal mol^{-1} by Vina.

Overall, the docking study for all proposed compounds **2.12a-f** and **2.13a-f** suggest that these compounds interact with DNA as groove binders. Althought, the calculated binding affinites obtained using AutoDock Vina are not necessarily related to the real values. The results can be used to compare between each solubilizing group and to compare the effect of using different linkers.

According to Table 2.1, the binding affinites for primary amine and thiol group are similar but secondary amines exhibit more negative value for their binding affinities, i.e. these componds are predicted to be stronger binders. This stronger predicted binding is probably the result of the fact that the secondary amines are also larger molecules. This pattern is not strictly observed for the shorter linker (Table 2.2) although secondary amines still appear to be amongst the stronger binders but the effect is less clear-cut. The effect of the change of the linker between the two Tables appears to be relatively small and doesn't follow a particular pattern.

2.2.2 Synthesis of ferrocene-naphthalimide conjugates with a 2,2-(ethylenedioxy)bisethyl linker (2.12a-f)

The proposed compounds in Scheme 2.13 were synthesized via multistep reactions. The first step involves attaching the ferrocene moiety to the linker. This is achieved by turning ferrocene carboxylic acid into the corresponding acid chloride using oxalyl chloride (Scheme 2.15, step A) followed by reaction with the required terminal diamine to form the amide bond (Scheme 2.15, step B), thus forming compound **2.15**. Next, the terminal amino group in **2.15** reacts with 4-chloro-1,8-naphthalic anhydride to form the naphthalimide compound with a linked ferrocene moiety, **2.16** (Scheme 2.15, step C). In the last step, several solubilizing groups were used to

substitute the chlorine atom on the naphthalimide moiety to form the final target compounds (**2.12a-f**, step D). We refer to these groups as solubilising groups because solubility is the main reason for introducing them but these groups will obviously also affect the spectroscopic properties of the naphthalimide chromophore so they could also be referred to as auxochromes.

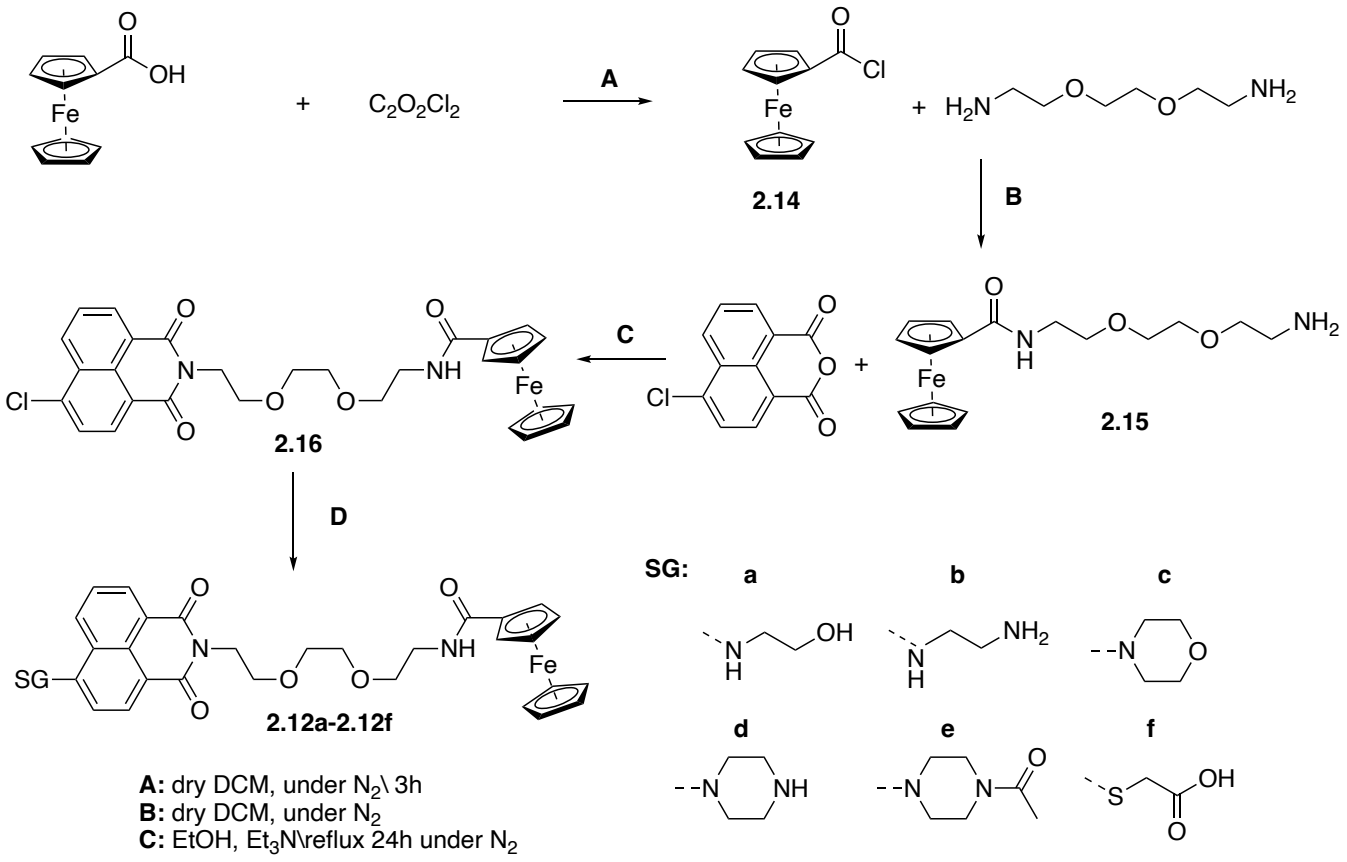

Scheme 2.15 The synthetic scheme for compounds 2.12a-f

The different steps are now briefly discussed.

Step 1. Synthesis of ferrocene amide using 2,2-(ethylenedioxy)bisethylamine (2.15)

To form the ferrocene-linker moiety **2.15**, one equivalent of commercially available ferrocene carboxylic acid was reacted with 2.5 equivalents of oxalyl chloride in dry DCM under inert atmosphere for 3h.[46, 47] The solvent was evaporated to afford ferrocenoyl chloride **2.14** in a 98 % yield (Scheme 2.16).

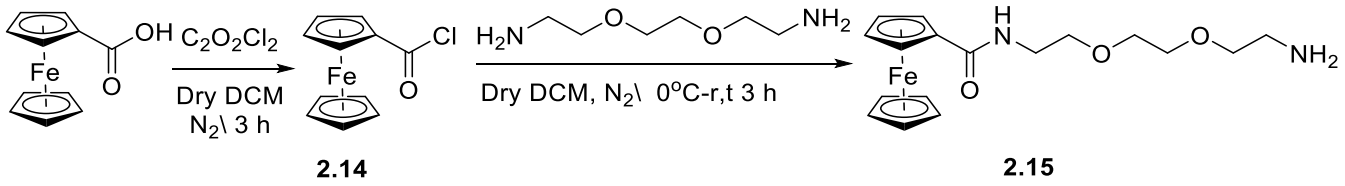

2.14 **2.15**

Scheme 2.16

After that, the obtained ferrocenoyl chloride **2.14** was redissolved in dry DCM and added to an excess of terminal diamine 2,2-(ethylenedioxy)bisethylamine and stirred at room temperature under N_2 for 3 h to form the amide bond and obtain **2.15** with a good yield (72 %).

The chemical structure was confirmed via ^{1}H- and ^{13}C-NMR spectroscopy and mass spectrometry. **2.15** has three distinguishing signals related to the ferrocene moiety in addition to linker signals. These three Fc-related signals are two triplet signals with two-proton integration related to protons a and b, and one singlet with five protons integration related to protons b (Figure 2.4). Since the plan is to synthesise ferrocene-naphthalimide dervatives, signals related to these three distinguishing signals will appear in the ^{1}H-NMR spectra for all synthesized compounds.

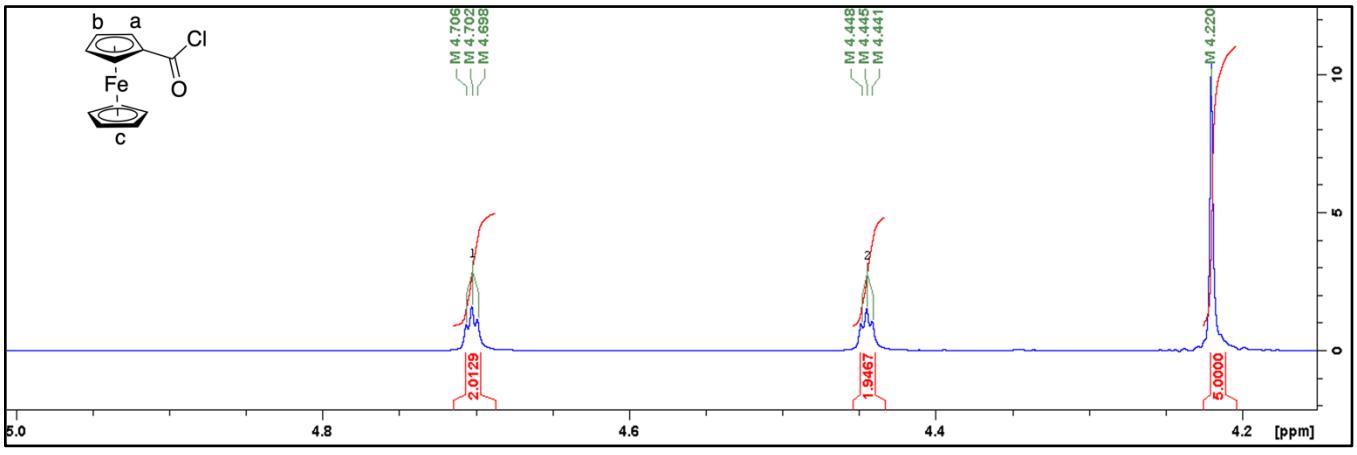

Figure 2.4 ^{1}H NMR spectrum for 2.14

Step 2. Synthesis of the ferrocene-naphthalimide conjugate 2.16

The key step in this scheme is to synthesize the ferrocene-naphthalimide conjugate **2.16** as a main skeleton to be used further in synthesizing the final target naphthalimide-ferrocene conjugates.

A reaction mixture consisting of two equivalents of **2.15** with one equivalent of 4-chloro-1,8-naphthalic anhydride in EtOH and in the presence of a catalytical amount of Et_3N was heated to reflux for 24 h. The reaction yielded 92% of the target compound **2.16** as a brown oil (Scheme 2.17).

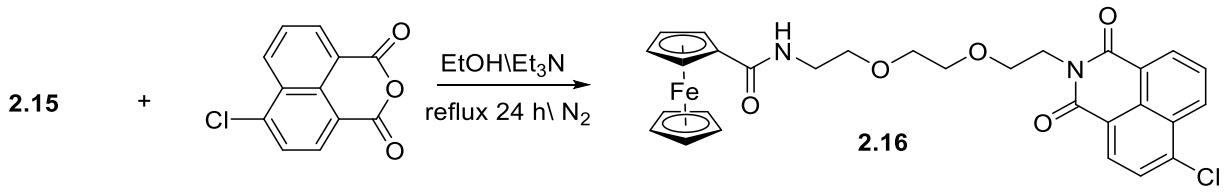

Scheme 2.17

As mentioned above, **2.16** is the scaffold to synthesise the target compounds **2.12a-f**. Therefore, the NMR spectrum for this compound will be another distinguishing pattern for all synthesized compounds in this scheme. The NMR pattern involves five distinguishable signals related to naphthalimide moiety (Scheme 2.5). These five signals comprise of three doublets of doublets signals and two doublets signals. The coupling constants of the two doublets of doublets (H_a and H_b) found between 8.5 and 8.6 ppm are equal to $J_{ortho}\approx 8$ and $J_{meta}\approx 1$. The coupling constants thus suggest that these signals are related to H5 and H7. The other doublet of doublets (H_d) at 7.75-7.78 ppm, which partially overlaps with the signal around 7.73, shows coupling constants $J_{ortho}\approx 8$, $J_{ortho}\approx 8$, which suggests that this signal is related to H6. The last two doublets (H_c and H_e) present around 7.73 and around 8.40 ppm have a coupling constant $J_{ortho}\approx 8$ which suggests that these signals are related to H2 and H3.

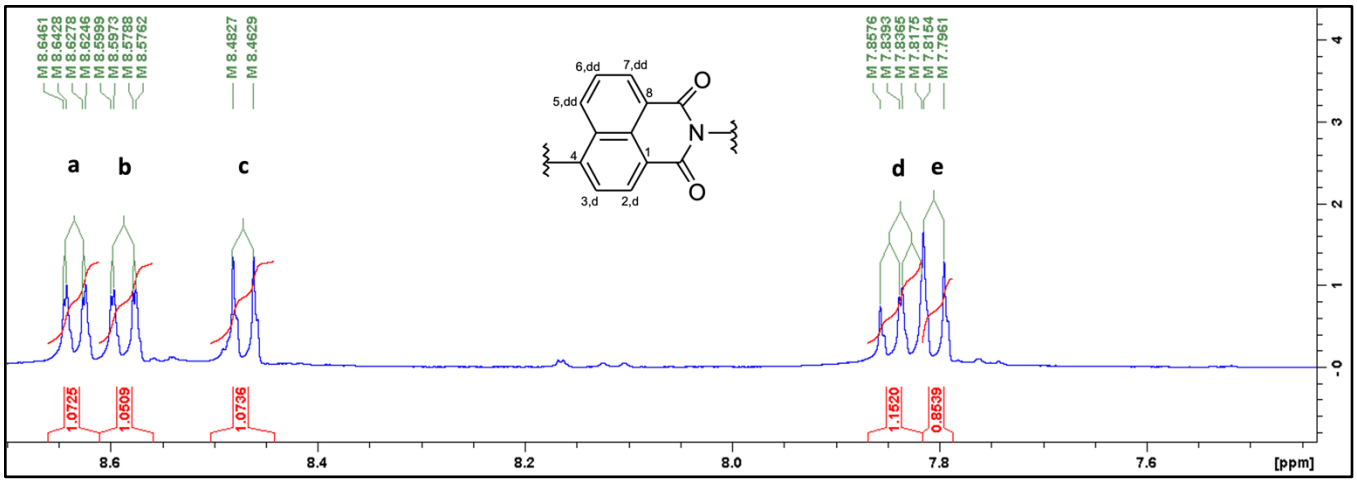

Figure 2.5 The ^{1}H-NMR spectrum for the aromatic naphthalimide moiety for 2.16

The purity of **2.16** is very important, and it has been checked by TLC (using chloroform: ethanol 9:1 as eluent) and showed one spot. However, the ^{1}H-NMR spectrum showed a trace of impurity as three additional signals appeared in the "ferrocene region" of the spectrum. These additional signals are small "mirror" signals for the ferrocene signals, i.e. they follow the same pattern of the expected ferrocence moiety but integrate to a fractional number of protons (Figure 2.6).

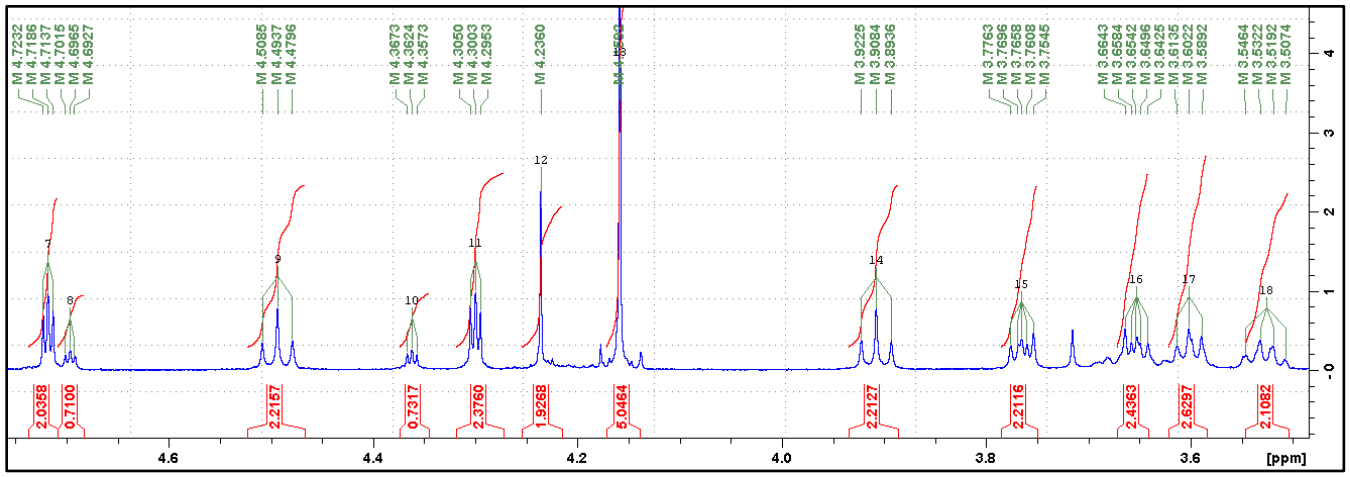

Figure 2.6 The ^{1}H-NMR spectrum for the aliphatic region of 2.16

Initially, it appeared as if the extra three mirror signals together with the anticipated signals for ferrocene integrated to the correct number of protons relative to the aromatic region. In addition, the compound showed up as one spot on TLC. Since the compound contains a redox-active ferrocene we thought that the oxidation state for iron might be affected, and we proposed the presence of one compound with two different oxidation states. However, this later turned out not to be the case.

As a result of this misinterpretation of the ^{1}H-NMR spectra, initially, this compound was used *as is* to introduce the solubilizing groups (ethanol amine and morpholine) without further purification. The small signals were then observed in the new compounds too. Therefore, the search of the right mobile phase was continued to purify **2.16** using column chromatography over silica. Eventually, **2.16** was purified using column chromatography (chloroform - acetone 1:1) (R_f= 0.69). However, the yield after column chromatography was not determined because not all material from the original reaction was purified.

Step 3. Synthesis of ferrocene-naphthalimide derivatives carrying solubilising groups

After synthesizing the ferrocene-naphthalimide skeleton **2.16**, different groups were introduced at the C-4 position that can change the solubility and widen the absorption spectrum to allow the use of a variety of detection techniques that can be used for studying the binding properties for these compounds with the DNA.

Step 3.1 Introduction of solubilizing groups through S_NAr reactions with 1^o amines

Primary amines such as ethanol amine and ethylene diamine were introduced to **2.16** as solubilizing groups. A reaction mixture involving **2.16** in neat ethanol amine was heated at reflux under N_2 atmosphere for 24 h. The reaction mixture was left to cool and then extracted using DCM and water. After extraction, the DCM from the organic layer was removed *in vacuo* to obtain **2.12a** as a brown oil. The crude **2.12a** was purified using column chromatography (silica, chloroform: acetone 1:1) (Scheme 2.18).

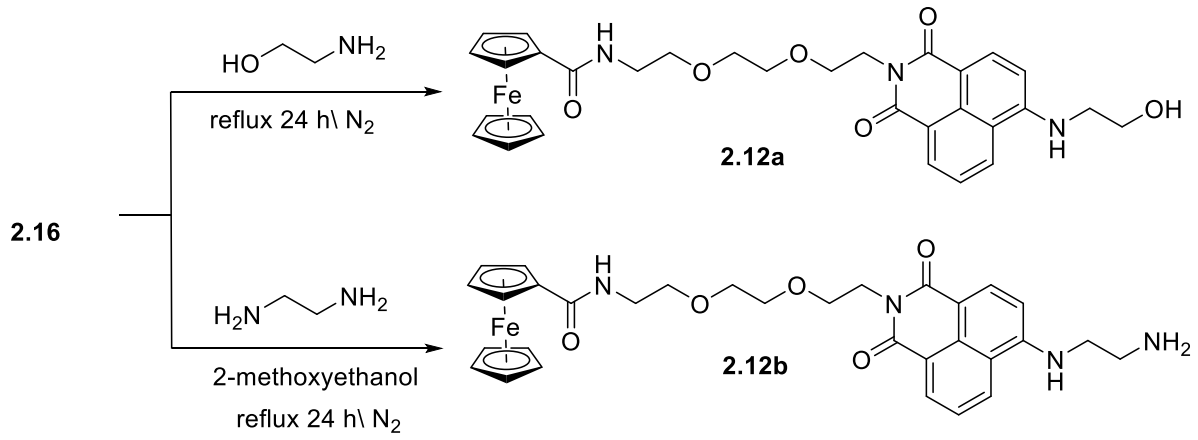

Scheme 2.18

Analogously, 7.75 equivalents of ethylene diamine were reacted with one equivalent of **1.16** using 2-methoxyethanol as a solvent. The reaction mixture was heated at reflux under N_2 for 24 h and the solvent removed *in vacuo*. The target compound was extracted using DCM and water (Scheme 2.18). The DCM from the organic layer was removed to obtain **2.12b** as a brown oil which was purified using column chromatography (silica, chloroform: acetone 1:1). Compounds **2.12a** and **2.12b** were characterized using NMR spectroscopy and mass spectrometry.

Step 3.2 Introduction of solubilizing groups through S_NAr reactions with 2^o amines

Compound **2.16** was further used as a skeleton to synthesise naphthalimide-ferrocene conjugates using secondary amines as solubilizing groups. Morpholine, piperazine and 1-acetyl piperazine were used to substitute the chlorine in **2.16** to form **2.12c**, **2.12d** and **2.12e**, respectively.

Morpholine was added to **2.16** dissolved in DMSO. The reaction mixture was heated to 100 °C for 48 hours under nitrogen. The mixture was neutralized with 1 M of HCl, and the resulting solution was dissolved in 50 mL DCM and rinsed several times with water. The solvent was evaporated *in vacuo* to obtain **2.12c** as a brown oil (Scheme 2.19).

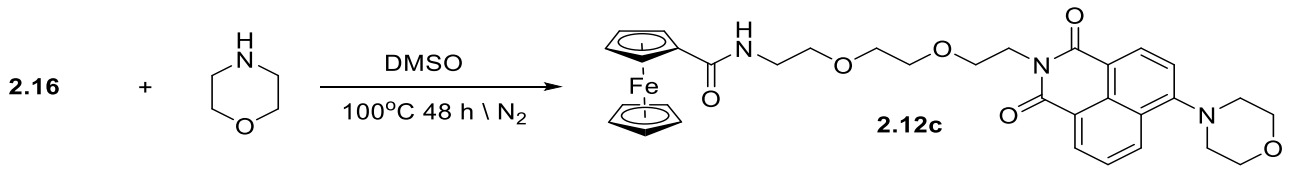

Scheme 2.19

The same protocol was successfully applied to synthesise **2.12d** and **2.12e** (Scheme 2.20) using piperazine and 1-acetyl piperazine as a solubilizing groups, respectively.

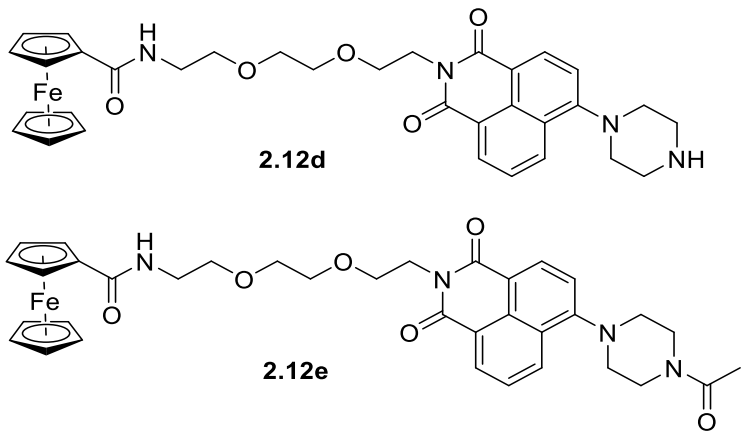

Scheme 2.20

The chemical structures for obtained compounds **2.12c-e** were confirmed using NMR spectra and mass spectrometry.

Step 3.3 Introduction of solubilizing groups through S_NAr reactions with thiol

In addition to primary and secondary amines, introducing solubilizing group via different nucleophilic atoms, such as sulfur nucleophiles, more likely changes geometry, polarisability, stability, steric and electronic characteristics of these comjpounds which could affect their DNA-binding properties.[48] Therefore, the thiol-containing compound 2-mercaptoethanol was used to synthesise a new target compound.

One equivalent of **2.16** was dissolved in 2-methoxyethanol and 1.5 equivalents of 2-mercaptoethanol were added. The reaction mixture was heated at reflux for 24 h under inert atmosphere (Scheme 2.21). After that, the reaction mixture was acidified using 1 M HCl and compound **2.12f** was extracted from the resulting aqueous phase using

DCM. The solvent from the organic fraction was removed *in vacuo* to obtain **2.12f** as a brown oil. The crude was purified using column chromatography (DCM: acetone 1:1).

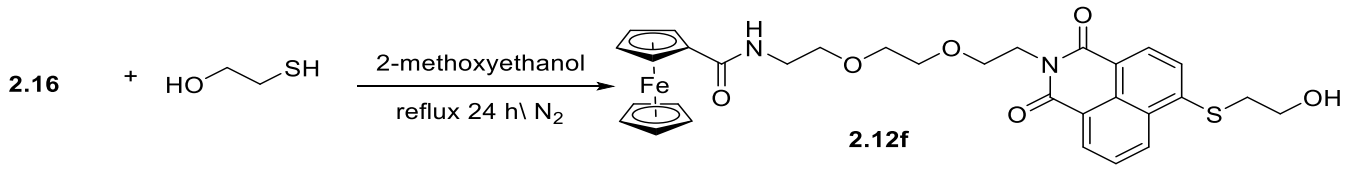

Scheme 2.21

2.2.3 Synthesis of ferrocene-naphthalimide conjugates with a propyl linker (2.13a,c,e)

Based on the successful synthetic protocols that we used to synthesise the first set of target compounds **2.12a-f**, this class of compounds were explored further using a different terminal diamine as the linker (Scheme 2.22).

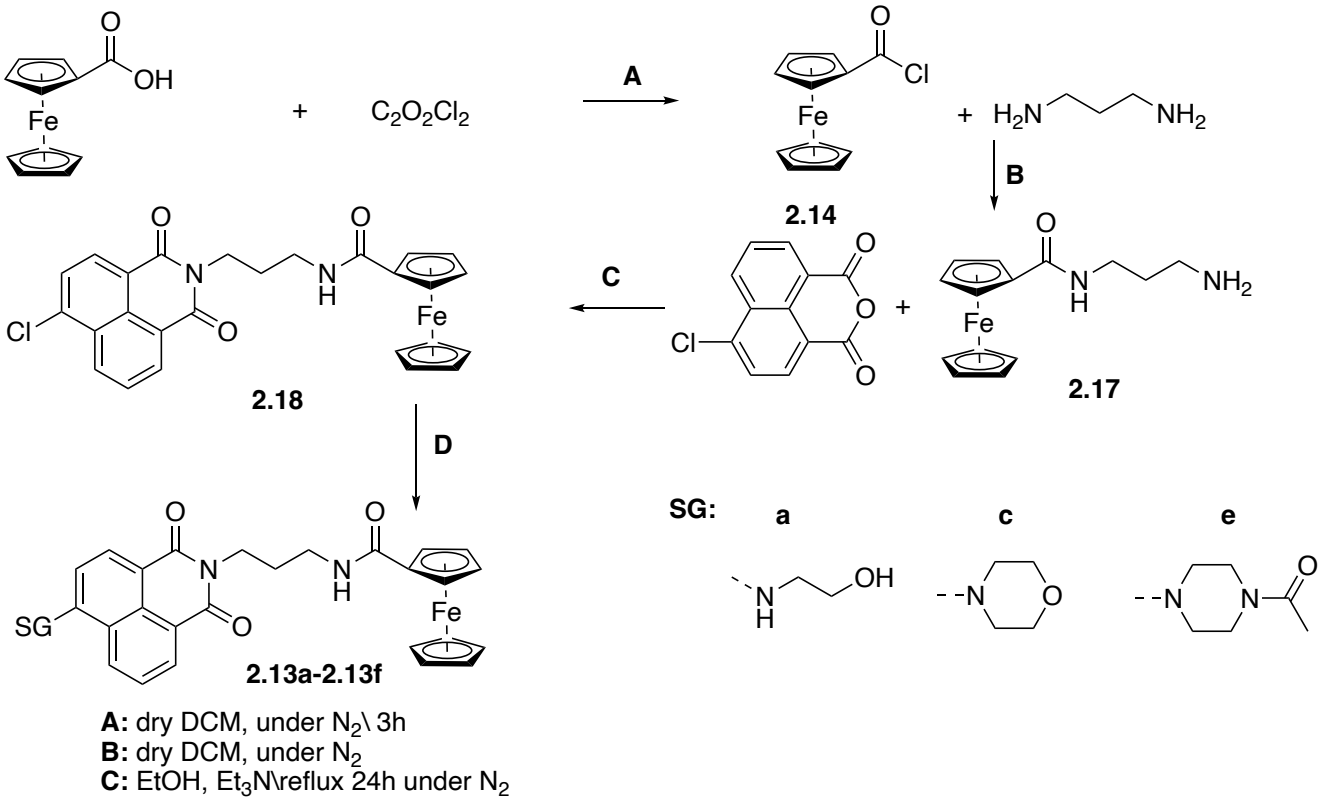

Scheme 2.22 synthetic scheme for compounds 2.13a,c,e

1,3-diaminopropane was chosen for the second series of compounds **2.13a,c,e**. The three steps involved in the synthetic procedures are outlined in Scheme 2.24.

Step 1. Synthesis of ferrocene amide using 1,3-diaminopropane

Like the first scheme, ferrocenoyl chloride **2.14** was synthesised using ferrocene carboxylic acid and oxalyl chloride. the obtained ferrocenoyl chloride was dissolved again in dry DCM and added to an excess of terminal diamine 1,3-diaminopropane and stirred under N_2 for 3 h to form the amide bond and obtain compound **2.17** in 36 % yield (Scheme 2.23).

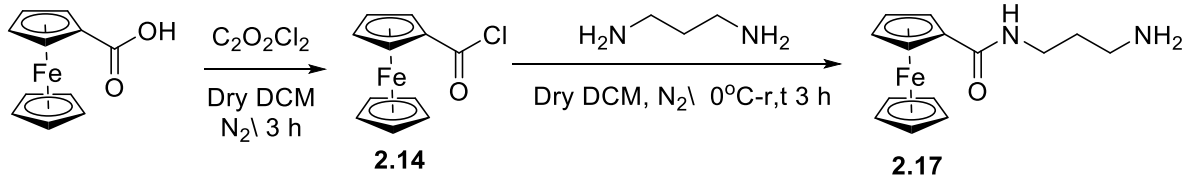

Scheme 2.23

Step 2. Synthesis of the propyl-linked ferrocene-naphthalimide conjugate

The main step for this scheme involves the synthesis of a new ferrocene-naphthalimide skeleton **2.18**. To obtain **2.18**, **2.17** was condensed with 4-chloro-1,8-naphthalic anhydride in EtOH and in the presence of a catalytic amount of Et_3N for 24 h (Scheme 2.24).

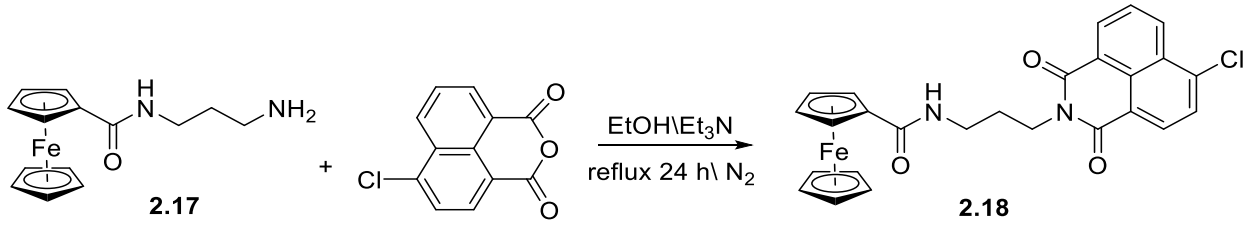

Scheme 2.24

Pure **2.18** was obtained as a brown solid (97 %) and the purity was checked using TLC (chloroform-acetone 1:1). The compound was used as a main skeleton to synthesise the final target naphthalimide-ferrocene conjugates **2.13a,c,e**.

Step 3. Synthesis of ferrocene-naphthalimide derivatives

As for the previous series of compounds, several groups were used to substitute the chlorine in **2.18** to enhance the solubility in water and to study their effect on spectroscopic and DNA-binding properties.

Introduction of solubilizing groups through S_NAr reactions with 1° amines

The primary amine ethanol amine was used as a solubilizing group. The reaction between **2.18** neat ethanolamine was carried out and heated at reflux under an N_2 atmosphere for 24 h. The reaction mixture was left to cool, poured into water and extracted with DCM. After that, the solvent was evaporated from the organic layer to obtain **2.13a** as a brown solid which was purified using column chromatography (DCM: acetone, 1:1, over silica) (Scheme 2.25).

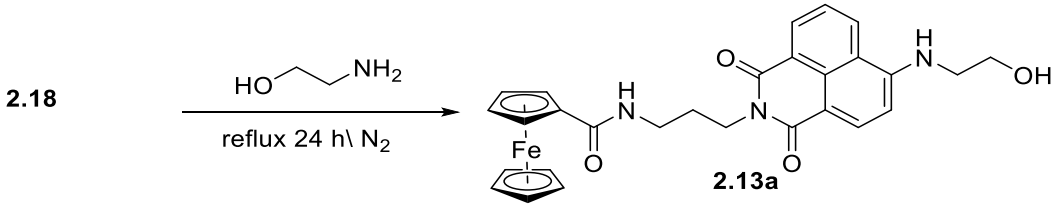

Scheme 2.25

Introduction of solubilizing groups through S_NAr reactions with 2° amines

In addition to the primary amine, secondary amines morpholine and 1-acetyl piperazine were used to substitute the chlorine in an S_NAr reaction.

Four equivalents of morpholine were added to a solution of one equivalent of **2.18** in DMSO. The reaction mixture was heated to 100 °C for 48 hours under nitrogen. At the end of the reaction, the mixture was neutralized with 1 M HCl and the resulting solution was extracted in DCM and water where the organic layer was washed with water several times. The solvent was removed to obtain **2.13c** as a brown solid (Scheme 2.26).

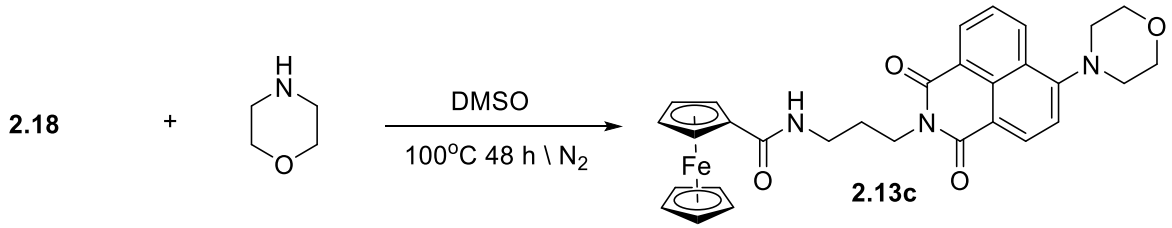

Scheme 2.26

The same protocol was successfully applied to synthesise **2.13e** using 1-acetyl piperazine as a solubilizing group (Scheme 2.29).

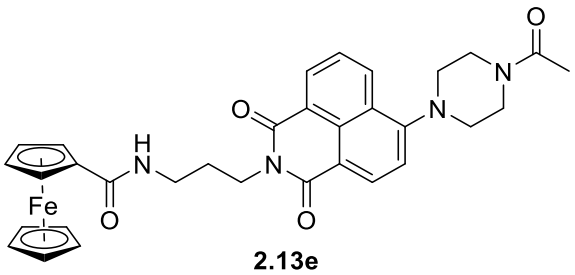

Scheme 2.27

2.2.4 Overview of NMR spectra.

To support further synthetic efforts involving naphthalimides, we wanted to identify the distinguishing NMR signals for these conjugates. Table 2.3 summarises the key signals in the ^{1}H-NMR spectra for the synthesized compounds **2.12a-f** and **2.13a,c,e**.

Table 2.3 The ^{1}H NMR spectra details for 2.12a-f, 2.13a,c,e

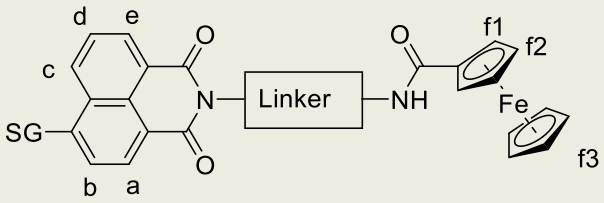

comp.	linker protons
2.16, 2.12a-f	6x CH_2
2.14, 2.13a,c,e	3x CH_2

	solvent	Aromatic protons			NH	Aliphatic CH_2	Ferrocene protons			SG
		a,b	c,e	d	i		f1	f2	f3	
2.16	$CDCl_3$	8.47, 7.80	8.63, 8.58	7.83	6.44	4.46, 3.87, 3.72, 3.61, 3.56, 3.48	4.68	4.27	4.12	
2.12a	DMSO-d_6	8.30, 6.86	8.71, 8.48	7.72	7.79	4.24, 3.67, 3.56, 3.50, 3.28	4.80	4.33	4.16	4.92, 3.73, 3.62
2.12b	$CDCl_3$	8.18 , 6.70	8.58, 8.45	7.62	6.57	4.46, 3.87, 3.73, 3.62, 3.55, 3.41	4.73	4.27	4.16	6.20, 3.47, 3.18
2.12c	$CDCl_3$	8.51, 7.21	8.59, 8.41	7.69	6.48	4.46, 3.87, 3.72, 3.62, 3.56, 3.47	4.71	4.27	4.15	4.01, 3.26
2.12d	$CDCl_3$	8.47, 7.16	8.53, 8.37	7.65	6.65	4.42, 3.83, 3.68, 3.58, 3.53, 3.44	4.70	4.24	4.11	4.73, 3.22,3.17
2.12e	DMSO-d_6	8.52, 7.38	8.55, 8.44	7.86	7.78	4.26, 3.69, 3.62, 3.55, 3.49,3.21.	4.78	4.32	4.14	3.79, 3.27, 2.12
2.12f	DMSO-d_6	8.41 7.84	8.61, 8.57	7.92	7.79	4.27, 3.70, 3.62, 3.56, 3.49, 3.29.	4.78	4.32	4.14	5.17, 3.78, 3.40
2.18	DMSO-d_6	8.47, 8.07	8.63 8.62	8.04	7.87	4.16, 3.30, 1.92	4.80	4.37	4.23	
2.13a	DMSO-d_6	8.32, 6.87	8.75 8.50	7.73	7.85	4.15, 3.27, 1.88	4.79	4.37	4.22	7.79,4.92 3.74,3.52
2.13c	DMSO-d_6	8.47, 7.40	8.54, 8.54.	7.86	7.86	4.16, 3.30, 1.90	4.79	4.37	4.22	3.95, 3.26
2.13e	DMSO-d_6	8.47, 7.41	8.57, 8.55	7.88	7.86	4.16, 3.21, 1.90	4.79	4.37	4.22	3.80, 3.28, 2.12

Table 2.3 immediately reveals some of the patterns that we would expect to see. The linker signals are consistent in all compounds. The ferrocene signals are also consistent but not completely the same between **2.12a-f** and **2.13a,c,e**, with signals varying up to approximately 0.1 ppm. It is worth to mention that using different solvent can shift the signal slightly. On the other hand, the five signals related to naphthalimide protons change a bit more due to the different solubilizing groups and especially when we used 2-mercaptoethanol as a solubilizing group. These characteristic patterns of naphthalimides signals are important since we are interested in synthesisng more naphthalimide dervatives in the following chapters and established patterns will allow us to quickly decide whether a compound has likely been made or not.

2.2.5 The aqueous solubility and UV-visible spectroscopic properties of the synthesized compounds

For these compounds to be used as sensitisers, sufficient aqueous solubility is needed. Initial exploration showed that solubilities were limited. Normally, known weights of potential binders need to (completely) dissolve in MOPS buffer to prepare standard solutions of the potential binders which can be used to determine, e.g., an extinction coefficient allowing quantitative studies of compound solubility. The lack of the solubility of these synthesized DNA binders **2.12a-f** and **2.13a,c,e** in water was an obstacle to prepare such standard solutions. Therefore, to be able to calculate the concentrations for all solutions, the molar extinction coefficient for the chromophores needs to be experimentally determined.

2.2.5.1 Determination of molar extinction coefficient for compounds 2.19-2.21

Since we used three classes of solubilizing groups (1°-amine, 2°-amine, thiol-group), compounds **2.19-21** were synthesized as a standard chromophore that can completely dissolve in aqueous solution and used to determine the molar extinction coefficient for three different naphthalimide chromophores.

The UV-visable spectra for the three naphthalimide chromophores **2.19-21** (Figure 2.7) show where the synthesized ferrocene-naphthalimide conjugates are expected to absorb.

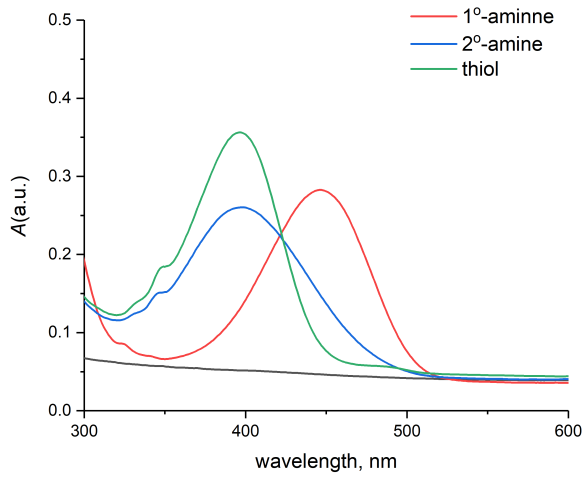

Figure 2.7. UV-visible spectra for a 20 μM solution of 2.19 (red), a 22.6 μM solution of 2.20 (blue), and a 25 μM solution of 2.21 (green) in buffer (25 mM MOPS, 50 mM NaCl, pH 7) at 25 °C

For each compound, three stock solutions were prepared in buffer and three dilution series were prepared from each stock. UV-visible spectra were recorded for all diluted solutions. According to the Beer-Lambert law, the molar extinction coefficient ε can be calculated by plotting the absorbance at λ_{max} for each solution against concentration (Figure 2.8). The best-fit line through these data is the molar extinction coefficient ε.

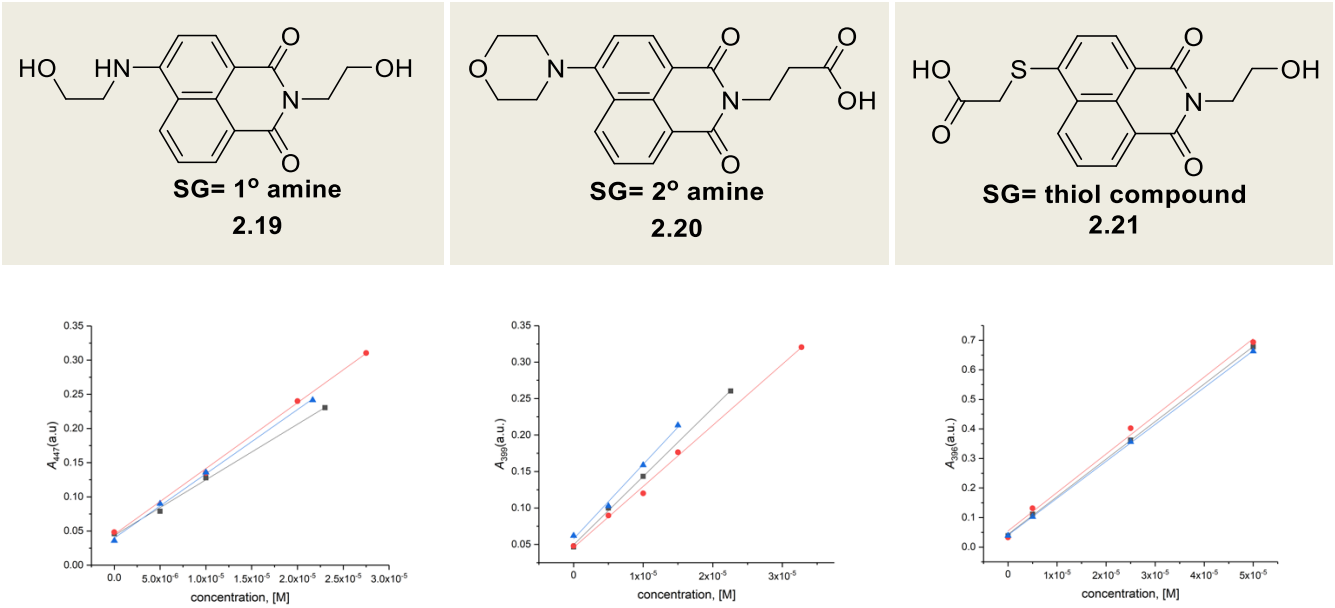

Figure 2.8 The absorbance at λ_{max} for compounds (2.19-21) solution in buffer (25 mM MOPS, 50 mM NaCl, pH 7) against concentration at 25 °C

These steps were applied for all compounds **2.19-21** where three stock solutions were prepared in buffer (25 mM MOPS, 50 mM NaCl, pH 7) and the UV-vis spectra were recorded at 25 °C. Compound **2.19** exhibited lower solubility compared to compounds **2.20-21** and therefore **2.19** required a large volume of buffer to make sure that this compound is completely dissolved. Therefore, after preparing the first stock in MOPS we have decided to prepare the second and third stocks in DI water for **2.19** since there is no risk of (de)protonation in aqueous solutions in any case. Table 2.4 illustrates the concentrations of all stocks; diluted concentrations and the extinction coefficients obtained after analyzing the data.

Table 2.4 The stocks concentrations, diluted concentrations and the extinction coefficients of 2.19-21

2.19	**Diluted solutions concentration / μM**			**extinction coefficient ε / M^{-1} cm^{-1}**	**Average ε / M^{-1} cm^{-1}**
Stock 1 (23 μM)	5	10	23	8.14×10^3	$(9.1\pm0.8)\times10^3$ at 447 nm
Stock 2 (27.5 μM) *	10*	20*	27.5*	9.64×10^3	
Stock 3 (21.66 μM) *	5*	10*	21.66*	9.40×10^3	
2.20	**Diluted solutions concentration, μM**			**extinction coefficient ε**	**Average ε**
Stock 1 (22.59 μM)	5	10	22.59	9.37×10^3	$(9.3\pm0.9)\times10^3$ at 399 nm
Stock 2 (32.757 μM)	5	10	32.757	8.37×10^3	
Stock 3 (15.8139 μM)	5	10	15.8139	10.21×10^3	
2.21	**Diluted solutions concentration, μM**			**extinction coefficient ε**	**Average ε**
Stock 1 (160.096 μM)	5	25	50	12.71×10^3	$(12.3\pm0.3)\times10^3$ at 396 nm
Stock 2 (84.579 μM)	5	25	50	12.37×10^3	
Stock 3 (169.16 μM)	5	25	50	11.88×10^3	

*** solution prepared in DI water**

These values for the molar extinction coefficients were used to calculate the solubility limits for the corresponding synthesized compounds.

The solubility of all synthesized ferrocene-naphthalimide conjugates was tested by trying to dissolve these compounds in MOPS buffer (typically approximately 5 mg in 10 mL). These compounds were only partially dissolved and therefore the obtained saturated solutions were filtered (0.2 μm). After filtration, the UV-vis spectra of the resulting solutions were recorded, and the concentrations were calculated using Beer Lambert law and the extinction coefficients as determined above (Table 2.4). Some of these compounds are not sufficiently spontaneously soluble in MOPS. Therefore, we dissolved these compounds in DMSO and used 100 μL of these stock solutions with 9900 μL of MOPS to obtain a solution for these compounds with 1% DMSO. The solutions were filtered, and the UV-vis spectra were recorded, and the concentrations were calculated using the Beer Lambert law (Table 2.6).

Table 2.5 The solublity for synthesised ferrocene-naphthalimide conjugates in MOPS buffer at room temperature

Compound	λ_{max}, nm	Solubility limit, M		Compound	λ_{max}, nm	Solubility limit, M	
		In MOPS	In MOPS (1% DMSO)			In MOPS	In MOPS (1% DMSO)
2.12a	448	4.24×10^{-5}	2.79×10^{-5}	**2.12f**	396	-	1.18×10^{-5}
2.12b	426	-	0.79×10^{-5}	**2.13a**	447	-	1.24×10^{-5}
2.12c	404	1.58×10^{-5}	1.57×10^{-5}	**2.13c**	405	3.52×10^{-6}	1.35×10^{-5}
2.12d	394	1.68×10^{-5}	2.97×10^{-5}	**2.13e**	401	1.12×10^{-5}	1.33×10^{-5}
2.12e	405	6.19×10^{-5}	4.73×10^{-5}	-	-	-	-

Compounds **2.12a**, **2.12c**, **2.12d**, **2.12e**, **2.13c**, **2.13e** are sufficiently soluble in MOPS and the solubility order is **2.12e**>**2.12a**>**2.12d**>**2.12c**>**2.13e**>**2.13c,** although some of these solubilities are probably within error margins. On the other hand, **2.12b**, **2.12f**, **2.13a**, **2.13c** are not sufficiently soluble in MOPS alone. All compounds are sufficiently soluble in MOPS with 1% DMSO, with the solubilities following this order **2.12e**>**2.12a**,**d**>**2.12c**>**2.13c**>**2.13e**>**2.13a**>**2.13f**>**2.12b**, again with the caveat that several of these are within error from eachother. Generally, there is a reasonable agreement between the solubility determined in MOPS buffer alone and the solubility resulting from diluting a stock solution in DMSO. The spectra for these compounds

confirm the chemical structures since they follow the signature UV-visible absorbances for the standard chromophore spectra in Figure 2.7.

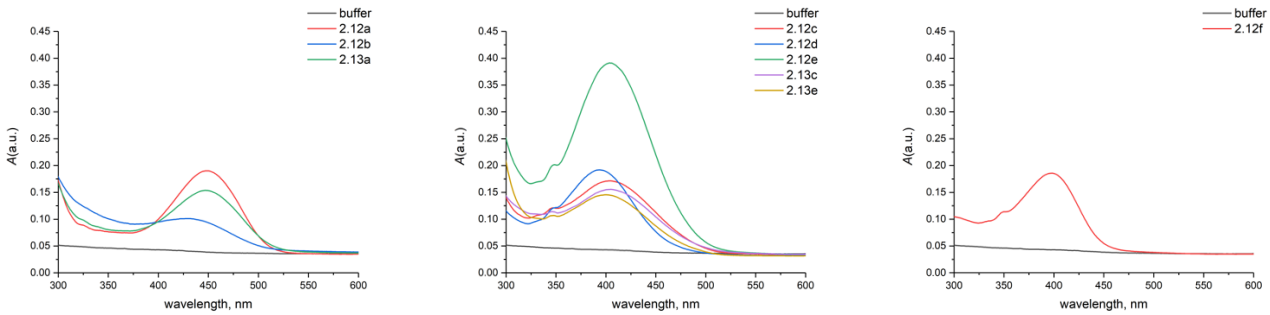

Figure 2.9 UV-visible spectra for a 16.7 μM solution of 2.12a (red, left); 7.1 μM solution of 2.12b (blue, left); 12.9 μM solution of 2.13a (green, left); 14.5 μM solution of 2.12c (red, middle); 16.7 μM solution of 2.12d (blue, middle); 37.6 μM solution of 2.12e (green, middle); 12.6 μM solution of 2.13c (purple, middle); 11.0 μM solution of 2.13e (orange, middle); and 12.1 μM solution of 2.12f (red, left) in buffer (25 mM MOPS, 50 mM NaCl, pH 7) at 25 °C

Generally, electronic properties of 4-substituted naphthalimides are changed by the nature of the substituent on the aromatic ring. Pavel Kucheryavy *et al.*[49] have studied the electronic properties for several 4-substituted naphthalimides with varied substitutent such as Cl, MeS, Me_2N, and NO_2 in CH_2Cl_2. The excited-state character of each NI derivative was studied using steady-state absorption and fluorescence spectra. Furthermore, time-dependent density functional theory (TD-DFT) was used to study the excited-state. According to their findings, the absorption of a photon by all substituted naphthalimides, except Nap-Cl, produces the second excited state (S2) and the transition was found to have a n,π* character. The authors concluded that Nap-SMe, Nap-NMe_2, and Nap-NO_2 show bands belonging to CT n-π* transitions at 391, 416, and 405 nm, respectively. However, the transition to S_1 in case of Nap-Cl has a π,π* character and undergoes intersystem crossing to produce the T1 state at 356 nm within 400 ps.

A similar pattern was observed in case of our synthesized ferrocene-naphthalimide conjugates **2.12a-f, 2.13a,c,e** in MOPS. The UV spectra for ferrocene-naphthalimide conjugates with 2°-amine and thiol as a solubilizing group **2.12c-f, 2.13c,e** show a band with λ_{max} between 394-405 nm (Fig 2.9). These wavelengths are in agreement with those for MeS-, Me_2N-, and NO_2-substituted compounds in Pavel Kucheryavy's study. This suggests that these bands are related to n-π* charge transfer in our compounds as well. Althought Pavel Kucheryavy study did not

include 1°-amine as a substitutent, the UV spectrum for ferrocene-naphthalimide conjugates with 1°-amine as a solubilizing group **2.12a-b, 2.13a** show a band around 448-426 nm. The red shift relative to secondary amines may indicate increased conjugation due to decreased steric hindrance. We tentatively attribute this band for primary amines to a n-π* transition as well.

2.2.6 UV-Visible titration

The main goal of synthesizing these compounds is to study their ability to bind with DNA. Therefore, the binding properties were investigated through UV-visible absorption titrations. As mentioned in Chapter 1, the changes in the UV-visible spectra during the titration, i.e. decreases or increases in the absorbance or shifts in λ_{max}, can be used to determine if the compounds interact with DNA or not. The titration was performed twice for each compound and the obtained data were plotted and analyzed in terms of the multiple independent binding sites (MIS) model to give binding affinities and binding site sizes (stoichiometries).

2.2.6.1 UV-visible spectroscopy DNA-binding studies of compounds 2.12a-f

The binding properties of our ferrocene-naphthalimide conjugates **(2.12a-f)** were studied using UV-visible titrations. The UV-visible absorption spectra of the water-soluble compounds were recorded with addition of FSDNA in MOPS buffer (25 mM MOPS, 50 mM NaCl, pH 7) at 25 °C. The titration was performed twice for each compound and the obtained data were plotted and analyzed in terms of the multiple independent binding sites (MIS) model to give binding affinities and binding site sizes (stoichiometries).[50] Datasets were analysed both individually and globally.

The titration results for **2.12a** are shown in Figure 2.10.

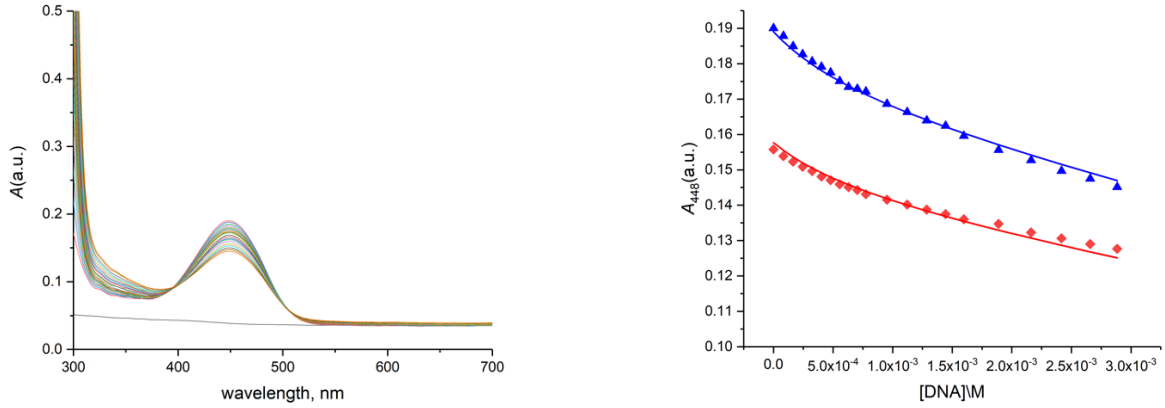

Figure 2.10 Titration spectra of 2.12a upon addition of FSDNA (left); and absorbance at 448 nm for 16.7 μM (▲) and 12.9 μM (◆) solutions of 2.12a as a function of FSDNA concentration in buffer (25 mM MOPS, 50 mM NaCl) at 25 °C. (▲) 1st titration, (◆) 2nd titration, the solid lines represent a global fit of a multiple independent sites model to the data (right)

The spectra for **2.12a** exhibit a hypochromic shift in absorbance at the λ_{max} of 448 nm upon addition of DNA. Plotting the absorbance at 448 nm as a function of DNA concentration yields the titration curves (Figure 2.10). The results of the data analysis are shown in Table 2.6.

Table 2.6 The DNA-binding affinity *K* (*n*=3) / M^{-1} of 2.12a

2.12a	1st titration	2nd titration	Global fit
***K* (*n*=3) / M^{-1}**	$(1.7\pm0.7)\times10^4$	$(3.6\pm0.5)\times10^3$	$(3.7\pm2.0)\times10^3$

Based on the global fit for the two titration curves in terms of the MIS model, the binding affinity and the binding site size appears unrealistically large (see appendix) and accordingly, the error margin on the global fit is large. Since **2.12a** is most likely a monointercalator, a more reasonable value for the binding site (*n*) is 3 basepairs. Thus, the data were analysed again with restricting the binding site size to 3 basepairs, even though we note that this value does not fall within the error margins of the initial fit. According to the fitting, the binding affinity $K_{binding}$ equals $(3.7\pm2.0)\times10^3$ M^{-1} (*n*=3) which indicates that **2.12a** is a weak binder.

Similarly, the titration for **2.12c-e** exhibit hypochromic shifts in absorbance at λ_{max}. Titration curves where extracted from the spectroscopic data by plotting the absorbance at 404 nm as a function of concentration (Figure 2.11).

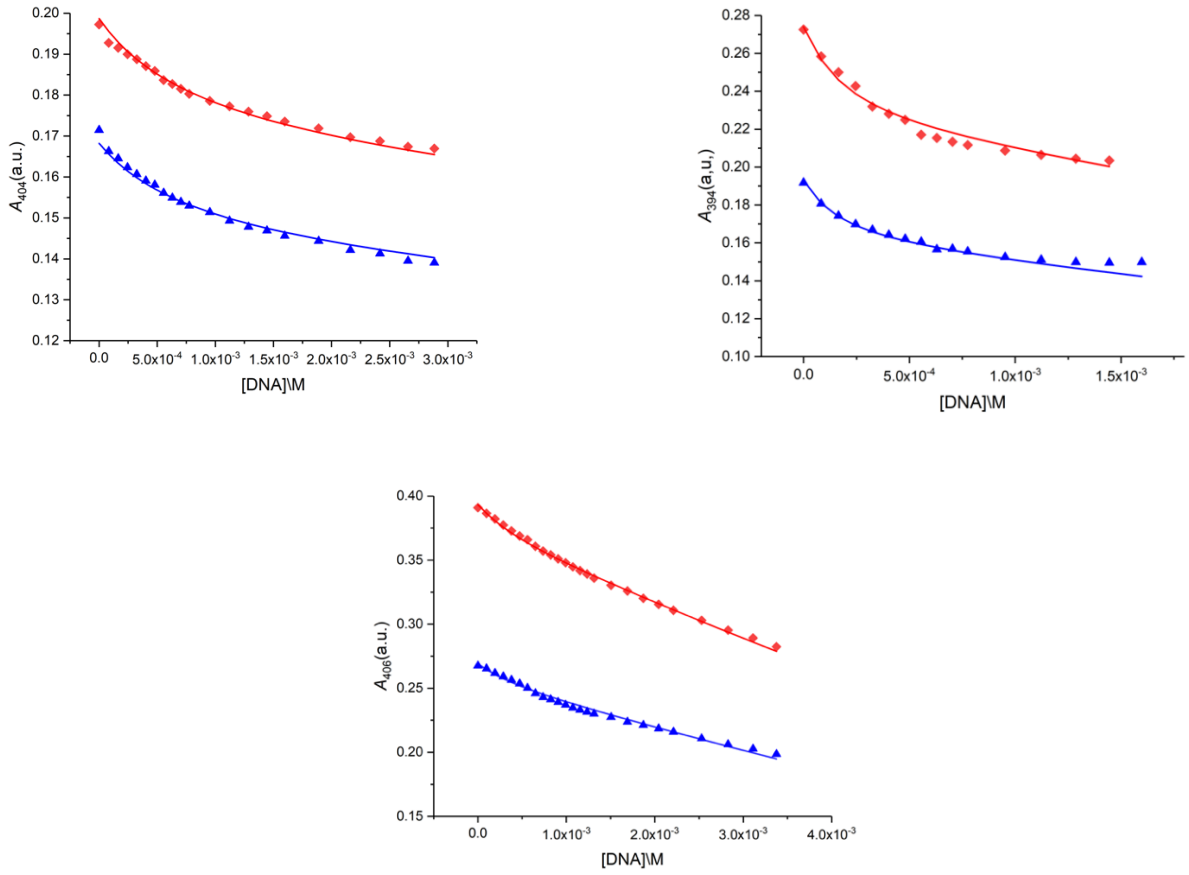

Figure 2.11 Absorbance at 404 nm for a 14.5 μM (▲) and 17.2 μM (◆) solutions of 2.12c as a function of FSDNA concentration (top left); absorbance at 394 nm for a 16.7 μM (▲) and 25.3 μM (◆) solutions of 2.12d as a function of FSDNA concentration (top right); and absorbance at 406 nm for a 24.4 μM (▲) and 37.6 μM (◆) solution of 2.12e as a function of FSDNA concentration (bottom) in buffer (25 mM MOPS, 50 mM NaCl) at 25 °C. (▲) 1st titration, (◆) 2nd titration, the solid lines represent a global fit of a multiple independent sites model to the data

The change in the absorbance in the titration curves for compound **2.12c** shows strong decreases at the beginning of the titration, which suggest that this compound binds strongly compare to **2.12c,e**, which exihibit less significant changing in the absorbance. The obtained titration curves for **2.12c-e** were analysed twice, with and without

restricting the stoichiometry at 3 basepairs (Table 2.7). Table 2.7 illustrates the binding affinities *K* (*n*=3) for compounds **2.12c-e**.

Table 2.7 The DNA-binding affinities *K* (*n*=3) / M^{-1} for compounds 2.12c-e

K (*n*=3) / M^{-1}	1st titration	2nd titration	Global fit
2.12c	$(4.8\pm0.7)\times10^3$	$(3.0\pm0.7)\times10^3$	$(3.7\pm1.2)\times10^3$
2.12d	$(2.5\pm0.5)\times10^4$	$(1.4\pm0.3)\times10^4$	$(2.0\pm0.5)\times10^4$
2.12e	$(8.3\pm3.5)\times10^3$	$(5.7\pm1.3)\times10^3$	$(6.6\pm1.5)\times10^3$

The binding affinities suggest that these compounds are weak binders. However, compound **2.12d** exhibits stronger DNA binding compared to **2.12c** and **2.12e**. The higher affinity is likely caused by the non-anilinic piperazine nitrogen becoming protonated at pH 7, resulting in a cationic compound with additional electrostatic interactions with DNA when binding.

Compounds **2.12b** and **2.12f** were not sufficiently soluble in MOPS buffer alone. Therefore, the alternative approach is to perform the titration by diluting 25 μL of a DMSO stock solution for these compounds with 2500 μL MOPS (resulting in a solution of MOPS with 1 vol-% DMSO). The titration results for **2.12b** are shown in Figure 2.12.

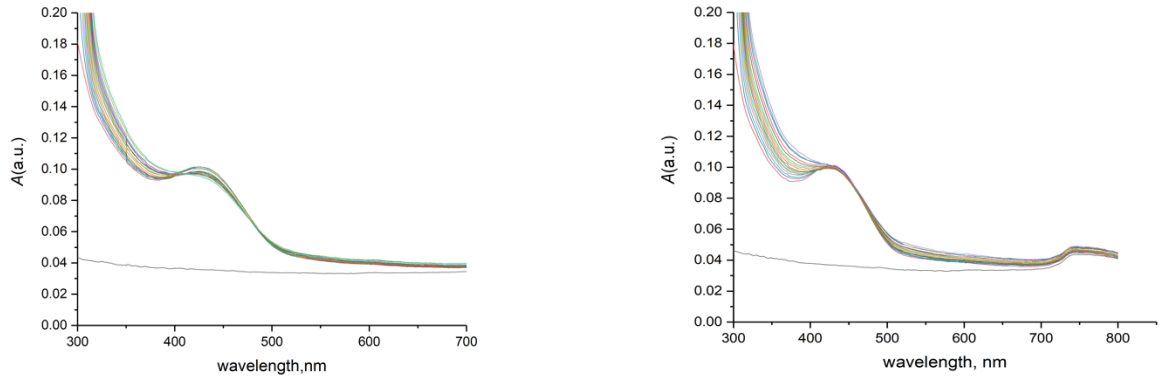

Figure 2.12 The Titration spectra for 7.1 μM (left) and 6.8 μM (right) solutions of 2.12b upon addition of FSDNA in buffer (25 mM MOPS, 50 mM NaCl) with 1% DMSO at 25 °C.

Figure 2.12 shows that the titration spectra for **2.12b** exhibit a limited hypochromic shift in absorbance at the λ_{max} of 426 nm. In addition, some experiments show a small increase in the baseline (600 – 800 nm) where the compound is unlikely to absorb. This baseline increase is attributed to precipitation, resulting in scattering of light. Nevertheless, as before, titrations curves where extracted (Figure 2.13).

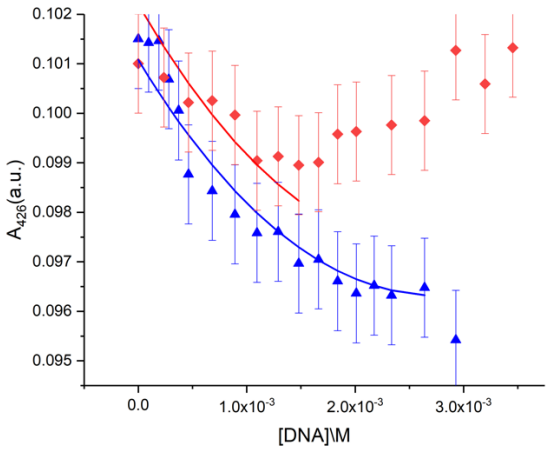

Figure 2.13 Absorbance at 426 nm for 7.1 μM (▲) and 6.8 μM (◆) solutions of 2.12b as a function of FSDNA concentration in buffer (25 mM MOPS, 50 mM NaCl) with 1% DMSO at 25 °C. (▲) 1st titration, (◆) 2nd titration, the solid lines represent a global fit of a multiple independent sites model to the data, right

Figure 2.13 shows that the decrease in absorbance is less than 0.01 absorbance units. The data are reproducible only at the first half of the titrations with one dataset showing an increase in absorbance after the initial decrease. We attribute the increase in absorbance to precipitation and resulting scattering of light, as also observed at higher wavelengths. Therefore, we analyzed the data based on the part where we observed less scattering. Like the previous compounds, the data for both titrations were analysed twice, with and without restricting the stoichiometry to 3 basepairs (Table 2.8). Based on the global fit, the binding affinity equals 122.4±1503 M^{-1} when the stoichiometry is restricted to 3 basepairs, which suggests that this compound is not binding with FSDNA, at least not to an extent that can be quantified in the current experiment.

Titrations curves for **2.12f** were created by plotting the absorbance at 396 nm as a function of DNA concentration (Figure 2.14).

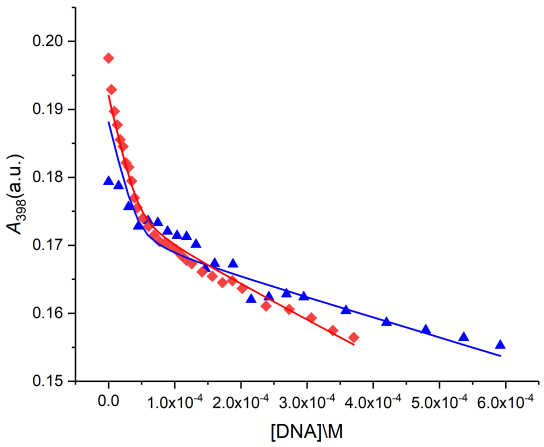

Figure 2.14 Absorbance at 398 nm for 12.0 μM (◆) and 11.6 μM (▲) solutions of 2.12f as a function of FSDNA concentration in buffer (25 mM MOPS, 50 mM NaCl) with 1% DMSO at 25 °C. (◆) 1st titration, (▲) 2nd titration, the solid lines represent a global fit of a multiple independent sites model to the data, right

The titration curves for **2.12f** are not as reproducible as the other compounds. The first titration curve (in red in Figure 2.14) shows a promising binding curve where the first part exhibits a strong decease in the absorbance at λ_{max}=398 nm followed by a clear change in slope, which suggest that this compound is a good binder. However, the second titration curve was surprisingly different where the decrease in the absorbance at λ_{max}=398 nm was not as high as in the first titration and there is far less of a change in curvature in the titration curve. The obtained titration curves for **2.12f** were analysed twice, with and without restricting the binding site size to 3 baspairs (Table 2.8). The binding affinity equals 3.8×10^5 M^{-1} which means that this compound should be considered a good binder, but this comes with the caveat that the fit appears to be dominated by the first dataset so this result needs to be considered somewhat doubtful. Table 2.8 summarises the binding affinities and the stoichimetries for compounds **2.12b,f**.

Table 2.8. The DNA-binding affinity *K* (*n*=3) / M^{-1} for compounds (2.12b,f)[a]

K (*n*=3) / M^{-1}	1st titration	2nd titration	Global fit
2.12b	$(2.6\pm0.2)\times10^3$	0.04±6.50 (not binding)	$(0.1\pm1.5)\times10^3$
2.12f	$(9.2\pm2.4)\times10^5$	$(1.9\pm2.0)\times10^5$	$(3.8\pm2.2)\times10^5$

a) In 25 mM MOPS pH 7, 50 mM NaCl with 1% DMSO at 25 °C

2.2.6.2 UV-visible spectroscopy DNA-binding studies of compounds 2.13a,c,e

The binding properties of the ferrocene-naphthalimide derivatives **2.13a,c,e** were studied using UV-visible titrations. The UV-visible absorption spectra of water-soluble compounds were recorded upon addition of FSDNA in MOPS buffer (25 mM MOPS, 50 mM NaCl, pH 7) at 25 °C.

The titrations for **2.13e** were performed in MOPS only, whereas titrations for **2.13a** and **2.13c** were performed using solutions resulting from diluting 25 μL of DMSO stock solution for these compounds with 2500 μL MOPS (resulting in a solution containing MOPS buffer with 1% DMSO). Generally, the spectra exhibit hypochromic shifts in absorbance at λ_{max}.

Titrations curves were extracted by plotting the absorbance at λ_{max} as a function of DNA concentration (Figure 2.15).

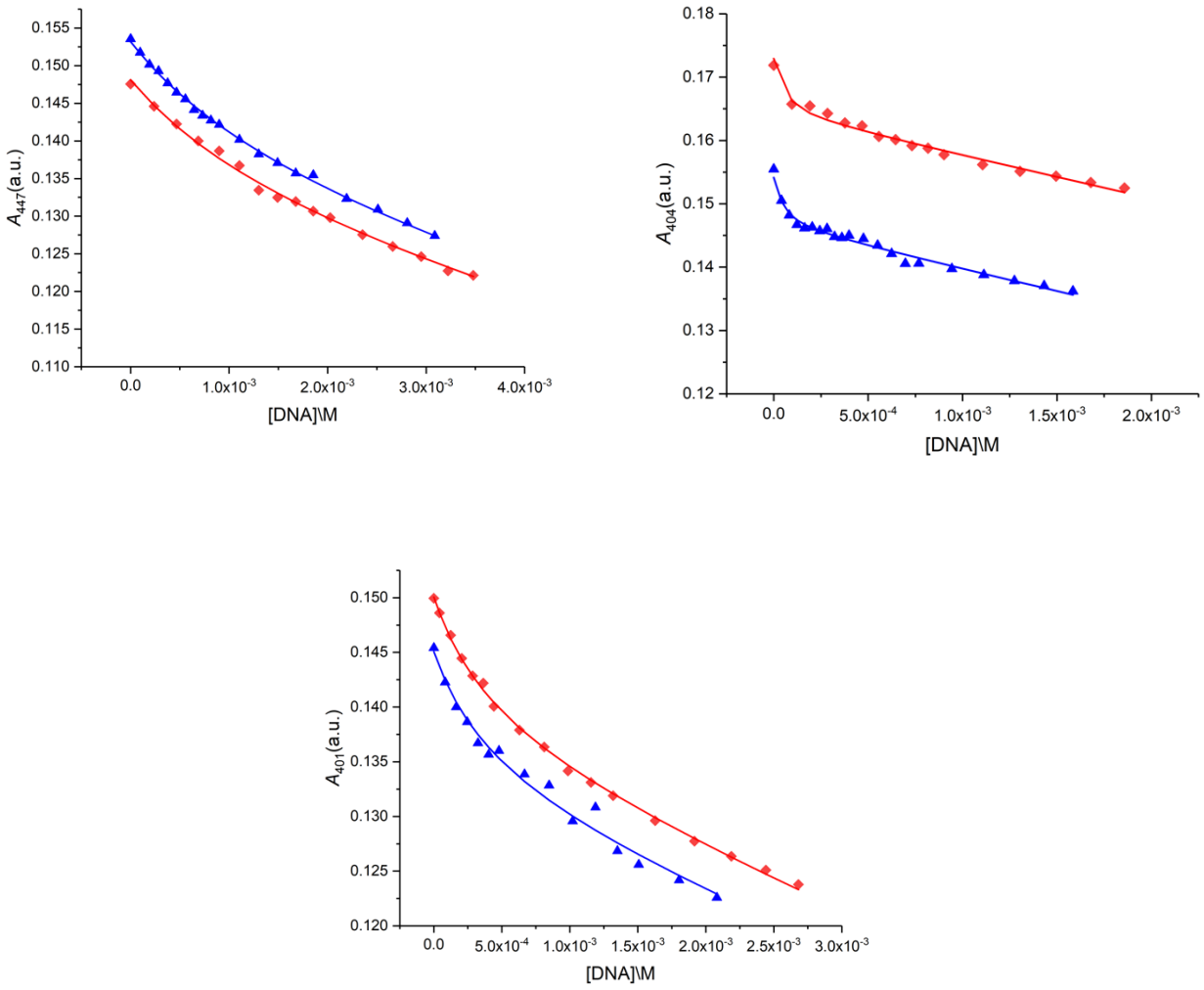

Figure 2.15 Absorbance at 447 nm for 12.9 μM (▲) and 12.1 μM (◆) solutions of 2.13a as a function of FSDNA concentration (top left); absorbance at 404 nm for 12.6 μM (▲) and 14.4 μM (◆) solutions of 2.13c as a function of FSDNA concentration (top right) in buffer (25 mM MOPS pH 7, 50 mM NaCl with 1% DMSO) at 25 °C; and absorbance at 401 nm for 11.0 μM (▲) and 11.5 μM (◆) solutions of 2.13e as a function of FSDNA concentration in buffer (25 mM MOPS, 50 mM NaCl) at 25 °C. (▲) 1st titration, (◆) 2nd titration, the solid lines represent a global fit of a multiple independent sites model to the data

The same protocol as previously used was applied to analyse the obtained titration curves for these compounds (Table 2.9).

Table 2.9 The binding affinities *K* (*n*=3) / M^{-1} for 2.13a,c,e

K (*n*=3) / M^{-1}	1st titration	2nd titration	Global fit
2.13a, DMSO[a]	$(2.7\pm0.7)\times10^{3}$	$(2.4\pm1.0)\times10^{44}$	$(1.7\pm0.5)\times10^{3}$
2.13c, DMSO[a]	$(16.7\pm6.9)\times10^{4}$	$(3.5\pm1.7)\times10^{4}$	$(1.0\pm0.4)\times10^{5}$
2.13e, MOPS[b]	$(6.8\pm5.5)\times10^{4}$	$(4.5\pm0.6)\times10^{3}$	$(6.9\pm2.0)\times10^{3}$

a) In 25 mM MOPS pH 7, 50 mM NaCl with 1% DMSO at 25 °C
b) In 25 mM MOPS pH 7, 50 mM NaC at 25 °C

The binding affinities suggests that compounds **2.13a** and **2.13e** are weak binders whereas compound **2.13c** exhibits stronger binding properties.

In conclusion, several interesting observations can be made in terms of binding properties for synthesized compounds **2.12a-f** and **2.13a,c,e**. Table 2.10 illustrates the binding affinities based on the global fits for comparison.

Table 2.10 The binding affinities based on the global fits for all synthesized compounds (2.12a-f) and (2.13a,c,e)

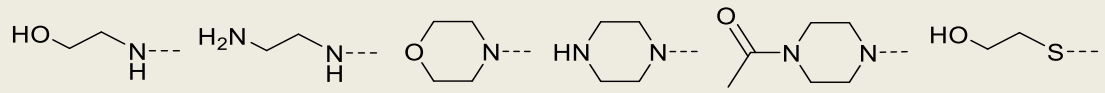

Compound	Binding affinity *	Compound	Binding affinity *
2.12a	$(3.7\pm2.0)\times10^{3}$	**2.13a**	$(1.7\pm0.5)\times10^{3}$
2.12b	$(0.1\pm1.5)\times10^{3}$		
2.12c	$(3.7\pm1.2)\times10^{3}$	**2.13c**	$(1.0\pm0.4)\times10^{5}$
2.12d	$(2.0\pm0.5)\times10^{4}$		
2.12e	$(6.6\pm1.5)\times10^{3}$	**2.13e**	$(6.9\pm2.0)\times10^{3}$
2.12f	$(3.8\pm2.2)\times10^{5}$		

* The stoichiometry is restricted (3)

Generally, ferrocene-naphthalimide derivatives behave as a weak binder with some exceptions. Compounds **2.12a** and **2.12f** are structurally similar, however, **2.12f** seems to bind more strongly with DNA compared to **2.12a**.

Interestingly, comparing the binding affinities for compounds with the same solubilizing groups but with different length of linker shows similar binding affinities except for one case. In the case of morpholine as solubilizing group (i.e. comparing **2.12c** and **2.13c**), changing the length of the linker has a remarkable effect on improving the binding affinity where the compound with a short aliphatic linker **2.13c** exhibits stronger binding affinity than the compound with the longer ether-based linker.

Additional interesting observations can be made by comparing the binding affinities for **2.12c**, **2.12d** and **2.12e**. Using the same linker (long linker) with different secondary amines, the compounds exhibit different binding proprieties, where piperazine shows higher binding affinity and morpholine shows lower binding affinity (**2.12d** **2.12e**>**2.12c**). This observation is attributed to protonation of the piperazine, resulting in a cationic binder with a higher affinity for negatively charged DNA.

2.2.7 Confocal microscopy studies

DNA is primarily localized in the cell nucleus. Therefore, some DNA binders are used as fluorescent nuclear stains and widely employed in cell life cycle analysis and nuclear imaging.[10] We wanted to know whether our compounds enter cells and, if so, where they accumulate. Exploratory fluorescence confocal microscopy studies were therefore carried out using the MCF-7 human breast adenocarcinoma cell line (Figure 2.16).

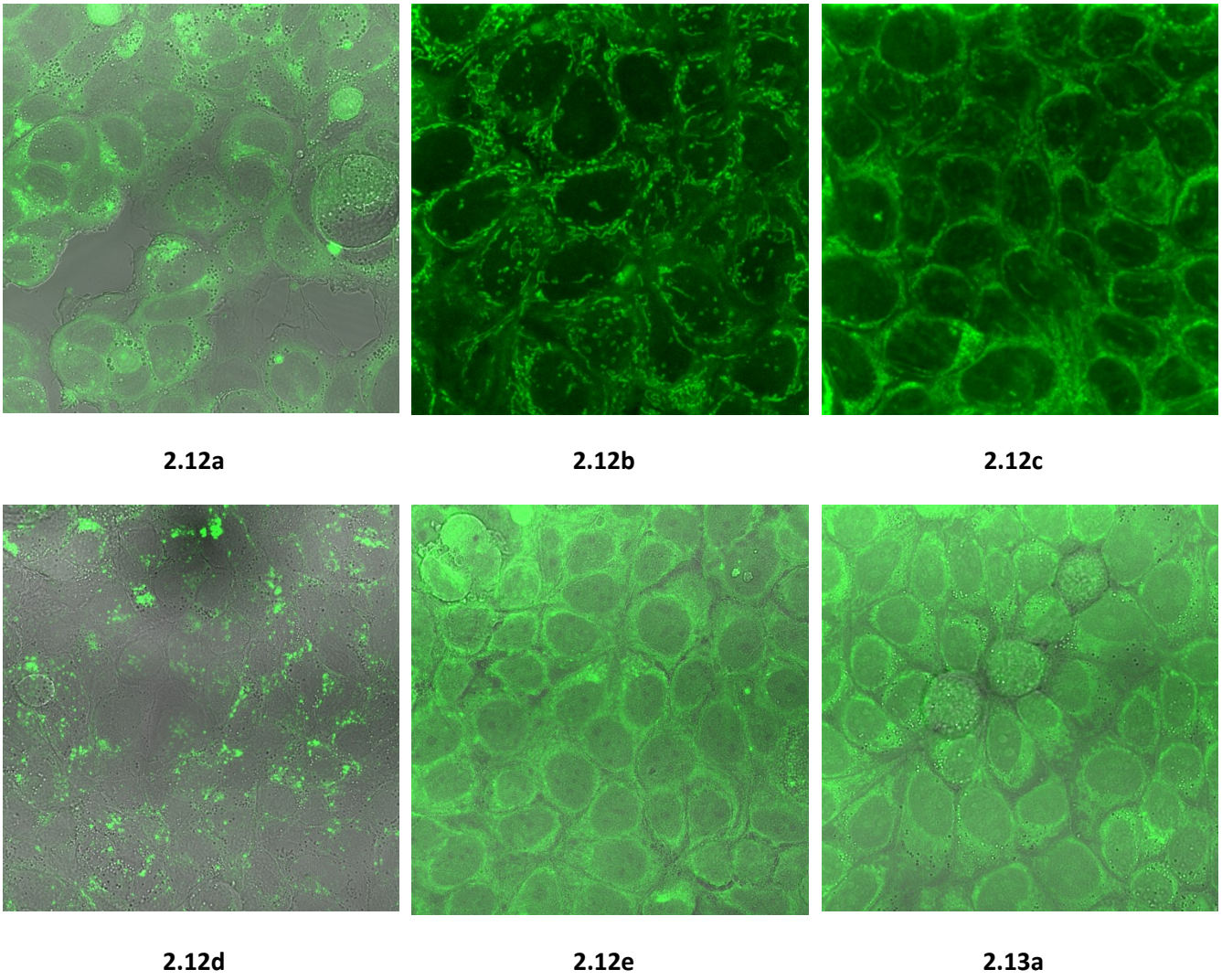

2.12a **2.12b** **2.12c**

2.12d **2.12e** **2.13a**

Figure 2.16 Fluorescence confocal microscopy images of MCF-7 human breast cancer cells with 2.12a-e and 2.13a

First of all, the MCF-7 cells looked confluent and healthy under all observations. Photobleaching was a problem for all compounds tested. The confocal microscopy studies (Figure 2.16) showed the following.

Compound **2.12b** shows punctate localisation which seem to cluster around the nuclei. This could indicate Golgi or lysosomal localisation. Some diffuse nuclear localisation is also possible in some of the images. Compounds **2.12a,c** show probable mitochondrial localisation wheras **2.12d** is more selectively localised in larger sub-cellular compartments e.g. lysosomes. Compound **2.12e** is mostly diffusely localised through the cytoplasm and nucleus (but not the nucleoli). Some punctate localisation is visible also in the cytoplasm. On the other hand, **2.13a** shows

punctate (e.g. mitochondrial) localisation, diffuse nuclear and nucleolar localisation also. Compound **2.12f** does not appear to be taken up in cells.

Although these exploratory results provide a reasonable suggestion of where these compounds might accumulate, to definitively characterise the sub-cellular compartment to which the compounds have localised, follow-up imaging will be required using known fluorophores so that co-localisation studies can be conducted.

2.2.8 Conclusions

Several ferrocene-linker-naphthalimide conjugates **(2.12a-f)**, **(2.13a,c,e)** were synthesized using two terminal diamine linkers and characterized using NMR spectroscopy and mass spectroscopy. The compounds all show some aqueous solubility and typically moderate affinity for DNA, which is reasonable considering the relatively small hydrophobic surface area of the naphthalimide intercalating moiety.

Based on the DNA-binding study, the binding affinities increase in the following order (weakest binder) **2.12b** < **2.13a** < **2.12a** < **2.12c** < **2.12e** < **2.13e** <**2.12d** < **2.13c** < **2.12 f** (strongest binder). Accordingly, compounds **2.12f** and **2.13c** are the most promising DNA-binding compounds. The binding affinities for these compounds are 3.8×10^5 and 1.0×10^5 M^{-1}, respectively. Unfortunatly the confocal study for compound **2.12f** has been performed without modifying the $\lambda_{excitation}$ to be suitable for the naphthalimide with thiol as a solublising group. Using an incorrect $\lambda_{excitation}$ lead to a misleading result that suggests that **2.12f** does not appear to be taken up in cells. In the other hand, **2.13c** has not been studied due to COVID-19 restriction which caused limited accessability of the confocal micropscopy equipment.

Exploratory confocal microscopy studies suggest that all compounds except **2.12e** are taken up in the cells, with varying extents of cellular localization.

The assumption that needs to be addressed is whether binders with higher DNA-binding affinities are more likely to localize in the cell nucleus where the DNA is primarily localized. According to the confocal study for some of ferrocene-linker-naphthalimide conjugates, this pattern is not observed. There is no correlation between the DNA-binding affinities and the localization of these binders in the cell nucleus. This could be attributed to transportation limitation for the binders across the nuclear membrane.

2.3 Experimental

2.3.1 Materials and measurements

All chemicals, including FS DNA, were procured from Sigma-Aldrich, Fisher or TCI and were used without further purification. DCM was dried using an MBraun solvent purification system. Flash column chromatography was carried out using 60 Å silica. All compounds show strong fluorescence and were readily visualized on TLC plates using UV light. ^{1}H-NMR and ^{13}C-NMR spectra were recorded utilizing a Bruker AV 400 UltraShield spectrometer and Bruker AV 500 UltraShield spectrometer using the solvent as an internal standard. All chemical shifts are reported with respect to TMS. High resolution mass spectra were recorded using a Waters Micromass LCT Premier. UV-visible spectra were recorded using a Jasco V-650 spectrophotometer at controlled temperature using an air-cooled EHCS-716 Peltier Thermostatted Cell Holder at 25 °C. The pH of buffers was recorded using Hanna microprocessor pH-meter equipped with a VWR 662-1382 glass electrode. The pH meter was calibrated using a two-point calibration with buffers of known pH obtained from Fisher scientific. Deionized water was obtained from an Elga Purelab Flex.

2.3.2 Experimental procedures

2.3.2.1 Synthesis of 2.14

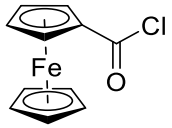

In an ice-bath, a capped round bottom flask was charged with one equivalent of ferrocene carboxylic acid (2 g, 8.69 mmol) dissolved in dry DCM. Then, 2.5 equivalents of oxalyl chloride (17.38, 2.2 g) were added at 0 °C. After that, the ice-bath was removed and the mixture was stirred for 3 hours at room temperature under nitrogen. The solvent was removed under reduced pressure. The product was obtained as a dark brown solid in 98 % yield. **^{1}H NMR (500 MHz, d6-DMSO) δ(ppm):** 4.70 (t, *J*=1.85, 2H, Fc), 4.44 (t, *J*=1.85, 2H, Fc), 4.22 (s, 5H, Fc). **^{13}C NMR (125 MHz, d6-DMSO) δ(ppm):** 172.6, 72.3, 71.5, 70.4, 70.0. **TOF MS ASAP+** 247.97 (100%), 248.97 (37%), 249.97 (55%), expected mass: 247.97 (100%), 248.97 (12%), 249.97 (32%).

2.3.2.2 Synthesis of 2.15

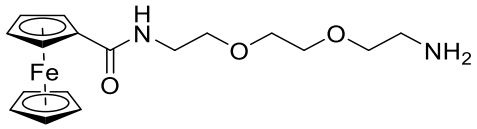

In an ice-bath, one equivalent of ferrocenoyl chloride **2.14** (2.12 g, 8.53 mmol) was dissolved in 25 mL dry DCM. This solution was then added dropwise over 10 minutes to a round-bottom flask containing a solution of 10.18 eq of 2,2-(ethylenedioxy)bisethylamine (12.86 g, 86.9 mmol) dissolved in 50 mL dry DCM. The obtained reaction mixture was allowed to warm to room temperature and left to stir under nitrogen atmosphere for 4 hours. A saturated solution of $NaHCO_3$ (25 mL) was used to quench the reaction. After that, the compound was extracted with DCM. The organic layer was washed with water (2 x 30 mL) and brine (30 mL) and dried over $MgSO_4$. The solvent was removed *in vacuo* to afford (Fc-PEG) as a brown oil in 72 % yield. **^{1}H NMR (400 MHz, $CDCl_3$) δ(ppm):** 6.45 (br.s, 1H, NH), 4.65 (br.s, 2H, CH, Fc), 4.26 (br.s, 2H, CH, Fc), 4.14 (s, 5H, Fc), 3.66-3.55 (m, 6H, CH_2), 3.52 (t, *J*=4.78, 2H, CH_2), 3.46 (t, *J*=4.40, 2H, CH_2), 1.16(t, *J*=7.52, 2H, CH_2). **^{13}C NMR (125 MHz, $CDCl_3$) δ(ppm):** 170.5, 76.1, 72.3, 70.4, 70.3, 70.1, 69.7, 68.3, 68.2, 41.3, 39.3. **TOF MS ES+** calc for [$C_{17}H_{25}N_2O_3Fe$] 361.1215 found 361.1227.

2.3.2.3 Synthesis of 2.16

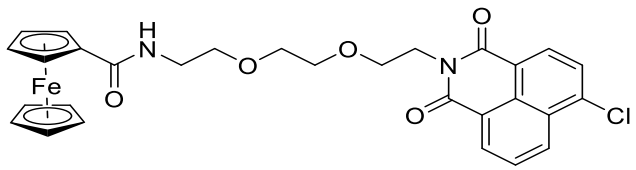

In round-bottom flask, two equivalents of **2.15** (2.25g, 6.25 mmol) were dissolved in EtOH. To this solution one equivalent of 4-chloro-1,8-naphthalic anhydride (0.72 g, 3.12 mmol) was added in addition to a few drops of triethylamine. The resulting mixture was heated to reflux under N_2 atmosphere for 24 h. At the end of the reaction, the solution was left to cool, and the solvent was removed under reduced pressure. The crude product was redissolved into DCM (50 mL), washed with water (2 x 50 mL), washed with brine (2 x 50mL) and dried over magnesium sulfate. After removing the solvent, the crude product was purified using column chromatography over silica gel using DCM and acetone (1:1) as eluent (R_f=0.69). The compound **2.16** was obtained as a brown oil in 93 % yield. **^{1}H-NMR (400 MHz, $CDCl_3$-d): δ(ppm):** 8.63(dd, *J*=7.3, *J*=1.3, Hz, 1H, Ar-H), 8.58(dd, *J*=8.4, *J*=1.0 Hz, 1H, Ar-H), 8.47 (d, 1H, *J*=7.9 Hz, Ar-H), 7.83 (dd, *J*=8.6, *J*=7.5 Hz,1H, Ar-H), 7.80 (t, *J*=7.7 Hz, 1H, Ar-H), 6.44(t, 1H, N-H), 4.68 (t, 2H, *J*=1.8, Hz, Fc), 4.46 (t, 2H, *J*=6.0 Hz, CH_2), 4.27 (t, 2H, *J*=1.80 Hz, Fc), 4.12 (s, 5H, Fc), 3.87 (t, 2H, *J*=5.8 Hz, CH_2), 3.73-3.71 (m, 2H, CH_2), 3.63-3.60 (m,2H, CH_2), 3.57-3.55 (m, 2H, CH_2), 3.51-3.47 (m, 2H, CH_2). **^{13}C-NMR (125 MHz, DMSO-d_6): δ(ppm):** 169.3, 163.5, 163.2, 138, 132.1, 131.4, 130.6, 129.1, 128.9, 128.9, 128.2,

123.1, 121.8, 77.0, 70.3, 70.1, 70.0, 69.8, 69.7, 68.6, 67.3, 39.3, 39.1. **TOF MS ES+** calc for $[C_{29}H_{27}N_2O_5ClFe]$+Na 595.0902 found 595.0911.

2.3.2.4 Synthesis of 2.12a

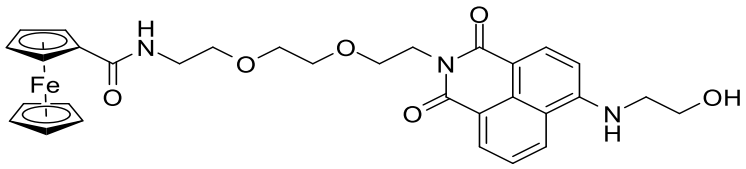

In a round-bottom flask, 0.22 g (0.39 mmol) of **2.16** was dissolved in ethanolamine (10 mL) and heated at reflux under nitrogen atmosphere overnight. The mixture was cooled. After that, 50 mL of water was added and the compound was extracted into DCM (2 x 50mL), and the organic layer is then washed with water (2 x 50 mL). Finally, the solution is dried with magnesium sulfate and the solvent removed *in vacuo* and the crude product was purified using column chromatography over silica gel using $CHCl_3$ and acetone (1:1) as eluent (R_f=0.31). The compound **2.12a** was obtained as a brown oil in 74 % yield. **^{1}H-NMR (400 MHz, DMSO-d_6): δ(ppm):** 8.71 (dd, *J*=8.7, *J*=0.9 Hz, 1H, Ar-H), 8.48(dd, *J*=7.3, *J*=0.8 Hz,1H, Ar-H), 8.30 (d, 1H, *J*=8.4 Hz, Ar-H), 7.80-7.78 (m, 1H, NH), 7.72 (dd, *J*=8.3, *J*=7.3 Hz,1H, Ar-H), 6.86(d, J=8.9, 1H, Ar-H), 4.92 (t,1H, *J*=5.7 Hz, OH), 4.80 (t,2H, *J*=1.9, CH, Fc), 4.33 (t, 2H, *J*=1.9 Hz, CH, Fc), 4.24 (t, 2H, *J*=6.5 Hz, CH_2), 4.16 (s, 5H, Fc), 3.73 (q, 2H, *J*=5.8, CH_2), 3.67 (t, 2H, *J*=6.3 Hz, CH_2), 3.63-3.61 (m,2H, CH_2), 3.58-3.55 (m,2H, CH_2), 3.53-3.49 (m, 4H, CH_2), 3.30-3.27 (m, 2H, CH_2).

2.3.2.5 Synthesis of 2.12b

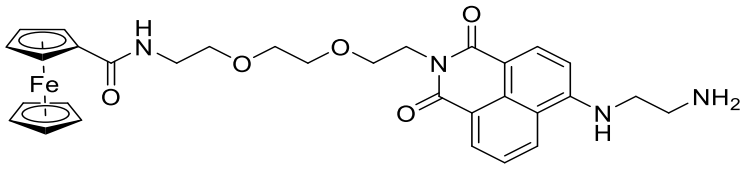

In round-bottom flask, one equivalent of **2.16** (0.18 g, 0.31 mmol) and 7.75 equivalents of ethylenediamine (0.16 mL, 2.4 mmol) were dissolved in 2-methoxyethanol (≈ 20 mL). The mixture was heated at reflux under nitrogen atmosphere overnight. The solution was allowed to cool, then the solvent was removed with a rotary evaporator. 50 mL of DCM was used to dissolve the crude solid. The solution was washed two times with 50 mL of water. The organic layer was dried in *vacuo*. The final compound was obtained as an orange oil and the crude was purified using column chromatography (DCM, acetone 1:1) R_f=0.35 (23 % yield). **^{1}H-NMR (400 MHz, $CDCl_3$-d): δ(ppm):** 8.58(d, *J*=7.5 Hz, 1H, Ar-H), 8.45(d, 1H, *J*=8.2 Hz, Ar-H), 8.18 (d, *J*=8.20 Hz, 1H, Ar-H), 7.62 (at, *J*=8.8 Hz,1H, Ar-H), 6.70 (d, *J*=9.1 Hz,1H, Ar-H), 6.58-6.56 (m,1H, N-H), 6.21-6.19 (m,1H, N-H), 4.74-4.72 (m, 2H,Fc), 4.46 (t, *J*=6.1 Hz, 2H, CH_2), 4.28-4.26 (m, 2H, Fc), 4.16 (s, 5H, Fc), 3.88-3.86 (t, *J*=5.9 Hz,2H, CH_2), 3.74-3.72 (m,2H, CH_2), 3.63-3.61

(m,2H, CH_2), 3.55 (t, *J*=4.2 Hz, 2H, CH_2), 3.48-3.46 (m, 2H, CH_2), 3.41 (q, *J*=5.4 Hz,2H, CH_2), 3.18 (t, *J*=5.4 Hz,2H, CH_2). **TOF MS ES+** calc for $[C_{31}H_{34}N_4O_5Fe]$+Na 619.1823 found 619.1826.

2.3.2.6 Synthesis of 2.12c

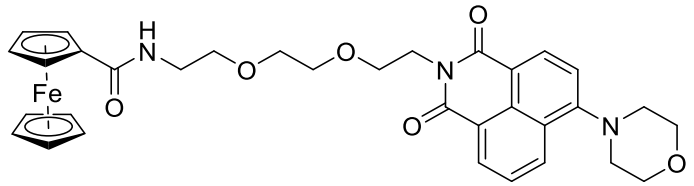

In a round-bottom flask, one equivalent of **2.16** (0.45 g, 0.79 mmol) was dissolved in ≈50 mL DMSO in the presence of four equivalents of morpholine (0.27 mL, 3.14 mmol). The reaction mixture was stirred and heated at 100 °C under N_2 atmosphere for 48 hours. The resulting solution was left to cool, then water was added and finally the solution was neutralized using 1 M HCl. The mixture was extracted into DCM, washed with water, and dried with $MgSO_4$. The solvent was removed under reduced pressure and the crude was purified using column chromatography (DCM: acetone 1:1, over silica) to yield **2.12c** as a brown oil (92 % yield). **^{1}H-NMR (400 MHz, $CDCl_3$-d): δ(ppm):** 8.59(dd, *J*=7.0, *J*=1.1 Hz, 1H, Ar-H), 8.51(d, 1H, *J*=8.0 Hz, Ar-H), 8.41 (dd, *J*=8.5, *J*=1.1 Hz, 1H, Ar-H), 7.69 (dd, *J*=8.4, *J*=7.5 Hz,1H, Ar-H), 7.21 (d, *J*=8.3 Hz,1H, Ar-H), 6.48(t, *J*=5.0 Hz,1H, N-H), 4.71 (t, *J*=1.2 Hz, 2H,Fc), 4.46 (t, *J*=5.9 Hz, 2H, CH_2), 4.27 (t, *J*=1.9 Hz, 2H, Fc), 4.15 (s, 5H, Fc), 4.01(t, *J*=4.5 Hz,4H, morpholine), 3.87 (t, *J*=5.9 Hz,2H, CH_2), 3.73-3.71 (m,2H, CH_2), 3.63-3.61 (m,2H, CH_2), 3.56 (t, *J*=4.8 Hz, 2H, CH_2), 3.48-3.46 (m,2H, CH_2), 3.26 (t, *J*=4.3 Hz,4H, morpholine). **TOF MS ES+** calc for $[C_{33}H_{35}N_3O_6Fe]$+Na 646.1820 found 646.1819.

2.3.2.7 Synthesis of 2.12d

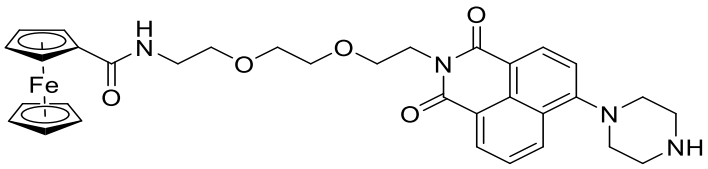

In a round-bottom flask, one equivalent of **2.16** (0.05 g, 0.087 mmol) and four equivalents of piperazine (0.03 g, 0.348 mmol) were dissolved in ≈ 10 mL DMSO. The mixture was heated at 100 °C under N_2 atmosphere for 48 hours. After that, the resulting solution was cooled and water was added and, finally, the solution was neutralized using 1 M HCl. The mixture was extracted into DCM, washed with water and dried with $MgSO_4$. The solvent was removed under reduced pressure to yield **2.12d** as a brown oil (64 % yield). **^{1}H-NMR (500 MHz, $CDCl_3$): δ(ppm):** 8.53 (d, *J*=7.4 Hz, 1H, Ar-H), 8.46 (d, 1H, *J*=8.3 Hz, Ar-H), 8.37 (d, *J*=8.4 Hz, 1H, Ar-H), 7.65 (t, *J*=7.62 Hz,1H, Ar-H), 7.16 (d, *J*=8.3 Hz,1H, Ar-H), 6.65 (t, *J*=5.4 Hz, 1H, N-H), 4.73 (s, 4H, CH_2x2), 4.71-4.68 (m, 2H,Fc), 4.42 (t, *J*=5.7 Hz, 2H, CH_2), 4.24 (t, *J*=1.6 Hz, 2H, Fc), 4.11 (s, 5H, Fc), 3.83 (t, *J*=5.7 Hz,2H, CH_2), 3.68 (m, 2H, CH_2), 3.59-3.57 (m,2H,

CH_2), 3.53 (t, *J*=4.7 Hz,2H, CH_2), 3.45-3.43 (m, 2H, CH_2), 3.23-3.21 (m, 2H, CH_2), 3.18-3.3.16 (m,2H, CH_2). **TOF MS ES+** calc for $[C_{33}H_{36}N_4O_5Fe]$+Na 645.1980 found 645.1990.

2.3.2.8 Synthesis of 2.12e

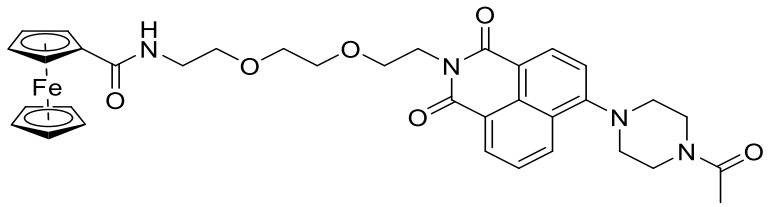

In a round-bottom flask, one equivalent of **2.16** (0.335 g, 0.58 mmol) and four equivalents of 1-acetyl piperazine (0.299 g, 2.33 mmol) were dissolved in ≈ 10 mL DMSO. The reaction mixture was heated at 100 °C under N_2 atmosphere for 48 hours. After that, the resulting solution was cooled and water was added, and the solution was neutralized using 1 M HCl. The mixture was extracted into DCM, washed with water and dried with $MgSO_4$. The solvent was removed under reduced pressure to yield **2.12e** as a brown oil (86 % yield). The crude was purified using column chromatography over silica using chloroform, acetone 1:1 as eluent (R_f=0.53). **^{1}H-NMR (400 MHz, DMSO): δ(ppm):** 8.55(d, *J*=8.6 Hz, 1H, Ar-H), 8.52 (d, 1H, *J*=7.8 Hz, Ar-H), 8.44 (d, *J*=8.1 Hz, 1H, Ar-H), 7.86(t, *J*=8.1 Hz,1H, Ar-H), 7.78 (t, *J*=5.24 Hz, 1H, N-H), 7.38 (d, *J*=8.1 Hz,1H, Ar-H), 4.78 (br.s, 2H, Fc), 4.32 (br.s, 2H,Fc), 4.26 (t, *J*=6.10 Hz, 2H, CH_2), 4.14 (s, 5H, Fc), 3.80-3.78 (br.s,4H, CH_2), 3.69 (t, *J*=6.28, 2H, CH_2), 3.62 (t, *J*= 4.04, 2H, CH_2), 3.55-3.54 (m, 2H, CH_2), 3.49(t, *J*=5.76 Hz, 2H, CH_2), 3.35 (s, 3H, CH_3), 3.28-3.27 (m,4H, CH_2), 3.22-3.20 (m,2H, CH_2).**^{13}C-NMR (125 MHz, $CDCl_3$): δ(ppm):** 175.4, 169.3, 164.5, 164.0, 155.3, 132.5, 131.3, 130.0, 129.9, 126.2, 126.2, 123.2, 117.4, 115.4, 70.4, 70.2, 69.9, 68.0, 53.1, 52.9, 46.4, 41.5, 39.1, 38.9, 29.7, 29.3, 21.5. **TOF MS ES+** calc for $[C_{35}H_{39}N_4O_6Fe]$ 665.2266 found 665.2260.

2.3.2.9 Synthesis of 2.12f

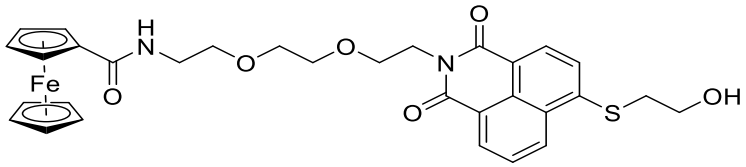

In a round-bottom flask, one equivalent of **2.16** (0.357 g, 0.621 mmol) and 1.5 equivalents of 2-mercaptoethanol (0.072 g, 0.931 mmol) and one equivalent of $NaHCO_3$ (0.052 g, 0.621) were dissolved in ≈ 20 mL 2-methoxyethanol. The mixture was heated at reflux under nitrogen atmosphere for 24h. After that, the solvent was removed with a rotary evaporator and DCM (≈50 mL) was used to dissolve the crude solid. The solution was washed twice with ≈ 50 mL of water. The organic layer was collected and the solvent evaporated *in vacuo*. The

crude was purified using column chromatography over silica ($CHCl_3$: acetone 1:1), R_f=0.5. The final compound was obtained as a brown oil in 62 % yield. **^{1}H-NMR (400 MHz, DMSO): δ(ppm):** 8.61 (dd, *J*=8.4 Hz, *J*= 1.0 Hz, 1H, Ar-H), 8.57 (dd, 1H, *J*=7.3 Hz, J=1.0 Hz, Ar-H), 8.41 (d, *J*=8.00 Hz, 1H, Ar-H), 7.92 (d.d, *J*=8.32, *J*=7.4 Hz,1H, Ar-H), 7.84 (d, *J*=8.2 Hz,1H, Ar-H), 7.79 (t,1H, *J*=5.7 Hz, N-H), 5.17 (t, *J*=5.4, 1H, OH), 4.78 (t, *J*=1.9 Hz, 2H, Fc), 4.32 (t, *J*=1.9 Hz, 2H, Fc), 4.27 (t, *J*=6.4 Hz, 2H, CH_2), 4.14 (s, 5H, Fc), 3.78 (q, *J*=6.0 Hz, 2H, CH_2), 3.70 (t, *J*=6.2 Hz, 2H, CH_2), 3.63-3.61 (m, 2H, CH_2), 3.57-3.55 (m, 2H, CH_2), 3.49 (t, *J*= 5.7 Hz, 2H, CH_2), 3.40 (t, *J*= 6.5 Hz, 2H, CH_2), 3.30-3.28 (m, 2H, CH_2). **TOF MS ES$^+$** calc for [$C_{31}H_{32}N_2O_6SFe$] 617.1330 found 616.1343.

2.3.2.10 Synthesis of 2.17

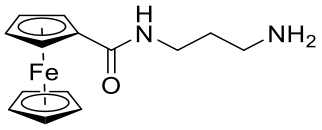

In an ice-bath, one equivalent of ferrocenoyl chloride **2.14** (2.07 g, 8.32 mmol) was placed in a round-bottom flask and dissolved in 25 mL dry DCM. This solution was then added dropwise over 10 minutes to a round-bottom flask containing a solution of 10.44 eq of 1,3-diaminopropane (6.43 g, 86.9 mmol) dissolved in dry DCM. The obtained solution was warmed to room temperature and left to stir under nitrogen atmosphere for 4 hours. A saturated solution of $NaHCO_3$ (25 mL) was used to quench the reaction. After that, the compound was extracted with DCM. The organic phase was washed with water (2 x 30 mL) and brine (30 mL) and dried over $MgSO_4$. The solvent was removed *in vacuo* to afford **2.17** as a brown solid in 36 % yield. **^{1}H-NMR (500 MHz, DMSO): δ(ppm):** 7.81(t, *J*= 5.14, 1H, N-H), 4.77 (t,2H, *J*=1.70, Hz, Fc), 4.32 (t, 2H, *J*=1.77 Hz, Fc), 4.14 (s, 5H, Fc), 3.25 (q, 2H, *J*=6.68 Hz, CH_2), 3.20 (t, 2H, *J*=7.20 Hz, CH_2), 1.76 (quin,2H, *J*=6.18 Hz, CH_2). **HR TOF MS ES+** calc for [$C_{14}H_{19}N_2OFe$] 287.0847 found 287.0833.

2.3.2.11 Synthesis of 2.18

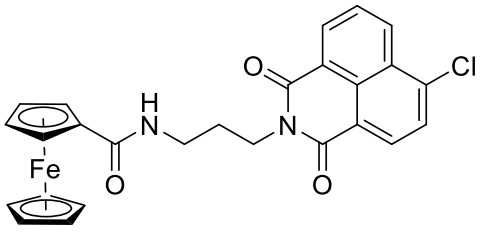

In a round-bottom flask, 1.5 equivalents of **2.17** (1.58 g, 5.33 mmol) were dissolved in EtOH. To this solution one equivalent of 4-chloro-1,8-naphthalic anhydride (0.82 g, 3.55 mmol) was added in addition to several drops of triethylamine. The resulting mixture was refluxed under N_2 atmosphere for 24 h. At the end of the reaction, the solution was left to cool and pure **2.18** was obtained as brown solid (97 % yield). The purity was checked by TLC

using DCM and acetone (1:1) as eluent (R_f=0.66). **^{1}H-NMR (500 MHz, DMSO): δ(ppm):** 8.63(d, *J*= 8.7, Hz, 1H, Ar-H), 8.62(d, *J*= 6.8 Hz,1H, Ar-H), 8.47 (d, 1H, *J*= 8.2 Hz, Ar-H), 8.07 (d, *J*=8.0 Hz,1H, Ar-H), 8.04 (dd, *J*=8.5, *J*=7.7 Hz,1H, Ar-H), 7.87(t, *J*= 5.9, 1H, N-H), 4.80 (t,2H, *J*=1.8, Hz, Fc), 4.37 (t, 2H, *J*=1.9 Hz, Fc), 4.23 (s, 5H, Fc), 4.16 (t, 2H, *J*=7.5 Hz, CH_2), 3.30 (q, 2H, *J*=6.4 Hz, CH_2), 1.92 (quin,2H, *J*=7.2 Hz, CH_2). **^{13}C-NMR (125 MHz, DMSO): δ(ppm):** 169.3, 163.6, 163.3, 137.9, 132.1, 131.4, 130.5, 129.1, 129.0, 128.2, 123.3, 122.1, 77.3, 70.3, 69.8, 68.5, 38.6, 37.2, 28.7. **HR MS EI** calc for [$C_{26}H_{21}N_2O_3ClFe$] 500.05846 found 500.0585.

2.3.2.12 Synthesis of 2.13a

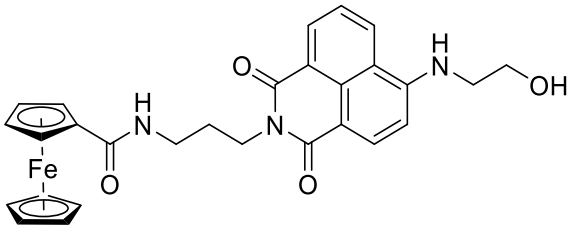

In a round-bottom flask, 0.25 g (0.5 mmol) of **2.18** was dissolved in ethanolamine (3 mL) and heated at reflux under nitrogen atmosphere overnight. The mixture was cooled. After that, 50 mL of water was added and the compound was extracted into DCM (2 x 20 mL), and the combined organic layer was then washed with water (≈30 mL x 2), and brine (≈30 mL x 2), then dried using $MgSO_4$. The solvent was removed under reduced pressure and purified using column chromatography over silica ($CHCl_3$: acetone 1:1, R_f=0.35). The product was obtained as a brown solid in 34 % yield. **^{1}H-NMR (500 MHz, DMSO): δ(ppm):** 8.75 (dd, *J*= 8.9, *J*=0.8 Hz, 1H, Ar-H), 8.50 (dd, *J*= 7.4, *J*=0.9 Hz,1H, Ar-H), 8.32 (d, 1H, *J*= 8.4 Hz, Ar-H), 7.85 (t, *J*= 6.1, 1H, N-H), 7.79 (t, *J*=5.5, 1H, N-H), 7.73 (dd, *J*=8.3, *J*=7.4 Hz,1H, Ar-H), 6.87 (d, *J*=8.7 Hz,1H, Ar-H), 4.92 (t, *J*=5.6 Hz, 1H,OH), 4.79 (t, *J*=2 Hz, 2H, Fc), 4.37 (t, *J*=1.9 Hz, 2H, Fc), 4.22 (s, 5H, Fc), 4.15 (t, 2H, *J*=7.4 Hz, CH_2), 3.74 (q, 2H, *J*=5.8 Hz, CH_2), 3.52 (q, 2H, *J*=5.9 Hz, CH_2), 3.27 (q, 2H, *J*=6.9 Hz, CH_2), 1.88 (quin,2H, *J*=6.9 Hz, CH_2). **^{13}C-NMR (125 MHz, DMSO): δ(ppm):** 169.3, 163.6, 163.3, 137.9, 132.1, 131.4, 130.5, 129.1, 128.9, 128.2, 123.3, 122.1, 77.3, 70.3, 69.8, 68.5, 38.6, 37.2, 28.7. **HR MS EI** calc for [$C_{28}H_{28}N_3O_4Fe$] 526.1429 found 526.1432.

2.3.2.13 Synthesis of 2.13c

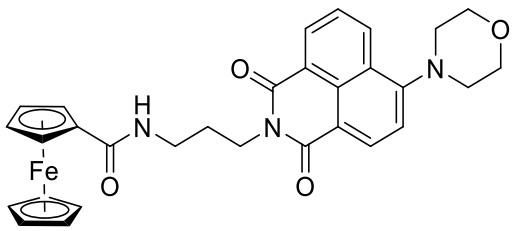

In a round-bottom flask, one equivalent of **2.18** (0.25 g, 0.5 mmol) was dissolved in ≈ 20 mL DMSO together with four equivalents of morpholine (0.17 g, 2 mmol). The reaction mixture was stirred and heated at 100 °C under N_2 atmosphere for 48 hours. The resulting solution was left to cool, then water was added and finally the solution was neutralized using 1 M HCl. The mixture was extracted into DCM, washed with water (≈30 ml x 2), and brine (≈30 ml x 2), then dried using $MgSO_4$. The solvent was removed under reduced pressure and the purity was checked using TLC (DCM: acetone 1:1, R_f= 0.84). The product was obtained as a brown solid in 83 % yield. **^{1}H-NMR (400 MHz, DMSO): δ(ppm):** 8.54(d, *J*= 8.7, Hz, 1H, Ar-H), 8.54(d, *J*= 7.3 Hz,1H, Ar-H), 8.47 (d, 1H, *J*= 8.1 Hz, Ar-H), 7.86 (t, *J*=7.7 Hz,2H, Ar-H and N-H), 7.40(d, *J*= 8.3, 1H, Ar-H), 4.79 (t,2H, *J*=1.9, Hz, Fc), 4.37 (t, 2H, *J*=1.8 Hz, Fc), 4.22 (s, 5H, Fc), 4.16 (t, 2H, *J*=7.2 Hz, CH_2), 3.95 (t, 4H, CH_2, *J*=4.4 Hz, morpholine), 3.3 (t, *J*=6.6, 2H, CH_2), 3.26 (t, 4H, *J*=4.2 Hz, CH_2, morpholine), 1.90 (quin,2H, *J*= 7.0 Hz, CH_2). **^{13}C-NMR (100 MHz, DMSO): δ(ppm):** 169.3, 164.1, 163.6, 156.1, 132.7, 131.1, 129.7, 126.6, 125.8, 123.1, 116.4, 115.6, 77.3, 70.3, 69.8, 68.5, 66.7, 53.5, 38.3, 37.2, 28.9. **HR MS** calc for [$C_{30}H_{30}N_3O_4Fe$] 550.1629 found 550.1632.

2.3.2.14 Synthesis of 2.13e

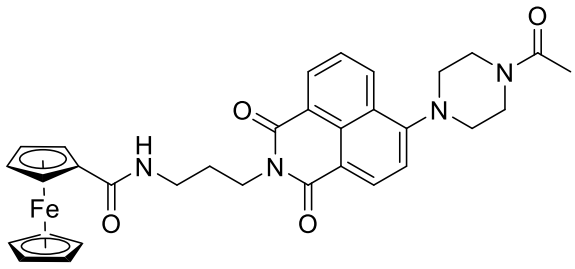

In a round-bottom flask, one equivalent of **2.18** (0.25 g, 0.5 mmol) was dissolved in ≈ 20 mL DMSO in the presence of four equivalents of 1-acetyl piperazine (0.256 mL, 2 mmol). The reaction mixture was stirred and heated at 100 °C under N_2 atmosphere for 48 hours. The resulting solution was left to cool, then water was added and finally the solution was neutralized using 1 M HCl. The mixture was extracted into DCM, washed with water (≈30 ml x2), and brine (≈30 ml x2), then dried using $MgSO_4$. The solvent was removed under reduced pressure and the purity was checked using TLC ($CHCl_3$: acetone 1:1, R_f=0,63). The product was obtained as a brown solid in 72% yield. **^{1}H-NMR (400 MHz, DMSO): δ(ppm):** 8.57 (d, *J*= 7.9, Hz, 1H, Ar-H), 8.55 (d, *J*= 6.5 Hz,1H, Ar-H), 8.47 (d, 1H, *J*= 8.2 Hz, Ar-H), 7.88 (dd, *J*=8.4, *J*=7.4 Hz,1H, Ar-H), 7.86 (t, *J*=5.5, *J*=5.20 Hz,1H, N-H), 7.41(d, *J*= 8.2, 1H, Ar-H), 4.79 (t,2H, *J*=1.9, Hz, Fc), 4.37 (t, 2H, *J*=1.8 Hz, Fc), 4.22 (s, 5H, Fc), 4.16 (t, 2H, *J*=7.3 Hz, CH_2), 3.81-3.79 (m, 4H, CH_2), 3.28 (t, *J*=6.0, 4H, CH_2), 3.21 (t, 2H, *J*=4.9 Hz, CH_2), 2.12 (s, 3H, CH_3), 1.90 (quin,2H, *J*=4.9 Hz, CH_2). **^{13}C-NMR (400 MHz, DMSO): δ(ppm):** 169.3, 169.0, 164.1, 163.6, 155.8, 132.6, 131.2, 129.6, 126.7, 125.9, 123.1, 116.5, 115.9, 79.7, 77.3, 70.3, 69.8, 68.5, 53.2, 53.0, 46.2, 41.4, 38.3, 37.2, 28.9, 21.8. **HR MS** calc for [$C_{32}H_{33}N_4O_4Fe$] 593.1851 found 593.1848.

2.3.3 Molar extinction coefficient determination for reference compounds

Three stock solutions were prepared for **2.19-21** by dissolving a weighable amount of these compounds in MOPS buffer. A series of three diluted solutions were prepared from each stock solution. 2500μL of each diluted solution was placed in a 1 cm pathlength thermostated quartz cuvette and the UV-vis spectra were recorded at 25 °C (Table 2.11). The molar extinction coefficient was calculated by plotting the absorbance at λ_{max} for each solution against concentration. The best-fit line using Origin 2017 through these data gives the slope, i.e. the molar extinction coefficient.

Table 2.11

	C, M	**A_{447}, 1st stock**	**C, M**	**A_{447}, 2nd stock**	**C, M**	**A_{447}, 3rd stock**
2.19	buffer	0.04602	buffer	0.04832	buffer	0.03587
	5×10^{-6}	0.07888	1×10^{-5}	0.13497	5×10^{-6}	0.09001
	1×10^{-5}	0.12785	2×10^{-5}	0.2401	1×10^{-5}	0.13586
	2.3×10^{-5}	0.23054	2.75×10^{-5}	0.31046	2.166×10^{-5}	0.2415
	C, M	**A_{399}, 1st stock**	**C, M**	**A_{399}, 2nd stock**	**C, M**	**A_{399}, 3rd stock**
2.20	buffer	0.04664	buffer	0.04791	buffer	0.06203
	5×10^{-6}	0.1	5×10^{-6}	0.08966	5×10^{-6}	0.10273
	1×10^{-5}	0.14343	1×10^{-5}	0.12015	1×10^{-5}	0.15877
	2.259×10^{-5}	0.26031	1.5×10^{-5}	0.17643	1.58139×10^{-5}	0.21353
			3.2757×10^{-5}	0.32038		
	C, M	**A_{396}, 1st stock**	**C, M**	**A_{396}, 2nd stock**	**C, M**	**A_{396}, 3rd stock**
2.21	buffer	0.0383	buffer	0.03294	buffer	0.03894
	5×10^{-6}	0.11201	5×10^{-6}	0.13134	5×10^{-6}	0.10264
	2.5×10^{-5}	0.36208	2.5×10^{-5}	0.40233	2.5×10^{-5}	0.35636
	5×10^{-5}	0.67799	5×10^{-5}	0.69329	5×10^{-5}	0.66289

2.3.4 Solubility tests of synthesized compounds

For each compound, two stock solutions were prepared, using MOPS and DMSO as solvents. The first series of solutions were prepared by placing approximately 10 mg of synthesized compounds **2.12a-f,2.13a,c,e** in 20 mL MOPS buffer (Table 2.12). Then the solutions were filtered using a 3 mm 0.2 μm syringe filter. The solution was placed in a 1 cm pathlength thermostatted quartz cuvette and the spectra were recorded at 25 °C and the concentrations were calculated using Beer Lambert law.

Table 2.12

Comp.	2.12a	2.12b	2.12c	2.12d	2.12e	2.12f	2.13a	2.13c	2.13e
w, mg [a]	9.6	18.2	4.9	10.5	4.2	9	10.2	12.9	17.3

[a] in 20 mL MOPS

Similarly, The second series of solutions were prepared by placing approximately 5 mg of synthesized compounds **2.12a-f,2.13a,c,e** in 1 mL DMSO. Then 100 μL of these stocks were diluted with 9900 μL MOPS and the resulting solutions/suspensions were filtered using a 3 mm 0.2 μm syringe filter. The resulting solutions were placed in a 1 cm pathlength thermostatted quartz cuvette and the spectra were recorded at 25 °C and the concentrations were calculated using Beer Lambert law.

2.3.5 UV-Visible titrations

2.3.5.1 Preparation of buffer solution

In a 2 litre beaker, 50 mmol (10.463 g) of 3-(*N*-morpholino)propanesulfonic acid (MOPS) and 100 mmol (5.844g) of sodium chloride were dissolved in 1500 mL of distilled water . The mixture was stirred until all solid had dissolved. The pH of the solution was tested with a calibrated pH meter and adjusted to pH 7.00±0.02 by addition of a sodium hydroxide solution. The solution was then transferred to a 2 litre volumetric flask and made up to 2 litres with distilled water. The flask was inverted to make sure the solution was completely homogenous before transferring to a bottle for storage.

2.3.5.2 Preparation of DNA solution

Fish sperm DNA (FSDNA) (~0.1 g) was placed in a 10 mL falcon tube with MOPS buffer (10 mL). The solution was sonicated to dissolve the solid then left to stand overnight to ensure all material was in solution. The solution was dialysed overnight using 3.5 kDa MWCO (molecular weight cut-off) dialysis tubing (Visking from Medicell) against 1 litre of buffer. The concentration of the DNA solution was determined spectrophotometrically by placing 10 μL of the dialysed solution in 2500 μL of buffer and recording a UV-visible spectrum between 200-800 nm. A molar absorptivity at 260 nm of 12,600 M^{-1} (bp) cm^{-1} was used to calculate concentrations (0.01047, 0.01225, 0.00384 mol dm^{-3}).

2.3.5.3 UV-visible titration

Concentrated stock solutions of sufficiently soluble compounds in MOPS **(2.12a,c-e), (2.13e)** were diluted by adding different volumes of these solutions to a 1 cm pathlength quartz cuvette and completing the volume with MOPS buffer until 2500 μl. Table 2.13 illustrates the details for each compound. The cuvette was placed in the spectrophotometer, thermostated at 25 °C and a UV-visible spectrum was recorded. The DNA solution was added stepwise in small aliquots (5-10 μl) and the UV-visible spectra were recorded within the range 200-600 nm before and after each addition of DNA. The absorptions at maximum wavelengths as a function of DNA and ligand concentrations were extracted from the UV-visible spectra. The obtained data for each titration were analysed using Origin 2017 by plotting the absorption as a function of DNA concentration. The multiple independent binding sites model[50] was used to determine the binding properties.

Table 2.13

	First titration		Second titration	
	At the beginning	**DNA concentration, M**	**At the beginning**	**DNA concentration , M**
2.12a	1500μL buffer+ 1000μL buffer stock	0.01047	1750μL buffer + 750μL stock solution	0.01047
2.12b	2500 μL buffer + 50 μL DMSO stock	0.01225	2500 μL buffer + 50 μL DMSO stock	0.01225
2.12c	2500μL buffer stock	0.01047	2500μL buffer stock	0.01047
2.12d	1000 μL buffer +1500 μL buffer stock	0.01047	500 μL buffer +2000 μL buffer stock	0.01047
2.12e	1500μL buffer+ 1000μL buffer stock	0.01225	1000μL buffer+ 1500μL buffer stock	0.01225
2.12f	2500 μL buffer + 25 μL DMSO stock	0.00224	2500 μL buffer + 25 μL DMSO stock	0.00384
2.13a	2500 μL buffer + 25 μL DMSO stock	0.01225	2500 μL buffer + 25 μL DMSO stock	0.01225
2.13c	2500 μL buffer + 25 μL DMSO stock	0.01047	2500 μL buffer + 25 μL DMSO stock	0.01225
2.13e	2500μL buffer stock	0.01047	2500μL buffer stock	0.01047

2.3.6 Molecular Docking study

To be able to dock ferrocene-naphthalimide conjugates using AutoDock vina, the chemical structures for the the proposed compounds need to be created in PDBQT format. In order to do that, we followed the procedure introduced by Vatsadze, Sergey *et al*.[51] Accordingly, the structure of the ferrocene moiety was downloaded (PDB: 1A3L) and the chemical structures for the remainder of the compounds were drawn using ChemDraw Professional 16.0 and subjected to geometrical optimization using MM2 (molecular dynamics and energy minimized) in Chem3D 16.0. The ferrocene moiety and the rest of the compound were linked together in Avogadro. The ferrocene moiety was selected and its geometry was fixed while the rest of compound was subjected to geometrical optimization with the UFF force field. The final structure was saved in MOL2 format and converted to a PDBQT file in AutoDock Tools after checking the torsions for all the bonds.[51] The structure of DNA with pre-

formed intercalation gap[45] d(ATCGAGACGTCTCGAT)$_2$ was used for the docking using AutoDock Vina[44] with the below parameters (Figure 2.17).

center_x = -2.152 center_y = 2.953 center_z = 24.92 size_x = 40 size_y = 40 size_z = 60 exhaustiveness = 200 num_modes = 10	**Definition:** **Center [x][y][z]**: box center in the receptor coordinate system. **Size [x][y][z]**: box dimensions along X, Y, and Z in the receptor coordinate system. **num_modes**: maximum number of binding modes to generate. **Exhaustiveness:** the time spent on the search is already varied heuristically depending on the number of atoms, flexibility, etc

Figure 2.17 The docking parameters

2.3.7 Confocal fluorescence microscopy

The ferrocene-naphthalimide conjugates 2.12a-f and 2.13a,c,e were dissolved in DMSO (final concentration of 5 mg/ml). the cells tested: MCF-7 human breast adenocarcinoma cell line.

Protocol: MCF-7: Cells were grown on glass (size 0) coverslips until confluent in RPMI medium incubated at 37°C (under 5% CO2 and 95% air). Adherent cells were then incubated with 100 µg/ml of each test compound for 30 min in fresh RPMI under the conditions specified previously. Following incubation, cells were washed three times in PBS (pH 7.2) and transferred to glass microscope slides for imaging. Imaging parameters: λex 405 nm diode laser, λem 520 for all compounds

2.4 Acknowledgment

I thank Catrin Williams and Tony Hayes for their work in confocal fluorescence microscopy for some of the compounds.

2.5 References

1. Tian, Z. Y.; Li, J. H.; Li, Q.; Zang, F. L.; Zhao, Z. H.; Wang, C. J., Study on the synthesis, biological activity and spectroscopy of naphthalimide-diamine conjugates. *Molecules* **2014,** *19* (6), 7646-68.

2. Wang, K.-R.; Qian, F.; Wang, X.-M.; Tan, G.-H.; Rong, R.-X.; Cao, Z.-R.; Chen, H.; Zhang, P.-Z.; Li, X.-L., Cytotoxic activity and DNA binding of naphthalimide derivatives with amino acid and dichloroacetamide functionalizations. *Chinese Chemical Letters* **2014,** *25* (7), 1087-1093.

3. Brider, T.; Redko, B.; Oron-Herman, M.; Cohen-Matzlich, A.; Gerlitz, G.; Gellerman, G.; Grynszpan, F., Synthesis and in vitro anticancer evaluation of 1,8-naphthalimide N(4) and S(4)-derivatives combining DNA intercalation and alkylation capabilities. *Research on Chemical Intermediates* **2015,** *42* (3), 1741-1757.

4. Lu, Y. T.; Chen, T. L.; Chang, K. S.; Chang, C. M.; Wei, T. Y.; Liu, J. W.; Hsiao, C. A.; Shih, T. L., Synthesis of novel C4-benzazole naphthalimide derivatives with potent anti-tumor properties against murine melanoma. *Bioorg Med Chem* **2017,** *25* (2), 789-794.

5. Banerjee, S.; Veale, E. B.; Phelan, C. M.; Murphy, S. A.; Tocci, G. M.; Gillespie, L. J.; Frimannsson, D. O.; Kelly, J. M.; Gunnlaugsson, T., Recent advances in the development of 1,8-naphthalimide based DNA targeting binders, anticancer and fluorescent cellular imaging agents. *Chem Soc Rev* **2013,** *42* (4), 1601-18.

6. Sarma, R. J.; Devi, K., Cystine-derived bis-naphthalimides as stimuli-responsive fluorescent gelators. *New Journal of Chemistry* **2015,** *39* (6), 4375-4383.

7. Antonini, I.; Volpini, R.; Dal Ben, D.; Lambertucci, C.; Cristalli, G., Design, synthesis, and biological evaluation of new mitonafide derivatives as potential antitumor drugs. *Bioorg Med Chem* **2008,** *16* (18), 8440-6.

8. Gudeika, D., A review of investigation on 4-substituted 1,8-naphthalimide derivatives. *Synthetic Metals* **2020,** *262*, 116328.

9. Gopikrishna, P.; Meher, N.; Iyer, P. K., Functional 1,8-Naphthalimide AIE/AIEEgens: Recent Advances and Prospects. *ACS Appl Mater Interfaces* **2018,** *10* (15), 12081-12111.

10. Zhou, J.; Chang, A.; Wang, L.; Liu, Y.; Liu, X.; Shangguan, D., Effects of side chains on DNA binding, cell permeability, nuclear localization and cytotoxicity of 4-aminonaphthalimides. *Org Biomol Chem* **2014,** *12* (45), 9207-15.

11. Yin, H.; Zhu, W.; Xu, Y.; Dai, M.; Qian, X.; Li, Y.; Liu, J., Novel aliphatic N-oxide of naphthalimides as fluorescent markers for hypoxic cells in solid tumor. *European Journal of Medicinal Chemistry* **2011,** *46* (7), 3030-3037.

12. Yu, H.; Guo, Y.; Zhu, W.; Havener, K.; Zheng, X., Recent advances in 1,8-naphthalimide-based small-molecule fluorescent probes for organelles imaging and tracking in living cells. *Coordination Chemistry Reviews* **2021,** *444*, 214019.

13. Korzec, M.; Kotowicz, S.; Gawecki, R.; Malarz, K.; Mrozek-Wilczkiewicz, A.; Siwy, M.; Schab-Balcerzak, E.; Grzelak, J.; Maćkowski, S., 1,8-Naphthalimides 3-substituted with imine or β-ketoenamine unit evaluated as compounds for organic electronics and cell imaging. *Dyes and Pigments* **2021,** *193*, 109508.

14. Li, M.; Du, F.; Xue, P.; Tan, X.; Liu, S.; Zhou, Y.; Chen, J.; Bai, L., An AIE fluorescent probe with a naphthalimide derivative and its application for detection of hypochlorite and imaging inside living cells. *Spectrochimica Acta Part A: Molecular and Biomolecular Spectroscopy* **2020,** *227*, 117760.

15. Bojinov, V. B.; Georgiev, N. I.; Bosch, P., Design and Synthesis of Highly Photostable Yellow–Green Emitting 1,8-Naphthalimides as Fluorescent Sensors for Metal Cations and Protons. *Journal of Fluorescence* **2009,** *19* (1), 127-139.

16. Dai, H.; Xu, H., A water-soluble 1,8-naphthalimide-based 'turn on' fluorescent chemosensor for selective and sensitive recognition of mercury ion in water. *Bioorg Med Chem Lett* **2011,** *21* (18), 5141-4.

17. J, N.; J, M., Evaluation of New Naphthalimides as Potential Anticancer Agents against Breast Cancer MCF-7, Pancreatic Cancer BxPC-3 and Colon Cancer HCT- 15 Cell Lines. *Organic Chemistry: Current Research* **2015,** *04* (03).

18. Brana, M. F.; Cacho, M.; Gradillas, A.; Pascual-Teresa, B. d.; Ramos, A., Intercalators as Anticancer Drugs. *Current Pharmaceutical Design* **2001,** *7* (17), 1745-1780.

19. Costanza, M. E.; Berry, D.; Henderson, I. C.; Ratain, M. J.; Wu, K.; Shapiro, C.; Duggan, D.; Kalra, J.; Berkowitz, I.; Lyss, A. P., Amonafide: An active agent in the treatment of previously untreated advanced breast cancer--a cancer and leukemia group B study (CALGB 8642). *Clinical Cancer Research* **1995,** *1* (7), 699-704.

20. Rosell, R.; Carles, J.; Abad, A.; Ribelles, N.; Barnadas, A.; Benavides, A.; Martín, M., Phase I study of mitonafide in 120 hour continuous infusion in non-small cell lung cancer. *Investigational New Drugs* **1992,** *10* (3), 171-175.

21. Duke, R. M.; Veale, E. B.; Pfeffer, F. M.; Kruger, P. E.; Gunnlaugsson, T., Colorimetric and fluorescent anion sensors: an overview of recent developments in the use of 1,8-naphthalimide-based chemosensors. *Chemical Society reviews* **2010,** *39* (10), 3936-3953.

22. Casado, A.; Rosell, R.; García-Gómez, R.; Díaz-Rubio, E.; Pérez-Manga, G.; Font, A.; Benavides, A.; Martín, M., Phase II study of mitonafide in non-small cell lung cancer (NSCLC). *Investigational New Drugs* **1996,** *14* (4), 415-417.

23. Malviya, V. K.; Liu, P. Y.; Alberts, D. S.; Surwit, E. A.; Craig, J. B.; Hannigan, E. V., Evaluation of amonafide in cervical cancer, phase II. A SWOG study. *Am J Clin Oncol* **1992,** *15* (1), 41-4.

24. Ratain, M. J.; Mick, R.; Berezin, F.; Janisch, L.; Schilsky, R. L.; Vogelzang, N. J.; Lane, L. B., Phase I study of amonafide dosing based on acetylator phenotype. *Cancer research* **1993,** *53* (10 Suppl), 2304-2308.

25. Laurent, I.; Florence, L.; Robert, K.; Tatjana, M., Naphthalimides and Azonafides as Promising Anti-Cancer Agents. *Current Medicinal Chemistry* **2009,** *16* (10), 1192-1213.

26. Min, L.; Hui, X., Overview of Naphthalimide Analogs as Anticancer Agents. *Current Medicinal Chemistry* **2009,** *16* (36), 4797-4813.

27. Waring, M. J.; González, A.; Jiménez, A.; Vázquez, D., Intercalative binding to DNA of antitumour drugs derived from 3-nitro-1,8-naphthalic acid. *Nucleic Acids Res* **1979,** *7* (1), 217-30.

28. Tomczyk, M. D.; Walczak, K. Z., l,8-Naphthalimide based DNA intercalators and anticancer agents. A systematic review from 2007 to 2017. *Eur J Med Chem* **2018,** *159*, 393-422.

29. Tandon, R.; Luxami, V.; Kaur, H.; Tandon, N.; Paul, K., 1,8-Naphthalimide: A Potent DNA Intercalator and Target for Cancer Therapy. *Chem Rec* **2017,** *17* (10), 956-993.

30. Xie, L.; Xu, Y.; Wang, F.; Liu, J.; Qian, X.; Cui, J., Synthesis of new amonafide analogues via coupling reaction and their cytotoxic evaluation and DNA-binding studies. *Bioorganic & Medicinal Chemistry* **2009,** *17* (2), 804-810.

31. Nayab, P. S.; Pulaganti, M.; Chitta, S. K.; Abid, M.; Uddin, R., Evaluation of DNA Binding, Radicals Scavenging and Antimicrobial Studies of Newly Synthesized N-Substituted Naphthalimides: Spectroscopic and Molecular Docking Investigations. *J Fluoresc* **2015,** *25* (6), 1905-20.

32. Kang, J.; Tangadanchu, V. K. R.; Gopala, L.; Gao, W.-W.; Cheng, Y.; Liu, H.-B.; Geng, R.-X.; Li, S.; Zhou, C.-H., Novel potentially antibacterial naphthalimide-derived metronidazoles: Design, synthesis, biological evaluation and supramolecular interactions with DNA, human serum albumin and topoisomerase II. *Chinese Chemical Letters* **2017,** *28* (7), 1369-1374.

33. Geraghty, C.; Wynne, C.; Elmes, R. B. P., 1,8-Naphthalimide based fluorescent sensors for enzymes. *Coordination Chemistry Reviews* **2021,** *437*, 213713.

34. Chinapang, P.; Ruangpornvisuti, V.; Sukwattanasinitt, M.; Rashatasakhon, P., Ferrocenyl derivative of 1,8-naphthalimide as a new turn-on fluorescent sensor for Au(III) ion. *Dyes and Pigments* **2015,** *112*, 236-238.

35. Georgiev, N. I.; Dimitrova, M. D.; Mavrova, A. T.; Bojinov, V. B., Synthesis, fluorescence-sensing and molecular logic of two water-soluble 1,8-naphthalimides. *Spectrochim Acta A Mol Biomol Spectrosc* **2017,** *183*, 7-16.

36. Xie, Z.; Zhou, Y.; Fu, M.; Ni, L.; Tong, Y.; Yu, Y.; Li, N.; Yang, Z.; Zhu, Q.; Wang, J., A 1,8-naphthalimide-based lysosome-targeting dual-analyte fluorescent probe for the detection of pH and palladium in biological samples. *Talanta* **2021,** *231*, 122365.

37. Bag, S. S.; Pradhan, M. K.; Kundu, R.; Jana, S., Highly solvatochromic fluorescent naphthalimides: Design, synthesis, photophysical properties and fluorescence switch-on sensing of ct-DNA. *Bioorganic & Medicinal Chemistry Letters* **2013,** *23* (1), 96-101.

38. Tikum, A. F.; Lim, W.; Fortibui, M. M.; Lee, S.; Park, S.; Kim, J., Palladium Probe Consisting of Naphthalimide and Ethylenediamine for Selective Turn-On Sensing of CO and Cell Imaging. *Inorganic Chemistry* **2021,** *60* (10), 7108-7114.

39. Wang, Z.; Tian, H.; Chen, K., Synthesis of novel dyes containing ferrocene. *Dyes and Pigments* **2001,** *51* (2), 161-165.

40. Zhang, J.; Cui, H.; Wei, G.; Cheng, L.; Lin, Y.; Ma, G.; Hong, N.; Liao, F.; Fan, H., A double signal amplification electrochemical MicroRNA biosensor based on catalytic hairpin assembly and bisferrocene label. *Journal of Electroanalytical Chemistry* **2020,** *858*, 113816.

41. Gan, J.; Tian, H.; Wang, Z.; Chen, K.; Hill, J.; Lane, P. A.; Rahn, M. D.; Fox, A. M.; Bradley, D. D. C., Synthesis and luminescence properties of novel ferrocene–naphthalimides dyads. *Journal of Organometallic Chemistry* **2002,** *645* (1), 168-175.

42. Gaiji, H.; Jolly, P.; Ustuner, S.; Goggins, S.; Abderrabba, M.; Frost, C. G.; Estrela, P., A Peptide Nucleic Acid (PNA)-DNA Ferrocenyl Intercalator for Electrochemical Sensing. *Electroanalysis* **2017,** *29* (3), 917-922.

43. Takenaka, S.; Yamashita, K.; Takagi, M.; Uto, Y.; Kondo, H., DNA Sensing on a DNA Probe-Modified Electrode Using Ferrocenylnaphthalene Diimide as the Electrochemically Active Ligand. *Analytical Chemistry* **2000,** *72* (6), 1334-1341.

44. Trott, O.; Olson, A. J., AutoDock Vina: improving the speed and accuracy of docking with a new scoring function, efficient optimization, and multithreading. *J Comput Chem* **2010,** *31* (2), 455-461.

45. Jones, J. E.; Amoroso, A. J.; Dorin, I. M.; Parigi, G.; Ward, B. D.; Buurma, N. J.; Pope, S. J. A., Bimodal, dimetallic lanthanide complexes that bind to DNA: the nature of binding and its influence on water relaxivity. *Chemical communications (Cambridge, England)* **2011,** *47* (12), 3374-3376.

46. names, *Manuscript in preparation*.

47. Yang, Z.; d'Auriac, M. A.; Goggins, S.; Kasprzyk-Hordern, B.; Thomas, K. V.; Frost, C. G.; Estrela, P., A Novel DNA Biosensor Using a Ferrocenyl Intercalator Applied to the Potential Detection of Human Population Biomarkers in Wastewater. *Environmental Science & Technology* **2015,** *49* (9), 5609-5617.

48. Luo, Y.-L.; Baathulaa, K.; Kannekanti, V. K.; Zhou, C.-H.; Cai, G.-X., Novel benzimidazole derived naphthalimide triazoles: synthesis, antimicrobial activity and interactions with calf thymus DNA. *Science China Chemistry* **2015,** *58* (3), 483-494.

49. Kucheryavy, P.; Li, G.; Vyas, S.; Hadad, C.; Glusac, K. D., Electronic properties of 4-substituted naphthalimides. *J Phys Chem A* **2009,** *113* (23), 6453-61.

50. Hahn, L.; Buurma, N. J.; Gade, L. H., A Water-Soluble Tetraazaperopyrene Dye as Strong G-Quadruplex DNA Binder. *Chemistry – A European Journal* **2016,** *22* (18), 6314-6322.

51. Vatsadze, S. Z.; Shulga, D. A.; Loginova, Y. D.; Vatsadze, I. A.; Wang, L.; Yu, H.; Kudryavtsev, K. V., Computer modeling of ferrocene-substituted 3,7-diazabicyclo[3.3.1]nonanes as serine protease inhibitors. *Mendeleev Communications* **2016,** *26* (3), 212-213.

Chapter 3 Synthesis of bis-naphthalimides as DNA- intercalators

Abstract

A series of bisnaphthalimide derivatives has been synthesized where two naphthalimide units were connected via several different linkers, including aliphatic, aromatic, and ether-containing linkers. Several solubilizing groups, viz. 1°-amine, 2°-amine and thiol groups, were introduced to both C4 positions in the resulting bisnaphthalimide scaffolds. The solubility for these compounds has been tested in MOPS buffer with solubilities typically in the range of 10^{-6} M^{-1} ~10^{-5} M^{-1} except in case of using thioglycolic acid as a solubilizing group where the solubility is higher and in the range of ~10^{-4} M. DNA-binding affinities were investigated using UV-visible titrations. According to the DNA-binding affinities, most tested bisnaphthalimide such as **3.9e** and **3.12d** can be considered good DNA binders with binding affinities of 6.13×10^{4} and 1.24×10^{4} M^{-1}, respectively. On the other hand, compound **3.10b** is the most promising compound among this series as it binds relatively strongly with DNA with binding affinity of 3.95×10^{5} M^{-1}. Unsurprisingly, bisnaphthalimides connected with thioglycolic acid do not bind with DNA due to the negatively charged carboxylates when the carboxylic acids get deprotonated in solution and electrostatically prevent bisnaphthalimide from binding with negatively charged DNA.

3.1 Introduction

3.1.1 Bisnaphthalimides as bis intercalators

The naphthalimide-based DNA binders in Chapter 2 are relatively weak binders. One of the approaches that has been proposed to develop naphthalimide derivatives with enhanced DNA-binding properties is connecting two units of naphthalimide via linkers.[1, 2] For example, bisnaphthalimides have been found to have higher antitumor activity and present higher DNA-binding affinities compared to the corresponding monomers.[1, 3-5] Several bisnaphthalimides have been reported as bis-intercalators.[4, 6-8]

3.1.2 Bisnaphthalimide derivatives in medicinal chemistry

Developing bisnaphthalimide dervatives has received considerable attention from resarchers who have an interest in the development of anticancer drugs.[9-11] Several bisnaphthalimides have been synthesized and their binding affinities for DNA have been studied. Compounds such as bisnafide (DMP-840, **3.1**) show interesting binding properties since it intercalates with high affinity with DNA in a sequence-specific manner (targeting G-C-rich regions) which has been reported to lead to single-strand DNA breaks,[12, 13] presumably through a reaction involving the intercalated compound. The compound was examined for treatment of human colorectal, lung, prostate, and breast cancers.[9-11] Elinafide (Lu-79553, **3.2**) is another example of a bisnaphthalimide that has been studied against a panel of human and murine cell lines.[14] Both compounds (Scheme 3.1) have reached clinical trials for solid tumor treatment. However, most clinical trials were unsuccessful because of a poor therapeutic index, poor water-solubility, or dose-limiting bone marrow toxicity. [15]

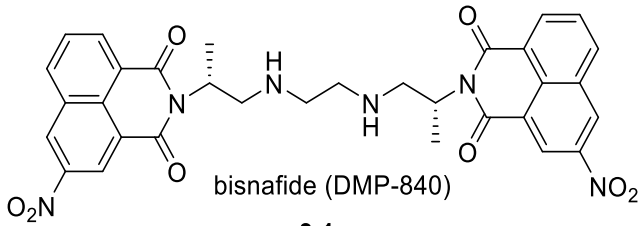

3.1

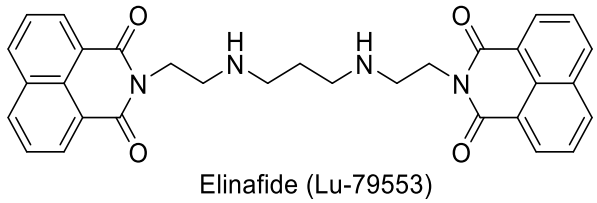

3.2

Scheme 3.1

Thus, significant efforts have been made to modify the naphthalimide skeleton to improve the therapeutic properties of bisnaphthalimides.[4, 16, 17]

Ippolito Antonini *et al*.[8] have synthesized a series of bisnaphthalimide derivatives (Scheme 3.2). Two naphthalimide units were connected using a N^1-(3-aminopropyl)-N^1-methylpropane-1,3-diamine linker to construct the bisnaphthalimide and subsequently two primary amines have been introduced through an S_NAr reaction to produce two final compounds **(3.3a-b)**.

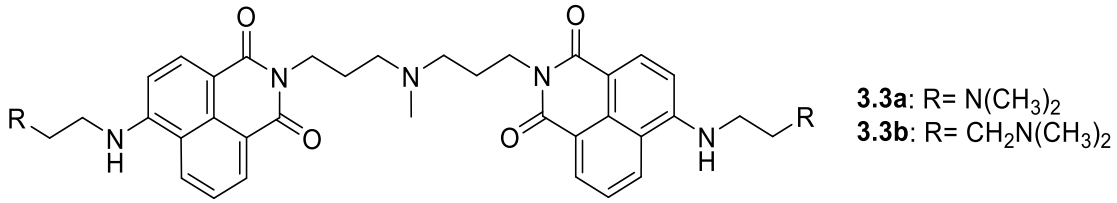

Scheme 3.2

According to this study, 'apparent'[1] binding constants (K_{app}) for **3.3a-b** equal 2.3×10^8 M^{-1} and 1.1×10^8 M^{-1}, respectively, which indicate that these compounds are promising leads in the field of anticancer drug discovery.

Rui-Xue Rong *et al*.[15] have synthesized a series of bisnaphthalimide derivatives were two naphthalimide units were connected via the same N^1-(3-aminopropyl)-N^1-methylpropane-1,3-diamine linker as used by Ippolito Antonini (Scheme 3.3). The cytotoxic activity of compounds **3.4a-f** was investigated against Hela, MCF-7, SGC-7901 and A549 cells. According to their findings, **3.4a** exhibits better activity against the tested cell lines compared to the control drug (amonafide). Therefore, the binding properties for this compound with calf thymus DNA (ct-DNA) were studied by UV–visible, fluorescence and circular dichroism spectroscopies and thermal denaturation experiments. The study shows that **3.4a** interacts with (ct-DNA) with a binding constant of $1.2\times 10^5\ M^{-1}$.

[1] The affinity constants have been reported as apparent affinity constants, but it is not clear why these are considered "apparent".

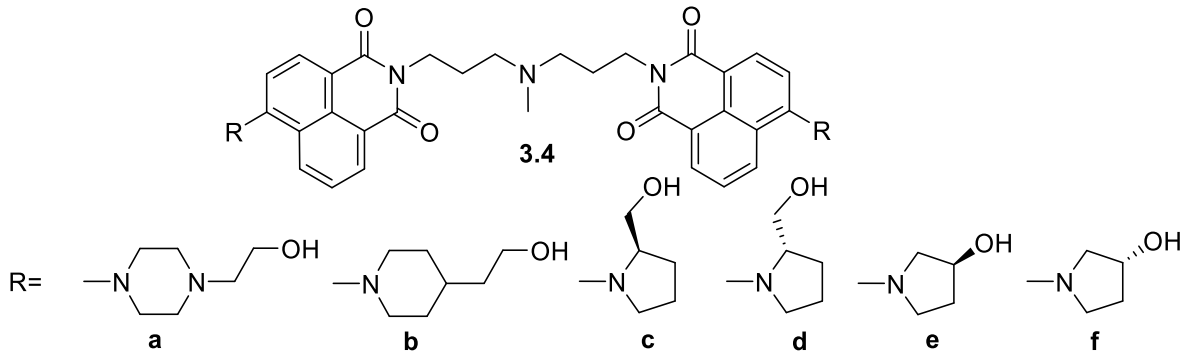

Scheme 3.3

Yu Huang *et al.*[18] have synthesized bisnaphthalimide derivatives **3.5a-e** were the length, and the nature of the linker is changed (Scheme 3.4). The DNA-binding affinities were determined using UV–vis titration using ct-DNA.

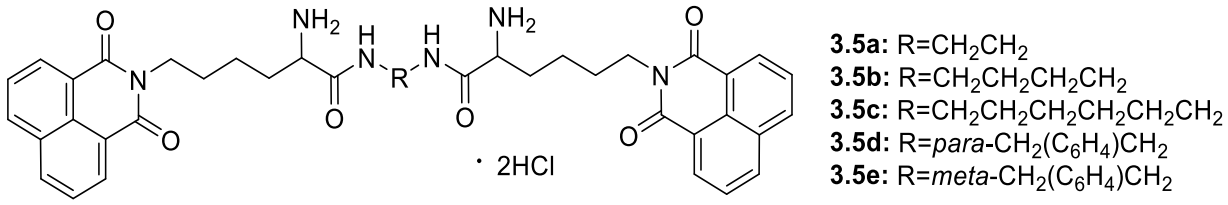

Scheme 3.4

According to their findings, compounds with short linkers bind more strongly with ct-DNA ($K_{binding}$= 3.40 × 10^4 M^{-1}) compared to the other linkers, with the compounds with rigid linkers (**3.5d,e**) being the weaker binders in this series.

3.1.3 bisnaphthalimides as fluorescent probes and sensitisers

As mentioned in Chapter 2, 3- and 4-substituted naphthalimide derivatives exhibit interesting photochemical and spectroscopic properties.[6] Naphthalimide is a chromophore with strong absorption and good fluorescence yields.[19] Hence, naphthalimide derivatives play a significant role as a fluorescent probes to detect different species in several areas.[20-23]

For example, Jean-MarcChovelon *et al.*[20] have synthesized bisnaphthalimide derivative **3.6** (Scheme 3.5) and its photophysical properties were investigated in organic solvents with different polarity (chloroform, acetonitrile).

The quantum yield for this compound is sensitive to interactions with solvents and metal ions. For example, the quantum yield is much lower in acetonitrile compared to chloroform. The formation of complexes for this compound with a series cation (Zn^{2+}, Ni^{2+}, Ce^{3+}, Co^{2+}, Cu^{2+} and Ag^{+}) and protons has been studied and the fluorescence enhancement factor on the quantum yield have been calculated in acetonitrile. The fluorescence enhancement factors for these complexes increases as following Zn^{2+}>Ni^{2+}>Ce^{3+}>Cu^{2+}>Co^{2+}>Ag^{+}. Therefore, this compound could be used as a fluorescence sensor which can be used to detect these cations in the environment.

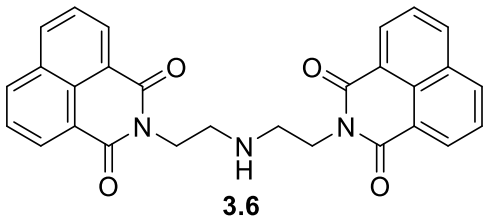

3.6

Scheme 3.5

Stanislava Yordanova *et al*.[21] have synthesized bisnaphthalimide derivative **3.7** using the same linker that has been used in Jean-MarcChovelon's study with a substitution in C4 of the naphthalimide scaffold (Scheme 3.6). The photophysical properties for this compound were studied for the purpose of detecting protons and several metal cations (Ag^{+}, Cu^{2+}, Co^{2+}, Ni^{2+}, Fe^{3+} and Zn^{2+}) using fluorescence spectroscopy.

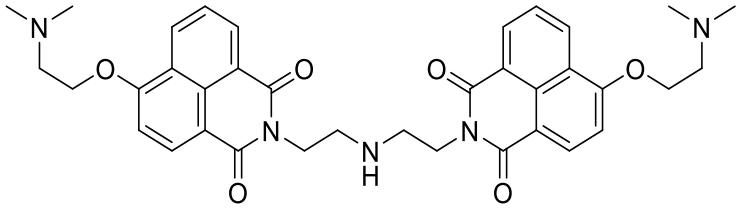

3.7

Scheme 3.6

The formation of metal complexes has been studied and the relative affinity between **3.7** and metal cations increases as following (highest affinity) Zn^{2+}>Ni^{2+}>Cu^{2+}> Co^{2+}>Fe^{3+}>Ag^{+} (lowest affinity). The result implies that this compound can be suitable for detection of metal cations and protons based on the quenching of photoinduced electron transfer processes.

3.1.4 Aims

Based on previous studies that reported that bisintercalators have improved binding affinities for DNA, this chapter aims to synthesise several bisnaphthalimides using different linkers. The synthesis also involves introducing several solubilizing groups on the C-4 position of the naphthalimide core (Scheme 3.7) which improve the solubility and affect the spectroscopic properties of the naphthalimide chromophore. The second aim of this chapter is to explore the aqueous solubilities and DNA-binding properties for these bisnaphthalimides.

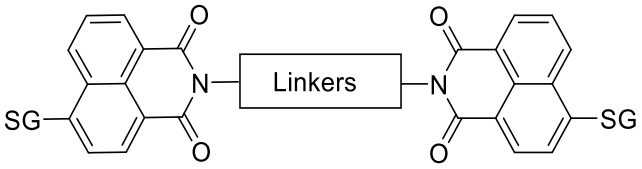

Scheme 3.7

3.2 Result and discussion

3.2.1 Design and docking study for proposed bisnaphthalimide derivatives.

A series of bisnaphthalimide derivatives with two variable factors that could affect the binding, viz. the linkers and the solubilizing groups (Scheme 3.8), was proposed.

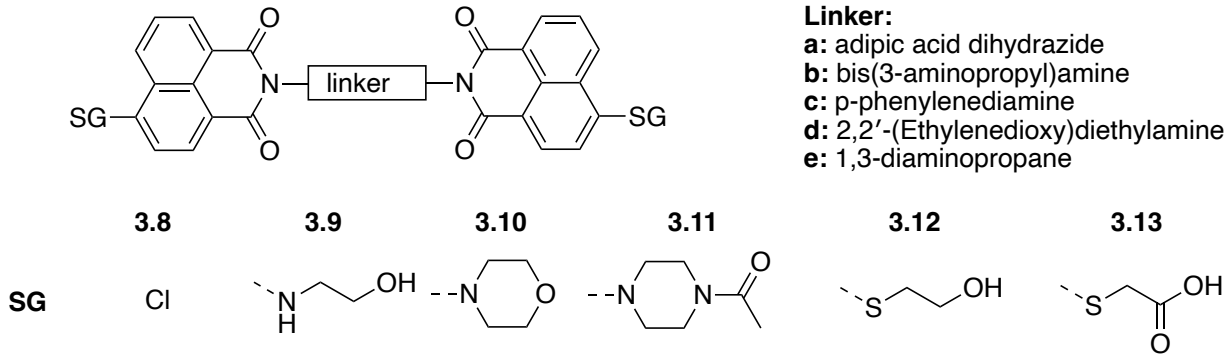

Scheme 3.8 The proposed bisnaphthalimide derivatives

An exploratory docking study for the 4-chloro substituted intermediates *en route* to the proposed dimers was carried out using AutoDock Vina [24] against a duplex DNA structure with a pre-formed intercalation gap[25]. The top 10 binding modes were ranked by the binding affinity. For each compound, the three best binding modes are presented in Figure 3.1.

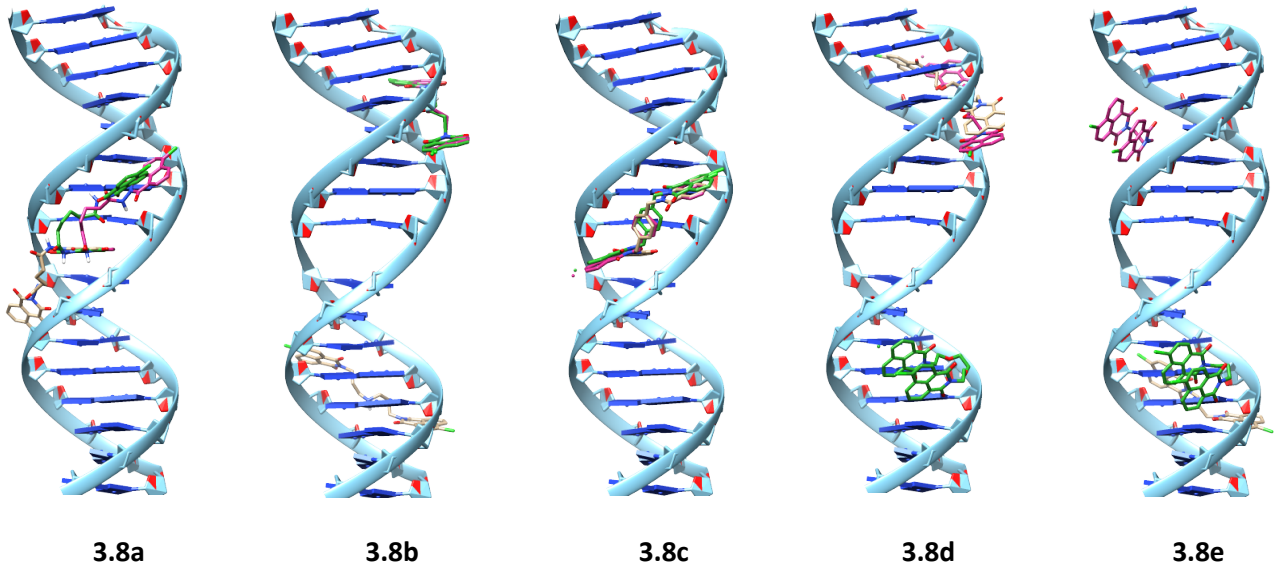

Figure 3.1 top 3 binding mode for peoposed compounds 3.8a-e with open d(ATCGAGACGTCTCGAT)$_2$.

The docking study shows that **3.8a** and **3.8c** are more likely to intercalate with DNA compared to the other dimers. Table 3.1 summarises the binding affinities for the top three binding modes of **3.8a-e**

Table 3.1 The DNA-binding affinities for the top three binding modes of compounds 3.8a-e according to AutoDock Vina

		3.8a	3.8b	3.8c	3.8d	3.8e
The binding affinity (kcal/mol)[b]	1st binding mode[a]	-11.2 (I)	-10.5 (GB)	-11.4 (I)	-10.2 (GB)	-10.6 (GB)
	2nd binding mode	-11.1 (I)	-10.4 (GB)	-10.5 (GB)	-10.2 (GB)	-10.5 (GB)
	3rd binding mode	-11.1 (I)	-10.3 (GB)	-10.5 (GB)	-10.2 (GB)	-10.4 (GB)

(I): intercalator, (GB): groove binder

a) The ranking of the binding modes is as produced by Vina

b) Binding affinities are only reported to 0.1 kcal mol^{-1} by Vina.

To explore this class of compounds further and improve the aqueous solubility, several nucleophilic groups were proposed to substitute the chlorine atom. As an example of primary amines, ethanol amine was proposed as a solubilizing group. The top three binding modes for the dimers carrying an ethanolamine solubilizing group are presented in Figure 3.2.

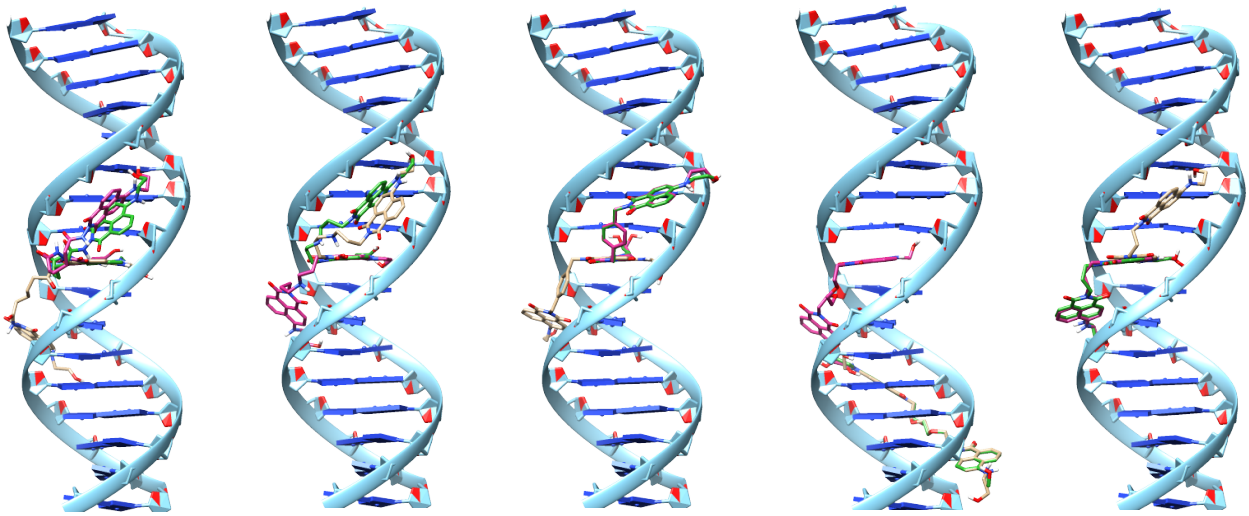

3.9a **3.9b** **3.9c** **3.9d** **3.e**

Figure 3.2 The top three binding modes of compounds 3.9a-e using AutoDock Vina

The docking study shows improvement on the possibility of intercalation in comparison with the parent compound. Table 3.2 illustrates the binding affinity for the top three binding modes of **3.9a-e** according to AutoDock Vina.

Table 3.2 The DNA-binding affinity for the top three binding mode of compounds (3.9a-e) according to AutoDock Vina

		3.9a	3.9b	3.9c	3.9d	3.9e
The binding affinity (kcal/mol)[b]	1st binding mode[a]	-10.5 (I)	-9.5 (I)	-10.0 (I)	-9.8 (GB)	-10.4 (I)
	2nd binding mode	-10.4 (I)	-9.5 (I)	-9.8 (I)	-9.7 (I)	-10.1 (I)
	3rd binding mode	-10.3 (I)	-9.3 (I)	-9.8 (I)	-9.7 (GB)	-10.0 (I)

(I): intercalator, (GB): groove binder

a) The ranking of the binding modes is as produced by Vina

b) Binding affinities are only reported to 0.1 kcal mol^{-1} by Vina.

In addition to a primary amine, cyclic secondary amines such as morpholine and 1-acetyl piperazine were proposed as a solubilizing group. Docking studies were again carried out for the proposed compounds **3.10a-e**. The top binding modes for the morpholine-based compounds are presented in Figure 3.3.

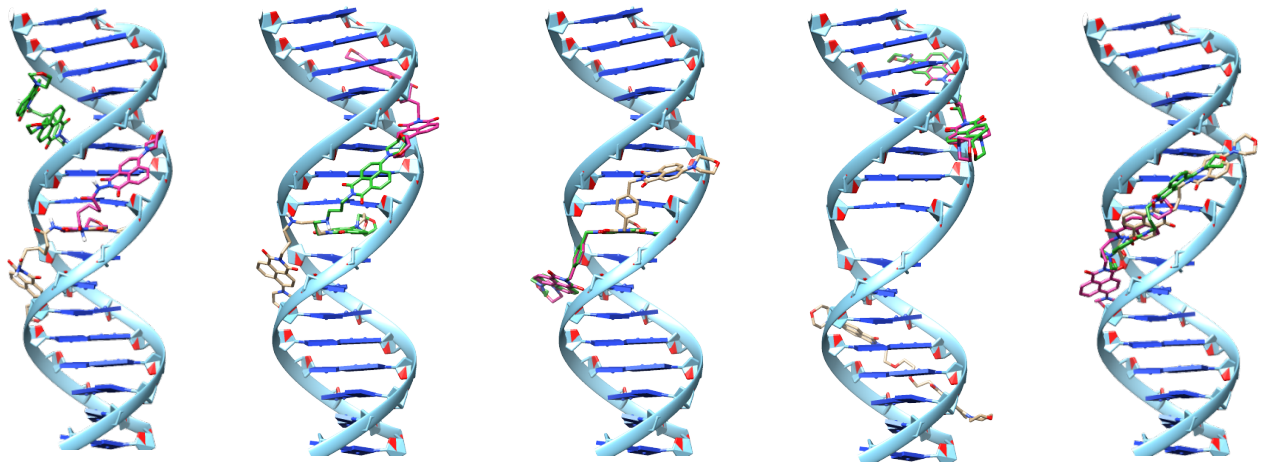

3.10a **3.10b** **3.10c** **3.10d** **3.10e**

Figure 3.3 The top three binding modes of compounds 3.10a-e using AutoDock Vina

Table 3.3 illustrates the binding affinity for the top three binding modes of **3.10a-e** using AutoDock Vina.

Table 3.3 The DNA-binding affinity for the top three binding modes of compounds 3.10a-e using AutoDock Vina

		3.10a	3.10b	3.10c	3.10d	3.10e
The binding affinity (kcal/mol)[b]	1st binding mode[a]	-12.5 (I)	-11.2 (I)	-11.8 (I)	-11.2 (GB)	-11.2 (GB)
	2nd binding mode	-12.4 (I)	-11.2 (GB)	-11.8 (I)	-11.0 (GB)	-11.2 (GB)
	3rd binding mode	-12.1 (GB)	-11.1 (I)	-11.7 (I)	-10.9 (GB)	-11.2 (GB)

(I): intercalator, (GB): groove binder

a) The ranking of the binding modes is as produced by Vina

b) Binding affinities are only reported to 0.1 kcal mol^{-1} by Vina.

Comparison of Tables 3.2 and 3.3 shows that more of the compounds are now predicted to act as groove binders. We attribute this finding to steric hindrance resulting from the sterically more demanding cyclic secondary amines making intercalation less favourable.

Secondary amine 1-acetyl piperazine was also proposed as a solubilizing group. Docking studies were carried out for these proposed compounds **3.11a-e** too. The top binding modes are presented in Figure 3.4.

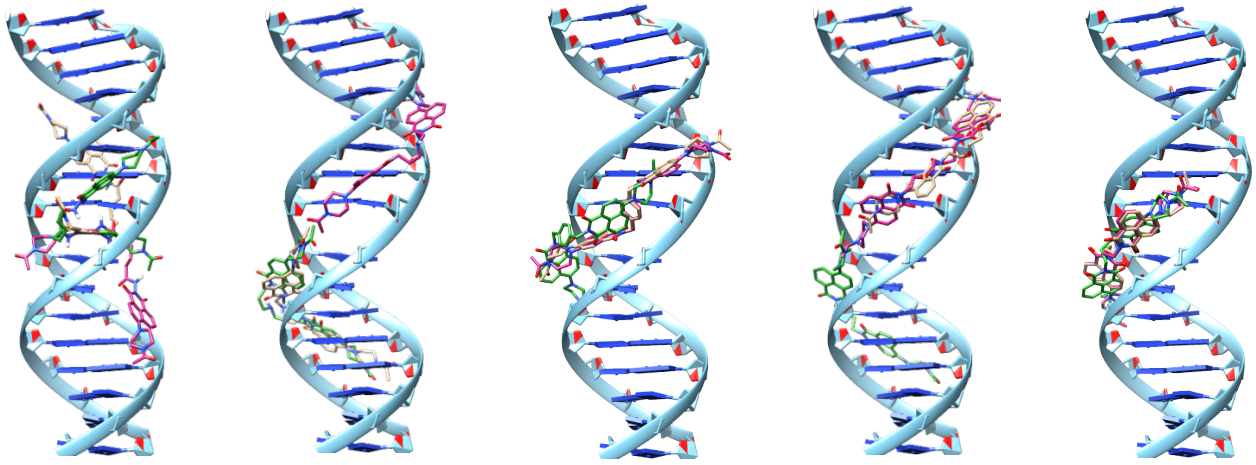

3.11a **3.11b** **3.11c** **3.11d** **3.11e**

Figure 3.4 The top three binding modes of compounds 3.11a-e using AutoDock Vina

Table 3.4 illustrates the binding affinities for the top three binding modes of compounds **3.11a-e** according to AutoDock Vina.

Table 3.4 The DNA-binding affinity for the top three binding modes of compounds 3.11a-e using AutoDock Vina

		3.11a	3.11b	3.11c	3.11d	3.11e
The binding affinity (kcal/mol)[b]	1st binding mode[a]	-13.6 (I)	-11.4 (GB)	-12.3 (GB)	-11.3 (GB)	-12.0 (GB)
	2nd binding mode	-13.5 (I)	-11.4 (GB)	-12.3 (GB)	-11.3 (GB)	-11.8 (GB)
	3rd binding mode	-13.2 (I)	-11.4 (GB)	-12.1 (GB)	-11.3 (GB)	-11.7 (GB)

(I): intercalator, (GB): groove binder

a) The ranking of the binding modes is as produced by Vina

b) Binding affinities are only reported to 0.1 kcal mol^{-1} by Vina.

Table 3.4 shows that now the majority of these compounds is predicted to bind in the minor groove. This observation suggests that N-acetyl piperazine affects the intercalative binding mode even more than morpholine.

In addition to primary and secondary amines, introducing solubilizing groups via different atom such as sulfur was proposed. 2-Mercaptoethanol was suggested **(3.12a-e)** as a SG and the docking study was carried out. The top binding modes are presented in Figure 3.5.

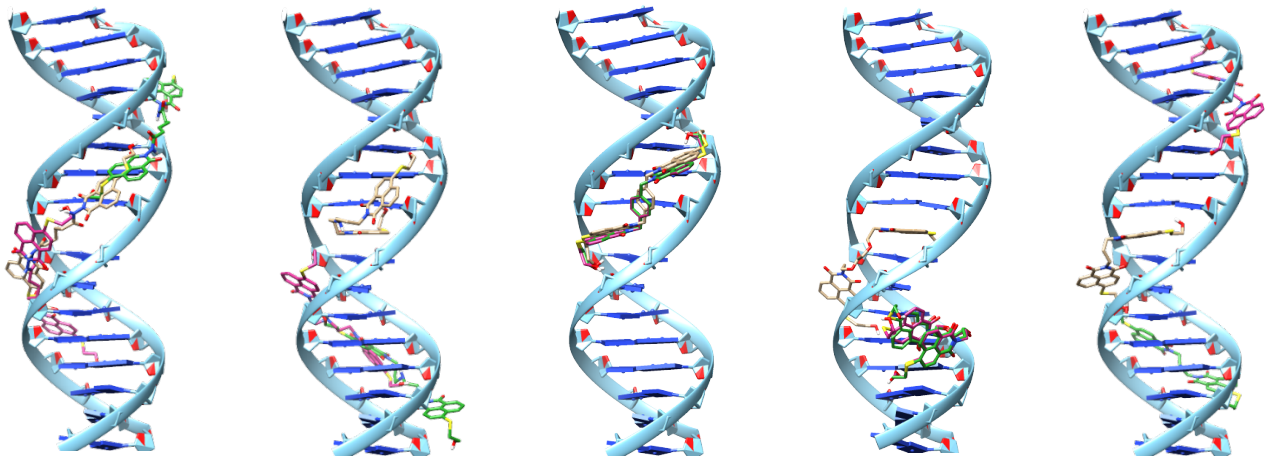

3.12a **3.12b** **3.12c** **3.12d** **3.12e**

Figure 3.5 The top three binding modes of compounds 3.12a-e using AutoDock Vina

Table 3.5 illustrates the binding affinities for the top three binding modes of **3.12a-e** according to AutoDock Vina.

Table 3.5 The DNA-binding affinities for the top three binding modes of 3.12a-e according to AutoDock Vina

		3.12a	**3.12b**	**3.12c**	**3.12d**	**3.12e**
The binding affinity (kcal/mol)[b]	1st binding mode[a]	-9.7 (GB)	-9.3 (I)	-9.9 (GB)	-9.5 (I)	-9.7 (I)
	2nd binding mode	-9.6 (GB)	-9.1 (GB)	-9.7 (GB)	-8.9 (GB)	-9.6 (GB)
	3rd binding mode	-9.6 (GB)	-9.0 (GB)	-9.6 (GB)	-8.8 (GB)	-9.6 (GB)

(I): intercalator, (GB): groove binder

a) The ranking of the binding modes is as produced by Vina

b) Binding affinities are only reported to 0.1 kcal mol^{-1} by Vina.

2-Mercaptoethanol and ethanol amine are structurally similar, however, docking results show that the possibility of the dimers to intercalate is better in case of using ethanol amine as solubilising group.

Thioglycolic acid was also proposed as a solubilizing group and docking studies were carried out for these proposed compounds **(3.13a-e)** too. The top binding modes are presented in Figure 3.6.

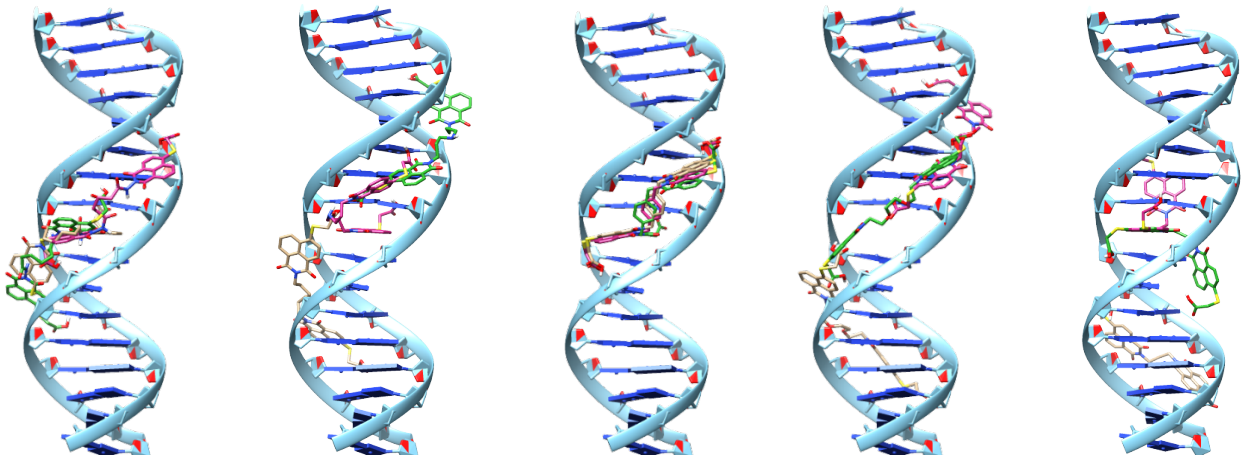

3.13a **3.13b** **3.13c** **3.13d** **3.13e**

Figure 3.6 The top three binding modes of compounds 3.13a-e according to AutoDock Vina

Table 3.6 illustrates the binding affinities for the top three binding modes of **3.13a-e** according to AutoDock Vina.

Table 3.6 The DNA-binding affinities for the top three binding modes of compounds 3.13a-e predicted using AutoDock Vina

		3.13a	**3.13b**	**3.13c**	**3.13d**	**3.13e**
The binding affinity (kcal/mol)[b]	1st binding mode[a]	-10.4 (I)	-9.4 (GB)	-10.3 (GB)	-9.7 (GB)	-9.6 (GB)
	2nd binding mode	-10.1 (GB)	-9.3 (I)	-9.9 (GB)	-9.7 (GB)	-9.6 (I)
	3rd binding mode	-10.0 (GB)	-9.3 (GB)	-9.9 (I)	-9.6 (GB)	-9.4 (I)

(I): intercalator, (GB): groove binder

a) The ranking of the binding modes is as produced by Vina

b) Binding affinities are only reported to 0.1 kcal mol^{-1} by Vina.

Overall, the docking studies suggest that all proposed compounds should bind to duplex DNA but that the binding mode may be sensitive to the substitution pattern on the naphthalimide moiety. Ethanolamine and morpholine appears to improve the ability of bisnaphthalimide to intercalate while 1-acetyl piperazine, 2-mercaptoethanol, and thioglycolic acid tend to bind as a groove binders. The difference in preference for binding more between, e.g., ethanolamine and 2-mercaptoethanol is surprising considering the relatively small difference in structure.

However, this finding should be considered in the context that docking results for many of the compounds explored here suggest relatively small binding energy differences between intercalation and groove binding so the predictions of the binding modes should not be considered conclusive.

The docking results for the proposed bisnaphthalimides in this chapter suggest that bisnaphthalimides have better DNA binding properties reflected by more negative binding affinities and more often bind as intercalators comparing to the ferrocene-naphthalimide conjugates in chapter 2. This observation is in agreement with the literature (See Chapter 1) that stated that bisnaphthalimides presented higher DNA-binding affinities compared to the corresponding monomers.[3-5]

3.2.2 Synthesis of bis-intercalator naphthalimides

The proposed synthetic scheme to the bis-naphthalimide derivatives involves two possible paths (Scheme 3.9). The first path starts with the dimerization step, using two equivalents of 4-chloro-1,8-naphthalic anhydride with one equivalent of each of the different terminal diamines as a linker, then introducing the solubilizing groups. The second path starts with introducing the solubilizing groups to the naphthalic anhydride unit and then carrying out the dimerization.

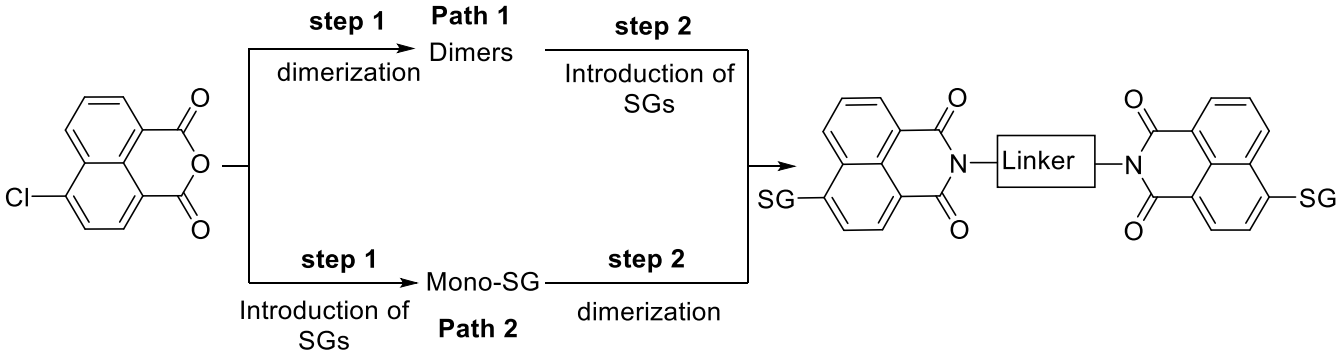

Scheme 3.9 The proposed synthetic scheme for all proposed bisnaphthalimides

Path 1, step 1: the dimerization of two units of naphthalimide

Linkers with different chain lengths and involving several functional groups (2°-amine and ether) were chosen. Varying linkers could affect binding affinities.

The dimerizations of the two naphthalimide units were carried out by refluxing 2.25 equivalents of 4-chloro-1,8-naphthalic anhydride with one equivalent of the chosen linkers in ethanol as a solvent (Scheme 3.10). A catalytic amount of triethylamine was added to the reaction mixture. To make sure that the naphthalimide reacts at both ends of the linkers, a slight excess of the anhydride was used, and the reaction mixture was refluxed for 24 h.

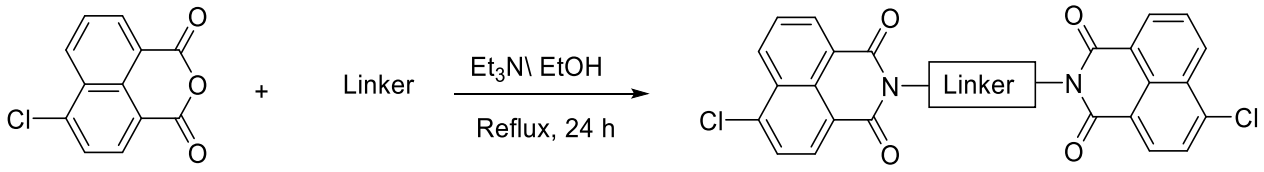

Linker

a adipic dihydrazide
b bis(3-aminopropyl)amine
c p-Phenylenediamine
d 2,2'-(ethylenedioxy)diethylamine
e 1,3-diamino propane

3.8a-e

Scheme 3.10 Dimerization of two units of naphthalic anhydride

Bisnaphthalimides **3.8a-e** were obtained with a good yield (70-90 %, Scheme 3.11) and characterized using IR, ^{1}H- and ^{13}C-NMR spectroscopy and mass spectrometry.

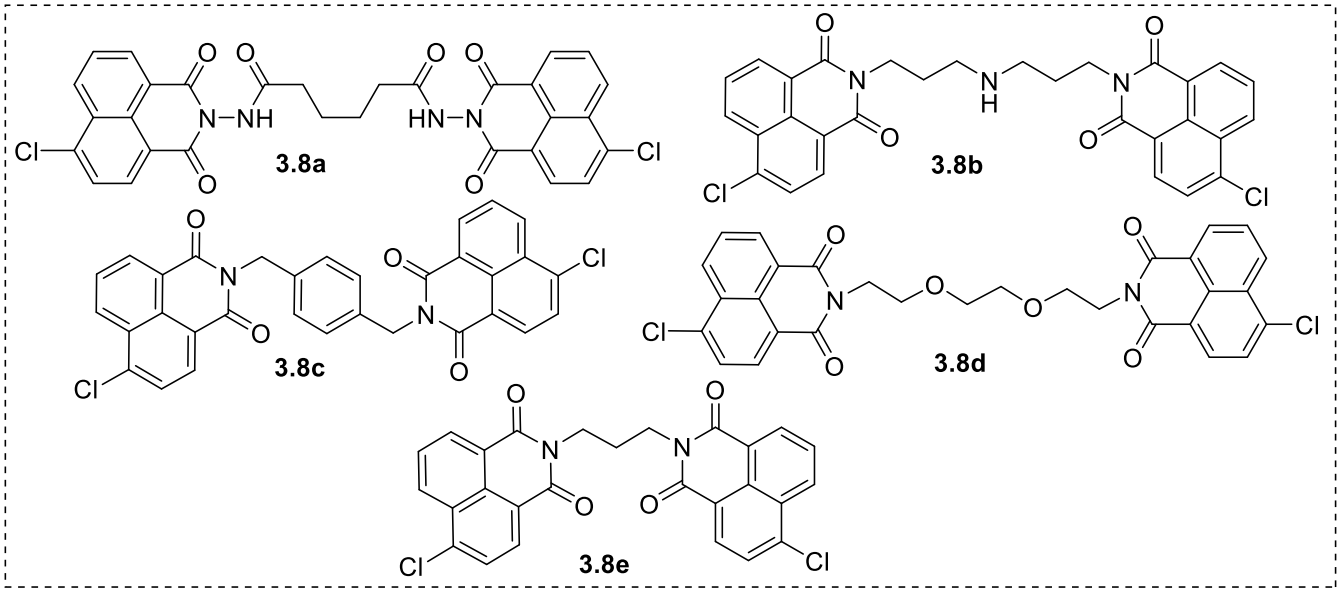

Scheme 3.11

All obtained dimers show five signature signals in ^{1}H-NMR spectroscopy with two proton integrations for each signal related to the naphthalimide moiety (Figure 3.7). These five signals comprise of three doublets of doublets signals and two doublet signals. The coupling constants of the two doublets of doublet between 8.45 and 8.65 ppm (H_a and H_b) are equal to $J_{ortho} \approx 8$ Hz and $J_{meta} \approx 1$ Hz which indicates that these signals are related to H5 and H7. The other doublets of doublet (H_d) is found between 7.65 and 8.00 pm with coupling constants $J_{ortho} \approx 8$ Hz and $J_{ortho} \approx 8$ Hz which indicates that this signal is related to H6. The last two doublets (H_c and H_e) present around 7.75-5.5 ppm, both with $J_{ortho} \approx 8$ Hz which indicates that these signals are related to H2 and H3. These signals correspond with the analogous signals found for monomeric naphthalimides as described in Chapter 2. Synthesized bisnaphthalimides also exhibit 12 signals in ^{13}C-NMR spectroscopy between 110 and 165 ppm. Seeing this pattern in ^{1}H- and ^{13}C-NMR spectroscopy for all synthesized bisnaphthalimides in this chapter is an easy way to make sure that the reaction has occurred. Since we synthesise symmetric bisnaphthalimide, these signals reflect the purity of the obtained products.

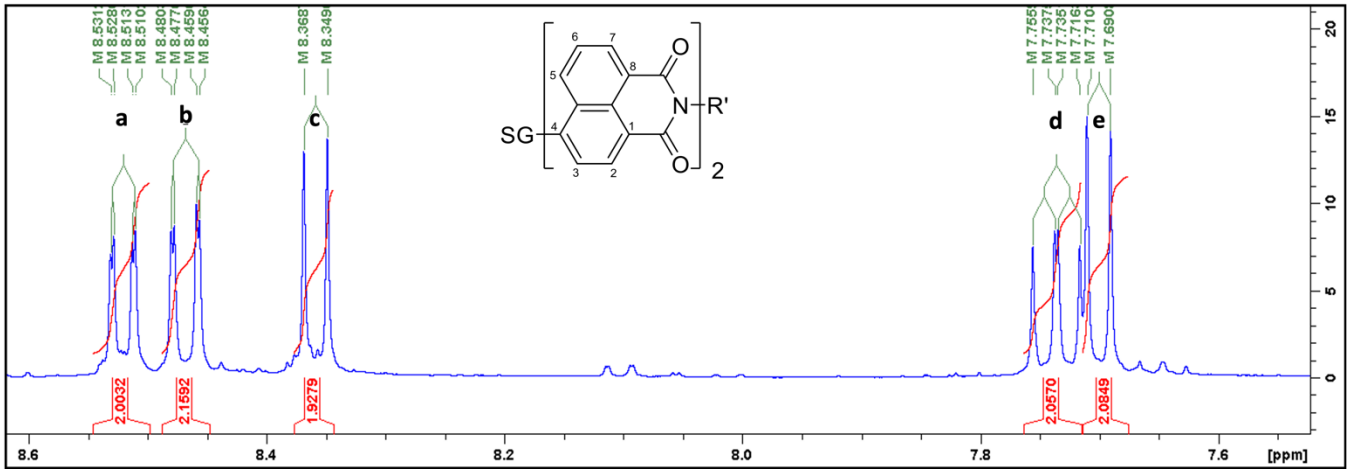

Figure 3.7. The ^{1}H-NMR spectrum for aromatic naphthalimide moiety

Path 1, step 2: Introduction of the solubilizing group

The obtained bisnaphthalimides **3.8a-e** are understandably only partially soluble in water due to their hydrophobic nature (See Section 3.2.3). To improve the solubility for this class of compound, the obtained bisnaphthalimides **3.8a-e** were subjected to S_NAr reactions. Several nucleophilic groups were used to substitute the chlorine atom at the C4-position.

introduction of solubilizing groups through S_NAr reactions with 1° amines

The obtained dimers **3.8a-e** were subjected to aromatic nucleophilic substitution reaction using ethanol amine. The chlorine atoms at both ends of the molecule are substituted by the amino group of the nucleophile. This reaction is enabled by the presence of the electron-withdrawing anhydride group in conjugation with the site of substitution. Generally, bisnaphthalimides **3.8a-e** were dissolved in 10 mL ethanol amine (excess of the nucleophile) and refluxed for 24 h under N_2 (Scheme 3.12).

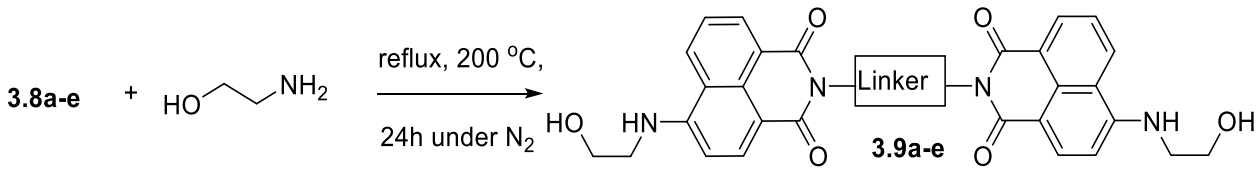

Scheme 3.12 Synthetic route of the dimers 3.9a-e

After the reaction was completed, DCM and water were added to extract the target compounds **3.9a-e** into the aqueous layer. The products were obtained in reasonable yields (Scheme 3.13) and characterized using ^{1}H- and ^{13}C-NMR spectroscopy and mass spectrometry.

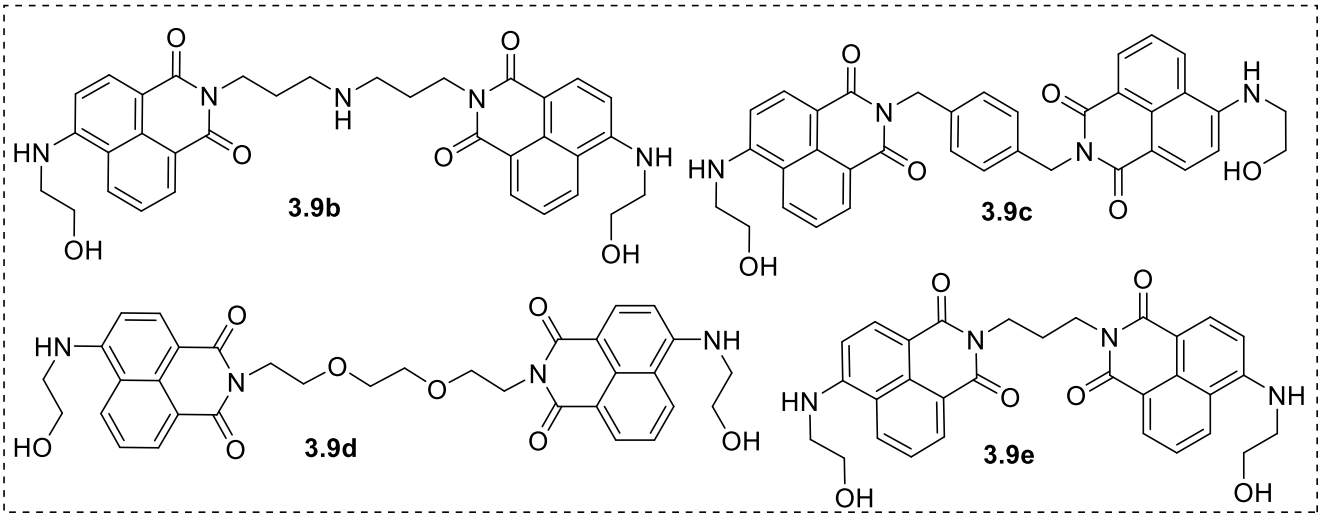

Scheme 3.13

Although **3.9b-e** in Scheme 3.13 were successfully synthesized, the stability of some of the linkers is not sufficient under the harsh S_NAr reaction conditions. The amino group in ethanol amine can attack the amide bond and break the linker in case of **3.9a**, leading to a monomeric naphthalimide as the only product (Scheme 3.14). The identity of this product was confirmed by comparison with intentionally synthesized **3.9**.

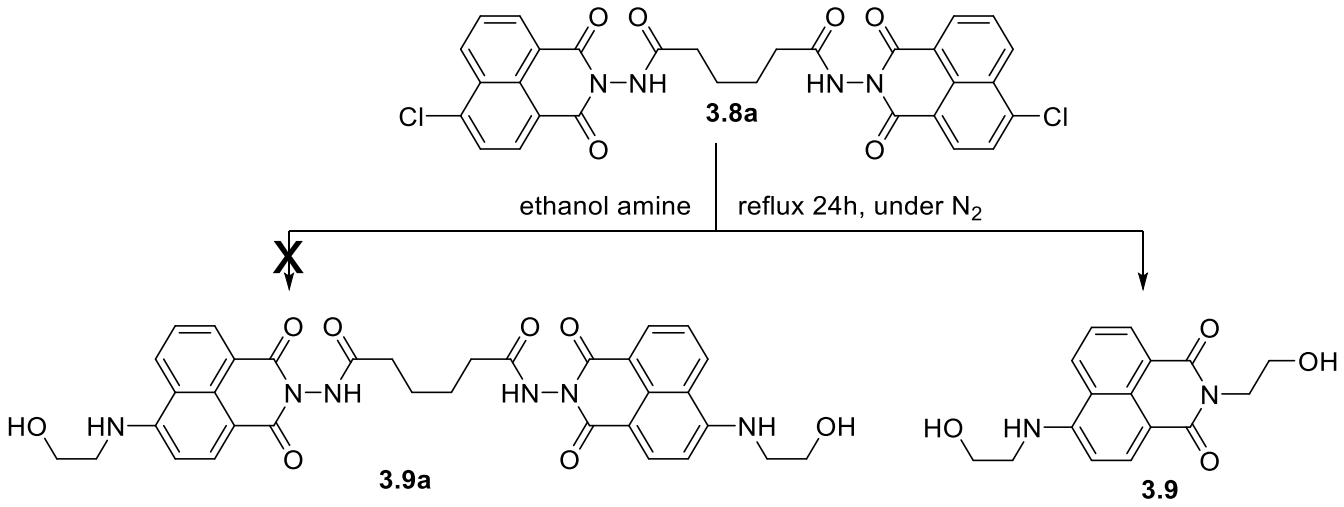

Scheme 3.14

The same reaction condition was successfully applied to the synthesis of **3.9d**. However, the final product was a mixture of both **3.9d** and **3.9**, which indicates that this dimer is not as stable as the other dimers (Scheme 3.15).

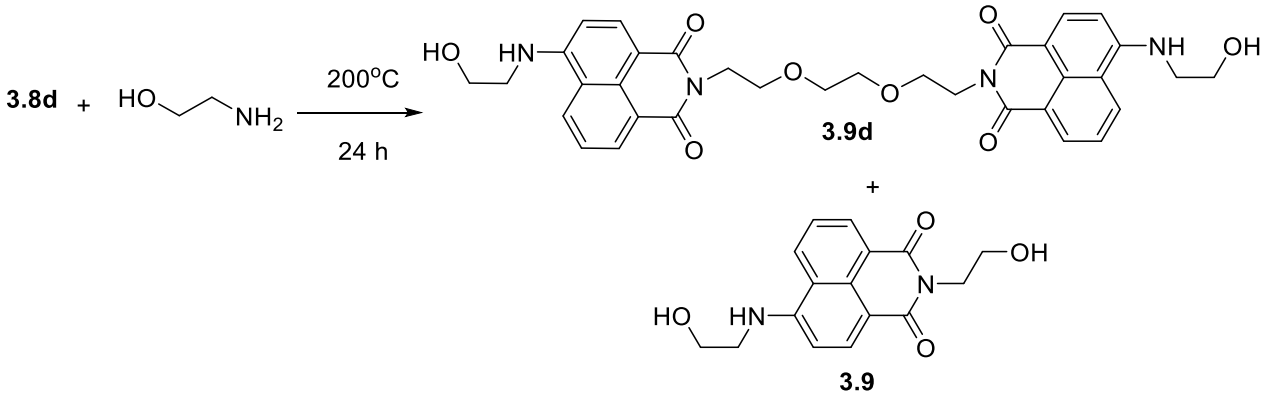

Scheme 3.15

Introduction of solubilizing groups through S_NAr reactions with 2° amines

To avoid any chance of linkers breaking, and to explore this class of compounds further, reaction with cyclic 2°-amine morpholine as a solubilizing group was attempted with the hypothesis that a 2°-amine would not affect the linkers because it cannot react to form an imide.

The reaction was carried out in DMF, using one equivalent of the bisnaphthalimides with ten equivalents (excess) of morpholine and heated at 100 °C for 24 h (Scheme 3.16). At the end of the reaction the solvent was removed, and methanol was added to allow the target compounds **3.10a-e** to precipitate. DMF (polar aprotic solvent) was chosen for this reaction since it does not hinder the attack of the amino group on carbon 4 of the naphthalimide. An excess of morpholine was used to minimize the opportunity for mono-substituted compounds to form.

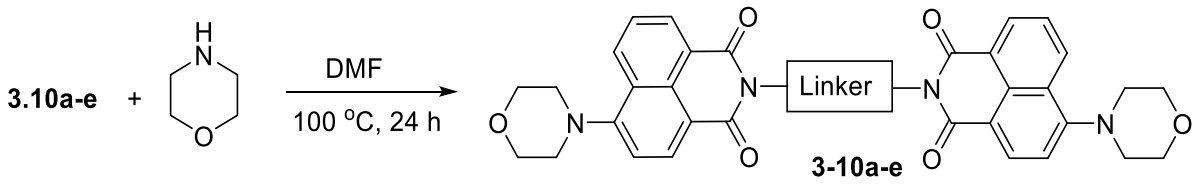

Scheme 3.16

This reaction condition was successfully applied to synthesise **3.10a,c-e** as pure yellow products with good yields (Scheme 3.17) and the resulting products were characterized using ^{1}H- and ^{13}C-NMR spectroscopy and mass spectrometry.

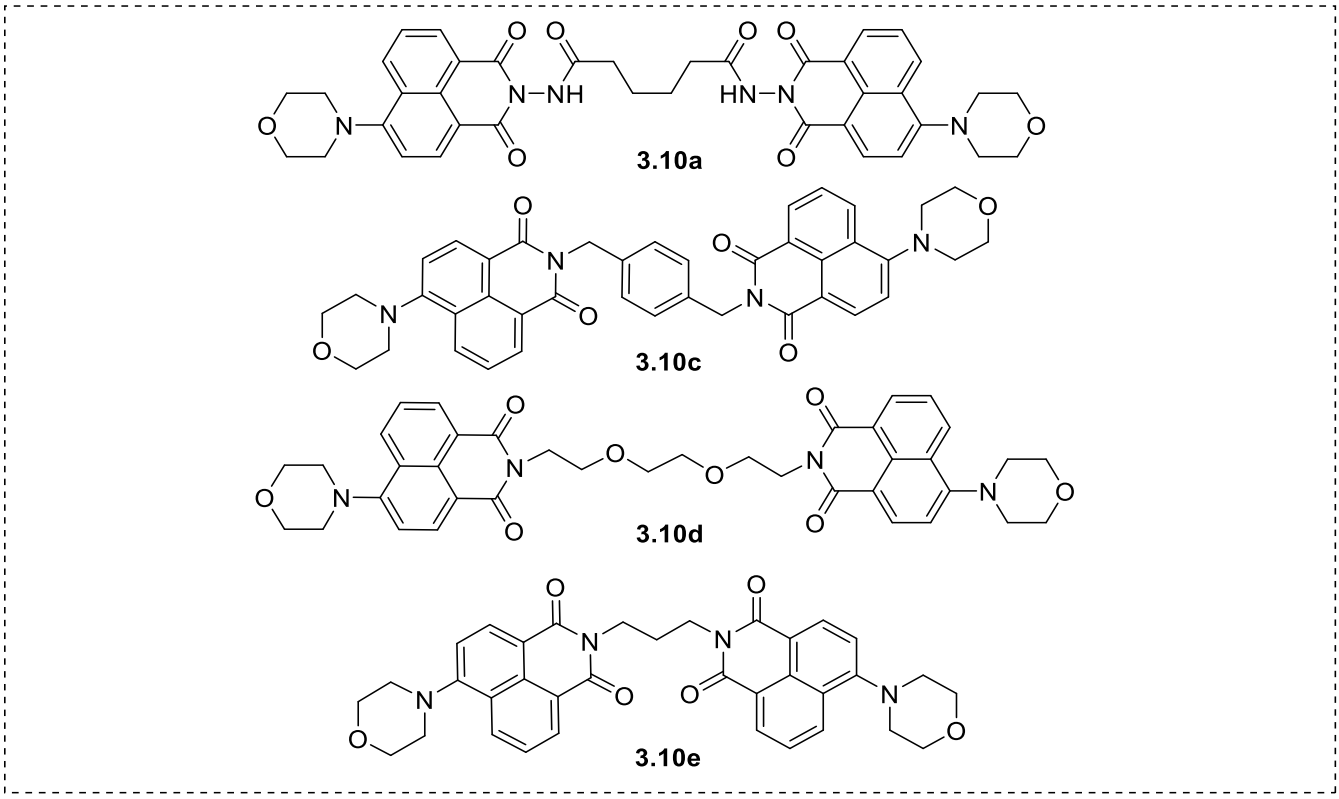

Scheme 3.17

Although the same reaction condition was applied to synthesise **3.10b**, the obtained crude product was a very sticky oil that did not precipitate as a yellow powder as we expected. Several solvents such as methanol, ethanol, ether, and water in ice-bath were used and failed to precipitate this compound. We therefore considered the second path, where the solubilizing group (morpholine) was introduced first to 4-chloro-1,8-naphthalic anhydride then the obtained monomer was used to synthesise **3.10b** (See below).

In addition to morpholine, 1-acetyl piperazine was used as a 2°-amine solubilizing group. The reaction was carried out in DMF using one equivalent of the bisnaphthalimides with ten equivalents of 1-acetyl piperazine and heated to 100 °C for 72 h (Scheme 3.18). At the end of the reaction the solvent was removed, and water was added instead of methanol to precipitate the target compounds **3.11d,e** (Scheme 3.18).

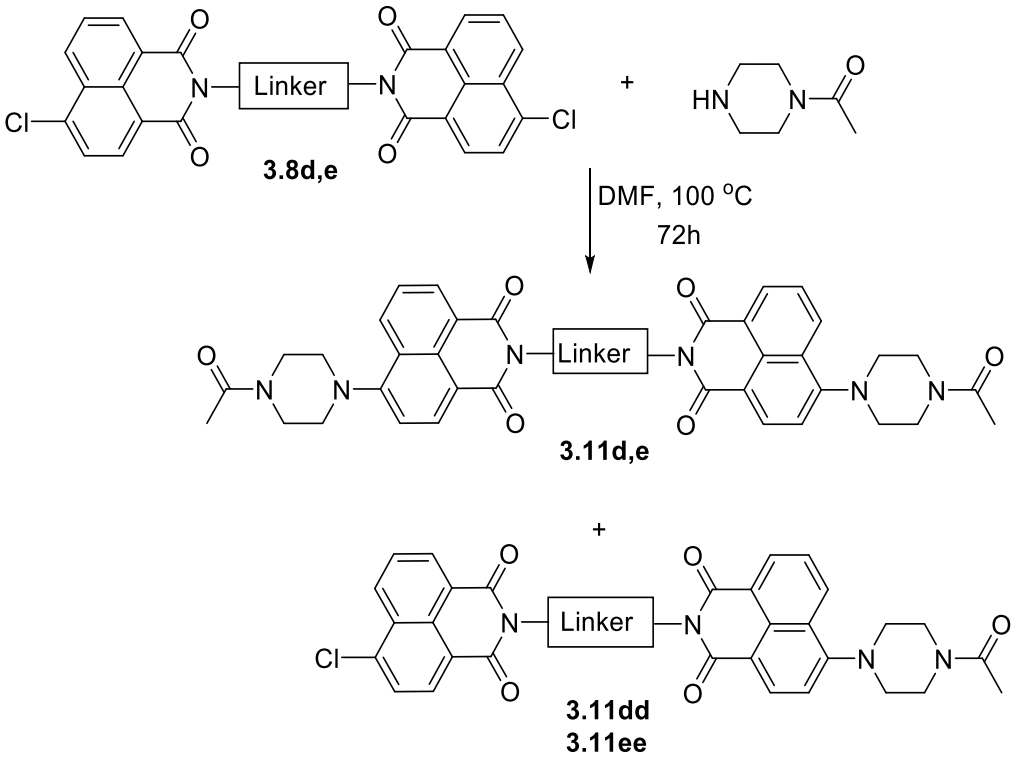

Scheme 3.18

The interesting difference between using morpholine and 1-acetyl piperazine in these reactions is the formation of asymmetrical substituted dimers in the case of using 1-acetyl piperazine. This difference is due to the strong nucleophilicity of morpholine compared to 1-acetyl piperazine. Nucleophiles need electron density to react with electrophiles, therefore the acetyl group in 1-acetyl piperazine appears to make it less reactive since it is taking away the source of the nucleophile's strength.

Compounds **3.11d,e** were synthesized by heating one equivalent of **3.8d,e** respectively with ten equivalents of 1-acetyl piperazine in DMF for 72 h. At the end of the reaction DMF was removed and water was added to precipitate the crude. The obtained crudes were a mixture of symmetric and asymmetric dimers. The two compounds were separated using column chromatography using DCM: ethanol (9.5:0.5) as eluent.

introduction of solubilizing groups through S_NAr reactions with thiol

In addition to primary and secondary amines, introducing solubilizing group via a different atom such as sulfur is more likely to change the compound geometry, polarisability, stability, steric and electronic characteristics which

could affect the binding properties.[26] Therefore, 2-mercaptoethanol was used to synthesise another series of target compounds.

One equivalent of the bisnaphthalimides **3.8a-e** and ten equivalents of 2-mercaptoethanol were dissolved in DMF and heated at 100 °C for 6 h (Scheme 3.19). After that the reaction mixture was acidified using HCl (5%)

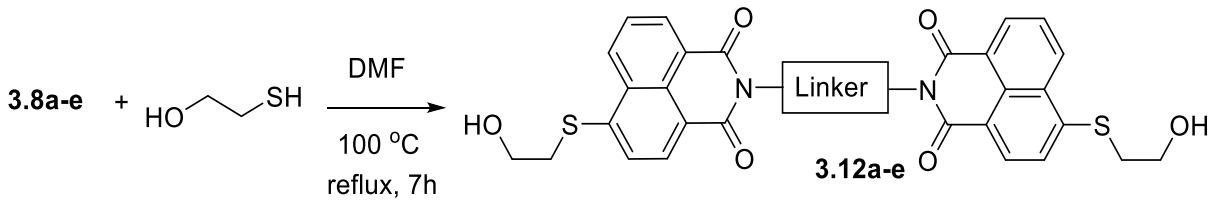

Scheme 3.19

These conditions were successfully used to obtain **3.12b,d,e** (Scheme 3.20) as pure yellow products in good yields (41-79%). Compounds **3.12b,d,e** were characterized using ^{1}H- and ^{13}C-NMR spectroscopy and mass spectrometry. On the other hand, **3.12a** and **3.12c** were not obtained as pure products. The ^{1}H-NMR spectra for these compounds show more signals than we expected in both the aliphatic and aromatic regions. This mean that the obtained product is a mixture of symmetric disubstituted and asymmetric monosubstituted bisnaphthalimide. Due to the lack of solubility of these compounds and the difficulty that we faced trying to separate previous symmetric and asymmetric bisnaphthalimide **3.11d,e** and **3.11dd,ee** using column chromatography, we decided to use the second synthetic path to obtain these compounds.

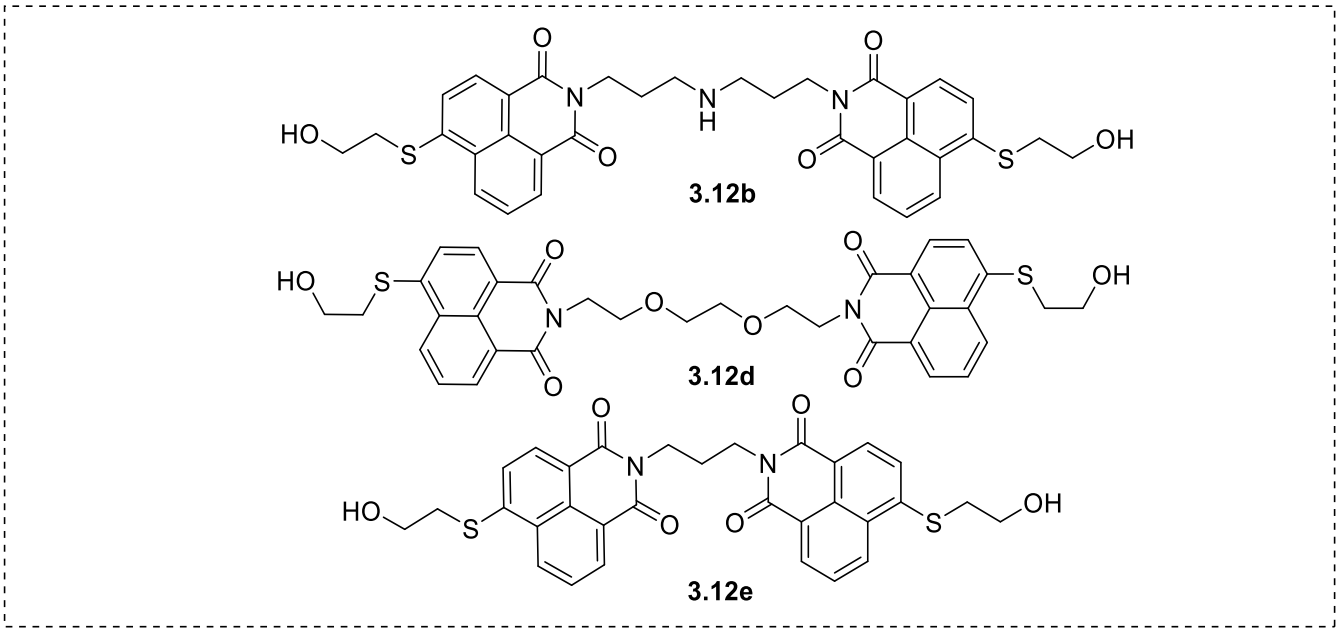

Scheme 3.20

Thioglycolic acid was also used as a solubilizing group. This class of compound is not expected to bind with DNA due to the negatively charged carboxylate group in neutral aqueous solutions which causes electrostatic repulsion with the phosphate groups in DNA. The reason behind using thioglycolic acid as a solubilizing group is to be used as starting material in chapter 5.

One equivalent of each of the obtained dimers **3.8a-e** was subjected to nucleophilic substitution using ten equivalents of thioglycolic acid using DMF as a solvent (Scheme 3.21). The reaction mixture was refluxed for 1-5 h and then the solution was left to cool and acidified using 5 % HCl to obtain a yellow powder.

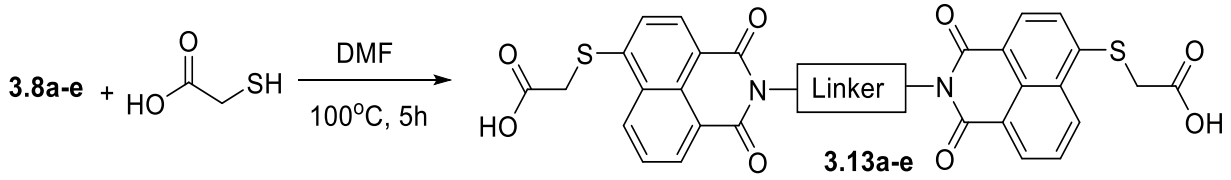

Scheme 3.21

This reaction condition was successfully carried out to synthesise **3.13a,c-e** as pure yellow products with good yields. All products were characterized using ^{1}H- and ^{13}C-NMR spectroscopy and mass spectrometry (Scheme 3.22).

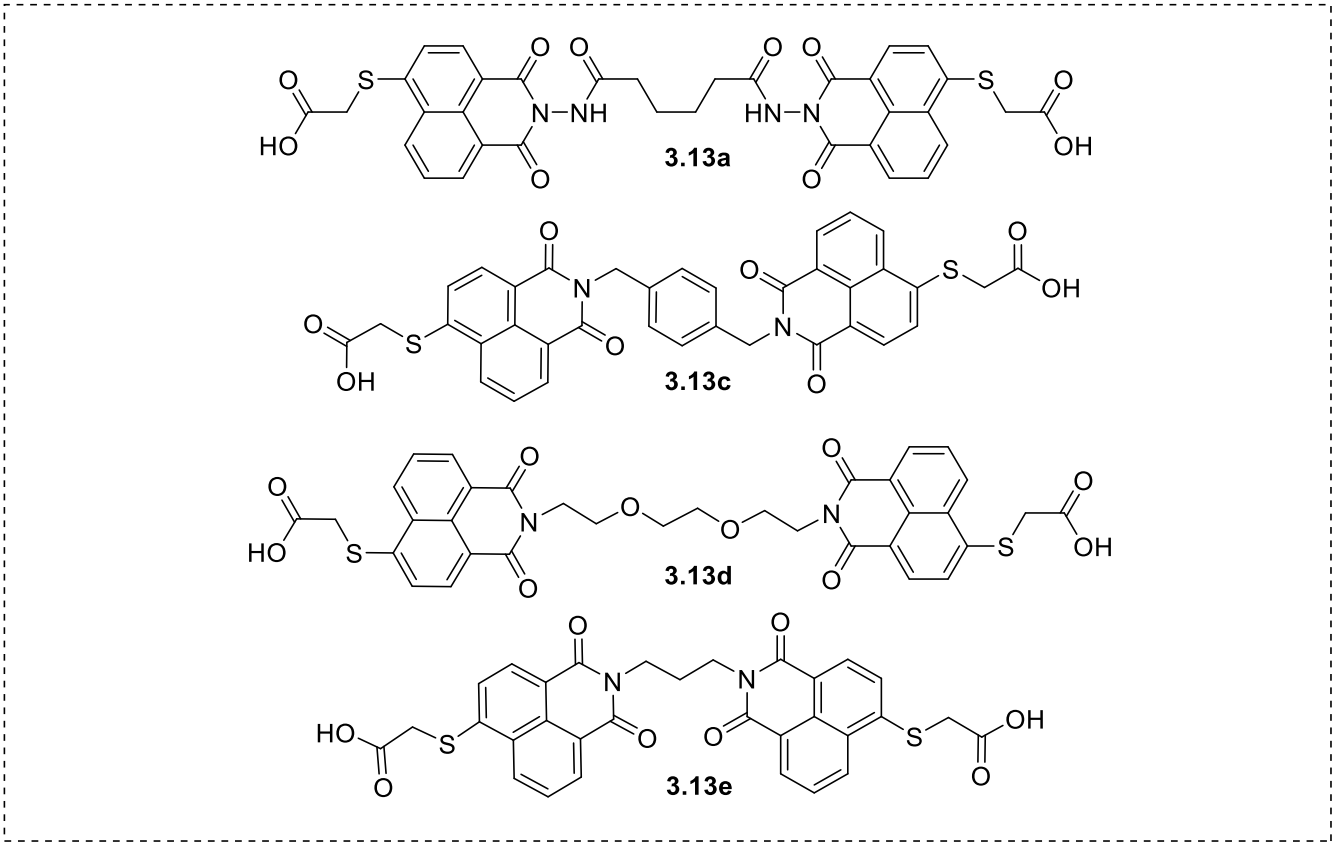

Scheme 3.22

Applying these reaction conditions to compound **3.8b** produced an asymmetric dimer where only one chlorine has been substituted (Scheme 3.23).

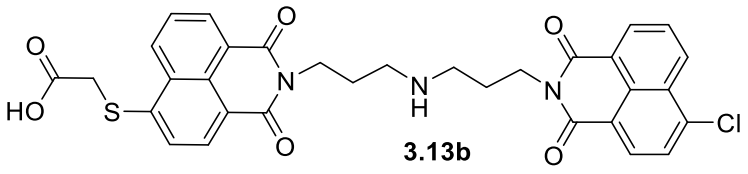

Scheme 3.23

It is worth to mention that when **3.13b-c** were dissolved in DMSO-d_6 to record the NMR spectra, the color of the solution was red at the beginning, and it changed to yellow after ≈5 min exposing to light. The NMR spectra were recorded twice, with and without shielding the tube from light as long as possible. When the solution in the NMR tube was shielded from the light, the colour of the solution did not change. However, the NMR spectra were the same, but this is likely because of exposure of the sample to light while in the queue on the NMR instrument. It is therefore currently not clear what causes the colour change.

Synthesis according to Path 2

As indicated above, for several compounds, synthetic path 1 yielded unsatisfactory results so path 2 was explored.

Path 2, step 1: S_NAr reaction

The solubilizing groups were introduced to 4-chloro 1,8-naphthalic anhydride to synthesise the new monomeric naphthalimide derivatives. This reaction can only be carried out with the secondary amines and the thiols because these can't react to form the naphthalimides.

One equivalent of 4-chloro-1,8-naphthalic anhydride was heated at 100 °C with two equivalents of morpholine in DMF for 24 h. After that, the solvent was removed, and methanol was added to precipitate **3.10** as an orange solid in 45% yield. Other substituted naphthalic anhydrides were synthesized analogously (Scheme 3.24).

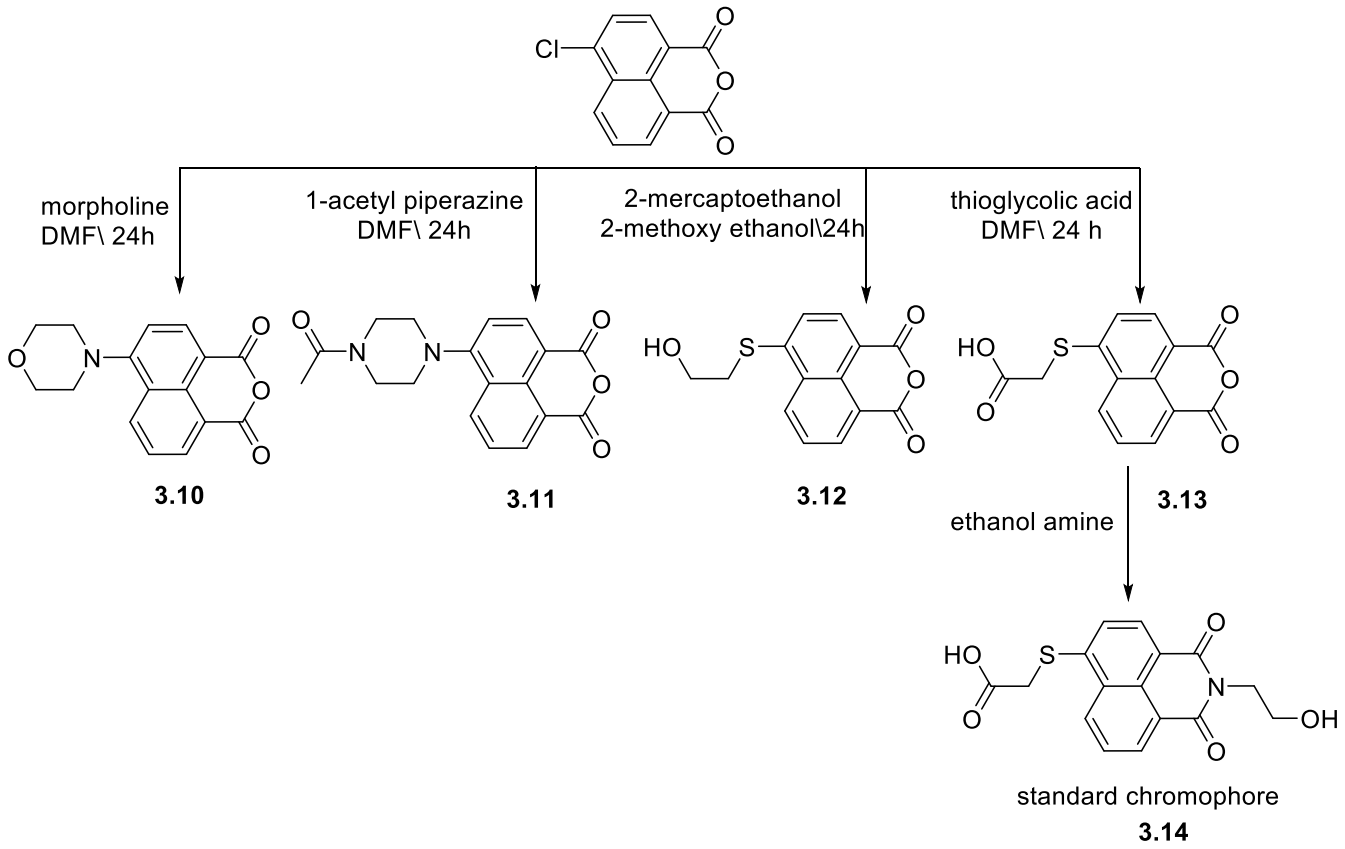

Scheme 3.24

Path 2, step 2: linking the naphthalimide units

The dimerization of 2.15 equivalents of new naphthalic anhydride monomer **3.10** with one equivalent of bis(3-aminopropyl)amine (linker b) was carried out in ethanol in the presence of a catalytic amount of triethylamine (Scheme 3.25). The reaction mixture was refluxed for 24 h to obtain a yellow solid **3.10b** at the end of the reaction in 32 % yield.

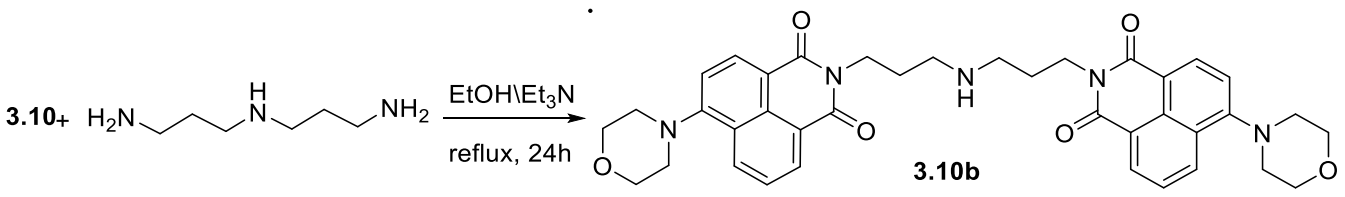

Scheme 3.25

The linking of 2 units of the new monomer **3.12** was carried out to synthesise **3.12a** and **3.12c**. A slight excess of 2.15 equivalents of **3.12** were dissolved in ethanol with one equivalent of the corresponding linkers in the presence of a catalytic amount of triethylamine and heated under reflux. However, the obtained crude cannot be characterized due to the lack of solubility for these compounds in DMSO-d_6 and chloroform-d.

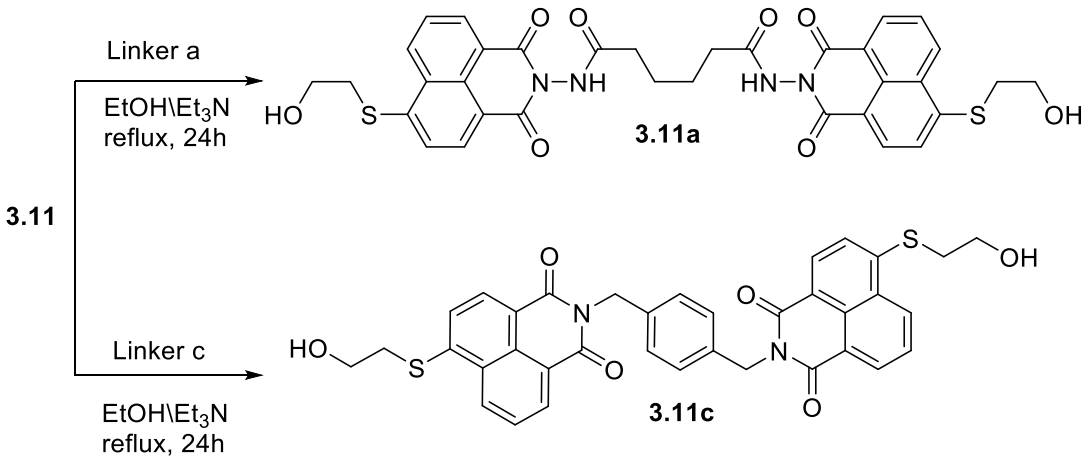

Scheme 3.26

3.2.3 Solubility of synthesized bisnaphthalimides

The solubility of all synthesized dimers was tested by placing a small amount of each dimer in MOPS buffer and stirring the mixture at least for 2 days. None of the materials has dissolved completely. The obtained suspensions were filtered to obtain saturated solutions. The UV-visible spectra were recorded, and the concentrations were calculated using the Beer Lambert law with the extinction coefficients for the various chromophores as determined in Chapter 2 for sufficiently soluble compounds **2.19-21**. Dimers **3.8a-e** are partially soluble in MOPS and show a band with λ_{max} at 301-302 nm (Table 3.7).

Table 3.7. The λ_{max} of 3.8a-e

	3.8a	**3.8b**	**3.8c**	**3.8d**	**3.8e**
λ_{max}, nm	302	302	302	301	301

The spectra of compounds **3.8b,d** show an unexpected band at 347 nm (Figure 3.8).

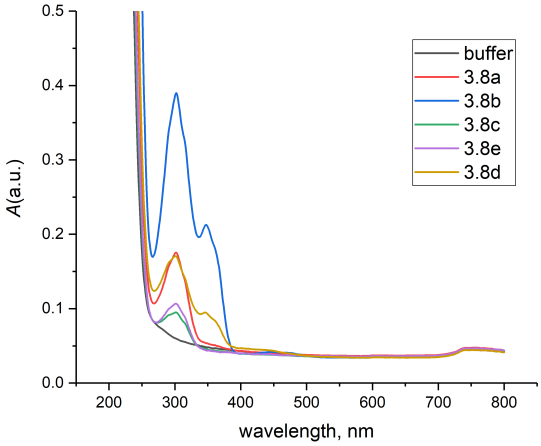

Figure 3.8. UV-visible spectra of bisnaphthalimides 3.8a-e in buffer (25 mM MOPS pH 7.0, 50 mM NaCl, 1 mM EDTA) at 25 °C.

There are three scenarios that could explain this additional band, viz.

- presence of impurities.
- intermolecular stacking of chromophores.
- intramolecular stacking of chromophores.

The first scenario involves the presence of an impurity in these compounds, despite the fact that the recorded NMR spectra for this compound did not show significant impurities. We note, however, that even a minor impurity with a sufficiently high extinction coefficient may result in a significant UV-visible absorbance.

The second and third scenarios involve stacking of the chromophores (Figure 3.9), which could cause a red-shift in absorbance in case of J-aggregate or blue-shift in absorbance in case of H-aggregate.[27, 28]

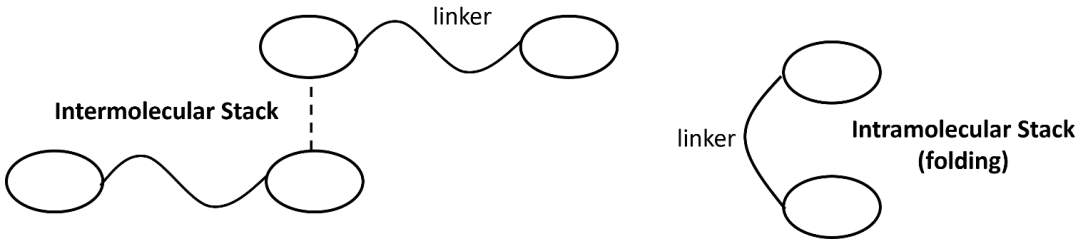

Figure 3.9. Intermolecular stacking and intramolecular stacking of chromophores

To identify which of the three scenarios causes the additional band, the solutions of **3.8b,d** were diluted, and the spectra were recorded again. The absorbances for both bands decrease with the dilution in the same pattern (Figure 3.10 a). This observation eliminates the possibility of intermolecular stacking because in case of dilution the band caused by intermolecular stacking should disappear to a larger extent than the absorbance for the monomer as a result of deaggregation at lower concentrations. Therefore, as a second test, the remaining solids that did not dissolve when the material was exposed to the buffer the first time (which was supposed to be non-dissolved **3.8b,d**) were dissolved in MOPS buffer and filtered again. The spectra for these new solutions were recorded (Figure 3.10 b). These spectra for the remaining materials show the two bands with different intensity which indicates that the second bands are related to the presence of impurities with a lower solubility than the desired compound.

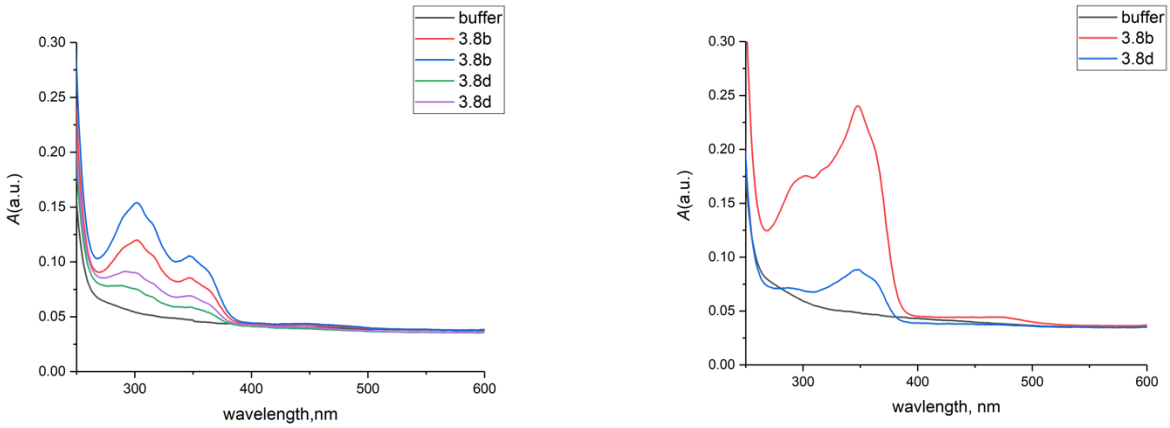

a **b**

Figure 3.10. UV-visible spectra of 3.8b stock solution (blue,left), 3.8b diluted solution (red,left), 3.8d stock solution (purble,left), 3.8d diluted solution (green,left), in buffer (25 mM MOPS pH 7.0, 50 mM NaCl, 1 mM EDTA) at 25 °C. UV-visible spectra of 3.8b second stock (red, right) 3.8d second stock (blue, right)

Table 3.8 illustrates the solubility limit for all synthesized dimers.

Table 3.8. The solubility limit for all synthesised compounds (3.9and 3.9be), (3.10a-e), (3.11d,e), (3.12b,d,e), and (3.13a,d,e)

	3.9	3.10	3.11	3.12	3.13
SG	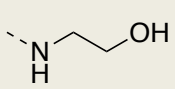	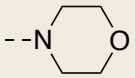	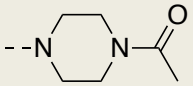	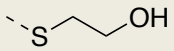	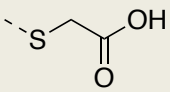
SG= ethanol amine	**3.9**	**3.9b**	**3.9c**	**3.9d**	**3.9e**
λ_{max}, nm	448	444	447	448	448
Solubility limit, M	8.67×10^{-5}	6.60×10^{-5}	2.60×10^{-5}	2.34×10^{-6}	6.99×10^{-6}
SG= morpholine	**3.10a**	**3.10b**	**3.10c**	**3.10d**	**3.10e**
λ_{max}, nm	-	401	-	-	-
Solubility limit, M	NS	7.88×10^{-6}	NS	NS	NS
SG= 1-acetyl piperazine	**3.11a**	**3.11b**	**3.11c**	**3.11d**	**3.11e**
λ_{max}, nm	-	-	-	403	-
Solubility limit, M	N	N	N	2.61×10^{-6}	NS
SG= 2-mercapto ethanol	**3.12a**	**3.12b**	**3.12c**	**3.12d**	**3.12e**
λ_{max}, nm	-	397	-	395	-
Solubility limit, M	N	8.11×10^{-6}	N	4.84×10^{-6}	NS
SG= thioglycolic acid	**3.13a**	**3.13b**	**3.13c**	**3.13d**	**3.13e**
λ_{max}, nm	401	-	-	401	394
Solubility limit, M	2.88×10^{-4}	N	NT	7.57×10^{-4}	3.24×10^{-4}

N: Not synthesized

NS: not sufficiently soluble

NT: not tested

As expected, using thioglycolic acid as the solubilising group has tremendously improved the solubility for bisnaphthalimides due to deprotonation of the carboxylic acid groups in the buffer at pH 7. Ethanol amine is the next solubilizing group that has positive effect in improving the solubility. 2-mercaptoethanol, morpholine and 1-acetyl piperazine show moderate improvement in the solubility. Although, we managed to introduce morpholine in all synthesized bisnaphthalimides, unfortunately only one compound, viz. **3.10b**, was sufficiently soluble. This observation means that morpholine is not a recommended group to improve the solubility for this class of compounds.

It is worth to mention that the electronic properties for substituted bisnaphthalimides follow the same pattern observed by Pavel Kucheryavy *et al*.[29] (see chapter 2). Applying this pattern to synthesized bisnaphthalimides in this chapter, the λ_{max} for the absorption of substituted bisnaphthalimides with chlorine as substituent is around 301-302 nm which suggest this band has a π-π* character. As in Chapter 2, using 1°, 2°-amine and thiol groups as a solubilizing group lead to chromophores that show a band that we attribute to n-π* charge-transfer character on the basis of Kucheryavy's work. Bisnaphthalimides with 2°-amine as a solubilizing group show a red-shift in λ_{max} relative to the Cl-substituted compound (between 401-403 nm). A similar shift is observed in case of using thiol groups where the λ_{max} = 394-401 nm. When using ethanol amine as a solubilizing group, a further red shift is observed, probably as a result of improved conjugation, resulting in a band around 448-444 nm.

3.2.4 UV-visible titrations

One of the aims of this chapter is to investigate the DNA-binding properties of the synthesized compounds. Like in Chapter 2, the binding properties were investigated through UV-visible absorption titrations. The changes in the UV-visible spectra during the titration, i.e. decreases or increases in the absorbance or shifts in λ_{max}, can be utilized to determine whether these compounds are interacting with the DNA or not.

Based on the spectra as recorded for the solubility tests for synthesized compounds **3.8a-e**, the λ_{max} for the dimers with chlorine in C4 is around 301-302 nm. Therefore, the binding properties for compounds **3.8a-e** cannot be studied using UV-visible spectroscopy since the λ_{max} for DNA is 260 nm with the absorbance peak going up to approximately 300 nm. As a result, the increasing concentration of DNA results in increasing absorbance of light up to a wavelength of around 300 nm as well. For each soluble compound, The titration was performed three times and the obtained data were plotted and analyzed using the MIS model [30] individually and globally to obtain the binding affinity and stoichiometry.

3.2.4.1 UV-visible spectroscopy studies of compounds (3.9,3.9b-e)

The binding properties of soluble **3.9** and bisnaphthalimide derivatives **3.9b-e** were studied using UV-visible titrations. UV-visible spectra were recorded in MOPS buffer (25 mM MOPS pH 7.0, 50 mM NaCl, 1 mM EDTA) at 25 °C upon addition of aliquots of FSDNA. The titration was performed three times for each compound and the obtained data were plotted and analyzed using the MIS model[30] individually and globally to obtain the binding affinity and stoichiometry.

The titration results for **3.9** are shown in Figure 3.11.

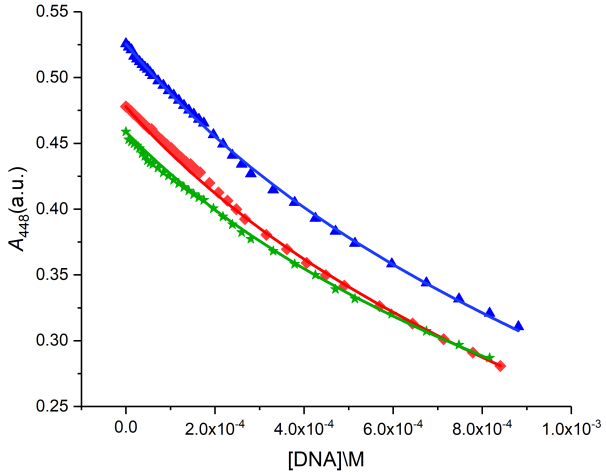

Figure 3.11 Absorbance at 448 nm for 53.2 μM (▲), 48.4 μM (◆), and 42.2 μM (★) solutions of 3.9 as a function of FSDNA concentration in buffer (25 mM MOPS pH 7.0, 50 mM NaCl, 1 mM EDTA) at 25 °C. (▲) 1st titration, (◆) 2nd titration, and (★) 3rd titration. The solid lines represent a global fit of a multiple independent sites model to the data.

The titration curves for **3.9** exhibit hypochromic shifts in absorbance at λ_{max}=448 nm. The obtained data were plotted and analyzed using the multiple independent binding sites model, individually and globally (Table 3.9).

Table 3.9 DNA-binding affinity *K* (*n*=3) / M^{-1} of 3.9

K (*n*=3) / M^{-1}	1st titration	2nd titration	3rd titration	Global fit
3.9	$(5.6\pm0.5)\times10^3$	$(3.7\pm0.4)\times10^3$	$(4.5\pm0.4)\times10^3$	$(4.7\pm0.4)\times10^3$
Bathochromic shift, nm	(448 - 451 nm)			

According to the global fit, the binding affinity $K_{binding}$ is $(4.0\pm1.4)\times10^4$ M^{-1} if the binding site size *n* is 8.8±0.9 basepairs (see appendix). However, since this compound is mono-intercalator, the reasonable binding site size for binding is 3 basepairs. Thus, the data were analyzed again with restricting the stoichiometry to 3 basepairs and according to this fitting $K_{binding}$ equals $(4.7\pm0.4)\times10^3$ M^{-1}. This compound is therefore a relatively weak binder, in line with the monomeric compounds reported in Chapter 2.

In general, the titration curves for **3.9b-e** exhibit a hypochromic shift in absorbance at λ_{max} and show negligible bathochromic shift. Titration curves were extracted from the spectroscopic data for these compounds by plotting the absorbance at λ_{max} as a function of DNA concentration (Figure 3.12).

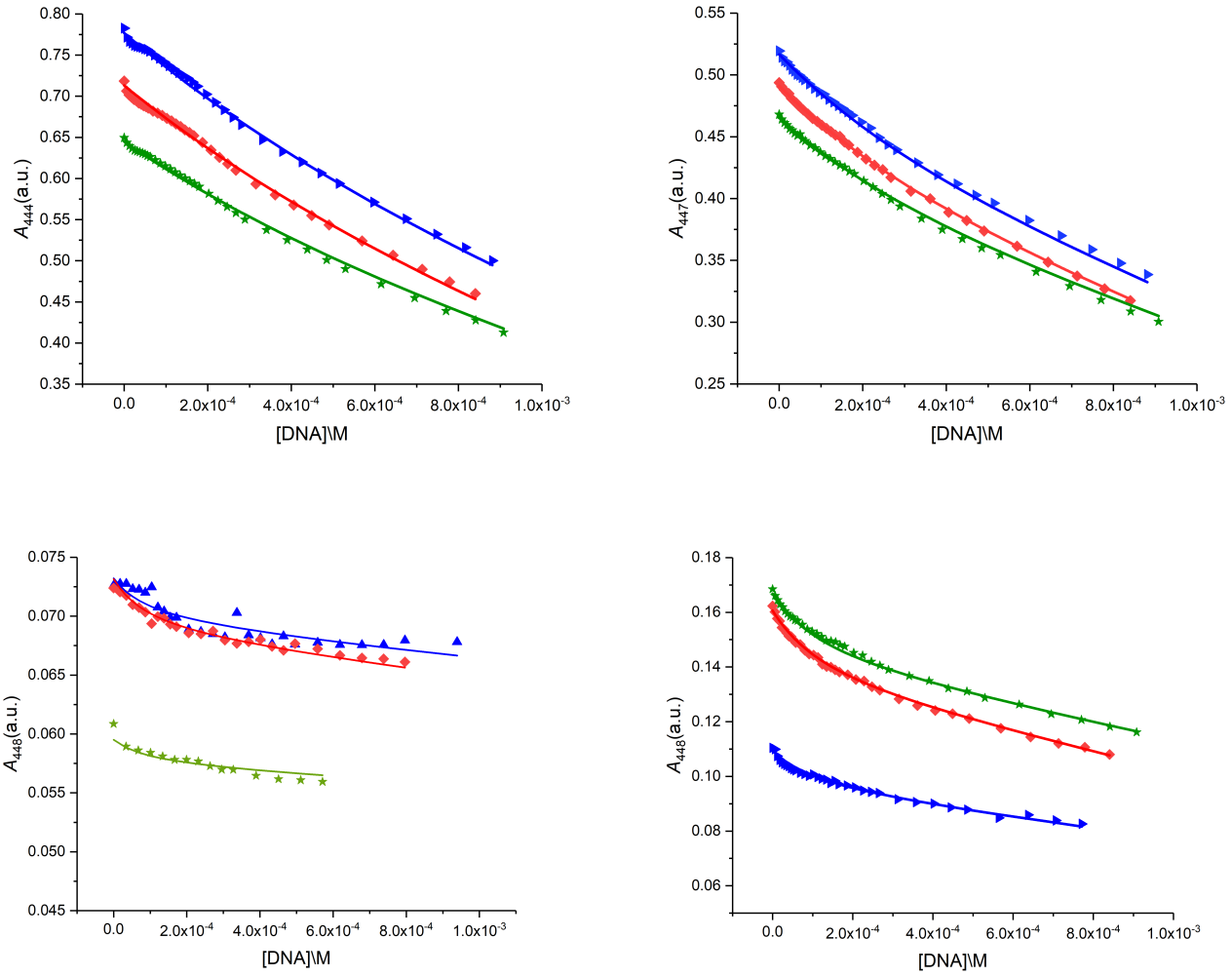

Figure 3.12 Absorbance at 444 nm for 40.8 μM (▲), 32.6 μM (◆), and 37.7 μM (★) solutions of 3.9b as a function of FSDNA concentration (top left); absorbance at 447 nm for 26.7 μM (▲), 25.1 μM (◆), and 23.2 μM (★) solutions of 3.9c as a function of FSDNA concentration (top right); absorbance at 448 nm for 1.6 μM (▲), 2.0 μM (◆), and 1.0 μM (★) solutions of 3.9d as a function of FSDNA concentration (bottom left); absorbance at 448 nm for 3.9 μM (▲), 6.7 μM (◆), and 7.0 μM (★) solutions of 3.9e as a function of FSDNA concentration in buffer (25 mM MOPS pH 7.0, 50 mM NaCl, 1 mM EDTA) at 25 °C. (▲) 1st titration, (◆) 2nd titration, and (★) 3rd titration, and the solid lines represent a global fit of a multiple independent sites model to the data.

The shape of the titration curves suggests that **3.9e** binds more strongly with DNA than the other compounds. The obtained titration curves data were analyzed twice, with and without restricting the stoichiometry at 6 basepairs

per binder. The stoichiometry was restricted to 6 basepairs since these compounds are considered as bis-intercalators (Table 3.10, see appendix for unrestricted stoichiometry and binding affinities). Using the same binding site size for all compounds also ensures that the resulting affinities are comparable.

Table 3.10 DNA-binding affinity *K* (n=6) / M^{-1} for compounds 3.9b-e

***K* (n=6) / M^{-1}**	**1st titration**	**2nd titration**	**3rd titration**	**Global fit**
3.9b	$(7.8\pm2.1)\times10^3$	$(8.8\pm2.6)\times10^3$	$(6.7\pm1.2)\times10^3$	$(7.5\pm1.3)\times10^3$
Bathochromic shift, nm	(444-447 nm)			
3.9c	$(2.3\pm0.3)\times10^4$	$(1.9\pm0.2)\times10^4$	$(1.4\pm0.1)\times10^4$	$(1.9\pm0.2)\times10^4$
Bathochromic shift, nm	(447-449)			
3.9d	$(2.48\pm0.89)\times10^4$	$(3.08\pm0.6)\times10^4$	$(4.62\pm0.93)\times10^4$	$(4.48\pm1.92)\times10^4$
Bathochromic shift, nm	444-448			
3.9e	$(9.81\pm1.62)\times10^4$	$(7.38\pm0.57)\times10^4$	$(4.30\pm0.36)\times10^4$	$(6.13\pm0.43)\times10^4$
Bathochromic shift, nm	448-450			

The resulting binding affinities indicate that this class of compounds is binding with FSDNA and the strength of the binding is **3.9e**>**3.9d**>**3.9c**>**3.9b**. Creating the linked bisnaphthalimides has also resulted in higher binding affinities than the corresponding monomeric compounds.

3.2.4.2 UV-visible spectroscopy studies of 3.10b

Of the morpholine-appended compounds, **3.10b** is the only compound that is sufficiently soluble in aqueous solution. The binding properties of this compound were studied using UV-vis titrations. The measurement of UV-visible absorption spectra was conducted in MOPS buffer (25 mM MOPS pH 7.0, 50 mM NaCl, 1 mM EDTA) at 25 °C. UV-visible spectra were recorded upon addition of aliquots of FSDNA. The titration was performed three times.

The titration spectra of this compound exhibit hypochromic and bathochromic shifts upon FSDNA addition (Figure 3.13).

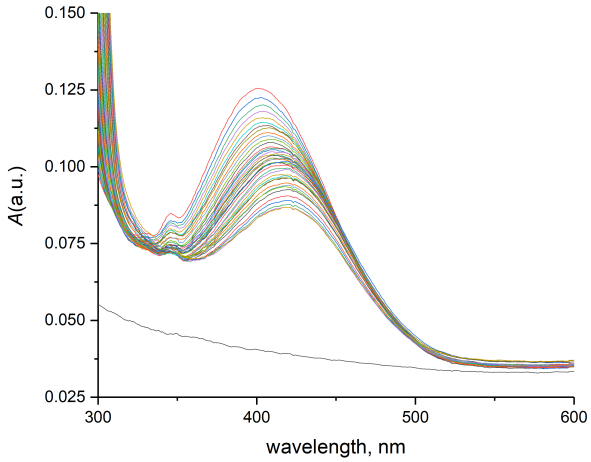

Figure 3.13. The titration spectra for a 4.4 μM solution of 3.10b upon FS DNA addition in buffer (25 mM MOPS pH 7.0, 50 mM NaCl, 1 mM EDTA) at 25 °C.

Titrations curves were created by plotting the absorbance at 401 nm as a function of DNA concentration. The three titration curves were analyzed individually and globally (Figure 3.14).

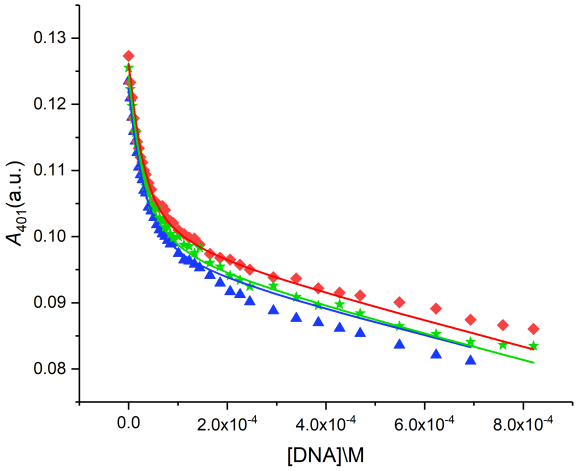

Figure 3.14 Absorbance at 401 nm for 4.4 μM (▲), 4.5 μM (◆), and 4.5 μM (★) solutions of 3.10b as a function of FSDNA concentration in buffer (25 mM MOPS, 50 mM NaCl, 1mM EDTA) at 25 °C. (▲) 1st titration, (◆) 2nd titration, and (★) 3rd titration, and the solid lines represent a global fit of a multiple independent sites model to the data.

Table 3.11 illustrates the obtained DNA-binding parameters of **3.10b**.

Table 3.11 DNA-binding affinity *K* (*n*=6) / M^{-1} of 3.10b

K (*n*=6) / M^{-1}	1st titration	2nd titration	3rd titration	Global fit
3.10b	(2.70±0.16)×10^5	(5.19±0.51)×10^5	(4.18±0.29)×10^5	(4.0±0.3)×10^5
Bathochromic shift, nm	(401-421 nm)			

Based on the global fit, the DNA-binding affinity $K_{binding}$ for **3.10b** equals (4.0±0.3)×10^5 M^{-1} after restricting the size of the binding site to 6 basepairs which indicates that this compound is a good binder.

3.2.4.3 UV-visible titrations of 3.11d interacting with FSDNA

Compound **3.11d** is the only compound of the series of substituted naphthalic anhydrides that is sufficiently soluble in aqueous solution. The binding properties of this compound were studied using UV-visible titrations. The compound was dissolved in MOPS buffer (25 mM MOPS pH 7.0, 50 mM NaCl, 1 mM EDTA) at 25 °C and UV-visible spectra were recorded upon addition of aliquots of a FSDNA stock solution. The titration curves of **3.11d** exhibit a hypochromic shift but an insignificant bathochromic shift upon DNA addition (Figure 3.15).

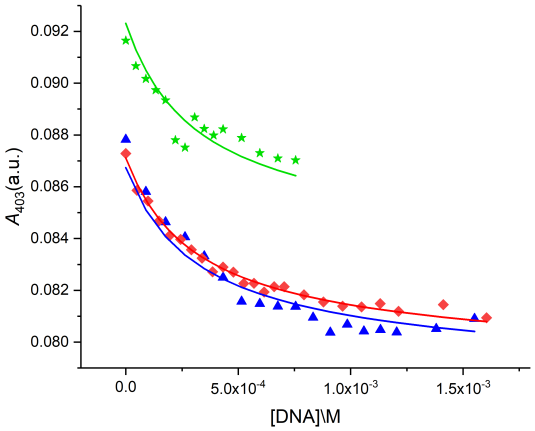

Figure 3.15 Absorbance at 403 nm for 2.4 µM (▲), 2.4 µM (◆), and 2.7 µM (★) solutions of 3.11d as a function of FSDNA concentration in buffer (25 mM MOPS, 50 mM NaCl, 1mM EDTA) at 25 °C. (▲) 1st titration, (◆) 2nd titration, and (★) 3rd titration, and the solid lines represent a global fit of a multiple independent sites model to the data.

The obtained data of the three titrations for this compound were plotted and analyzed both individually and globally (Table 3.12).

Table 3.12 DNA Binding affinity *K* (*n*=6) / M^{-1} of 3.11d

***K* (*n*=6) / M^{-1}**	**1st titration**	**2nd titration**	**3rd titration**	**Global fit**
3.11d	$(8.99\pm5.36)\times10^4$	$(9.18\pm2.93)\times10^4$	$(4.32\pm4.33)\times10^4$	$(2.04\pm0.7)\times10^4$
Bathochromic shift, nm	403-405			

Based on the global fit, the binding affinity ($K_{binding}$) for compound **3.11d** is $(2.0\pm0.7)\times10^4$ M^{-1} after restricting the size of the binding site at 6 basepairs which indicates that this compound is a reasonably good binder.

3.2.4.4 UV-visible spectroscopy studies of 3.12b,d interacting with FSDNA

The binding properties of **3.12b,d** were also studied using UV-visible titrations. The measurement of UV-visible absorption spectra for the compounds was conducted in MOPS buffer (25 mM MOPS pH 7.0, 50 mM NaCl, 1 mM EDTA) at 25 °C. Further UV-visible spectra were recorded following addition of aliquots of FSDNA. The titration was preformed three times.

The titrations for **3.12b,d** exhibit hypochromic shifts upon the addition of FSDNA (Figure 3.16).

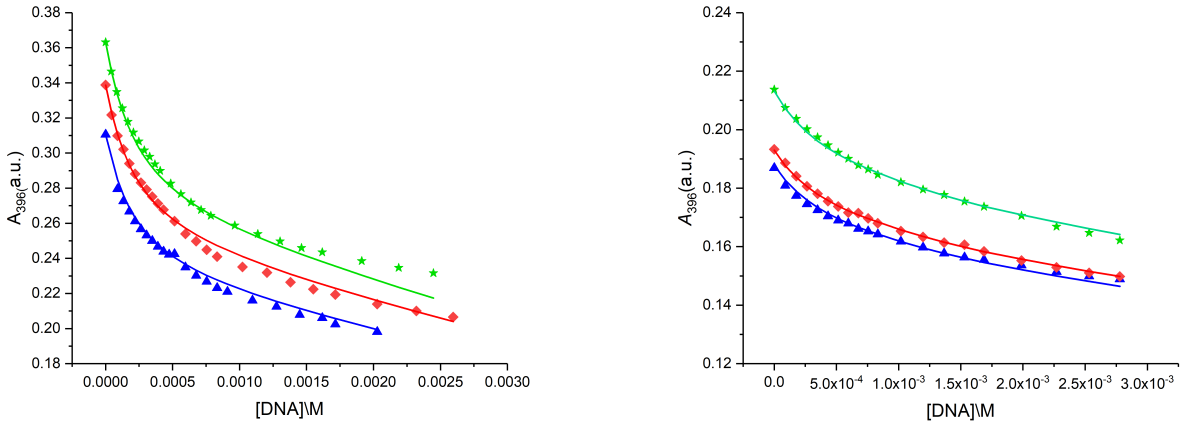

Figure 3.16 Absorbance at 396 nm for 10.9 μM (▲), 12.1 μM (◆), and 13.1 μM (★) solutions of 3.12b as a function of FSDNA concentration (left); absorbance at 396 nm for 5.9 μM (▲), 6.1 μM (◆), and 7.0 μM (★) solutions of 3.12d as a function of FSDNA concentration in buffer (25 mM MOPS, 50 mM NaCl, 1mM EDTA) at 25 °C. (▲) 1st titration, (◆) 2nd titration, and (★) 3rd titration, and the solid lines represent a global fit of a multiple independent sites model to the data.

The obtained data for the three titrations for these two compounds were plotted and analyzed individually and globally (Table 3.13).

Table 3.13 DNA binding affinity *K* (*n*=6) / M^{-1} of 3.12b,d

***K* (*n*=6) / M^{-1}**	**1st titration**	**2nd titration**	**3rd titration**	**Global fit**
3.12b	(3.21±0.24)×10^4	(2.86±0.25)×10^4	(1.96±0.13)×10^4	(3.38±0.28)×10^4
Bathochromic shift, nm	396-406			
3.12d	(1.37±0.13)×10^4	(1.27±0.14)×10^4	(1.14±0.14)×10^4	(1.24±0.17)×10^4
Bathochromic shift, nm	396-400			

Based on the global fit, the binding affinities for compounds **3.12b,d** are (3.38±0.28)×10^4 M^{-1} and (1.24±0.17)×10^4 M^{-1}, respectively, when the stoichiometry is restricted to 6 basepairs. The binding affinities indicate that these compounds bind with FSDNA and that **3.12b** may bind better than **3.12d** but the difference is relatively small.

3.2.4.5 UV-visible spectroscopy studies of 3.13a,d,e

The binding properties of **3.13a,d,e** were studied using UV-visible titrations. The measurement of UV-visible absorption spectra was conducted in MOPS buffer (25 mM MOPS pH 7.0, 50 mM NaCl, 1 mM EDTA) at 25 °C, with a UV-visible spectrum recorded following each addition of FSDNA. The titration was performed three times and the obtained absorbances at λ_{max} were plotted as a function of DNA concentration (Figure 3.17) and analyzed individually and globally, giving the binding affinity.

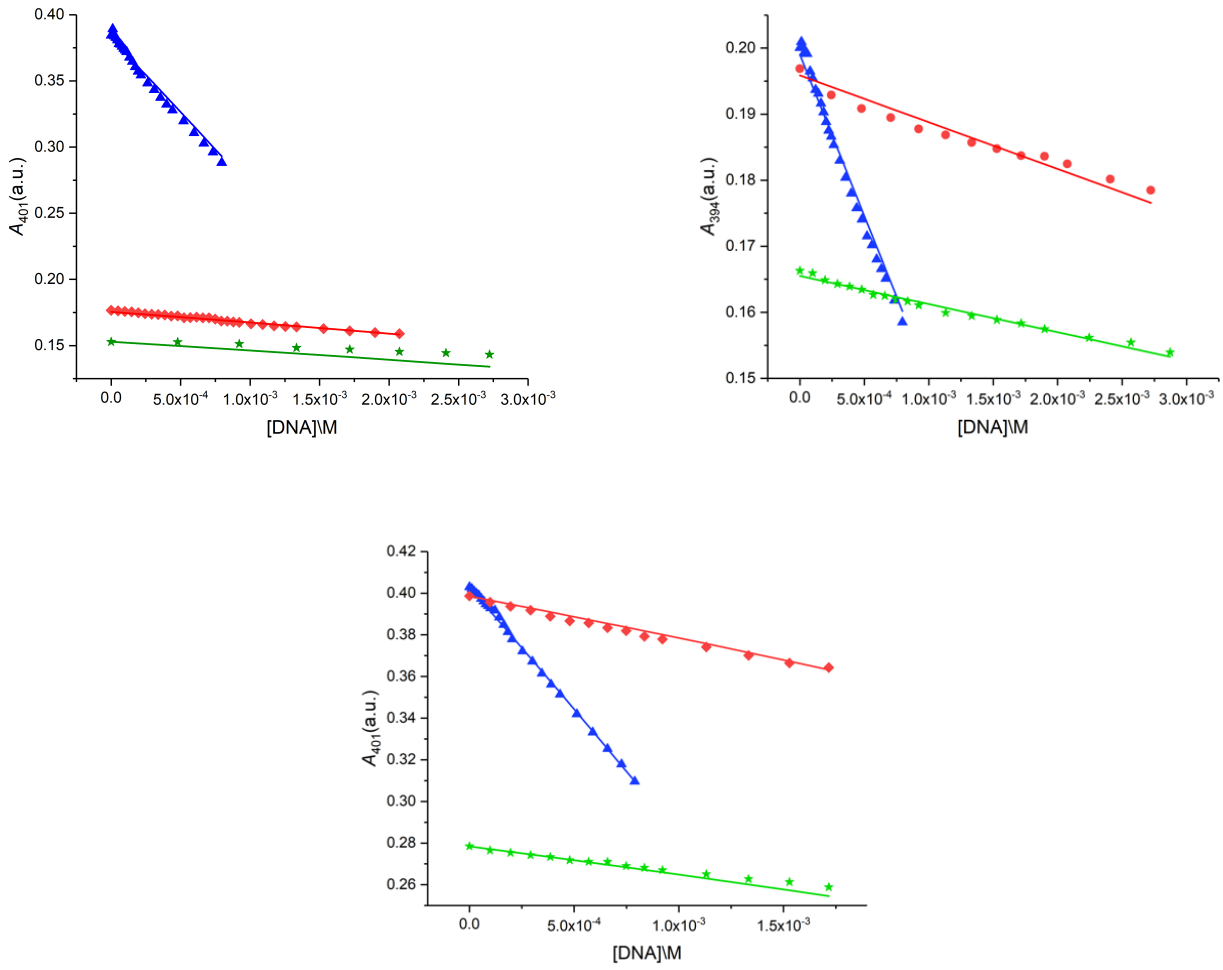

Figure 3.17 Absorbance at 401 nm for 13.8 μM (▲), 5.4 μM (◆), and 4.5 μM (★) solutions of 3.13a as a function of FSDNA concentration (top left); absorbance at 394 nm for 6.4 μM (▲), 6.4 μM (◆), and 4.11 μM (★) solutions of 3.13e as a function of FSDNA concentration (top right), and absorbance at 401 nm for 14.7 μM (▲), 14.5 μM (◆), and 9.8 μM (★) solutions of 3.13d as a function of FSDNA concentration (bottom) in buffer (25 mM MOPS pH 7.0, 50 mM NaCl, 1 mM EDTA) at 25 °C. (▲) 1st titration, (◆) 2nd titration, and (★) 3rd titration. The solid lines represent a global fit of a multiple independent sites model to the data.

The binding parameters from analysis are summarized in Table 3.14.

Table 3.14 DNA binding affinity *K* (*n*=6) / M^{-1} of 3.13a,d,e

***K* (*n*=6) / M^{-1}**	**1st titration**	**2nd titration**	**3rd titration**	**Global fit**
3.13a	$0.32\pm6.23\times10^{10}$	0.47±490.2	0.42±155.8	0.3±272.0
3.13d	0.83±2634	0.34±207.7	0.44±133.0	0.40±278.8
3.13e	$0.10\pm1.11\times10^{10}$	0.37±176.8	0.35±80.68	0.31±81.77

Based on the global fit, the binding affinity for compound **3.13a** is 0.3±272.0 M^{-1} when the stoichiometry is restricted at 6 basepairs. The binding affinities unsurprisingly indicate that this compound is not binding to DNA. This is more than likely due to the negatively charged carboxylate group which causes electrostatic repulsion with the phosphate groups in DNA. The featureless decreases in absorbance in Figure 3.17 therefore represent simple dilution of the compound upon addition of the FSDNA solution. In fact, the reason behind synthesizing this compound was to be use as starting material in Chapter 5.

Similarly, the titration curves for the other examples of this class of compounds exhibit decreases in absorbance at λ_{max} (Figure 3.18). Based on the global fits with the binding site sizes restricted to 6 basepairs, the binding affinities for compounds **3.13d,e** indicate that this class of compounds do not bind with DNA.

Comparison of binding affinities

Table 3.16 summarises the DNA-binding affinities based on the global fit for all aqueous-buffer-soluble synthesized compounds.

Table 3.15 DNA-binding affinities based on the global fits for all soluble synthesized compounds

Compound	Binding affinity * / M^{-1}	Compound	Binding affinity * / M^{-1}
3.9**	$(4.7\pm0.4)\times10^3$	**3.11d**	$(2.0\pm0.7)\times10^4$
3.9b	$(7.5\pm1.3)\times10^3$	**3.12b**	$(3.4\pm0.3)\times10^4$
3.9c	$(1.9\pm0.2)\times10^4$	**3.12d**	$(1.2\pm0.2)\times10^4$
3.9d	$(4.5\pm1.9)\times10^4$	**3.13a**	0.3±272.0
3.9e	$(6.1\pm0.4)\times10^4$	**3.13d**	0.40±278.8
3.10b	$(4.0\pm0.3)\times10^5$	**3.13e**	0.31±81.77

* The stoichiometry is restricted to 6 basepairs

** The stoichiometry is restricted to 3 basepairs

Several interesting observations can be made in terms of binding properties for the synthesized compounds. A general look at the table confirms that thioglycolic acid groups are not recommended in terms of binding with DNA due to the negatively charged carboxylate that form at neutral pH. The morpholine solubilizing group appears to make a positive impact on the DNA-binding affinity of **3.10b**, but at the same time appears to reduce water solubility considering that **3.10b** was the only example of this series of compounds that dissolved sufficiently. Using 2-mercaptoethanol and 1-acetyl piperazine as solubilizing groups results in compounds showing moderate binding properties with DNA.

3.2.5 Conclusion

A series of bisnaphthalimide derivatives have been synthesized where two units of naphthalimide were connected via several linkers. Several solubilizing groups (1°-amine, 2°-amine, thiol group) were introduced to C4 in the naphthalimide scaffold. The solubility of these compounds has been tested in MOPS buffer and the DNA-binding affinities were investigated using UV-visible titrations. Using thioglycolic acid as solubilizing group has improved the solubility tremendously due to the deprotonation of the carboxylic acid. However, for the same reason using this solubilizing group causes electrostatic repulsion with the negatively charged DNA and therefore this repulsion does not allow this class of compounds to bind with DNA. Ethanolamine is the second group that has improved the solubility for synthesized bisnaphthalimides. 2-Mercaptoethanol also has a good influence on aqueous

solubility. Both ethanolamine and 2-mercaptoethanol appended bisnaphthalimides show moderate binding affinities with FSDNA. Unfortunately, using morpholine and piperazine as solubilizing groups results in little aqueous solubility, which is a pity considering the very good binding properties for the soluble members of these families, especially the morpholine-appended bisnaphthalimide that shows strong binding affinity with FS DNA.

3.3 Experimental:

3.3.1 Materials and measurements:

All chemicals, including FS DNA, were procured from Sigma-Aldrich, Fisher or TCI and were used without further purification. Flash column chromatography was carried out using 60 Å silica. All compounds show strong fluorescence and were readily visualized on TLC plates using UV light. ^{1}H-NMR and ^{13}C-NMR spectra were recorded utilizing a Bruker AV 400 UltraShield spectrometer and Bruker AV 500 UltraShield spectrometer using the solvent as an internal standard. All chemical shifts are reported with respect to TMS. High resolution mass spectra were recorded using a Waters Micromass LCT Premier. UV-visible spectra were recorded using a Jasco V-650 spectrophotometer at controlled temperature using an air-cooled EHCS-716 Peltier Thermostatted Cell Holder at 25 °C. The pH of buffers was recorded using Hanna microprocessor pH-meter equipped with a VWR 662-1382 glass electrode. The pH meter was calibrated using a two-point calibration with buffers of known pH obtained from Fisher scientific. Deionized water was obtained from an Elga Purelab Flex.

3.3.2 Synthetic Procedures

Synthesis of N^1,N^6-bis(6-chloro-1,3-dioxo-1H-benzo[de]isoquinolin-2(3H)-yl)adipamide 3.8a

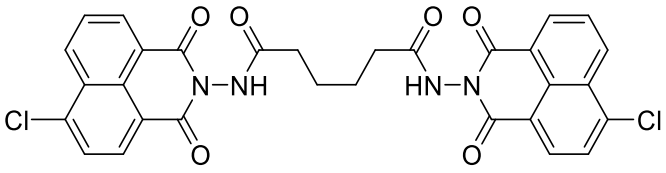

A suspension of 2.25 equivalents of 4-chloro-1,8-naphtalic anhydride (2.61 g, 11.25 mmol) in ethanol was placed in a round-bottom flask. One equivalent of triethylamine Et_3N (0.36 g, 5 mmol) and one equivalent of adipic dihydrazide (0.87 g, 5 mmol) were added. The reaction mixture was heated under reflux for 24 h, after that the resulting mixture was left to cool. The solid was filtered, washed with cold ethanol and dried in an oven (75 °C) to give the pure N^1,N^6-bis(6-chloro-1,3-dioxo-1H-benzo[de]isoquinolin-2(3H)-yl)adipamide **3.8a** as off-white solid (89 % yield). **m.p.** >300 °C, **IR** (C=O) 1669.46 cm^{-1}, **^{1}H-NMR (400 MHz, DMSO-d_6): δ(ppm)** 10.67 (s, 2H, NH), 8. 61 (dd,2H, *J* =8.54 Hz, *J* =1.02 Hz, Ar-CH), 8.56 (dd, 2H, *J* = 7.30 Hz, *J* = 0.98 Hz, Ar-CH), 8.41 (d, 2H, *J* = 8.00 Hz, Ar-CH), 8.01 (d, 2H, *J* = 7.92 Hz, Ar-CH), 7.97 (dd, 2H, *J* = 8.42 Hz, *J* =7.46 Hz, Ar-CH), 2.35 (br.signal, 4H, CH_2), 1.67 (br.signal, 4H, CH_2). **^{13}C-NMR (100 MHz, DMSO-d_6): δ(ppm)** 171.4, 161.7, 161.4, 138,7. 132.8. 132.1, 131.3, 129.3, 129.2, 128.8, 128.4, 122.9, 121.6, 33.3, 24.9. **TOF MS ES+** calc for [$C_{30}H_{21}N_4O_6Cl_2$] 603.0838 found 603.0845.

Synthesis of 2,2'-(azanediylbis(propane-3,1-diyl))bis(6-chloro-1H-benzo[de]isoquinoline-1,3(2H)-dione) 3.8b

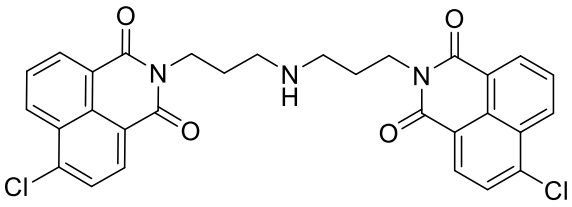

In a round-bottom flask, a suspension of 2.25 equivalents of 4-chloro-1,8-naphtalic anhydride (2.61 g, 11.25 mmol) in ethanol was placed. One equivalent of triethylamine Et_3N (0.36 g, 5 mmol) and one equivalent of bis(3-aminopropyl)amine (0.65 g, 5 mmol) were added. The reaction mixture was heated under reflux for 24 h, after that the resulting mixture was left to cool. The solid was filtered, washed with cold ethanol and dried in a oven (75 °C) to give pure 2,2'-(azanediylbis(propane-3,1-diyl))bis(6-chloro-1H-benzo[de]isoquinoline-1,3(2H)-dione) **3.8b** as yellow solid (96 % yield). **m.p.** 150-155 °C, **IR** (C=O) 1655.96 cm^{-1}, **^{1}H-NMR (400 MHz, $CDCl_3$-d): δ(ppm):** 8.52 (dd, 2H, *J* =7.30 Hz, *J* =1.00 Hz, Ar-CH), 8.46 (dd, 2H, *J* = 8.50 Hz, *J* = 1.06 Hz, Ar-CH), 8.35 (d, 2H, *J* =7.88 Hz, Ar-CH), 7.73 (dd, 2H, *J* = 8.40 Hz, *J* = 7.44 Hz, Ar-CH), 7.70 (d, 2H, *J* = 7.80 Hz, Ar-CH), 4.15 (t, 4H, *J*=7.16 Hz, CH_2), 2.65 (t, 4H, *J* = 6.54 Hz, CH_2), 1.87 (quint, 4H, *J* = 6.88 Hz, CH_2). **^{13}C-NMR (100 MHz, $CDCl_3$-d): δ (ppm):** 163.7, 163.4, 138.9, 132.0, 131.1, 130.5, 129.2, 129.0, 127.8, 127.3, 123.0, 121.5, 46.9, 38.4, 28.1. **HR TOF MS ES$^+$** calc for $[C_{30}H_{24}N_3O_4Cl_2]$ 560.1144 found 560.1157.

Synthesis of 2,2'-(1,4-phenylenebis(methylene))bis(6-chloro-1H-benzo[de]isoquinoline-1,3(2H)-dione) 3.8c

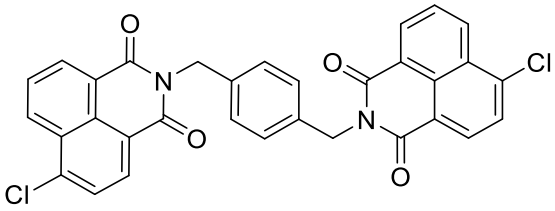

In a round-bottom flask, a suspension of 2.25 equivalents of 4-chloro-1,8-naphtalic anhydride (2.61 g, 11.25 mmol) in ethanol was placed, one equivalent of triethylamine Et_3N (0.36 g, 5 mmol) and one equivalent of p-xylylenediamine (0.67 g, 5 mmol) were added. The reaction mixture was heated under reflux for 24 h, after that the resulting mixture was left to cool. The solid was filtered, washed with cold ethanol and dried in an oven (75°C) to give pure 2,2'-(1,4-phenylenebis(methylene))bis(6-chloro-1H-benzo[de]isoquinoline-1,3(2H)-dione) **3.8c** as off-white solid (75 % yield). **m.p.** >300 °C, **IR** (C=O) 1661.75 cm^{-1}, **^{1}H-NMR (400 MHz, $CDCl_3$-d): δ(ppm):** 8. 65 (d, 2H, *J* = 7.12 Hz, Ar-CH), 8.60 (dd, 2H, *J* = 8.50Hz, *J* = 0.94 Hz, Ar-CH), 8.49 (d, 2H, *J* =7.72 Hz, Ar-CH), 7.84 (dd, 2H, *J* = 8.22 Hz, *J* = 7.17 Hz, Ar-CH), 7.82 (d, 2H, *J* = 7.56 Hz, Ar-CH), 7.50 (s,4H, Ar-CH), 5.33 (s, 4H, CH_2). **^{13}C-NMR (125 MHz,**

$CDCl_3$-d): δ(ppm): 163.7, 163.4, 139.2, 136.3, 132.2, 131.3, 130.8, 129.3, 129.1, 129.0, 127.8, 127.4, 123.0, 121.5, 43.3. **HR TOF MS ES+** calc for $[C_{32}H_{19}N_2O_4Cl_2]$ 565.0722 found 565.0729.

Synthesis of 2,2'-((ethane-1,2-diylbis(oxy))bis(ethane-2,1-diyl))bis(6-chloro-1H-benzo[de]isoquinoline-1,3(2H)-dione) 3.8d

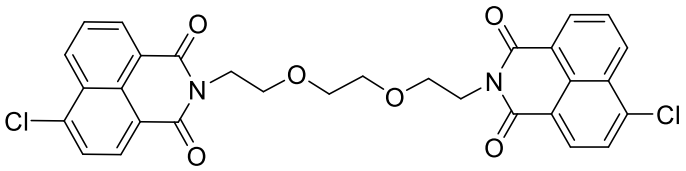

In a round-bottom flask, a suspension of 2.25 equivalents of 4-chloro-1,8-naphtalic anhydride (2.61 g, 11.25 mmol) in ethanol was placed, one equivalent of triethylamine Et_3N (0.36 g, 5 mmol) and one equivalent of 2,2'-(ethylenedioxy)diethylamine (0.74 g, 5 mmol) were added. The reaction mixture was heated under reflux for 24 h, after that the resulting mixture was left to cool. The solid was filtered, washed with cold ethanol and dried in an oven (75 °C) to give pure 2,2'-((ethane-1,2-diylbis(oxy))bis(ethane-2,1-diyl))bis(6-chloro-1H-benzo[de]isoquinoline-1,3(2H)-dione) **3.8d** as off-white solid (81 % yield). **m.p.** >205-209 °C, **IR** (C=O) 1655.96 cm^{-1}. **^{1}H-NMR (400 MHz, $CDCl_3$-d): δ(ppm):** 8.50 (dd, 2H, *J* =7.28 Hz, *J* =1.12 Hz, Ar-H), 8.43 (dd, 2H, *J* = 8.48 Hz, *J* =1.12 Hz, Ar-H), 8.35 (d, 2H, *J* =7.88 Hz, Ar-H), 7.71 (dd, 2H, *J* = 8.50 Hz, *J* = 7.34 Hz, Ar-H), 7.68 (d, 2H, *J* = 7.92 Hz, Ar-H), 4.27 (t, 4H, *J*=6.04 Hz, CH_2), 3.69 (t, 4H, *J* = 6.06 Hz, CH_2), 3.59 (s,4H, CH_2). **^{13}C-NMR (100 MHz, $CDCl_3$-d): δ(ppm):** 163.6, 163.4, 138.9, 131.9, 131.1, 130.5, 129.1, 129.0, 127.7, 127.3, 122.9, 121.4, 70.1, 67.8, 39.1. **HR TOF MS ES+** calc for $[C_{30}H_{22}N_2O_6Cl_2]$+Na 599.0753 found 599.0753.

Synthesis of 2,2'-(propane-1,3-diyl)bis(6-chloro-1H-benzo[de]isoquinoline-1,3(2H)-dione) 3.8e

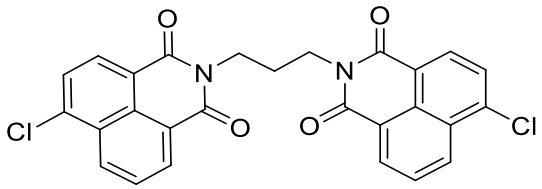

In a round-bottom flask, a suspension of 2.25 equivalents of 4-chloro-1,8-naphtalic anhydride (2.61 g, 11.25 mmol) in ethanol was placed. One equivalent of triethylamine Et_3N (0.36 g, 5 mmol) and one equivalent of 1,3-diaminopropane (0.37 g, 5 mmol) were added. The reaction mixture was heated under reflux for 24 h, after that the resulting mixture was left to cool. The solid was filtered, washed with cold ethanol and dried in an oven (75 °C) to give pure 2,2'-(propane-1,3-diyl)bis(6-chloro-1H-benzo[de]isoquinoline-1,3(2H)-dione) **3.8e** as off-white solid (98 % yield). **m.p.** >269-272 °C, **IR** (C=O) 1654.03 cm^{-1}. **^{1}H-NMR (400 MHz, $CDCl_3$-d): δ(ppm):** 8.54 (dd, 2H, *J* =7.32 Hz, *J* =1.04 Hz, Ar-CH), 8.51 (dd, 2H, *J* = 8.46 Hz, *J* =1.06 Hz, Ar-CH), 8.37 (d, 2H, *J* =7.92 Hz, Ar-CH), 7.75 (dd,

2H, *J* = 8.50 Hz, *J* = 7.50 Hz, Ar-CH), 7.72 (d, 2H, *J* = 7.96 Hz, Ar-CH), 4.27 (t, 4H, *J*=7.18, CH_2), 2.16 (quint, 2H, *J* = 7.09 Hz, CH_2). **^{13}C NMR (400 MHz, $CDCl_3$-d): δ(ppm):** 163.7, 163.4, 139.0, 132.0, 131.1, 130.6, 129.3, 129.1, 127.8, 127.3, 123.0, 121.5, 38.4, 26.8. **HR TOF MS ES+** calc for [$C_{27}H_{17}N_2O_4Cl_2$] 503.0565 found 503.0569.

Synthesis of 2-(2-hydroxyethyl)-6-((2-hydroxyethyl)amino)-1H-benzo[de]isoquinoline-1,3(2H)-dione 3.9

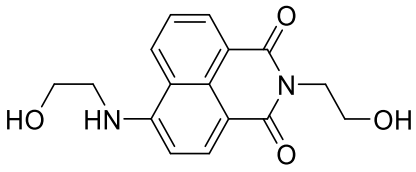

In a round-bottom flask, 0.60g of N^1,N^6-bis(6-chloro-1,3-dioxo-1H-benzo[de]isoquinolin-2(3H)-yl)adipamide **3.8a** (1 mmol) was dissolved in 10 ml ethanolamine and refluxed for 24 h under N_2. The solution was left to cool, and then 20 ml of DCM and 20 ml of water were added into separatory funnel. A yellow solid crashed out in the aqueous layer and this solid was vacuum filtered to give pure 2-(2-hydroxyethyl)-6-((2-hydroxyethyl)amino)-1H-benzo[de]isoquinoline-1,3(2H)-dione **3.9** as a yellow solid (96 % yield). **^{1}H-NMR (400 MHz, DMSO-d_6):δ(ppm):** 8.69 (dd, *J* =8.54 Hz, *J* = 1.06 Hz, 1H, Ar-CH), 8.43 (dd, *J* = 7.30 Hz, *J* = 0.90 Hz, 1H, Ar-CH), 8.26 (d, *J* = 8.56 Hz, 1H, Ar-CH), 7.72 (t, *J*=5.36,1H, N-H), 7.68 (dd, *J* = 8.32 Hz, *J* = 7.56 Hz, 1H, Ar-CH), 7.38 (d, *J* = 8.68 Hz, 1H, Ar-CH), 4.89 (t, *J*=5.60, 1H, N-H), 4.78 (t, *J*=5.86, 1H, O-H), 4.12 (t, *J* = 7.04 Hz, 2H, CH_2), 3.70 (q, *J* = 5.86 Hz, 2H, CH_2) 3.58 (q, *J* = 6.40 Hz, 2H, CH_2), 3.47 (q, *J* = 5.76 Hz, 2H, CH_2). **^{13}C-NMR (100 MHz, DMSO-d_6):δ(ppm):** 164.3, 163.5, 151.2, 134.6, 131.1, 129.9, 129.0, 124.7, 122.4, 120.6, 108.1, 104.3, 59.2, 58.4, 46.0, 41.8. **HR TOF MS ASAP+** calc for [$C_{16}H_{17}N_2O_4$] 301.1188 found 301.1189.

Synthesis of 2,2'-(azanediylbis(propane-3,1-diyl))bis(6-((2-hydroxyethyl)amino)-1H-benzo[de]isoquinoline-1,3(2H)-dione) 3.9b

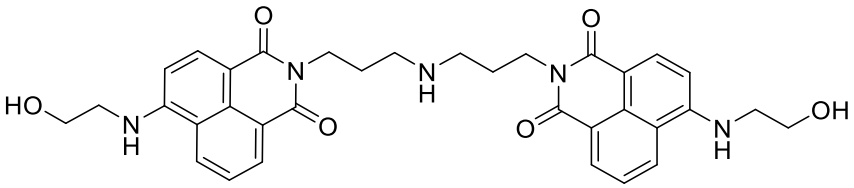

In a round-bottom flask, 0.56 g (1 mmol) of 2,2'-(azanediylbis(propane-3,1-diyl))bis(6-chloro-1H-benzo[de]isoquinoline-1,3(2H)-dione) **3.8b** was dissolved in 10 ml ethanolamine and refluxed for 24h under N_2. The solution was left to cool, and then 20 ml of DCM and 20 ml of water were added into separatory funnel. A yellow solid crashed out in the aqueous layer and this solid was vacuum filtered to give pure 2,2'-(azanediylbis(propane-3,1-diyl))bis(6-((2-hydroxyethyl)amino)-1H-benzo[de]isoquinoline-1,3(2H)-dione) **3.9b** as a yellow solid (41 % yield). **^{1}H-NMR (400 MHz, DMSO-d_6): δ(ppm):** 8. 69 (dd,2H, *J* = 8.72, Hz, *J* = 0.96 Hz), 8.42 (dd,

2H, *J* = 7.32 Hz, *J* = 0.96 Hz), 8.25(d, 2H, *J*=8.64), 7.71 (t, 2H, *J* = 7.92 Hz), 7.67 (dd, 2H, *J* = 8.32 Hz, *J* = 7.44 Hz), 6.81 (d, 2H, *J* = 8.84 Hz), 4.88 (t, 2H, *J* = 5.04 Hz), 4.05 (t, 2H, *J* = 6.92 Hz), 3.70 (q, 4H, J=5.92), 3.47 (q, 4H, *J*=5.72), 3.47 (quint,4H, J=7.32).

Synthesis of 2,2'-(1,4-phenylenebis(methylene))bis(6-((2-hydroxyethyl)amino)-1H-benzo[de]isoquinoline-1,3(2H)-dione) 3.9c

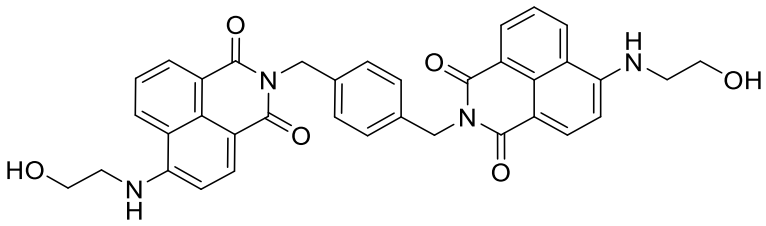

In a round-bottom flask, 0.11 g of 2,2'-(1,4-phenylenebis(methylene))bis(6-chloro-1H-benzo[de]isoquinoline-1,3(2H)-dione) **3.8c** (0.2 mmol) was dissolved in 10 ml ethanolamine and refluxed for 24 h under N_2. The solution was left to cool, and then 20 ml of DCM and 20 ml of water were added into separatory funnel. A yellow solid crashed out in the aqueous layer and this solid was vacuum filtered to give 2,2'-(1,4-phenylenebis(methylene))bis(6-((2-hydroxyethyl)amino)-1H-benzo[de]isoquinoline-1,3(2H)-dione) **3.9c** as a yellow solid (46 % yield). **^{1}H-NMR (400 MHz, DMSO-d_6): δ(ppm):** 8. 71 (d,2H, *J* = 8.8, Hz), 8.42 (d, 2H, *J* = 7.04 Hz, *J* = 0.96 Hz), 8.26(d, 2H, *J*=8.8), 7.77 (br.s, 2H), 7.68 (t, 2H, *J* = 7.72 Hz), 7.25(s, 4H), 6.82 (d, 2H, *J*=9.24), 5.17 (s, 4H, CH_2), 4.88 (t, 2H), 3.71 (q, 4H, *J*=5.4), 3.47 (q, 4H, *J*=5.44).

Synthesis of 2,2'-((ethane-1,2-diylbis(oxy))bis(ethane-2,1-diyl))bis(6-((2-hydroxyethyl)amino)-1H-benzo[de]isoquinoline-1,3(2H)-dione) 3.9d

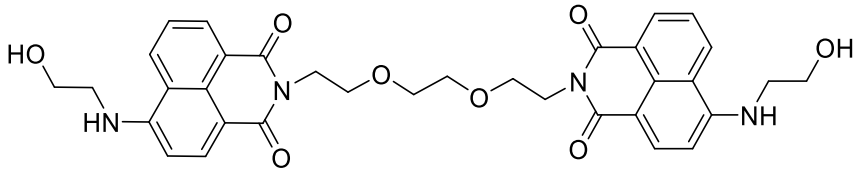

In a round-bottom flask, 0.12 g (0.2 mmol) of 2,2'-((ethane-1,2-diylbis(oxy))bis(ethane-2,1-diyl))bis(6-chloro-1H-benzo[de]isoquinoline-1,3(2H)-dione) **3.8d** was dissolved in 10 ml ethanolamine and refluxed for 24 h under N_2. The solution was left to cool, and then 20 ml of DCM and 20 ml of water were added into separatory funnel. A yellow solid crashed out in the aqueous layer and this solid was vacuum filtered to 2,2'-((ethane-1,2-diylbis(oxy))bis(ethane-2,1-diyl))bis(6-((2-hydroxyethyl)amino)-1H-benzo[de]isoquinoline-1,3(2H)-dione) **3.9d** as a yellow solid (Yield 34 %). The compound was purified using column chromatography over silica (chloroform: ethanol 9:1) (R_f=0.2). **^{1}H-NMR (400 MHz, $CDCl_3$-d): δ(ppm):** 8.38 (dd, *J* = 7.32 Hz, *J* = 1.04 Hz, 2H, Ar-CH), 8.36 (dd,

J = 8.66 Hz, J=0.94 Hz, 2H, Ar-CH), 8.22 (d, *J* = 7.92 Hz, 2H, Ar-CH), 7.74 (dd, *J* = 8.40 Hz, *J* = 7.36 Hz, 2H, Ar-CH), 7.63 (d, *J* = 8.04 Hz, 2H, Ar-CH), 5.14 (t, *J*=5.50, 2H, OH), 4.10 (t, *J* = 6.24 Hz, 4H, CH_2), 3.73 (q, *J* = 5.98 Hz, 4H, CH_2), 3.59 (t, *J* = 6.30 Hz, 4H, CH_2), 3.54 (s, ,CH2), 3.28 (t, *J* = 6.44 Hz, 4H, CH_2). **^{13}C-NMR (100 MHz, $CDCl_3$-d): δ (ppm):** 163.5, 163.4, 145.1, 131.3, 130.8, 129.9, 128.9, 127.8, 127.4, 122.9, 122.8, 118.5, 70.0, 67.3, 59.5, 39.1, 34.5. **HR TOF MS ES+** calc for [$C_{34}H_{33}N_2O_8S_2$] 661.1678 found 661.1691.

Synthesis of 2,2'-(propane-1,3-diyl)bis(6-((2-hydroxyethyl)amino)-1H-benzo[de]isoquinoline-1,3(2H)-dione) 3.9e

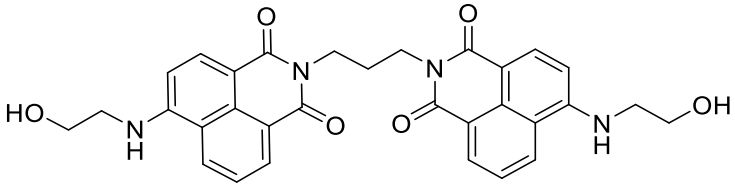

In a round-bottom flask, (0.1 g, 0.2 mmol) of 2,2'-(propane-1,3-diyl)bis(6-chloro-1H-benzo[de]isoquinoline-1,3(2H)-dione) **3.8e** was dissolved in 10 ml ethanolamine and refluxed for 24h under N_2. The solution was left to cool, and then 20 ml of DCM and 20 ml of water were added into separatory funnel. A yellow solid crashed out in the aqueous layer and this solid was vacuum filtered to give 2,2'-(propane-1,3-diyl)bis(6-((2-hydroxyethyl)amino)-1H-benzo[de]isoquinoline-1,3(2H)-dione) **3.9e** as a yellow solid (Yield= 51 %). **^{1}H-NMR (400 MHz, DMSO-d_6): δ (ppm):** 8.69 (dd, *J* =8.56 Hz, *J* = 0.84 Hz, 2H, Ar-CH), 8.40 (dd, *J* = 7.24 Hz, *J* = 1.00 Hz, 2H, Ar-CH), 8.22 (d, *J* = 8.56 Hz, 2H, Ar-CH), 7.76 (t, *J*=5.54,2H, N-H), 7.67 (dd, *J* = 8.30 Hz, *J* = 7.50 Hz, 2H, Ar-CH), 6.80 (d, *J* = 8.56 Hz, 2H, Ar-CH), 4.90 (t, *J*=5.42, 2H, N-H), 4.09 (t, *J* = 7.12 Hz, 4H, CH_2), 3.69 (q, *J* = 5.52 Hz, 4H, CH_2) 3.47 (q, *J* = 5.52 Hz, 4H, CH_2), 1.97 (quint, *J* = 5.52 Hz, 2H, CH_2). **HR TOF MS ES+** calc for [$C_{31}H_{29}N_4O_6$] 553.2087 found 553.2087.

Synthesis of 6-morpholino-1H,3H-benzo[de]isochromene-1,3-dione 3.10

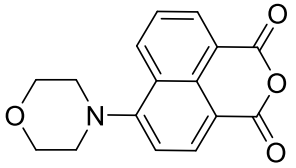

In a round-bottom flask, one equivalent of 4-chloro-1,8-naphthalic anhydride (2.32 g, 10 mmol) was dissolved in DMF with two equivalents of morpholine (1.74 g, 20 mmol) and heated to 100 °C for 24 h. After the reaction was completed, the solvent was evaporated, and methanol was added to obtain 6-morpholino-1H,3H-benzo[de]isochromene-1,3-dione **3.10** as a yellow powder that was filtered and recrystallized from methanol (45 % yield). **^{1}H-NMR (400 MHz, DMSO-d_6): δ(ppm):** 8.55 (dd, *J* =8.48 Hz, *J* = 0.96 Hz, 1H, Ar-CH), 8.50 (dd, *J* = 7.24 Hz, *J* = 0.96 Hz, 1H, Ar-CH), 8.43 (d, *J* = 8.12 Hz, 1H, Ar-CH), 7.85 (dd, *J* = 8.42 Hz, *J* = 7.38 Hz, 1H, Ar-CH), 7.38 (d, *J* =

8.20 Hz, 1H, Ar-CH), 3.92 (t, *J* = 4.50 Hz, 4H), 3.28 (t, *J* = 4.50 Hz, 4H). **^{13}C-NMR (100 MHz, DMSO-d_6): δ (ppm):** 161.6, 160.8, 156.8, 134.6, 133.0, 132.3, 132.1, 126.8, 125.6, 119.8, 115.7, 112.1, 66.5, 53.3. **HR TOF MS ASAP+** calc for [$C_{16}H_{14}NO_4$] 284.0923 found 284.0924.

Synthesis of N^1,N^6-bis(6-morpholino-1,3-dioxo-1H-benzo[de]isoquinolin-2(3H)-yl)adipamide 3.10a

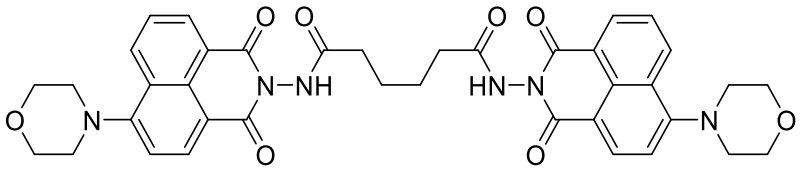

In a round-bottom flask, one equivalent of N^1,N^6-bis(6-chloro-1,3-dioxo-1H-benzo[de]isoquinolin-2(3H)-yl)adipamide **3.8a** (0.603 g, 1 mmol) was dissolved in 50 ml DMF with 10 eq of morpholine (0.87g, 10 mmol) and heated to 100 °C for 24 h. After cooling to room temperature, the solvent was removed under vacuum to obtain highly viscus oil. Then methanol was added to allow N^1,N^6-bis(6-morpholino-1,3-dioxo-1H-benzo[de]isoquinolin-2(3H)-yl)adipamide **3.10a** to precipitate as yellow solid (73 % yield). **^{1}H-NMR (400 MHz, $CDCl_3$-d): δ (ppm):** 9.34 (s, 2H, NH), 8. 50 (d,2H, *J* = 7.20 Hz, Ar-CH), 8.44 (d, 2H, *J* = 8.16 Hz, Ar-CH), 8.33 (d, 2H, *J* = 8.44 Hz, Ar-CH), 7.59 (t, 2H, *J* = 7.84 Hz, Ar-CH), 7.11 (d, 2H, *J* = 8.16 Hz, Ar-CH), 3.92 (t, 8H, CH_2, *J* = 4.40 Hz, morpholine), 3.16 (br.s, 8H,CH_2, morpholine), 2.65 (br.s, 4H, CH_2), 2.02 (br.s, 4H, CH_2). **^{13}C-NMR (100 MHz, $CDCl_3$-d): δ (ppm):** 171.8, 156.4, 156.1, 133.7, 132.2, 131.0, 130.4, 130.0, 126.1, 125.8, 122.8, 116.3, 114.9, 66.8, 53.4, 34.0, 23.7. **HR TOF MS ES+** calc for [$C_{38}H_{37}N_6O_8$] 705.2673 found 705.2672.

Synthesis of 2,2'-(azanediylbis(propane-3,1-diyl))bis(6-morpholino-1H-benzo[de]isoquinoline-1,3(2H)-dione) 3.10b

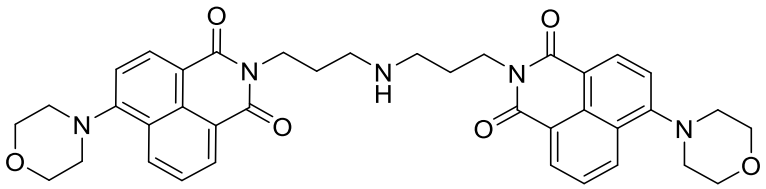

In a round-bottom flask, 2.15 equivalents of 6-morpholino-1H,3H-benzo[de]isochromene-1,3-dione **3.10** (0.61 g, 2.15 mmol) and one equivalent of bis(3-aminopropyl)amine (1 mmol, 0.13 g) were dissolved in ethanol with ≈ 5 drops of Et_3N and the resulting mixture was heated to reflux for 24 h. After that the solvent was removed and cold ethanol was added which allow 2,2'-(azanediylbis(propane-3,1-diyl))bis(6-morpholino-1H-benzo[de]isoquinoline-1,3(2H)-dione) **3.10b** to precipitate as yellow solid in 32 % yield. **^{1}H-NMR (400 MHz, $CDCl_3$-d): δ (ppm):** 8. 59 (dd,2H, *J* = 7.28, *J* = 1.20 Hz, Ar-CH), 8.04 (d, 2H, *J* = 8.04 Hz, Ar-CH), 8.43 (dd, 2H, *J* = 8.46, *J*=1.22 Hz, Ar-CH), 7.71 (dd, 2H, *J* = 8.44, *J*=7.28 Hz, Ar-CH), 7.24 (d, 2H, *J* = 8.08 Hz, Ar-CH), 4.26 (t, 4H, *J*=7.02, CH_2), 4.03(t, 8H, *J*=4.54 Hz,

CH_2, morpholine), 3.27 (t, *J*=4.56, 8H, CH_2, morpholine), 2.72 (t, *J*=6.92, 4H,CH_2), 1.95 (quint, *J*=6.98, 4H,CH_2). **^{13}C-NMR (100 MHz, $CDCl_3$-d): δ ν(ppm):** 164.5, 164.0, 155.6, 132.6, 131.2, 130.0, 129.9, 126.1, 125.9, 117.2, 115.0, 67.0, 53.5, 47.1, 38.3, 28.5. **LR TOF MS ES+** 662.30 (100%), **HR TOF MS ES+** calc for [$C_{38}H_{40}N_5O_6$] 662.2979 found 662.3005.

Synthesis of 2,2'-(1,4-phenylenebis(methylene))bis(6-morpholino-1H-benzo[de]isoquinoline-1,3(2H)-dione) 3.10c

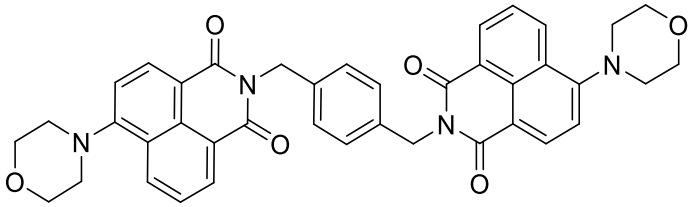

In a round-bottom flask, one equivalent of the 2,2'-(1,4-phenylenebis(methylene))bis(6-chloro-1H-benzo[de]isoquinoline-1,3(2H)-dione) **3.8c** (1 mmol, 0.56 g) was dissolved in 50 ml DMF with 10 eq of morpholine (0.87g, 10 mmol) and heated to 100 °C for 24 h. After cooling to RT, the solvent was removed under vacuum. Then methanol were added to allow 2,2'-(1,4-phenylenebis(methylene))bis(6-morpholino-1H-benzo[de]isoquinoline-1,3(2H)-dione) **3.10c** to precipitate as a yellow powder (80 % yield). **^{1}H-NMR (400 MHz, $CDCl_3$-d): δ (ppm):** 8.50 (d, *J* = 8.04 Hz, 2H, Ar-CH), 8.47 (d, *J* = 8.04 Hz, 2H, Ar-CH), 8.41 (d, *J*=8.40, 2H,Ar-CH), 7.80 (t, *J*=7.94, 2H, Ar-CH), 7.34 (d, *J* = 8.28 Hz, 2H, Ar-CH), 7.27(s, 4H, Ar-CH), 5.19 (s, 4H, CH_2), 3.90 (t, *J*=4.18, 8H, CH_2), 3.32 (t, 3.70, *J*=3.70, 8H, CH_2). **HR TOF MS ES+** calc for [$C_{40}H_{35}N_4O_6$] 667.2557 found 667.2561.

Synthesis of 2,2'-((ethane-1,2-diylbis(oxy))bis(ethane-2,1-diyl))bis(6-morpholino-1H-benzo[de]isoquinoline-1,3(2H)-dione) 3.10d

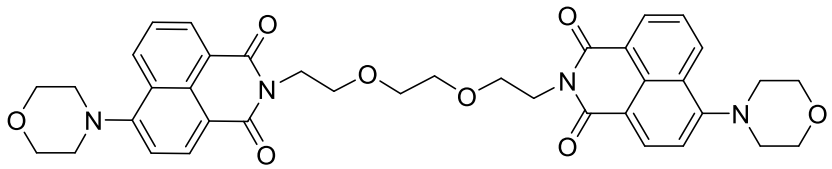

In a round-bottom flask, one equivalent 2,2'-((ethane-1,2-diylbis(oxy))bis(ethane-2,1-diyl))bis(6-chloro-1H-benzo[de]isoquinoline-1,3(2H)-dione) **3.8d** (1 mmol, 0.57 g) was dissolved in 50 ml DMF with 10 equivalents of morpholine (0.87g, 10 mmol) and heated to 100 °C for 24 h. After cooling to RT, the solvent was removed under vacuum. Then methanol were added to allow 2,2'-((ethane-1,2-diylbis(oxy))bis(ethane-2,1-diyl))bis(6-morpholino-1H-benzo[de]isoquinoline-1,3(2H)-dione) **3.10d** to precipitate as a yellow powder (67 % yield). **^{1}H-NMR (400 MHz, $CDCl_3$-d): δ (ppm):** 8.58 (d, 2H, *J* =7.20 Hz, Ar-CH), 8.52 (d, 2H, *J* = 8.00 Hz, Ar-CH), 8.41 (d, 2H, *J*

=8.40 Hz, Ar-CH), 7.70 (t, 2H, *J* = 7.86 Hz, Ar-CH), 7.23 (d, 2H, *J* = 8.08 Hz, Ar-CH), 4.38 (t, 4H, *J*=6.12 Hz, CH_2), 4.03 (t,8H, *J*=4.30 Hz, CH_2), 3.77 (t, 4H, *J*=6.04 Hz, CH_2), 3.68 (s, 4H, CH_2), 3.27 (t, 8H, *J*=4.10 Hz, CH_2). **^{13}C-NMR (100 MHz, $CDCl_3$-d): δ(ppm):** 164.39, 163.92, 155.56, 132.55, 131.21, 130.02, 129.93, 126.13, 125.82, 123.31, 117.19, 114.94, 70.12, 67.94, 66.99, 53.44, 38.93. **HR TOF MS ASAP+** calc for [$C_{38}H_{39}N_4O_8$] 679.2768 found 679.2767.

Synthesis of 2,2'-(propane-1,3-diyl)bis(6-morpholino-1H-benzo[de]isoquinoline-1,3(2H)-dione) 3.10e

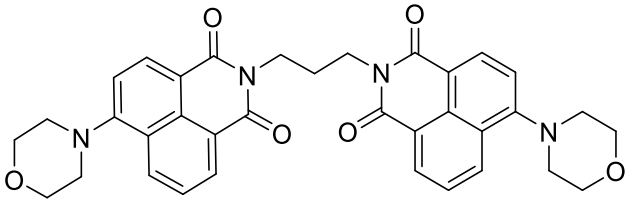

In a round-bottom flask, one equivalent of 2,2'-(propane-1,3-diyl)bis(6-chloro-1H-benzo[de]isoquinoline-1,3(2H)-dione) **3.8e** (1 mmol, 0.50 g) was dissolved in 50 ml DMF with 10 eq of morpholine (0.87g, 10 mmol) and heated to 100 °C for 24 h. After cooling to RT, the solvent was removed under vacuum. Then methanol were added to allow 2,2'-(propane-1,3-diyl)bis(6-morpholino-1H-benzo[de]isoquinoline-1,3(2H)-dione) **3.10e** to precipitate as yellow solid (83 % yield). **^{1}H-NMR (400 MHz, $CDCl_3$-d): δ (ppm):** 8.58 (d,2H, *J* = 7.28, Hz, Ar-CH), 8.52 (d, 2H, *J*=8.08 Hz, Ar-CH), 8.43(d, 2H, *J*=8.44, Ar-CH), 7.70(t, *J*=7.80, 2H, Ar-CH), 7.23 (t, 2H, *J* = 8.00 Hz, Ar-CH), 4.36 (t, J= 7.12, 4H, CH_2), 4.04 (t, 8H, *J*= 4.28, CH_2), 3.28 (t, *J*=4.30 Hz, 8H, CH_2), 2.23 (quint, J=7.04, 2H, CH_2). **HR TOF MS ASAP+** calc for [$C_{35}H_{33}N_4O_6$] 605.2400 found 605.2402.

Synthesis of 6-(4-acetylpiperazin-1-yl)-1H,3H-benzo[de]isochromene-1,3-dione 3.11:

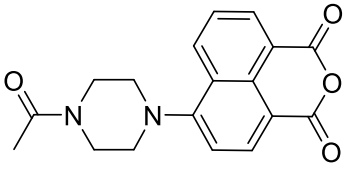

In a round-bottom flask, one equivalent of 4-chloro-1,8-naphthalic anhydride (10 mmol, 2.32 g) and one equivalent of 1-acetyl piperazine (10 mmol, 1.28 g) were dissolved in DMF and heated to 100 °C for 24h. After the reaction completed, the solvent was evaporated, and methanol was added to obtain 6-(4-acetylpiperazin-1-yl)-1H,3H-benzo[de]isochromene-1,3-dione **3.11** as yellow powder that filtered and crystalized in methanol (68 %). **^{1}H-NMR (400 MHz, DMSO-d_6): δ(ppm):** 8.55 (d, 2H, *J* =8.32 Hz, Ar-CH), 8.50 (d, 2H, *J* = 7.24 Hz, Ar-CH), 8.41 (d, 2H, *J* =7.72 Hz, Ar-CH), 7.85 (t, 2H, *J* = 8.26 Hz, Ar-CH), 7.36 (d, 2H, *J* = 8.76 Hz, Ar-CH), 3.77 (br.s, 4H, CH_2), 3.30 (br.s, 2H, CH_2), 3.23 (br.s, 2H, CH_2), 2.08 (s, 3H, CH_3). **^{13}C-NMR (100 MHz, DMSO-d_6): δ(ppm):** 169.0, 161.6, 160.8, 156.7, 134.6, 133.0, 132.3, 132.1, 126.9, 125.7, 119.9, 116.0, 112.3, 53.0, 52.8, 46.1, 41.3, 21.8.

Synthesis of 2,2'-((ethane-1,2-diylbis(oxy))bis(ethane-2,1-diyl))bis(6-(4-acetylpiperazin-1-yl)-1H-benzo[de]isoquinoline-1,3(2H)-dione) 3.11d

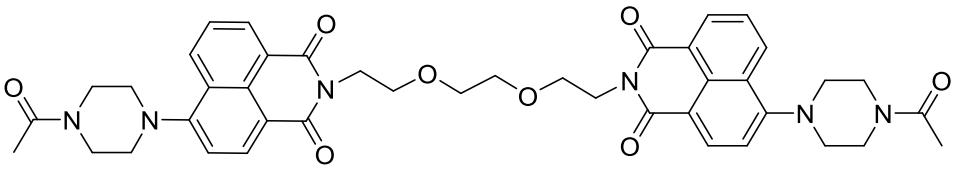

In a round-bottom flask, one equivalent of 2,2'-((ethane-1,2-diylbis(oxy))bis(ethane-2,1-diyl))bis(6-chloro-1H-benzo[de]isoquinoline-1,3(2H)-dione) **3.8d** (0.57 g, 1 mmol) was dissolved in DMF with 10 eq of 1-acetyl piperazine (1.28 g, 10 mmol) and heated to 100 °C for 72h. Then the solvent was removed under vacuum, and methanol was added to obtain a yellow powder which was purified with column chromatography over silica (chloroform: ethanol 9:1) (45 %). The product was mixture of symmetric (R_f=0.5) and asymmetric (R_f=0.55) dimer. The NMR for symmetric dimer is following **^{1}H-NMR (500 MHz, DMSO-d_6): δ(ppm):** 8.49 (dd, 2H, *J* =7.22 Hz, *J* = 0.87 Hz Ar-CH), 8.42 (d, 2H, *J* = 8.00 Hz, Ar-CH), 8.32 (dd, 2H, *J* = 8.40Hz, *J*=0.90 Hz, Ar-CH), 7.63 (dd, 2H, *J* = 8.30, *J*= 7.40 Hz, Ar-CH), 7.12 (d, 2H, *J* = 8.05 Hz, Ar-CH), 4.27(t, *J*=6.17, 4H, CH_2), 3.85 (br.s, 4H, CH_2), 3.71 (br.s, 4H, CH_2), 3.67(t, *J*=6.17, 4H, CH_2), 3.58 (s, 4H, CH_2), 3.15 (br.s, 8H, CH_2), 2.12 (s, 6H, CH_3). **^{13}C-NMR (125 MHz, DMSO-d_6): δ(ppm):** 169.2, 164.3, 163.8, 155.0, 132.3, 131.2, 129.8, 129.7, 126.2, 126.0, 123.3, 117.6, 115.3, 70.1, 67.9, 52.9(2C), 46.4, 41.5, 38.9, 21.4. **HR TOF MS ES+** calc for[$C_{42}H_{45}N_6O_8$] 761.3299 found 761.3333.

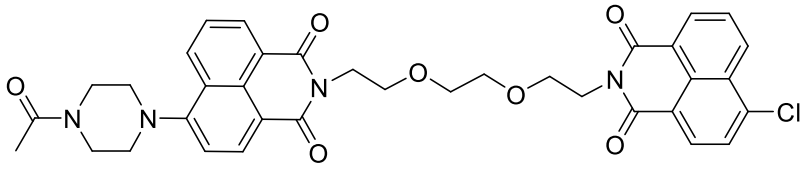

The NMR for asymmetric dimer **^{1}H-NMR (500 MHz, DMSO-d_6): δ(ppm):** 8.50 (dd, 1H, *J* =7.32 Hz, *J* = 1.12 Hz Ar-CH), 8.48 (dd, 1H, *J* =7.32 Hz, *J* = 1.12 Hz Ar-CH), 8.43 (d, 1H, *J* = 9.00 Hz, Ar-CH), 8.43 (d, 1H, *J* = 7.90 Hz, Ar-CH), 8.39 (d, 1H, *J* = 8.15 Hz, Ar-CH), 8.32 (dd, 1H, *J* = 8.42Hz, *J*=0.97 Hz, Ar-CH), 7.63 (dd, 1H, *J* = 8.25, *J*= 7.40 Hz, Ar-CH), 7.59 (dd, 1H, *J* = 8.35, *J*= 7.35 Hz, Ar-CH), 7.13 (d, 1H, *J* = 8.00 Hz, Ar-CH), 7.09 (d, 1H, *J* = 8.20 Hz, Ar-CH), 4.29 (t, *J*=6.05, 2H, CH_2), 4.27(t, *J*=6.00, 2H, CH_2), 3.85 (br.s, 2H, CH_2), 3.71 (br.s, 2H, CH_2), 3.69(t, *J*=5.60, 2H, CH_2), 3.67 (t, *J*=6.00, 2H, CH_2), 3.59 (s, 2H, CH_2), 3.17 (br.s, 2H, CH_2), 3.13 (br.s, 2H, CH_2), 3.05 (s, 2H, CH_2), 2.12 (s, 3H, CH_3). **HR TOF MS ES+** calc for [$C_{36}H_{34}N_4O_7Cl$] calc 669.2116 found 669.2131

Synthesis of 2,2'-(propane-1,3-diyl)bis(6-(4-acetylpiperazin-1-yl)-1H-benzo[de]isoquinoline-1,3(2H)-dione) 3.11e

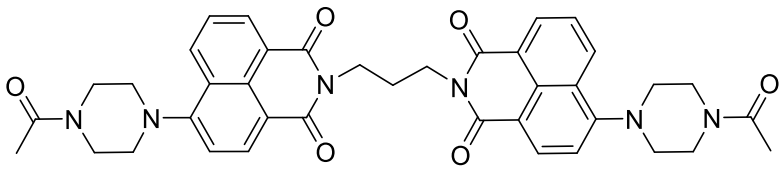

In a round-bottom flask, one equivalent of 2,2'-(propane-1,3-diyl)bis(6-chloro-1H-benzo[de]isoquinoline-1,3(2H)-dione) **3.8e** (0.52 g, 1 mmol) was dissolved in DMF with ten equivalents of 1-acetyl piperazine (1.28 g, 10 mmol) and heated to 100 °C for 72 h. Then the solvent was removed under vacuum, and methanol was added to obtain a yellow powder which was purified with column chromatography over silica (chloroform: ethanol 9:1) (80 %). The product was mixture of symmetric (R_f=0.3) and asymmetric (R_f=0.4) dimer. The NMR for symmetric dimer is following **^{1}H-NMR (500 MHz, DMSO-d_6): δ(ppm):** 8.49 (dd, 2H, *J* =7.32 Hz, *J* = 1.12 Hz Ar-CH), 8.43 (d, 2H, *J* = 8.05 Hz, Ar-CH), 8.34 (dd, 2H, *J* = 8.47Hz, *J*=1.22 Hz, Ar-CH), 7.65 (dd, 2H, *J* = 8.40, *J*= 7.35 Hz, Ar-CH), 7.14 (d, 2H, *J* = 8.15 Hz, Ar-CH), 4.26(t, *J*=7.22, 4H, CH_2), 3.87 (br.s, 4H, CH_2), 3.72 (br.s, 4H, CH_2), 3.19 (s, 4H, CH_2), 3.15 (br.s, 4H, CH_2), 2.12 (s, 6H, CH_3), 2.12(quin, 2H, *J*=7.95, CH_2). **^{13}C-NMR (125 MHz, DMSO-d_6): δ(ppm):** 169.4, 164.3, 163.9, 155.1, 132.4, 131.3, 129.8, 129.8, 126.2, 126.1, 123.3, 117.5, 115.4, 53.0, 52.9, 46.4, 41.6, 38.3, 27.1, 21.4. **HR TOF MS ES+** calc for [$C_{39}H_{39}N_6O_6$] 687.2931 found 687.2960.

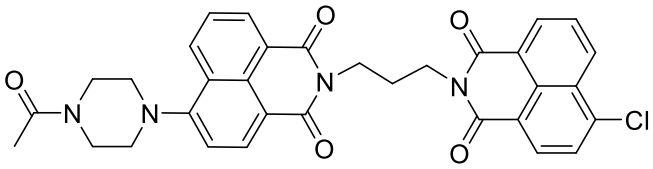

The NMR for asymmetric dimer **^{1}H-NMR (500 MHz, DMSO-d_6): δ(ppm):** 8.50 (dd, 1H, *J* =7.25 Hz, *J* = 0.95 Hz, Ar-CH), 8.46 (dd, 2H, *J* = 7.22 Hz, *J*=1.27 Hz, Ar-CH),), 8.41 (d, 1H, *J* = 8.05 Hz, Ar-CH), 8.37 (d, 1H, *J* = 8.30 Hz, Ar-CH), 8.37 (d, 1H, *J*=7.40, Ar-CH), 8.34 (dd, 1H, *J* = 8.42 Hz, *J*=1.27 Hz, Ar-CH), 7.64 (dd, 2H, *J* = 8.40, *J*= 7.35 Hz, Ar-CH), 7.57 (dd, 2H, *J* = 8.47 Hz, *J*= 7.42, Ar-CH), 7.13 (d, 1H, *J* = 8.05 Hz, Ar-CH), 7.03 (d, 1H, *J*=8.35, Ar-CH), 4.27 (t, *J*=6.87, 2H, CH_2), 4.26 (d, 2H, J=6.72, CH_2), 3.87 (br.s, 2H, CH_2), 3.72 (t, *J*=4.65, 2H, CH_2), 3.18 (br.s, 2H, CH_2), 3.14 (br.s, 2H, CH_2), 2.12 (s, 3H, CH_3), 1.59(br.s, 2H, CH_2). **^{13}C-NMR (500 MHz, DMSO-d_6): δ(ppm):** 169.2, 164.6, 164.3, 164.0, 163.8, 155.0, 133.9, 132.6, 132.4, 131.3, 131.1, 131.1, 130.2, 129.8, 129.7, 126.2, 126.1, 125.3, 124.9, 123.3, 123.0, 117.6, 115.3, 115.1, 113.4, 53.0, 52.9, 46.4, 41.5, 38.4, 38.2, 27.1, 21.5. **HR TOF MS ES+** calc for [$C_{33}H_{29}N_4O_5$] 561.2138 found 561.2129.

Synthesis of 6-((2-hydroxyethyl)thio)-1H,3H-benzo[de]isochromene-1,3-dione (3.12):

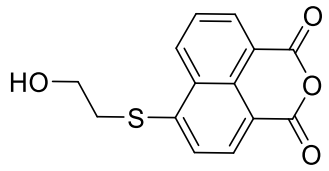

In a round-bottom flask, one equivalent of 4-chloro-1,8-naphtalic anhydride (50 mmol, 11.6 g) and 1.5 equivalents of 2-mercaptoethanol (75 mmol, 5.85) in addition to 2 equivalents of sodium bicarbonate (100 mmol, 8.4 g) were dissolved in 2-methoxy ethanol. The reaction mixture was heated to reflux for 6 h. The solution was cooled down to ambient temperature, yielding 6-((2-hydroxyethyl)thio)-1H,3H-benzo[de]isochromene-1,3-dione **3.12** as yellow precipitate, which was filtered and washed with ethanol (Yield 94 %). **^{1}H-NMR (400 MHz, $CDCl_3$): δ(ppm):** 8.63 (dd, *J* = 8.48 Hz, *J* = 0.72 Hz, 1H), 8.55 (d, *J* = 7.28 Hz, 1H), 8.39 (d, *J* = 8 Hz, 1H), 7.92 (dd, *J* = 8.4 Hz, *J* = 7.44 Hz, 1H), 7.83 (d, *J* = 8 Hz, 1H), 5.20 (s,1H, OH), 3.76 (t, *J* = 6.32 Hz, 2H, CH_2), 3.40 (t, *J* = 6.32 Hz, 2H, CH_2). **^{13}C-NMR (100 MHz, $CDCl_3$): δ (ppm):** 161.2, 161.0, 147.0, 133.2, 132.6, 131.1, 130.3, 129.1, 128.0, 123.2, 120.1, 115.2, 59.4, 34.5. **HR TOF MS ES+** calc for [$C_{14}H_{11}O_4S$] 275.0378 found 275.0372.

Synthesis of 2,2'-(azanediylbis(propane-3,1-diyl))bis(6-((2-hydroxyethyl)thio)-1H-benzo[de]isoquinoline-1,3(2H)-dione) 3.12b

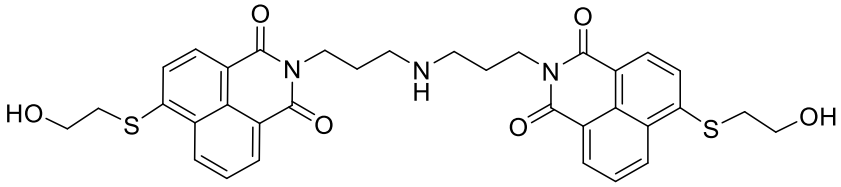

In a round-bottom flask, one equivalent of 2,2'-(azanediylbis(propane-3,1-diyl))bis(6-chloro-1H-benzo[de]isoquinoline-1,3(2H)-dione) **3.8b** (0.56 g, 1 mmol,) and ten equivalents of 2-mercaptoethanol (10 mmol, 0.78 g) in addition to ten equivalents of sodium bicarbonate (0.84 g, 10 mmol) were dissolved in ≈50 mL DMF. The reaction mixture was heated at 100 °C for 6 h. The solution was cooled down to room temperature and a yellow precipitate formed, which was filtered and washed with ethanol to yield 2,2'-(azanediylbis(propane-3,1-diyl))bis(6-((2-hydroxyethyl)thio)-1H-benzo[de]isoquinoline-1,3(2H)-dione) **3.12b** in 79 %. **^{1}H-NMR (400 MHz, $CDCl_3$-d): δ (ppm):** 8.85 (dd, *J* = 8.55 Hz, *J* = 0.95 Hz, 2H, Ar-CH), 8.50 (dd, *J* = 7.42, *J* = 1.12 Hz, 2H, Ar-CH), 8.34 (d, *J* = 7.95 Hz, 2H, Ar-CH), 7.89 (dd, *J* = 8.65 Hz, *J* = 7.40 Hz, 2H, Ar-CH), 7.80 (d, *J* = 8.10 Hz, 2H, Ar-CH), 4.09 (t, *J* = 6.50 Hz, 4H, CH_2), 3.75 (t, *J* = 6.50 Hz, 4H, CH_2), 3.37 (t, *J* = 6.05 Hz, 4H, CH_2). 2.99 (br signal, 4H, CH_2), 2.00 (quin, *J* = 7.15 Hz, 4H, CH_2).**^{13}C-NMR (125 MHz, DMSO-d_6): δ(ppm):** 163.9, 163.9, 145.3, 131.5, 130.9, 130.2, 129.2, 128.1, 127.7, 123.3, 123.2, 118.8, 59.5, 45.0, 37.4, 34.6, 25.0.

Synthesis of 2,2'-((ethane-1,2-diylbis(oxy))bis(ethane-2,1-diyl))bis(6-((2-hydroxyethyl)thio)-1H-benzo[de]isoquinoline-1,3(2H)-dione) 3.12d

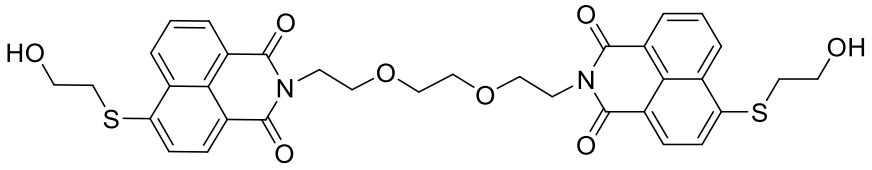

In a round-bottom flask, one equivalent of 2,2'-(azanediylbis(propane-3,1-diyl))bis(6-chloro-1H-benzo[de]isoquinoline-1,3(2H)-dione) **3.8d** (1 mmol, 0.56 g) and ten equivalents of 2-mercaptoethanol (10 mmol, 0.78) in addition to ten equivalents of sodium bicarbonate (10 mmol, 0.84 g) were dissolved in ≈50 mL DMF. The reaction mixture was heated at 100 °C for 6 h. The solution was cooled down to ambient temperature resulting in formation of 2,2'-((ethane-1,2-diylbis(oxy))bis(ethane-2,1-diyl))bis(6-((2-hydroxyethyl)thio)-1H-benzo[de]isoquinoline-1,3(2H)-dione) **3.12d** as yellow precipitate, which was filtered and washed with ethanol Yield (65 %). **^{1}H-NMR (400 MHz, $CDCl_3$-d): δ (ppm):** 8.38 (dd, *J* = 7.32 Hz, *J* = 1.04 Hz, 2H, Ar-CH), 8.36 (dd, *J* = 8.66 Hz, J=0.94 Hz, 2H, Ar-CH), 8.22 (d, *J* = 7.92 Hz, 2H, Ar-CH), 7.74 (dd, *J* = 8.40 Hz, *J* = 7.36 Hz, 2H, Ar-CH), 7.63 (d, *J* = 8.04 Hz, 2H, Ar-CH), 5.14 (t, *J*=5.50, 2H, OH), 4.10 (t, *J* = 6.24 Hz, 4H, CH_2), 3.73 (q, *J* = 5.98 Hz, 4H, CH_2), 3.59 (t, *J* = 6.30 Hz, 4H, CH_2), 3.54 (s, ,CH2), 3.28 (t, *J* = 6.44 Hz, 4H, CH_2). **^{13}C-NMR (100 MHz, $CDCl_3$-d): δ (ppm):** 163.5, 163.4, 145.1, 131.3, 130.8, 129.9, 128.9, 127.8, 127.4, 122.9, 122.8, 118.5, 70.0, 67.3, 59.5, 39.1, 34.5. **HR TOF MS ES+** calc for [$C_{34}H_{33}N_2O_8S_2$] 661.1678 found 661.1691.

Synthesis of 2,2'-(propane-1,3-diyl)bis(6-((2-hydroxyethyl)thio)-1H-benzo[de]isoquinoline-1,3(2H)-dione) 3.12e

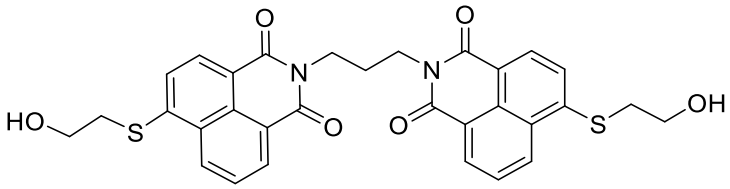

In a round-bottom flask, one equivalent of 2,2'-(azanediylbis(propane-3,1-diyl))bis(6-chloro-1H-benzo[de]isoquinoline-1,3(2H)-dione) **3.8e** (0.56 g, 1 mmol) and ten equivalents of 2-mercaptoethanol (0.78, 10 mmol) in addition to ten equivalents of sodium bicarbonate (0.84 g, 10 mmol) were dissolved in ≈ 50 mL 2-DMF. The reaction mixture was heated at 100 °C for 6 h. The solution was cooled down to an ambient temperature, forming 2,2'-(propane-1,3-diyl)bis(6-((2-hydroxyethyl)thio)-1H-benzo[de]isoquinoline-1,3(2H)-dione) **3.12e** as yellow precipitate, which was filtered and washed with chloroform Yield (41 %). **^{1}H-NMR (400 MHz, $CDCl_3$-d): δ (ppm):** 8.50 (dd, *J* = 8.46 Hz, *J* = 1.02 Hz, 2H, Ar-CH), 8.42 (dd, *J* = 7.32 Hz, *J*=1.00 Hz, 2H, Ar-CH), 8.25 (d, *J* = 7.96

Hz, 2H, Ar-CH), 7.82 (dd, *J* = 8.42 Hz, *J* = 7.38 Hz, 2H, Ar-CH), 7.71 (d, *J* = 8.12 Hz, 1H), 5.14 (t, *J*=5.50, 2H, OH), 4.12 (t, *J* = 7.08 Hz, 4H, CH_2), 3.75 (q, *J* = 6.05 Hz, 4H, CH_2), 3.35 (t, *J* = 6.38 Hz, 4H, CH_2), 2.06 (quint, *J* = 6.89 Hz, 2H, CH_2). **^{13}C-NMR (100 MHz, $CDCl_3$-d): δ(ppm):** 163.6, 163.5, 145.1, 131.4, 130.8, 130.0, 129.0, 127.9, 127.5, 123.1, 123.0, 118.6, 59.5, 38.1, 34.5. **HR TOF MS ES+** calc for [$C_{31}H_{27}N_2O_6S_2$] 587.1311 found 587.1320.

Synthesis of 2-(1,3-dioxo-1H,3H-benzo[de]isochromen-6-yl)acetic acid 3.13

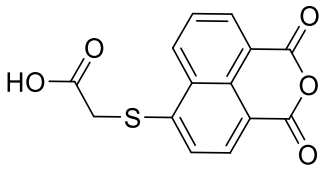

In a round-bottom flask, one equivalent of 4-chloro-1,8-naphtalic anhydride (4.64 g, 20 mmol,) and 1.5 equivalents of thioglycolic acid (2.09 ml, 30 mmol,) in addition to 1.5 equivalents of sodium bicarbonate (2.52 g, 30 mmol) were dissolved in DMF. The reaction mixture was refluxed for 2 h. The solution was left to cool to room temperature and the reaction mixture was acidified using HCl (5%) to obtain 2-(1,3-dioxo-1H,3H-benzo[de]isochromen-6-yl)acetic acid **3.13** as a yellow precipitate in 46 % yield. **^{1}H-NMR (400 MHz, DMSO-d_6): δ(ppm):** 13.15 (s, 1H, OH), 8.63 (dd, *J* =8.48 Hz, *J* = 1.04 Hz, 1H, Ar-CH), 8.56 (dd, *J* = 7.30 Hz, *J* = 1.02 Hz, 1H, Ar-CH), 8.40 (d, *J* = 7.92 Hz, 1H, Ar-CH), 7.93 (dd, *J* = 8.46 Hz, *J* = 7.34 Hz, 1H, Ar-CH), 7.73 (d, *J* = 8.00 Hz, 1H, Ar-CH), 4.26 (s, 2H, CH_2). **^{13}C-NMR (100 MHz, DMSO-d_6): δ(ppm):** 170.0, 161.1, 160.9, 145.6, 133.2, 132.5, 131.0, 130.2, 128.8, 128.1, 123.6, 120.2, 115.8, 34.1. **HR TOF MS ES$^+$** calc for [$C_{14}H_9O_5S$] 289.0171 found 289.0161.

Synthesis of 2,2'-(((adipoylbis(azanediyl))bis(1,3-dioxo-2,3-dihydro-1H-benzo[de]isoquinoline-2,6-diyl))bis(sulfanediyl))diacetic acid 3.13a

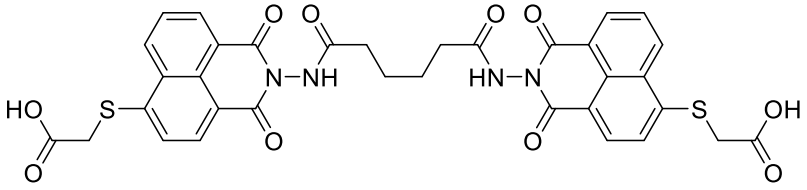

In a round-bottom flask, one equivalent of N^1,N^6-bis(6-chloro-1,3-dioxo-1H-benzo[de]isoquinolin-2(3H)-yl)adipamide **3.8a** (0.603 g, 1 mmol) was dissolved in 50 ml DMF. After that, ten equivalents of thioglycolic acid (0.92 g, 10 mmol) in addition to ten equivalents of sodium bicarbonate (0.84 g, 10 mmol) were added. The reaction mixture was heated at 100 °C for 5 h then left to cool down to room temperature. At the end the reaction mixture was acidified using HCl (5%) to obtain 2,2'-(((adipoylbis(azanediyl))bis(1,3-dioxo-2,3-dihydro-1H-benzo[de]isoquinoline-2,6-diyl))bis(sulfanediyl))diacetic acid **3.13a** as a yellow precipitate in 83 % yield. **^{1}H-NMR (400 MHz, DMSO-d_6): δ (ppm):** 12.99 (s, 2H, OH), 10.58 (s, 2H, N-H), 8.54 (dd, *J* =8.46 Hz, *J* = 0.98 Hz, 2H, Ar-CH),

8.50 (dd, *J* = 7.30 Hz, *J* = 0.90 Hz, 2H, Ar-CH), 8.34 (d, *J* = 7.92 Hz, 2H, Ar-CH), 7.86 (dd, *J* = 8.37 Hz, *J* = 7.42 Hz, 2H, Ar-CH), 7.67 (d, *J* = 8.12 Hz, 2H, Ar-CH), 4.16 (s, 4H, CH_2), 2.35 (br.s, 4H, CH_2), 1.68 (br.s, 4H, CH_2). **^{13}C-NMR (100 MHz, DMSO-d_6): δ (ppm):** 171.4, 170.1, 161.9, 161.8, 144.9, 132.3, 131.5, 130.7, 129.1, 128.0, 127.8, 123.8, 122.9, 118.9, 34.3, 33.4, 24.9. **HR TOF MS ES+** calc for [$C_{34}H_{27}N_4O_{10}S_2$] 715.1169 found 715.1181.

Synthesis of 2-((2-(3-((3-(6-chloro-1,3-dioxo-1H-benzo[de]isoquinolin-2(3H)-yl)propyl)amino)propyl)-1,3-dioxo-2,3-dihydro-1H-benzo[de]isoquinolin-6-yl)thio)acetic acid 3.13b

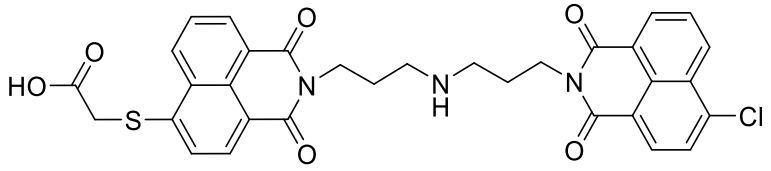

In a round-bottom flask, one equivalent of 2,2'-(azanediylbis(propane-3,1-diyl))bis(6-chloro-1H-benzo[de]isoquinoline-1,3(2H)-dione) 3.8b (0.56 g, 1 mmol) was dissolved in 50 ml DMF. After that, ten equivalents of thioglycolic acid (0.92 g, 10 mmol) in addition to ten equivalents of sodium bicarbonate (0.84 g, 10 mmol) were added. The reaction mixture was heated at 100 °C for 5 h then left to cool down to room temperature. At the end the reaction mixture was acidified using HCl (5%) to 2-((2-(3-((3-(6-chloro-1,3-dioxo-1H-benzo[de]isoquinolin-2(3H)-yl)propyl)amino)propyl)-1,3-dioxo-2,3-dihydro-1H-benzo[de]isoquinolin-6-yl)thio)acetic acid **3.13bba** as a yellow precipitate in 84 % yield. **^{1}H-NMR (500 MHz, DMSO-d_6): δ (ppm):** 8.59 (dd, *J* =8.5, *J* =1.0 Hz, 1H, Ar-CH), 8.57-8.54 (m, 1H, Ar-CH), 8.51 (dd, *J*=7.30, *J*=1.2 Hz, 1H,Ar-CH), 8.46-8.44 (m, 1H, Ar-CH), 8.35 (d, *J* = 7.9 Hz, 2H, Ar-CH), 8.29 (dd, *J* = 8.0, J = 7.5 Hz, 1H, Ar-CH), 7.90 (dd, *J* = 8.5, *J* = 7.5 Hz, 1H, Ar-CH), 7.88-7.85 (m, 1H, Ar-CH), 7.72 (d, *J* = 8.6 Hz, 1H, Ar-CH), 7.707.68 (m, 1H, Ar-CH), 4.21 (s, 2H, CH_2), 4.09 (t, *J* = 6.3 Hz, 2H, CH_2), 4.02-4.00(m, 2H, CH_2), 3.00 (b. signal, 2H, CH_2), 1.99 (quin, *J* = 7.3 Hz, 2H, CH_2), 1.85 (quin, *J* = 7.6 Hz, 2H, CH_2).

Synthesis of 2,2'-(((1,4-phenylenebis(methylene))bis(1,3-dioxo-2,3-dihydro-1H-benzo[de]isoquinoline-2,6-diyl))bis(sulfanediyl))diacetic acid 3.13c

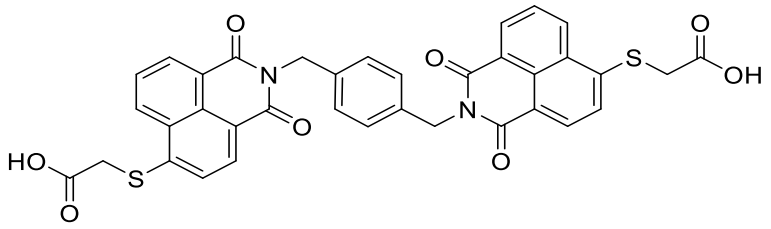

In a round-bottom flask, one equivalent of 2,2'-(1,4-phenylenebis(methylene))bis(6-chloro-1H-benzo[de]isoquinoline-1,3(2H)-dione) **3.8c** (1 mmol, 0.56 g) was dissolved in 50 ml DMF. After that, ten

equivalents of thioglycolic acid (10 mmol, 0.92 g) in addition to ten equivalents of sodium bicarbonate (10 mmol, 0.84 g) were added. The reaction mixture was refluxed for 5 h, then left to cool down to room temperature. At the end the reaction mixture was acidified using HCl (5%) and the obtained product was filtered and washed with chloroform to yield 2,2'-(((1,4-phenylenebis(methylene))bis(1,3-dioxo-2,3-dihydro-1H-benzo[de]isoquinoline-2,6-diyl))bis(sulfanediyl))diacetic acid **3.13c** as a yellow precipitate in 77 % yield. **^{1}H-NMR (400 MHz, DMSO-d_6): δ(ppm):** 8.59 (d, *J* =8.60 Hz, 2H, Ar-CH), 8.54 (d, *J* = 7.30 Hz, 2H, Ar-CH), 8.38 (d, *J* = 7.55 Hz, 2H, Ar-CH), 7.90 (dd, *J* = 8.30 Hz, *J* = 7.65 Hz, 2H, Ar-CH), 7.72 (d, *J* = 8.05 Hz, 2H, Ar-CH), 7.29 (s, 4H, Ar-CH), 7.29 (s, 4H, Ar-CH), 5.19 (s, 4H, CH_2), 4.16 (s, 4H, CH_2), 4.21 (s, 4H, CH_2).

Synthesis of S,S'-(((ethane-1,2-diylbis(oxy))bis(ethane-2,1-diyl))bis(1,3-dioxo-2,3-dihydro-1H-benzo[de]isoquinoline-2,6-diyl)) bis(2-hydroxyethanethioate) 3.13d

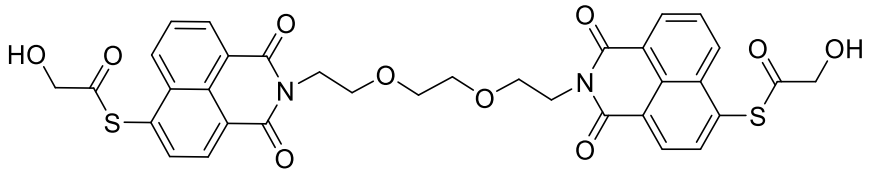

In a round-bottom flask, one equivalent of 2,2'-((ethane-1,2-diylbis(oxy))bis(ethane-2,1-diyl))bis(6-chloro-1H-benzo[de]isoquinoline-1,3(2H)-dione) **3.8d** (1 mmol, 0.688 g) was dissolved in 50 ml DMF. After that, ten equivalents of thioglycolic acid (10 mmol, 0.92 g) in addition to ten equivalents of sodium bicarbonate (10 mmol, 0.84 g) were added. The reaction mixture was refluxed for 5 h and then left to cool down to room temperature. At the end the reaction mixture was acidified using HCl (5%) to obtain S,S'-(((ethane-1,2-diylbis(oxy))bis(ethane-2,1-diyl))bis(1,3-dioxo-2,3-dihydro-1H-benzo[de]isoquinoline-2,6-diyl)) bis(2-hydroxyethanethioate) **(3.13d)** as a yellow precipitate in 63 % yield. **^{1}H-NMR (500 MHz, DMSO-d_6): δ(ppm):** 13.16 (s, 2H, OH), 8.47 (d, *J* =7.20 Hz, 2H, Ar-CH), 8.46 (d, *J* = 8.50 Hz, 2H, Ar-CH), 8.33 (d, *J* = 7.90 Hz, 2H, Ar-CH), 7.84 (dd, *J* = 8.40 Hz, *J*=7.30 2H, Ar-CH), 7.66 (d, *J* = 8.05 Hz, 2H, Ar-CH), 4.20 (s, 4H, CH_2), 4.18 (t, *J*=6.70 Hz, 4H, CH_2), 3.65 (t, *J*= 6.35, 4H, CH_2), 3.59 (s,4H, CH_2). **^{13}C-NMR (125 MHz, DMSO-d_6): δ(ppm):** 170.1, 163.5, 163.4, 143.8, 131.4, 130.8, 129.8, 128.7, 127.7, 127.6, 123.5, 122.9, 119.1, 70.0, 67.3, 39.1, 34.3. **HR TOF MS ES$^+$** calc for [$C_{34}H_{29}N_2O_{10}S_2$] 689.1264 found 689.1272.

Synthesis of 2,2'-((propane-1,3-diylbis(1,3-dioxo-2,3-dihydro-1H-benzo[de]isoquinoline-2,6-diyl))bis(sulfanediyl))diacetic acid 3.13e

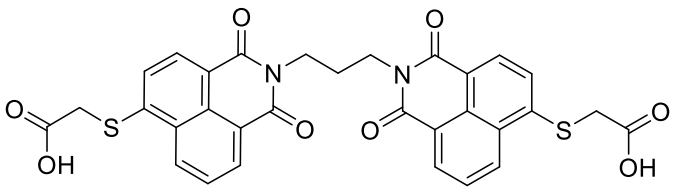

In a round-bottom flask, one equivalent of 2,2'-(propane-1,3-diyl)bis(6-chloro-1H-benzo[de]isoquinoline-1,3(2H)-dione) **3.8e** (0.50 g, 1 mmol) was dissolved in 50 ml DMF. After that, ten equivalents of thioglycolic acid (0.92 g, 10 mmol) in addition to ten equivalents of sodium bicarbonate (0.84 g, 10 mmol) were added. The reaction mixture was refluxed for 1 h and subsequently left to cool down to room temperature. At the end, the reaction mixture was acidified using HCl (5%) to obtain 2,2'-((propane-1,3-diylbis(1,3-dioxo-2,3-dihydro-1H-benzo[de]isoquinoline-2,6-diyl))bis(sulfanediyl))diacetic acid **3.13e** as a yellow precipitate in 88 % yield. **^{1}H-NMR (400 MHz, DMSO-d_6): δ(ppm):** 13.12 (s, 2H, OH), 8.51 (d, *J* =8.28 Hz, 2H, Ar-CH), 8.43 (d, *J* = 7.24 Hz, 2H, Ar-CH), 8.27 (d, *J* = 7.92 Hz, 2H, Ar-CH), 7.84 (t, *J* = 7.90 Hz, 2H, Ar-CH), 7.65 (d, *J* = 8.08 Hz, 2H, Ar-CH), 4.21 (s, 4H, CH_2), 4.12 (t, *J*=7.00 Hz, 4H, CH_2), 2.06 (quin, *J*= 7.10, 2H, CH_2). **^{13}C-NMR (100 MHz, DMSO-d_6): δ(ppm):** 170.1, 163.6, 163.5, 143.8, 131.4, 130.7, 129.9, 128.8, 127.8, 127.7, 123.6, 123.0, 119.1, 38.2, 34.2, 26.3. **HR TOF MS ES$^+$** calc for [$C_{31}H_{23}N_2O_8S_2$] 615.0896 found 615.0898.

Synthesis of 2-((2-(2-hydroxyethyl)-1,3-dioxo-2,3-dihydro-1H-benzo[de]isoquinolin-6-yl)thio)acetic acid 3.14

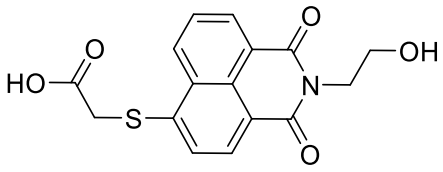

In a round-bottom flask, one equivalent of 2-(1,3-dioxo-1H,3H-benzo[de]isochromen-6-yl)acetic acid **3.13** (0.50 g, 1.7 mmol) was dissolved in ≈ 30 mL ethanol. Ten equivalents of ethanolamine (0.65 mL, 10.7 mmol) and five equivalents of (0.62 mL, 8.5 mmol) were added and the mixture was heated under reflux for 10 h. the reaction mixture was lef to cool then it was acidified with 5% HCl (aq.) to precipitate a yellow solid and the mixture left to stand overnight. The mixture was filtered, the solid washed with distilled water and left to dry to obtain 2-((2-(2-hydroxyethyl)-1,3-dioxo-2,3-dihydro-1H-benzo[de]isoquinolin-6-yl)thio)acetic acid **3.14** as yellow solid (yield 84%). **^{1}H-NMR (400 MHz, DMSO-d_6): δ(ppm):** 8.60 (1H, dd, *J*=8.5, *J*=1.0, Ar-CH), 8.55 (1H, dd, *J*= 7.2, 0.9, Ar-CH), 8.38 (1H, d, *J*= 7.9 Hz, Ar-CH), 7.91 (1H, dd, *J*=8.5, *J*=7.4 Hz, Ar-CH), 7.73 (1H, d, *J*= 8.0, Ar-CH), 4.81 (1H, s, OH),

4.19 (2H, s, CH_2), 4.15 (2H, t, *J*= 6.3 Hz, CH_2). 3.63 (2H, br signal, CH_2). **^{13}C-NMR (100 MHz, DMSO-d_6): δ (ppm):** 170.2, 163.8, 163.7, 143.7, 131.5, 130.8, 129.9, 129.0, 128.0, 127.8, 123.8, 123.4, 119.5, 58.3, 42.3, 34.4.

3.3.3 Solubility tests of synthesized compounds

To prepare ligands solution, several milligrams were dissolved in MOPS buffer and stirred for 3-5 days. Then the solutions were filtered using a 3 mm 0.2 μm syringe filter. The solution was placed in a 1 cm pathlength thermostatted quartz cuvette and the spectra were recorded at 25 °C and the concentrations were calculated using Beer Lambert law.

3.3.4. UV-visible titrations

3.3.4.1 Preparation of buffer

3-(*N*-morpholino)propanesulfonic acid (MOPS) (10.463 g, 50 mmol), ethylenediaminetetraacetic acid (EDTA) (0.584 g, 2 mmol) and sodium chloride (5.844 g, 100 mmol) were placed in a 2 litre beaker with a magnetic stirrer bar. 1500 mL of deionised water was added, and the mixture was stirred until all solid had dissolved. The pH of the solution was tested with a calibrated pH meter and adjusted to pH 7.00±0.02 by addition of a concentrated aqueous sodium hydroxide solution. The solution was then transferred to a 2 litre volumetric flask and made up to 2 litres with deionised water. The flask was inverted to make sure the solution was completely homogenous before transferring to a bottle for storage.

3.3.4.2 Preparation of DNA Solution

Fish sperm DNA (FSDNA) (~0.1 g) was placed in a 10 mL falcon tube with MOPS buffer (10 mL). The mixture was sonicated to dissolve the solid, then left to stand overnight to ensure all material was in solution. The solution was dialysed overnight using 3.5 kDa MWCO (molecular weight cut-off) dialysis tubing (Visking from Medicell Membranes Ltd.) against 1 litre of buffer. The dialysis buffer was replaced with a fresh litre of buffer, and the DNA solution was dialysed for a further night. The concentration of the DNA solution was determined spectrophotometrically by placing 10 μL of the DNA stock solution in 2500 μL of buffer and recording a UV-visible spectrum between 200-800 nm. A molar absorptivity of 12,600 M^{-1} (bp) cm^{-1} at 260 nm was used to calculate the concentration

2.3.4.3 UV-visible titration

Concentrated stock solutions of sufficiently soluble bisnaphthalimides were diluted by adding different volumes of these solutions to a 1 cm pathlength quartz cuvette and completing the volume with MOPS buffer until 2500 μl. The absorbance in the range of 0.08-0.8 a.u. was recorded in the cuvette. Even if solubility allowed higher concentrations to be used, this was avoided to avoid self-aggregation and precipitation of the ligand and to remain in within the range of absorbance where the spectrophotometer generates a linear response with concentration. The cuvette was placed in the spectrophotometer, thermostated at 25 °C and a UV-visible spectrum was recorded. The DNA solution was added stepwise in small aliquots (5-10 μl) and the UV-visible spectra were recorded within the range 200-600 nm after each addition of DNA. The absorptions at maximum wavelengths as a function of DNA and ligand concentrations were extracted from the UV-visible spectra. The obtained data for each titration were analysed using Origin 2017 by plotting the absorption as a function of DNA concentration. The multiple independent binding sites model[30] was used to determine the binding properties.

3.3.5 Molecular Docking study

The chemical structures for the proposed compounds were drawn using ChemDraw Professional 16.0 and they were subjected to geometrical optimization using MM2 (molecular dynamics and energy minimized) in Chem3D 16.0. The final structure was saved as PDB format and converted to PDBQT file in AutoDock Tools after checking the torsions for all the bonds. The structure of DNA with a pre-formed intercalation gap[25] called "open $d(ATCGAGACGTCTCGAT)_2$ " was used as the docking target with docking carried out using AutoDock Vina[24] with the below parameters (figure 3.18).

center_x = -2.152 center_y = 2.953 center_z = 24.92 size_x = 40 size_y = 40 size_z = 60 exhaustiveness = 200 num_modes = 10	**Definition:** **Center [x][y][z]**: box center in the receptor coordinate system. **Size [x][y][z]**: box dimensions along X, Y, and Z in the receptor coordinate system. **num_modes**: maximum number of binding modes to generate. **Exhaustiveness:** the time spent on the search is already varied heuristically depending on the number of atoms, flexibility, etc

Figure 3.18 The docking parameters

References

1. Zhao, J.; Li, W.; Ma, R.; Chen, S.; Ren, S.; Jiang, T., Design, synthesis and DNA interaction study of new potential DNA bis-intercalators based on glucuronic acid. *Int J Mol Sci* **2013,** *14* (8), 16851-65.

2. Huang, Y.; Song, Y.; Huang, M.; Fan, Y.-R.; Tian, D.-N.; Zhao, Q.-P.; Yang, X.-B.; Zhang, W.-N., Synthesis, DNA binding, and cytotoxicity activity of bis-naphalenyl compounds with different diamine linkers. *Research on Chemical Intermediates* **2016,** *42* (10), 7329-7344.

3. Tandon, R.; Luxami, V.; Kaur, H.; Tandon, N.; Paul, K., 1,8-Naphthalimide: A Potent DNA Intercalator and Target for Cancer Therapy. *Chem Rec* **2017,** *17* (10), 956-993.

4. Braña, M. F.; Castellano, J. M.; Morán, M.; Pérez de Vega, M. J.; Qian, X. D.; Romerdahl, C. A.; Keilhauer, G., Bis-naphthalimides. 2. Synthesis and biological activity of 5,6-acenaphthalimidoalkyl-1,8-naphthalimidoalkyl amines. *European Journal of Medicinal Chemistry* **1995,** *30* (3), 235-239.

5. Yang, P.; Yang, Q.; Qian, X., Novel DNA bis-intercalators of isoquinolino[4,5-bc]acridines: design, synthesis and evaluation of cytotoxic activity. *Tetrahedron* **2005,** *61* (50), 11895-11901.

6. Banerjee, S.; Veale, E. B.; Phelan, C. M.; Murphy, S. A.; Tocci, G. M.; Gillespie, L. J.; Frimannsson, D. O.; Kelly, J. M.; Gunnlaugsson, T., Recent advances in the development of 1,8-naphthalimide based DNA targeting binders, anticancer and fluorescent cellular imaging agents. *Chem Soc Rev* **2013,** *42* (4), 1601-18.

7. Braña, M. F.; Castellano, J. M.; Perron, D.; Maher, C.; Conlon, D.; Bousquet, P. F.; George, J.; Qian, X. D.; Robinson, S. P., Chromophore-Modified Bis-Naphthalimides: Synthesis and Antitumor Activity of Bis-Dibenz[de,h]isoquinoline-1,3-diones. *Journal of Medicinal Chemistry* **1997,** *40* (4), 449-454.

8. Antonini, I.; Volpini, R.; Dal Ben, D.; Lambertucci, C.; Cristalli, G., Design, synthesis, and biological evaluation of new mitonafide derivatives as potential antitumor drugs. *Bioorg Med Chem* **2008,** *16* (18), 8440-6.

9. Thompson, J.; Pratt, C. B.; Stewart, C. F.; Avery, L.; Bowman, L.; Zamboni, W. C.; Pappo, A., Phase I study of DMP 840 in pediatric patients with refractory solid tumors. *Investigational New Drugs* **1998,** *16* (1), 45-49.

10. McRipley, R. J.; Burns-Horwitz, P. E.; Czerniak, P. M.; Diamond, R. J.; Diamond, M. A.; Miller, J. L.; Page, R. J.; Dexter, D. L.; Chen, S. F.; Sun, J. H.; et al., Efficacy of DMP 840: a novel bis-naphthalimide cytotoxic agent with human solid tumor xenograft selectivity. *Cancer Res* **1994,** *54* (1), 159-64.

11. Nitiss, J. L.; Zhou, J.; Rose, A.; Hsiung, Y.; Gale, K. C.; Osheroff, N., The Bis(naphthalimide) DMP-840 Causes Cytotoxicity by Its Action against Eukaryotic Topoisomerase II. *Biochemistry* **1998,** *37* (9), 3078-3085.

12. LoRusso, P.; Demchik, L.; Dan, M.; Polin, L.; Gross, J. L.; Corbett, T. H., Comparative efficacy of DMP 840 against mouse and human solid tumor models. *Investigational New Drugs* **1995,** *13* (3), 195-203.

13. Lai, C.-M.; Garner, D. M.; Gray, J. E.; Brogdon, B. L.; Peterman, V. C.; Pieniaszek Jr, H. J., Determination of bisnafide, a novel bis-naphthalimide anticancer agent, in human plasma by high-performance liquid chromatography with UV detection. *Journal of Pharmaceutical and Biomedical Analysis* **1998,** *17* (3), 427-434.

14. Bousquet, P. F.; Braña, M. F.; Conlon, D.; Fitzgerald, K. M.; Perron, D.; Cocchiaro, C.; Miller, R.; Moran, M.; George, J.; Qian, X.-D.; Keilhauer, G.; Romerdahl, C. A., Preclinical Evaluation of LU 79553: A Novel Bis-naphthalimide with Potent Antitumor Activity. *Cancer Research* **1995,** *55* (5), 1176-1180.

15. Rong, R.-X.; Sun, Q.; Ma, C.-L.; Chen, B.; Wang, W.-Y.; Wang, Z.-A.; Wang, K.-R.; Cao, Z.-R.; Li, X.-L., Development of novel bis-naphthalimide derivatives and their anticancer properties. *MedChemComm* **2016,** *7* (4), 679-685.

16. Tian, Z. Y.; Li, J. H.; Li, Q.; Zang, F. L.; Zhao, Z. H.; Wang, C. J., Study on the synthesis, biological activity and spectroscopy of naphthalimide-diamine conjugates. *Molecules* **2014,** *19* (6), 7646-68.

17. Ge, C.; Chang, L.; Zhao, Y.; Chang, C.; Xu, X.; He, H.; Wang, Y.; Dai, F.; Xie, S.; Wang, C., Design, Synthesis and Evaluation of Naphthalimide Derivatives as Potential Anticancer Agents for Hepatocellular Carcinoma. *Molecules* **2017,** *22* (2).

18. Huang, Y.; Wu, C. X.; Song, Y.; Huang, M.; Tian, D. N.; Yang, X. B.; Fan, Y. R., Synthesis, DNA Binding, and Anticancer Properties of Bis-Naphthalimide Derivatives with Lysine-Modified Polyamine Linkers. *Molecules* **2018,** *23* (2).

19. Licchelli, M.; Biroli, A. O.; Poggi, A.; Sacchi, D.; Sangermani, C.; Zema, M., Excimer emission induced by metal ion coordination in 1,8-naphthalimide-tethered iminopyridine ligands. *Dalton Transactions* **2003,** (23).

20. Chovelon, J.-M.; Grabchev, I., A novel fluorescent sensor for metal cations and protons based of bis-1,8-naphthalimide. *Spectrochimica Acta Part A: Molecular and Biomolecular Spectroscopy* **2007,** *67* (1), 87-91.

21. Yordanova, S.; Stoianov, S.; Grabchev, I.; Petkov, I., Detection of Metal Ions and Protons with a New Blue Fluorescent Bis(1,8-Naphthalimide). *International Journal of Inorganic Chemistry* **2013,** *2013*, 1-6.

22. Lee, M. H., Bis(Naphthalimide-Piperazine)-Based Off-On Fluorescent Probe for Acids. *Journal of Fluorescence* **2016,** *26* (3), 807-811.

23. Dai, H.; Xu, H., Selective and Sensitive Fluorescent Chemosensors for Cu2+ Ion Based upon Bis-1,8-naphthalimide Dyads. *Chinese Journal of Chemistry* **2012,** *30* (2), 267-272.

24. Trott, O.; Olson, A. J., AutoDock Vina: improving the speed and accuracy of docking with a new scoring function, efficient optimization, and multithreading. *J Comput Chem* **2010,** *31* (2), 455-461.

25. Jones, J. E.; Amoroso, A. J.; Dorin, I. M.; Parigi, G.; Ward, B. D.; Buurma, N. J.; Pope, S. J. A., Bimodal, dimetallic lanthanide complexes that bind to DNA: the nature of binding and its influence on water relaxivity. *Chemical communications (Cambridge, England)* **2011,** *47* (12), 3374-3376.

26. Luo, Y.-L.; Baathulaa, K.; Kannekanti, V. K.; Zhou, C.-H.; Cai, G.-X., Novel benzimidazole derived naphthalimide triazoles: synthesis, antimicrobial activity and interactions with calf thymus DNA. *Science China Chemistry* **2015,** *58* (3), 483-494.

27. Zhao, Q.; Lai, H.; Chen, H.; Li, H.; He, F., H- and J-aggregation inspiring efficient solar conversion. *Journal of Materials Chemistry A* **2021,** *9* (2), 1119-1126.

28. Nicholas, J. H., Expanded Theory of H- and J-Molecular Aggregates: The Effects of Vibronic Coupling and Intermolecular Charge Transfer. *Chemical reviews* **2018,** *v. 118* (no. 15), pp. 7069-7163-2018 v.118 no.15.

29. Kucheryavy, P.; Li, G.; Vyas, S.; Hadad, C.; Glusac, K. D., Electronic properties of 4-substituted naphthalimides. *J Phys Chem A* **2009,** *113* (23), 6453-61.

30. Hahn, L.; Buurma, N. J.; Gade, L. H., A Water-Soluble Tetraazaperopyrene Dye as Strong G-Quadruplex DNA Binder. *Chemistry – A European Journal* **2016,** *22* (18), 6314-6322.

Chapter 4 Synthesis of fused-ring-extended 1,8-naphthalimide derivatives

Abstract

A series of fused-ring-extended 1,8-naphthalimide derivatives were successfully synthesized. The synthesis involves synthesizing and separating two isomers of a building block for potential intercalators. Several solubilizing groups were introduced in C4 of the naphthalene ring. The DNA-binding properties for these compounds were studied using UV-visible titrations. It is found that this class of compounds binds strongly with DNA, however the titration curves show unusual behavior where we had to analyse the data in a slightly different way to obtain apparent DNA-binding affinities K_{app}. In general, there is no difference between these isomers in terms of binding with DNA. The binding properties for two isomers has remarkably improved when we used different groups (1°-amin, 2°-amine, thiol group) compared to bromo-substituted isomers. Compound **4.16a**, with ethanolamine as the solubilizing group, is the most promising compound among this series with an apparent DNA-binding affinities K_{app} of 8.45×10^4 M^{-1}. Using 2-mercaptoethanol **4.16d** and **4.17d** on the other hand show the lowest DNA-binding affinities ($\sim10^3$ M^{-1}). We note, however, that these binding affinities are apparent binding affinities and therefore likely underestimate the actual affinities of these compounds for DNA.

4.1 Introduction

One of the approaches that has been utilized to enhance the potency of mononaphthalimides to be better intercalators involves modifying the intercalating chromophore to generate a larger flat aromatic system, such as an anthracene moiety rather than the simpler naphthalene. Expanding the flat aromatic system can improve the ability for the compounds to intercalate.[1-3]

4.1.1 Fused-ring-extended 1,8-naphthalimide derivatives in medicinal chemistry

Increasing the aromatic surface for naphthalic anhydride via fusing one or more aromatic rings to the naphthalene core means increasing the surface that participates in π-stacking interactions which leads to improved DNA-binding properties.[3-6] Azonafide **4.2** has an anthracene core instead of a naphthalene core and therefore bears a resemblance to amonafide **4.1**. The antitumor activity for **4.2** has improved compared to **4.1.**[2]

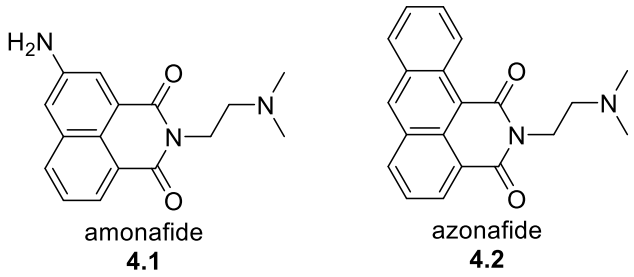

Scheme 4.1

Efforts have been made to modify the naphthalimide skeleton by increasing the aromatic surface that can intercalate and therefore improve their therapeutic properties. [3, 7-9]

Qing Yang *et al*.[9] have synthesized several heterocyclic-fused naphthalimide intercalators **4.3-4.6** carrying chiral substituents (Scheme 4.2). DNA-binding activities have been studied using fluorescence spectroscopy. The result shows that S-enantiomers binds better to ct-DNA (calf thymus DNA) compared to R-enantiomers and the racemic mixture, and the binding increases as following **4.5** > **4.6** > **4.4** > **4.3**.

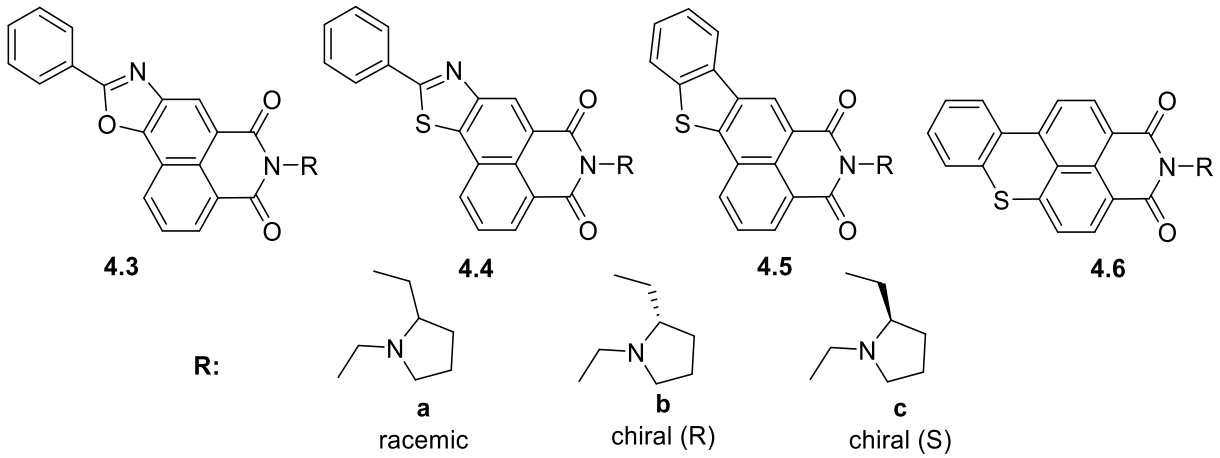

Scheme 4.2

Zhigang Li *et al*. [10] have synthesized series of 2-aminothiazonaphthalimides **4.7a-b** and **4.8a-b** with two different length of aminoalkyl side chains (Scheme 4.3). The binding constant for these compounds with ct-DNA was determined using a fluorescence-based method. The results show that all compounds bind with DNA with different strength. Using long aminoalkyl side chain exhibits higher binding affinities with DNA. Moreover, the **4.8** scaffold presents better DNA-binding properties. Accordingly, **4.8b** (Scatchard binding constant of 4.73×10^{4} M^{-1}) is the most promising compound to bind with DNA among this series.[10]

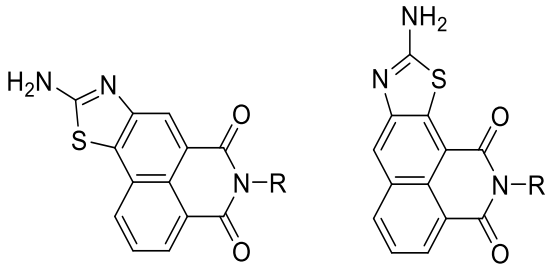

a: R= $CH_2CH_2N(CH_3)_2$
b: R= $CH_2CH_2CH_2N(CH_3)_2$

Scheme 4.3

Chaochao Ge *et al*. [8] have developed the previous promising scaffold **4.8** using different alkylamines as a side chains **4.9a-e** (Scheme 4.4). The anti-cancer properties for these compounds were investigated *in vitro* against four tumor cell lines using amonafide as the reference drug. Compound **4.9a** showed promising antitumor activity and was therefore selected for study *in vivo* trials

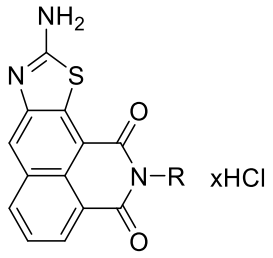

4.9

a: R= $CH_2CH_2CH_2NH_2$
b: R= $CH_2CH_2CH_2CH_2NH_2$
c: R= $CH_2CH_2CH_2NHCH_2CH_2CH_2NH_2$
d: R= $CH_2CH_2CH_2CH_2NHCH_2CH_2CH_2CH_2NH_2$
e: R= $CH_2CH_2CH_2CH_2N(CH_2CH_2)_2NH$

Scheme 4.4

Yufang Xu *et a*l.[11] have synthesized several five-membered thio-heterocyclic fused naphthalimide derivatives **4.10a-d** with different lengths of side chains (Scheme 4.5). The photocleaving abilities of these compounds were investigated and the binding properties with ct-DNA were studied. The result shows that this class of compounds bind strongly with DNA and cause DNA damage. The DNA-binding affinities for **4.10a-d** were compared with other series of compounds contain six-member fused ring **4.11a-d** that have been synthesized by the same group. Five-membered thio-fused naphthalimide derivatives bind better (~10^5 M^{-1}) than six-membered thio-fused naphthalimide derivatives (~10^3 M^{-1}).

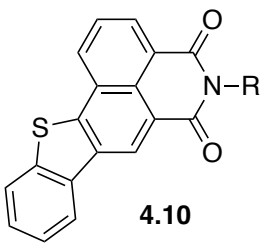

4.10

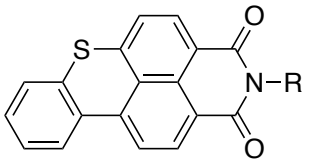

4.11

R:

a

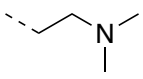

b

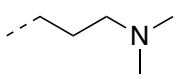

c

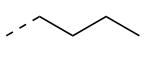

d

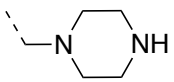

Scheme 4.5

Shaoying Tan *et al.*[12] from the same group have synthesized two series of compounds related to their previous compound (Scheme 4.6) where five/six-membered oxo-heterocycle-fused naphthalimide derivatives **4.12a-d** and **4.13a-d** (Scheme 4.6) were synthesized. The antitumor activities were investigated against several tumor cell lines and show better antiproliferative activity compared to amonafide. **4.12a** and **4.13a** show promising activities therefore, the DNA-binding affinities for these compounds were studied using CD spectroscopy. According to the binding affinities **4.12a** and **4.13a** bind with DNA but not as strong as the corresponding thio-heterocycle naphthalimide derivatives **4.10a** and **4.11a** from the previous study.

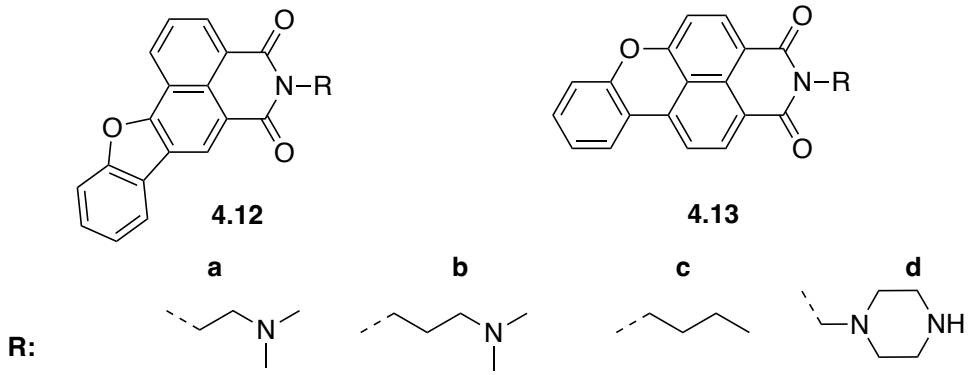

Scheme 4.6

Meenakshi Verma, *et al.*[13] have synthesized a series of fused-ring-extended 1,8-naphthalimide derivatives **4.14a-j** (Scheme 4.7) where several primary and secondary amines were used as substituents in C4 of the naphthalene ring. The antitumour activities were investigated against 60 tumour cell lines using 5-fluorouracil as a reference drug. Compound **4.14d** is the most active compound among this series compared to the standard drug. The DNA binding affinity for this compound was further studied using UV-visible and fluorescence spectroscopy. The addition of ct-DNA caused a bathochromic shift (420-430 nm). The interaction type was determined as intercalation using thermal denaturation experiments that show increases in melting points for ct-DNA from 60 °C to 68 °C. However, it is unclear how the authors determined that the extending fused ring has formed isomer **4.14** and not isomer **4.15** or a mixture of both isomers.

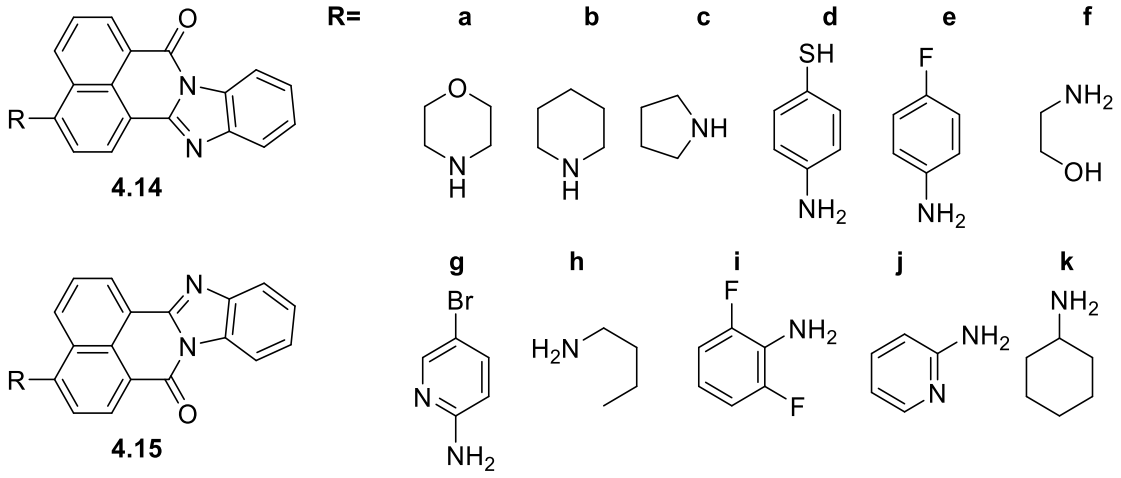

Scheme 4.7

4.1.2 Aims

This chapter aims to synthesise naphthalimide derivatives via expanding the aromatic system. The proposed compounds have two variable factors. The first factor is to synthesise and separate two isomers, where the first isomer involves a fused ring on the same side as the C4 substituents on the naphthalene ring (Scheme 4.8, compound **4.16**) and the other isomer is where the fused ring is in the other side (Scheme 4.8, compound **4.17**). The second factor is introducing the same pattern of solubilizing groups that has been used in the previous chapters (1° amine, 2° amine, thiol compounds).

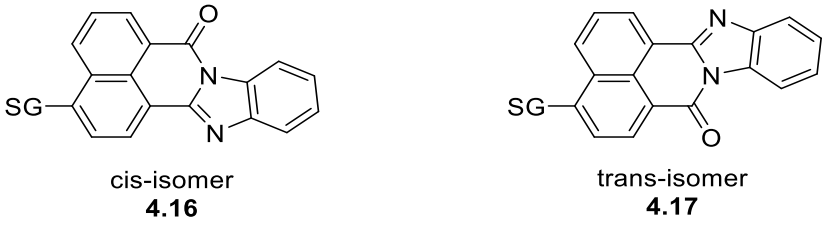

Scheme 4.8

The second aim of this chapter is to study the DNA-binding properties for the synthesized compounds using UV-visible titrations.

4.2 Result and Discussion

4.2.1 Design and docking study for fused-ring-extended 1,8-naphthalimide derivatives

In our search for higher affinities for DNA and inspired by the effect of fusing an aromatic ring to the naphthalimide skeleton, several compounds with larger potentially intercalating aromatic systems were proposed (Scheme 4.9). These proposed mono-naphthalimide derivatives involve increasing the aromatic surface and then introducing the solubilizing groups.

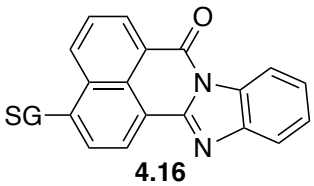

4.16

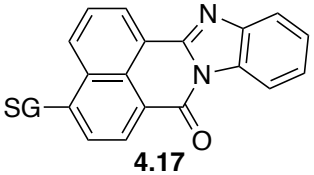

4.17

	4.16-17	**4.16-17a**	**4.16-17b**	**4.16-17c**	**4.16-17d**	**4.16-17e**
SG	Br	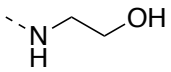	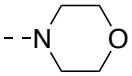	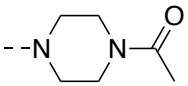	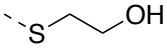	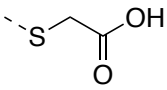

Scheme 4.9

A docking study for the proposed fused-ring-extended 1,8-naphthalimide derivatives **4.16** and **4.16a-e** was carried out using AutoDock Vina[14] against a DNA structure with a pre-formed intercalation gap[15] . The docking produces the top 10 binding modes ranked by the binding affinity. However, only the top three binding mode are presented in Figure 4.1.

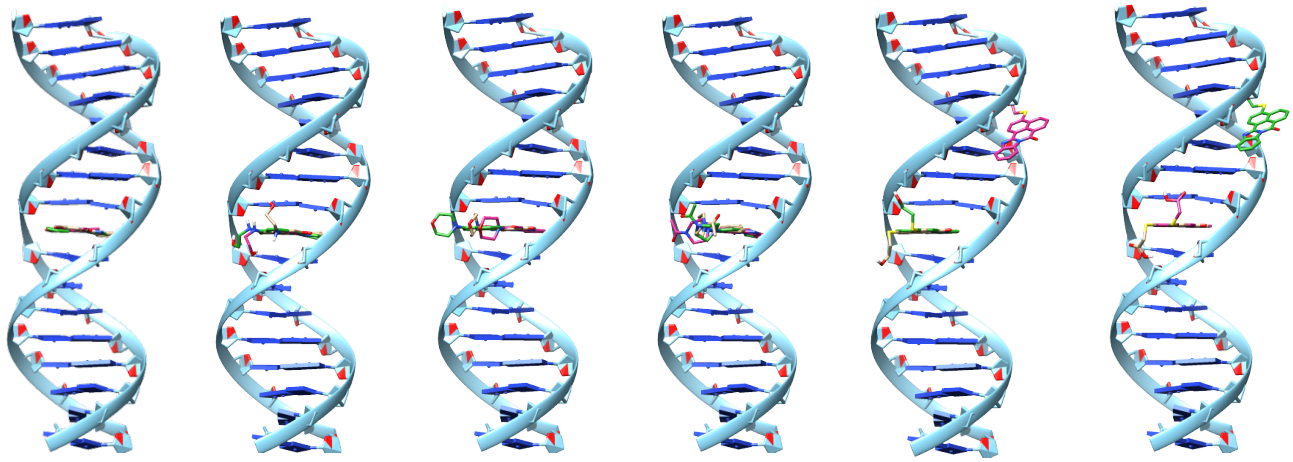

4.16 **4.16a** **4.16b** **4.16c** **4.16d** **4.16e**

Figure 4.1 top 3 binding modes for proposed 4.16 and 4.16a-e with open d(ATCGAGACGTCTCGAT)$_2$

The docking study suggest that all proposed compounds bind with the DNA as an intercalator. Table 4.1 illustrates the binding affinity for the top three binding modes of **4.16** and **4.16a-e** using AutoDock Vina.

Table 4.1 The DNA-binding affinities for the top three binding modes of 4.16 and 4.16a-e using AutoDock Vina

		4.16	4.16a	4.16b	4.16c	4.16d	4.16e
The binding affinity (kcal/mol)[b]	1st binding mode[a]	-10.2 (I)	-9.7 (I)	-10.8 (I)	-11.4 (I)	-8.9 (I)	-10.1 (I)
	2nd binding mode	-10.2 (I)	-9.7 (I)	-10.7 (I)	-11.4 (I)	-8.7 (GB)	-9.9 (I)
	3rd binding mode	-10.0 (I)	-9.3 (I)	-9.8 (I)	-11.2 (I)	-8.7 (I)	-9.1 (GB)

(I): intercalator, (GB): groove binder

a) The ranking of the binding modes is as produced by Vina

b) Binding affinities are only reported to 0.1 kcal mol^{-1} by Vina.

In addition to exploring the DNA-binding properties for the cis-isomer derivatives, the trans-isomer derivatives **4.17** and **4.17a-e** were proposed, and the docking study were carried out using AutoDock Vina (Figure 4.2).

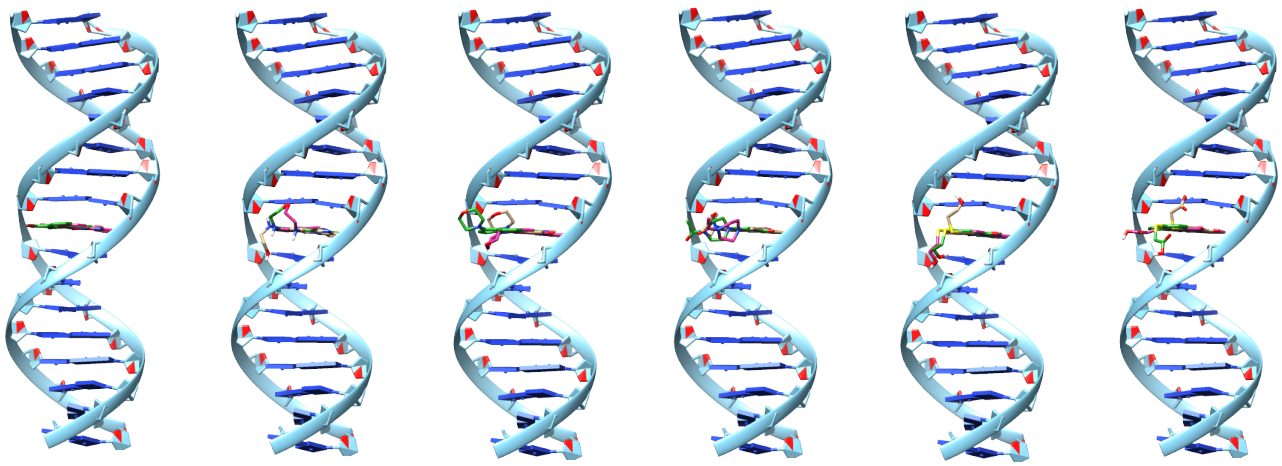

4.17 **4.17a** **4.17b** **4.17c** **4.17d** **4.17e**

Figure 4.2 The top three binding modes of 4.17 and 4.17a-e using AutoDock Vina

Based on docking study results, proposed trans-isomer derivatives also bind with the DNA as an intercalator. Table 4.2 illustrates the binding affinities for the top three binding modes of **4.17** and **4.17a-e** using AutoDock Vina.

Table 4.2 The binding affinity for the top three binding modes of 4.17 and 4.17a-e using AutoDock Vina

		4.17	4.17a	4.17b	4.17c	4.17d	4.17e
The binding affinity (kcal/mol)[b]	1st binding mode[a]	-10.1 (I)	-9.7 (I)	-11.0 (I)	-11.4 (I)	-9.8 (I)	-9.7 (I)
	2nd binding mode	-10.1 (I)	-9.7 (I)	-11.0 (I)	-11.3 (I)	-9.6 (I)	-8.7 (I)
	3rd binding mode	-9.7 (I)	-9.3 (I)	-10.4 (I)	-11.3 (I)	-9.5 (I)	-8.7 (I)

(I): intercalator, (GB): groove binder

a) The ranking of the binding modes is as produced by Vina

b) Binding affinities are only reported to 0.1 kcal mol^{-1} by Vina.

Overall, all proposed compounds show high ability to intercalate in the DNA as expected. The predicted binding affinities for both isomers with the solubilizing groups are almost the same except for thiol-based solubilising groups where the values show some variation.

This class of compounds understandably shows higher ability to intercalate with DNA, as quantified by the predicted binding affinity, compared to ferrocene-naphthalimide conjugates in chapter 2 due to the increased aromatic surface. However, the bisnaphthalimide derivatives in chapter 3 exhibits better binding affinities as a consequence of existing of two units of intercalator. Nevertheless, avoiding the use of dimers may be interesting, for example for reasons of ease of synthesis and solubility.

4.2.2 Synthesis of fused-ring-extended 1,8-naphthalimide derivatives

The synthesis route for this class of compounds includes two steps. The first step involves increasing the aromatic system of 4-bromo-1,8-naphthalic anhydride (note, in several experiments, the 4-bromo-substituted compound is used in this Chapter, not the 4-chloro-substituted compound) using ortho-phenylenediamine. The second step involves the nucleophilic aromatic substitution (S_NAr) of the halogen with different solubilizing groups. The synthetic procedure is outlined in Scheme 4.10.

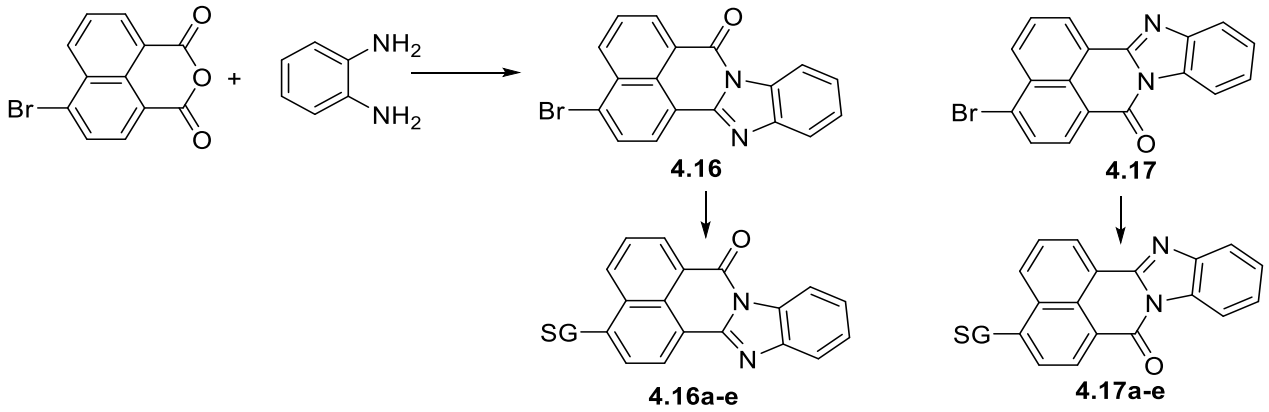

Scheme 4.10 synthetic scheme of 4.16a-e and 4.17a-e

Step 1. Increasing the aromatic surface area

To increase the surface are of the planar aromatic system, 4-chloro-1,8-naphthalic anhydride was fused with o-phenylenediamine to form the two isomers **4.16-Cl** and **4.17-Cl**. This reaction was carried out using acetic acid as the solvent and the reaction mixture was heated to reflux for 2 h. The ^{1}H-NMR spectrum for the obtained yellow product shows the presence of 18 protons, which is consistent with a mixture of the two structural isomers (Scheme 4.11)

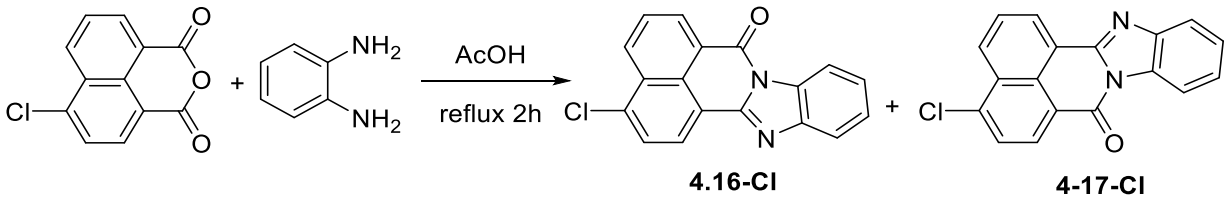

Scheme 4.11

Although this reaction was conveniently carried out, separating the two obtained isomers using column chromatography was a challenging step since the two isomers have the very similar R_f. Fortunately, using 4-bromo- instead of 4-chloro-1,8-napthalic anhydride under the same conditions provided an alternative way to obtain the desired compounds (Scheme 4.12). [16]

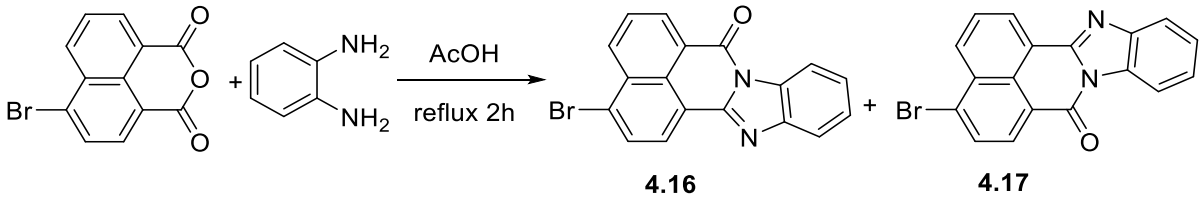

Scheme 4.12

Separating the two isomers using column chromatography was a problematic step. Although it was stated in the literature that toluene: ethyl acetate 5:1 was successfully used as a mobile phase. We face two problems, one of them is the lack of solubility of the isomers in the mobile phase and the second issue was related to the similarity of the R_f for the two isomers. These two issues forced us to perform the column chromatography for the mixture many times just to obtain enough amount of both isomers in a pure state.

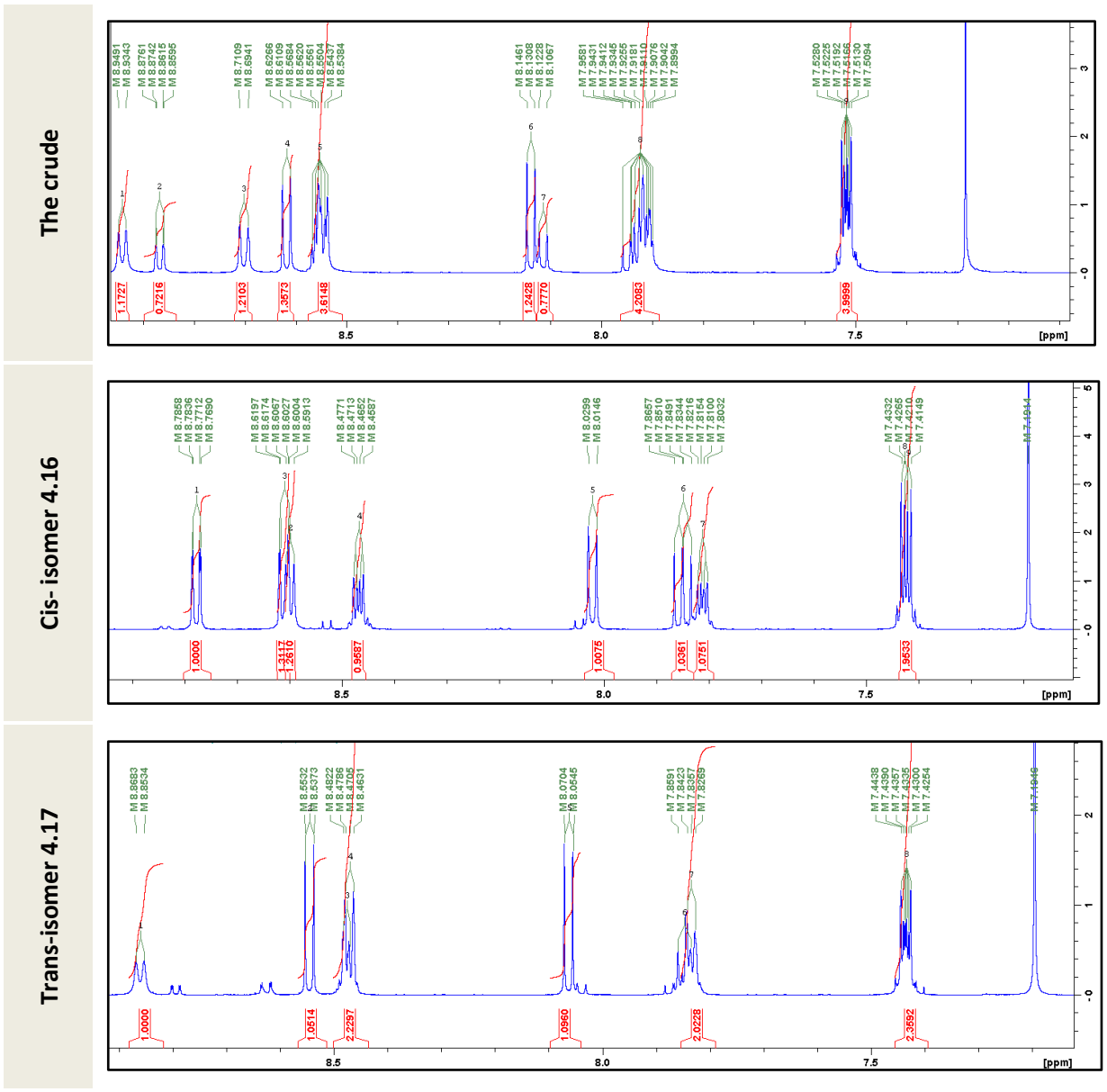

Figure 4.3 ^{1}H-NMR spectra for the crude, 4.16 and 4.17

To be able to differentiate between both pure isomers, we tried and succeeded to grow crystals of one of these isomers allowing X-ray crystallography. X-ray crystallography (Figure 4.4) confirmed that the first compound that gets out the column is the cis isomer **4.16**. The data collection parameters for the X-ray structure is available in the Appendix (see appendix section 4.4)

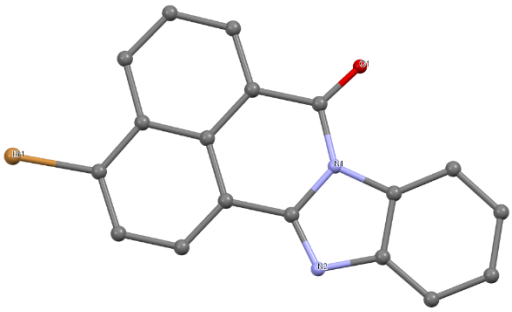

Figure 4.4 X-ray structre of 4.16 (cis-isomer)

Step 2. introduction of solubilizing groups through S_NAr reactions

After increasing the aromatic surface area of the intercalating part of the molecule, the next step is to introduce the same pattern of solubilizing groups that have been used in previous chapters. Based on the solubility and DNA binding study for synthesized compounds in Chapter 2 and 3, It can be said that solubilizing group play a role in improving the solubility and affecting the binding affinities with DNA.

Step 2.1 introduction of solubilizing groups through S_NAr reactions with 1° amine

The two isomers were used as a skeleton to synthesise mono-intercalators with a solubilizing group using ethanol amine as a nucleophile.

One equivalent of **4.16** was dissolved in 10 ml of ethanol amine and heated to reflux for 24 h. At the end of the reaction, the reaction mixture was left to cool and then extracted in DCM and water. The organic layer was dried over $MgSO_4$ and the solvent was evaporated to obtain the crude product in 31% yield. The crude product was then purified using column chromatography (DCM-ethanol 9:1) with R_f=0.5.

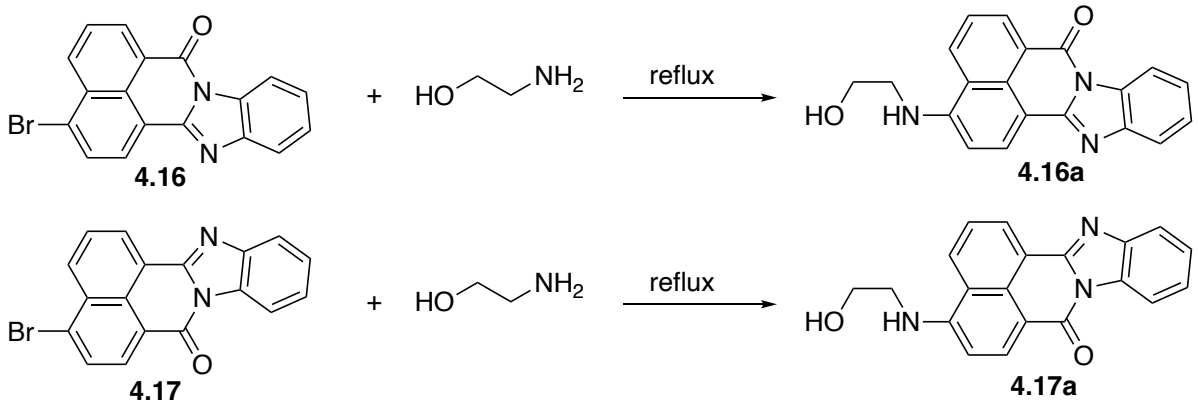

Scheme 4.13

The same reaction condition were used in an attempt to synthesise **4.17a** (Scheme 4.13) but this failed. The NMR spectrum for the obtained crude product is not consistent with the expected NMR spectrum and no further attempt was carried out to synthesise this compound.

Step 2.2 introduction of solubilizing groups through S_NAr reactions with 2° amines

Secondary amine morpholine was also used as a solubilizing group with both isomers (cis and trans) to produce **4.16b** and **4.17b**. One equivalent of **4.16** with ten equivalents of morpholine in DMF were heated at 100 °C for 24 h (Scheme 4.14). At the end of the reaction, the solvent was evaporated and then methanol was added to obtain pure **4.16b** in a good yield. Similarly, the same condition was successfully used to synthesise **4.17b**.

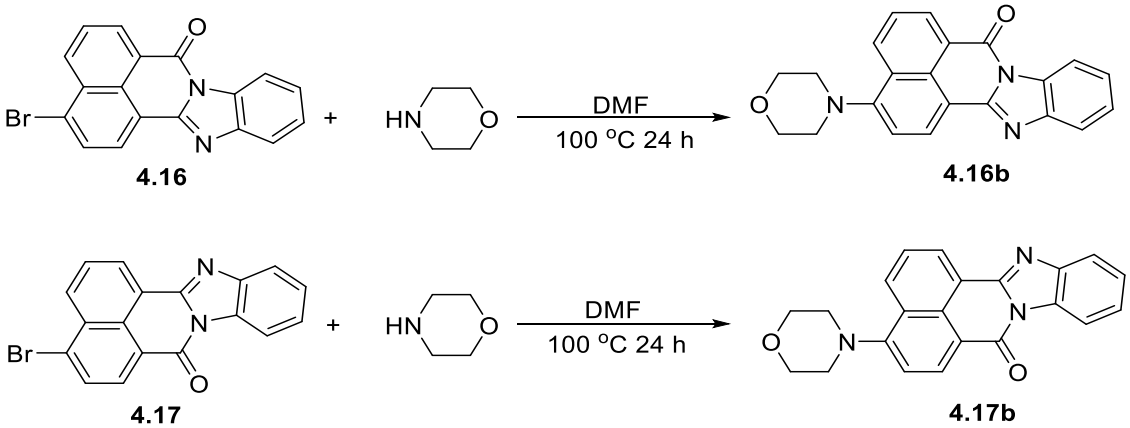

Scheme 4.14

The chemical structures of **4.16c** and **4.17c** were confirmed using ^{1}H-, ^{13}C-NMR spectroscopy and mass spectrometry. However, the ^{1}H-NMR spectrum for **4.17c** shows extra four signals in the aliphatic region. These signals are not related to the chemical structure of **4.17c**, and these signals were identified as belonging to an impurity. The 2D NMR (COSY and HSQC) was used to confirm that these signals are not in any way correlated to the signals related to **7.17c** (Figure 4.5).

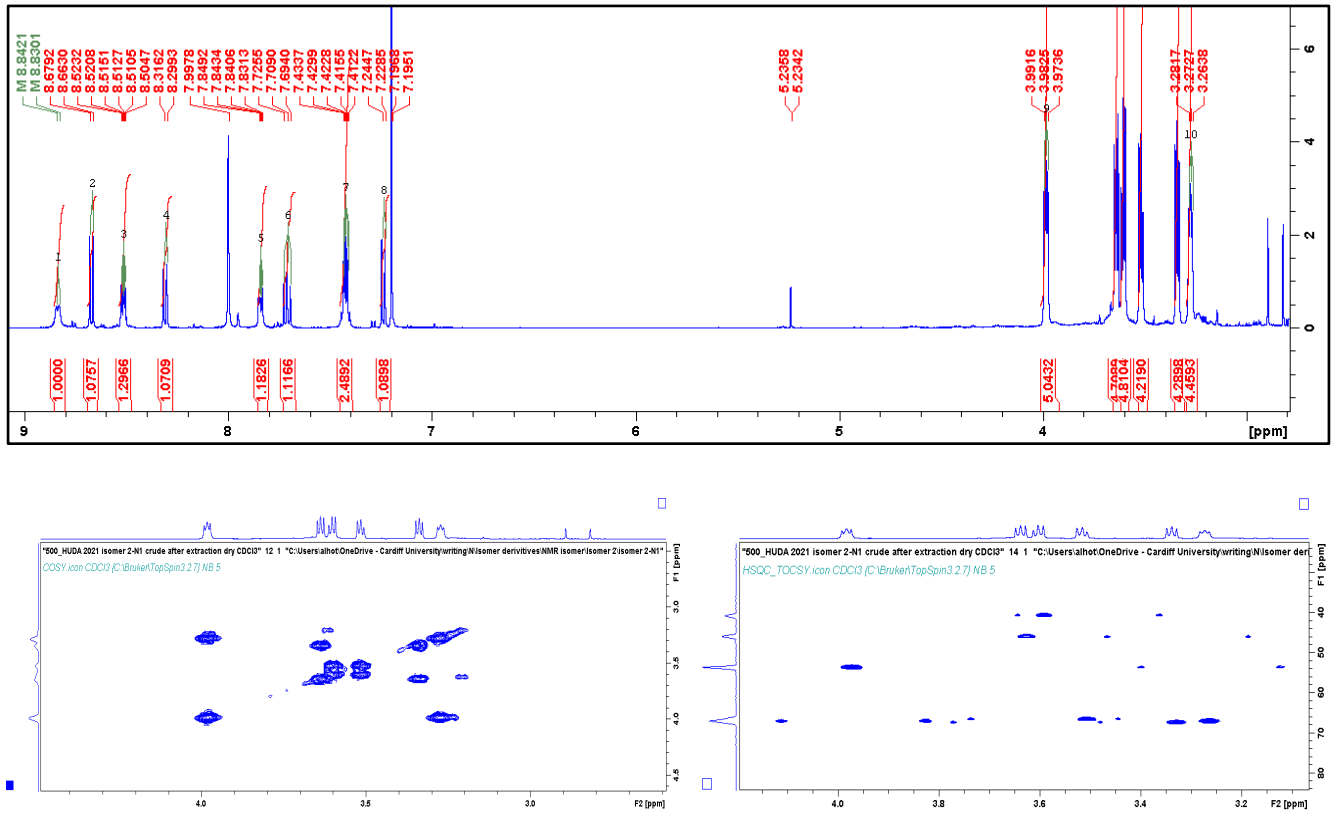

Figure 4.5 1D,2D NMR (COSY and HSQC) of 4.17c

Based on the 2D NMR spectrum, two of these signals are identified as excess morpholine whereas the other two signals we could not recognize. It is worth mentioning that according to mass spectrometry the found mass is exactly the mass that we expected (calculated: 356.1399 found 356.1399) which confirms the chemical structure of **4.17c**. Since all the signals for the impurity suggest an aliphatic compound, we expect that it will not interfere with the UV-visible titrations.

Next, 1-acetyl piperazine was introduced as a solubilizing group using the same reaction conditions to obtain **4.16c** and **4.17c** where one equivalent of each isomer was heated with ten equivalents of 1-acetyl piperazine in DMF for 24 h (Scheme 4.15). The final products were characterized using ^{1}H- and ^{13}C-NMR spectroscopy and mass spectrometry.

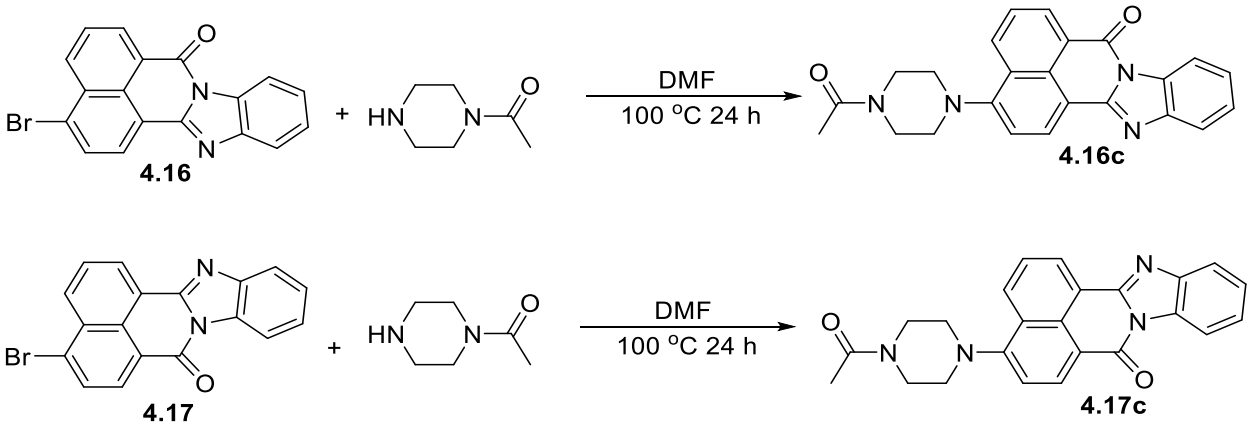

Scheme 4.15

Step 2.3 Introduction of solubilizing groups through S_NAr reactions with thiol

To create thioethers, one equivalent of **4.16** was dissolved in 2-methoxyethanol with ten equivalents of 2-mercaptoethanol and the reaction mixture was heated to reflux for 24 h (Scheme 4.16). At the end of the reaction, the reaction mixture was left to cool and then acidified using 5% HCl to yield 92 % of **4.16d**. The crude product was purified using column chromatography (toluene : ethyl acetate 1:9, R_f=0.33).

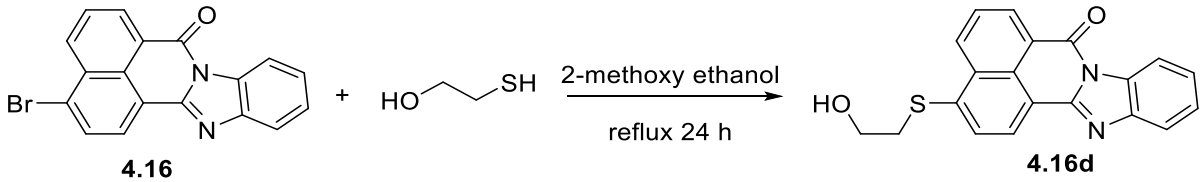

Scheme 4.16

The same protocol was successfully followed to synthesise **4.17d** (Scheme 4.17).

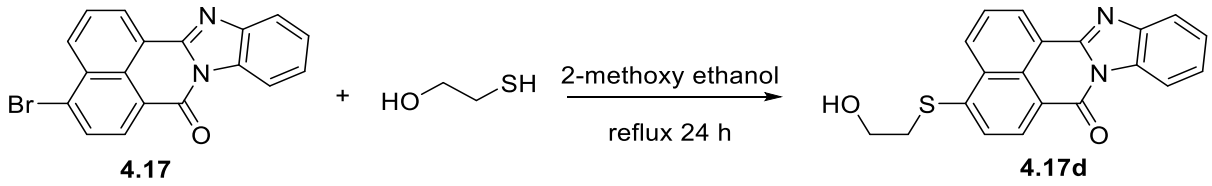

Scheme 4.17

4.2.3 The solubility of all synthesized compounds

The solubility of the synthesized fused-ring-extended 1,8-naphthalimide derivatives was tested by dissolving these compounds in DMSO. Next, 25μL of these stock solutions were added to cuvettes contain 2500 μL of buffer (25 mM MOPS pH 7.0, 50 mM NaCl, 1 mM EDTA). The UV-visible spectra were recorded, and the concentrations were calculated using the Beer Lambert law with the extinction coefficients for the various chromophores as determined in Chapter 2 for sufficiently soluble compounds **2.19-21**. Since the extinction coefficients for the isomers cannot be determined experimentally due to the lack of solubility, the extinction coefficients for the standard chromophore in Chapter 2 were used as an estimation for these compounds. It is an educated guess that this should not cause an error in the concentration of more than a factor of 2. Table 4.3 illustrates the solubility and λ_{max} for the obtained compounds.

Table 4.3 the solubility of compounds 4.16,4.16a-d and 4.17,4-17b-d in MOPS with 1% DMSO

Comp.	**4.16**	**4.16a**	**4.16b**	**4.16c**	**4.16d**
λ_{max}, nm	390	476	441	431	427
Solubility limit, M	5.44×10^{-6}	1.12×10^{-5}	9.04×10^{-6}	3.91×10^{-6}	3.62×10^{-6}
Comp.	**4.17**	**4.17a**	**4.17b**	**4.17c**	**4.17d**
λ_{max}, nm	375	NS	426	425	421
Solubility limit, M	3.86×10^{-6}	NS	9.37×10^{-6}	9.80×10^{-6}	2.74×10^{-6}

NS: not synthesized

4.2.4 UV-visible titrations

The DNA-binding properties of fused-ring-extended 1,8-naphthalimide derivatives **4.16,4.16a-d** and **4.17,4.17b-d** were studied using UV-visible titrations. The measurement of UV-visible absorption spectra of all compounds was conducted during addition of aliquots of a FSDNA stock solution in MOPS buffer (25 mM MOPS pH 7.0, 50 mM NaCl, 1 mM EDTA) with 1% DMSO at 25 °C. The titration was performed twice for each compound and the obtained data were plotted and analyzed using the MIS model,[15] individually and globally, to determine the binding affinity and stoichiometry.

4.2.4.1 UV-visible spectroscopy studies of 4.16 and 4.17

The DNA-binding properties of **4.16** and **4.17** were studied using UV-visible titrations. The titrations were performed twice for each compound and the titration spectra are shown in Figure 4.6.

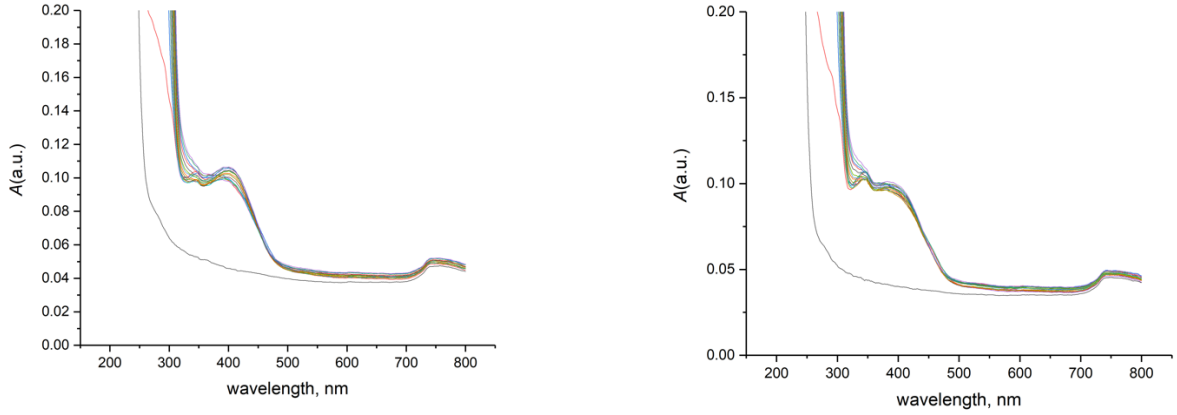

Figure 4.6. The titration spectra for a 5.7 μM solution of 4.16 (left) and a 4.0 μM solution of 4.17 (right) upon addition of aliquots of a FSDNA stock solution in MOPS buffer (25 mM MOPS pH 7.0, 50 mM NaCl, 1 mM EDTA) with 1% DMSO at 25 °C

The titration spectra show small a decrease in the absorbance at λ_{max} at the beginning of the titration, followed by increases in the absorbance with a bathochromic shift. The titration spectra also show some scattering during the titration, probably due to precipitation. Therefore, when extracting the titration curves, the absorbance at the selected wavelength was corrected by subtracting the increase in the baseline absorbance at 600 nm which increases because of the scattering. Since the titrations show bathochromic shift, the obtained data for **4.16** and **4.17** were plotted at 402 and 432 nm, respectively, where the spectra show the highest change in the absorbance.

This choice generates data with a wider range, which reflects the binding better than if the absorbance were plotted at the λ_{max} for **4.16** and **4.17**. Finally, the obtained data were analyzed in terms of the multiple independent binding sites (MIS) model to give binding affinities and binding site sizes (stoichiometries).[15] Datasets were analyzed both individually and globally. The titration curves of **4.16** and **4.17** are shown in Figure 4.7.

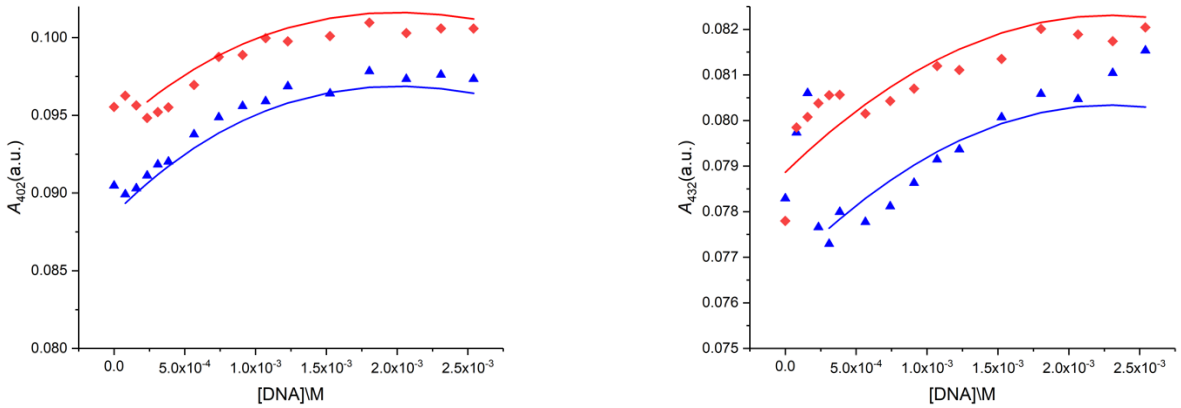

Figure 4.7 Absorbance (corrected for scattering) at 402 nm for 5.7 μM (▲) and 5.2 μM (◆) solutions of 4.16 as a function of FSDNA concentration (left), and absorbance (corrected for scattering) at 432 nm for 4.0 μM (▲), and 3.8 μM (◆) solutions of 4.17 as a function of FSDNA concentration (right) in buffer (25 mM MOPS pH 7.0, 50 mM NaCl, 1 mM EDTA) with 1% DMSO at 25 °C. (▲) 1st titration, (◆) 2nd titration, and the solid lines represent a global fit of a multiple independent sites model to the data.

Table 4.4 illustrates the binding affinity and the binding site size of **4.16** and **4.17**.

Table 4.4 DNA-binding affinity *K* (*n*=3) / M^{-1} of 4.16 and 4.17

***K* (*n*=3) / M^{-1}**	**1st titration**	**2nd titration**	**Global fit**
4.16	390.6±70.72	540.8±123.9	362.4±144.0
4.17	0.31±38.64	0.49±107.7	0.31±48.38

Based on the global fit, the binding affinity of **4.16** equals 362.4±144.0 M^{-1} when the binding site size is restricted to 3 basepairs. Similarly, the binding affinity of **4.17** equals 0.31±48.38 M^{-1} when the binding site size is restricted to 3 basepairs. These binding affinities and the bathochromic shift indicate that **4.16** and **4.17** show negligible, or at best very weak, affinity for DNA (see appendix for unrestricted analysis for the data).

4.2.4.2 UV-visible spectroscopy studies of 4.16a

The binding properties of **4.16a** were studied using UV-visible titrations. The UV-visible absorption spectra were recorded upon addition of FSDNA in MOPS (25 mM MOPS pH 7.0, 50 mM NaCl, 1 mM EDTA) with 1% DMSO at 25 °C. The titration was performed twice and the spectra for one of the titrations of this compound are shown in Figure 4.8, separating the early and later parts of the titration.

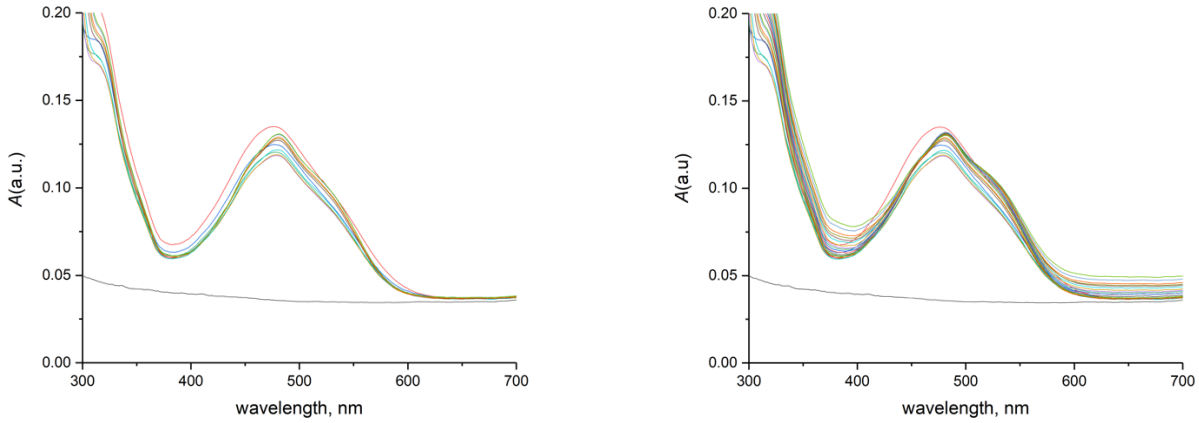

Figure 4.8 The titration spectra for a 11.5 μM solution of 4.16a upon addition of aliquots of a FSDNA stock solution in MOPS buffer (25 mM MOPS pH 7.0, 50 mM NaCl, 1 mM EDTA) with 1% DMSO at 25 °C at the beginning of the titration (left); and at the end of the titration (right).

The titration spectra for **4.16a** exhibit an interesting behavior where the absorbance at λ_{max}=476 nm quickly decreases at the beginning of the titration. After that, the absorbance starts to increase after each addition of FSDNA with a bathochromic shift (476-482 nm). The quick decrease at the beginning of the titration and the bathochromic shift are a strong indication that this compound strongly binds with the DNA. However, this may well involve non-specific binding because of the high ligand:DNA ratios for this initial quick decrease in absorbance. During the titration, some scattering was observed in the spectra due to precipitation. Surprisingly, the increase in scattering does not coincide with the quick decrease in absorbance around λ_{max} at the start of the titration but rather occurs during the later stages of the titration, i.e. in the presence of an excess of DNA. It is

therefore not clear what causes this scattering. To analyze the data, the absorbance was corrected by subtracting the baseline absorbance at 600 nm as affected by the scattering. The obtained data were plotted and the second phase of the data (excluding the initial rapid decrease) was analyzed in terms of the multiple independent binding sites (MIS) model to give apparent DNA-binding affinities K_{app} and binding site sizes (stoichiometries).[15] Datasets were analyzed both individually and globally (Figure 4.9).

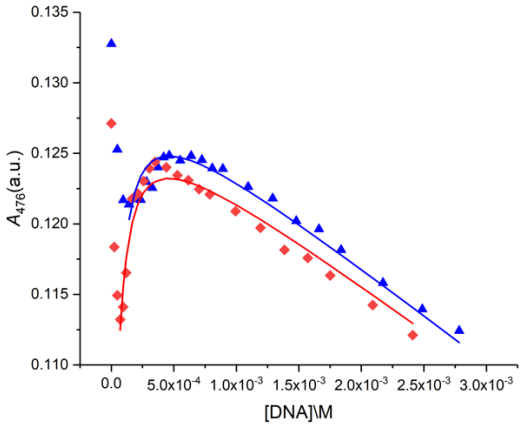

Figure 4.9 Absorbance (corrected for scattering) at 476 nm for 11.5 μM (▲), and 10.9 μM (◆) solutions of 4.16a as a function of FSDNA concentration in buffer (25 mM MOPS pH 7.0, 50 mM NaCl, 1 mM EDTA) with 1% DMSO at 25 °C. (▲) 1st titration, (◆) 2nd titration, the solid lines represent a global fit of a multiple independent sites model to the second part of the data.

The results of the data analysis are shown in Table 4.5.

Table 4.5 The DNA-binding affinity K_{app} (n=3) / M^{-1} of 4.16a

K_{app} (n=3) / M^{-1}	1st titration	2nd titration	Global fit
4.16a	(1.09±0.21)×10^4	(8.55±2.40)×10^4	(8.45±3.11)×10^4
Bathochromic shift, nm	476-482nm		

As indicated above, due to the strange behavior for this compound, the binding affinities were obtained by analyzing the second half of the titrations which is not ideal and does not completely reflect the binding strength

for this compound with DNA. Based on the global fit, the apparent DNA-binding affinity for this compound equals $(8.45\pm3.11)\times10^4$ M^{-1} when the binding site size is restricted to 3 basepairs, which indicates that this compound is a good binder.

4.2.4.3 UV-visible spectroscopy studies of 4.16b and 4.17b

The binding properties of **4.16b** and **4.17b** were studied using UV-visible titrations. The UV-visible absorption spectra were recorded upon addition of aliquots of a FSDNA stock solution in MOPS buffer (25 mM MOPS pH 7.0, 50 mM NaCl, 1 mM EDTA) with 1% DMSO at 25 °C. The titration was performed twice for each compound and the spectra for the first titration for both compounds are shown in Figure 4.10.

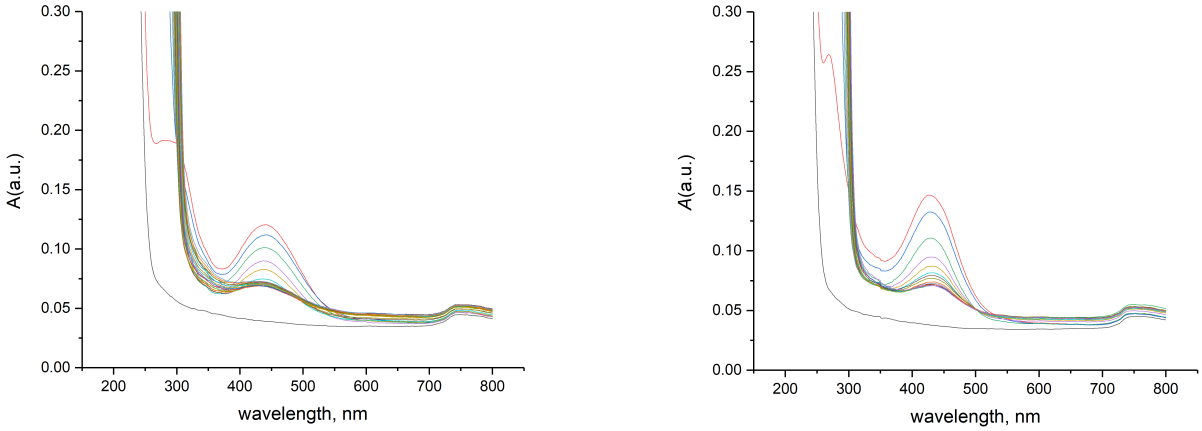

Figure 4.10 The titration spectra for a 8.7 μM solution of 4.16b (left) and a 11.1 μM solution of 4.17b (right) upon addition of aliquots of a FSDNA stock solution in MOPS buffer (25 mM MOPS pH 7.0, 50 mM NaCl, 1 mM EDTA) with 1% DMSO at 25 °C.

The titration spectra for both compounds show strong decreases in the absorbance which indicate that these compounds are interacting strongly with DNA. However, the absorbance then slightly increases in the second half of the titration. During the titration, some scattering was observed in the spectra at higher wavelengths due to precipitation. Overall, this pattern may indicate initial non-specific binding followed by a second phase where non-specifically bound ligand molecules bind in tighter binding sites. To analyze the data, the absorbance was corrected by subtracting the scattering as quantified by the absorbance at 600 nm as before. The obtained data

were plotted and analyzed in terms of the multiple independent binding sites (MIS) model to give binding affinities and binding site sizes (stoichiometries).[15] Datasets were analyzed both individually and globally (Figure 4.11).

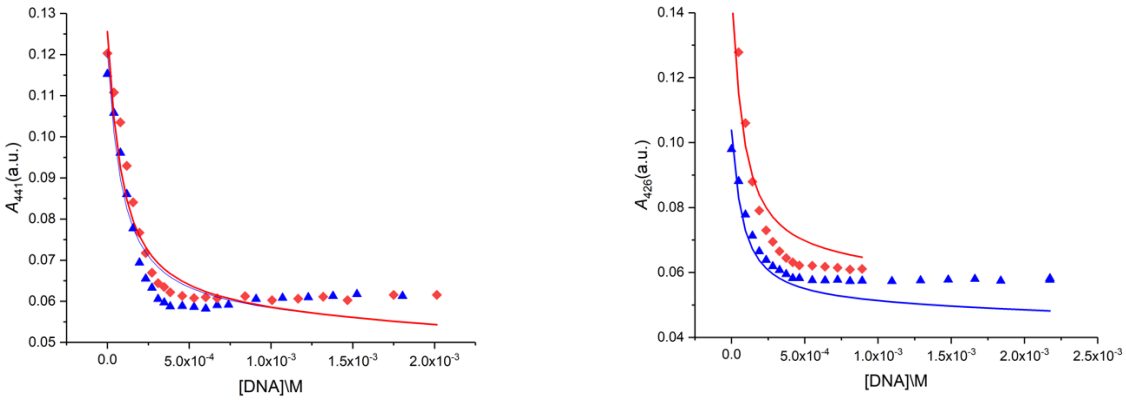

Figure 4.11 Absorbance (corrected for scattering) at 441 nm for 8.7 μM (▲), and 9.4 μM (◆) solutions of 4.16b as a function of FSDNA concentration; and Absorbance (corrected for scattering) at 426 nm for 7.1 μM (▲), and 11.1 μM (◆) solutions of 4.17b as a function of FSDNA concentration in buffer (25 mM MOPS pH 7.0, 50 mM NaCl, 1 mM EDTA) with 1% DMSO at 25 °C. (▲) 1st titration, (◆) 2nd titration, the solid lines represent a global fit of a multiple independent sites model to the data.

Figure 4.11 shows that the titration curves do not follow the expected shape of the graph according to the multiple independent binding sites (MIS) model. This finding is in agreement with the hypothesis that the binding curves in Figure 4.10 do not represent a simple binding event. Nevertheless, MIS model was used to analyze the data in order to get an estimate of the binding affinity and the results of the data analysis are shown in Table 4.6.

Table 4.6 DNA-binding affinity *K* (*n*=3) / M^{-1} of 4.16b and 4.17b.

***K* (*n*=3) / M^{-1}**	**1st titration**	**2nd titration**	**Global fit**
4.16b	(2.18±0.46)×10^4	(3.59±0.89)×10^4	(4.01±0.74)×10^4
4.17b	(5.04±1.09)×10^4	(3.29±0.69)×10^4	(4.65±1.16)×10^4

According to the global fit, both compounds can be considered as a good binder with binding affinities of (4.01±0.74)×10^4 and (4.65±1.16)×10^4 M^{-1} (for *n*=3), respectively. The titration spectra and the titration curves and the binding affinities suggest that **4.16b** and **4.17b** behave similarly in terms of binding to DNA.

4.2.4.4 UV-visible spectroscopy studies of 4.16c and 4.17c

The binding properties of **4.16c** and **4.17c** were studied using UV-vis titrations. The UV-visible absorption spectra were recorded upon addition of FSDNA in MOPS buffer (25 mM MOPS pH 7.0, 50 mM NaCl, 1 mM EDTA) with 1% DMSO at 25 °C. The titration was performed twice for each compound and the titration spectra (Figure 4.12).

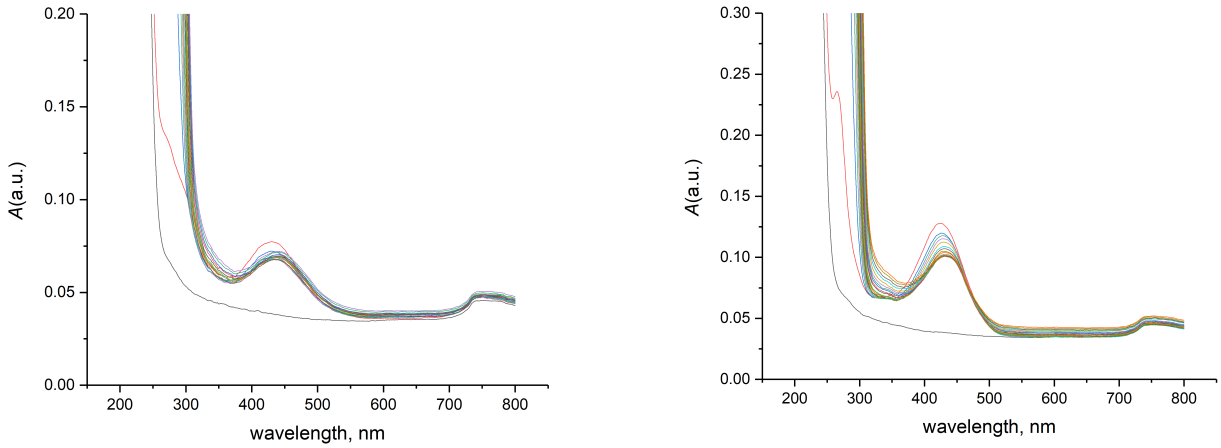

Figure 4.12 The titration spectra for a 4.1 μM solution of 4.16c and a 9.4 μM solution of 4.17c in buffer (25 mM MOPS pH 7.0, 50 mM NaCl, 1 mM EDTA) with 1% DMSO at 25 °C upon addition of aliquots of FSDNA.

The titrations spectra show that **4.17c** exhibits a higher hypochromic shift at the beginning of the titration than **4.16c** which suggests that **4.17c** binds more strongly with DNA than **4.16c**. Figure 4.11 also shows an increase in the baseline at higher wavelength which we attribute to scattering due to precipitation. Therefore, the absorbance was corrected by subtracting the baseline absorbance as affected by scattering. The obtained data were plotted and analyzed in terms of the multiple independent binding sites (MIS) model to give binding affinities and binding site sizes (stoichiometries).[15] Datasets were analysed both individually and globally (Figure 4.13).

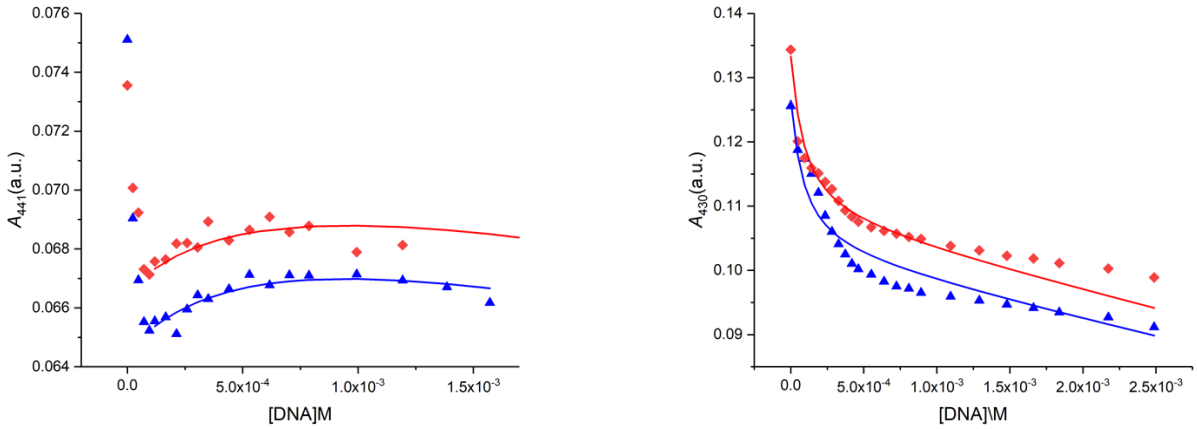

Figure 4.13 Absorbance (corrected for scattering) at 441 nm for 4.1 μM (▲) and 3.7 μM (◆) solutions of 4.16c as a function of FSDNA concentration (left), and absorbance (corrected for scattering) at 430 nm for 9.4 μM (▲) and 10.1 μM (◆) solutions of 4.17c as a function of FSDNA concentration in buffer (25 mM MOPS pH 7.0, 50 mM NaCl, 1 mM EDTA) with 1% DMSO at 25 °C. (▲) 1st titration, (◆) 2nd titration. Solid lines represent a global fit of a multiple independent sites model to the data.

Interestingly, these isomeric compounds don't behave in the same way in terms of binding with DNA. Compound **4.16c** exhibits a small hyperchromic shift in the second half of the titration whereas **4.17c** shows a relatively normal binding graph. The results of the data analysis are shown in Table 4.7.

Table 4.7 Binding affinity *K* (*n*=3) / M^{-1} of 4.16c and 4.17c.

K_{app} (*n*=3) / M^{-1}	1st titration	2nd titration	Global fit
4.16c	(0.39±0.10)×10^4	(0.11±0.04)×10^4	(4.5±3.6)×10^3
4.17c	(2.49±0.62)×10^4	(8.90±2.20)×10^4	(4.07±0.90)×10^4

Based on the global fit, the binding affinities of **4.16c** and **4.17c** equal (4.5±3.6)×10^3 and (4.07±0.90)×10^4 M^{-1} (for *n*=3), respectively. This suggests that **4.17c** binds better with DNA compared to **4.16c**, but this comes with the caveat that both datasets were analysed in very different manner. In fact, the binding affinity for **4.16** is an apparent affinity K_{app} based only on the second phase of the binding curve and thus ignores the stronger binding

during the first phase of the experiment. The fact that the fitted line for **4.17c** in Figure 4.12 doesn't follow the data points suggests that even **4.15** may show a second phase in these titrations but the increase in absorbance associated with this second phase is more than cancelled by the decrease in absorbance caused by dilution of the sample upon the addition of the DNA stock solution.

4.2.4.5 UV-visible spectroscopy studies of 4.16d and 4.17d

The binding properties of **4.16d** and **4.17d** were studied using UV-visible titrations. The UV-visible absorption spectra were recorded upon addition of FSDNA in MOPS buffer (25 mM MOPS pH 7.0, 50 mM NaCl, 1 mM EDTA) with 1% DMSO at 25 °C. The titration was performed twice for each compound (Figure 4.14).

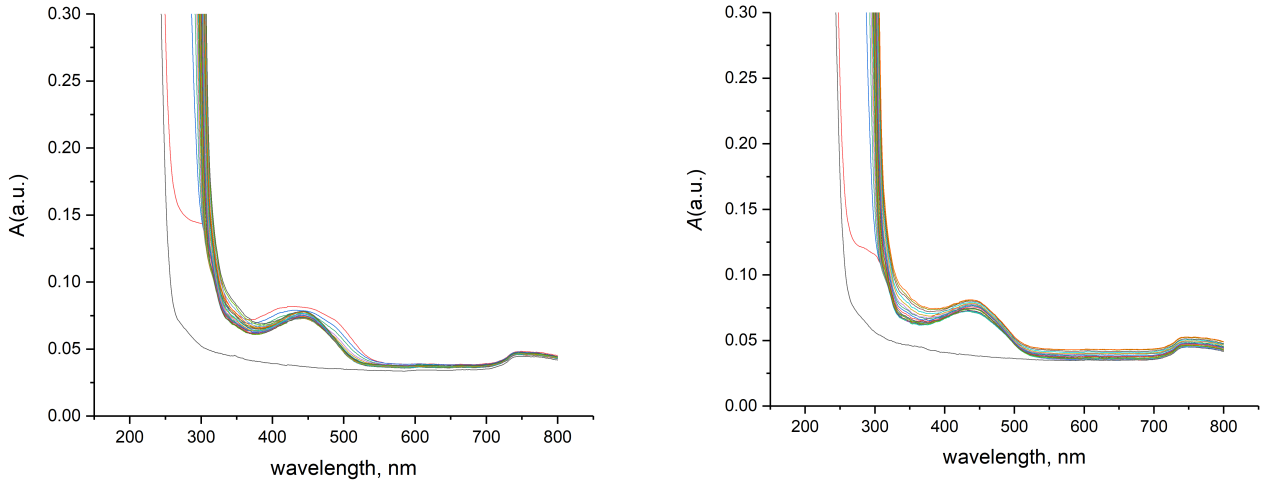

Figure 4.14 The FSDNA titration spectra for a 3.6 μM solution of a 4.16d (left) and a 2.8 μM solution of 4.17d (right) in buffer (25 mM MOPS pH 7.0, 50 mM NaCl, 1 mM EDTA) with 1% DMSO at 25 °C.

The titration spectra of **4.16d** and **4.17d** show a similar pattern as observed in case of **4.16a**, where the absorbance shows a hypochromic shift at the beginning of the titration followed by hyperchromic shift. As before, this pattern suggests two binding phases. In the first phase, the excess of ligand binds to all available binding sites, i.e. tight binding sites and weaker secondary binding sites. This corresponds to the steep decrease in absorbance at the start of the titration. During the second phase of the titration, weakly bound ligand in secondary binding sites moves to the additional tighter binding sites offered by the added DNA.

The absorbance was corrected for scattering as before and was plotted as a function on DNA concentration resulting in a graph that can analysed to obtain the apparent binding affinities and the binding site size. The obtained curves were analyzed in terms of the multiple independent binding sites (MIS) model to give apparent binding affinities and binding site sizes (stoichiometries).[15] Datasets were analysed both individually and globally (Figure 4.15).

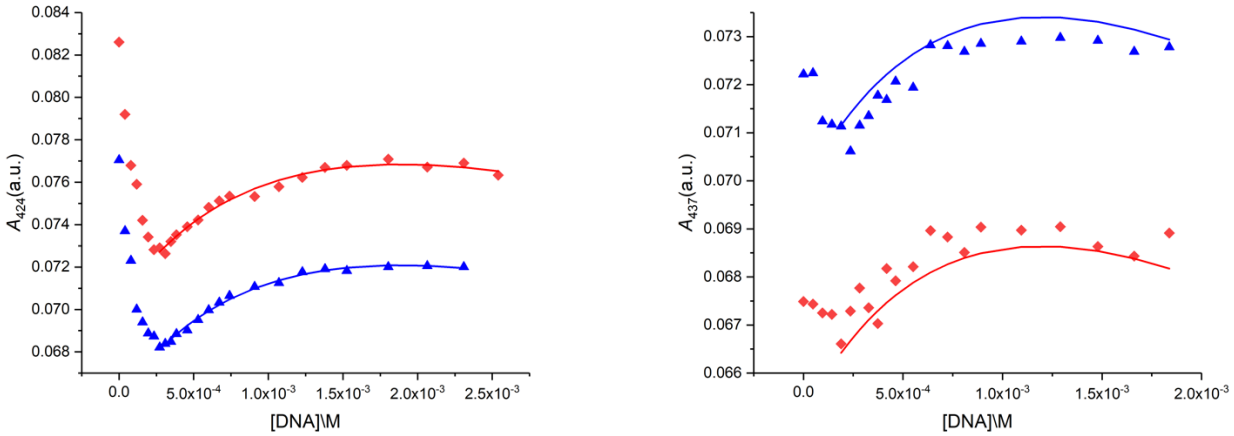

Figure 4.15 Absorbance (corrected for scattering) at 424 nm for 3.6 μM (▲) and 3.7 μM (◆) solutions of 4.16d as a function of FSDNA concentration (left); and absorbance (corrected for scattering) at 437 nm for 2.8 μM (▲) and 2.7 μM (◆) solutions of 4.17d as a function of FSDNA concentration (right) in buffer (25 mM MOPS pH 7.0, 50 mM NaCl, 1 mM EDTA) with 1% DMSO at 25 °C. (▲) 1st titration, (◆) 2nd titration, and the solid lines represent a global fit of a multiple independent sites model to the data.

The titration curves indicate that both compounds behave in a relatively similar way in terms of binding with DNA in the second phase of the titration. The results of the data analysis are shown in Table 4.8.

Table 4.8 DNA-binding affinity K_{app} (n=3) / M^{-1} of 4.16d and 4.17d

K_{app} (n=3) / M^{-1}	1st titration	2nd titration	Global fit
4.16d	$(0.21\pm0.08)\times10^4$	$(0.15\pm0.99)\times10^4$	$(1.8\pm0.7)\times10^3$
4.17d	$(2.0\pm0.5)\times10^3$	$(1.5\pm0.5)\times10^3$	$(2.0\pm0.9)\times10^3$

Based on the global fit, the apparent binding affinities of **4.16d** and **4.17d** equal 1.8×10^3 and 2.0×10^3 M^{-1} (for n=3) respectively which means that both compounds bind with DNA with the same strength. The presence of a first phase in the titration indicates that stronger binding also occurs, in particular for **4.16d**.

4.2.5 Conclusions

A series of compounds with extended aromatic surfaces was successfully synthesized. Generally, this class of compounds shows an interesting behavior with DNA where almost all compounds show high hypochromic shift at the beginning of the titration followed by an increase in absorbance in a second phase of the titration. This pattern suggests that these compounds tend to bind with the DNA through both specific and non-specific binding. Alternatively, or possibly in addition, aggregation may also play a role since this class of compounds is highly hydrophobic. DNA binding may therefore be associated with de-aggregation of aggregates present in solution, or DNA binding could template aggregation processes.

During the titration most of the compounds exhibit hyperchromic and bathochromic shift which we consider as an indication of binding. There is no clear difference in terms of binding with DNA between the two isomers, which is not unreasonable considering that selectivity resulting from an intercalative binding mode is not often observed.

This class of compounds exhibits different behavior compared to ferrocene-naphthalimide conjugates in chapter 2 and bisnaphthalimide derivatives in chapter 3. As mentioned above, it exhibits high hypochromic shift at the beginning of the titration followed by an increase in absorbance in a second phase of the titration which was not ideal to be analyzed using MIS model. Nevertheless, DNA-binding affinities K_{app} for this class show some improvement relative to the mononaphthalimides but these values are not be reliable to compare the binding properties for this class with ferrocene-naphthalimide conjugates in chapter 2 and bisnaphthalimide derivatives in chapter 3 because the compounds studied in this chapter display more complex binding equilibria.

4.3 Experimental

4.3.1 Materials and measurements

All chemicals, including FS DNA, were procured from Sigma-Aldrich, Fisher or TCI and were used without further purification. Flash column chromatography was carried out using 60 Å silica. All compounds show strong fluorescence and were readily visualized on TLC plates using UV light. ^{1}H-NMR and ^{13}C-NMR spectra were recorded utilizing a Bruker AV 400 UltraShield spectrometer and Bruker AV 500 UltraShield spectrometer using the solvent as an internal standard. All chemical shifts are reported with respect to TMS. High resolution mass spectra were recorded using a Waters Micromass LCT Premier. UV-visible spectra were recorded using a Jasco V-650 spectrophotometer at controlled temperature using an air-cooled EHCS-716 Peltier Thermostatted Cell Holder at 25 °C. The pH of buffers was recorded using Hanna microprocessor pH-meter equipped with a VWR 662-1382 glass electrode. The pH meter was calibrated using a two-point calibration with buffers of known pH obtained from Fisher scientific. Deionized water was obtained from an Elga Purelab Flex.

4.3.2 Synthetic Procedures

Synthesis of (3-chloro-7H-benzo[de]benzo[4,5]imidazo[2,1-a]isoquinolin-7-one) 4.16-Cl and (4-chloro-7H-benzo[de]benzo[4,5]imidazo[2,1-a]isoquinolin-7-one) 4.17-Cl

In a round bottom flask, one equivalent of 4-chloro-1,8-naphthalic anhydride (2.32 g, 10 mmol) and one equivalent of o-phenylene diamine (10 mmol, 1.08 g) were dissolved in ≈ 50 mL acetic acid and refluxed for 2 h. After that the solution was left to cool and poured in ≈50 mL water and the obtained solid was filtered and washed with ethanol to produce a mixture of two isomers in 91% yield. **^{1}H-NMR (400 MHz, DMSO-d$_6$): δ(ppm)** 8.85 (d, *J*= 7.20, 1H, Ar-CH), 8.80 (d, *J*= 7.28, 1H, Ar-CH), 8.73 (d, *J*= 8.44 Hz, 1H, Ar-CH), 8.70 (d, *J*= 7.88 Hz, 1H, Ar-CH), 8.65 (d, *J*= 7.88 Hz, 1H, Ar-CH), 8.57 (d, *J*= 8.56 Hz, 1H, Ar-CH), 8.45-8.43 (m, 2H, Ar-CH), 8.14 (d, *J*= 8.76 Hz, 1H, Ar-CH), 8.10 (d, *J*= 7.72 Hz, 2H, Ar-CH), 8.06 (d, *J*= 7.76 Hz, 1H, Ar-CH), 7.91-7.88 (m, 2H, Ar-CH), 7.53-7.51 (m, 4H, Ar-CH). **^{13}C-NMR (125 MHz, DMSO-d$_6$): δ(ppm)** 160.3, 160.1, 149.4, 149.1, 147.7, 147.5, 143.9, 143.9, 139.1, 135.5, 132.6, 132.0, 132.0, 131.9, 131.7, 129.7, 129.6, 129.5, 129.2, 128.6, 128.4, 128.3, 128.3, 128.2, 128.0, 127.2, 126.2, 125.9, 125.9, 124.2, 123.0, 121.6, 120.5, 120.4, 120.4, 115.8. **HR FTMS+** calc for [$C_{18}H_{10}N_2OCl$] 305.0482 found 305.0489.

Synthesis of (3-bromo-7H-benzo[de]benzo[4,5]imidazo[2,1-a]isoquinolin-7-one) 4.16 and (4-bromo-7H-benzo[de]benzo[4,5]imidazo[2,1-a]isoquinolin-7-one) 4.17

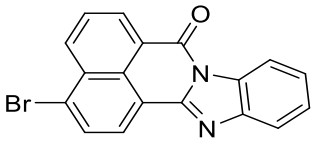

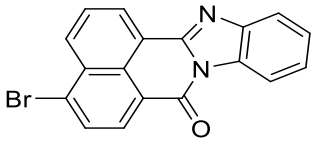

In a round bottom flask, one equivalent of 4-bromo-1,8-naphthalic anhydride (2.77 g, 10 mmol) and two equivalents of o-phenylene diamine (20 mmol, 2.16 g) were dissolved in 50 ml of acetic acid and refluxed for 2h. After that the solution was left to cool and poured in ≈50 mL water, the obtained solid was filtered and yielded a mixture of two isomers in 98 % yield. The two isomers were separated using column chromatography (toluene: ethyl acetate 5:1). **4.16 (cis): ^{1}H-NMR (500 MHz, $CDCl_3$-d): δ(ppm):** 8.77 (dd, *J*= 7.30, *J*= 1.10 Hz, 1H, Ar-CH), 8.60 (dd, *J*= 8.45, *J*= 1.15 Hz, 1H, Ar-CH), 8.59 (d, *J*= 7.90 Hz, 1H, Ar-CH), 8.46 (dd, *J*= 6.10, *J*= 3.15 Hz, 1H, Ar-CH), 8.01 (d, *J*= 7.85 Hz, 1H, Ar-CH), 7.84 (dd, *J*= 8.45, *J*= 7.30 Hz, 1H, Ar-CH), 7.80 (dd, *J*= 5.82, *J*= 3.37 Hz, 1H, Ar-CH), 7.42 (d, *J*= 6.05 Hz, 1H, Ar-CH), 7.42 (d, *J*= 6.10 Hz, 1H, Ar-CH). **^{13}C-NMR (125 MHz, $CDCl_3$-d): δ(ppm):** 160.0, 148.6, 134.7, 132.6, 131.7, 131.6, 131.3, 128.2, 128.1, 127.8, 127.4, 126.1, 125.8, 123.6, 120.2, 120.0, 115.9. **HR FTMS+** calc for [$C_{18}H_9N_2OBr$] 347.98928 found 347.9898.

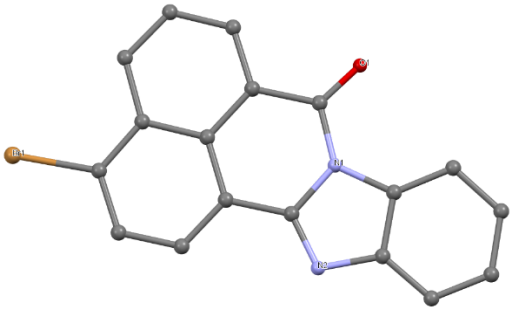

4.17 (trans): ^{1}H-NMR (500 MHz, $CDCl_3$-d): δ(ppm): 8.86 (dd, *J*= 7.45 Hz, 1H, Ar-CH), 8.54 (d, *J*= 7.95 Hz, 1H, Ar-CH), 8.47 (d, *J*= 5.85 Hz, 1H, Ar-CH), 8.47 (d, *J*= 7.55 Hz, 1H, Ar-CH), 8.06 (d, *J*= 7.95 Hz, 1H, Ar-CH), 7.84-7.82 (m, 2H, Ar-CH), 7.44-7.42 (m, 2H, Ar-CH). **^{13}C-NMR (125 MHz, $CDCl_3$-d): δ(ppm):** 160.1, 148.8, 134.9, 132.1, 131.8, 131.7, 131.5, 131.3, 128.7, 128.3, 128.1, 126.2, 125.9, 122.8, 120.9, 120.0, 115.9. **HR FTMS+** calc for [$C_{18}H_9N_2OBr$] 347.98928 found 347.9895.

Synthesis of 3-((2-hydroxyethyl)amino)-7H-benzo[de]benzo[4,5]imidazo[2,1-a]isoquinolin-7-one 4.16a

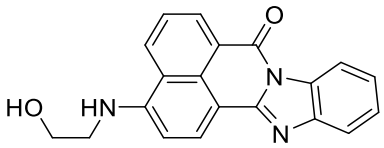

In a round bottom flask, one equivalent of 3-bromo-7H-benzo[de]benzo[4,5]imidazo[2,1-a]isoquinolin-7-one **4.16** (18 mg, 0.05 mmol) was dissolved in ≈10 mL ethanol amine. The reaction mixture was heated at 100 °C for 24 h. The reaction mixture was left to cool and then extracted in DCM and water. The organic layer was dried over $MgSO_4$ and the solvent was evaporated under vacuum. The crude **4.16a** was obtained in 31% and purified using column chromatography (DCM-ethanol 9:1) (R_f=0.5). **^{1}H-NMR (400 MHz, ACETONE-d_6): δ(ppm):** 8.82 (d, *J*= 8.32 Hz, 1H, Ar-CH), 8.79 (d, *J*= 6.80 Hz, 1H, Ar-CH), 8.67 (d, *J*= 8.36 Hz, 1H, Ar-CH), 8.51 (d, *J*= 8.72 Hz, 1H, Ar-CH), 7.83 (dd, *J*= 8.52 Hz, *J*= 7.48 Hz, 1H, Ar-CH), 7.75 (d, *J*= 8.08 Hz, 1H, Ar-CH), 7.47-7.43 (m, 1H, Ar-CH), 7.41-7.37 (m, 1H, Ar-CH), 7.02 (d, *J*= 8.72 Hz, 1H, Ar-CH), 4.31-4.27 (m, 1H, OH), 3.96 (q, *J*= 5.72 Hz, 2H, CH_2), 3.66 (q, *J*= 5.72 Hz, 2H, CH_2). **HR FTMS+** calc for [$C_{20}H_{16}N_3O_2$] 330.1242 found 330.1239.

Synthesis of 3-morpholino-7H-benzo[de]benzo[4,5]imidazo[2,1-a]isoquinolin-7-one 4.16b

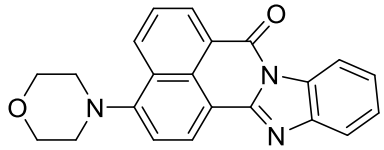

In a round bottom flask, one equivalent of 3-bromo-7H-benzo[de]benzo[4,5]imidazo[2,1-a]isoquinolin-7-one **4.16** (24.9 mg, 0.07 mmol) and ten equivalents of morpholine (62 mg, 0.72 mmol) were dissolved in ≈20 mL DMF. The reaction mixture was heated at 100 °C for 24 h. At the end the solvent was removed under vacuum and methanol was added to obtain pure 3-morpholino-7H-benzo[de]benzo[4,5]imidazo[2,1-a]isoquinolin-7-one **4.16b** as an orange solid in 70 % yield. **^{1}H-NMR (500 MHz, ACETONE-d_6): δ(ppm):** 8.66 (dd, J= 7.20, J= 1.30 Hz, 1H, Ar-CH), 8.64 (d, J= 7.90, 1H, Ar-CH), 8.63 (dd, J= 8.32, J= 1.22 Hz, 1H, Ar-CH), 8.38-8.36 (m, 1H, Ar-CH), 8.81 (dd, J= 8.45, J= 7.35 Hz, 1H, Ar-CH), 7.69-8.67 (m, 1H, Ar-CH), 7.39 (d, J= 7.75 Hz, 1H, Ar-CH), 7.36-7.34 (m, 2H, Ar-CH), 3.87 (t, J= 4.58 Hz, 4H, CH2), 3.18 (t, J= 4.12 Hz, 4H, CH2). **^{13}C-NMR (125 MHz, ACETONE-d_6): δ(ppm):** 160.7, 154.3, 144.4, 131.7, 131.3, 128.7, 128.1, 127.2, 126.2, 125.7, 125.4, 124.5, 119.6, 119.4, 116.0, 115.5, 115.4, 115.2, 66.7. **HR FTMS+** calc for [$C_{22}H_{18}N_3O_2$] 356.1399 found 356.1396.

Synthesis of 3-morpholino-7H-benzo[de]benzo[4,5]imidazo[2,1-a]isoquinolin-7-one 4.17b

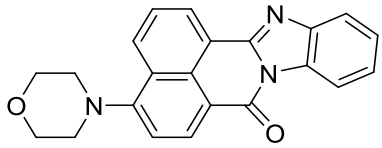

In round bottom flask, one equivalent of (4-bromo-7H-benzo[de]benzo[4,5]imidazo[2,1-a]isoquinolin-7-one) **4.17** (70.5 mg, 0.20 mmol) and ten equivalents of morpholine (176 mg, 2 mmol) were dissolved in ≈ 20 mL DMF. The reaction mixture was heated at 100 °C for 24 h. At the end the solvent was removed under vacuum and methanol was added to obtain pure 4-morpholino-7H-benzo[de]benzo[4,5]imidazo[2,1-a]isoquinolin-7-one **4.17b** as an orange solid in 58 % yield.**^{1}HNMR (500 MHz, ACETONE-d_6): δ (ppm):** 8.83 (d, *J*= 6.0, J= 1.30 Hz, 1H, Ar-CH), 8.66 (d, *J*= 8.1, 1H, Ar-CH), 8.52-8.50 (m, 1H, Ar-CH), 8.30 (d, *J*=8.5, 1H, Ar-CH), 7.84-7.83 (m, 1H, Ar-CH), 7.70 (t, *J*=7.8, 1H, Ar-CH), 7.43-7.41 (m, 1H, Ar-CH), 7.22 (d, *J*=8.10, 1H, Ar-CH), 3.98 (t, *J*= 4.50 Hz, 4H, CH_2), 4.47 (t, *J*= 4.5 Hz, 4H, CH_2). **^{13}C NMR (125 MHz, $CDCl_3$): δ (ppm):** 160.9, 160.6, 157.0, 133.5, 129.0, 128.3, 126.7, 126.4, 125.9, 125.4, 119.7, 118.5, 116.1, 115.2, 66.5, 53.7. **HR TOF MS ES+** calc for [$C_{22}H_{18}N_3O_2$] 356.1399 found 356.1399.

Synthesis of 3-(4-acetylpiperazin-1-yl)-7H-benzo[de]benzo[4,5]imidazo[2,1-a]isoquinolin-7-one 4.16c

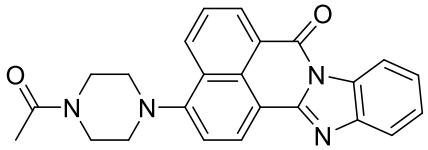

In a round bottom flask, one equivalent of 3-bromo-7H-benzo[de]benzo[4,5]imidazo[2,1-a]isoquinolin-7-one **4.16** (14.9 mg, 0.042 mmol) and ten equivalents of 1-acteyl piperazine (54.8 mg, 0.42 mmol) were dissolved in ≈20 mL DMF. The reaction mixture was heated at 100 °C for 48 h. Then the solvent was removed under vacuum and methanol was added to obtain an orange crude product (89 %). The crude product was purified with column chromatography over silica (toluene: ethyl acetate 1:1) to remove impurities and then the product was washed off the column with (DCM: ethanol 9:1) to obtain pure 3-(4-acetylpiperazin-1-yl)-7H-benzo[de]benzo[4,5]imidazo[2,1-a]isoquinolin-7-one **4.16c**. **^{1}H-NMR (500 MHz, ACETONE-d_6): δ(ppm):** 8.66 (d, *J*= 7.20 Hz, 1H, Ar-CH), 8.66 (d, *J*= 8.40 Hz, 1H, Ar-CH), 8.63 (d, *J*= 7.70 Hz, 1H, Ar-CH), 8.38-8.36 (m, 1H, Ar-CH), 7.82 (dd, *J*= 8.22, *J*= 7.32 Hz, 1H, Ar-CH), 7.69-7.67 (m, 1H, Ar-CH), 7.39 (d, *J*= 8.20 Hz, 1H, Ar-CH), 7.36-7.33 (m, 2H, Ar-CH), 3.77 (t, *J*= 4.72 Hz, 4H, CH_2), 3.22 (t, *J*= 4.85 Hz, 2H, CH_2), 3.14 (t, *J*= 4.50 Hz, 2H, CH_2), 2.00 (s, 3H, CH_3). **^{13}C-NMR (125 MHz, ACETONE-d_6): δ(ppm):** 168.3, 160.7, 154.1, 149.5, 144.3, 131.9, 131.6, 131.3, 129.7, 128.6, 128.0, 127.4, 126.3, 125.4, 124.5, 123.8, 119.6, 116.4, 115.5, 53.4, 53.2, 46.2, 41.2, 20.6. **HR TOF MS ES+** calc for [$C_{24}H_{21}N_4O_2$] 397.1674 found 397.1665.

Synthesis of 3-morpholino-7H-benzo[de]benzo[4,5]imidazo[2,1-a]isoquinolin-7-one 4.17c

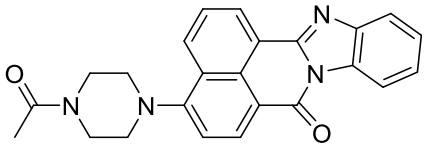

In a round bottom flask, one equivalent of 4-bromo-7H-benzo[de]benzo[4,5]imidazo[2,1-a]isoquinolin-7-one **4.17** (48.9 mg, 0.14 mmol) and ten equivalents of 1-acetyl piperazine (0.18 g, 1.4 mmol) were dissolved in ≈20 mL DMF. The reaction mixture was heated at 100 °C for 48 h. at the end the solvent was removed under vacuum and methanol was added to obtain an orange crude product (85 %). The crude product was purified by column chromatography over silica (toluene: ethyl acetate 1:1) to remove impurities then the compound was washed off the column with (DCM: ethanol 9:1) to obtain pure 4-(4-acetylpiperazin-1-yl)-7H-benzo[de]benzo[4,5]imidazo[2,1-a]isoquinolin-7-one **4.17c**. **^{1}H-NMR (500 MHz, $CDCl_3$-d): δ(ppm):** 8.91 (d, *J*= 6.85 Hz, 1H, Ar-CH), 8.76 (d, *J*= 8.05 Hz, 1H, Ar-CH), 8.60-8.58 (m, 1H, Ar-CH), 8.49 (dd, *J*= 8.50 Hz, *J*= 0.90 Hz, 1H, Ar-CH), 7.93-7.91 (m, 1H, Ar-CH), 7.82 (dd, *J*= 8.40 Hz, *J*= 7.45 Hz, 1H, Ar-CH), 7.52-7.50 (m, 2H, Ar-CH). 7.32 (d, *J*= 8.50 Hz, 1H, Ar-CH), 3.99 (br.signal, 2H, CH_2), 3.84 (t, *J*= 4.95 Hz, 2H,CH_2), 3.35 (t, *J*= 4.47 Hz, 2H,CH_2), 3.31 (t, *J*= 4.47 Hz, 2H,CH_2), 2.23 (s, 3H, CH_3). **^{13}C-NMR (125 MHz, $CDCl_3$-d): δ(ppm):** 169.3, 160.5, 156.4, 149.5, 133.2, 132.0, 131.9, 129.0, 127.9, 127.4, 126.8, 126.6, 125.8, 125.4, 119.8, 117.9, 116.0, 115.6, 53.2, 53.1, 46.5, 41.6, 21.6. **HR TOF MS ES+** calc for [$C_{24}H_{21}N_4O_2$] 397.1665 found 397.1666.

Synthesis of 3-((2-hydroxyethyl)thio)-7H-benzo[de]benzo[4,5]imidazo[2,1-a]isoquinolin-7-one 4.16d

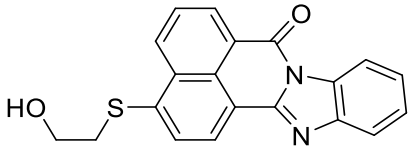

In a round bottom flask, one equivalent of 3-bromo-7H-benzo[de]benzo[4,5]imidazo[2,1-a]isoquinolin-7-one **4.16** (34.9 mg, 0.1 mmol) and 1.5 equivalents of 2-mercaptoethanol (11.7 mg, 0.15 mmol) and one equivalent of $NaHCO_3$ (8.4 mg, 0.1 mmol) were dissolved in ≈20 mL 2-methoxyethanol. The reaction mixture was heated at 100 °C for 24 h and then left to cool and acidified using 1 M HCl. The crude product 3-((2-hydroxyethyl)thio)-7H-benzo[de]benzo[4,5]imidazo[2,1-a]isoquinolin-7-one **4.16d** was obtained in 93 % yield. The crude product was purified using column chromatography (toluene-ethyl acetate, 1:9) R_f=0.3. **^{1}H-NMR (400 MHz, DMSO-d_6): δ(ppm):** 8.78 (dd, J= 7.44 Hz, J= 1.24 Hz, 1H, Ar-CH), 8.74 (dd, J= 8.46 Hz, J= 0.90 Hz, 1H, Ar-CH), 7.92 (d, J= 7.92 Hz, 1H, Ar-CH), 8.46-8.44 (m, 1H, Ar-CH), 8.01 (dd, *J*= 8.52 Hz, *J*= 7.24 Hz, 1H, Ar-CH), 7.92 (d, *J*= 8.04 Hz, 1H, Ar-CH), 7.89-

7.87 (m, 1H, Ar-CH), 7.51-7.49 (m, 2H, Ar-CH), 4.66 (s, 1H, OH), 3.75 (q, *J*= 5.88 Hz, 2H, CH_2), 3.38 (t, *J*= 6.38 Hz, 2H, CH_2). **HR FTMS$^+$** calc for [$C_{20}H_{14}N_2O_2S$] 346.07705 found 346.0776.

Synthesis of 3-((2-hydroxyethyl)thio)-7H-benzo[de]benzo[4,5]imidazo[2,1-a]isoquinolin-7-one 4.17d

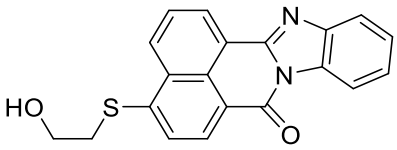

In a round bottom flask, one equivalent of 4-bromo-7H-benzo[de]benzo[4,5]imidazo[2,1-a]isoquinolin-7-one **4.17** (0.1 g, 0.3 mmol) and 1.5 equivalents of 2-mercaptoethanol (0.04 g, 0.45 mmol) and one equivalent of $NaHCO_3$ (0.03 g, 0.3 mmol) were dissolved in ≈20 mL 2-methoxyethanol. The reaction mixture was heated at 100 °C for 24 h and then left to cool and acidified using 1 M HCl. The product 4-((2-hydroxyethyl)thio)-7H-benzo[de]benzo[4,5]imidazo[2,1-a]isoquinolin-7-one **4.17d** was obtained in 77 % yield. The crude product was purified using column chromatography (toluene-ethyl acetate, 1:9) R_f= 0.3. **^{1}H-NMR (500 MHz, ACETONE-d_6): δ(ppm):** 8.85 (dd, *J*= 7.25, *J*= 1.20 Hz, 1H, Ar-CH), 8.50 (dd, *J*= 8.47, *J*= 1.17 Hz, 1H, Ar-CH), 8.76 (d, *J*= 7.85 Hz, 1H, Ar-CH), 8.53-8.51 (m, 1H, Ar-CH), 8.03 (dd, *J*= 8.42, *J*= 7.27 Hz, 1H, Ar-CH), 7.99 (d, *J*= 8.00 Hz, 1H, Ar-CH), 7.856-7.82 (m, 1H, Ar-CH), 7.51 (t, *J*= 5.57 Hz, 1H, Ar-CH), 7.51 (d, *J*= 7.30 Hz, 1H, Ar-CH), 4.28 (t, *J*=4.72 Hz, 1H, C-OH), 3.94 (q, *J*= 6.25 Hz, 2H, CH_2), 3.47 (t, *J*= 6.50 Hz, 2H, CH_2).**TOF MS ES+** calc for [$C_{20}H_{15}N_2O_2S$] 347.0854 found 347.0842.

4.3.3 Ligand solubility tests

To prepare the ligand solutions, several milligrams of the synthesized compounds were dissolved in DMSO (Table 4.9). 25 μl of the DMSO stock solution was added into a 1 cm pathlength thermostatted quartz cuvette containing 2500 μl buffer (25 mM MOPS, 50 mM NaCl, 1mM EDTA). The spectra were recorded at 25 °C and the concentrations were calculated using Beer Lambert law using the extinction coefficients for the reference compounds synthesized in Chapter 2.

Table 4.9 concentration of stock solution of (4.16,4.16a-d) and (4.17, 4.17b-d) in DMSO

Comp.	4.16	4.16a	4.16b	4.16c	4.16d
Concentration, mg\ml	2	0.8	0.36	0.4	7.38
Comp.	4.17	4.17a	4.17b	4.17c	4.17d
Concentration, mg\ml	2.34	NS	0.91	0.24	0.9

4.3.4 UV-Visible titration

4.3.4.1 Preparation of Buffer

3-(*N*-morpholino)propanesulfonic acid (MOPS) (10.463 g, 50 mmol), ethylenediaminetetraacetic acid (EDTA) (0.584 g, 2 mmol) and sodium chloride (5.844 g, 100 mmol) were placed in a 2 litre beaker with a magnetic stirrer bar. 1500 mL of deionised water was added, and the mixture stirred until all solid had dissolved. The pH of the solution was tested with a calibrated pH meter and adjusted to pH 7.00±0.02 by addition of a concentrated sodium hydroxide solution. The solution was then transferred to a 2 litre volumetric flask and made up to 2 litres with distilled water. The flask was inverted to make sure the solution was completely homogenous before transferring to a bottle for storage.

4.3.4.2 Preparation of DNA Solution

Fish sperm DNA (FSDNA) (~0.1 g) was placed in a 10 mL falcon tube with MOPS buffer (10 mL). The solution was sonicated to dissolve the solid then left to stand overnight to ensure all material was in solution. The solution was dialysed overnight using 3.5 kDa MWCO (molecular weight cut-off) dialysis tubing (Visking from Medicell) against 1 litre of buffer, then the dialysis buffer was replaced with a fresh litre of buffer, and the dialysis step repeated. The concentration of the DNA solution was determined spectrophotometrically by placing 10 µL of the resulting DNA stock solution in 2500 µL of buffer and recording a UV-visible spectrum between 200-800 nm. A molar absorptivity of 12,600 M^{-1} (bp) cm^{-1} at 260 nm was used. The concentrations of the solutions were determined to be 0.01008 and 0.01215 mol dm^{-3}.

4.3.4.3 UV-visible titration

The titrations were performed by placing 25 μl of the DMSO stock solution of ligand into a 1 cm pathlength quartz cuvette containing 2500 μl buffer (25 mM MOPS, 50 mM NaCl, 1mM EDTA). The UV-visible spectrum was recorded at 25 °C. The absorbance in the range of 0.06-0.1 a.u. was recorded in a cuvette to avoid self-aggregation and precipitation of the ligand The DNA solution was added stepwise in small aliquots (5-10 μl) and the UV-visible spectra were recorded within the range 200-600 nm after each addition of DNA. The absorptions at maximum wavelengths as a function of DNA and ligand concentrations were extracted from the UV-visible spectra. The obtained data for each titration were analysed using Origin 2017 by plotting the absorption as a function of DNA concentration. The multiple independent binding sites model[15] was used to determine the binding properties.

4.3.5 Molecular Docking study

The chemical structure for proposed compounds were drawn using ChemDraw Professional 16.0 and it was subjected for geometrical optimization using MM2 (molecular dynamics and energy minimized) in Chem3D 16.0 in separate file. The final structure was saved as PDB format and converted to PDBQT file in AutoDock Tools after checking the torsions for all the bonds. The crystal structure of DNA with pre-formed intercalation gap[17] d(ATCGAGACGTCTCGAT)$_2$ was used for the docking using AutoDock Vina[14] with the below parameters (Figure 4.16).

center_x = -2.152 center_y = 2.953 center_z = 24.92 size_x = 40 size_y = 40 size_z = 60 exhaustiveness = 200 num_modes = 10	**Definition:** **Center [x][y][z]**: box center in the receptor coordinate system. **Size [x][y][z]**: box dimensions along X, Y, and Z in the receptor coordinate system. **num_modes**: maximum number of binding modes to generate. **Exhaustiveness:** the time spent on the search is already varied heuristically depending on the number of atoms, flexibility, etc

Figure 4.16 The docking parameters

Acknowledgements

I thank Dr Benson Kariuki for the determination of the X-ray structure of **4.16.**

4.4 References

1. Brana, M. F.; Cacho, M.; Gradillas, A.; Pascual-Teresa, B. d.; Ramos, A., Intercalators as Anticancer Drugs. *Current Pharmaceutical Design* **2001,** *7* (17), 1745-1780.

2. Sami, S. M.; Dorr, R. T.; Solyom, A. M.; Alberts, D. S.; Remers, W. A., Amino-Substituted 2-[2-(Dimethylamino)ethyl]-1,2-dihydro-3H-dibenz[de,h]isoquinoline-1,3-diones. Synthesis, Antitumor Activity, and Quantitative Structure-Activity Relationship. *Journal of Medicinal Chemistry* **1995,** *38* (6), 983-993.

3. Chen, Z.; Xu, Y.; Qian, X., Naphthalimides and analogues as antitumor agents: A review on molecular design, bioactivity and mechanism of action. *Chinese Chemical Letters* **2018,** *29* (12), 1741-1756.

4. Li, S.; Zhong, W.; Li, Z.; Meng, X., Unprecedented synthesis, in vitro and in vivo anti-cancer evaluation of novel triazolonaphthalimide derivatives. *Eur J Med Chem* **2012,** *47* (1), 546-52.

5. Tandon, R.; Luxami, V.; Kaur, H.; Tandon, N.; Paul, K., 1,8-Naphthalimide: A Potent DNA Intercalator and Target for Cancer Therapy. *Chem Rec* **2017,** *17* (10), 956-993.

6. Qian, X.; Li, Z.; Yang, Q., Highly efficient antitumor agents of heterocycles containing sulfur atom: linear and angular thiazonaphthalimides against human lung cancer cell in vitro. *Bioorg Med Chem* **2007,** *15* (21), 6846-51.

7. Tian, Z. Y.; Li, J. H.; Li, Q.; Zang, F. L.; Zhao, Z. H.; Wang, C. J., Study on the synthesis, biological activity and spectroscopy of naphthalimide-diamine conjugates. *Molecules* **2014,** *19* (6), 7646-68.

8. Ge, C.; Chang, L.; Zhao, Y.; Chang, C.; Xu, X.; He, H.; Wang, Y.; Dai, F.; Xie, S.; Wang, C., Design, Synthesis and Evaluation of Naphthalimide Derivatives as Potential Anticancer Agents for Hepatocellular Carcinoma. *Molecules* **2017,** *22* (2).

9. Yang, Q.; Yang, P.; Qian, X.; Tong, L., Naphthalimide intercalators with chiral amino side chains: effects of chirality on DNA binding, photodamage and antitumor cytotoxicity. *Bioorg Med Chem Lett* **2008,** *18* (23), 6210-3.

10. Li, Z.; Yang, Q.; Qian, X., Novel 2-aminothiazonaphthalimides as visible light activatable photonucleases: effects of intercalation, heterocyclic-fused area and side chains. *Bioorg Med Chem Lett* **2005,** *15* (7), 1769-72.

11. Xu, Y.; Qu, B.; Qian, X.; Li, Y., Five-member thio-heterocyclic fused naphthalimides with aminoalkyl side chains: intercalation and photocleavage to DNA. *Bioorganic & Medicinal Chemistry Letters* **2005,** *15* (4), 1139-1142.

12. Tan, S.; Yin, H.; Chen, Z.; Qian, X.; Xu, Y., Oxo-heterocyclic fused naphthalimides as antitumor agents: Synthesis and biological evaluation. *European Journal of Medicinal Chemistry* **2013,** *62*, 130-138.

13. Verma, M.; Luxami, V.; Paul, K., Synthesis, in vitro evaluation and molecular modelling of naphthalimide analogue as anticancer agents. *Eur J Med Chem* **2013,** *68*, 352-60.

14. Trott, O.; Olson, A. J., AutoDock Vina: improving the speed and accuracy of docking with a new scoring function, efficient optimization, and multithreading. *J Comput Chem* **2010,** *31* (2), 455-461.

15. Hahn, L.; Buurma, N. J.; Gade, L. H., A Water-Soluble Tetraazaperopyrene Dye as Strong G-Quadruplex DNA Binder. *Chemistry – A European Journal* **2016,** *22* (18), 6314-6322.

16. El-Betany, A. M. M.; Vachova, L.; Bezzu, C. G.; Pope, S. J. A.; McKeown, N. B., The synthesis and study of fluorescent PAMAM-based dendritic molecules. *Tetrahedron* **2013,** *69* (39), 8439-8445.

17. Jones, J. E.; Amoroso, A. J.; Dorin, I. M.; Parigi, G.; Ward, B. D.; Buurma, N. J.; Pope, S. J. A., Bimodal, dimetallic lanthanide complexes that bind to DNA: the nature of binding and its influence on water relaxivity. *Chemical communications (Cambridge, England)* **2011,** *47* (12), 3374-3376.

Chapter 5 Naphthalimide-TEMPO derivatives

Abstract

A series of mono- and bisnaphthalimide-TEMPO conjugates has been successfully synthesized. The TEMPO moiety was connected to the naphthalimide scaffold using an amide-coupling reaction between 4-amino TEMPO and a carboxylic acid group connected to the naphthalimide unit. The solubility of the synthesized mono- and bisnaphthalimide TEMPO conjugates has been tested in MOPS buffer. Understandably, bisnaphthalimide derivatives were not sufficiently soluble but the mononaphthalimide-TEMPO conjugates are partially soluble. DNA-binding properties for the synthesized mononaphthalimide derivatives was studied using UV-visible titrations. Based on the binding affinities, this class of compound binds moderately with DNA. Among this series of compound, **5.12e** which contains two TEMPO moieties, binds with DNA better than the other compounds while **5.12b** that involve morpholine as SG binds with DNA with lower affinity.

5.1 Introduction

5.1.1 TEMPO derivatives as spin labels and probes

In the previous Chapters, we addressed the DNA-binding properties of naphthalimides and related compounds through structural variation. Naphthalimides were explored because of their interesting fluorescence properties which should allow their use as fluorescent sensitisers in genosensors. However, other detection opportunities with similar sensitivity might be offered by EPR spectroscopy (See Chapter 1).

Nitroxides are persistent cyclic radicals [1] that have been utilized in different applications, such as polymerization (e.g. nitroxide-mediated polymerization) [2, 3], diagnostic techniques such as electron paramagnetic resonance (EPR), trapping agents[4], spin markers[5], and spin-labelling[6, 7]. TEMPO (2,2,6,6-tetramethylpiperidine-N-oxyl, **5.2**) and its derivatives are prominent members of this class of compounds. As mentioned in Chapter 1, TEMPO can be used as a spin label and as a spin probe.

As a spin label, TEMPO can be covalently attached to DNA components (on the nucleobase, the ribose, or phosphate),[8] which can result in distinguishable differences in EPR spectra between unhybridised ssDNA and the hybridized dsDNA form.[9]

Dnyaneshwar B. Gophane *et al*.,[10] have synthesized isoindoline-derived benzimidazole nitroxide spin label (^{lm}Um, Figure 5.1 A, **5.1**) and used it to synthesise 14-mer oligoribonucleotide 5′-(CACGA^{lm}UmGCGAGGUC). The EPR

spectra for the free spin label are different from the EPR spectrum of the labeled oligoribonucleotide and there are further distinguishable differences when the hybridization event occurs to form a duplex (Figure 5.1).

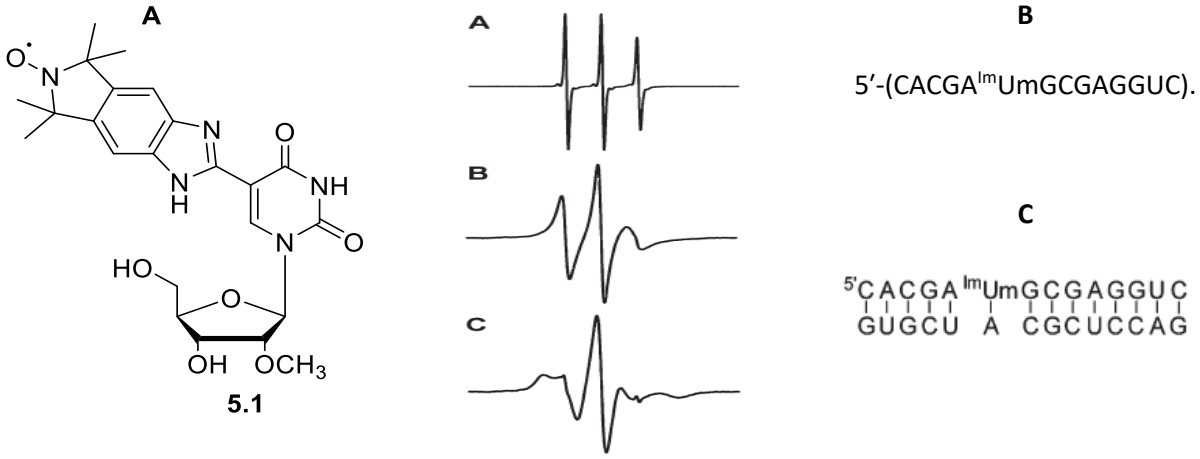

Figure 5.1 EPR spectra of A) free isoindoline-derived benzimidazole nitroxide spin label, B) 14-mer RNA single strand 5'-(CACGA^{Im}UmGCGAGGUC), and C) the duplex 5'-(CACGA^{Im}UmGC- GAGGUC)·5'-(GACCUCGCAUCGUG)

As spin probes, nitroxides were utilized in the form of nitroxide-containing intercalators and groove binders. Belmont *et al*.[11] have synthesized two labeled-acridine derivatives using nitroxyl radical (Figure 5.2). The DNA-binding affinities of these compounds were determined using two techniques, viz. fluorescence spectroscopy and electron paramagnetic resonance. This study shows that binding affinities calculated using EPR spectroscopy are very similar to those calculated using fluorescence spectroscopy (compound **5.2**, K_{fluo}=3×10^4 M^{-1}, K_{EPR}=2×10^4 M^{-1};

compound **5.3**, K_{fluo}=1.5×10^5 M^{-1}, K_{EPR}=2×10^5 M^{-1}). It also shows the differences in signal between free and bound species (Figure 5.2).

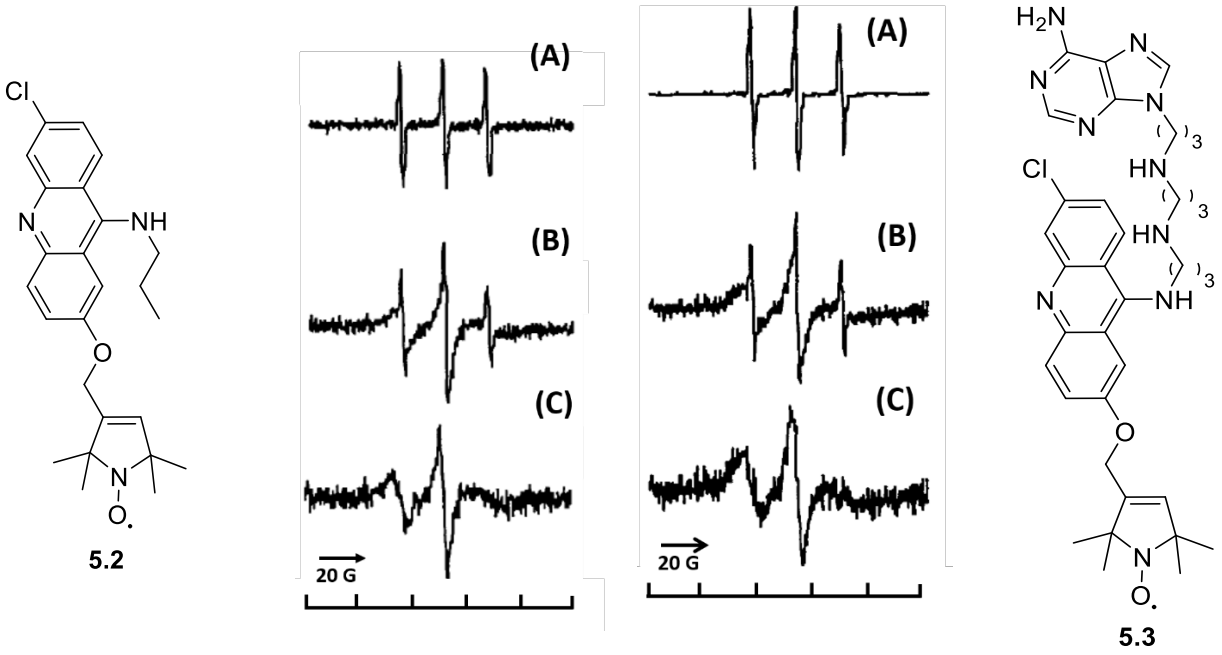

Figure 5.2 EPR spectra of the labelled acridine derivatives (5.1 and 5.2) in the absence (A) and presence of DNA (B) and difference spectrum (C).[11]

5.1.2 Synthesis of TEMPO derivatives

TEMPO derivatives with different functional groups are commercially available (Scheme 5.1). Therefore, any compound can in principle be connected to a TEMPO moiety using a choice of several reactions. A particularly interesting option is the amide-coupling reaction which could be carried out using either **5.6** or **5.7** with a complementary carboxylic acid or an amine, respectively.

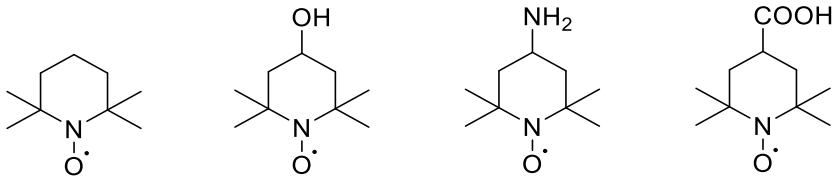

5.4 **5.5** **5.6** **5.7**

TEMPO

Scheme 5.1

Generally, formation of amide bonds is extensively studied in drug discovery. There are several coupling reagents used for this purpose.[12] Carbamides such as 1-ethyl-3-(3-dimethylaminopropyl) carbodiimide (EDC) is one of the well-known coupling agents that is used to activate a carboxylic acid group by transforming it to an activated ester which subsequently forms the amide bond (Scheme 5.2).[12, 13] In addition to EDC, using a combination of EDC and 1-hydroxybenzotriazole (HOBt) is usually used to avoid racemization of chiral molecules.[14]

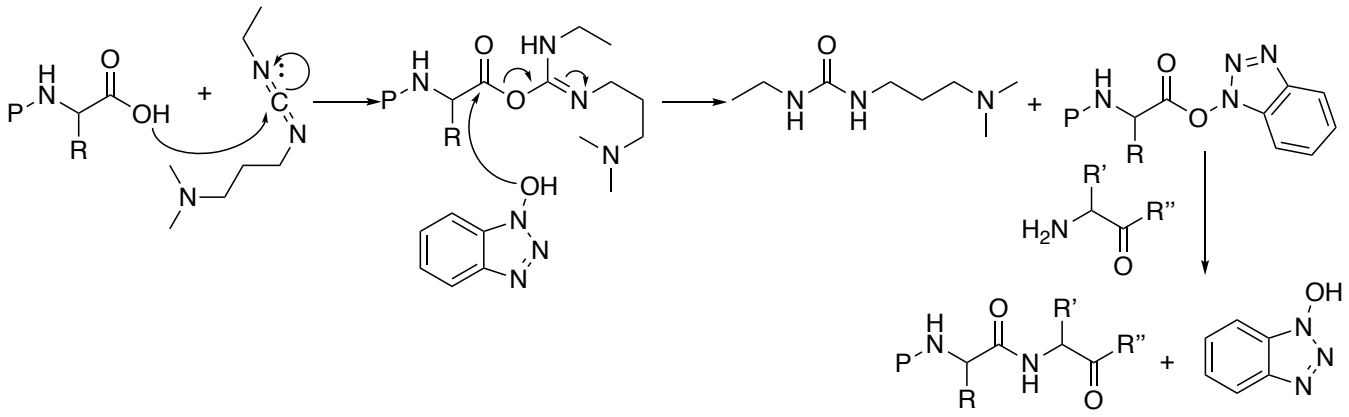

Scheme 5.2

In 2012, Li, Guo *et al.*[15] successfully synthesised TEMPO-derivatives **5.7a-c** and **5.9a-c** using both approaches to the coupling reaction. The first approach involves a coupling reaction between 4-amino-2,2,6,6-tetramethylpiperidine-N-oxyl (4-NH_2-TEMPO) and the carboxylic acid group in **5.8a-c** using EDC and HOBt as coupling agents (Figure 5.3).[15] Compounds **5.9a-c** were obtained in low yield (12-17%).

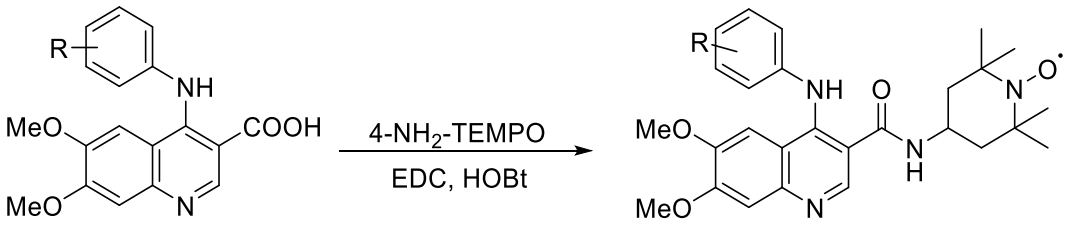

5.8a: R=3-Cl
5.8b: R=3-Br
5.8c: R=3-Cl,4-F

5.9a: R=3-Cl
5.9b: R=3-Br
5.9c: R=3-Cl,4-F

Scheme 5.3

The second approach involved the same reaction conditions but now the coupling occurs between 4-carboxy-2,2,6,6-tetramethylpiperidine-N-oxyl (4-COOH-TEMPO) and the amino group in **4.10a-c (Figure 5.4)**.

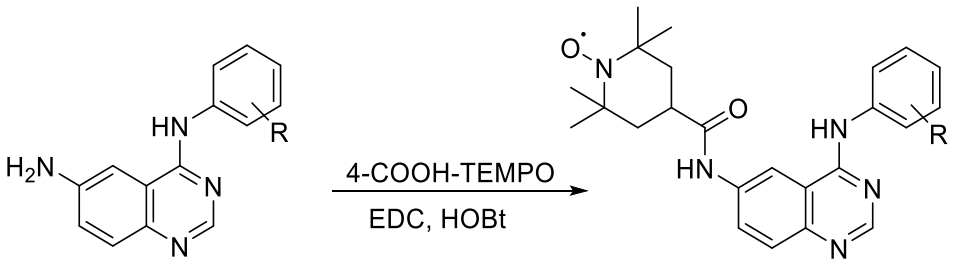

5.10a: R=3-Cl
5.10b: R=3-Br
5.10c: R=3-Cl,4-F

5.11a: R=3-Cl
5.11b: R=3-Br
5.11c: R=3-Cl,4-F

Scheme 5.4

Compounds **5.11a-c** were obtained in a slightly higher yields than using 4-amino TEMPO (18-30%). These results suggest that there is no fundamental difference in reactivity in amide-forming reactions between 4-amino-TEMPO and 4-carboxy-TEMPO. From this, we conclude that both 4-amino-TEMPO and 4-carboxy-TEMPO are viable coupling partners so that the synthetic scheme can be selected on the basis of difficulty of synthesising the required coupling partners.

5.1.3 Aims

As part of our efforts to develop and modify naphthalimide derivatives for sensing purposes, we decided to introduce a free radical moiety such as nitroxide to the naphthalimide scaffold. We selected the naphthalimide scaffold because at the time of starting this work, the development of the synthesis of the larger intercalators described in Chapter 4 had not sufficiently advanced to be considered as part of the synthesis of conjugates with TEMPO.

The reaction we decided to use is the coupling between a carboxylic acid and an amine to form a peptide (amide) bond. For the coupling reaction, we chose to use 4-amino TEMPO to react with intermediate A instead of 4-COOH-TEMPO to react with intermediate B. The reason behind this is to avoid any potentially challenging purifications we anticipated in case of using intermediate B (Scheme 5.5) which has a free primary amine group.

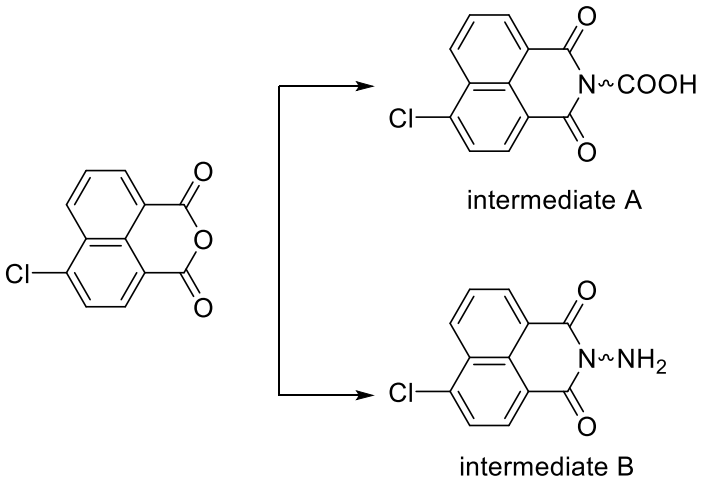

Scheme 5.5

This Chapter therefore aimed to synthesise several mono- and bis-naphthalimide-TEMPO derivatives via coupling reactions between carboxylic acid groups attached to naphthalimide derivatives and 4-amino-TEMPO. In addition, we wanted to study the aqueous solubility and DNA-binding ability for these compounds.

5.2 Result and discussion

5.2.1 Design and docking study for proposed compounds

Several mono-naphthalimide-TEMPO derivatives **5.12a-e** were proposed (Scheme 5.6).

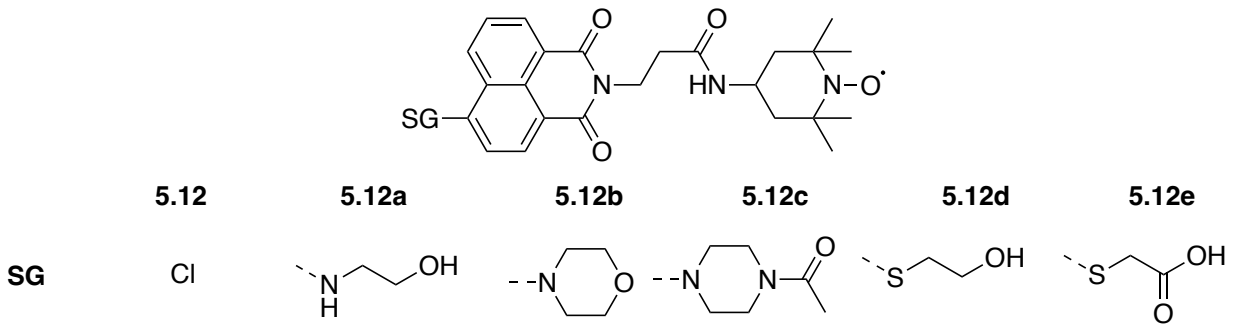

Scheme 5.6 proposed naphthalimide-TEMPO derivatives (5.12a-e)

In addition to mono-naphthalimide-TEMPO derivatives, bisnaphthalimide-TEMPO derivatives were proposed using previously synthesized bisnaphthalimides (See Chapter 3) leading to the compounds in Scheme 5.7.

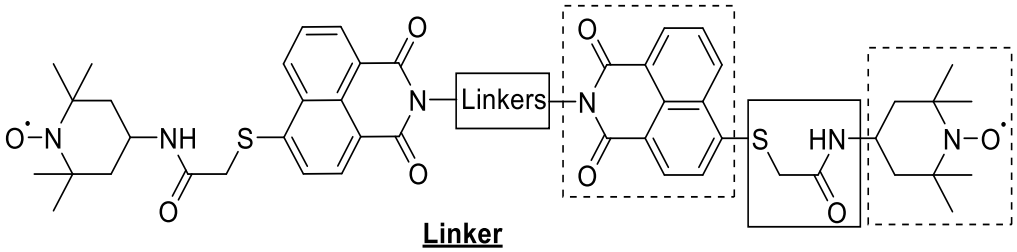

Linker

5.13a adipic dihydrazide
5.13b bis(3-aminopropyl)amine
5.13c p-Phenylenediamine
5.13d 2,2'-(ethylenedioxy)diethylamine
5.13e 1,3-diamino propane

Scheme 5.7

Docking studies for the proposed naphthalimide-TEMPO derivatives were carried out using AutoDock Vina against a DNA structure with a pre-formed intercalation gap[16] as in the previous Chapters. Figure 5.3 shows the top three binding modes for each compound.

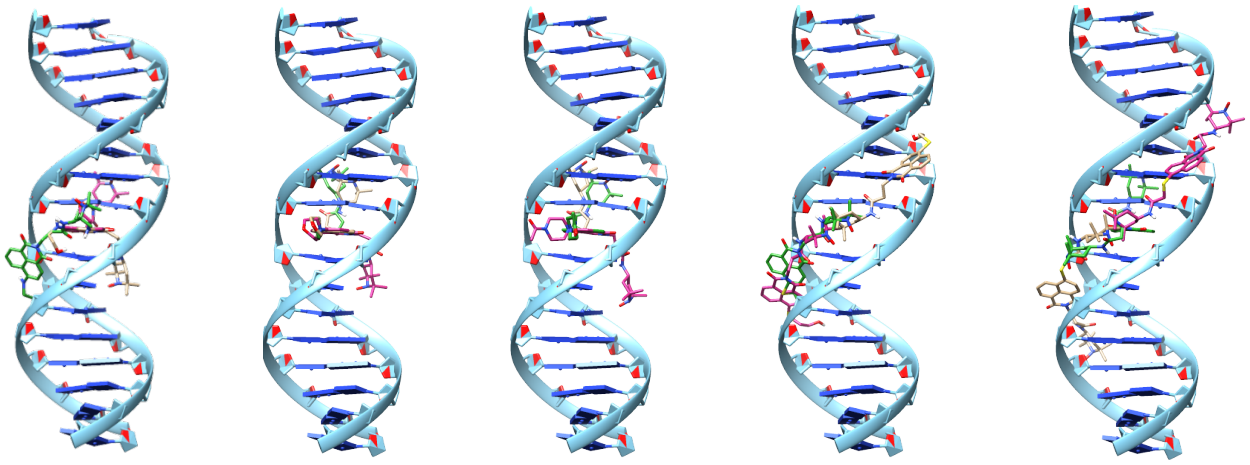

5.12a **5.12b** **5.12c** **5.12d** **5.12e**

Figure 5.3 The top three binding modes of 5.12a-e using AutoDock Vina

The docking study suggests that three members this class of compounds (SG= 1° and 2° amine) more likely bind with DNA as an intercalator whereas the other two prefer to bind in the minor groove. Table 5.1 illustrates the predicted binding affinity for the top three binding modes of **5.12a-e.**

Table 5.1 DNA binding affinities for the top three binding modes of 5.12a-e predicted using AutoDock Vina

		5.12a	5.12b	5.12c	5.12d	5.12e
The binding affinity (kcal/mol)[b]	1st binding mode[a]	-9.7 (I)	-10.9 (I)	-10.7 (I)	-9.3 (GB)	-11.3 (GB)
	2nd binding mode	-9.7 (I)	-10.9 (I)	-10.7 (I)	-9.2 (GB)	-11.2 (GB)
	3rd binding mode	-9.3 (I)	-10.8 (I)	-10.6 (I)	-9.1 (GB)	-11.2 (I)

(I): intercalator, (GB): groove binder

a) The ranking of the binding modes is as produced by Vina

b) Binding affinities are only reported to 0.1 kcal mol^{-1} by Vina.

The docking study for the proposed bisnaphthalimide-TEMPO derivatives was carried out analogously[16]. The top 10 binding modes were ranked by the binding affinity. The three best binding modes are presented in Figure 5.4

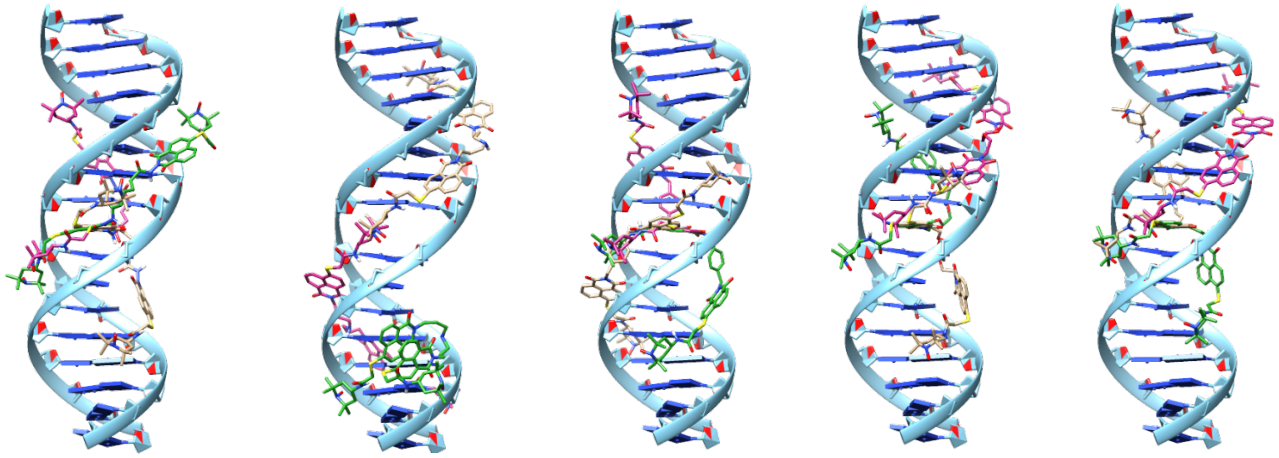

5.13a **5.13b** **5.13c** **5.13d** **5.13e**

Figure 5.4 The top three DNA-binding modes of compounds 5.13a-e using AutoDock Vina

The docking study suggests that most examples of this class of compounds are likely to bind with DNA as an intercalator. Table 5.2 illustrates the predicted binding affinities for the top three binding modes of **5.13a-e** using AutoDock Vina.

Table 5.2 The DNA-binding affinities for the top three binding modes of 5.13a-e predicted using AutoDock Vina

		5.13a	5.13b	5.13c	5.13d	5.13e
The binding affinity (kcal/mol)[b]	1st binding mode[a]	-12.6 (I)	-11.8(GB)	-12.2 (I)	-12.1 (I)	-12.1 (I)
	2nd binding mode	-12.5 (I)	-11.7 (GB)	-12.1 (I)	-11.8 (GB)	-12.1 (GB)
	3rd binding mode	-12.4 (I)	-11.6 (GB)	-12.1 (I)	-11.8 (I)	-11.9 (I)

(I): intercalator, (GB): groove binder

a) The ranking of the binding modes is as produced by Vina

b) Binding affinities are only reported to 0.1 kcal mol^{-1} by Vina.

As expected, the DNA-binding affinity of bisnaphthalimide-TEMPO derivatives is better than mono-naphthalimide-TEMPO derivatives. This improvement is due to the presence of two units of intercalator in bisnaphthalimides which cause higher DNA-binding affinities compared to the corresponding monomers. This finding is consistent with docking comparison that has been made between bisnaphthalimides and ferrocene-naphthalimide conjugates (see chapter 3).

5.2.2 Synthesis of mono-naphthalimide-TEMPO conjugates 5.12a-e

The proposed synthetic scheme for the mono-naphthalimide-TEMPO derivatives involves three steps (Scheme 5.8). The first step aims to introduce the carboxylic acid "anchor point" to the naphthalimide unit on the way to introduce the TEMPO moiety using an amide coupling reaction. Therefore, the first step in this scheme involves the reaction between 4-chloro-1,8-naphthalic anhydride and an amino acid, in this case β-alanine, to facilitate this reaction.

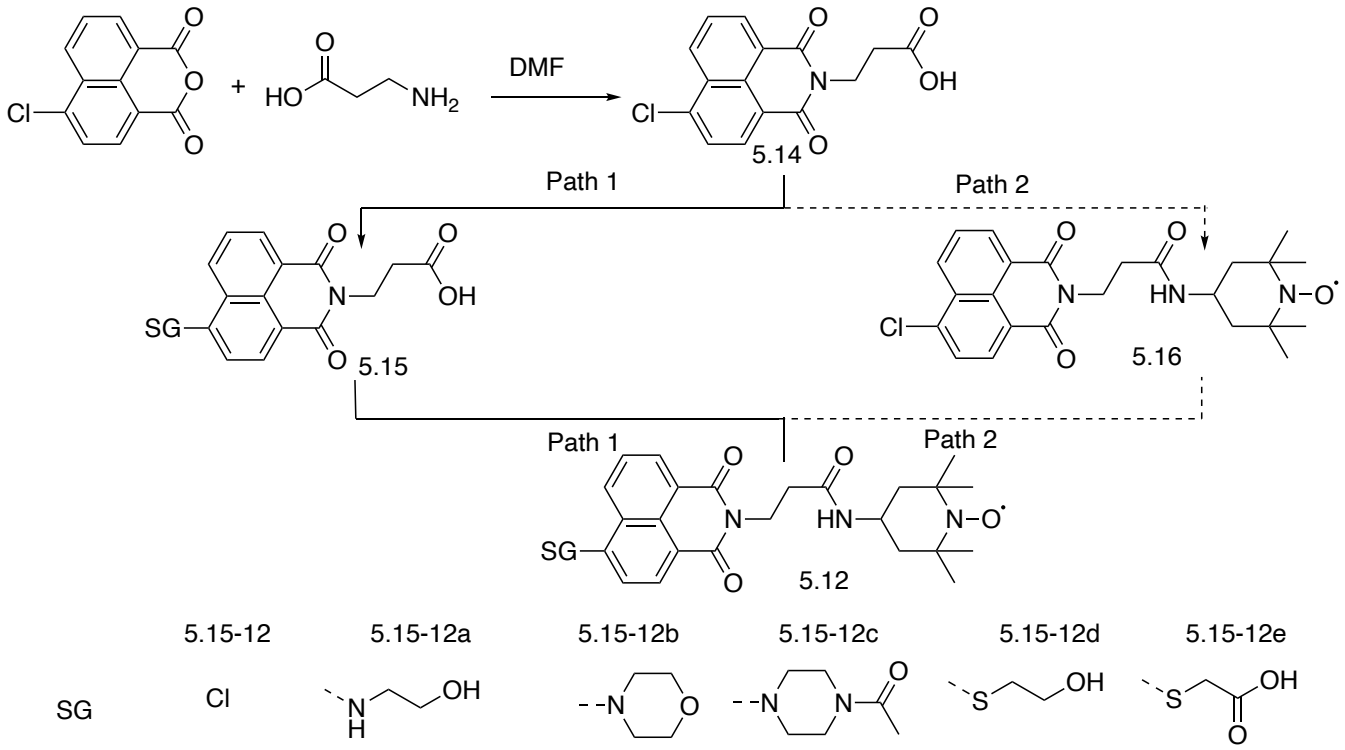

Scheme 5.8 proposed synthetic scheme for 5.12a-e

After the first step, two possible paths can be followed to eventually synthesise the target compounds **5.12a-e**. The first involves introducing the solubilizing groups to 3-(6-chloro-1,3-dioxo-1H-benzo[de]isoquinolin-2(3H)-yl)propanoic acid **5.14** before introducing the TEMPO moiety (Scheme 5.8, **5.15a-e**). The second path involves introducing the TEMPO moiety first before introducing the solubilizing groups (Scheme 5.8, **5.16**). It may appear easier if we selected the second path where the TEMPO-moiety was introduced first which involves performing the amide-coupling reaction once and then several solubilizing groups can be introduced. However, there are disadvantages to choosing this path, including the difficulty that can be faced in characterization of **5.16** and **5.12a-e** using NMR spectroscopy. Also, the harsh reaction conditions required for introducing the solubilizing groups may affect the stability of TEMPO.[17] Hence the first path has been chosen.

5.2.2.1 Synthesis of 3-(6-chloro-1,3-dioxo-1H-benzo[de]isoquinolin-2(3H)-yl)propanoic acid 5.14

The synthesis of 3-(6-chloro-1,3-dioxo-1H-benzo[de]isoquinolin-2(3H)-yl)propanoic acid **5.14** is an easy reaction that provides us with the carboxylic acid functionality that is needed for the amide coupling reaction.

One equivalent of 4-chloro-1,8-naphthalic anhydride and one equivalent of β-alanine were dissolved in DMF. The reaction mixture was heated to reflux for 24 h. The solvent was removed *in vacuo* and ethanol was added to produced **5.14** in 83% yield (Scheme 5.9). The product was characterized using ^{1}H- and ^{13}C-NMR spectroscopy and mass spectrometry.

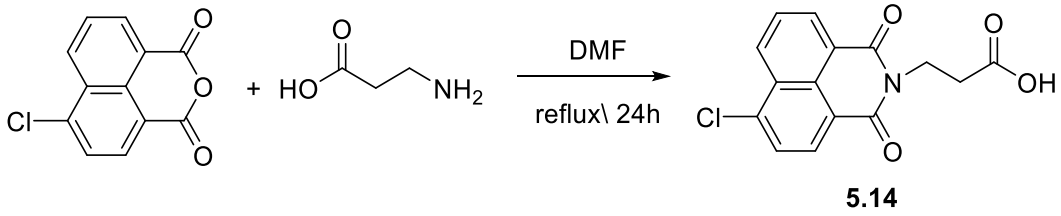

5.14

Scheme 5.9

The ^{1}H-NMR spectrum of **5.14** shows the five distinguishable signals for naphthalimide following the pattern in Table 2.3 (Chapter 2).

5.2.2.2 Introduction of the solubilizing groups

Like previous chapters, the same types of solubilizing groups (1°-amine, 2°-amine, and thiol compounds) were proposed to be introduced to compound **5.14**.

Introduction of solubilizing groups through S_NAr reactions with 1° amines

Like Chapter 3, the plan is to introduce ethanolamine to **5.14** where one equivalent of **5.14** was dissolved in neat ethanolamine and heated under reflux for 24 h (Scheme 5.10). The reaction mixture was left to cool followed by a failed attempt to extract the product using chloroform and water. We believe that the product did not precipitate due to the high solubility of **5.15a** in water. Although we evaporated the water, the crude was a highly viscous solution or oil (with residues of ethanolamine). We tried to acidify the solution as an attempt to precipitate **5.15a** but it did not achieve this purpose.

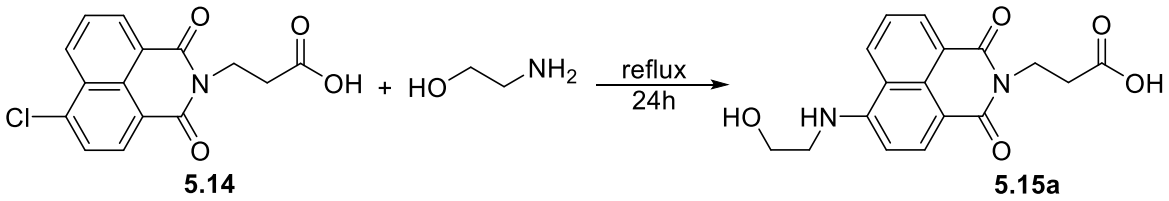

5.14 **5.15a**

Scheme 5.10

No further attempts at purifying **5.15a** were made.

Introduction of solubilizing groups through S_NAr reactions with 2°-amines

In our effort to introduce 2°-amine groups to the naphthalimide unit in **5.14**, excesses of morpholine and 1-acetyl piperazine were heated at 100 °C with 3-(6-chloro-1,3-dioxo-1H-benzo[de]isoquinolin-2(3H)-yl)propanoic acid **5.14** for 24 h using DMF as solvent (Scheme 5.11).

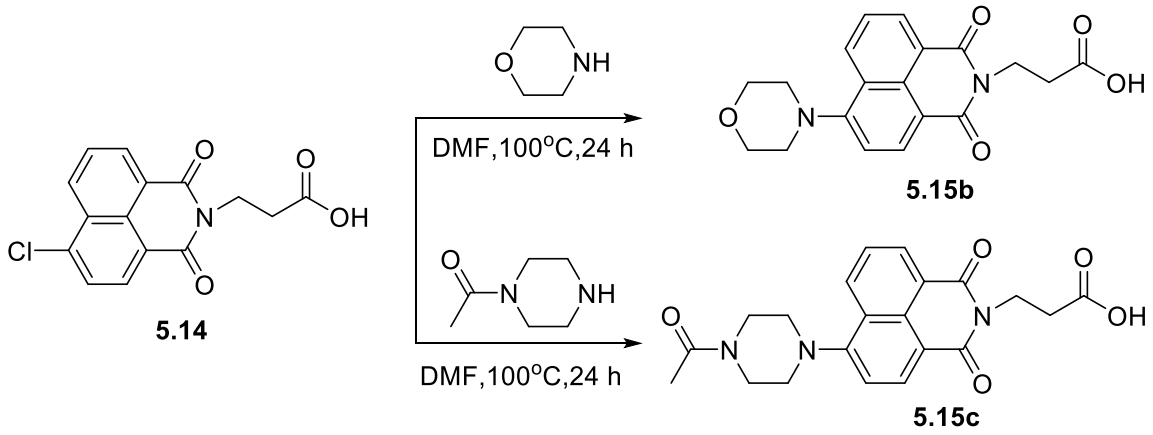

Scheme 5.11

Although, these reaction conditions were successfully used out in previous chapters, using this approach did not work with this class of compound. The ^{1}H-NMR spectrum shows signals related to the starting materials 3-(6-chloro-1,3-dioxo-1H-benzo[de]isoquinolin-2(3H)-yl)propanoic acid **5.14** with traces of desired compounds **5.15b-c**. The presence of the carboxylic acid in compound **5.14** is likely affecting the nucleophilicity of morpholine and 1-acetyl piperazine. Therefore, it interferes with the formation of desired compounds **5.15b-c**- via S_NAr reaction.

Therefore, we decided to swap the first and second reaction and use previously synthesized compounds **3.10** and **3.11** (Chapter 3) and use them to synthesise **5.15b-c** under the same conditions applied to the synthesis of **4.14** (Scheme 5.12)

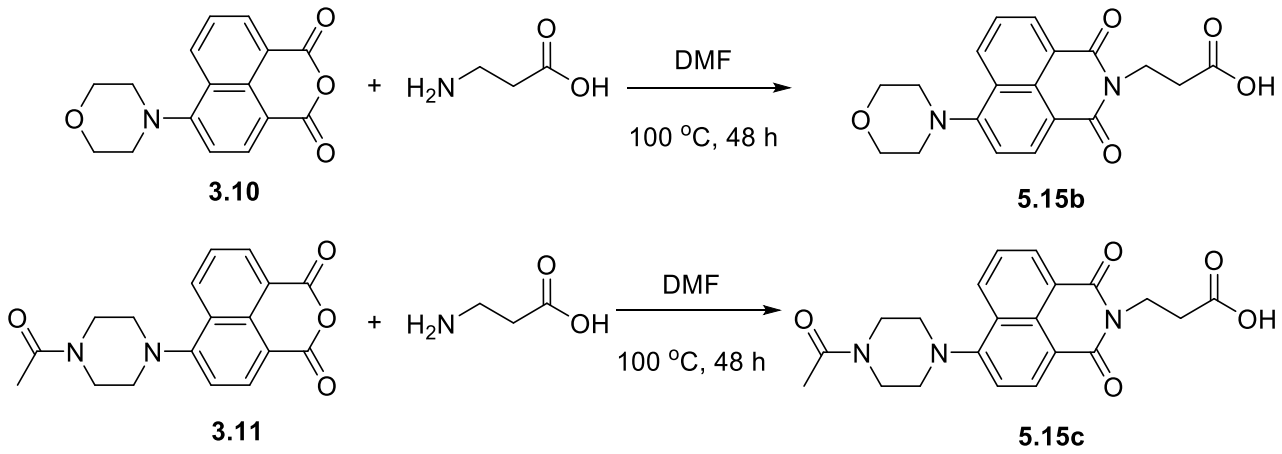

Scheme 5.12

One equivalent of **3.10** was dissolved in DMF with one equivalent of β-alanine and heated at 100 °C for 48 h. The solvent was removed, and we added ethanol to allow **5.15b** to precipitate. The same protocol was successfully carried out to synthesise compound **5.15c**. The obtained compounds **5.15b-c** were characterized using ^{1}H- and ^{13}C-NMR spectroscopy and mass spectrometry.

Introduction of solubilizing groups through S_NAr reactions with thiols

To one equivalent of 3-(6-chloro-1,3-dioxo-1H-benzo[de]isoquinolin-2(3H)-yl)propanoic acid **5.14**, two equivalents of 2-mercaptoethanol and a solvent were added and the resulting mixture was heated to reflux for 24 h. This reaction has been carried out twice using different solvents (2-methoxyethanol and DMF) (Scheme 5.13). At the end of the reaction, the reaction mixture was acidified using 5% HCl.

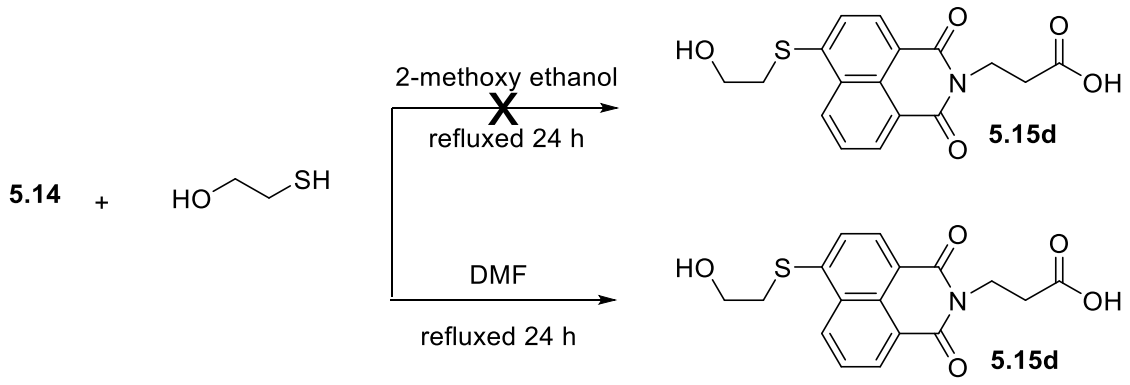

Scheme 5.13

Although it has been reported that 2-methoxyethanol was used for this reaction[18], the ^{1}H-NMR spectrum shows that using 2-methoxyethanol appeared to be unsuccessful. Compound **5.15d** was successfully synthesized in a good yield of 59 % using DMF as solvent.

On the other hand, one equivalent of **5.14** was refluxed with two equivalents of thioglycolic acid in DMF for 24 h. At the end of the reaction, the mixture was acidified using 5% HCl to obtain **5.15e** in 67 % yield (Scheme 5.14).

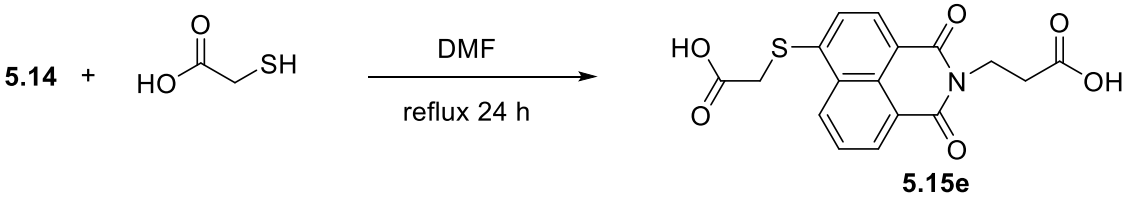

Scheme 5.14

5.2.2.3 Synthesis of naphthalimide-TEMPO derivatives 5.12b-e

After introducing the solubilizing groups to the naphthalimide unit, the next step is to add the sensitising TEMPO group via an amide coupling reaction (Scheme 5.15).

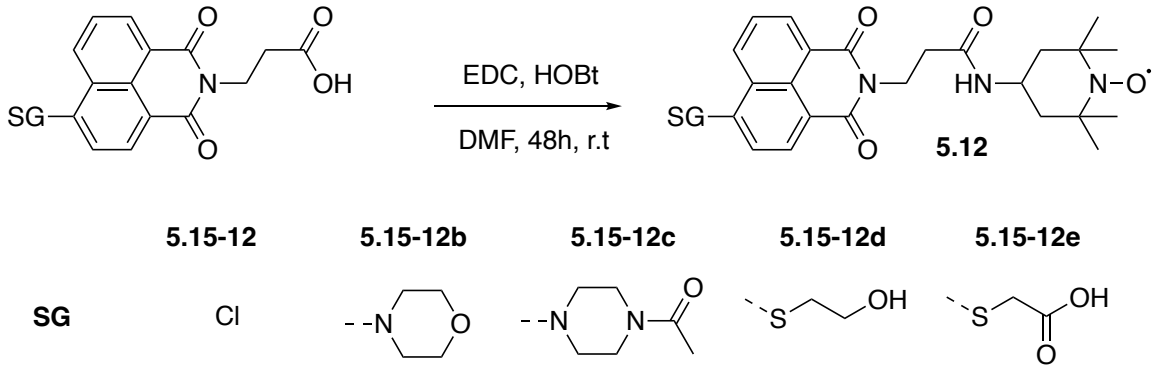

Scheme 5.15

One equivalent of **5.15b** with 1.5 equivalents of 4-amino TEMPO were dissolved in dry DMF. Additionally, EDC.HCl and HOBt were added as coupling agents to activate the carboxylic acid groups to nucleophilic attack by the amino group. The reaction mixture was stirred for 48 h at room temperature and the solvent was removed under vacuum. The completion of the reaction and purity of the obtained compounds **5.12b** was checked using TLC and the compounds were characterized using mass spectrometry. These conditions were successfully applied to synthesise **5.12c-e** (Scheme 5.16).

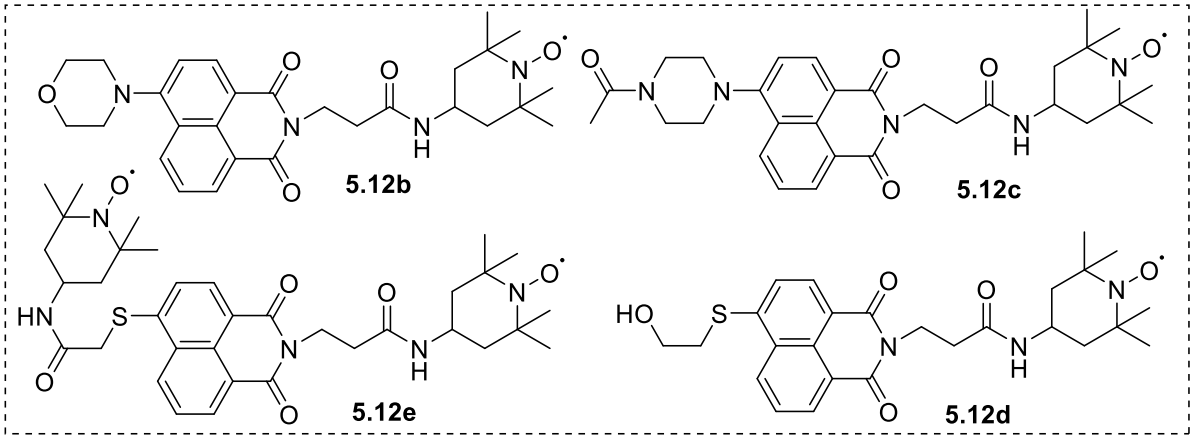

Scheme 5.16

The chemical structure of the obtained compounds **5.12b-e** were confirmed using mass spectrometry. The mass spectra show a M+1 peak. The isotope distribution for all compounds is relatively similar to expected mass (theoretical mass). Table 5.3 summarizes the mass spectrometry details of **5.12b-e.**

Table 5.3 The mass spectrometry details of 5.12b-e

	5.12b	5.12c	5.12d	5.12e
Expected mass	[M+1] 508.26 (100%) [M+2] 509.26 (30%) [M+3] 510.27 (2.7%)	[M+1] 549.29 (100%) [M+2] 550.29 (32%) [M+3] 551.29 (5.1%)	[M+1] 499.21 (100%) [M+2] 500.21 (28%) [M+3] 501.20 (4.5%).	[M+1] 666.32 (100%) [M+2] 667.33 (38%) [M+3] 668.33 (7%).
Found Mass	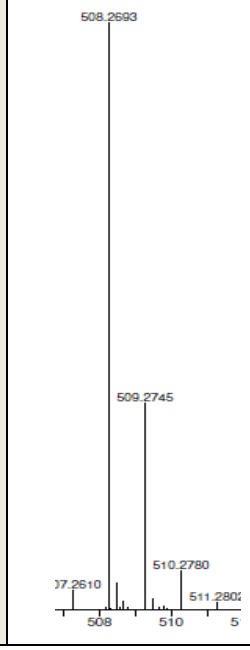	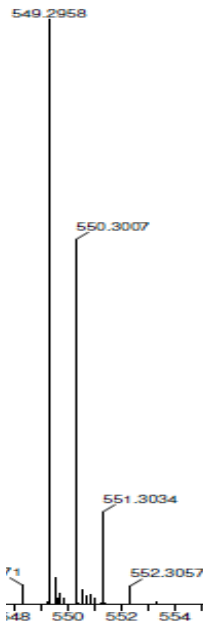	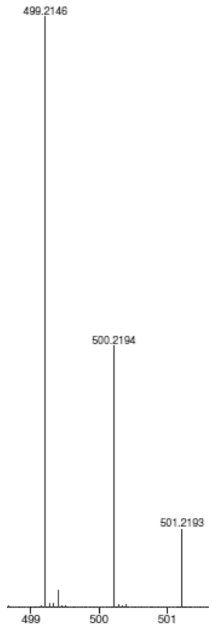	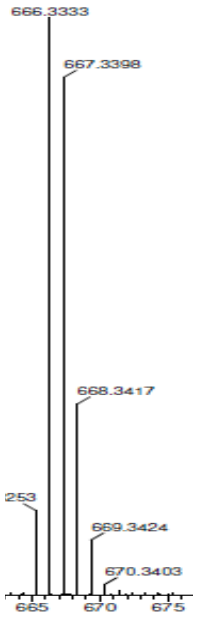

In addition to mass spectrometry, UV-visible spectra (Figure 5.5) show a band in the region that expected for the substituted naphthalimide chromophores in previous chapters (see chapter 2 and 3), and this also confirms the formation of the new compounds **5.12b-e**

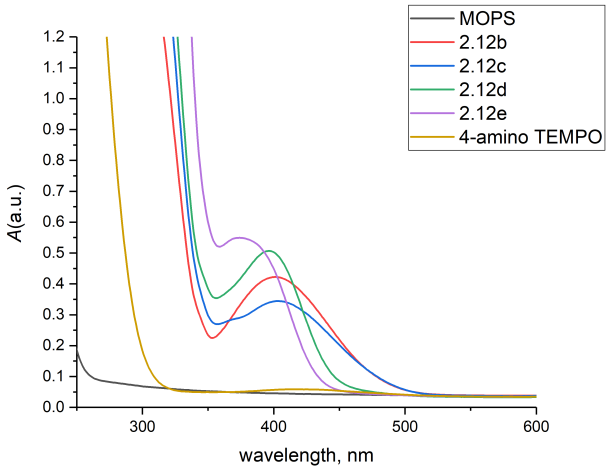

Figure 5.5 UV-visible spectra of a 40.4 µM solution of 5.12b (red); a 31.8 µM solution of 5.12c (blue); a 37.8 µM solution of 5.12d (green); a 41.6 µM solution of 5.12e (purple) in buffer (25 mM MOPS, 50 mM NaCl, 1 mM EDTA) at 25 °C

5.2.3 Synthesis of bis-naphthalimide-TEMPO derivatives 5.13a,d,e

The synthesis of the bisnaphthalimide-TEMPO derivatives **5.13a,d,e** was proposed using previously synthesized substituted dimers **3.13a,d,e** (Chapter 3 and Scheme 5.17).

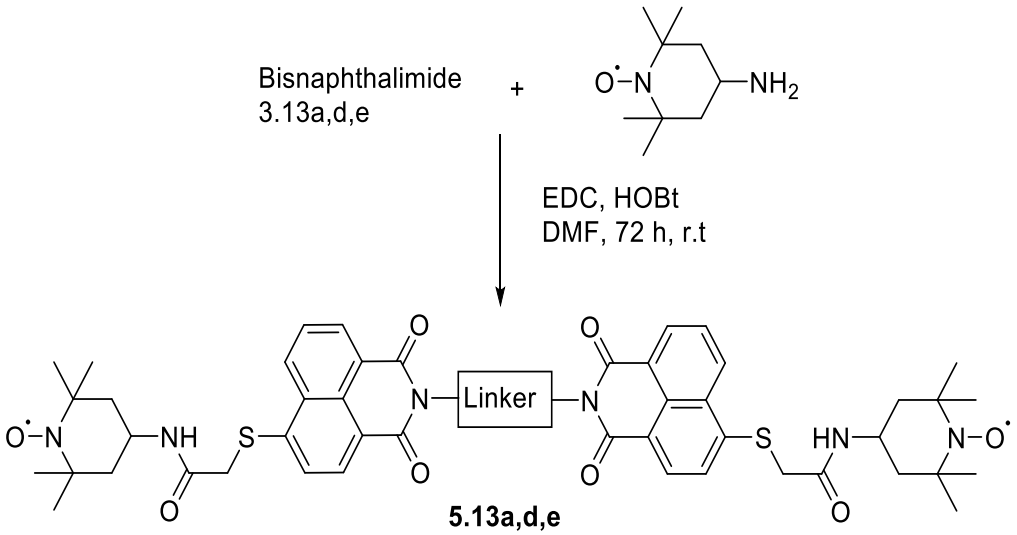

Scheme 5.17

Starting from bisnaphthalimide derivatives **3.13a,d,e**, the same coupling approach that has been used to synthesise **5.12b-e** was successfully applied to synthesise bis-naphthalimide-TEMPO derivatives **5.13a,d,f**. One equivalent of **3.13a** with three equivalents of 4-amino TEMPO were dissolved in DMF and three equivalents of each HOBt and EDC.HCl and two equivalents of N-ethyl-diisopropylamine were added. The reaction mixture was stirred at room temperature for 72 h The volume of solvent was reduced *in vacuo*, then methanol was added to precipitate a brown solid which was left to dry. The crude **5.13a** was obtained as a brown solid in 28% yield and purified using column chromatography over silica.

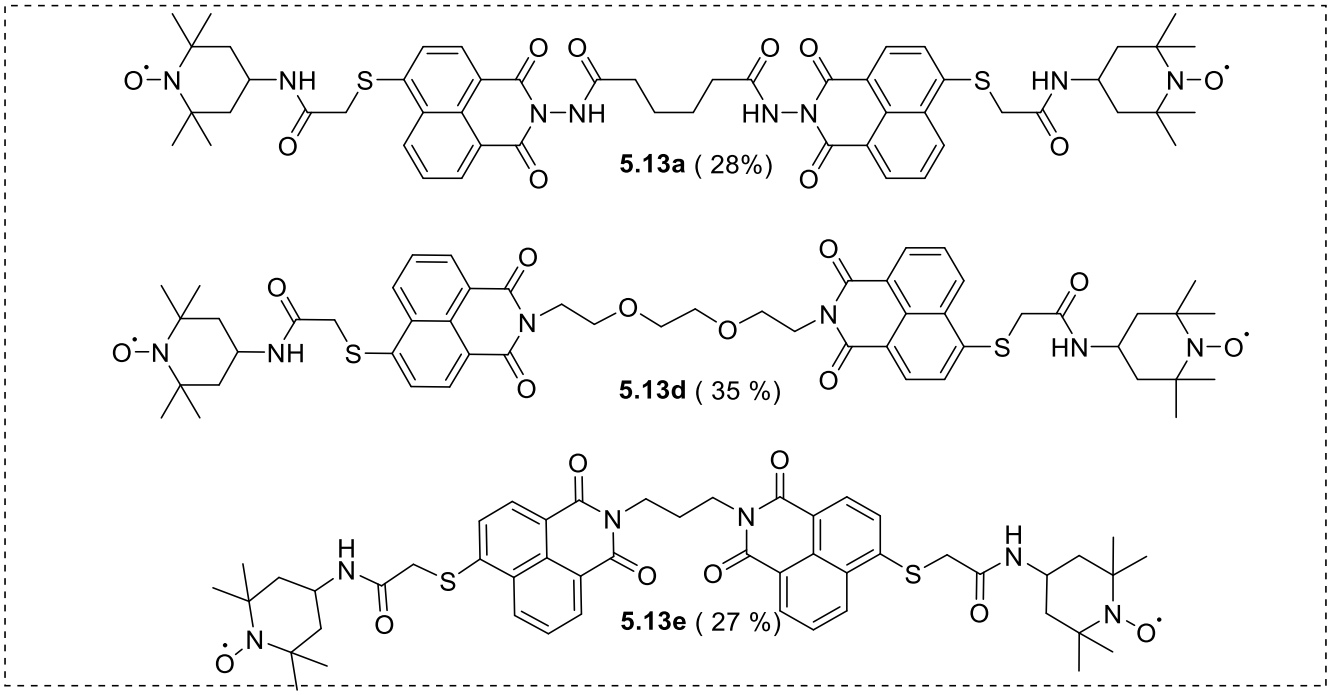

Scheme 5.18

The same conditions were used to synthesise **5.13d,e** (Scheme 5.18). All obtained compounds were characterized using mass spectrometry (Table 5.4).

Table 5.4 The mass spectrometry details of 5.13a,d,e

	5.13a	5.13d	5.13e
Expected mass	[M+1] 1021.39 (100%) [M+2] 1022.39 (56%)	[M+1] 995.40 (100%) [M+2] 996.40 (56%) [M+3] 997.40 (15%)	[M+1] 921.36 (100%) [M+2] 922.36 (53%) [M+3] 923.37 (14%).
Found Mass	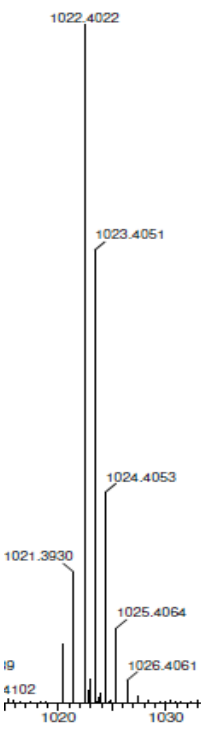	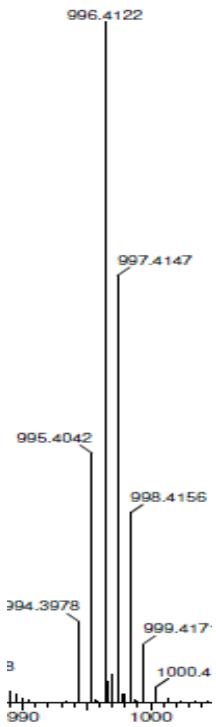	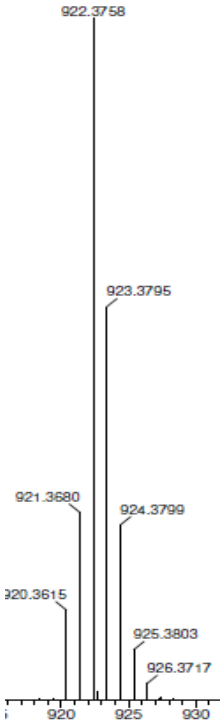

The mass spectra of bisnaphthalimide-TEMPO derivatives **5.13a,d,e** show an unexpected pattern. This pattern involves the isotope distribution for the molecular ion. The spectra show the [M+1] peak for all compounds, which indicates that these compounds were successfully synthesized. However, the abundance for the isotope peaks does not follow the expected pattern. One scenario can be presented here to rationalize the mass spectra which suggests that one of the TEMPO groups has been protonated, potentially following reduction (Scheme 5.19).

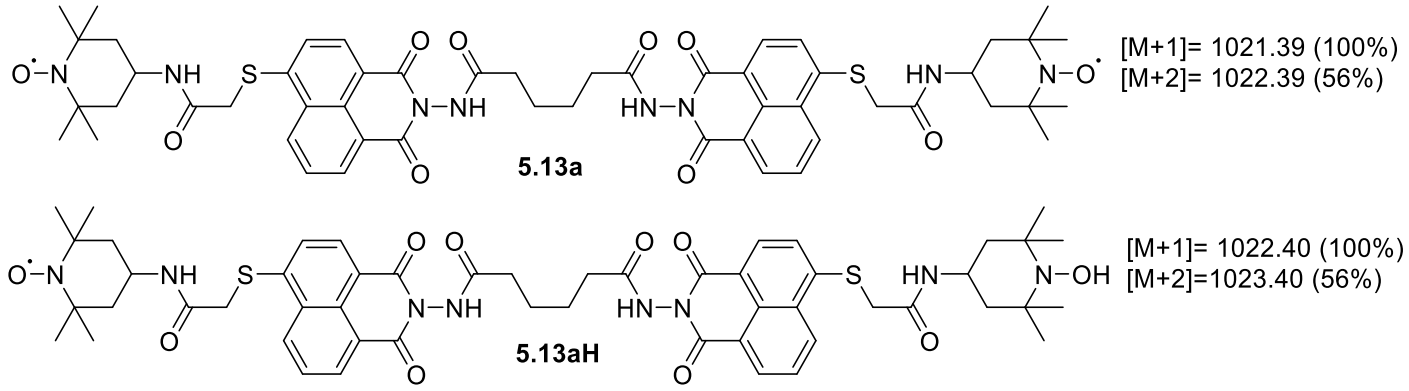

Scheme 5.19

Interestingly, the [M+1] peak and the isotope distribution of protonated bisnaphthalimide (Figure 5.19, **5.13H**) are consistent with the found molecular mass. Accordingly, the mixture might contain both of protonated and unprotonated bisnaphthalimide-TEMPO derivatives since the molecular ion for both are observed. However, it cannot be said whether this protonation took place during the reaction or during the ionization in the mass spectrometer. It is worth mentioning that the EPR spectra for TEMPO-bisnaphthalimide derivatives have been recorded by Dr. Emma Richards' group and show the expected EPR signal, which also confirms the formation of the bisnaphthalimide-TEMPO derivatives but does not exclude the possible presence of reduced forms of these compounds.

Comparison of the ^{1}H-NMR spectra for **5.13e** with the dimer **3.13e** also implied that the TEMPO-moiety had been incorporated into the molecule as signals were observed at similar chemical shift values but these signals were very broad due to the presence of the radicals

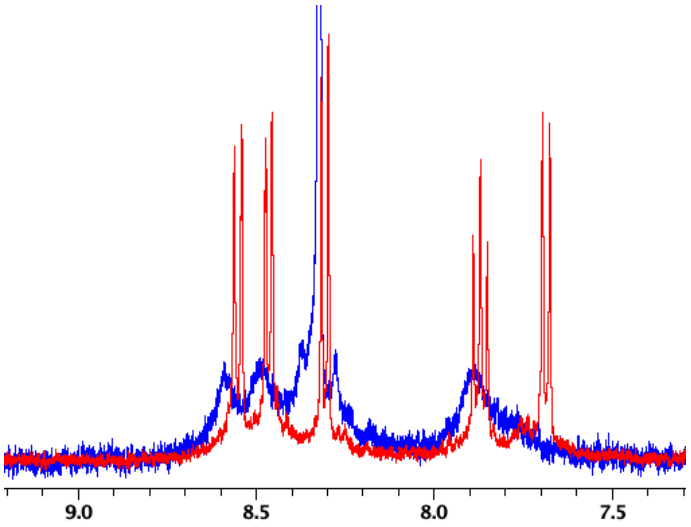

Figure 5.6 ^{1}H NMR aromatic region of 3.13e (red) and 5.13e (blue)

5.2.4 The solubility

The solubility of the synthesized naphthalimide-TEMPO derivatives was tested by placing approximately 5 mg of each compound in buffer (25 mM MOPS, 50 mM NaCl, pH 7) followed by stirring at room temperature for 2-5 days. The obtained suspensions were filtered (0.2 µm) to obtain saturated solutions. The UV-visible spectra of these solutions were recorded, and the concentrations were calculated using the Beer Lambert law with the extinction coefficients for the chromophores as determined in Chapter 2. Table 5.5 illustrates the solubility and λ_{max} for the obtained compounds.

Table 5.5 The solubility of 5.12b-e in MOPS buffer[a]

	5.12b	**5.12c**	**5.12d**	**5.12e**
λ_{max}, nm	401	403	396	374
Solubility limit, M	5.07×10^{-4}	8.00×10^{-5}	1.88×10^{-4}	5.19×10^{-4}

a) 25 mM MOPS pH 7.0, 50 mM NaCl, 1 mM EDTA at room temperature.

It is important to mention that **5.12b-e** were not completely dry when they were used because traces of the DMF (reaction solvent) still remained. This situation may have increased the solubility of these compounds in MOPS. Generally, the solubility for this class of compound is good where the compound containing two TEMPO moieties shows high solubility. Morpholine is the second group that has a good influence on the solubility in this class which is unexpected considering its effect on the solubility of bisnaphthalimides was not good. The compounds with 1-acetyl piperazine and 2-mercaptoethanol were the least soluble compounds among this series.

The solubility of bisnaphthalimide-TEMPO derivatives **5.13a,d,e** were tested by similarly placing these compounds in MOPS and the solutions were filtered (0.2 μm). The UV-visible spectra of these solutions were recorded and unfortunately these compounds are not sufficiently soluble in MOPS so no further experiments were carried out with these compounds.

5.2.5 Affinity for DNA

The primary goal of synthesizing these compounds is for use as sensitisers in EPR-based detection of DNA. Therefore, the next step is to study their ability with duplex DNA. The DNA-binding properties were investigated through UV-visible absorption titrations. The changes in the UV-visible spectra during the titration, i.e. decreases or increases in the absorbance or shifts in λ_{max}, can be used to determine if the compounds are interacting with the DNA or not.

5.2.5.1 UV-visible spectroscopy studies of 5.12b-e interacting with duplex DNA

The titration for **5.12b** was conducted three times in MOPS at 25 °C. The absorbances at 401 nm were plotted as a function of DNA concentration and analyzed using the MIS model[19], both individually and globally (Figure 5.7) to obtain the binding affinity and stoichiometry.

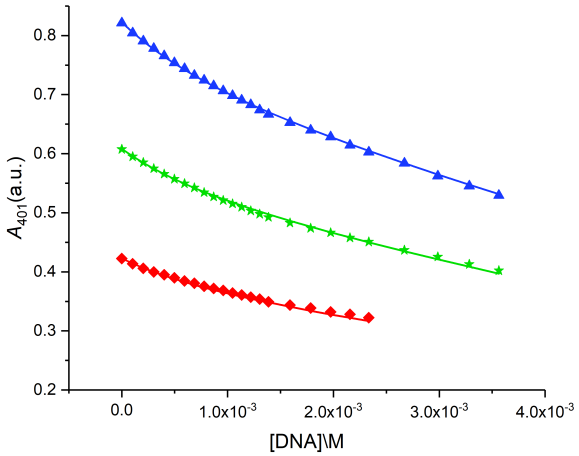

Figure 5.7 Absorbance at 401 nm for 83.0 µM (▲), 40.4 µM (◆), and 60.3 µM (★) solutions of 5.12b as a function of FSDNA concentration in buffer (25 mM MOPS, 50 mM NaCl, 1 mM EDTA) at 25 °C. (▲) 1st titration, (◆) 2nd titration, and (★) 3rd titration, and the solid lines represent a global fit of a multiple independent sites model to the data.

The titration curves exhibit a hypochromic shift in absorbance at 401 nm. The results of the analyses in terms of the MIS model are shown in Table 5.6.

Table 5.6 DNA-binding affinity *K* (n=3) / M^{-1} of 5.12b

***K* (n=3) / M^{-1}**	**1st titration**	**2nd titration**	**3rd titration**	**Global fit**
5.12b	(2.6±0.1) ×10^3	(3.6±0.4) ×10^3	(4.1±0.4) ×10^3	(3.0±0.2) ×10^3
Bathochromic shift, nm	401-405			

The titration data were analyzed with and without restricting the binding site size to 3 basepairs for each titration and in the global fit (see appendix). The individual fits show significant variation in *K* and *n*, including some surprising values for the binding site size. Restricting the binding site size to 3 basepairs results in more reproducible fits. Based on the global fit, the binding affinity $K_{binding}$ is (3.0±0.2) ×10^3 M^{-1} when the stoichiometry is restricted to 3 basepairs which indicates that this compound is a weak binder.

Similarly, titrations were carried out for **5.12c-e** and the titration curves were plotted and analyzed using the multiple independent binding sites model individually and globally (Figure 5.8).

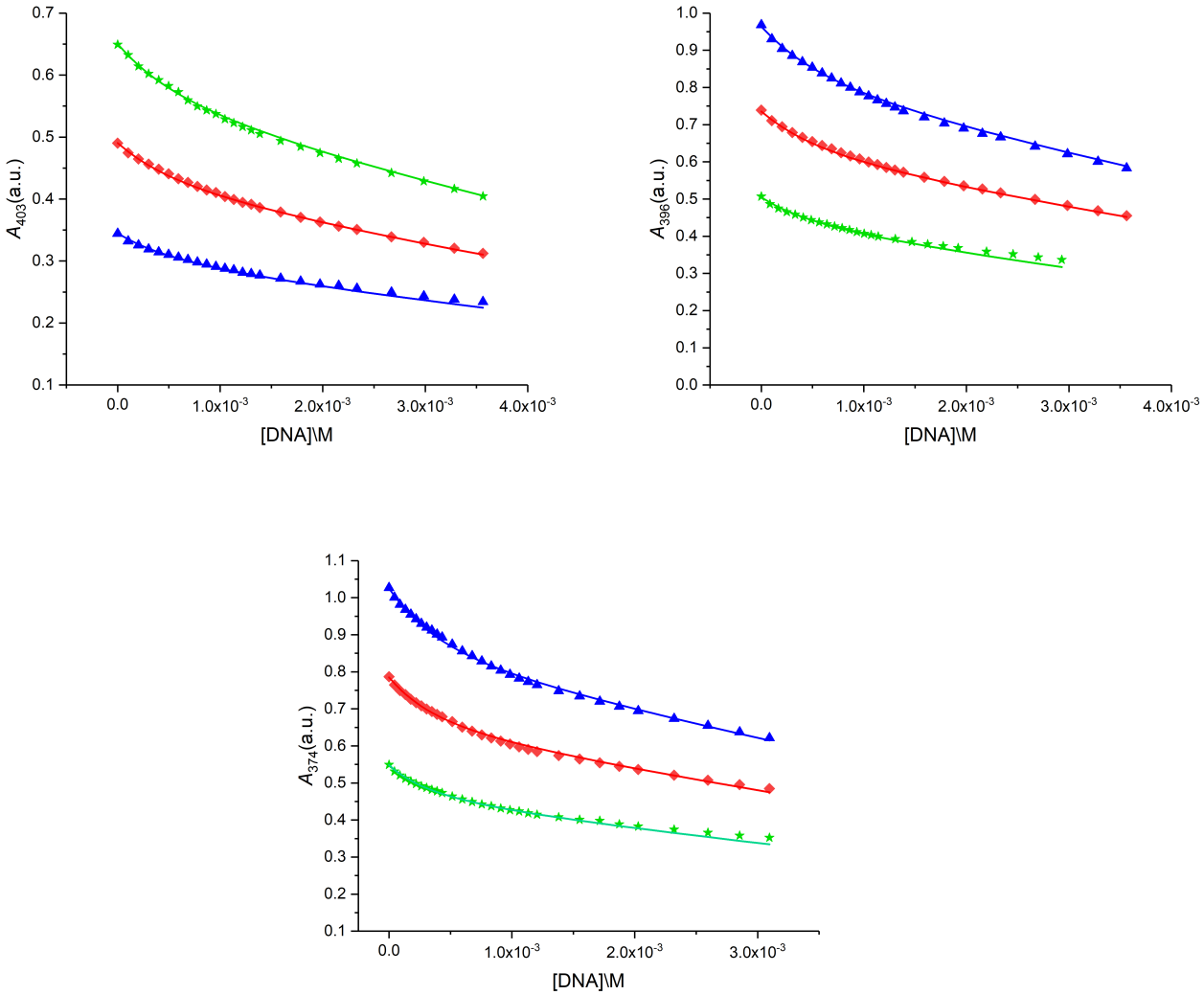

Figure 5.8 Absorbance at 403 nm for 31.8 μM (▲), 47.8 μM (◆), and 64.9 μM (★) solutions of 5.12c as a function of FSDNA concentration (top left), absorbance at 396 nm for 74.9 μM (▲), 56.6 μM (◆), and 37.8 μM (★) solutions of 5.12d as a function of FSDNA concentration (top right), and absorbance at 374 nm for 79.8 μM (▲), 60.2 μM (◆), and 41.6 μM (★) solutions of 5.12e as a function of FSDNA concentration in buffer (25 mM MOPS, 50 mM NaCl, 1mM EDTA) at 25 °C. (▲) 1st titration, (◆) 2nd titration, and (★) 3rd titration, the solid lines represent a global fit of a multiple independent sites model to the data.

The titration data for all compounds are reproducible. The curvature in the titration curves for **5.12e** looks more promising in terms of binding affinity for DNA compared to the other compounds. Table 5.7 illustrates the binding affinity and the stoichiometry of **5.12c-e**.

Table 5.7 DNA-binding affinities *K* (*n*=3) / M^{-1} of 5.12c-e

***K* (*n*=3) / M^{-1}**	**1st titration**	**2nd titration**	**3rd titration**	**Global fit**
5.12c	(6.5±0.8) ×10^3	(3.8±0.2) ×10^3	(4.3±0.3) ×10^3	(4.4±0.3) ×10^3
Bathochromic shift, nm	403-409			
5.12d	(4.4±0.3) ×10^3	(4.3±0.2) ×10^3	(11.5±1.9) ×10^3	(4.7±0.4) ×10^3
Bathochromic shift, nm	396-402			
5.12e	(8.2±0.7) ×10^3	(10.0±0.2) ×10^3	(13.9±1.9) ×10^3	(9.6±0.6) ×10^3
Bathochromic shift, nm	374-389			

According to the data analysis, the binding affinities of **5.12c-e** were obtained with and without restricting the binding site size to 3 basepairs (see appendix). Generally, this class of compound binds moderately with DNA. The most promising compound, among this series, in terms of binding with DNA is **5.12e** which contains two TEMPO moieties. The strength of binding increases in the following order **5.12b**< **5.12d**<**5.12c**<**5.12e**.

By comparing the DNA-binding affinities for this class of compounds with all synthesized compounds in previous chapters it appears that attaching a TEMPO group to naphthalimide does not seem to improve the DNA-binding properties. This observation is not unexpected, especially where the comparison involves bisnaphthalimide derivatives (chapter 3) and fused-ring-extended 1,8-naphthalimide derivatives (chapter 4). bisnaphthalimide derivatives contain two units of intercalators and fused-ring-extended 1,8-naphthalimide derivatives have a large aromatic surface to intercalate which improve the binding compared to mono-naphthalimide-TEMPO derivatives. It therefore appears as if the TEMPO group does not contribute significantly to the DNA-binding affinity.

Finally, due to the lack of solubility of bisnaphthalimide-TEMPO derivatives in MOPS, binding properties for this class of compounds has not been studied.

5.2.6 Conclusion

Several mono- and bisnaphthalimide-TEMPO conjugates have been synthesized using amide coupling reactions and the obtained compounds were characterized using mass spectrometry. The solubility for these compounds was tested and unsurprisingly bisnaphthalimide-TEMPO conjugates were not sufficiently soluble in MOPS whereas the mononaphthalimide derivatives were partially soluble. Therefore, the binding properties were only studied for mononaphthalimide-TEMPO derivatives using UV-visible titrations. The DNA-binding affinities show that compound **5.12e,** which contains two TEMPO moieties, binds with DNA better than the other compounds. Compound **5.12b** with morpholine as a solubilizing group binds least strongly with DNA.

5.3 Experimental

5.3.1 Materials and measurements

All chemicals, including FS DNA, were procured from Sigma-Aldrich, Fisher or TCI and were used without further purification. Flash column chromatography was carried out using 60 Å silica. All compounds show strong fluorescence and were readily visualized on TLC plates using UV light. ^{1}H-NMR and ^{13}C-NMR spectra were recorded utilizing a Bruker AV 400 UltraShield spectrometer and Bruker AV 500 UltraShield spectrometer using the solvent as an internal standard. All chemical shifts are reported with respect to TMS. High resolution mass spectra were recorded using a Waters Micromass LCT Premier. UV-visible spectra were recorded using a Jasco V-650 spectrophotometer at controlled temperature using an air-cooled EHCS-716 Peltier Thermostatted Cell Holder at 25 °C. The pH of buffers was recorded using Hanna microprocessor pH-meter equipped with a VWR 662-1382 glass electrode. The pH meter was calibrated using a two-point calibration with buffers of known pH obtained from Fisher scientific. Deionized water was obtained from an Elga Purelab Flex.

5.3.2 Experimental procedures

Synthesis of 3-(6-chloro-1,3-dioxo-1H-benzo[de]isoquinolin-2(3H)-yl)propanoic acid 5.14

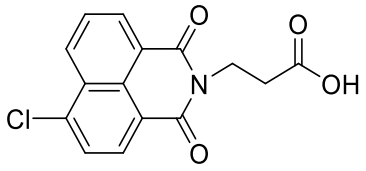

In a round-bottom flask, one equivalent of 4-chloro-1,8-naphthalic anhydride (6.97 g, 30 mmol) was mixed with one equivalent of β-alanine (2.67 g, 30 mmol) and dissolved in ≈50 mL DMF. The reaction mixture was heated to reflux for 24 h. The solvent was removed *in vacuo* and ethanol was added to obtain 3-(6-chloro-1,3-dioxo-1H-benzo[de]isoquinolin-2(3H)-yl)propanoic acid **5.14** as pale-yellow solid in 83% yield. **^{1}H-NMR (400 MHz, DMSO): δ(ppm):** 8.58 (dd, 1H, *J* = 8.38 Hz, *J* = 0.98 Hz, Ar-CH), 8.56 **(**dd, 1H, *J* = 7.36 Hz, *J* = 1.04 Hz, Ar-CH), 8.41 (d, 1H, *J* = 7.92 Hz, Ar-CH), 8.02 (d, 1H, *J* = 7.60 Hz, Ar-CH), 8.00 (dd, 1H, *J* = 8.36 Hz, *J* = 7.28 Hz, Ar-CH), 4.24 (t, 2H, *J* =7.88 Hz, CH_2), 2.60 (t, 2H, *J*=7.76, CH_2); **^{13}C-NMR (100 MHz, DMSO): δ(ppm):** 172.9, 163.3, 163.0, 137.9, 132.0, 131.3, 130.5, 129.1, 128.9, 128.8, 128.1, 123.2, 121.9, 36.3, 32.5. **HR TOF MS ES+** calc for [$C_{15}H_{11}NO_4Cl$] 304.0377 found 304.0368.

Synthesis of 3-(6-morpholino-1,3-dioxo-1H-benzo[de]isoquinolin-2(3H)-yl)propanoic acid 5.15b

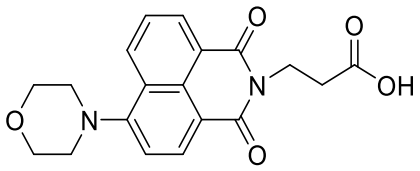

In a round-bottom flask, one equivalent of 6-morpholino-1H,3H-benzo[de]isochromene-1,3-dione **3.10** (0.13 g, 0.45 mmol) was mixed with one equivalent of β-alanine (0.04 g, 0.45 mmol) and dissolved in ≈50 mL DMF. The reaction mixture was heated to 100 °C for 48 h. The solvent was removed *in vacuo* and ethanol was added to produce 3-(6-morpholino-1,3-dioxo-1H-benzo[de]isoquinolin-2(3H)-yl)propanoic acid **5.15b** as a yellow powder in 92 % yield. **^{1}H-NMR (500 MHz, $CDCl_3$): δ(ppm):** 8.50 (dd, 1H, *J* =8.55 Hz, *J* =1.05 Hz), 8.48 (dd, 1H, *J* = 7.30 Hz, *J* =1.05 Hz), 8.42 (d, 1H, *J* = 8.15 Hz), 7.82 (dd, 1H, *J* = 8.30 Hz, *J* =7.40 Hz), 7.37 (d, 1H, *J* = 8.30 Hz), 4.25 (t, 2H, *J* =7.25 Hz), 3.91 (t, 4H, *J* =4.37 Hz), 3.23 (t, 4H, *J* =4.55 Hz), 2.57 (t, 2H, *J*=7.77); **^{13}C-NMR (125 MHz, DMSO-d_6)** δ 172.9, 163.9, 163.3, 155.9, 132.6, 131.1, 131.1, 129.6, 126.6, 125.7, 123.0, 116.3, 115.5, 66.6, 53.5, 36.0, 32.7. **HR TOF MS ES+** calc for [$C_{19}H_{19}N_2O_5$] 355.1294 found 355.1296.

Synthesis of 3-(6-(4-acetylpiperazin-1-yl)-1,3-dioxo-1H-benzo[de]isoquinolin-2(3H)-yl)propanoic acid 5.15c

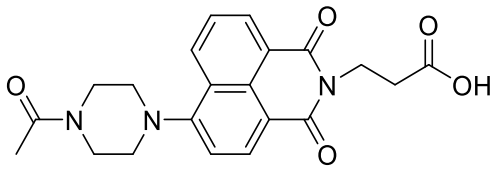

In a round-bottom flask, one equivalent of 6-(4-acetylpiperazin-1-yl)-1H,3H-benzo[de]isochromene-1,3-dione **3.11** (0.45 g, 1.38 mmol) was mixed with one equivalent of β-alanine (0.12 g, 1.38 mmol) and dissolved in ≈50 mL DMF. The reaction mixture was heated to 100 °C for 48 h. The solvent was removed *in vacuo* and ethanol was added to produced **5.15c** as a yellow powder in 33 % yield. **^{1}H-NMR (500 MHz, DMSO-d_6): δ(ppm):** 8.53 (dd, 1H, *J*= 8.50 Hz, *J*=1.05 Hz, Ar-CH), 8.50 (d, 1H, *J* = 7.27 Hz, *J*=1.07 Hz, Ar-CH), 8.42 (d, 1H, *J* = 8.00 Hz, Ar-CH), 7.85 (dd, 1H, *J* = 8.40 Hz, *J*=7.60 Hz, Ar-CH), 7.37 (d, 1H, *J* = 8.30 Hz, Ar-CH), 4.29 (t, 2H, *J* =8.02 Hz, CH_2), 3.78-3.75 (m, 4H, CH_2), 3.24 (t, 2H, *J* =4.97 Hz, CH_2), 3.17 (t, 4H, *J*=4.77, CH_2); 2.56 (t, 4H, *J*=8.00, CH_2); 2.09 (s, 3H, CH_3); **^{13}C-NMR (125 MHz, DMSO-d_6)** δ 172.9, 168.9, 163.9, 163.3, 155.8, 132.6, 131.1, 131.0, 129.5, 126.6, 125.8, 123.0, 118.6, 116.4, 115.9, 53.1, 53.0, 46.1, 41.3, 36.0, 32.8, 21.7. **HR TOF MS ES+** calc for [$C_{21}H_{22}N_3O_5$] 396.1559 found 396.1560.

Synthesis of 3-(6-((2-hydroxyethyl)thio)-1,3-dioxo-1H-benzo[de]isoquinolin-2(3H)-yl)propanoic acid 5.15d

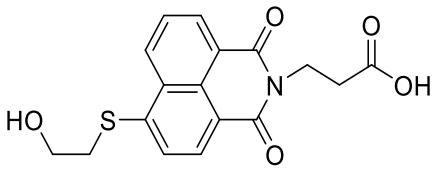

In a round-bottom flask, one equivalent of 3-(6-chloro-1,3-dioxo-1H-benzo[de]isoquinolin-2(3H)-yl)propanoic acid **5.14** (0.60 g, 2 mmol) was mixed with two equivalents of 2-mercaptoethanol (0.31 g, 4 mmol) and one equivalent of sodium hydrogen carbonate $NaHCO_3$ (0.16 g, 2 mmol) and dissolved in ≈ 50 mL DMF. The reaction mixture was heated to reflux for 24 h. After that the solvent was removed and the residue was acidified using HCl 5%. Diethyl ether was added with the sample placed in an ice-bath to allow a yellow solid to precipitate and the solid was filtered and **5.15d** was obtained in 59 % yield. **^{1}H-NMR (400 MHz, ACETONE): δ(ppm):** 8.60 (dd, 1H, J =8.50 Hz, J =1.10 Hz, Ar-CH), 8.56 (dd, 1H, J = 7.30 Hz, J = 1.10 H, Ar-CH), 8.41 (d, 1H, *J* = 7.88 Hz, Ar-CH), 7.87 (dd, 1H, *J* = 8.62 Hz, *J* = 7.34 Hz, Ar-CH), 7.82 (d, 1H, *J*= 8.12 Hz, Ar-CH), 4.42-4.39 (m, 2H, CH_2), 3.93 (t, 2H, *J*=6.62 Hz, CH_2), 3.44 (t, 2H, *J* =6.62 Hz, CH_2), 2.79-2.75 (m, 2H, CH_2); **^{13}C-NMR (100 MHz, ACETONE): δ(ppm):** 171.7, 163.3, 163.2, 144.8, 130.9, 130.4, 129.7, 129.4, 128.1, 126.8, 123.2, 123.1, 119.1, 59.8, 35.7, 34.5, 31.7. **HR TOF MS ES+** calc for [$C_{17}H_{16}NO_5S$] 346.0749 found 346.0745.

Synthesis of 3-(6-((carboxymethyl)thio)-1,3-dioxo-1H-benzo[de]isoquinolin-2(3H)-yl)propanoic acid 5.15e

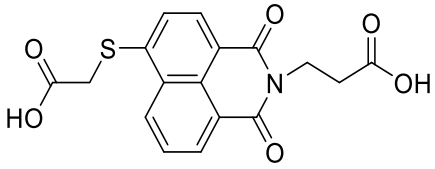

In a round-bottom flask, one equivalent of 3-(6-chloro-1,3-dioxo-1H-benzo[de]isoquinolin-2(3H)-yl)propanoic acid **5.14** (0.60 g, 2 mmol) was mixed with two equivalents of thioglycolic acid (0.36 g, 4 mmol) and 1.5 equivalents of sodium hydrogen carbonate $NaHCO_3$ (0.25 g, 3 mmol) and dissolved in ≈ 50 mL DMF. The reaction mixture was heated to reflux for 24 h. After that the solvent was removed and the crude residue was then acidified using HCl 5% and **5.15e** was obtained as yellow solid in 67 % yield. **^{1}H-NMR (500 MHz, DMSO): δ(ppm):** 8.59 (dd, 1H, *J*=8.30 Hz, J =1.20 Hz, Ar-CH), 8.54 (dd, 1H, *J*= 7.17 Hz, *J*= 1.07 H, Ar-CH), 8.39 (d, 1H, *J*= 7.90 Hz, Ar-CH), 7.92 (dd, 1H, *J* = 8.42 Hz, *J* = 7.27 Hz, Ar-CH), 7.73 (d, 1H, *J*= 8.15 Hz, Ar-CH), 4.25 (t, 2H, *J*=7.72 Hz, CH_2), 4.21 (s, 2H, CH_2), 2.59 (t, 2H, *J* =7.35 Hz, CH_2). **^{13}C-NMR (125 MHz, DMSO): δ(ppm):** 172.9, 170.1, 163.5, 163.4, 143.9, 131.5, 130.8, 130.0, 129.0, 128.0, 1527.8, 123.8, 123.2, 119.3, 36.1, 34.3, 32.6. **HR TOF MS ES+** calc for [$C_{17}H_{14}NO_6S$] 360.0542 found 360.0539.

Synthesis of 5.12b

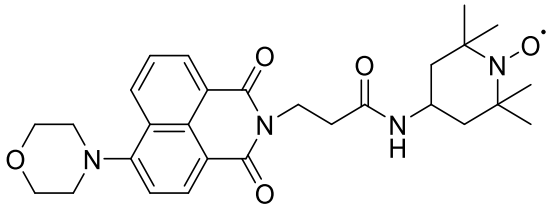

In a round-bottom flask, one equivalent of 3-(6-morpholino-1,3-dioxo-1H-benzo[de]isoquinolin-2(3H)-yl)propanoic acid **5.15b** (0.1 g, 0.3 mmol) and 1.5 equivalents of 4-amino-TEMPO (0.07 g, 0.45 mmol) were dissolved in DMF. Then, 1.5 equivalents of HOBt (0.06 g, 0.45 mmol) and 1.5 equivalents of EDC.HCl (0.08 g, 0.45 mmol) and 1.5 equivalents of N-ethyldiisopropylamine (0.038g, 0.45 mmol) were added. The flask was sealed and left to stir at room temperature for 48 h. The reaction mixture was concentrated *in vacuo* and the purity of **5.12b** was checked using TLC DCM, ethanol 9:1 as eluent (R_f=0.62). **HR TOF MS ES+** calc for [$C_{28}H_{36}N_4O_5$] 508.2686 found 508.2693, found isotope distribution: [M=1] 508.2693(100%), [M+2] 509.2745 (35%), [M+3] 510.2780 (7%). expected isotope distribution [M+1] 508.26 (100%), [M+2] 509.26 (30%) [M+3] 510.27 (2.7%)

Synthesis of 5.12c

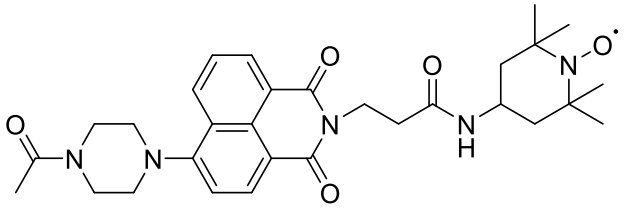

In a round-bottom flask, one equivalent of 3-(6-(4-acetylpiperazin-1-yl)-1,3-dioxo-1H-benzo[de]isoquinolin-2(3H)-yl)propanoic acid **5.15c** (0.11 g, 0.3 mmol) and 1.5 equivalent of 4-amino-TEMPO (0.07 g, 0.45 mmol) were dissolved in DMF. Then, 1.5 equivalent of HOBt (0.06 g, 0.45 mmol) and 1.5 equivalent of EDC.HCl (0.08 g, 0.45 mmol) and 1.5 equivalent of N-ethyldiisopropylamine (0.038g, 0.45 mmol) were added. The flask was sealed and left to stir at room temperature for 48 h. The reaction mixture was concentrated *in vacuo* and the purity of **5.12c** was checked using TLC using DCM: ethanol 9:1 as eluent (R_f=0.53). **HR TOF MS ES+** calc for [$C_{30}H_{39}N_5O_5$] 549.2951 found 549.2958. 549.2958 (100%), 550.3007 (63%), 551.3034 (20%). expected mass: 549.29 (100%), 550.29 (32%), 551.29 (5.1%).

Synthesis of 5.12d

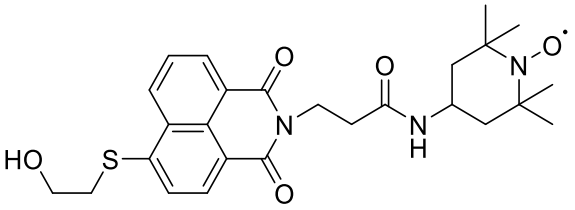

In a round-bottom flask, one equivalent of 3-(6-((2-hydroxyethyl)thio)-1,3-dioxo-1H-benzo[de]isoquinolin-2(3H)-yl)propanoic acid **5.15d** (0.09 g, 0.3 mmol) and 1.5 equivalent of 4-amino-TEMPO (0.07 g, 0.45 mmol) were dissolved in DMF. Then, 1.5 equivalent of HOBt (0.06 g, 0.45 mmol) and 1.5 equivalent of EDC.HCl (0.08 g, 0.45 mmol) and 1.5 equivalent of N-ethyldiisopropylamine (0.038g, 0.45 mmol) were added. The flask was sealed and left to stir at room temperature for 48 h. The reaction mixture was concentrated *in vacuo* The reaction mixture was concentrated *in vacuo* and the purity of **5.12d** was checked using TLC (R_f=0.7, DCM-acetone 1:1). **HR TOF MS ES+** calc. for [$C_{26}H_{33}N_3O_5S$] 499.2141, found 499.2146. Isotopes found: 499.2146 (100%), 500.2194 (45%), 501.2193 (15%); Expected mass of isotopes: 499.21 (100%), 500.21 (28%), 501.20 (4.5%).

Synthesis of 5.12e

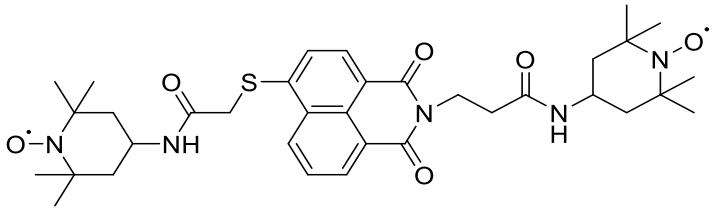

In a round-bottom flask, one equivalent of 3-(6-((carboxymethyl)thio)-1,3-dioxo-1H-benzo[de]isoquinolin-2(3H)-yl)propanoic acid **5.15e** (0.17 g, 0.5 mmol) and three equivalents of 4-amino-TEMPO (0.25 g, 1.5 mmol) were dissolved in DMF. Then, three equivalents of HOBt (0.22 g, 1.5 mmol) and three equivalents of EDC.HCl (0.28 g, 1.5 mmol) and one equivalent of N-ethyldiisopropylamine (0.06 g, 0.5 mmol) were added. The flask was sealed and left to stir at room temperature for 48 h. The reaction mixture was concentrated *in vacuo* and the purity of **5.12e** has been checked using TLC (R_f=0.8, DCM-acetone 1:1).

Synthesis of 5.13a

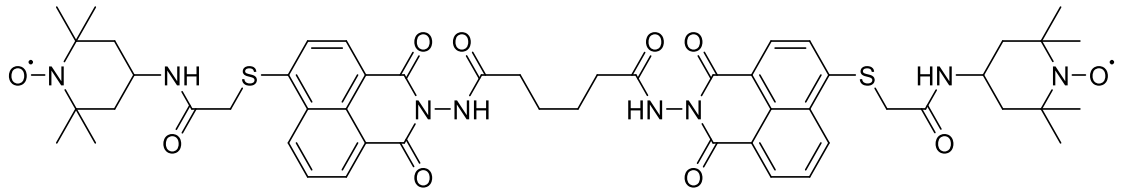

In a round-bottom flask, one equivalent of N^1,N^6-bis(6-chloro-1,3-dioxo-1H-benzo[de]isoquinolin-2(3H)-yl)adipamide **3.13a** (0.501 g, 0.81 mmol), three equivalents of 4-amino-TEMPO (0.402 g, 2.43 mmol), three equivalents of HOBt (0.328 g, 2.43 mmol) and three equivalents of EDC.HCl (0.465 g, 2.43 mmol) were dissolved in ≈ 20 mL dry DMF. Two equivalents of N-ethyl-diisopropylamine (0.23mL, 1.62 mmol) were added. The flask was sealed and left to stir at room temperature for 72 h. The volume of solvent was reduced *in vacuo* then methanol was added to separate a brown oil which was filtered and left to dry. Upon drying the oil solidified. The crude product **5.13a** was obtained as brown solid in 28% yield. *m/z* (TOF MS ES+) 1021.40 (58%), 1022.41 (100), 1023.41 (63), 1024.41 (30) (expected mass: 1020.39). **TOF MS ES+** 1022.4022 (100%), 1023.4051 (70%).

Synthesis of 5.13d

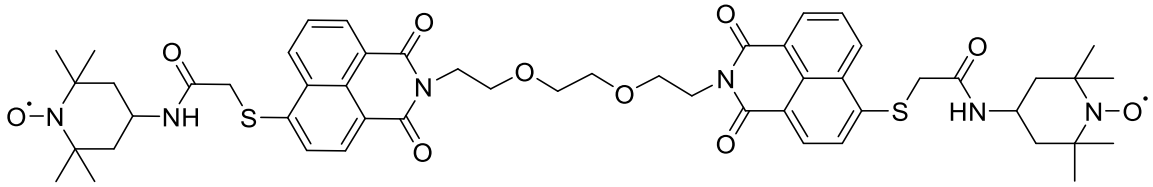

In a round-bottom flask, one equivalent of S,S'-(((ethane-1,2-diylbis(oxy))bis(ethane-2,1-diyl))bis(1,3-dioxo-2,3-dihydro-1H-benzo[de]isoquinoline-2,6-diyl)) bis(2-hydroxyethanethioate) **3.13d** (0.502 g, 0.81 mmol), three equivalents of 4-amino-TEMPO (0.401 g, 2.43 mmol), three equivalents of HOBt (0.328 g, 2.43 mmol) and three equivalents of EDC.HCl (0.465 g, 2.43 mmol) were dissolved in a ≈20 mL dry DMF. Two equivalents of N-ethyl-diisopropylamine (0.23 mL, 1.62 mmol) were added. The flask was sealed and left to stir at room temperature for 72 h. The reaction mixture was concentrated in vacuo and methanol was added to separate a brown oil which was filtered and left to dry. Upon drying the oil solidified. The crude product was obtained in 35 % yield was purified by column chromatography 9:1 chloroform-methanol (R_f=0.85) to give **5.13d** as yellow crystals, m/z (TOF MS ES+) 995.42 (50%), 996.41 (100), 997.41 (60), 998.41 (25) (expected mass: 994.40).

Synthesis of 5.13e

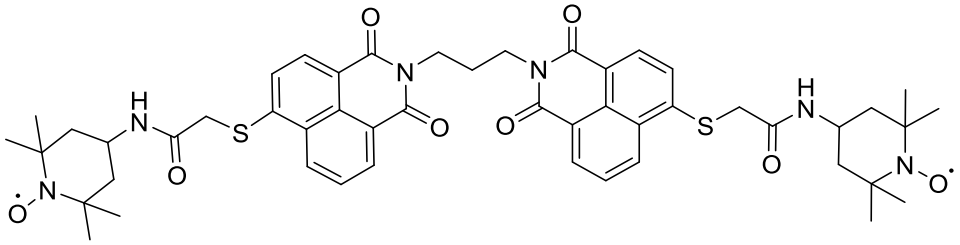

In a round-bottom flask, one equivalent of 2,2'-((propane-1,3-diylbis(1,3-dioxo-2,3-dihydro-1H-benzo[de]isoquinoline-2,6-diyl))bis(sulfanediyl))diacetic acid **3.13e** (0.502 g, 0.81 mmol), three equivalents of 4-amino-TEMPO (0.41 g, 2.43 mmol), three equivalents of HOBt (0.328 g, 2.43 mmol) and three equivalents of EDC.HCl (0.465 g, 2.43 mmol) were dissolved in ≈20 mL DMF. Two equivalents of N-ethyl-diisopropylamine (0.23 mL, 1.62 mmol) were added. The flask was sealed and left to stir at room temperature for 72 h. The reaction mixture was concentrated in vacuo and methanol was added to precipitate a yellow solid which was filtered and left to dry. The crude product was obtained in 27% yield and purified by column chromatography 9:1 chloroform: methanol (R_f= 0.81) to give the **5.13e** as yellow crystals, m/z (TOF MS ES+) 921.37 (45%), 922.37 (100), 923.38 (55), 924.38 (23) (expected mass: 920.36). **TOF MS ES+** 921.3680 (20%), 922.3758 (50%), 923.3795 (30%)

5.3.3. Solubility tests of synthesized compounds

To prepare ligand solutions, several milligrams of obtained compounds **5.12b-e** (not completely dry, DMF traces) was partially dissolved in MOPS buffer and stirred for 2-5 days. Then the solutions were filtered using a 0.2 µm syringe filter. The solution was placed in a 1 cm pathlength thermostatted quartz cuvette and the spectra were recorded at 25 °C and the concentrations were calculated using the Beer Lambert law using the extinction coefficients for the chromophores as determined in Chapter 2.

5.3.4 UV-visible titration

5.3.4.1 Preparation of buffer

3-(*N*-morpholino)propanesulfonic acid (MOPS) (10.463 g, 50 mmol), ethylenediaminetetraacetic acid (EDTA) (0.584 g, 2 mmol) and sodium chloride (5.844 g, 100 mmol) were placed in a 2 litre beaker with a magnetic stirrer bar. 1500 mL of distilled water was added, and the mixture was stirred until all solid had dissolved. The pH of the solution was tested with a calibrated pH meter and adjusted to pH 7.00±0.02 by addition of a concentrated sodium

hydroxide solution. The solution was then transferred to a 2 litre volumetric flask and made up to 2 litres with distilled water. The flask was inverted to make sure the solution was completely homogenous before transferring to a bottle for storage.

5.3.4.2 Preparation of DNA Solution

Fish sperm DNA (FSDNA) (~0.1 g) was placed in a 10 mL falcon tube with MOPS buffer (10 mL). The solution was sonicated to dissolve the solid and then left to stand overnight to ensure all material was in solution. The solution was dialysed overnight using 3.5 kDa MWCO (molecular weight cut-off) dialysis tubing (Visking, Medicell) against 1 litre of buffer, then the dialysis buffer was removed, and a fresh litre of buffer was added, and the dialysis step was repeated. The concentration of the DNA solution was determined spectrophotometrically by placing 10 µL of the concentrated DNA stock solution in 2500 µL of buffer and recording a UV-visible spectrum between 200-800 nm. A molar absorptivity of 12,600 M^{-1} (bp) cm^{-1} at 260 nm was used to determine the DNA concentration (0.0129, 0.010, 0.011 mol dm^{-3})

2.3.4.3 UV-visible titration

Concentrated stock solutions of sufficiently soluble naphthalimide-TEMPO derivatives were diluted by adding different volumes of these solutions to a 1 cm pathlength quartz cuvette and completing the volume with MOPS buffer until 2500 µl. The absorbance in the range of 0.2-1.1 a.u. was recorded in a cuvette to avoid self-aggregation and precipitation of the ligand. The cuvette was placed in the spectrophotometer, thermostated at 25 °C and a UV-visible spectrum was recorded. The DNA solution was added stepwise in small aliquots (5-10 µl) and the UV-visible spectra were recorded within the range 200-800 nm after each addition of DNA. The absorptions at maximum wavelengths were extracted from the UV-visible spectra and plotted as a function of DNA and ligand concentrations. The obtained data for each titration were analysed using Origin 2017 using the multiple independent binding sites model[19].

5.3.5 Molecular Docking study

The chemical structures for the proposed compounds were drawn using ChemDraw Professional 16.0 and they were subjected to geometrical optimization using MM2 (molecular dynamics and energy minimized) in Chem3D 16.0. The final structure was saved in PDB format and converted to a PDBQT file in AutoDock Tools after checking

the torsions for all the bonds. The structure of DNA with a pre-formed intercalation gap[20] called "open d(ATCGAGACGTCTCGAT)$_2$ " was used as the docking target with docking carried out using AutoDock Vina[16] with the parameters in Figure 5.9.

center_x = -2.152 center_y = 2.953 center_z = 24.92 size_x = 40 size_y = 40 size_z = 60 exhaustiveness = 200 num_modes = 10	**Definition:** **Center [x][y][z]**: box center in the receptor coordinate system. **Size [x][y][z]**: box dimensions along X, Y, and Z in the receptor coordinate system. **num_modes**: maximum number of binding modes to generate. **Exhaustiveness:** the time spent on the search is already varied heuristically depending on the number of atoms, flexibility, etc

Figure 5.9 The docking parameters

Acknowledgment

I thank Jai Noah Maxwell for the synthesis of compounds **5.13a,d,e.**

5.4 References

1. Samuni, A. M.; Barenholz, Y., 19 - Use of Nitroxides to Protect Liposomes Against Oxidative Damage. In *Methods in Enzymology*, Düzgüneş, N., Ed. Academic Press: 2004; Vol. 387, pp 299-314.

2. Monaco, A.; Becer, C. R., Synthesis, Characterization and Applications of Glycopolymers. In *Reference Module in Chemistry, Molecular Sciences and Chemical Engineering*, Elsevier: 2020.

3. Hasirci, V.; Huri, P. Y.; Tanir, T. E.; Eke, G.; Hasirci, N., 1.22 Polymer Fundamentals: Polymer Synthesis☆. In *Comprehensive Biomaterials II*, Ducheyne, P., Ed. Elsevier: Oxford, 2017; pp 478-506.

4. Wang, J.; He, C.; Wu, P.; Wang, J.; Duan, C., An Amide-Containing Metal–Organic Tetrahedron Responding to a Spin-Trapping Reaction in a Fluorescent Enhancement Manner for Biological Imaging of NO in Living Cells. *Journal of the American Chemical Society* **2011,** *133* (32), 12402-12405.

5. Simonet, J.; El Badre, M. C.; Cariou, M., The cathodic scission of aromatic derivatives in the presence of nitrones as spin markers: on the reactivity of transient nitroxides in weak H-donor solvents: Part 2. On the cleavage of aromatic sulphones and halides in benzonitrile. *Journal of Electroanalytical Chemistry* **1992,** *334* (1), 169-182.

6. Haugland, M.; Lovett, J.; Anderson, E., Advances in the synthesis of nitroxide radicals for use in biomolecule spin labelling. *Chemical Society Reviews* **2018,** *47*.

7. Hardwick, J. S.; Haugland, M. M.; El-Sagheer, A. H.; Ptchelkine, D.; Beierlein, F. R.; Lane, A. N.; Brown, T.; Lovett, J. E.; Anderson, E. A., 2'-Alkynyl spin-labelling is a minimally perturbing tool for DNA structural analysis. *Nucleic Acids Res* **2020,** *48* (6), 2830-2840.

8. Prior, C.; Danilāne, L.; Oganesyan, V. S., All-atom molecular dynamics simulations of spin labelled double and single-strand DNA for EPR studies. *Physical Chemistry Chemical Physics* **2018,** *20* (19), 13461-13472.

9. Bannwarth, W.; Schmidt, D., Oligonucleotides containing spin-labeled 2'-deoxycytidine and 5-methyl-2'-deoxycytidine as probes for structural motifs of DNA. *Bioorganic & Medicinal Chemistry Letters* **1994,** *4* (8), 977-980.

10. Gophane, D. B.; Endeward, B.; Prisner, T. F.; Sigurdsson, S. T., A semi-rigid isoindoline-derived nitroxide spin label for RNA. *Organic & Biomolecular Chemistry* **2018,** *16* (5), 816-824.

11. Belmont, P.; Chapelle, C.; Demeunynck, M.; Michon, J.; Michon, P.; Lhomme, J., Introduction of a nitroxide group on position 2 of 9-phenoxyacridine: Easy access to spin labelled DNA-binding conjugates. *Bioorganic & Medicinal Chemistry Letters* **1998,** *8* (6), 669-674.

12. Wang, Z.; Wang, X.; Wang, P.; Zhao, J., Allenone-Mediated Racemization/Epimerization-Free Peptide Bond Formation and Its Application in Peptide Synthesis. *Journal of the American Chemical Society* **2021**.

13. Chan, L. C.; Cox, B. G., Kinetics of Amide Formation through Carbodiimide/N-Hydroxybenzotriazole (HOBt) Couplings. *The Journal of Organic Chemistry* **2007,** *72* (23), 8863-8869.

14. Mahmoud, Khaled A.; Long, Y.-T.; Schatte, G.; Kraatz, H.-B., Rearrangement of the Active Ester Intermediate During HOBt/EDC Amide Coupling. *European Journal of Inorganic Chemistry* **2005,** *2005* (1), 173-180.

15. Li, S.; Guo, C.; Sun, X.; Li, Y.; Zhao, H.; Zhan, D.; Lan, M.; Tang, Y., Synthesis and biological evaluation of quinazoline and quinoline bearing 2,2,6,6-tetramethylpiperidine-N-oxyl as potential epidermal growth factor receptor(EGFR) tyrosine kinase inhibitors and EPR bio-probe agents. *European Journal of Medicinal Chemistry* **2012,** *49*, 271-278.

16. Trott, O.; Olson, A. J., AutoDock Vina: improving the speed and accuracy of docking with a new scoring function, efficient optimization, and multithreading. *J Comput Chem* **2010,** *31* (2), 455-461.

17. Ciriano, M. V.; Korth, H.-G.; van Scheppingen, W. B.; Mulder, P., Thermal Stability of 2,2,6,6-Tetramethylpiperidine-1-oxyl (TEMPO) and Related N-Alkoxyamines. *Journal of the American Chemical Society* **1999,** *121* (27), 6375-6381.

18. Beheshtiha, S. Y. S.; Hekmatshoar, R.; Soltani, F., SYNTHESIS AND ABSORPTION PROPERTIES OF SOME NEW 4-THIO-1,8-NAPHTHYLIMIDES AND 4-(THIO)-7H-BENZIMIDAZO [2,1-A] BENZ [D,E] ISOQUINOLIN-7-ONE DERIVATIVES. *Phosphorus, Sulfur, and Silicon and the Related Elements* **2004,** *179* (9), 1723-1729.

19. Hahn, L.; Buurma, N. J.; Gade, L. H., A Water-Soluble Tetraazaperopyrene Dye as Strong G-Quadruplex DNA Binder. *Chemistry – A European Journal* **2016,** *22* (18), 6314-6322.

20. Jones, J. E.; Amoroso, A. J.; Dorin, I. M.; Parigi, G.; Ward, B. D.; Buurma, N. J.; Pope, S. J. A., Bimodal, dimetallic lanthanide complexes that bind to DNA: the nature of binding and its influence on water relaxivity. *Chemical communications (Cambridge, England)* **2011,** *47* (12), 3374-3376.

EPILOGUE

6.1 General conclusions

In this thesis several classes of naphthalimide derivatives have been designed, inspired by approaches that had been proven to improve the DNA-binding affinities. The majority of these compounds are uncharged. Neutral binders were targeted in an attempt to avoid precipitation of DNA-binder complexes resulting from non-specific electrostatic binding of cationic binders with anionic DNA leading to neutral complexes. Most of proposed compounds have been successfully synthesized and characterized, typically using ^{1}H-, ^{13}C-NMR spectroscopy and mass spectrometry. Several solubilizing groups have been introduced for each class of compound. The resulting aqueous solubility for these compounds is varied. Solubilising groups have different effects on the solubility from one class to another; there is no clear pattern, as far as we have found, between each group and how much it improves the solubilities. Nevertheless, considering only the neutral compounds synthesized here, reasonable solubilities ranging from μM to tens of μM have been found.

The DNA- binding proprieties for all soluble compounds were evaluated using UV-visible titrations. Ferrocene-mononaphthalimide conjugates generally are weak binders. However, there are some exceptions, **2.12f** and **2.13c** bind strongly with DNA with binding affinities of 3.8×10^{5} and 1.01×10^{5} M^{-1}, respectively. Generally, using linkers with different lengths to connect the naphthalimide scaffold and ferrocene moieties did not play a significant role in terms of binding with DNA except for one case when morpholine was used as a solubilizing group. In this case changing the length of the linker between the ferrocene and the naphthalimide has a remarkable effect on improving the binding affinity where the compound with a short linker **2.13c** exhibits a higher binding affinity than the compound with the longer ether-based linker

Bisnaphthalimides on the other hand, can be considered as good binders. Most tested bisnaphthalimides, such as **3.9e** and **3.12d**, showed good affinities for DNA of 6.13×10^{4} and 1.24×10^{4} M^{-1}, respectively. On the other hand, compound **3.10b** is the most promising compound among this series as it binds relatively strongly with DNA with a binding affinity of 3.95×10^{5} M^{-1}. Unsurprisingly, bisnaphthalimides substituted with thioglycolic acid do not bind with DNA due to the negatively charged carboxylates when the carboxylic acids get deprotonated in solution and electrostatically prevent the bisnaphthalimide from binding with negatively charged DNA.

The next class of compounds are fused-ring-extended 1,8-naphthalimide derivatives, which come in two isomers. The DNA-binding properties for fused-ring-extended 1,8-naphthalimide derivatives look both promising and interesting since the titration curves show unusual behavior. In general, there is no difference between the two isomers of each compound in terms of binding with DNA. The binding properties for both isomers were remarkably improved when we introduced different groups (1°-amine, 2°-amine, thiol group) compared to the bromo-substituted isomers. Compound **4.16a**, with ethanolamine as the solubilizing group, is the most promising

compound among this series with an apparent DNA-binding affinity K_{app} of 8.45×10^4 M^{-1}. The 2-mercaptoethanol-substituted **4.16d** and **4.17d**, on the other hand, show the lowest DNA-binding affinities (~10^3 M^{-1}). We note, however, that these binding affinities are apparent binding affinities and therefore likely underestimate the actual affinities of these compounds for DNA.

Finally, mono-naphthalimide-TEMPO conjugates bind moderately with DNA. Among this series of compounds **5.12e**, which contains two TEMPO moieties, binds with DNA better than the other compounds while **5.12b**, that involves morpholine as solubilising group, binds with DNA with lower affinity.

6.2 Outlook

Since the DNA-binding proprieties for all soluble compounds were investigated using UV-visible titrations, it is worth considering other techniques to study the DNA-binding affinities. For instance, the binding affinities for the most promising ferrocene-naphthalimide conjugates such as **2.13c** and **2.12f** could be studied further using electrochemical techniques and these compounds should also be tested in electrochemical genosensors. Similarly the DNA affinity of naphthalimide-TEMPO conjugates **5.12e** can be studied using EPR and this would also establish the applicability of these compounds as sensitisers in EPR-based genosensors. To further study the interactions behind the complex binding curves for the fused-ring-extended 1,8-naphthalimide derivatives, isothermal titration calorimetry (ITC) could be used. The advantage of ITC is that the binder is titrated into the DNA solution. As a result, precipitation processes resulting from an excess of binder in the presence of a small amount of DNA occur at the end of the titration rather than at the beginning, which makes the data easier to interpret. In addition, ITC will allow us to study the self aggregation of these compounds in the absence and presence of DNA.

It is also interesting to study the binding affinities for the insoluble bisnaphthalimides by making solutions using DMSO stock solutions of the compounds. Although the resulting solutions may not be stable, it would be interesting to quantify the affinity of all compounds for DNA, especially the bisnaphthalimides with morpholine as a solubilizing group which show the most promising binding affinities for this class of compound.

In terms of compound design, in all synthesized compounds, the length and the nature of the linker affect binding affinities, which means that expanding the range of properties of the linkers is something that should be considered in the future. One class of linkers that might be of interest are short peptides or hairpin-polyamide like structures. This might allow interactions in the major or minor groove to strengthen the interactions beyond the effects of intercalation alone. Finally, it would be interesting to conjugate the fused-ring-extended 1,8-naphthalimide derivative with ferrocene and TEMPO to create functional sensitisers with a higher affinity for DNA.

Appendix

Table of Contents

Appendix for Chapter 2

A2.1 Characterization of compounds using NMR spectroscopy

NMR code: 500_HUDA 2021 Fc-Cl fcc acetone DMSO

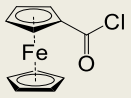

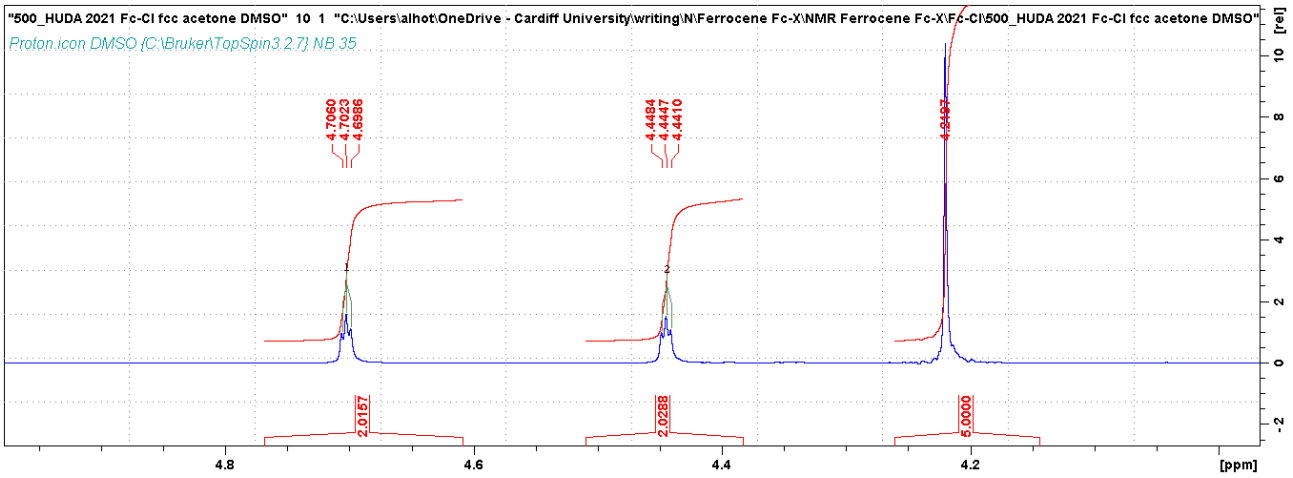

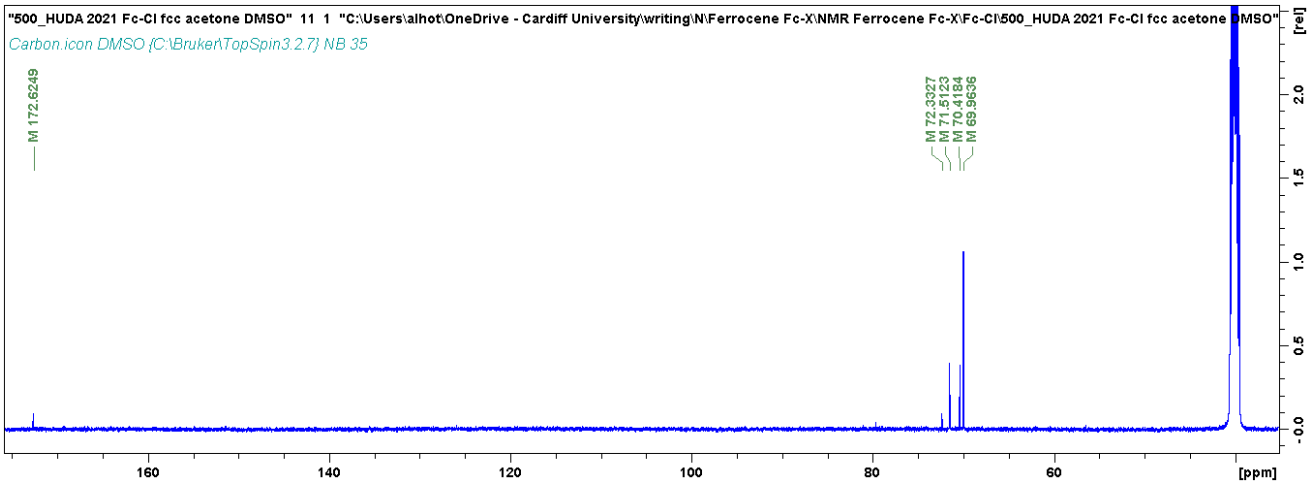

^{1}H NMR (500 MHz, DMSO): δ(ppm): 4.70 (t, *J*=1.85, 2H, Fc), 4.44(t, *J*=1.85, 2H, Fc), 4.22 (s, 5H, Fc). **^{13}C NMR (500 MHz, DMSO): δ(ppm):** 172.62, 72.33, 71.51, 70.41, 69.96. **TOF MS ASAP+** 247.97 (100%), 248.97 (37%), 249.97 (55%)

^{1}H NMR code: 400_HUDA 2020 Fc-PEG mine Flask 1 CDCl3\ ^{13}C NMR code: 500_HUDA 2021 Fc-PEG CDCL3

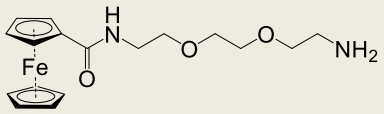

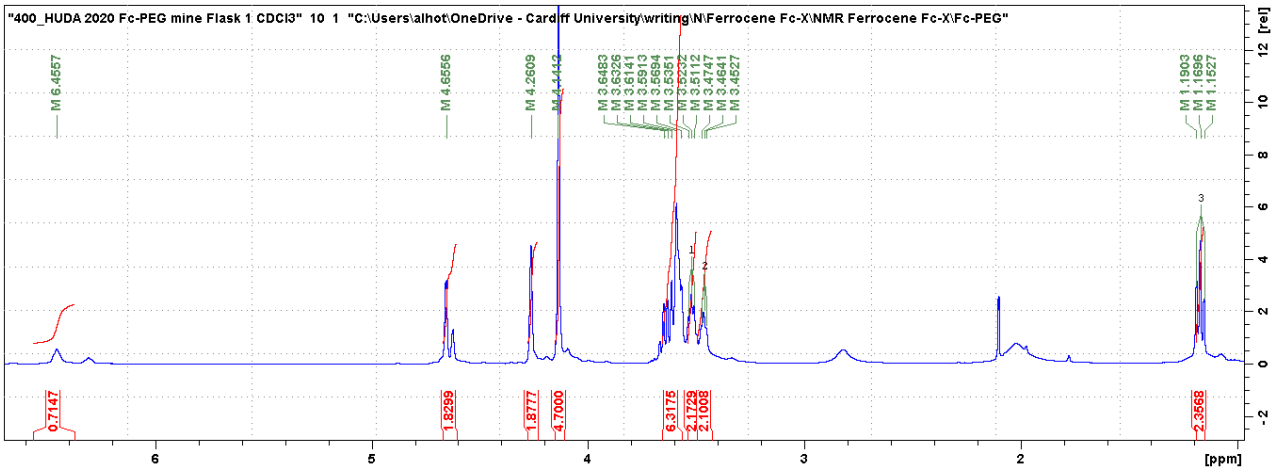

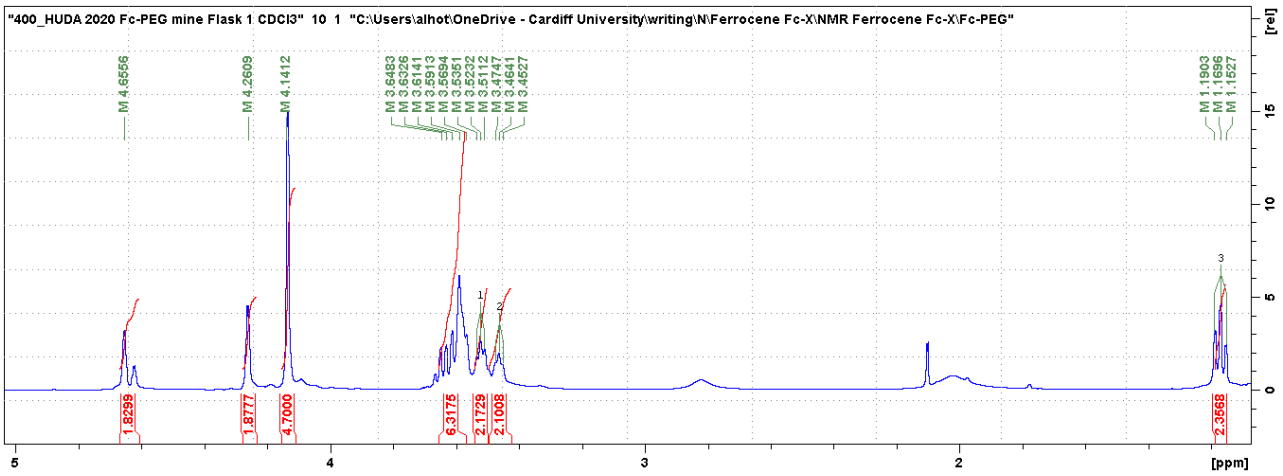

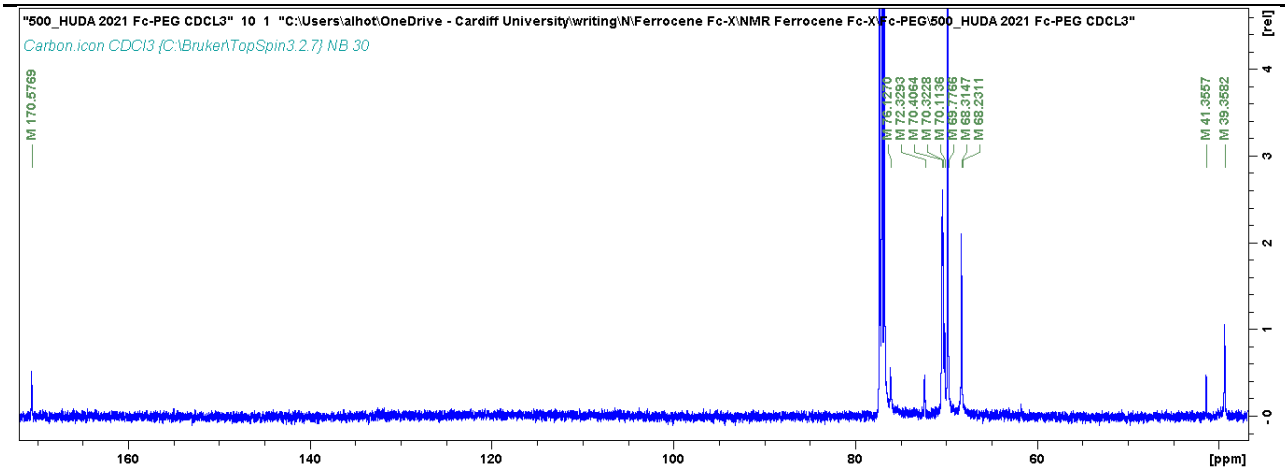

^{1}H NMR (400 MHz, CDCl3): δ(ppm): 6.45 (br.s, 1H, NH), 4.65 (br.s, 2H, CH, Fc), 4.26 (br.s, 2H, CH, Fc), 4.14 (s, 5H, Fc), 3.61 (m, 6H, CH_2), 3.52 (t, *J*=4.78, 2H, CH_2), 3.46 (t, *J*=4.40, 2H, CH_2), 1.16(t, *J*=7.52, 2H, CH_2). **^{13}C NMR (500 MHz, CDCl3): δ(ppm):** 170.57, 76.12, 72.32, 70.40, 70.32, 70.11, 69.77, 68.31, 68.23, 41.35, 39.35. **TOF MS ES+** calc for [$C_{17}H_{25}N_2O_3Fe$] 361.1215 found 361.1227.

^{1}H NMR code: 400_HUDA 2020 Fc-N2 mine 2nd col col 3\ ^{13}C NMR code: 500_HUDA 2021 conf Fc-Nap DMSO

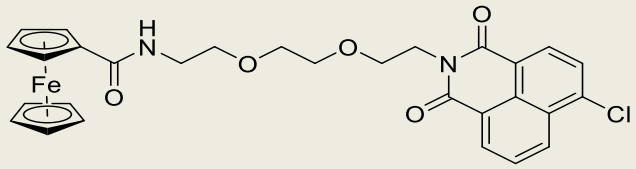

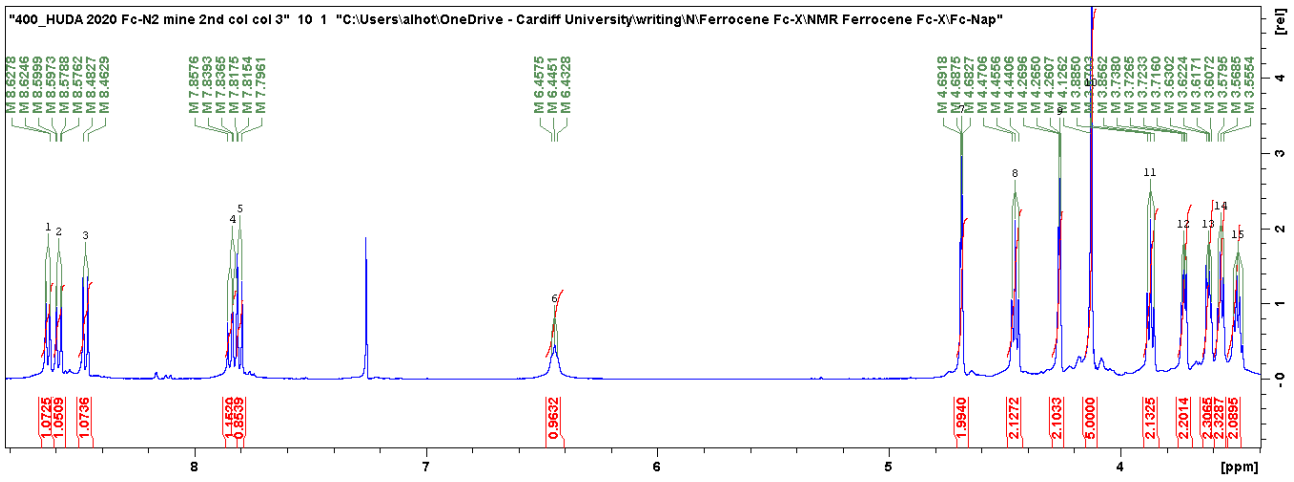

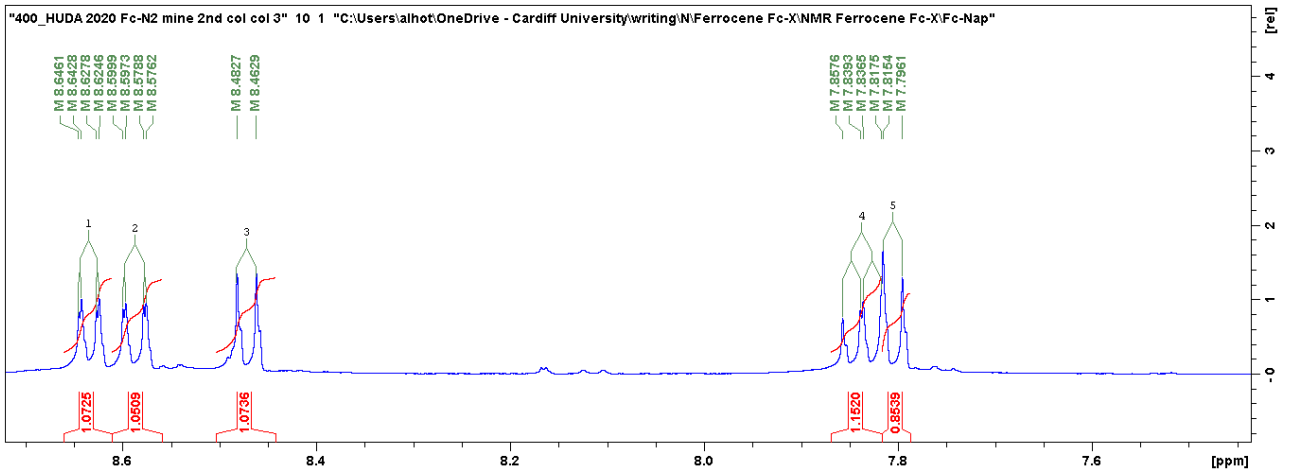

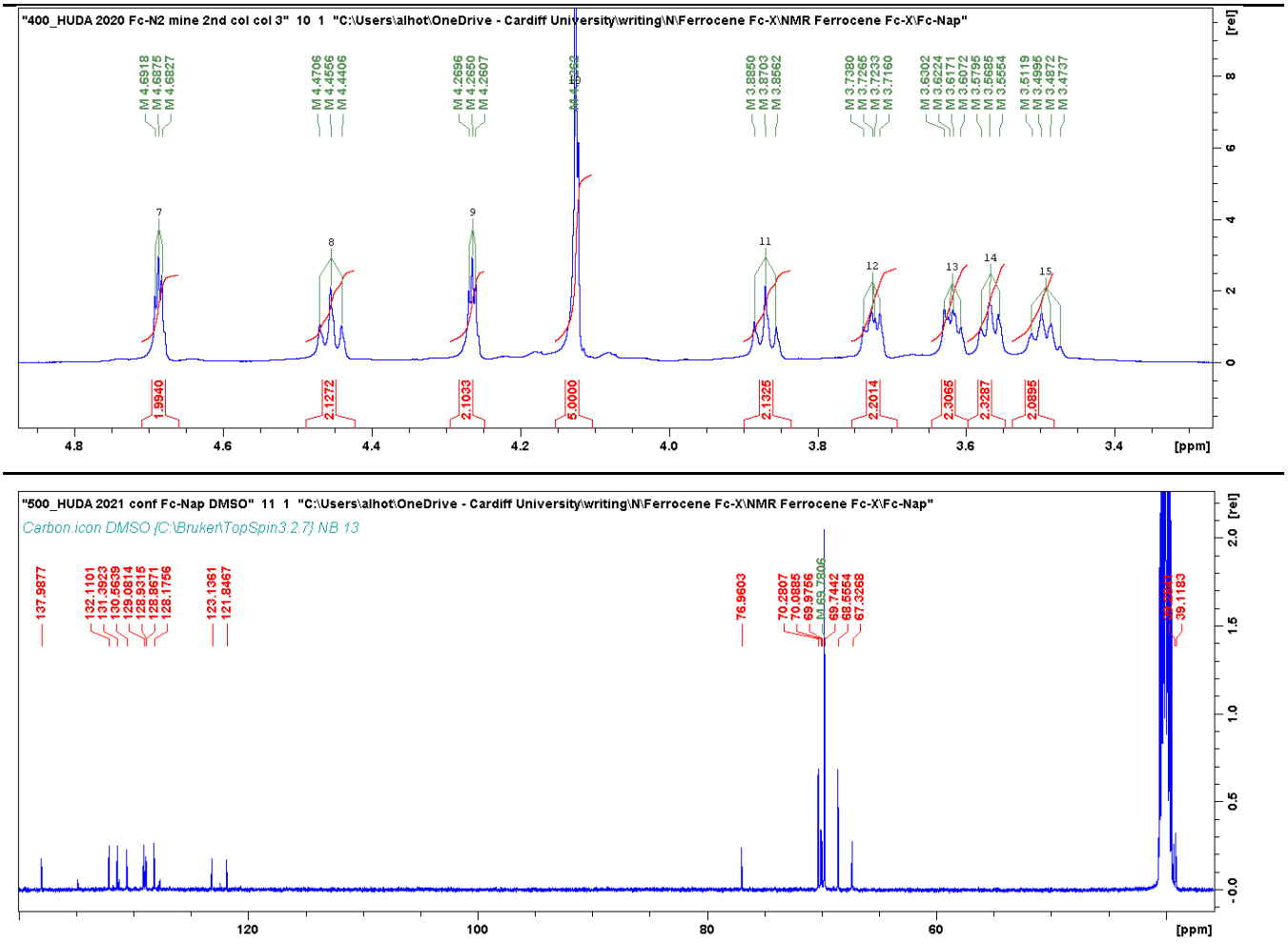

^{1}H NMR (400 MHz, CDCl3-d): δ(ppm): 8.63(dd, *J*=7.3, *J*=1.3, Hz, 1H, Ar-H), 8.58(dd, *J*=8.4, *J*=1.0 Hz, 1H, Ar-H), 8.47 (d, 1H, *J*=7.9 Hz, Ar-H), 7.83 (dd, *J*=8.6, *J*=7.5 Hz,1H, Ar-H), 7.80 (d, *J*=7.7 Hz, 1H, Ar-H), 6.44(t, 1H, N-H), 4.68 (t, 2H, *J*=1.8, Hz, Fc), 4.46 (t, 2H, *J*=6.0 Hz, CH_2), 4.27 (t, 2H, *J*=1.80 Hz, Fc), 4.12 (s, 5H, Fc), 3.87 (t, 2H, *J*=5.8 Hz, CH_2), 3.72 (m, 2H, CH_2), 3.61 (m,2H, CH_2), 3.56 (m, 2H, CH_2), 3.48 (m, 2H, CH_2). **^{13}C NMR (125 MHz, DMSO-d_6): δ(ppm):** 169.3, 163.5, 163.2, 138, 132.1, 131.4, 130.6, 129.1, 128.9, 128.9, 128.2, 123.1, 121.8, 77.0, 70.3, 70.1, 70.0, 69.8, 69.7, 68.6, 67.3, 39.3, 39.1. **TOF MS ES+** calc for $[C_{29}H_{27}N_2O_5ClFe]$+Na 595.0902 found 595.0911.

400_HUDA 2020 Fc-N1 mine col 8 DMSO

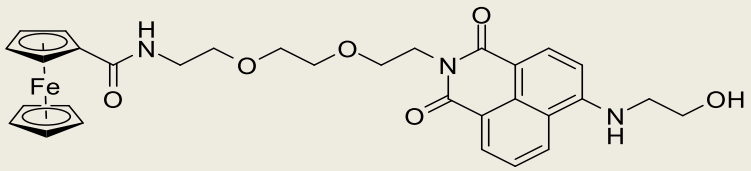

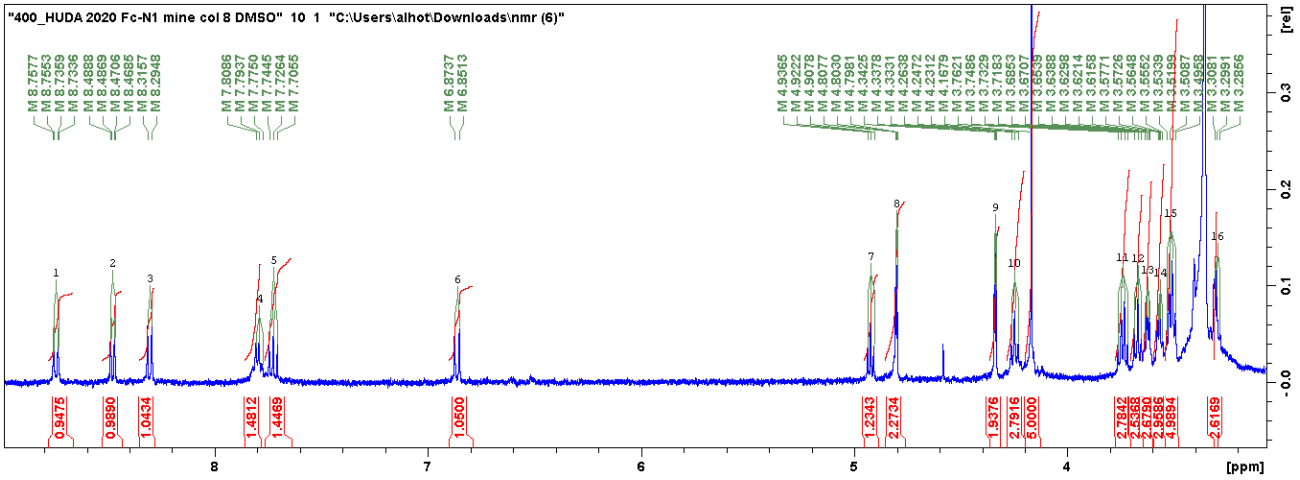

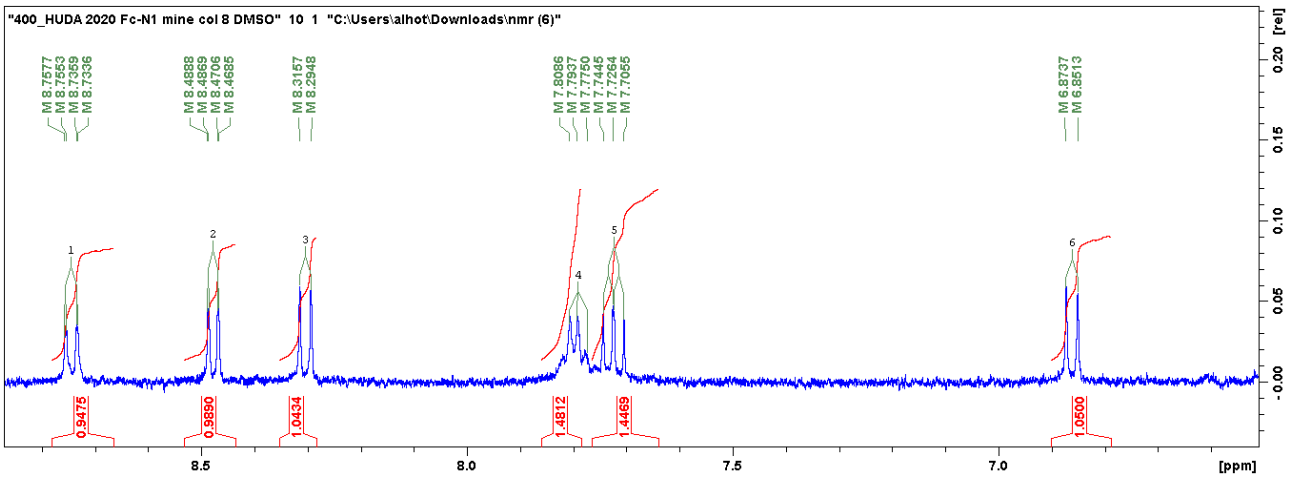

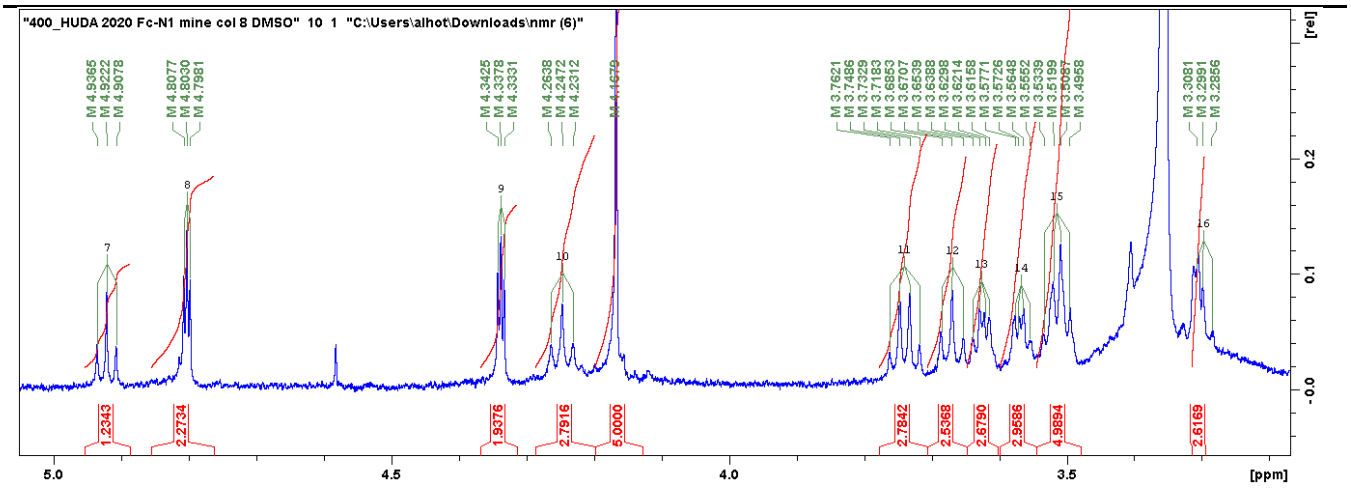

^{1}H NMR (400 MHz, DMSO-d_6): δ(ppm): 8.74 (d.d, *J*=8.7, *J*=0.9 Hz, 1H, Ar-H), 8.48(dd, *J*=7.3, *J*=0.8 Hz,1H, Ar-H), 8.30 (d, 1H, *J*=8.4 Hz, Ar-H), 7.79 (m, 1H, NH), 7.72 (d.d, *J*=8.3, *J*=7.3 Hz,1H, Ar-H), 6.86(d, J=8.9, 1H, Ar-H), 4.92 (t,1H, *J*=5.7 Hz, OH), 4.80 (t,2H, *J*=1.9, CH, Fc), 4.33 (t, 2H, *J*=1.9 Hz, CH, Fc), 4.24 (t, 2H, *J*=6.5 Hz, CH_2), 4.16 (s, 5H, Fc), 3.73 (q, 2H, *J*=5.8, CH_2), 3.67 (t, 2H, *J*=6.3 Hz, CH_2), 3.62 (m,2H, CH_2), 3.56 (m,2H, CH_2), 3.50 (m, 4H, CH_2), 3.28 (m, 2H, CH_2).

400_HUDA 2020 Fc-N2 mine col 13 CDCl3

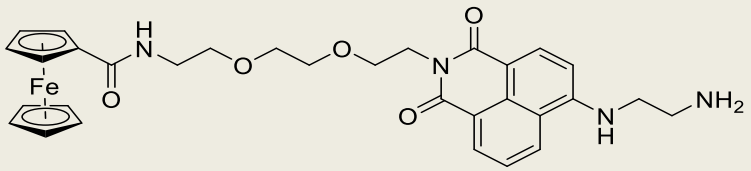

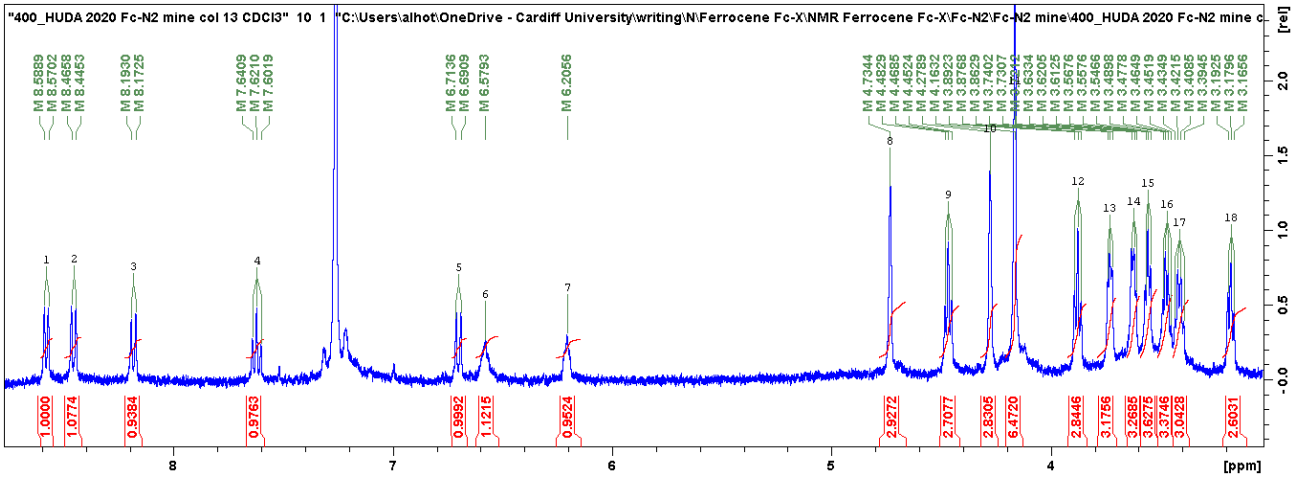

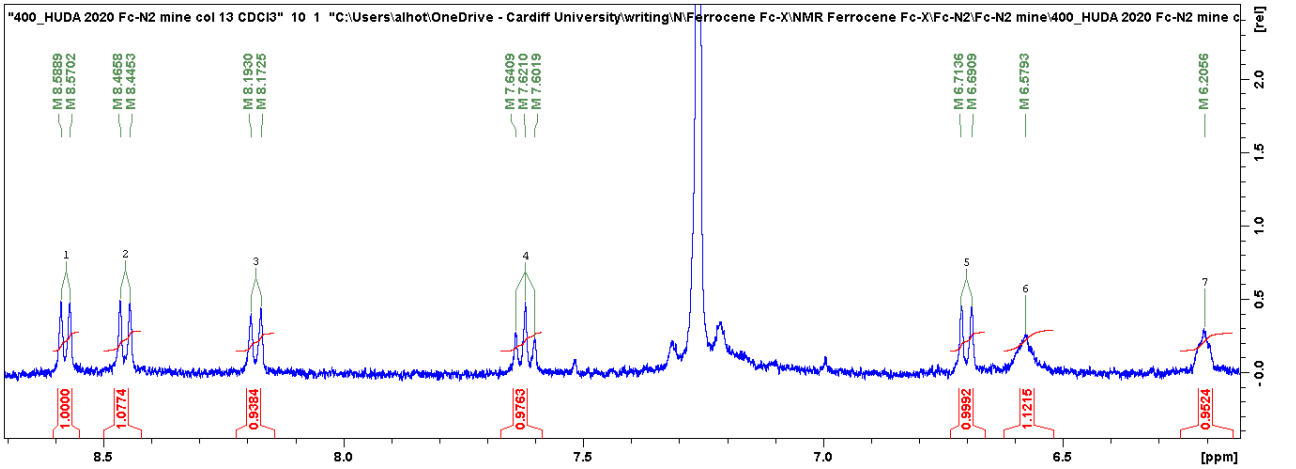

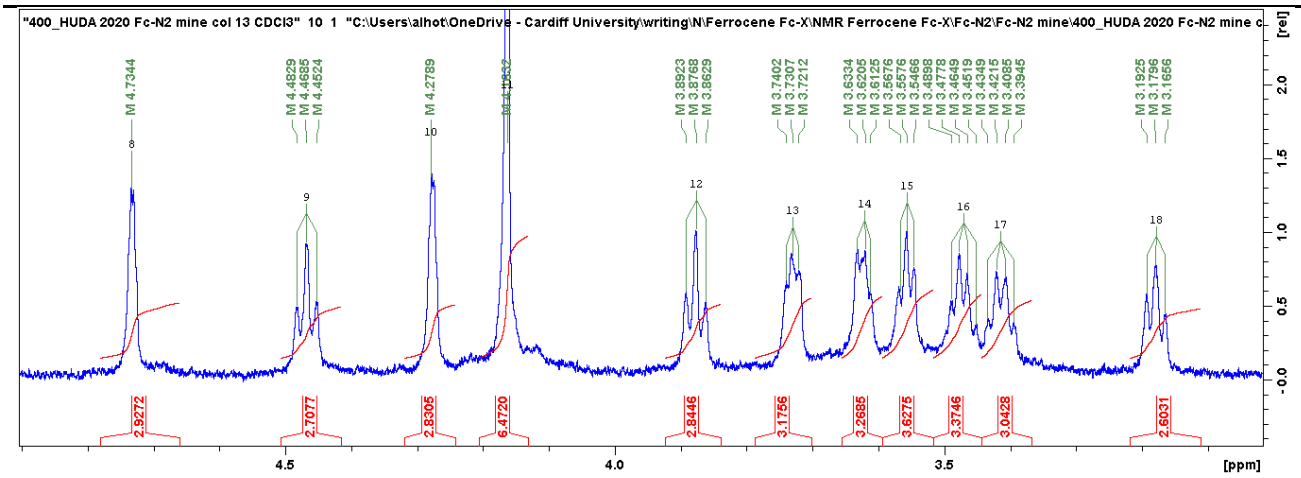

^{1}H NMR (400 MHz, $CDCl_3$-d): δ(ppm): 8.58(d, *J*=7.5 Hz, 1H, Ar-H), 8.45(d, 1H, *J*=8.2 Hz, Ar-H), 8.18 (d, *J*=8.20 Hz, 1H, Ar-H), 7.62 (at, *J*=8.8 Hz,1H, Ar-H), 6.70 (d, *J*=9.1 Hz,1H, Ar-H), 6.57 (m,1H, N-H), 6.20 (m,1H, N-H), 4.73 (m, 2H,Fc), 4.46 (t, *J*=6.1 Hz, 2H, CH_2), 4.27 (m, 2H, Fc), 4.16 (s, 5H, Fc), 3.87 (t, *J*=5.9 Hz,2H, CH_2), 3.73 (m,2H, CH_2), 3.62 (m,2H, CH_2), 3.55 (t, *J*=4.2 Hz, 2H, CH_2), 3.47 (m, 2H, CH_2), 3.41 (q, *J*=5.4 Hz,2H, CH_2), 3.18 (t, *J*=5.4 Hz,2H, CH_2). **TOF MS ES+** calc for $[C_{31}H_{34}N_4O_5Fe]$+Na 619.1823 found 619.1826.

400_HUDA 2020 Fc-N3 All sample col 3 CDCL3

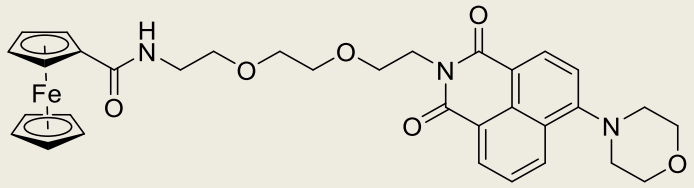

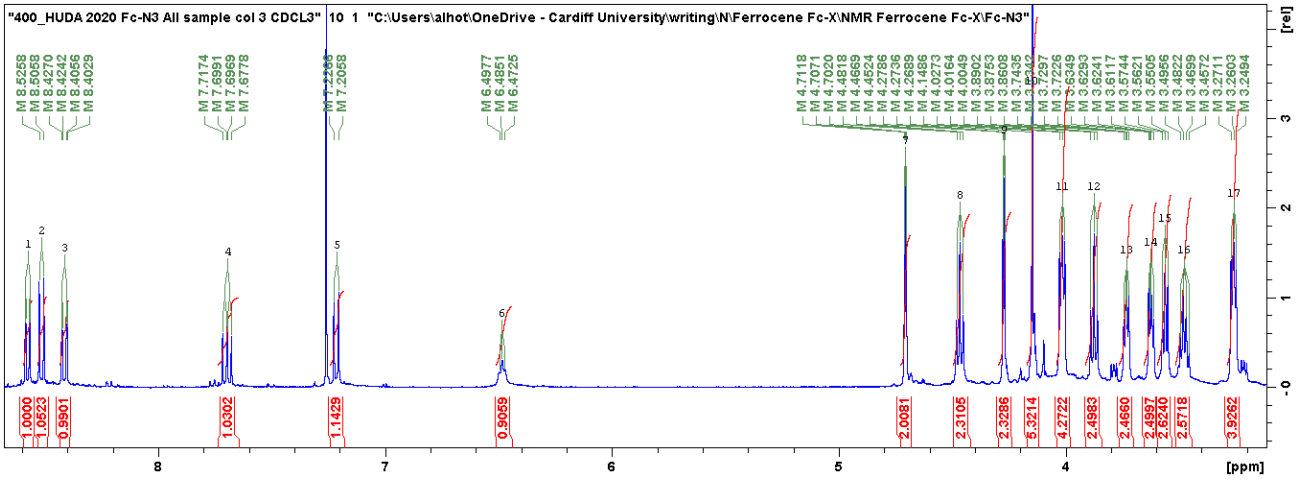

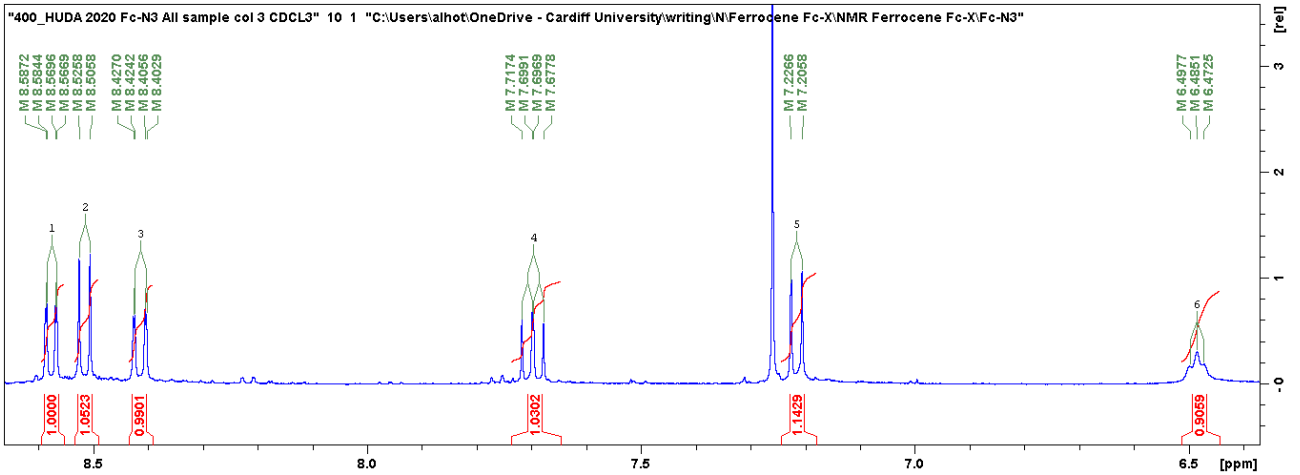

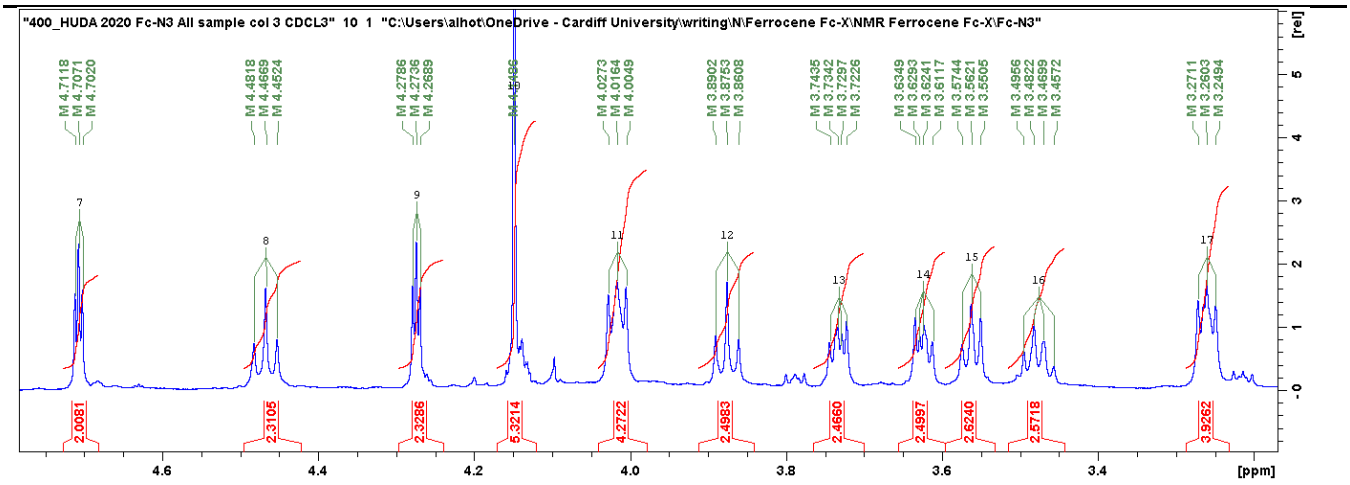

^{1}H NMR (400 MHz, $CDCl_3$-d): δ(ppm): 8.59(dd, *J*=7.0, *J*=1.1 Hz, 1H, Ar-H), 8.51(d, 1H, *J*=8.0 Hz, Ar-H), 8.41 (dd, *J*=8.5, *J*=1.1 Hz, 1H, Ar-H), 7.69 (dd, *J*=8.4, *J*=7.5 Hz,1H, Ar-H), 7.21 (d, *J*=8.3 Hz,1H, Ar-H), 6.48(t, *J*=5.0 Hz,1H, N-H), 4.71 (t, *J*=1.2 Hz, 2H,Fc), 4.46 (t, *J*=5.9 Hz, 2H, CH_2), 4.27 (t, *J*=1.9 Hz, 2H, Fc), 4.15 (s, 5H, Fc), 4.01(t, *J*=4.5 Hz,4H, morpholine), 3.87 (t, *J*=5.9 Hz,2H, CH_2), 3.72 (m,2H, CH_2), 3.62 (m,2H, CH_2), 3.56 (t, *J*=4.8 Hz, 2H, CH_2), 3.47 (m,2H, CH_2), 3.26 (t, *J*=4.3 Hz,4H, morpholine). **TOF MS ES+** calc for $[C_{33}H_{35}N_3O_6Fe]$+Na 646.1820 found 646.1819.

1H NMR: 500_HUDA 2020 Fc-N4-pip under N2 CDCl3

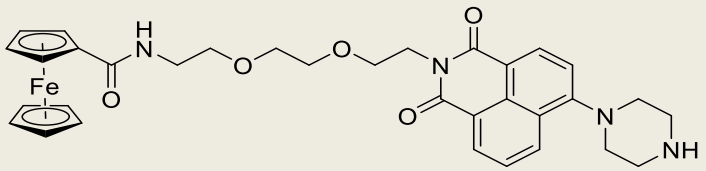

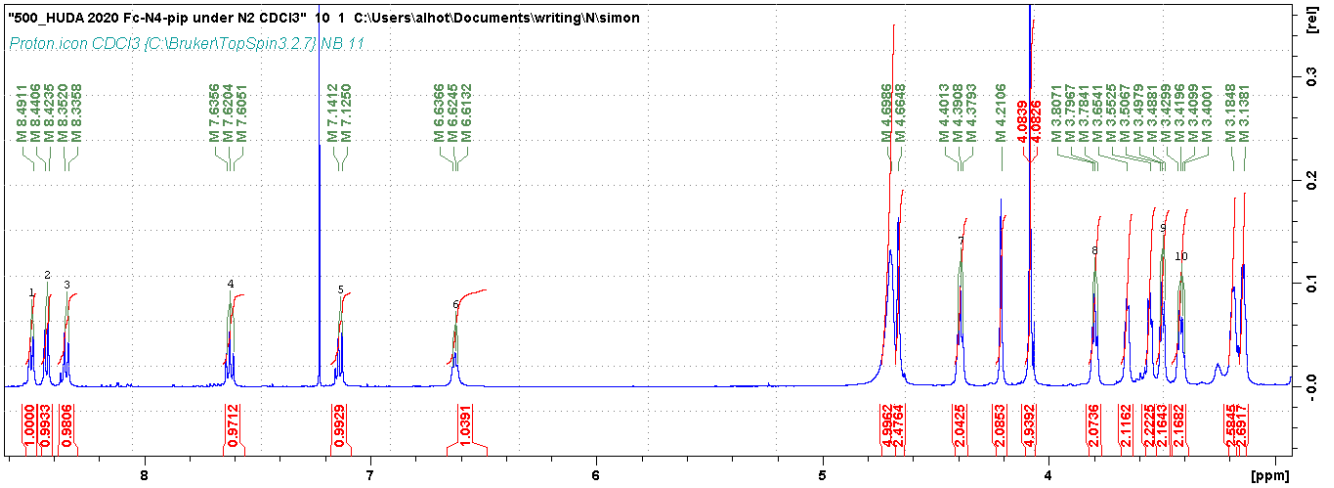

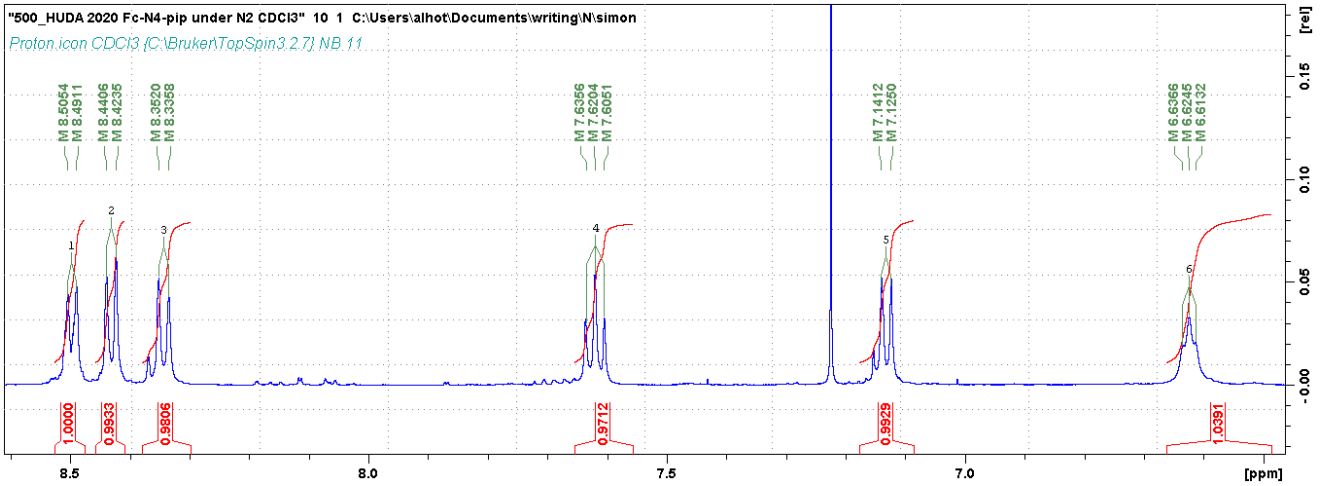

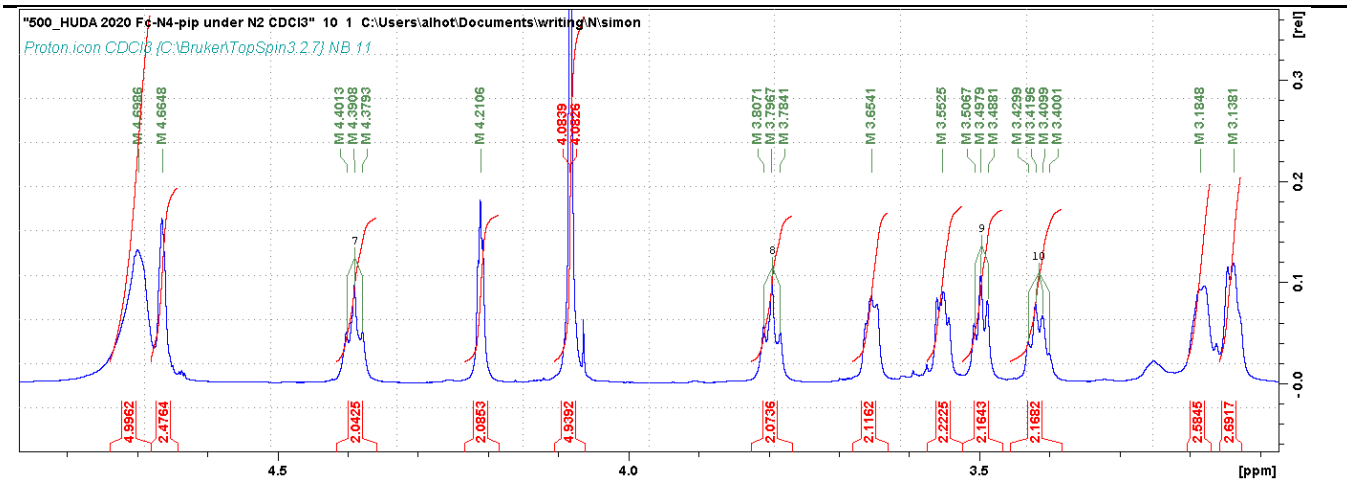

^{1}H NMR (500 MHz, CDCl3): δ(ppm): 8.53 (d, *J*=7.4 Hz, 1H, Ar-H), 8.46 (d, 1H, *J*=8.3 Hz, Ar-H), 8.37 (d, *J*=8.4 Hz, 1H, Ar-H), 7.65 (t, *J*=7.62 Hz,1H, Ar-H), 7.16 (d, *J*=8.3 Hz,1H, Ar-H), 6.65 (t, *J*=5.4 Hz, 1H, N-H), 4.73 (s, 4H, CH_2x2), 4.70 (m, 2H,Fc), 4.42 (t, *J*=5,7 Hz, 2H, CH_2), 4.24 (t, *J*=1.6 Hz, 2H, Fc), 4.11 (s, 5H, Fc), 3.83 (t, *J*=5.7 Hz,2H, CH_2), 3.68 (m, 2H, CH_2), 3.58 (m,2H, CH_2), 3.53 (t, *J*=4.7 Hz,2H, CH_2), 3.44 (m, 2H, CH_2), 3.22 (m, 2H, CH_2), 3.17 (m,2H, CH_2). **TOF MS ES+** calc for $[C_{33}H_{36}N_4O_5Fe]$+Na 645.1980 found 645.1990.

^{1}H NMR: 400_HUDA 2020 Fc-N5 col 5 DMSO\ 13C NMR: 500_HUDA 2021 Fc-N5 col 5 CDCl3

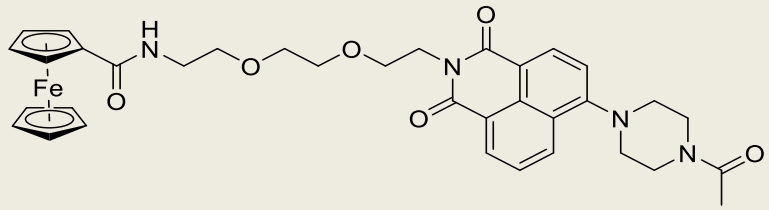

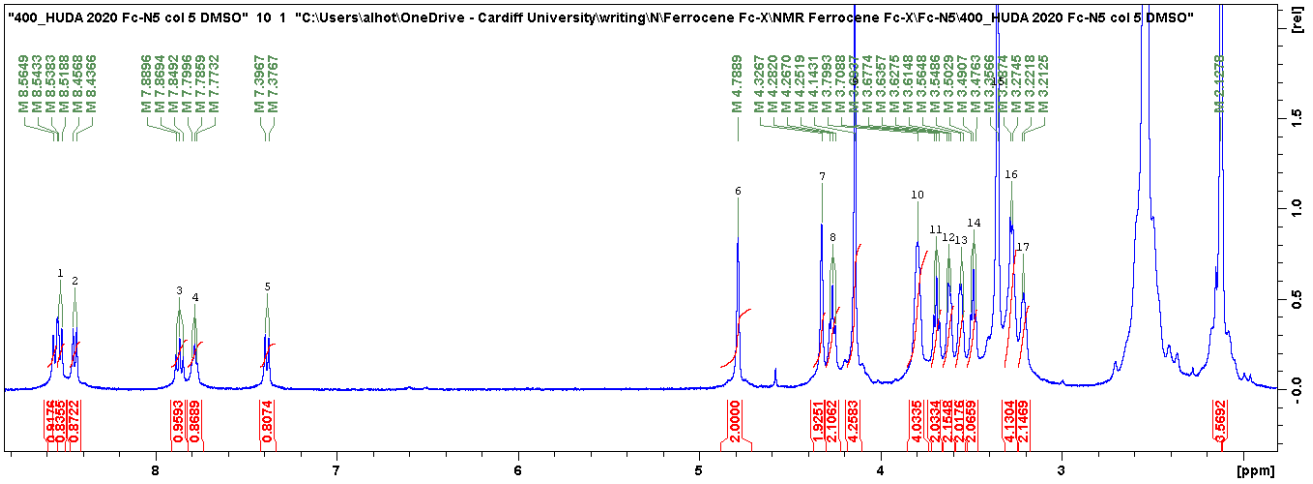

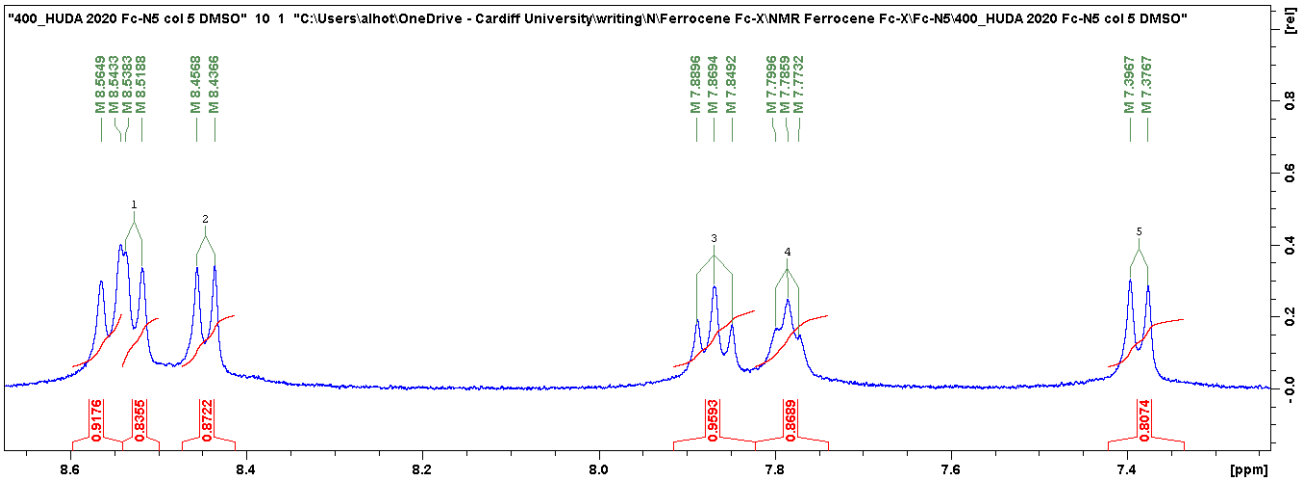

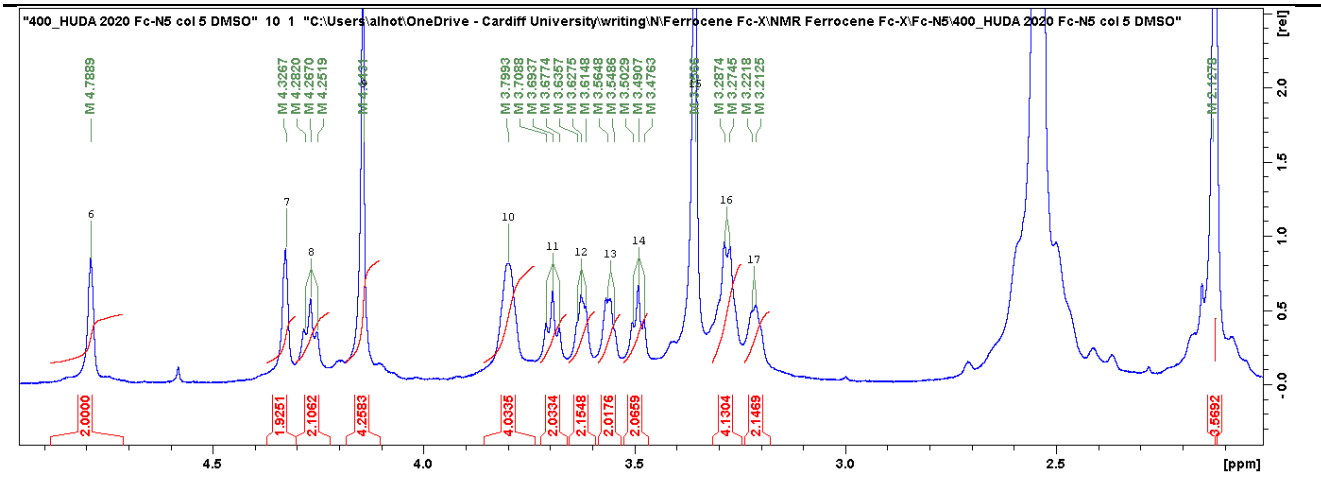

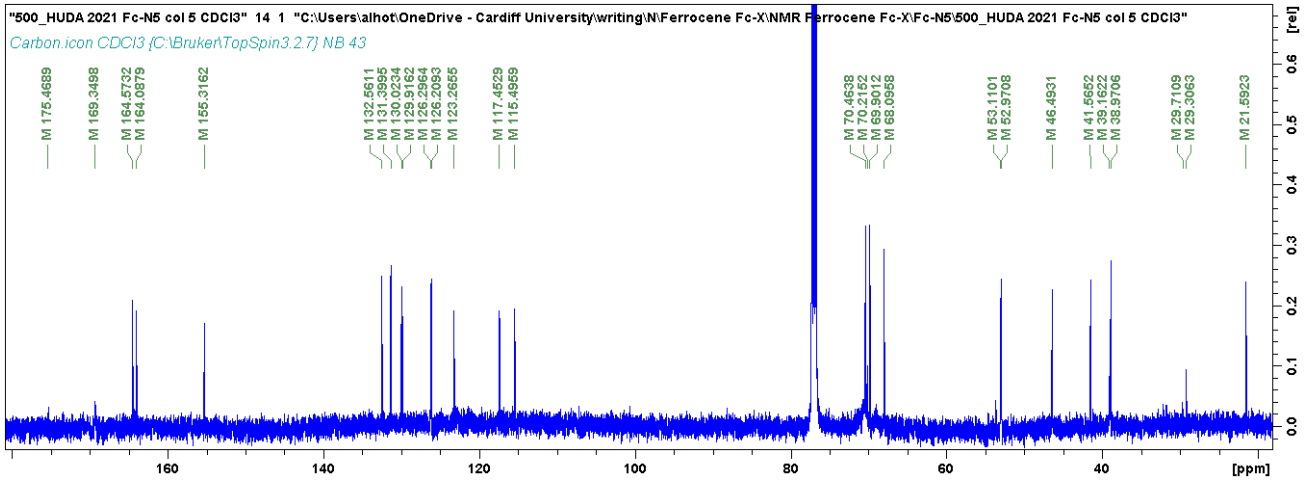

^{1}H NMR (400 MHz, DMSO): δ(ppm): 8.52(d, *J*=8.80 Hz, 1H, Ar-H), 8.49 (d, 1H, *J*=7.60 Hz, Ar-H), 8.41 (d, *J*=7.60 Hz, 1H, Ar-H), 7.83(t, *J*=7.98 Hz,1H, Ar-H), 7.75 (t, *J*=5.24 Hz, 1H, N-H), 7.35 (d, *J*=8.08 Hz,1H, Ar-H), 4.75 (br.s, 2H, Fc), 4.29 (br.s, 2H,Fc), 4.23 (t, *J*=6.10 Hz, 2H, CH_2), 4.11 (s, 5H, Fc), 3.76 (br.s,4H, CH_2), 3.66 (t, *J*=6.28, 2H, CH_2), 3.59 (t, *J*= 4.04, 2H, CH_2), 3.51 (m, 2H, CH_2), 3.45 (t, *J*=5.76 Hz, 2H, CH_2), 3.32 (s, 3H, CH_3), 3.24 (m,4H, CH_2), 3.18 (m,2H, CH_2). **^{13}C NMR (500 MHz, CDCl3): δ(ppm):** 175.46, 169.34, 164.57, 164.08, 155.31, 132.56, 131.39, 130.02, 129.91, 126.29, 126.20, 123.26, 117.45, 115.49, 70.46, 70.21, 69.90, 68.09, 53.11, 52.97, 46.49, 41.56, 39.16, 38.97, 29.71, 29.30, 21.59. **TOF MS ES+** calc for [$C_{35}H_{39}N_4O_6Fe$] 665.2266 found 665.2260.

400_HUDA 2020 Fc-Su1 2nd crude col 4 DMSO

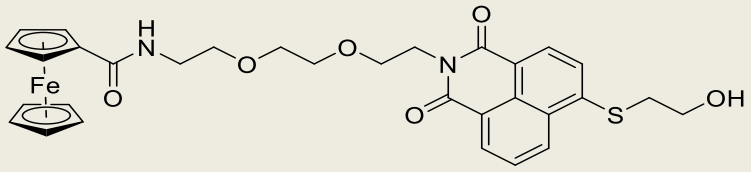

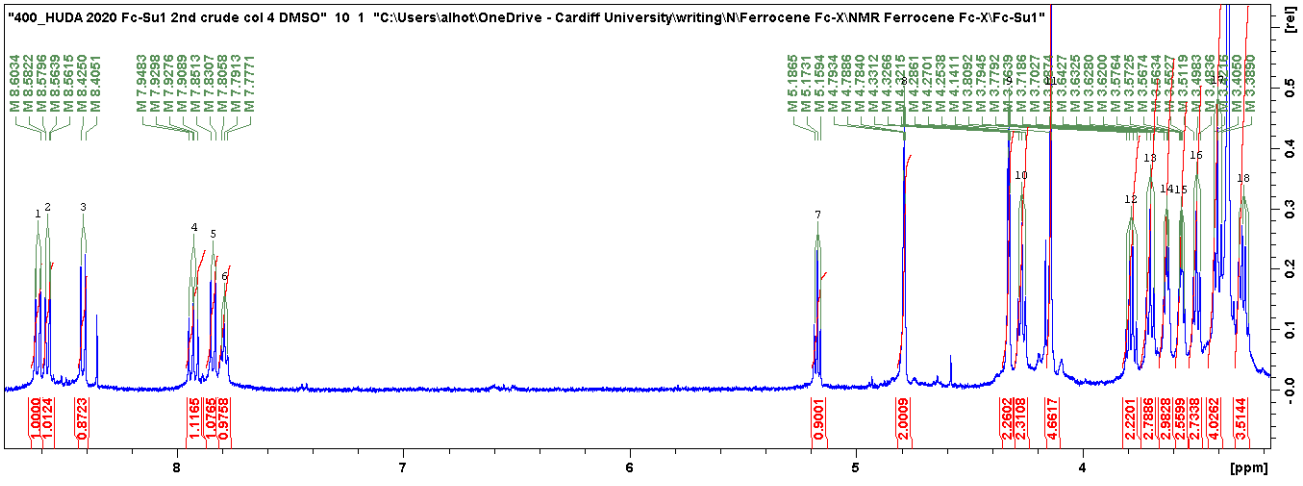

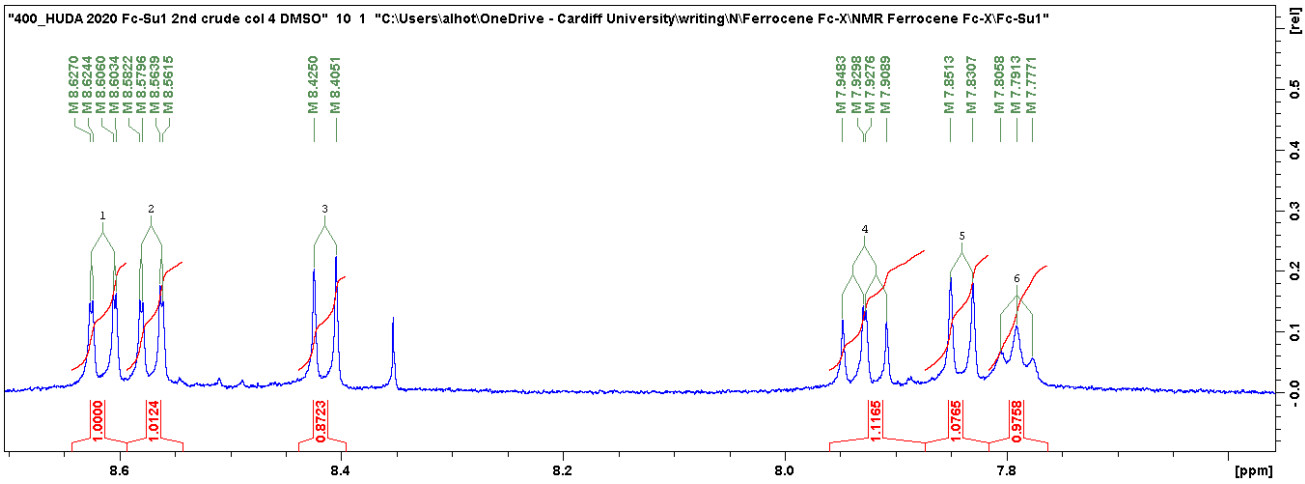

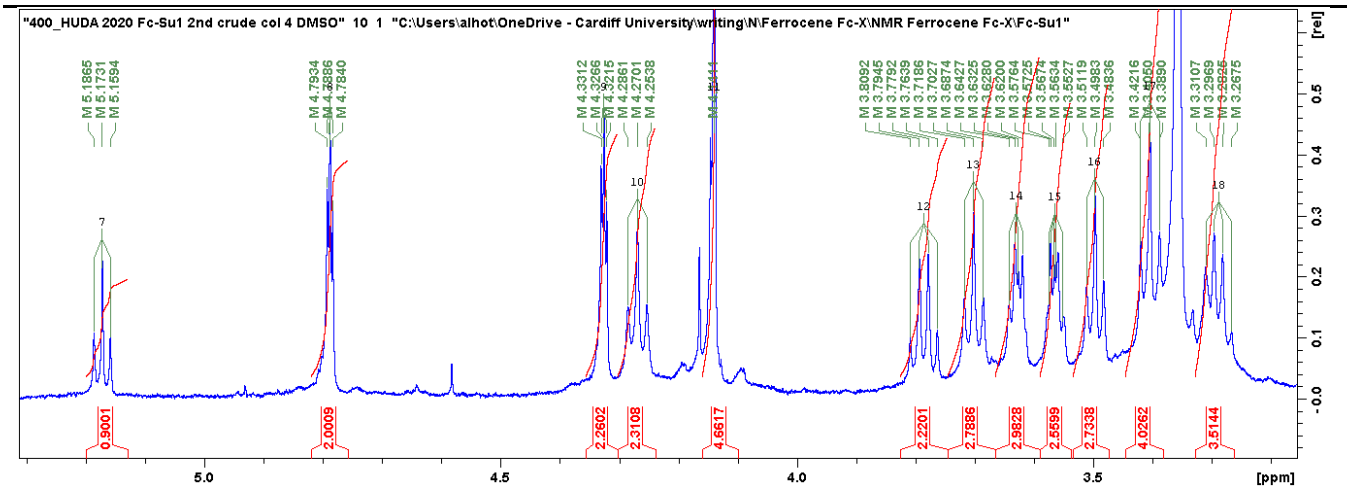

^{1}H NMR (400 MHz, DMSO): δ(ppm): 8.61 (dd, *J*=8.4 Hz, *J*= 1.0 Hz, 1H, Ar-H), 8.57 (dd, 1H, *J*=7.3 Hz, J=1.0 Hz, Ar-H), 8.41 (d, *J*=8.00 Hz, 1H, Ar-H), 7.92 (d.d, *J*=8.32, *J*=7.4 Hz,1H, Ar-H), 7.84 (d, *J*=8.2 Hz,1H, Ar-H), 7.79 (t,1H, *J*=5.7 Hz, N-H), 5.17 (t, *J*=5.4, 1H, OH), 4.78 (t, *J*=1.9 Hz, 2H, Fc), 4.32 (t, *J*=1.9 Hz, 2H, Fc), 4.27 (t, *J*=6.4 Hz, 2H, CH_2), 4.14 (s, 5H, Fc), 3.78 (q, *J*=6.0 Hz, 2H, CH_2), 3.70 (t, *J*=6.2 Hz, 2H, CH_2), 3.62 (m, 2H, CH_2), 3.56 (m, 2H, CH_2), 3.49 (t, *J*= 5.7 Hz, 2H, CH_2), 3.40 (t, *J*= 6.5 Hz, 2H, CH_2), 3.29 (m, 2H, CH_2). **TOF MS ES^{+}** calc for **[$C_{31}H_{32}N_2O_6SFe$]** 617.1330 found 616.1343.

500_HUDA 2021 Fc-E crude DMSO

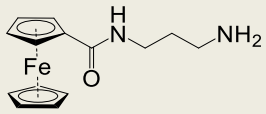

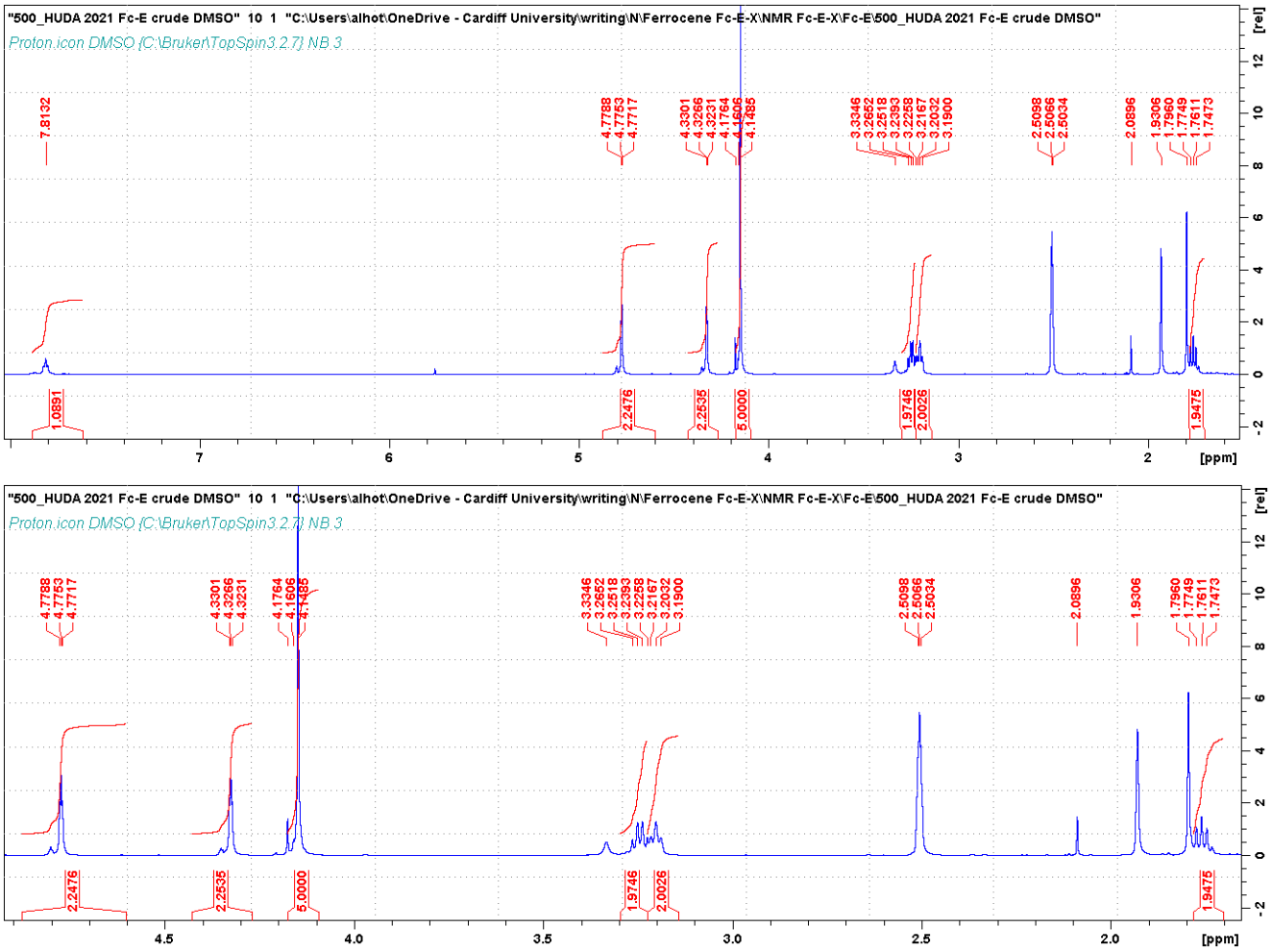

^{1}H NMR (500 MHz, DMSO): δ(ppm): 7.81(t, *J*= 5.14, 1H, N-H), 4.77 (t,2H, *J*=1.70, Hz, Fc), 4.32 (t, 2H, *J*=1.77 Hz, Fc), 4.14 (s, 5H, Fc), 3.25 (q, 2H, *J*=6.68 Hz, CH_2), 3.20 (t, 2H, *J*=7.20 Hz, CH_2), 1.76 (quin,2H, *J*=6.18 Hz, CH_2). **HR TOF MS ES+** calc for [$C_{14}H_{19}N_2OFe$] 287.0847 found 287.0833.

500_HUDA 2021 Fc-E-Nap 2nd crude DMSO

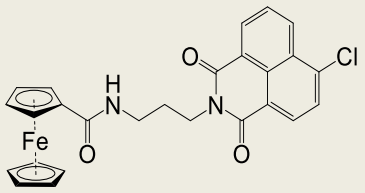

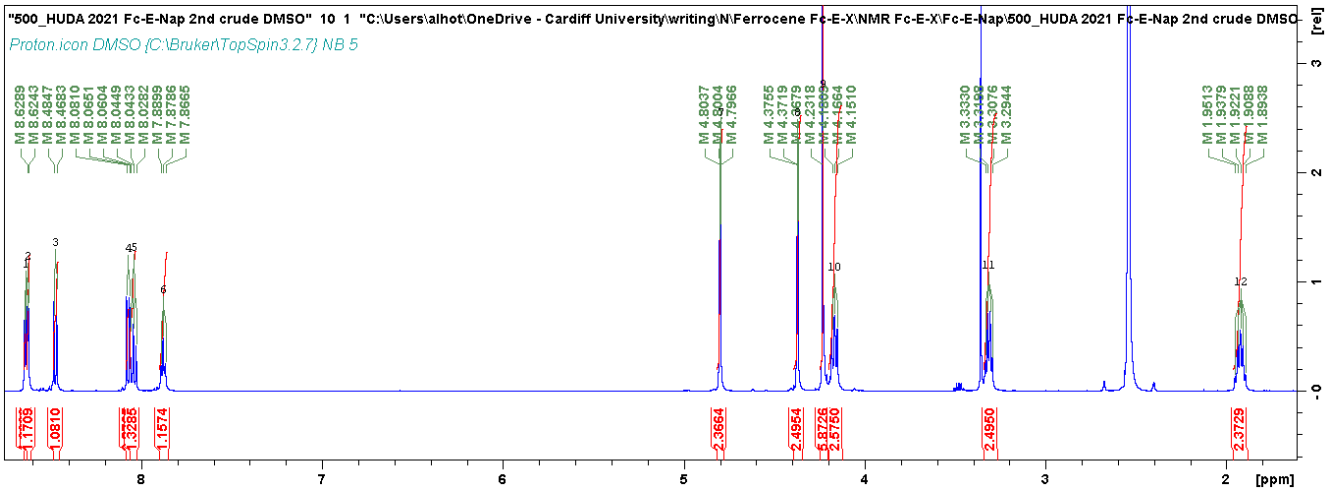

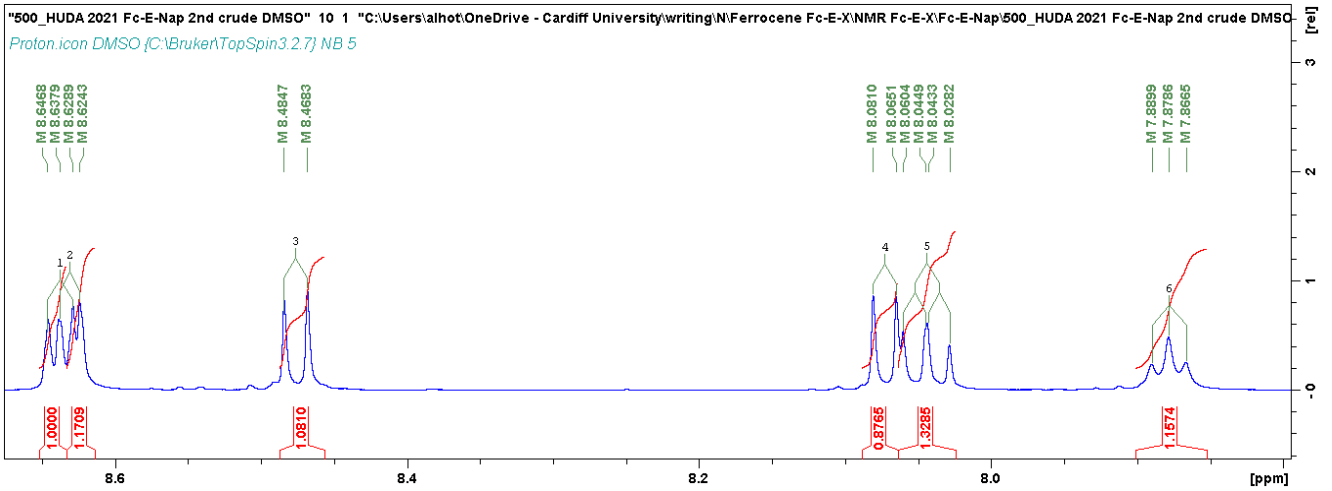

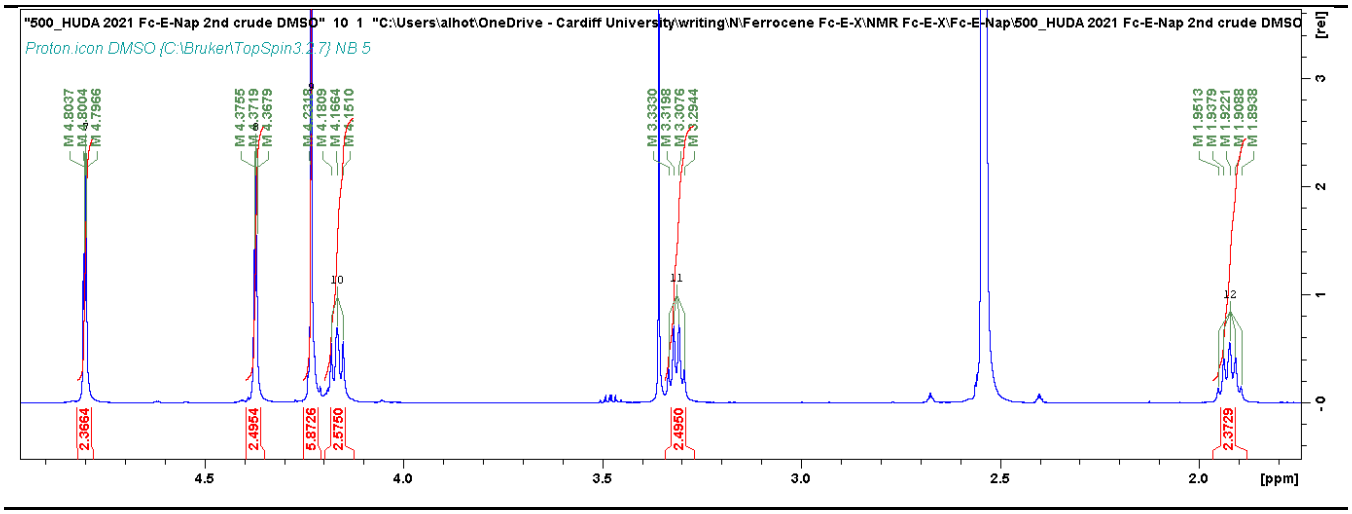

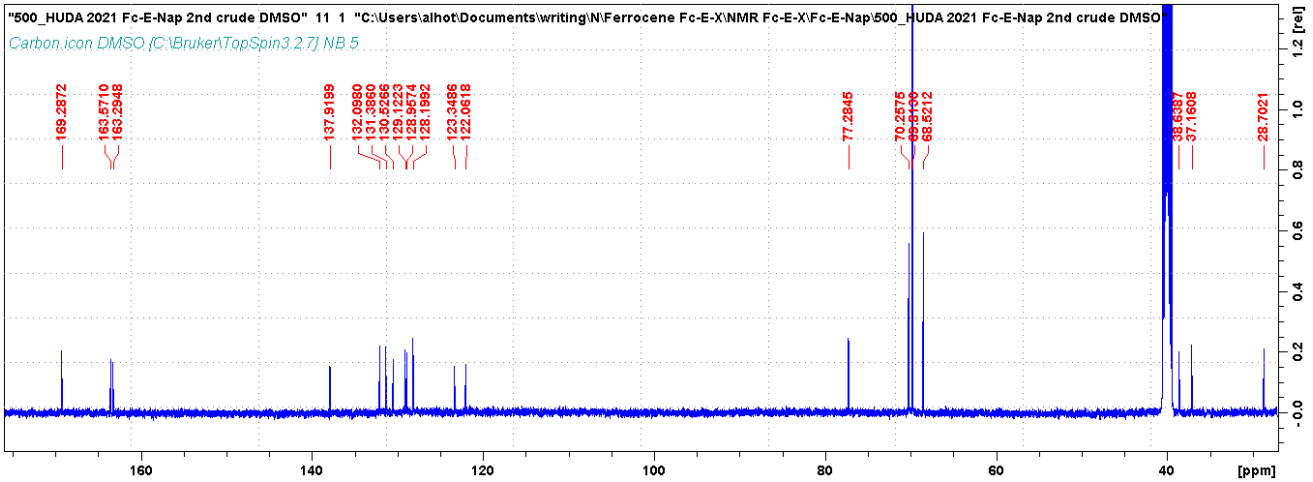

^{1}H NMR (500 MHz, DMSO): δ(ppm): δ 8.63(d, *J*= 8.7, Hz, 1H, Ar-H), 8.62(d, *J*= 6.8 Hz,1H, Ar-H), 8.47 (d, 1H, *J*= 8.2 Hz, Ar-H), 8.07 (d, *J*=8.0 Hz,1H, Ar-H), 8.04 (dd, *J*=8.5, *J*=7.7 Hz,1H, Ar-H), 7.87(t, *J*= 5.9, 1H, N-H), 4.80 (t,2H, *J*=1.8, Hz, Fc), 4.37 (t, 2H, *J*=1.9 Hz, Fc), 4.23 (s, 5H, Fc), 4.16 (t, 2H, *J*=7.5 Hz, CH_2), 3.30 (q, 2H, *J*=6.4 Hz, CH_2), 1.92 (quin,2H, *J*=7.2 Hz, CH_2). **^{13}C NMR (125 MHz, DMSO): δ(ppm):** 169.28, 163.57, 163.29, 137.91, 132.09, 131.38, 130.52, 129.12, 128.95, 128.19, 123.34, 122.06, 77.28, 70.25, 69.81, 68.52, 38.63, 37.16, 28.70. **HR MS EI** calc for [$C_{26}H_{21}N_2O_3ClFe$] 500.05846 found 500.0585.

500_HUDA 2021 Fc-E-N1 col 3 DMSO\ 500_HUDA 2021 conf Fc-E-N1 DMSO

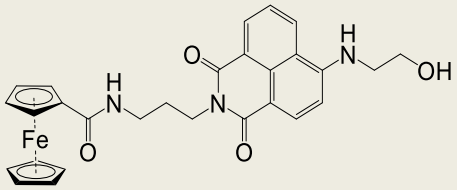

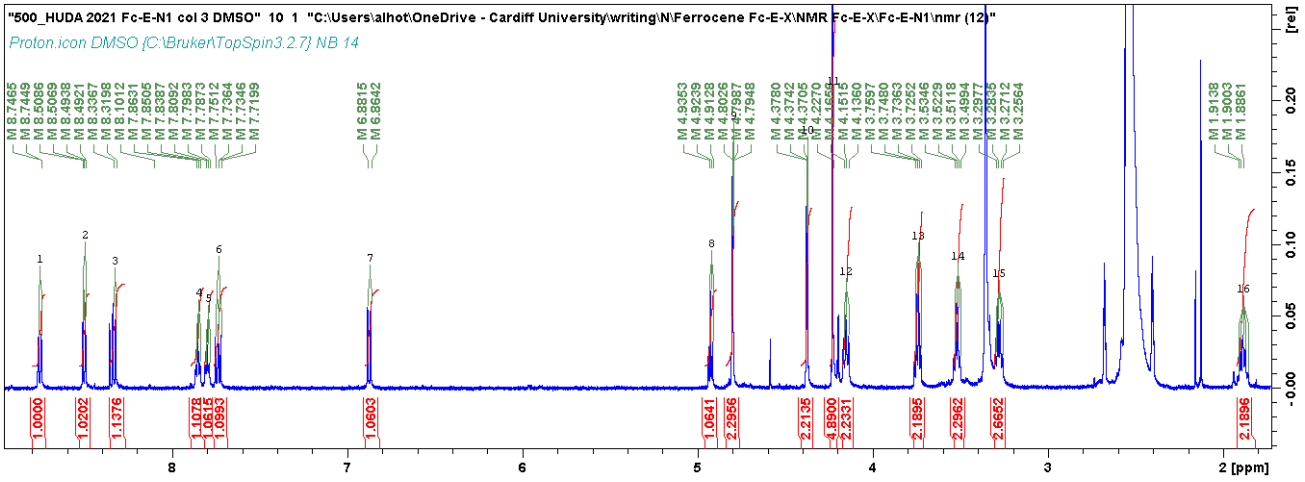

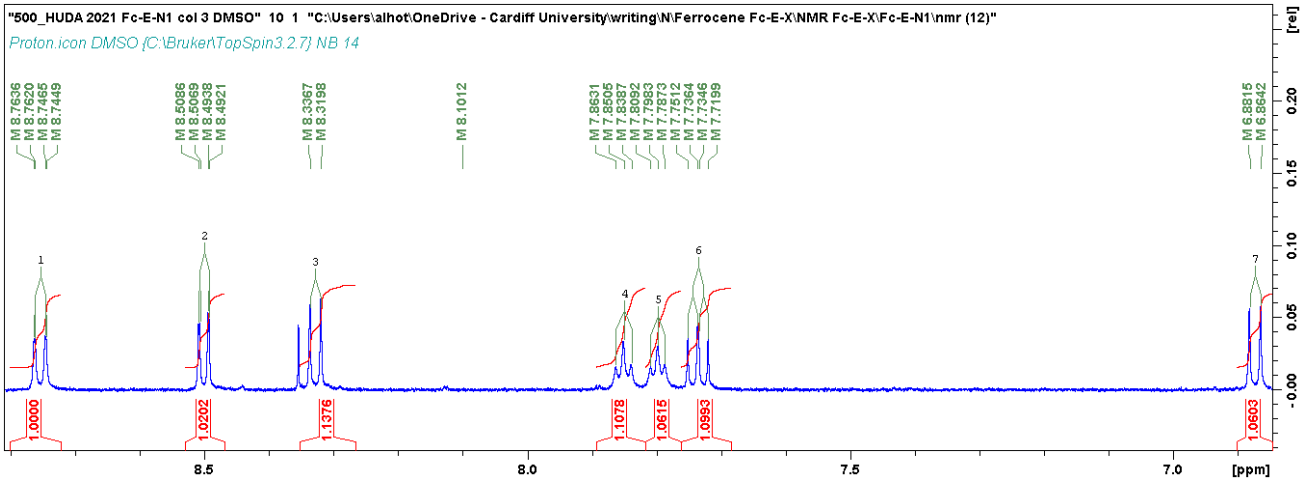

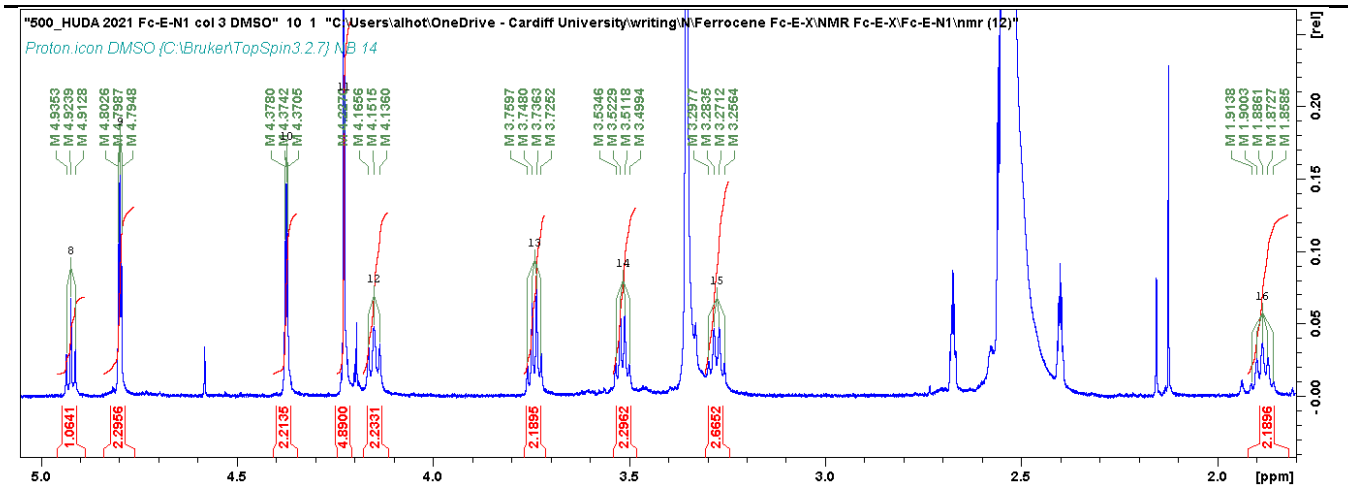

^{1}H NMR (500 MHz, DMSO): δ(ppm): δ 8.75(dd, *J*= 8.9, *J*=0.8 Hz, 1H, Ar-H), 8.50 (dd, *J*= 7.4, *J*=0.9 Hz,1H, Ar-H), 8.32 (d, 1H, *J*= 8.4 Hz, Ar-H), 7.85(t, *J*= 6.1, 1H, N-H), 7.79 (t, *J*=5.5, 1H, N-H), 7.73 (dd, *J*=8.3, *J*=7.4 Hz,1H, Ar-H), 6.87 (d, *J*=8.7 Hz,1H, Ar-H), 4.92 (t, *J*=5.6 Hz, 1H,OH), 4.79 (t, *J*=2 Hz, 2H, Fc), 4.37 (t, *J*=1.9 Hz, 2H, Fc), 4.22 (s, 5H, Fc), 4.15 (t, 2H, *J*=7.4 Hz, CH_2), 3.74 (q, 2H, *J*=5.8 Hz, CH_2), 3.52 (q, 2H, *J*=5.9 Hz, CH_2), 3.27 (q, 2H, *J*=6.9 Hz, CH_2), 1.88 (quin,2H, *J*=6.9 Hz, CH_2). **^{13}C NMR (125 MHz, DMSO): δ(ppm):** 169.28, 163.57, 163.29, 137.91, 132.09, 131.38, 130.52, 129.12, 128.95, 128.19, 123.34, 122.06, 77.28, 70.25, 69.81, 68.52, 38.63, 37.16, 28.70. **HR MS EI** calc for [$C_{28}H_{28}N_3O_4Fe$] 526.1429 found 526.1432.

400_HUDA 2021 Fc-E-N3 dry crude DMSO

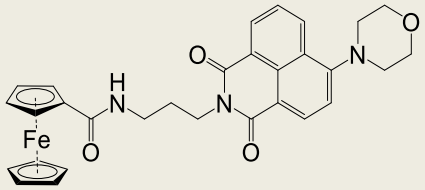

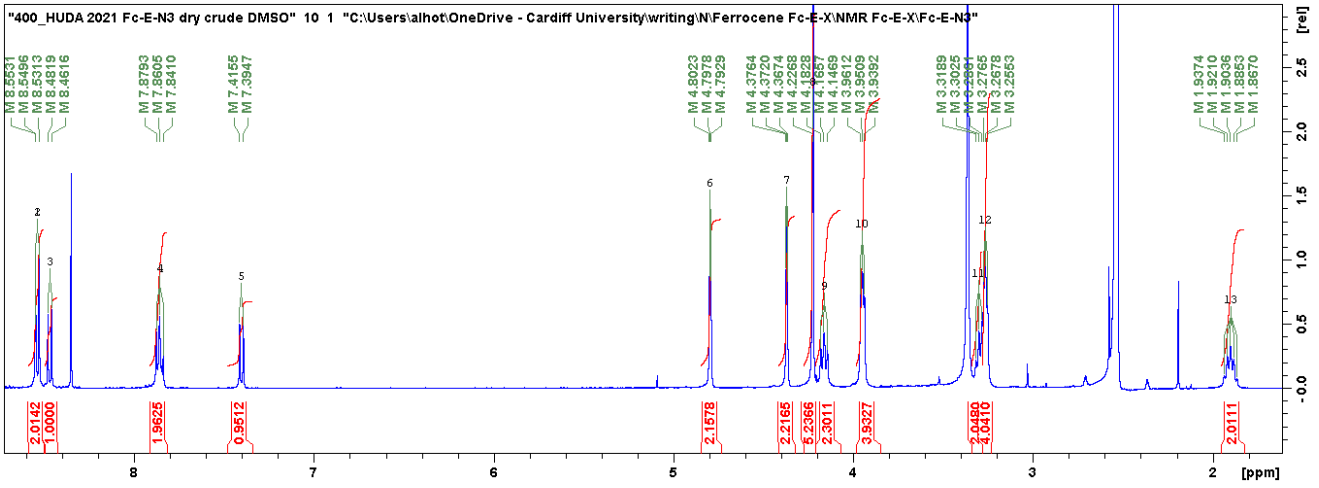

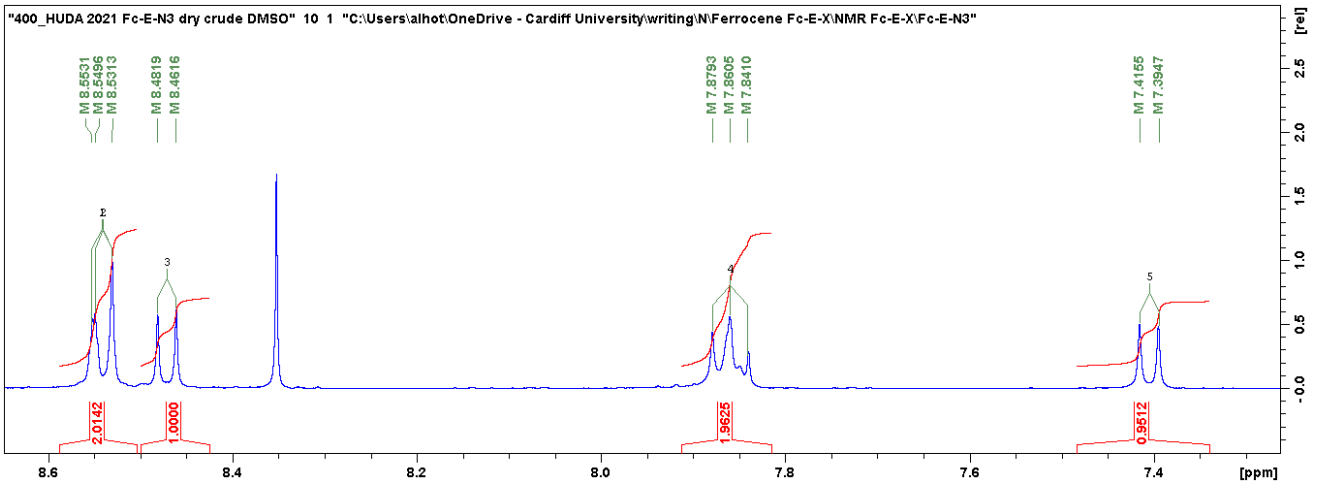

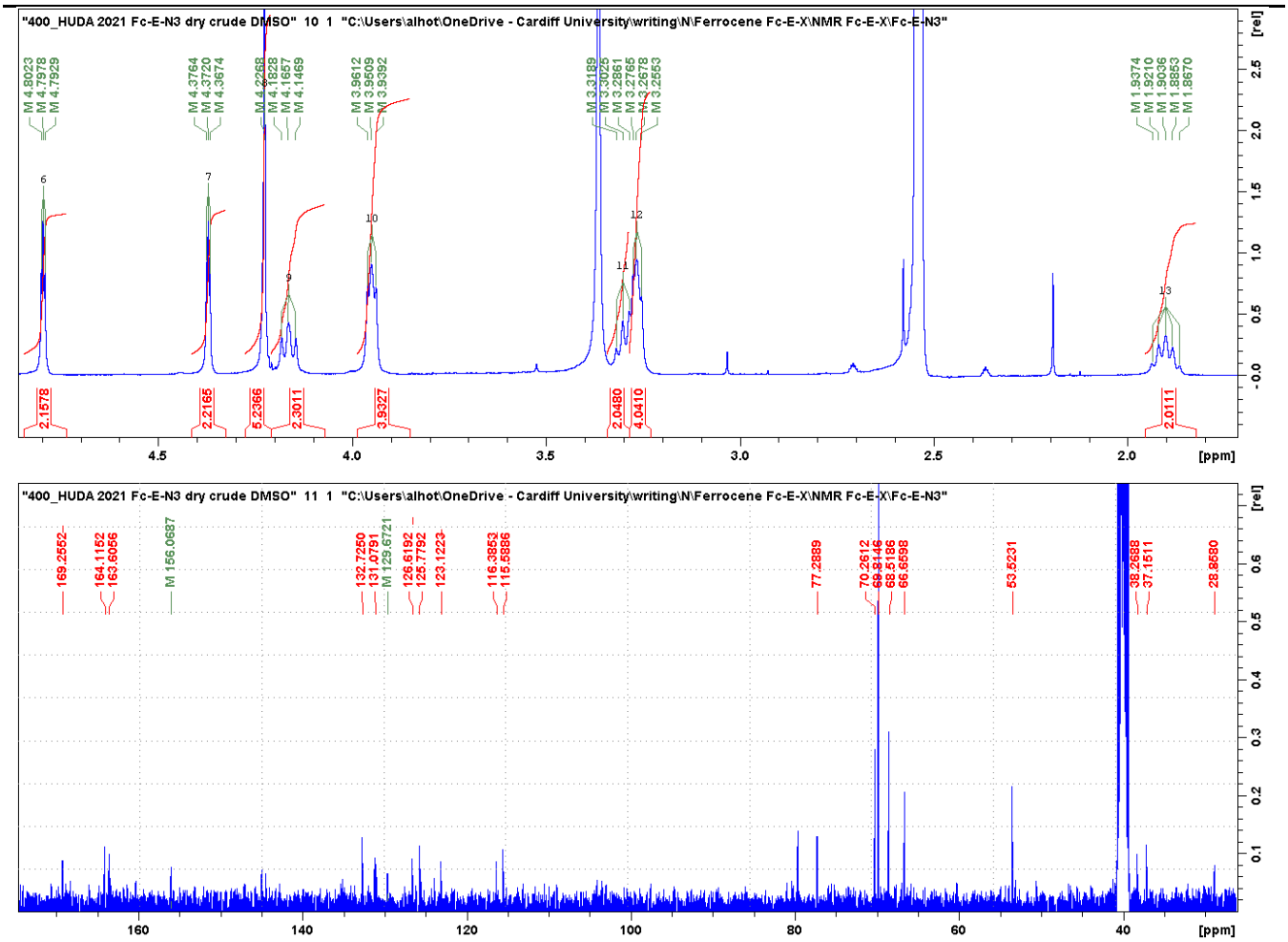

^{1}H NMR (400 MHz, DMSO): δ(ppm): 8.51(d, *J*= 8.48, Hz, 1H, Ar-H), 8.50(d, *J*= 7.37 Hz,1H, Ar-H), 8.43 (d, 1H, *J*= 8.08 Hz, Ar-H), 7.82 (t, *J*=7.96 Hz,2H, Ar-H and N-H), 7.37(d, *J*= 8.32, 1H, Ar-H), 4.76 (t,2H, *J*=1.88, Hz, Fc), 4.33 (t, 2H, *J*=1.86 Hz, Fc), 4.18 (s, 5H, Fc), 4.13 (t, 2H, *J*=7.16 Hz, CH_2), 3.91 (t, 4H, CH_2, *J*=4.38 Hz, morpholine), 3.27 (t, *J*=6.80, 2H, CH_2), 3.23 (t, 4H, *J*=4.36 Hz, CH_2, morpholine), 1.87 (quin,2H, *J*= 7.25 Hz, CH_2). **^{13}C NMR (100 MHz, DMSO): δ(ppm):** 169.25, 164.11, 163.60, 156.06, 132.72, 131.07, 129.67, 126.61, 125.77, 123.12, 116.38, 115.58, 77.28, 70.26, 69.81, 68.51, 66.65, 53.52, 38.26, 37.15, 28.85. **HR MS** calc for [$C_{30}H_{30}N_3O_4Fe$] 550.1629 found 550.1632.

400_HUDA 2021 Fc-E-N5 crude DMSO

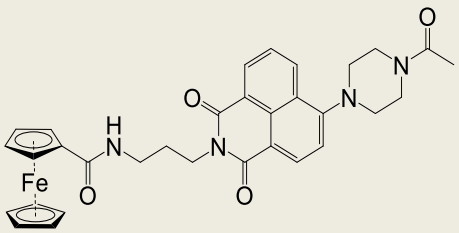

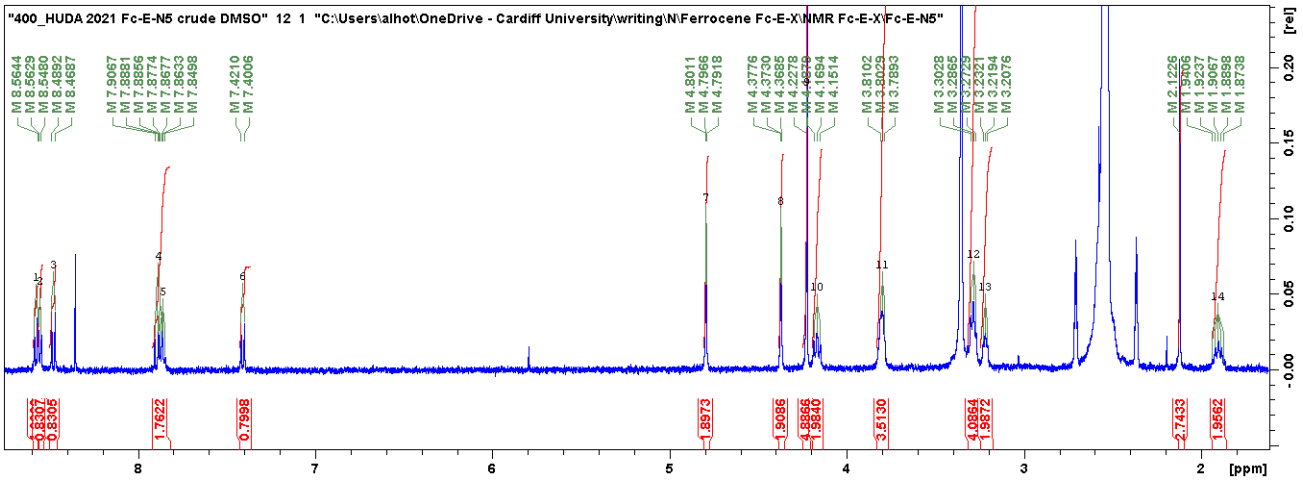

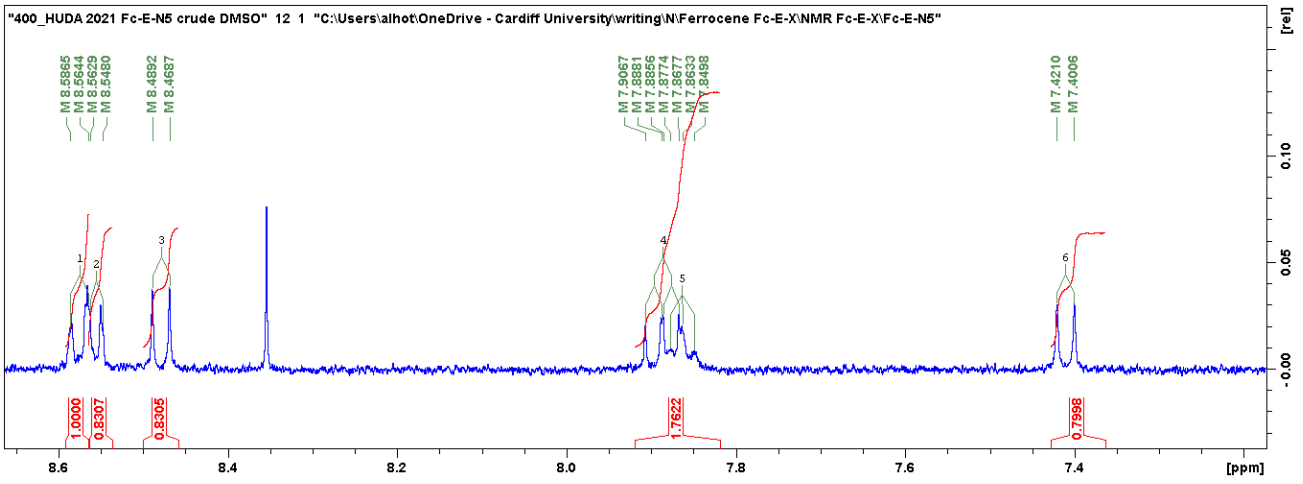

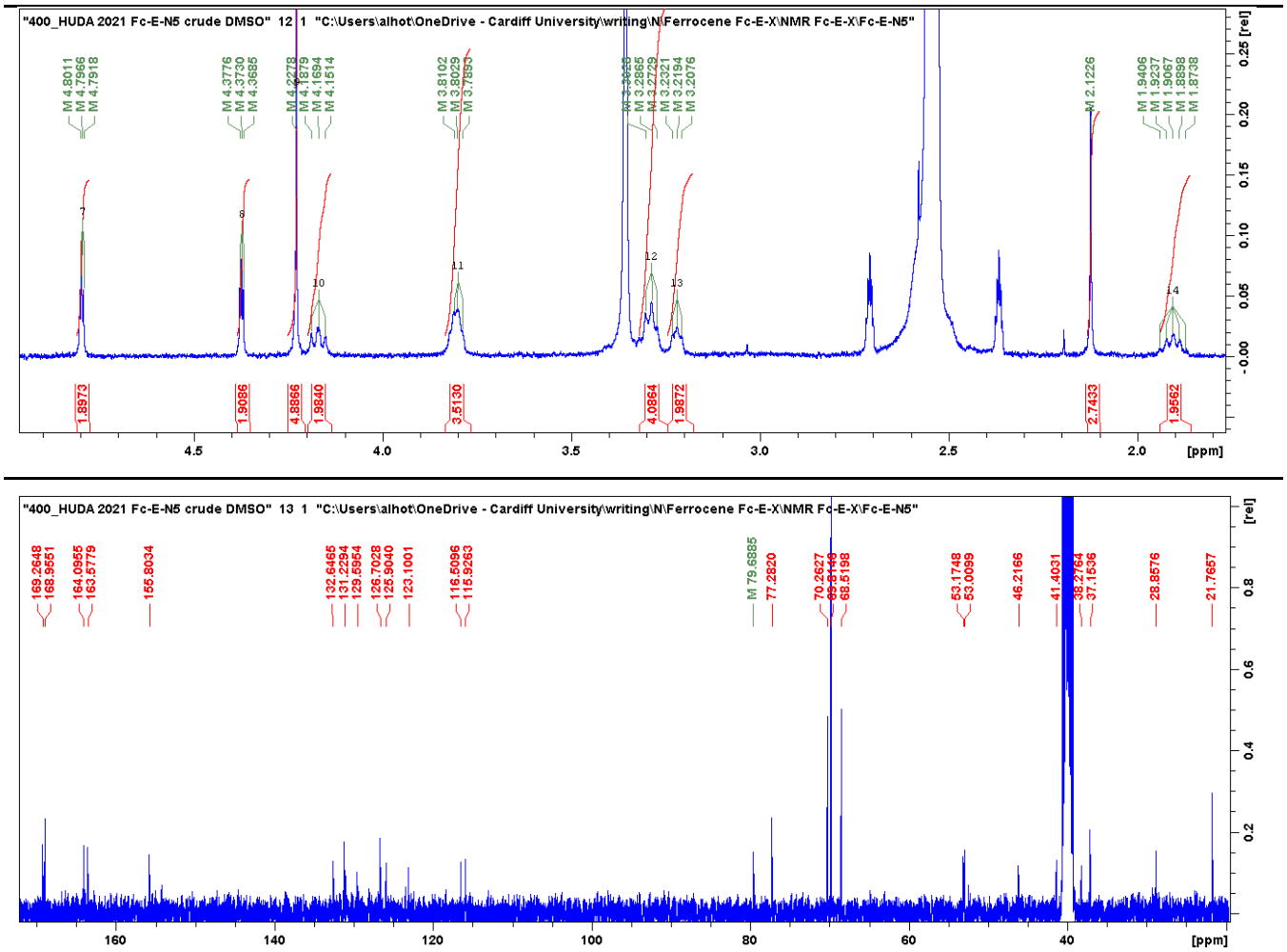

^{1}H NMR (400 MHz, DMSO): δ(ppm): 8.57(d, *J*= 7.9, Hz, 1H, Ar-H), 8.55(d, *J*= 6.5 Hz,1H, Ar-H), 8.47 (d, 1H, *J*= 8.2 Hz, Ar-H), 7.88 (dd, *J*=8.4, *J*=7.4 Hz,1H, Ar-H), 7.86 (t, *J*=5.5, *J*=5.20 Hz,1H, N-H), 7.41(d, *J*= 8.2, 1H, Ar-H), 4.79 (t,2H, *J*=1.9, Hz, Fc), 4.37 (t, 2H, *J*=1.8 Hz, Fc), 4.22 (s, 5H, Fc), 4.16 (t, 2H, *J*=7.3 Hz, CH_2), 3.80 (m, 4H, CH_2), 3.28 (t, *J*=6.0, 4H, CH_2), 3.21 (t, 2H, *J*=4.9 Hz, CH_2), 2.12 (s, 3H, CH_3), 1.90 (quin,2H, *J*= 4.9 Hz, CH_2). **^{13}C NMR (400 MHz, DMSO): δ(ppm):** 169.26, 168.95, 164.09, 163.57, 155.80, 132.64, 131.22, 129.59, 126.70, 125.90, 123.10, 116.50, 115.92, 79.68, 77.28, 70.26, 69.81, 68.51, 53.17, 53.00, 46.21, 41.40, 38.27, 37.15, 28.85, 21.76. **HR MS** calc for [$C_{32}H_{33}N_4O_4Fe$] 593.1851 found 593.1848.

A2.2 Characterization of compounds using mass spectrometry

Comp.	Mass spectrum code	Comp.	Mass spectrum code
2.14	NB_MS33791_LR_ASAP	2.12e	NB_MS33999_HR_ES
2.15	NB_MS30949_HR_ES	2.12f	NB_MS33958_HR_ES
2.16	NB_MS30389_HR_ES	2.17	NB_MS35141_HR_ES
2.12a	NB_MS34007_LR_ES	2.18	NB_MS35158_HR_EI
2.12b	NB_MS30329_HR_ES	2.13a	NB_MS36000_HR_ES
2.12c	NB_MS30330_HR_ES	2.13c	NB_MS33957_HR_ES
2.12d	NB_MS30331_HR_ES	2.13e	NB_MS35190_HR_ES

A2.3 UV-vis titration spectra

Comp.	1st titration	2nd titration
2.12a	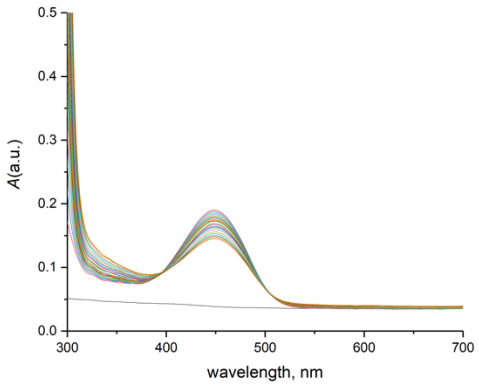	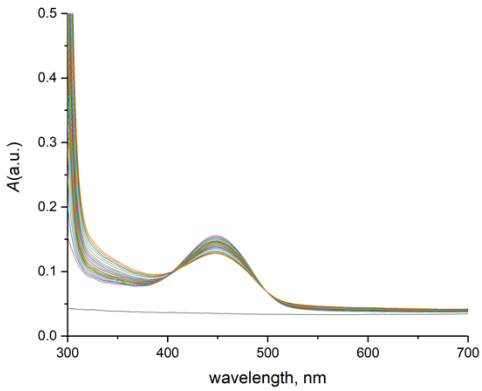
2.12b	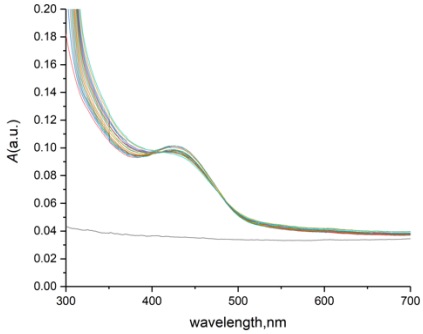	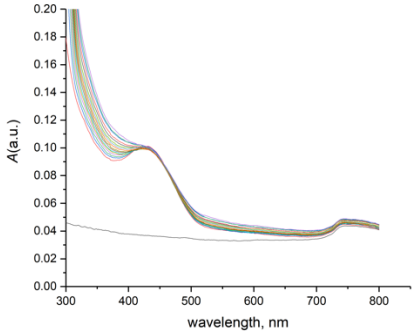
2.12c	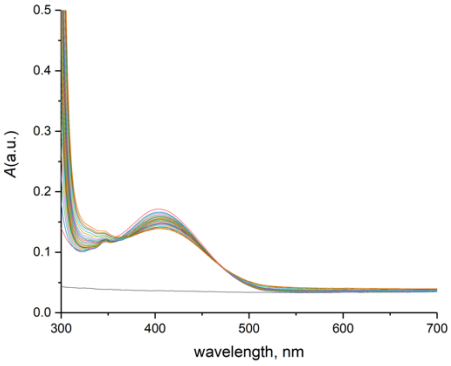	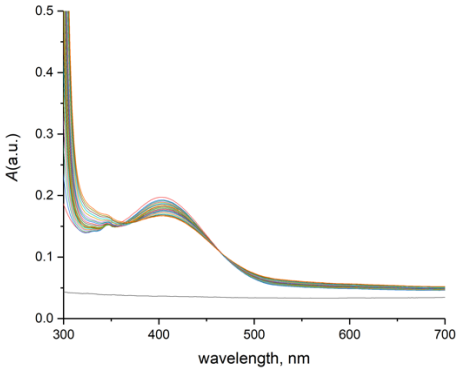

2.12d	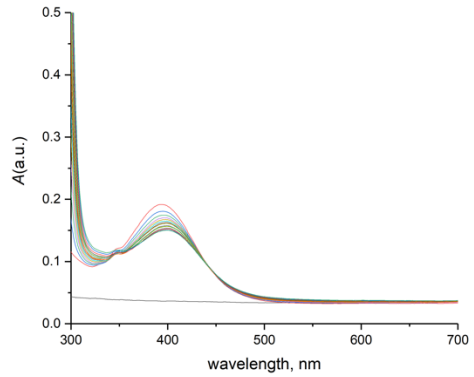	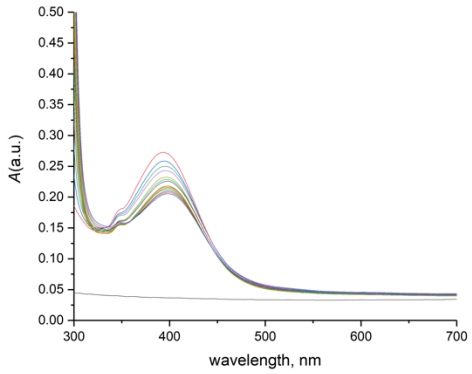
2.12e	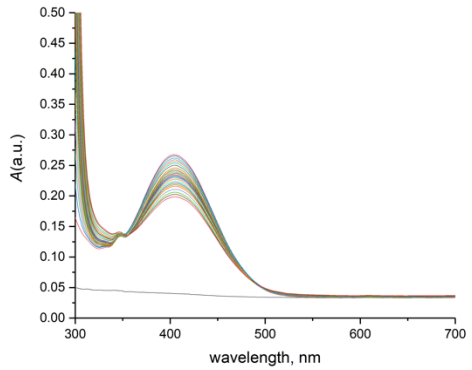	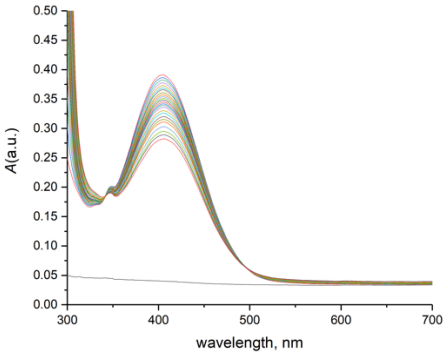
2.12f	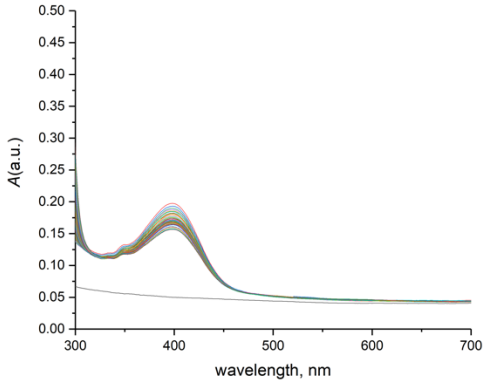	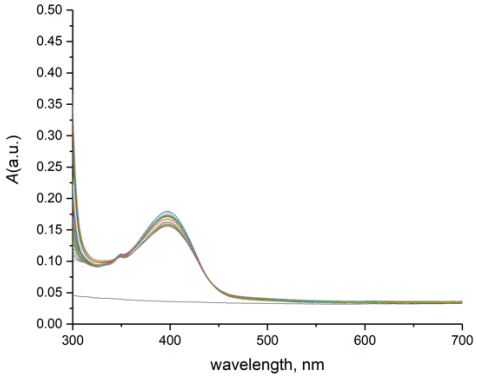

2.13a	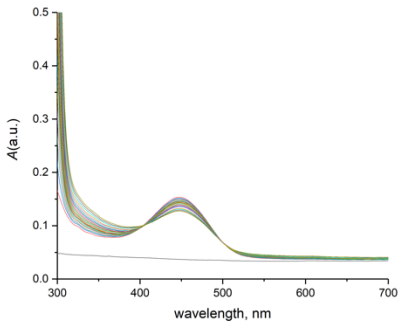	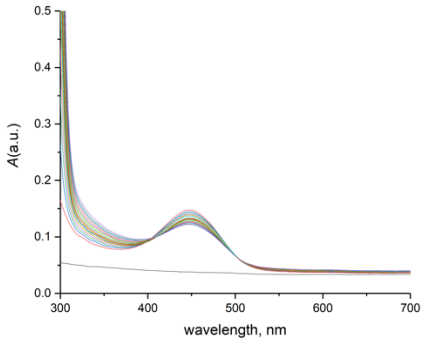
2.13c	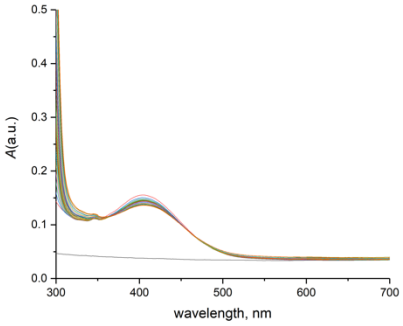	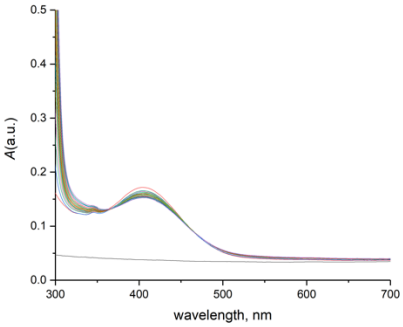
2.13e	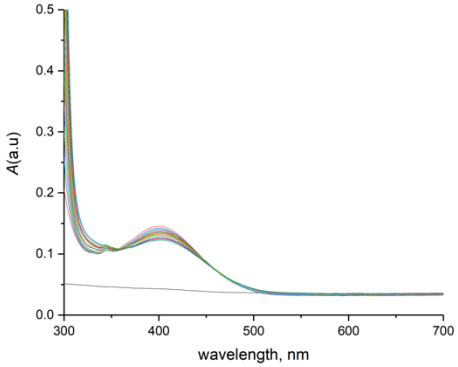	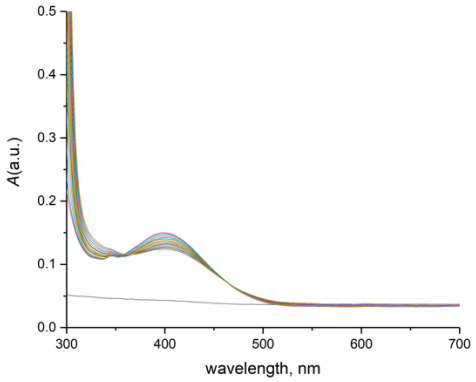

A2.4 Unrestricted preliminary fitting of UV-visible titration data

The binding affinity and the stoichiometry for compounds (2.12a)

2.12a	**1st titration**	**2nd titration**	**Global fit**
***K* / M^{-1}**	$3.96\times10^{8}\pm1.71\times10^{10}$	$(2.5\pm1.3)\times10^{5}$	$(8.2\pm15.8)\times10^{5}$
***n* / basepairs**	36.2±4.4	45.1±5.9	47.0±11.1
***K* (*n*=3) / M^{-1}**	$(1.7\pm0.7)\times10^{4}$	$(3.6\pm0.5)\times10^{3}$	$(3.7\pm2.0)\times10^{3}$
2.12c	**1st titration**	**2nd titration**	**Global fit**
***K* / M^{-1}**	$496.7\pm1.53\times10^{5}$	$2467\pm8.48\times10^{4}$	$93.73\pm1.74\times10^{4}$
n / basepairs	0.32±100.9	2.47±81.26	0.08±14.79
K (n=3) / M^{-1}	4822±739.9	3022±705.1	3729±1198
2.12d	**1st titration**	**2nd titration**	**Global fit**
***K* / M^{-1}**	$1.63\times10^{5}\pm1.45\times10^{5}$	$7.83\times10^{5}\pm6.35\times10^{5}$	$4.89\times10^{5}\pm4.18\times10^{5}$
n / basepairs	10.6±4.19	16.94±1.81	14.31±2.59
K (n=3) / M^{-1}	$2.48\times10^{4}\pm4711$	$1.43\times10^{4}\pm3597$	$2.04\times10^{4}\pm4605$
2.12e	**1st titration**	**2nd titration**	**Global fit**
***K* / M^{-1}**	$1.8\times10^{8}\pm2.87\times10^{9}$	$1.38\times10^{6}\pm1.14\times10^{6}$	$6.55\times10^{6}\pm1.08\times10^{7}$
n / basepairs	39.27±2.72	29.90±1.91	34.34±15.70
K (n=3) / M^{-1}	8294±3512	5738±1360	6631±1521
2.12b	**1st titration**	**2nd titration**	**Global fit**
***K* / M^{-1}**	$2.56\times10^{7}\pm1.34\times10^{8}$	$7.00\times10^{37}\pm1.16\times10^{44}$	$9.18\times10^{34}\pm0.0$
n / basepairs	107.8±19.12	383.6±0	73.77±149.4
K (n=3) / M^{-1}	2589±2022	0.04±6.50 (not binding)	122.4±1503
2.12f	**1st titration**	**2nd titration**	**Global fit**
***K* / M^{-1}**	$3.52\times10^{6}\pm2.86\times10^{6}$	$4.92\times10^{43}\pm9.68\times10^{40}$	$1.16\times10^{6}\pm1.78\times10^{6}$

n / basepairs	3.82±0.29	13.07±3.32	3.87±0.95
K (n=3) / M^{-1}	$9.18\times10^{5}\pm2.40\times10^{5}$	$1.87\times10^{5}\pm2.00\times10^{5}$	$3.8\times10^{5}\pm2.15\times10^{5}$
2.13a, DMSO[a]	**1st titration**	**2nd titration**	**Global fit**
***K* / M^{-1}**	$1.69\times10^{5}\pm2.12\times10^{5}$	$1.14\times10^{27}\pm1.06\times10^{38}$	$1.93\times10^{31}\pm2.96\times10^{42}$
***n* / basepairs**	51±18	130.0±11.79	56.06±11.46
***K* (*n*=3) / M^{-1}**	$(2.7\pm0.7)\times10^{3}$	$2.41\times10^{44}\pm1.01\times10^{44}$	$(1.7\pm0.5)\times10^{3}$
2.13c, DMSO[a]	**1st titration**	**2nd titration**	**Global fit**
***K* / M^{-1}**	$1.38\times10^{5}\pm3.1\times10^{5}$	$1.57\times10^{12}\pm8.81\times10^{20}$	$617.7\pm3.59\times10^{5}$
***n* / basepairs**	2.71±3.55	$1.43\pm6.04\times10^{8}$	0.03±17.9
***K* (*n*=3) / M^{-1}**	$(16.7\pm6.9)\times10^{4}$	$(3.5\pm1.7)\times10^{4}$	$(10.1\pm3.8)\times10^{4}$
2.13e, MOPS[b]	**1st titration**	**2nd titration**	**Global fit**
***K* / M^{-1}**	$1.09\times10^{7}\pm8.61\times10^{7}$	736.0±x5.79×10^{5}	$889.8\pm7.14\times10^{5}$
***n* / basepairs**	19.30±7.27	0.51±670.0	0.41±329.1
***K* (*n*=3) / M^{-1}**	$(6.8\pm5.5)\times10^{4}$	$(4.5\pm\pm0.6)\times10^{3}$	$(6.9\pm2.0)\times10^{3}$

Appendix for Chapter 3

A3.1 Characterization of compounds using NMR spectroscopy

400_Huda 2019 D1-A4 DMSO

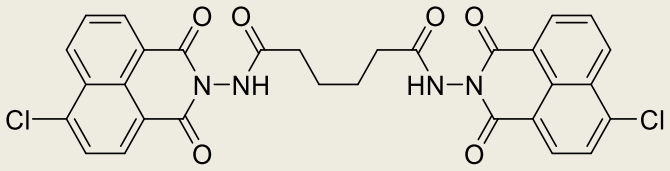

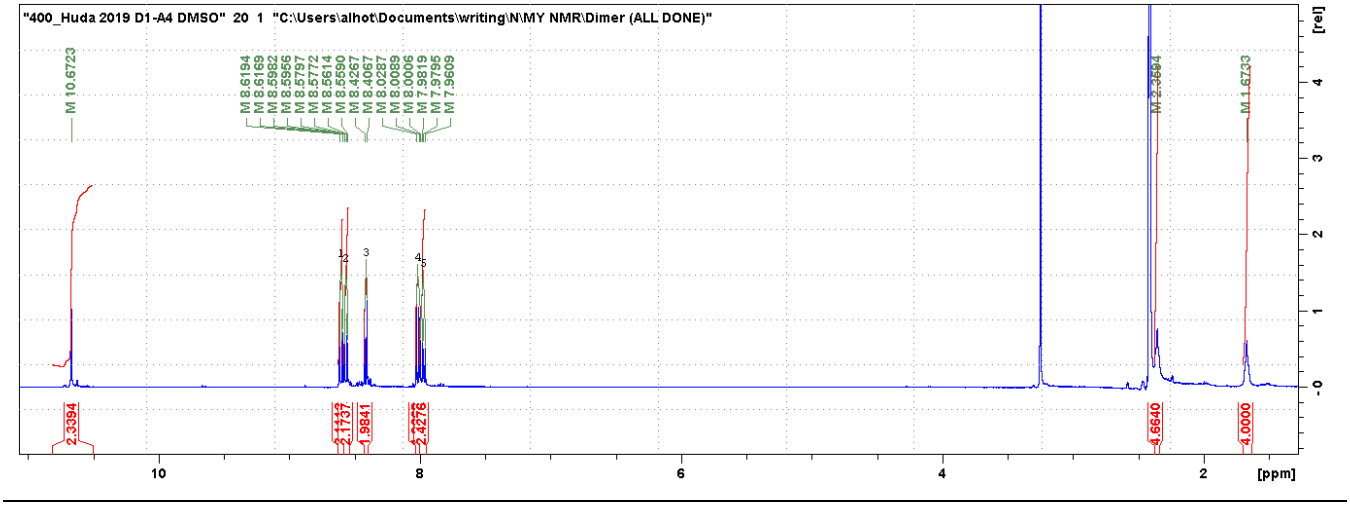

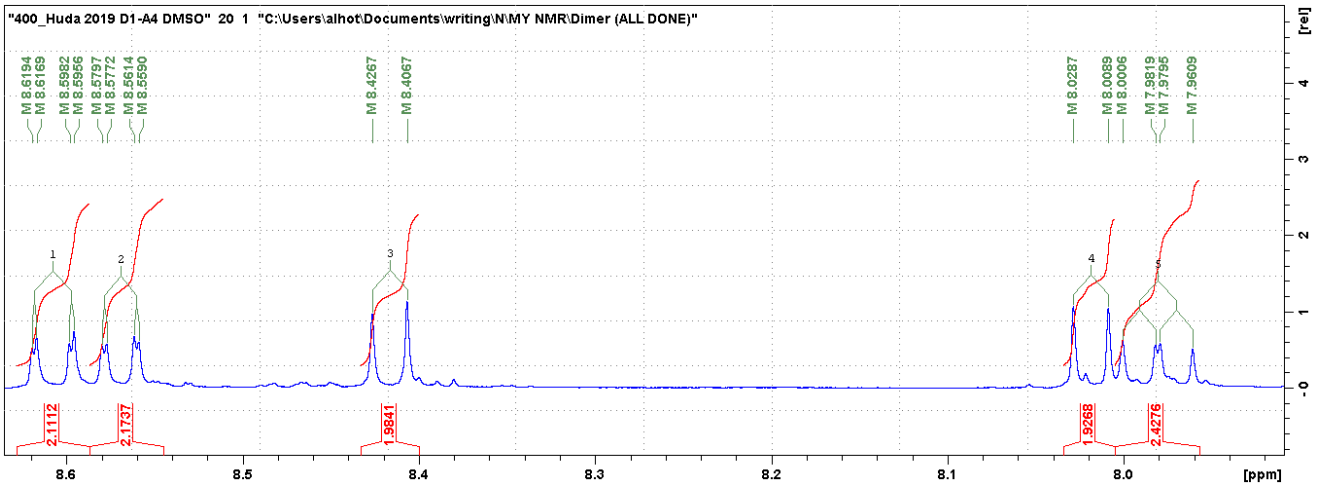

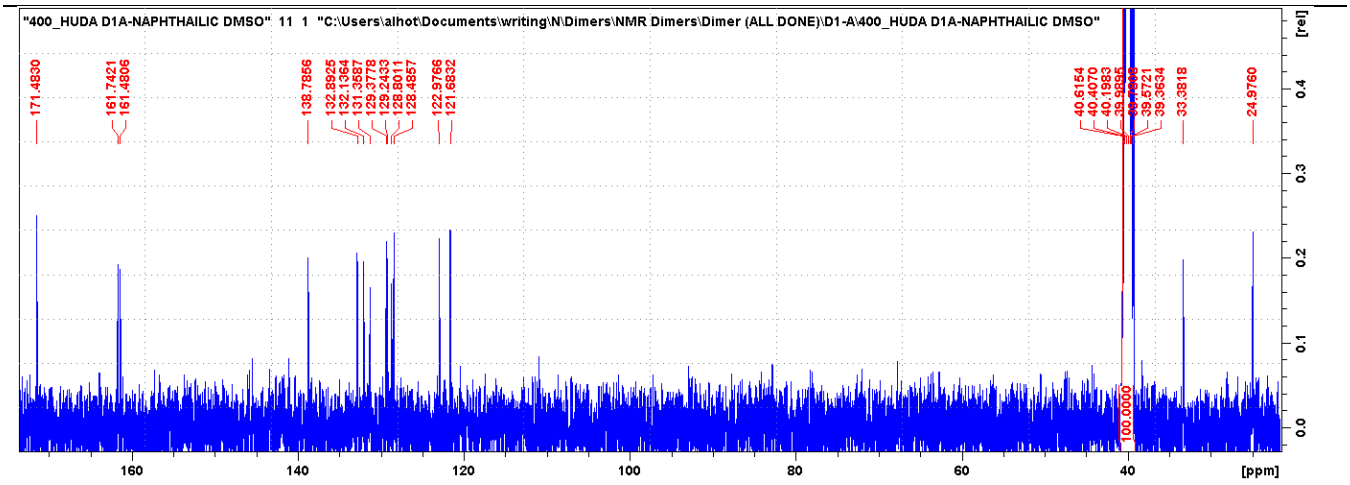

m.p >300 °C, **IR** (C=O) 1669.46 cm^{-1}, **^{1}HNMR (400 MHz, DMSO): δ(ppm)** 10.67 (s, 2H, NH), 8. 61 (dd,2H, *J* =8.54 Hz, *J* =1.02 Hz, Ar-CH), 8.56 (dd, 2H, *J* = 7.30 Hz, *J* = 0.98 Hz, Ar-CH), 8.41 (d, 2H, *J* = 8.00 Hz, Ar-CH), 8.01 (d, 2H, *J* = 7.92 Hz, Ar-CH), 7.97 (dd, 2H, *J* = 8.42 Hz, *J* =7.46 Hz, Ar-CH), 2.35 (br.signal, 4H,CH_2), 1.67 (br.signal, 4H,CH_2). **^{13}C NMR (400 MHz, DMSO): δ(ppm)** 171.48, 161.74, 161.48, 138,78. 132.89. 132.13, 131.35, 129.37, 129.24, 128.80, 128.48, 122.97, 121.68, 33.38, 24.97. **TOF MS ES+** calc for [$C_{30}H_{21}N_4O_6Cl_2$] 603.0838 found 603.0845.

400_Huda 2019 D1-B OLD CDCL3

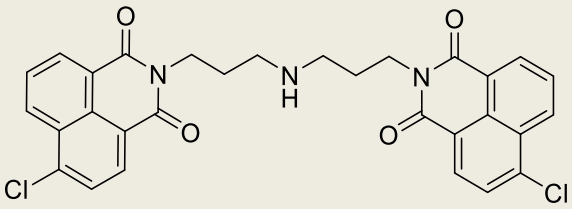

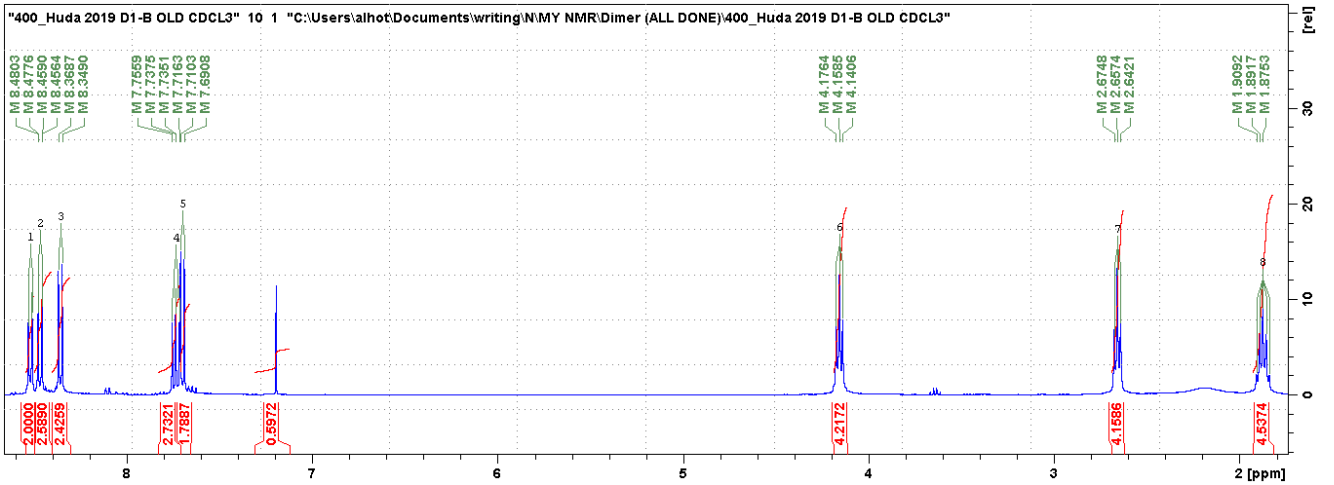

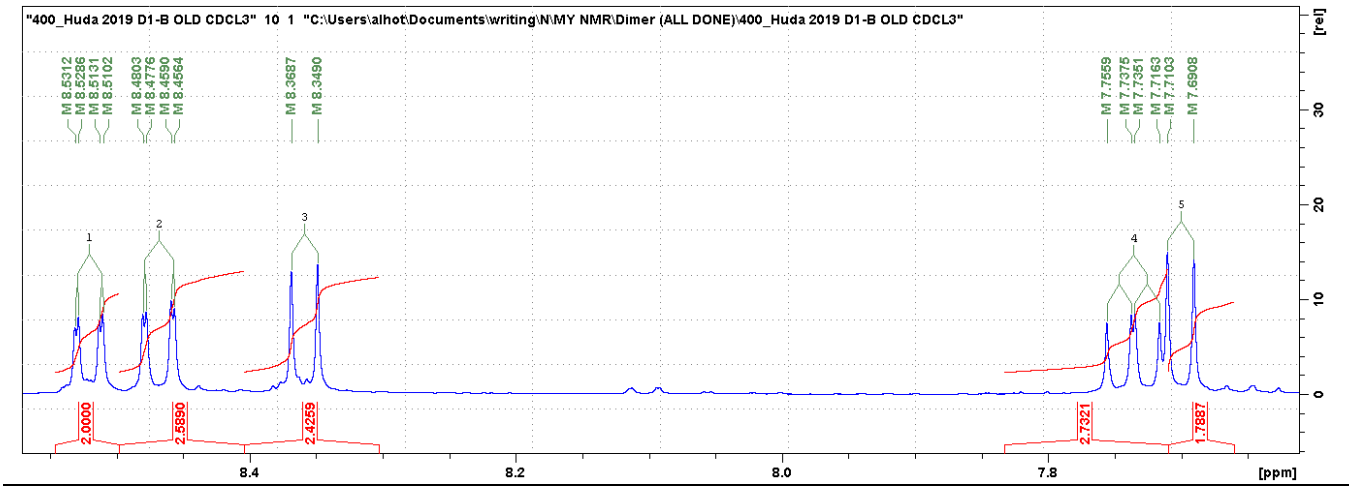

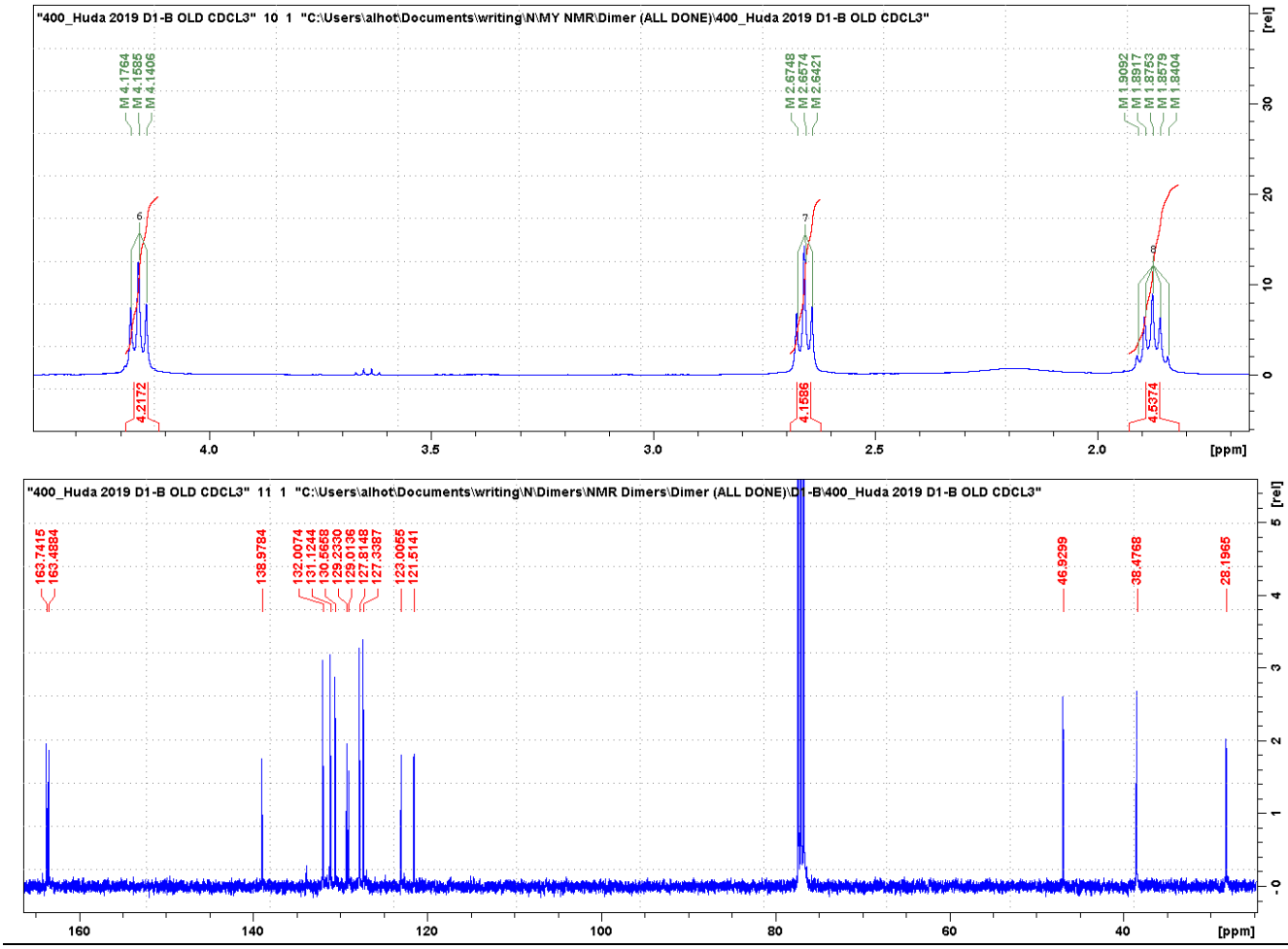

m.p 150-155 °C, **IR** (C=O) 1655.96 cm^{-1}, **^{1}H NMR (400 MHz, CDCl3): δ(ppm):** 8.52 (dd, 2H, *J* =7.30 Hz, *J* =1.00 Hz, Ar-CH), 8.46 (dd, 2H, *J* = 8.50 Hz, *J* = 1.06 Hz, Ar-CH), 8.35 (d, 2H, *J* =7.88 Hz, Ar-CH), 7.73 (dd, 2H, *J* = 8.40 Hz, *J* = 7.44 Hz, Ar-CH), 7.70 (d, 2H, *J* = 7.80 Hz, Ar-CH), 4.15 (t, 4H, *J*=7.16 Hz, CH_2), 2.65 (t, 4H, *J* = 6.54 Hz, CH_2), 1.87 (quint, 4H, *J* = 6.88 Hz, CH_2). **^{13}C NMR (400 MHz, CDCl3): δ(ppm):** 163.74, 163.48, 138.97, 132.00, 131.12, 130.56, 129.23, 129.01, 127.81, 127.38, 123.00, 121.51, 46.92, 38.47, 28.19. **HR TOF MS ES+** calc for [$C_{30}H_{24}N_3O_4Cl_2$] 560.1144 found 560.1157.

400_Robin_D1C_chloroform\500_HUDA 2021 conf D1-C CDCl3 C13

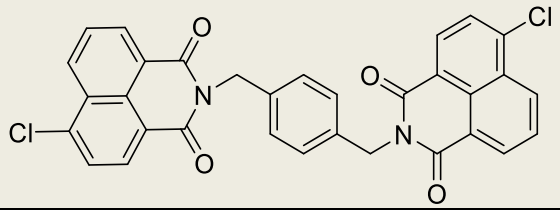

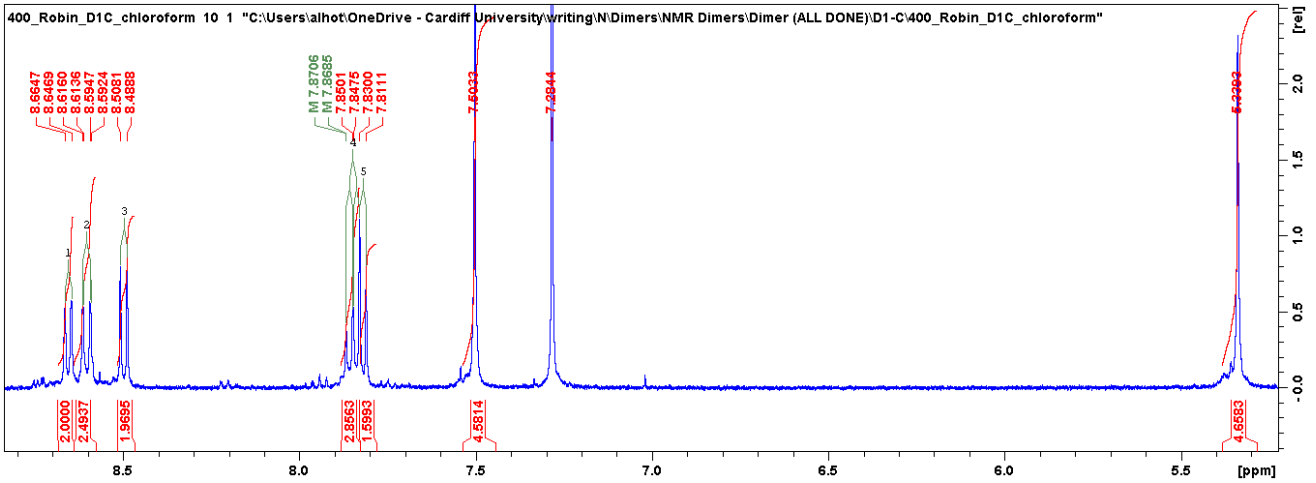

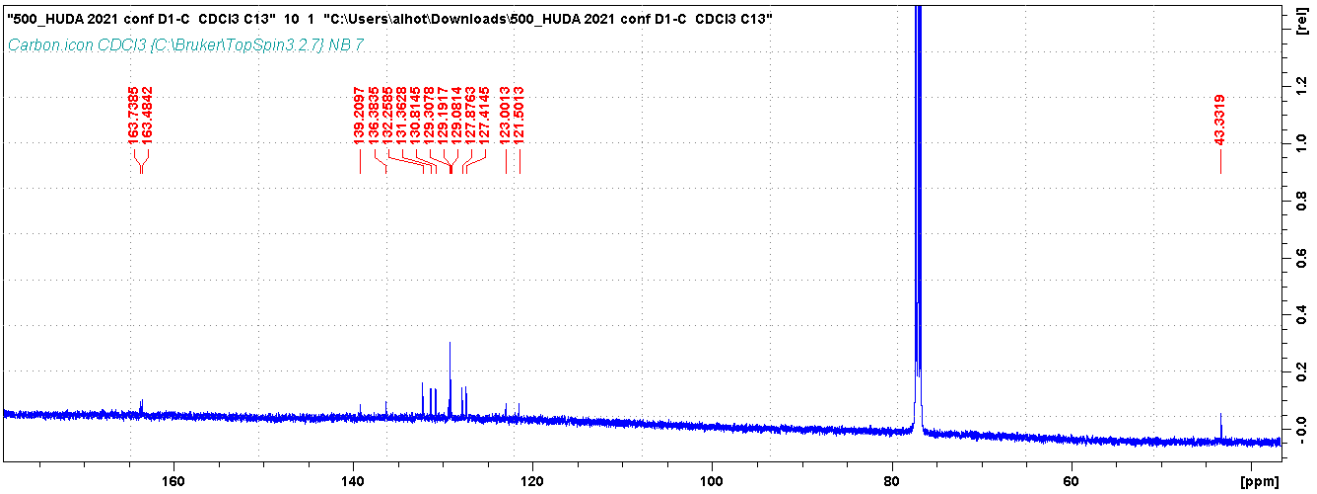

m.p >300 °C, **IR** (C=O) 1661.75 cm^{-1}, **^{1}H NMR (400 MHz, CDCl3): δ(ppm):** 8. 65 (d, 2H, *J* = 7.12 Hz, Ar-CH), 8.60 (dd, 2H, *J* = 8.50Hz, *J* = 0.94 Hz, Ar-CH), 8.49 (d, 2H, *J* =7.72 Hz, Ar-CH), 7.84 (dd, 2H, *J* = 8.22 Hz, *J* = 7.17 Hz, Ar-CH), 7.82 (d, 2H, *J* = 7.56 Hz, Ar-CH), 7.50 (s,4H, Ar-CH), 5.33 (s, 4H, CH_2). **^{13}C NMR (500 MHz, CDCl3): δ(ppm):** 163.73, 163.48, 139.20, 136.38, 132.25, 131.36, 130.81, 129.30, 129.19, 129.08, 127.87, 127.41, 123.00, 121.50, 43.33. **HR TOF MS ES+** calc for [$C_{32}H_{19}N_2O_4Cl_2$] 565.0722 found 565.0729.

400_Huda 2019 D1-E CDCl3

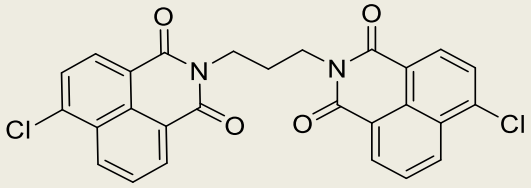

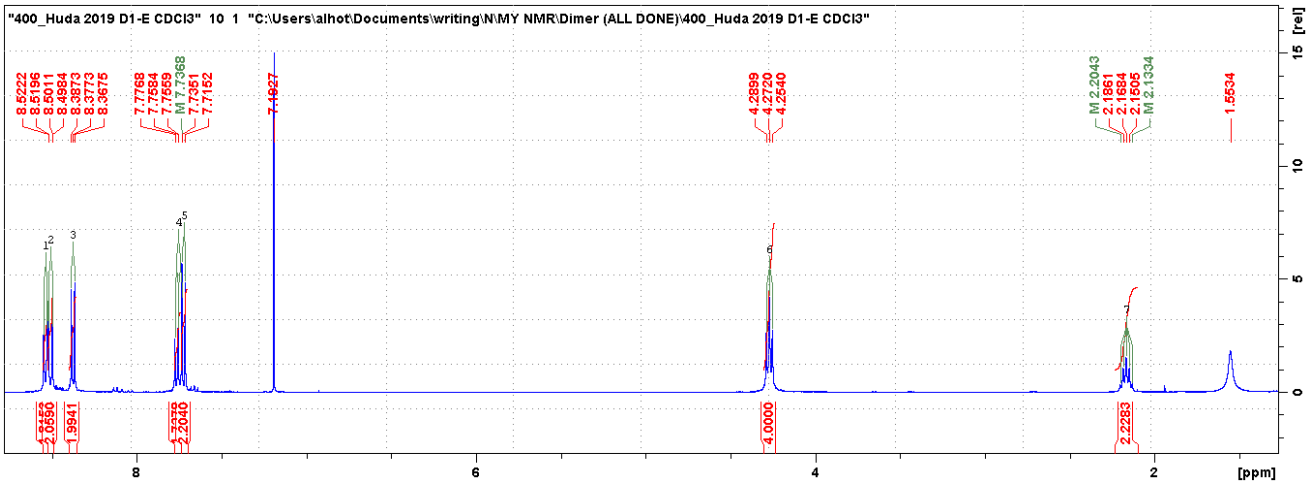

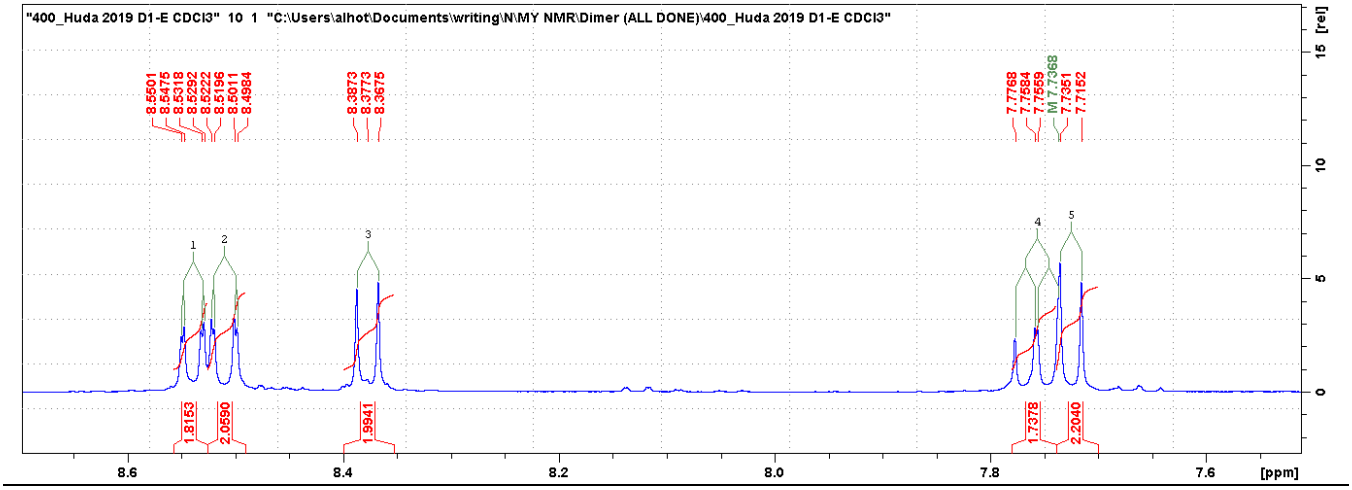

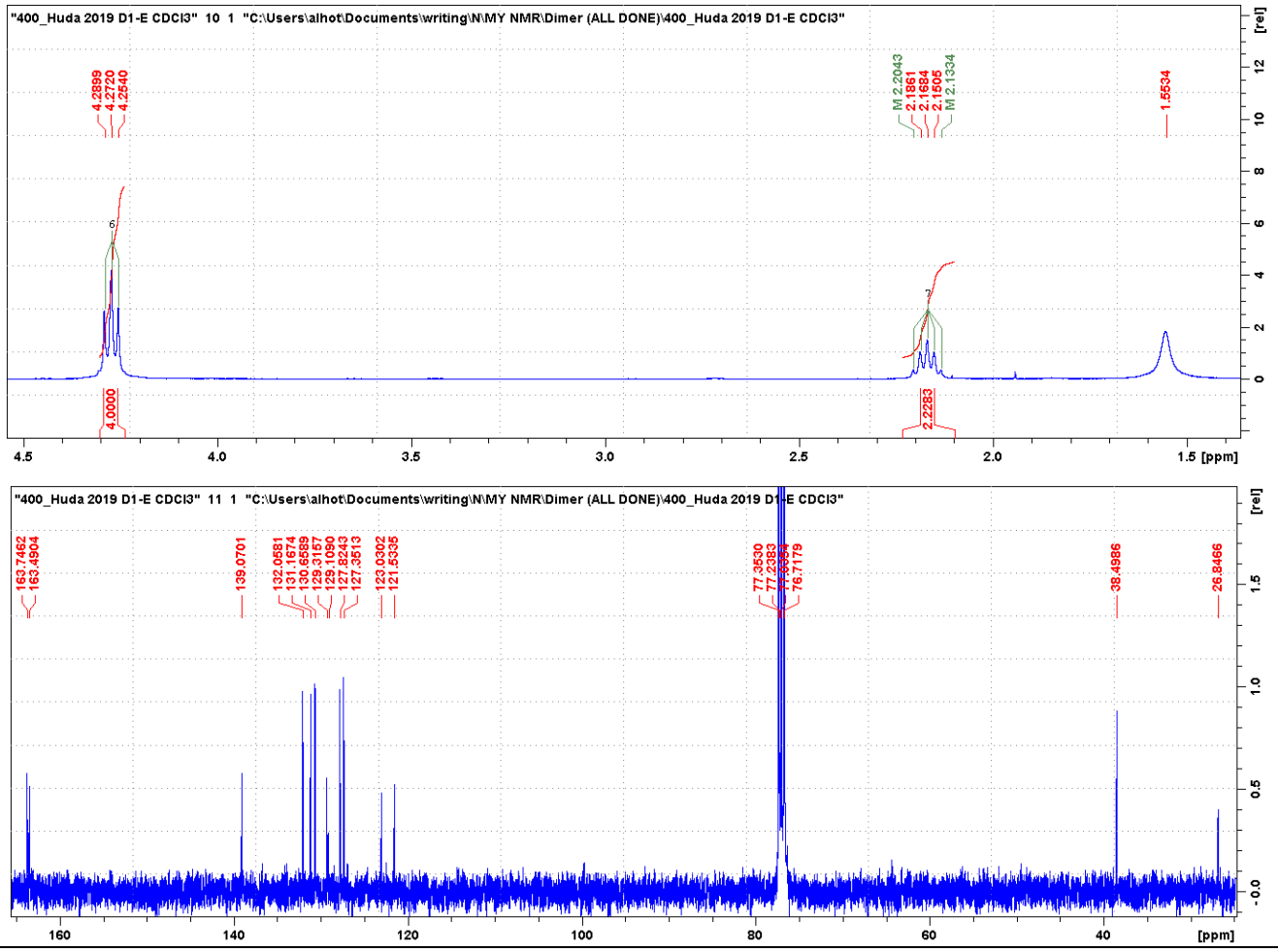

m.p >269-272 °C, **IR** (C=O) 1654.03 cm^{-1}. **^{1}H NMR (400 MHz, CDCl3): δ(ppm):** 8.54 (dd, 2H, *J* =7.32 Hz, *J* =1.04 Hz, Ar-CH), 8.51 (dd, 2H, *J* = 8.46 Hz, *J* =1.06 Hz, Ar-CH), 8.37 (d, 2H, *J* =7.92 Hz, Ar-CH), 7.75 (dd, 2H, *J* = 8.50 Hz, *J* = 7.50 Hz, Ar-CH), 7.72 (d, 2H, *J* = 7.96 Hz, Ar-CH), 4.27 (t, 4H, *J*=7.18, CH_2), 2.16 (quint, 2H, *J* = 7.09 Hz, CH_2). **^{13}C NMR (400 MHz, CDCl3): δ(ppm):** 163.74, 163.49, 139.07, 132.05, 131.16, 130.65, 129.31, 129.10, 127.82, 127.35, 123.03, 121.53, 38.49, 26.84. **HR TOF MS ES+** calc for [$C_{27}H_{17}N_2O_4Cl_2$] 503.0565 found 503.0569.

400_Huda 2019 D1-F CDCl3

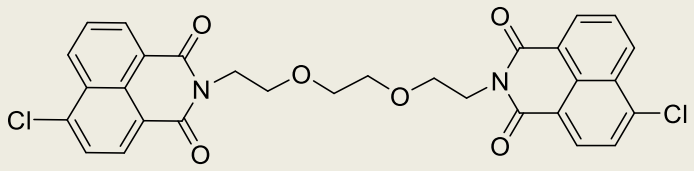

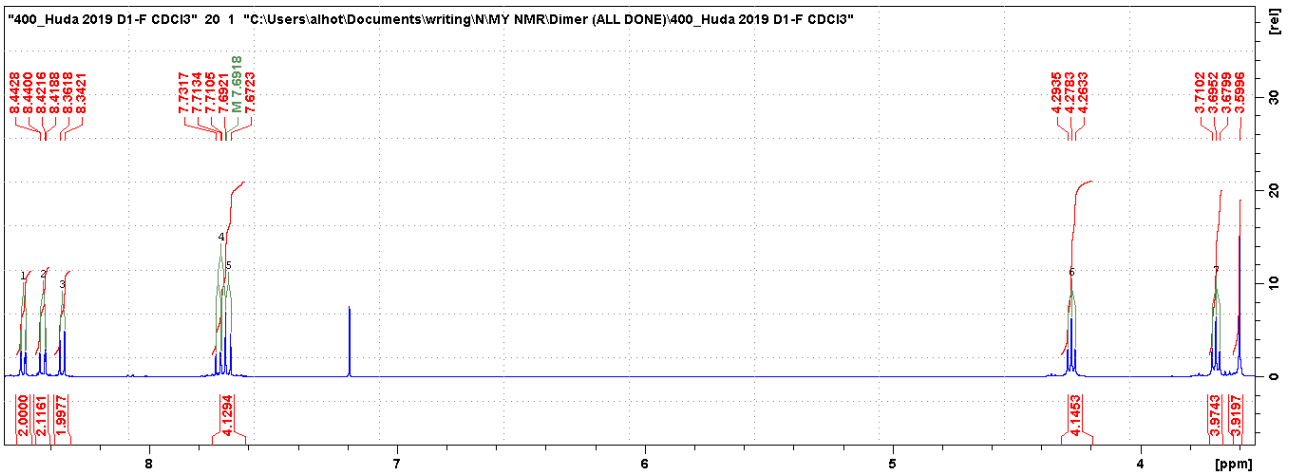

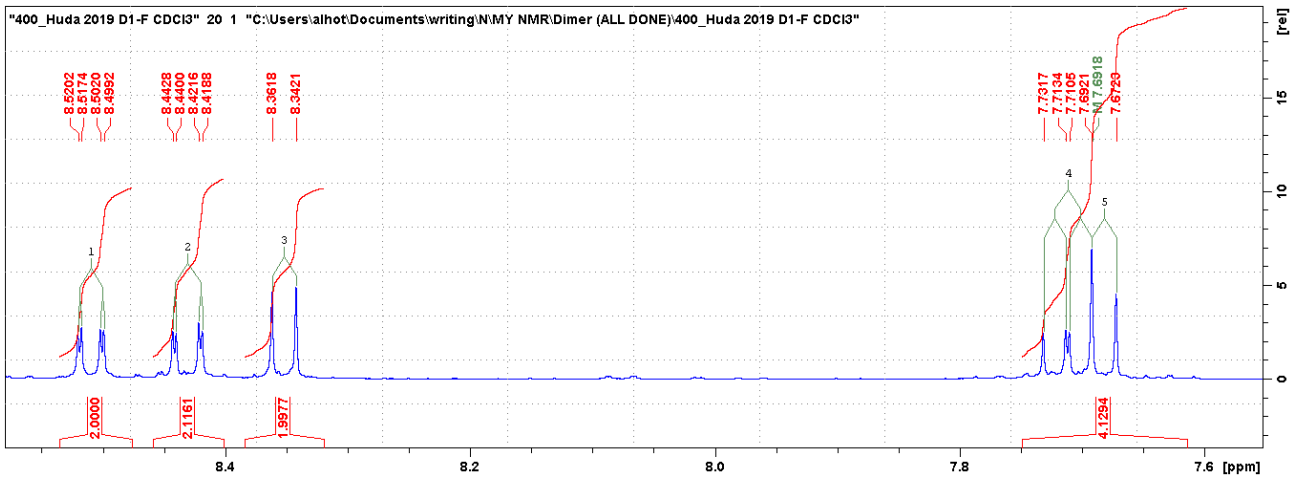

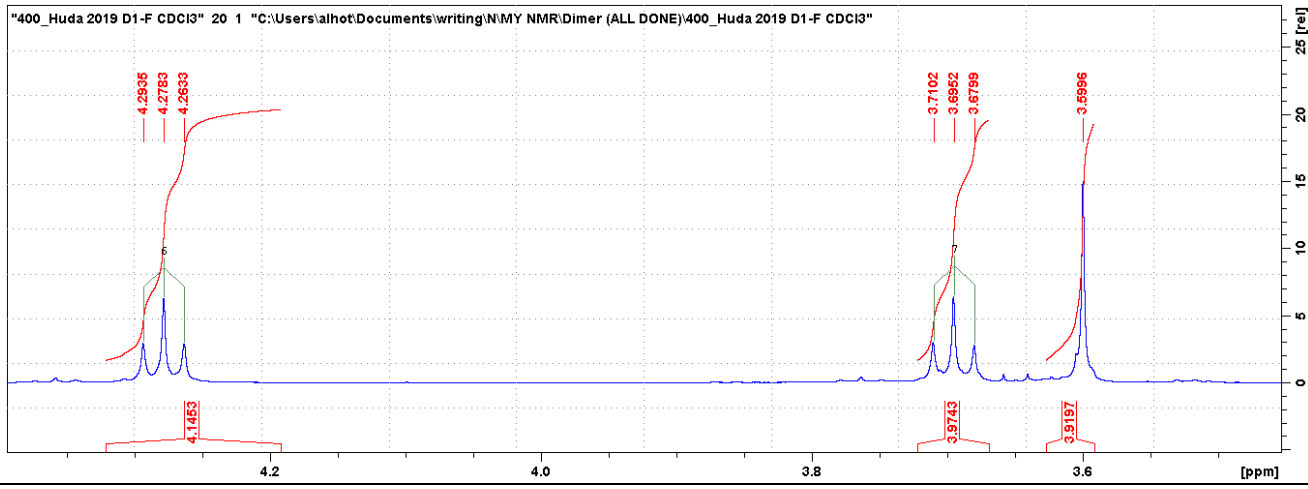

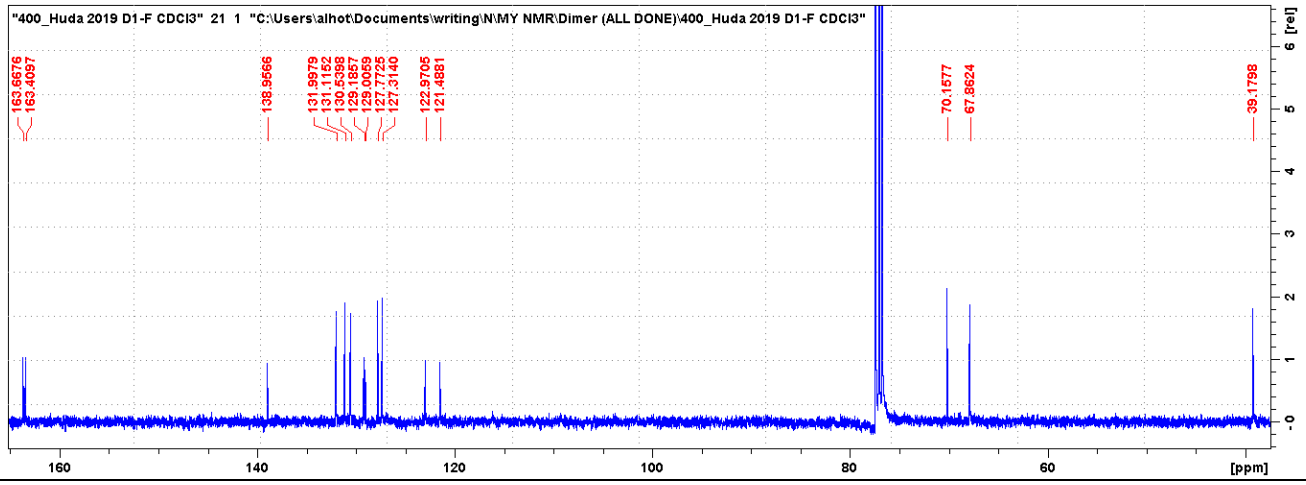

m.p >205-209 °C, **IR** (C=O) 1655.96 cm^{-1}. **^{1}H NMR (400 MHz, CDCl3): δ(ppm):** 8.50 (dd, 2H, *J* =7.28 Hz, *J* =1.12 Hz, Ar-H), 8.43 (dd, 2H, *J* = 8.48 Hz, *J* =1.12 Hz, Ar-H), 8.35 (d, 2H, *J* =7.88 Hz, Ar-H), 7.71 (dd, 2H, *J* = 8.50 Hz, *J* = 7.34 Hz, Ar-H), 7.68 (d, 2H, *J* = 7.92 Hz, Ar-H), 4.27 (t, 4H, *J*=6.04 Hz, CH_2), 3.69 (t, 4H, *J* = 6.06 Hz, CH_2), 3.59 (s,4H, CH_2). **^{13}C NMR (400 MHz, CDCl3): δ(ppm):** 163.66, 163.40, 138.95, 131.99, 131.11, 130.53, 129.18, 129.00, 127.77, 127.31, 122.97, 121.48, 70.15, 67.86, 39.17. **HR TOF MS ES+** calc for $[C_{30}H_{22}N_2O_6Cl_2]^{+Na}$ 599.0753 found 599.0753.

400_HUDA D1A S1 DMSO

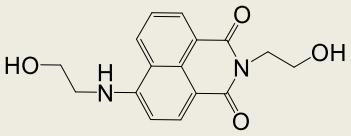

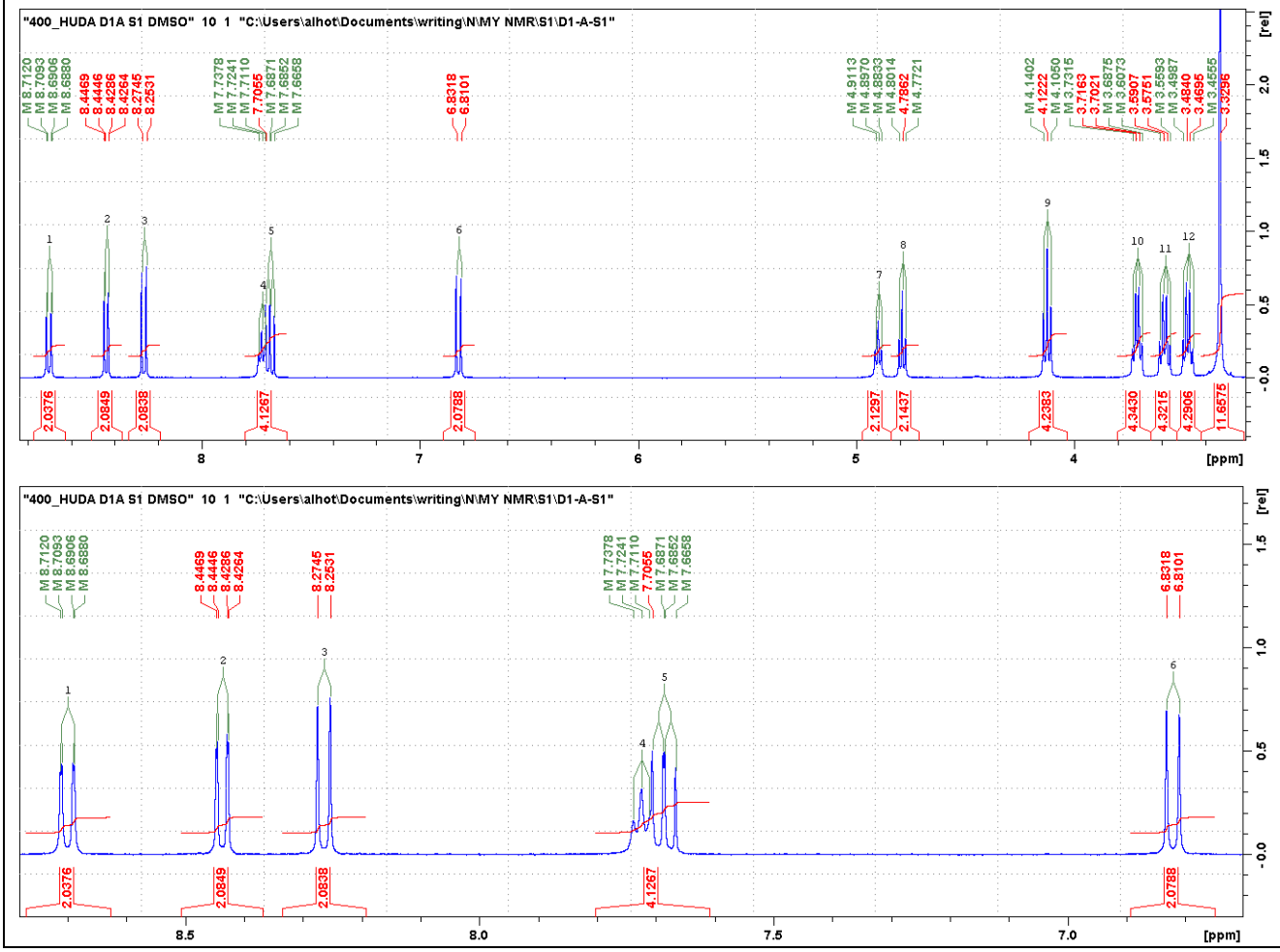

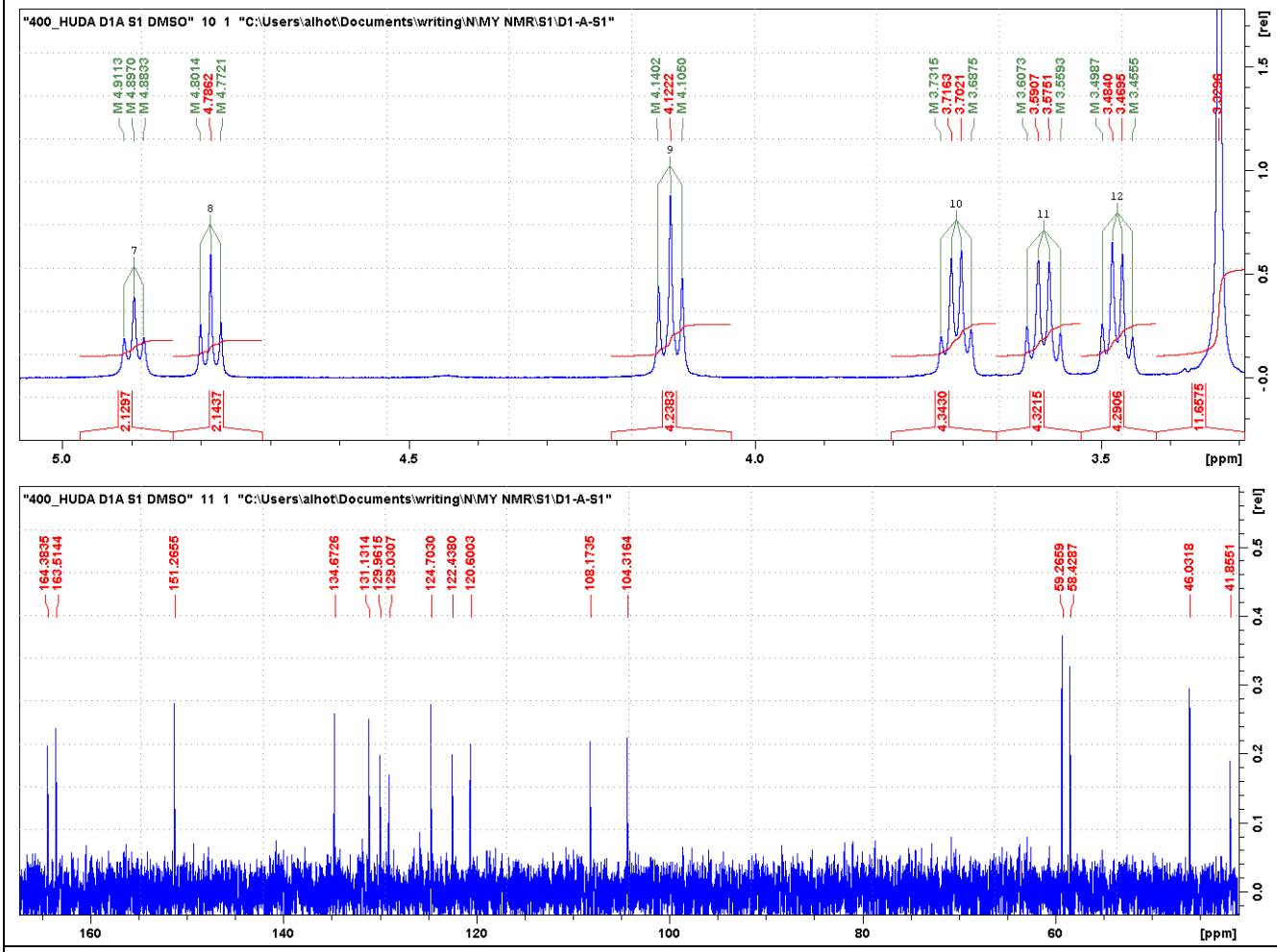

^{1}H NMR (400 MHz, DMSO): δ(ppm): 8.69 (dd, *J* =8.54 Hz, *J* = 1.06 Hz, 1H, Ar-CH), 8.43 (dd, *J* = 7.30 Hz, *J* = 0.90 Hz, 1H, Ar-CH), 8.26 (d, *J* = 8.56 Hz, 1H, Ar-CH), 7.72 (t, *J*=5.36,1H, N-H), 7.68 (dd, *J* = 8.32 Hz, *J* = 7.56 Hz, 1H, Ar-CH), 7.38 (d, *J* = 8.68 Hz, 1H, Ar-CH), 4.89 (t, *J*=5.60, 1H, N-H), 4.78 (t, *J*=5.86, 1H, O-H), 4.12 (t, *J* = 7.04 Hz, 2H, CH_2), 3.70 (q, *J* = 5.86 Hz, 2H, CH_2) 3.58 (q, *J* = 6.40 Hz, 2H, CH_2), 3.47 (q, *J* = 5.76 Hz, 2H, CH_2). **^{13}C NMR (400 MHz, DMSO): δ(ppm):** 164.38, 163.51, 151.26, 134.67, 131.13, 129.96, 129.03, 124.70, 122.43, 120.60, 108.17, 104.31, 59.26, 58.42, 46.03, 41.85. **HR TOF MS ES+** calc for [$C_{16}H_{17}N_2O_4$] 301.1188 found 301.1189.

400_HUDA 2020 conf D1-B-S1 DMSO

CH2 linker overlap with DMSO signal at 2.6 (Known that by the comparison with D1-B NMR)

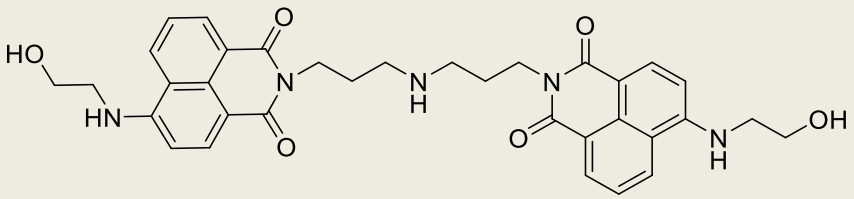

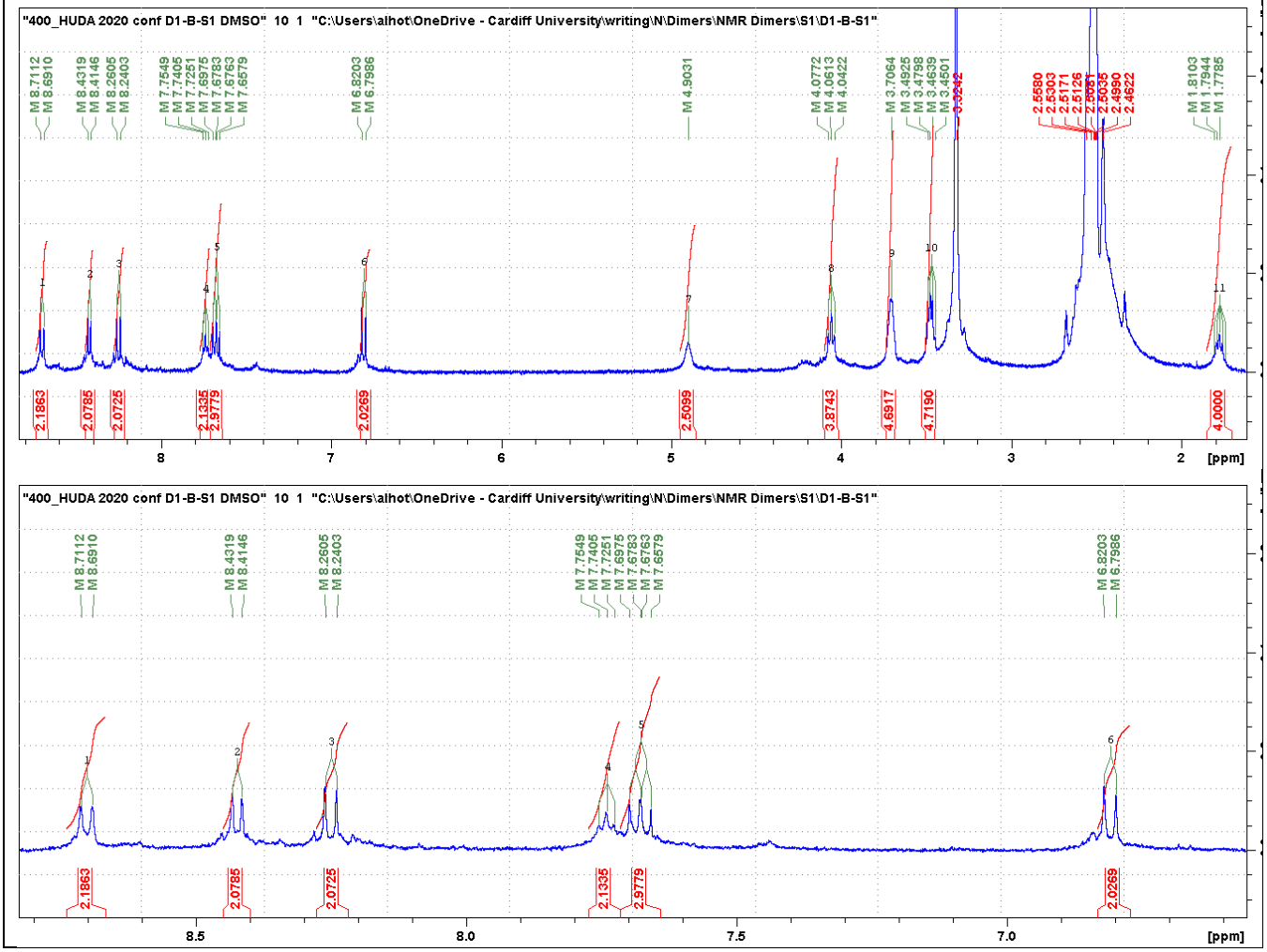

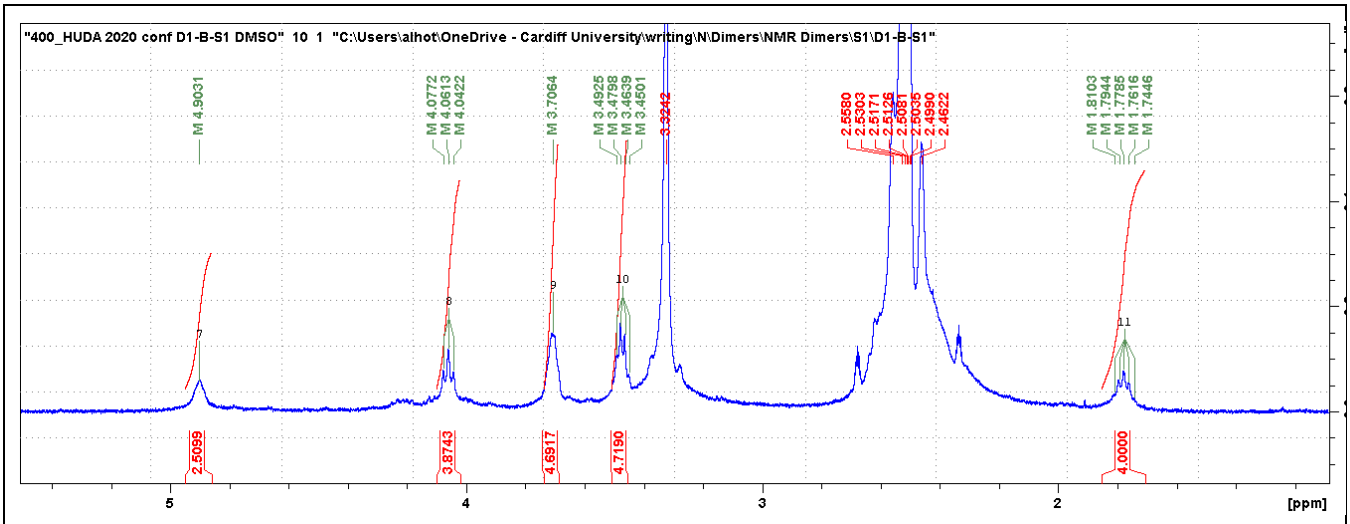

^{1}H NMR (400 MHz, DMSO): δ(ppm): 8.70 (d, *J* =8.08 Hz, 2H, Ar-CH), 8.42 (d, *J* = 6.92 Hz, 2H, Ar-CH), 8.25 (d, *J* = 8.08 Hz, 1H, Ar-CH), 7.74 (t, *J*=5.96, 2H, N-H), 7.67 (dd, *J* = 8.32 Hz, *J* = 7.52 Hz, 2H, Ar-CH), 6.79 (d, *J* = 8.68 Hz, 2H, Ar-CH), 4.90 (br.s, 2H, OH), 4.06 (t, *J*=7.00, 4H, CH_2), 3.70 (br.s, 4H, CH_2), 3.47 (q, *J* = 5.65 Hz, 4H, CH_2), 1.77 (quin, *J* = 6.57 Hz, 4H, CH_2). **^{13}C NMR (400 MHz, DMSO): δ(ppm):**. **HR TOF MS ES+** calc for [$C_{34}H_{36}N_5O_6$] 610.2666 found 610.2662.

400_HUDA 2020 conf D1-C-S1 DMSO

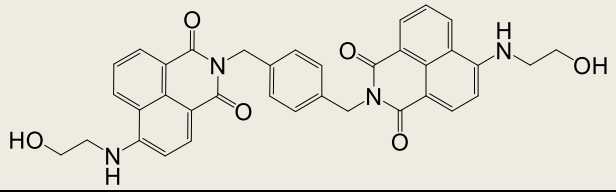

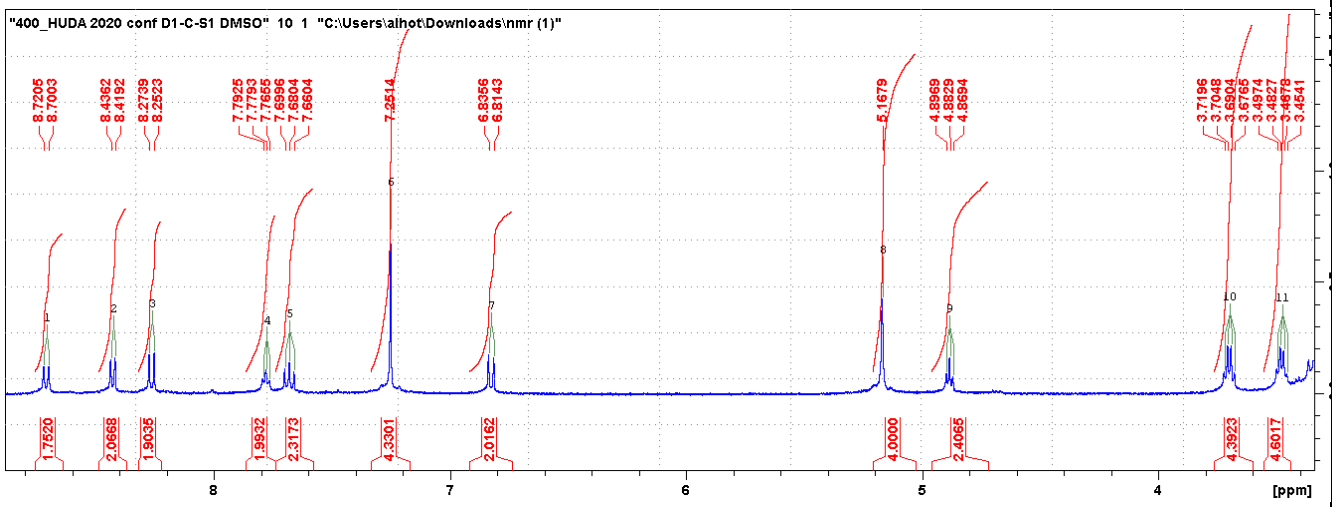

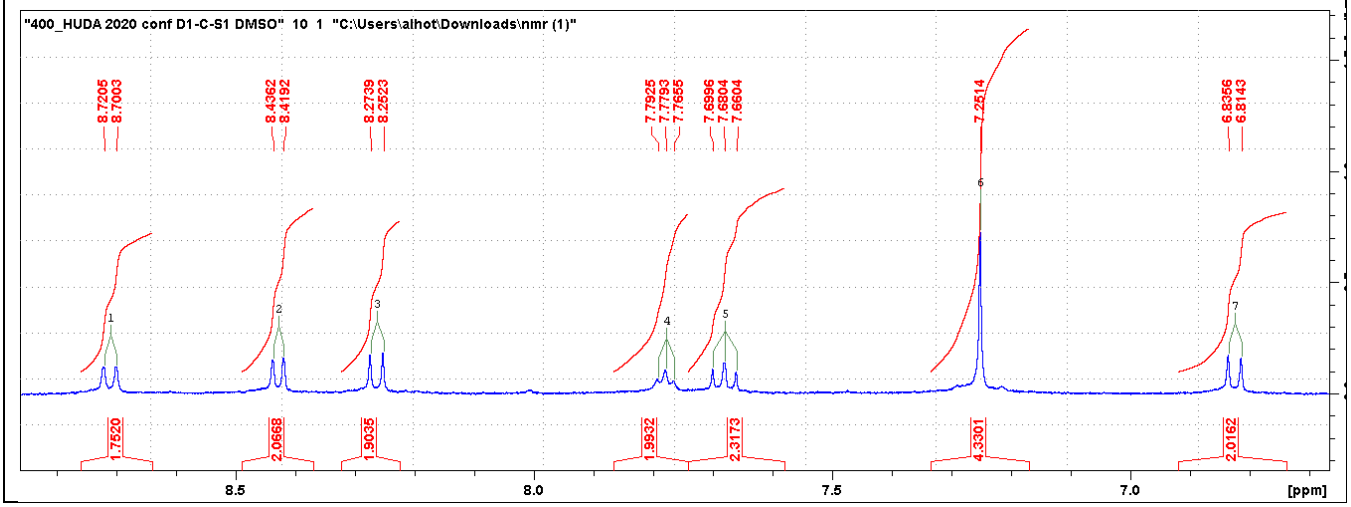

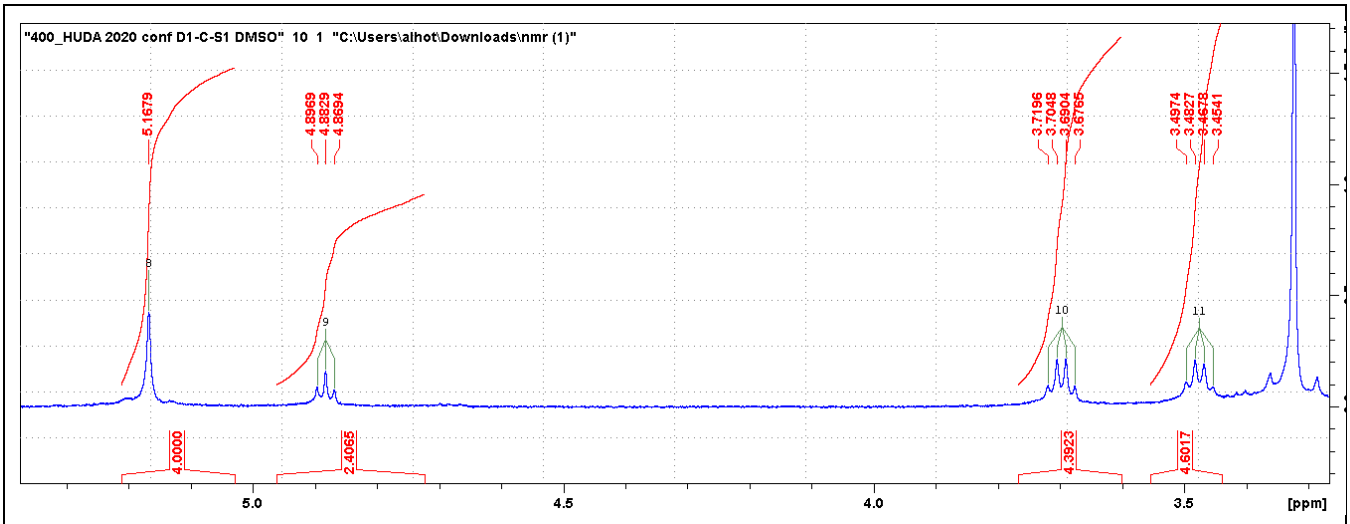

^{1}H NMR (400 MHz, DMSO): δ(ppm): 8.71 (d, *J* =8.08 Hz, 2H, Ar-CH), 8.42 (d, *J* = 6.80 Hz, 2H, Ar-CH), 8.26 (d, *J* = 8.64 Hz, 2H, Ar-CH), 7.77 (t, *J*=5.40,2H, N-H), 7.68 (t, *J* = 7.84 Hz, 2H, Ar-CH), 7.25 (s, 4H, Ar-CH), 6.82 (d, *J* = 8.52 Hz, 2H, Ar-CH), 5.16 (s, 4H, CH_2), 4.88 (t, *J*=5.50, 2H, O-H), 3.70 (q, *J* = 5.74 Hz, 4H, CH_2), 3.47 (q, *J* = 5.77 Hz, 4H, CH_2).

400_HUDA 2019 D1-E-S1 OLD DMSO\500_HUDA 2021 Conf 13C D1-E-S1 DMSO

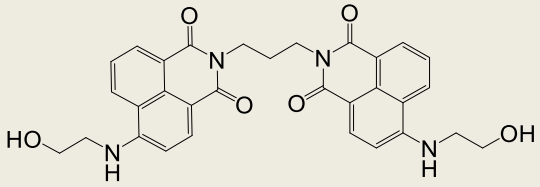

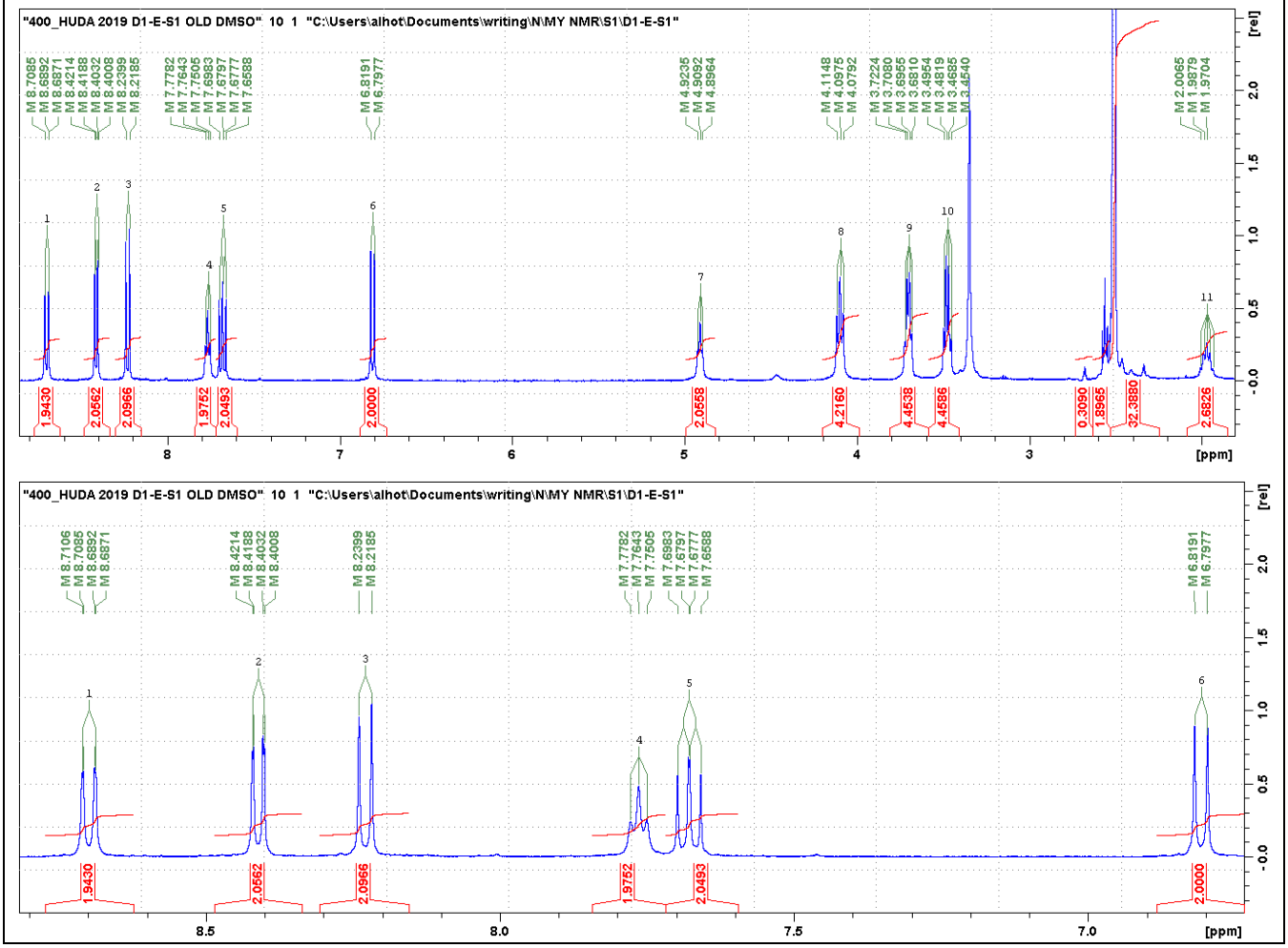

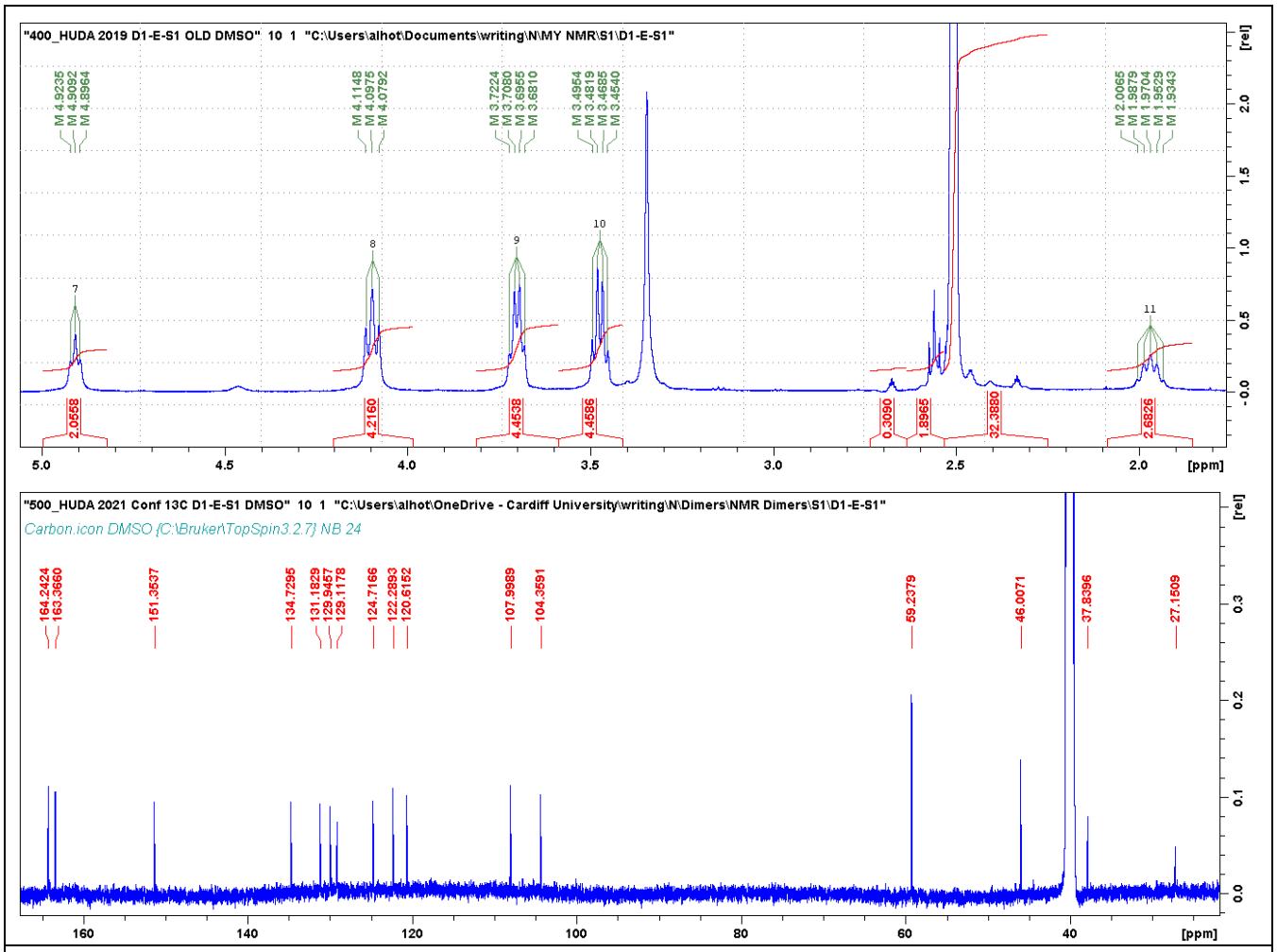

^{1}H NMR (400 MHz, DMSO): δ(ppm): 8.69 (dd, *J* =8.56 Hz, *J* = 0.84 Hz, 2H, Ar-CH), 8.40 (dd, *J* = 7.24 Hz, *J* = 1.00 Hz, 2H, Ar-CH), 8.22 (d, *J* = 8.56 Hz, 2H, Ar-CH), 7.76 (t, *J*=5.54,2H, N-H), 7.67 (dd, *J* = 8.30 Hz, *J* = 7.50 Hz, 2H, Ar-CH), 6.80 (d, *J* = 8.56 Hz, 2H, Ar-CH), 4.90 (t, *J*=5.42, 2H, N-H), 4.09 (t, *J* = 7.12 Hz, 4H, CH_2), 3.69 (q, *J* = 5.52 Hz, 4H, CH_2) 3.47 (q, *J* = 5.52 Hz, 4H, CH_2), 1.97 (quint, *J* = 5.52 Hz, 2H, CH_2). **^{13}C NMR (500 MHz, DMSO): δ(ppm):** 164.24, 163.36, 151.35, 134.72, 131.18, 129.94, 129.11, 124.71, 122.28, 120.61, 107.99, 104.35, 59.23, 46.00, 37.83, 27.15. **HR TOF MS ES+** calc for [$C_{31}H_{29}N_4O_6$] 553.2087 found 553.2087.

500_HUDA 2021 D1-F-S1 new 4 col DMSO\Acetone, chloroform, and DCM were observed.

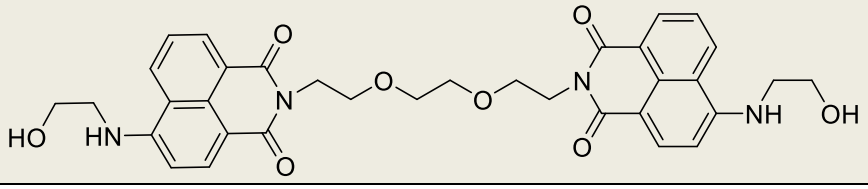

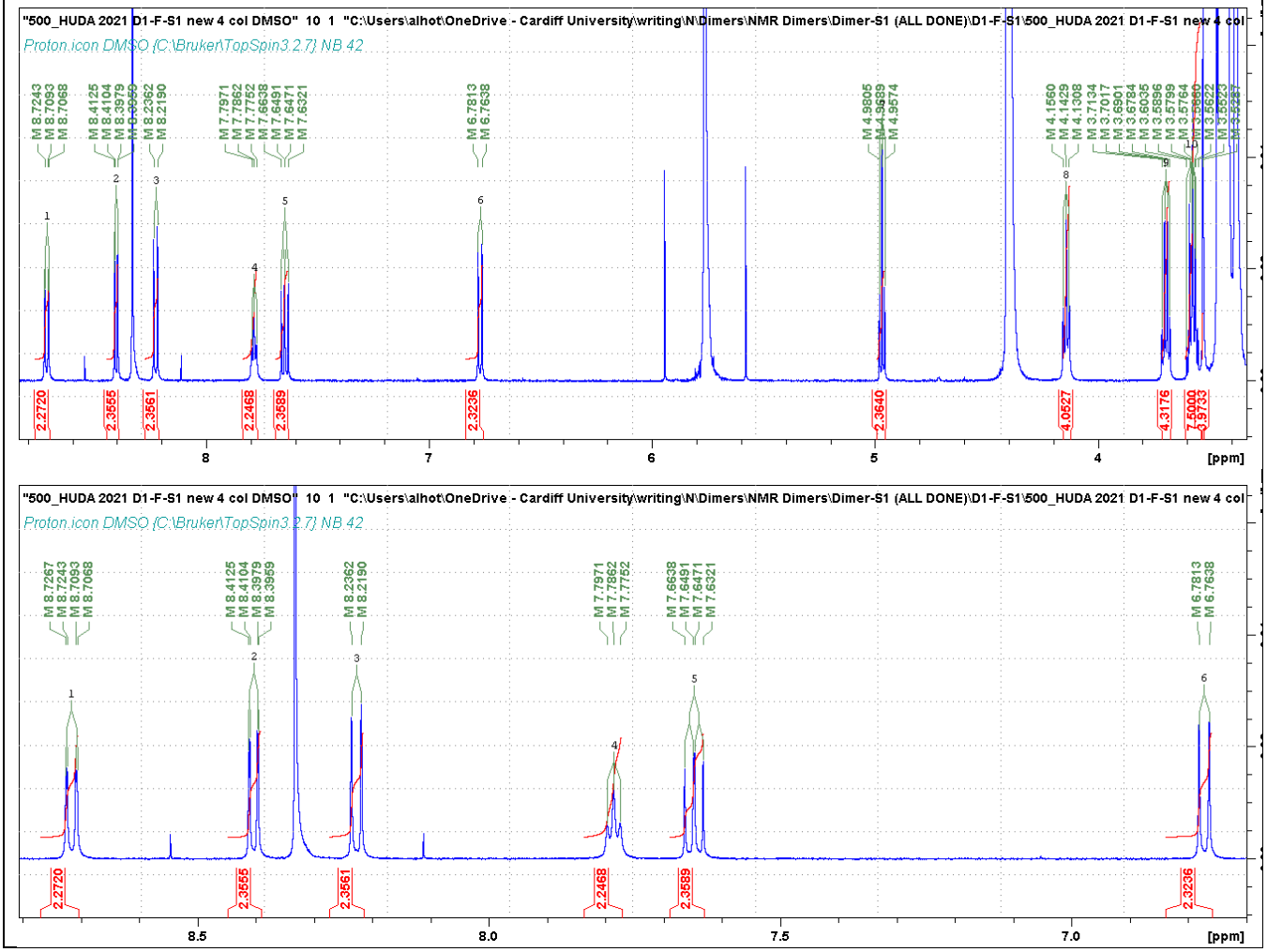

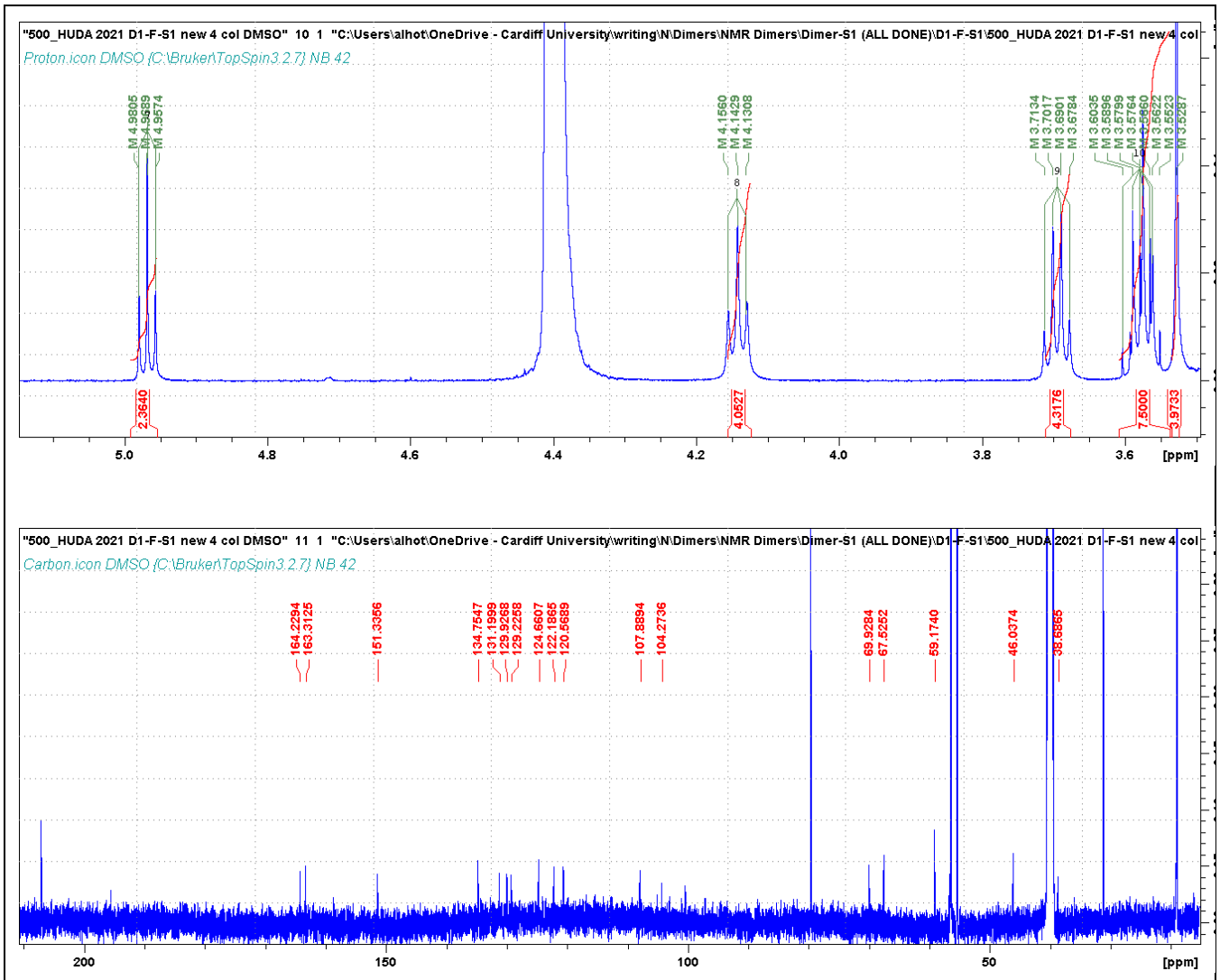

^{1}H NMR (500 MHz, DMSO): δ(ppm): 8.71 (dd, *J* =8.72 Hz, *J* = 1.22 Hz, 2H, Ar-CH), 8.40 (dd, *J* = 7.27 Hz, *J* = 1.02 Hz, 2H, Ar-CH), 8.22 (d, *J* = 8.60 Hz, 2H, Ar-CH), 7.78 (t, *J*=5.47,2H, N-H), 7.64 (dd, *J* = 8.42 Hz, *J* = 7.42 Hz, 2H, Ar-CH), 8.75 (d, *J* = 8.75 Hz, 2H, Ar-CH), 4.96 (t, *J*=5.77, 2H, N-H), 4.14 (t, *J* = 6.30 Hz, 4H, CH_2), 3.69 (q, *J* = 5.83 Hz, 4H, CH_2), 3.57 (m, 8H, CH_2), 3.52 (s, 4H, CH_2). **^{13}C NMR (500 MHz, DMSO): δ(ppm):** 164.22, 163.31, 151.33, 134.75, 131.19, 129.92, 129.22, 124.66, 122.18, 120.56, 107.88, 104.27, 69.92, 67.52, 59.17, 46.03, 38.68. **HR TOF MS ES+** calc for [$C_{34}H_{35}N_4O_8$] 627.2455 found 627.2463.

400_HUDA 2020 M1-N1 New method crystal MeOH DMSO

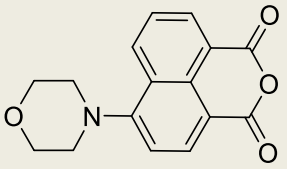

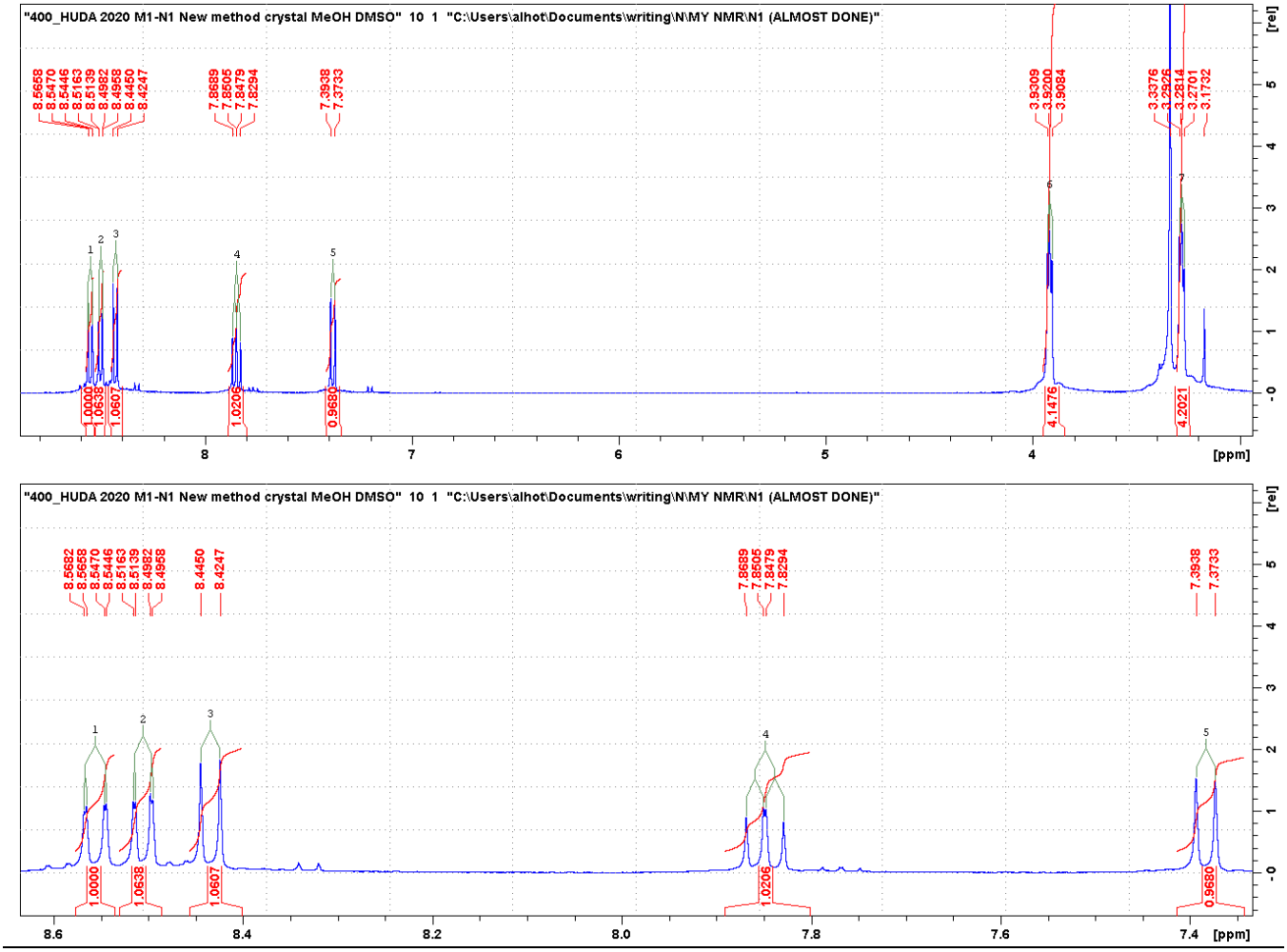

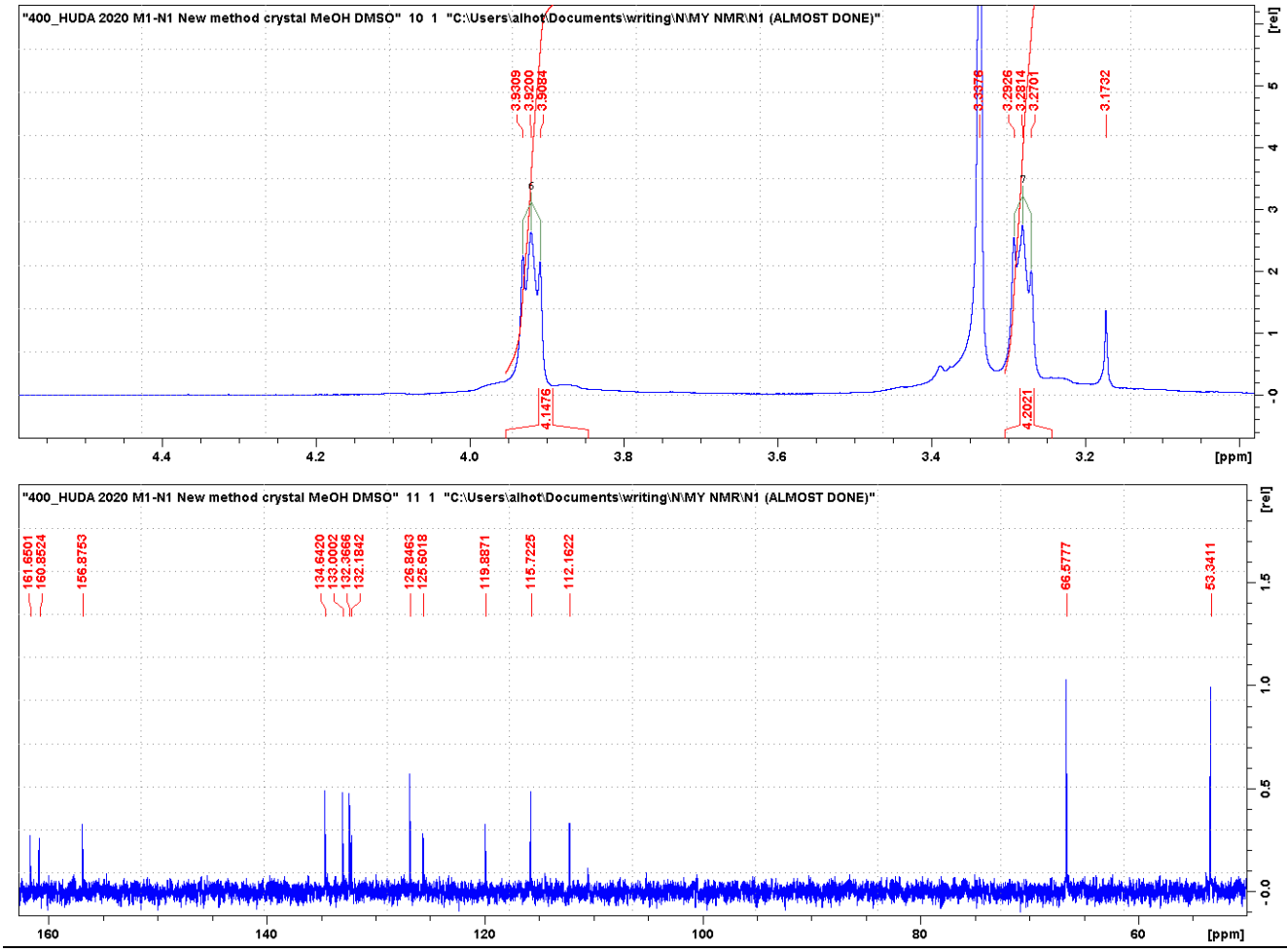

^{1}H NMR (400 MHz, DMSO): δ(ppm): 8.55 (dd, *J* =8.48 Hz, *J* = 0.96 Hz, 1H, Ar-CH), 8.50 (dd, *J* = 7.24 Hz, *J* = 0.96 Hz, 1H, Ar-CH), 8.43 (d, *J* = 8.12 Hz, 1H, Ar-CH), 7.85 (dd, *J* = 8.42 Hz, *J* = 7.38 Hz, 1H, Ar-CH), 7.38 (d, *J* = 8.20 Hz, 1H, Ar-CH), 3.92 (t, *J* = 4.50 Hz, 4H), 3.28 (t, *J* = 4.50 Hz, 4H). **^{13}C NMR (400 MHz, DMSO): δ(ppm):** δ 161.65, 160.85, 156.87, 134.64, 133.00, 132.36, 132.18, 126.84, 125.60, 119.88, 115.72, 112.16, 66.57, 53.34. **HR TOF MS ASAP+** calc for [$C_{16}H_{14}NO_4$] 284.0923 found 284.0924.

400_HUDA 2020 D1-A4-N1 new method CDCl3

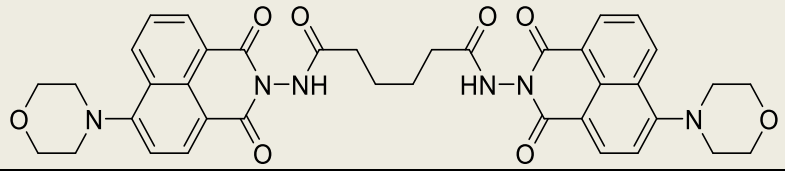

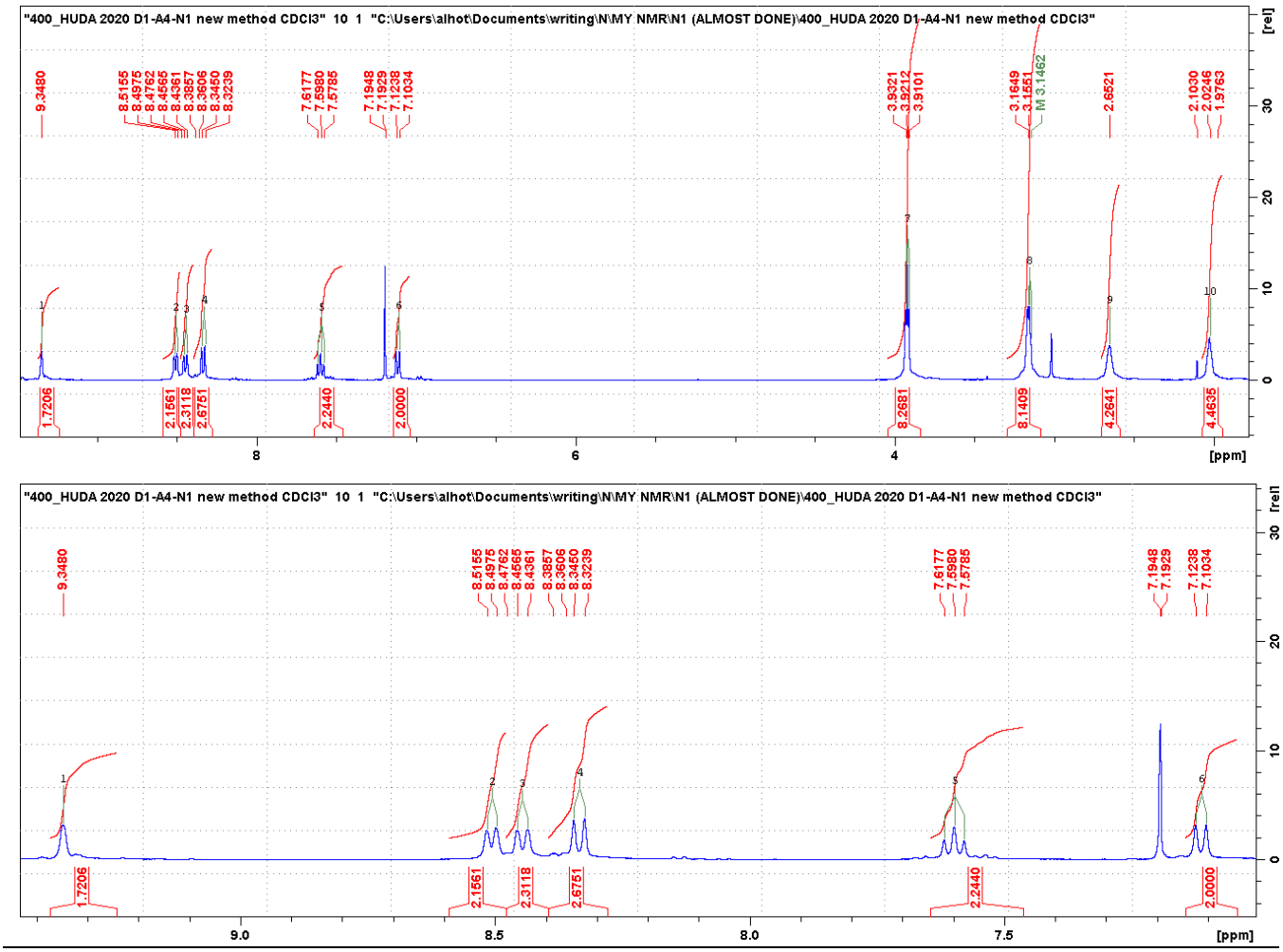

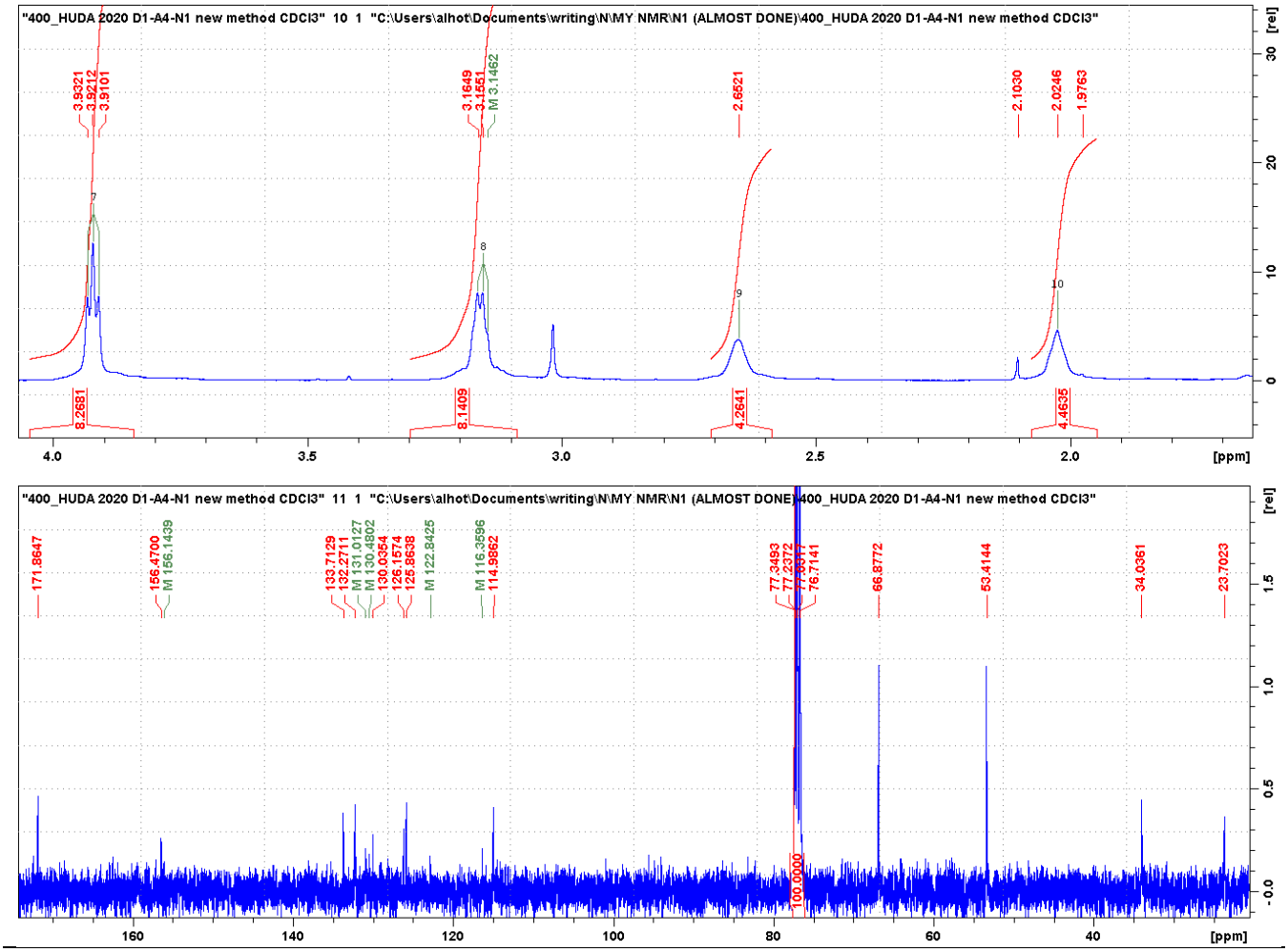

^{1}H NMR (400 MHz, $CDCl_3$): δ(ppm): 9.34 (s, 2H, NH), 8. 50 (d,2H, *J* = 7.20 Hz, Ar-CH), 8.44 (d, 2H, *J* = 8.16 Hz, Ar-CH), 8.33 (d, 2H, *J* = 8.44 Hz, Ar-CH), 7.59 (t, 2H, *J* = 7.84 Hz, Ar-CH), 7.11 (d, 2H, *J* = 8.16 Hz, Ar-CH), 3.92 (t, 8H, CH_2, *J* = 4.40 Hz, morpholine), 3.16 (br.signal, 8H,CH_2, morpholine), 2.65 (br.signal, 4H,CH_2), 2.02 (br.signal, 4H,CH_2). **^{13}C NMR (400 MHz, $CDCl_3$): δ(ppm):** 171.86, 156.47, 156.14, 133.71, 132.27, 131.01, 130.48, 130.03, 126.15, 125.86, 122.84, 116.35, 114.98, 66.87, 53.41, 34.03, 23.70. **LR TOF MS ES+** 705.27 (100%), **HR TOF MS ES+** calc for [$C_{38}H_{37}N_6O_8$] 705.2673 found 705.2672. (Yield= 73.23 %).

400_HUDA 2019 D1-N1-B CDCL3

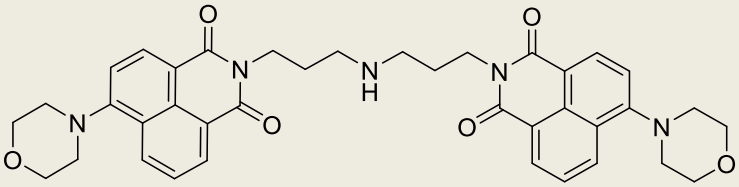

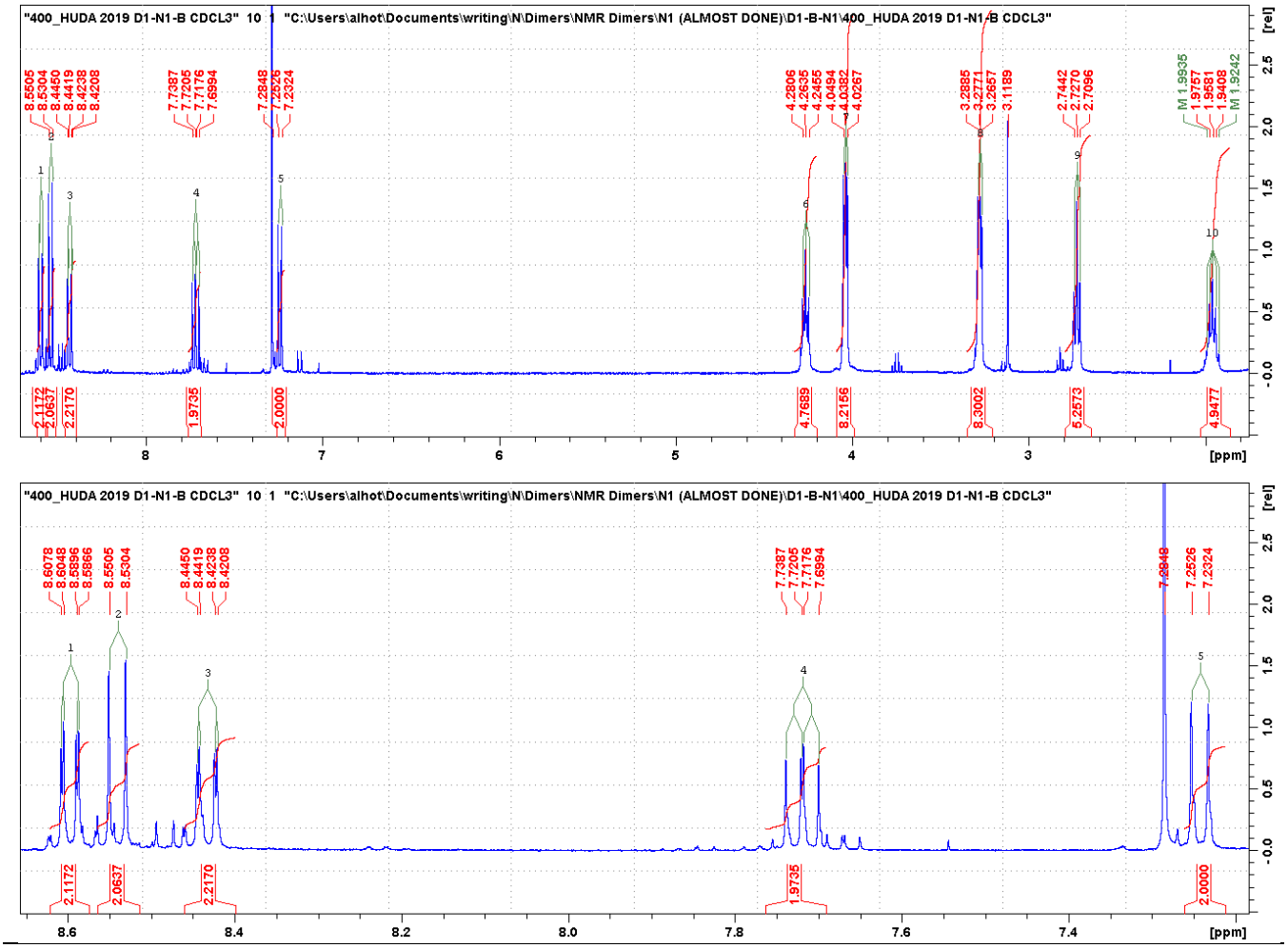

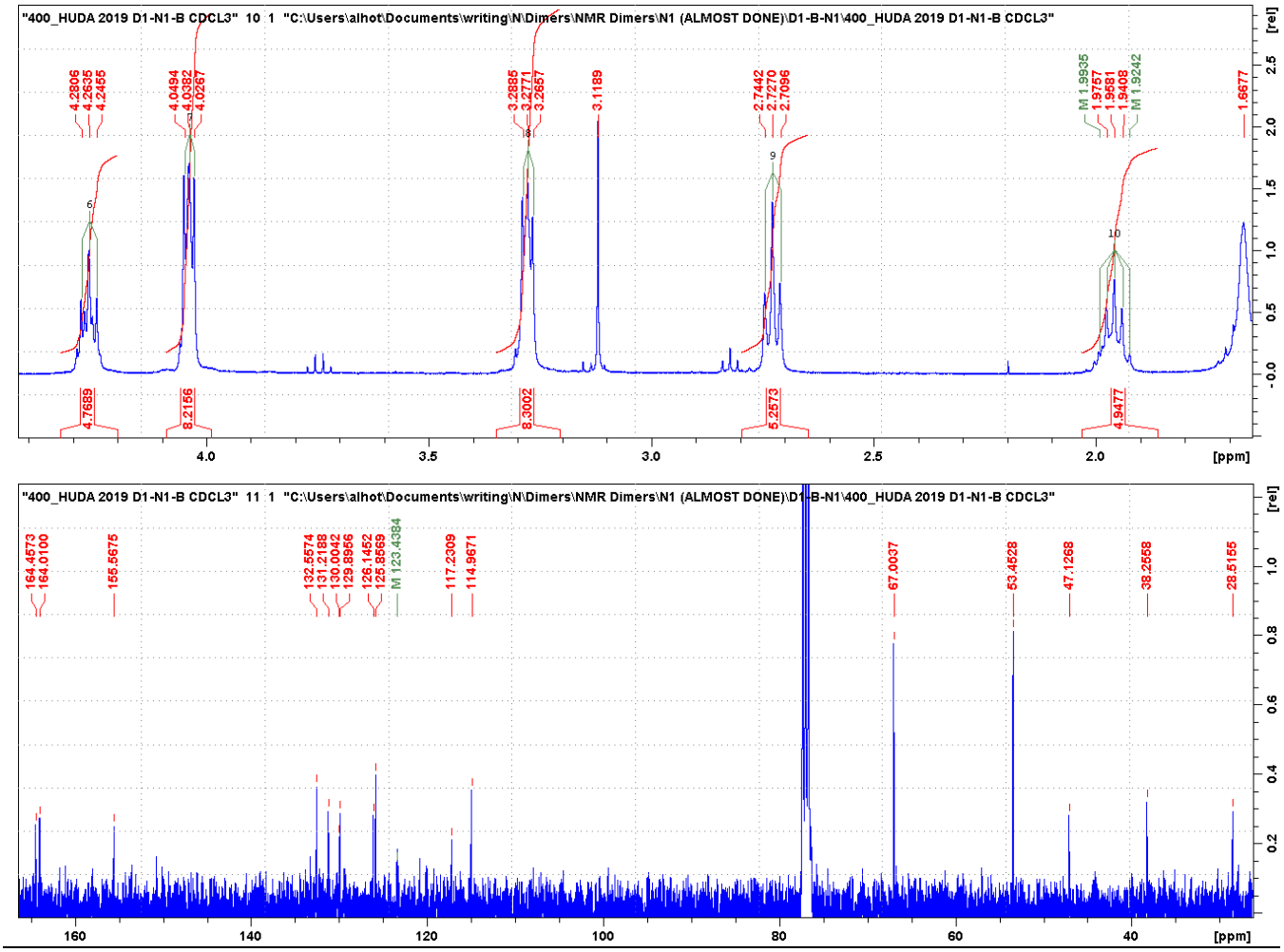

^{1}H NMR (400 MHz, $CDCl_3$): δ(ppm): 8. 59 (dd,2H, *J* = 7.28, *J* = 1.20 Hz, Ar-CH), 8.04 (d, 2H, *J* = 8.04 Hz, Ar-CH), 8.43 (dd, 2H, *J* = 8.46, *J*=1.22 Hz, Ar-CH), 7.71 (dd, 2H, *J* = 8.44, *J*=7.28 Hz, Ar-CH), 7.24 (d, 2H, *J* = 8.08 Hz, Ar-CH), 4.26 (t, 4H, *J*=7.02, CH_2), 4.03(t, 8H, *J*=4.54 Hz, CH_2, morpholine), 3.27 (t, *J*=4.56, 8H, CH_2, morpholine), 2.72 (t, *J*=6.92, 4H,CH_2), 1.95 (quint, *J*=6.98, 4H,CH_2). **^{13}C NMR (400 MHz, $CDCl_3$): δ(ppm):** 164.45, 164.01, 155.56, 132.55, 131.21, 130.00, 129.89, 126.14, 125.85, 117.23, 114.96, 67.00, 53.45, 47.12, 38.25, 28.51. **LR TOF MS ES+** 662.30 (100%), **HR TOF MS ES+** calc for [$C_{38}H_{40}N_5O_6$] 662.2979 found 662.3005.

Mass spectrum: NB_MS33561_HR_ES

400_HUDA 2020 D1-C-N1 new method 48h DMSO

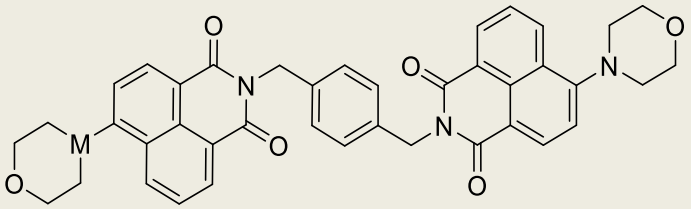

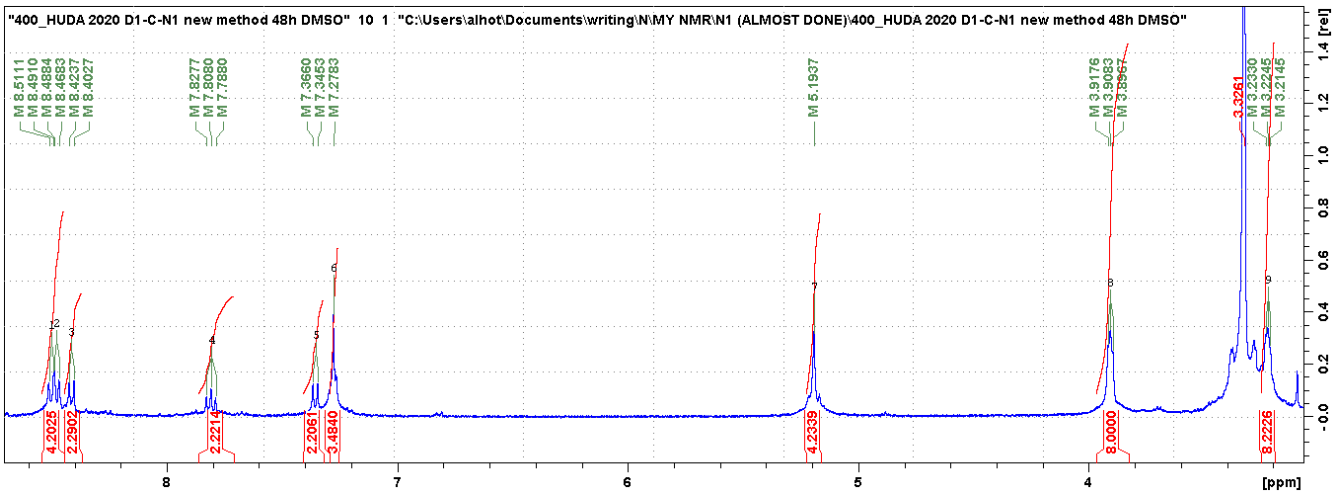

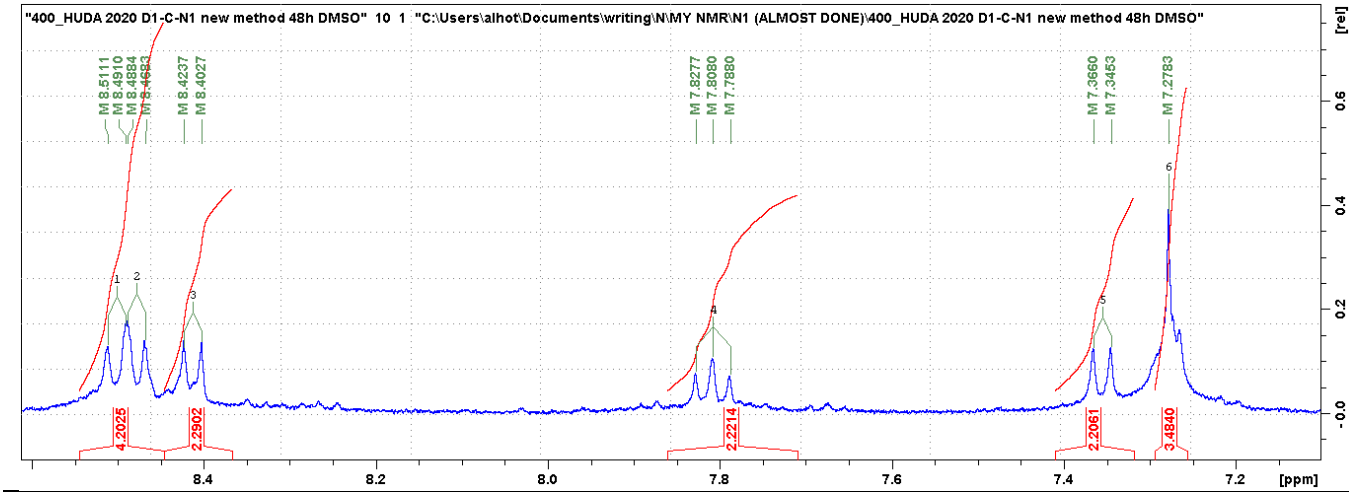

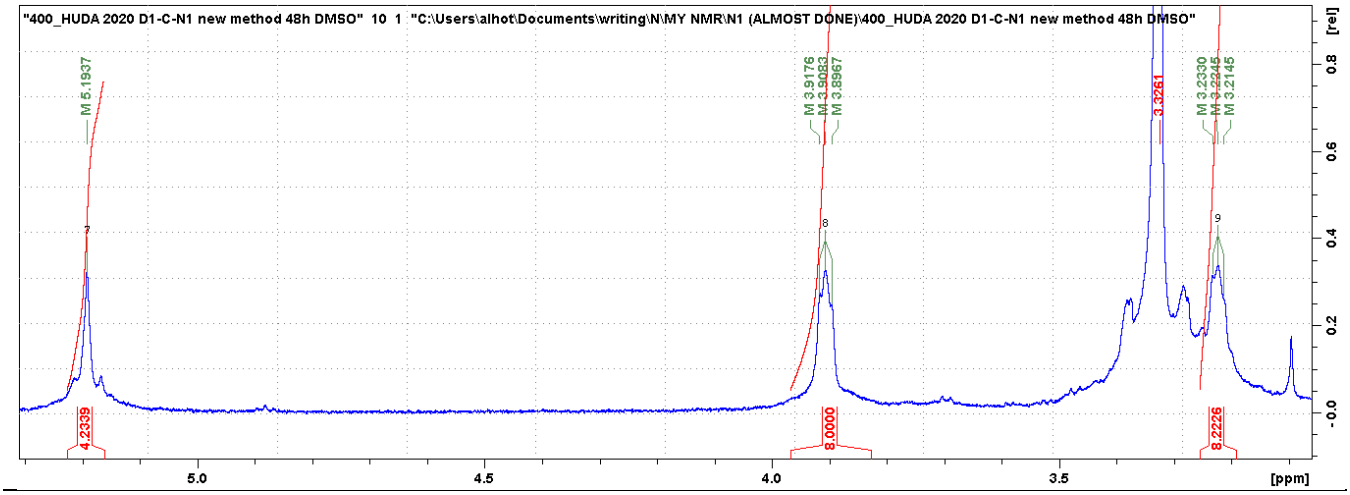

^{1}H NMR (400 MHz, $CDCl_3$): δ(ppm): 8. 50 (d, *J* = 8.04 Hz, 2H, Ar-CH), 8.47 (d, *J* = 8.04 Hz, 2H, Ar-CH), 8.41 (d, *J*=8.40, 2H,Ar-CH), 7.80 (t, *J*=7.94, 2H, Ar-CH), 7.34 (d, *J* = 8.28 Hz, 2H, Ar-CH), 7.27(s, 4H, Ar-CH), 5.19 (s, 4H, CH_2), 3.90 (t, *J*=4.18, 8H, CH_2), 3.32 (t, 3.70, *J*=3.70, 8H, CH_2). **HR TOF MS ES+** calc for [$C_{40}H_{35}N_4O_6$] 667.2557 found 667.2561.

400_HUDA 2020 D1-E-N1 new method CDCl3

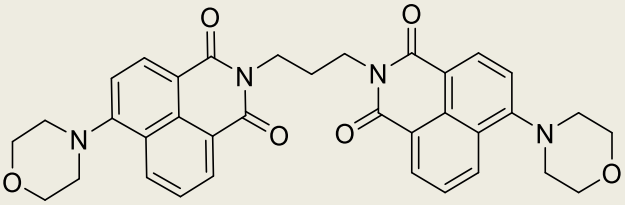

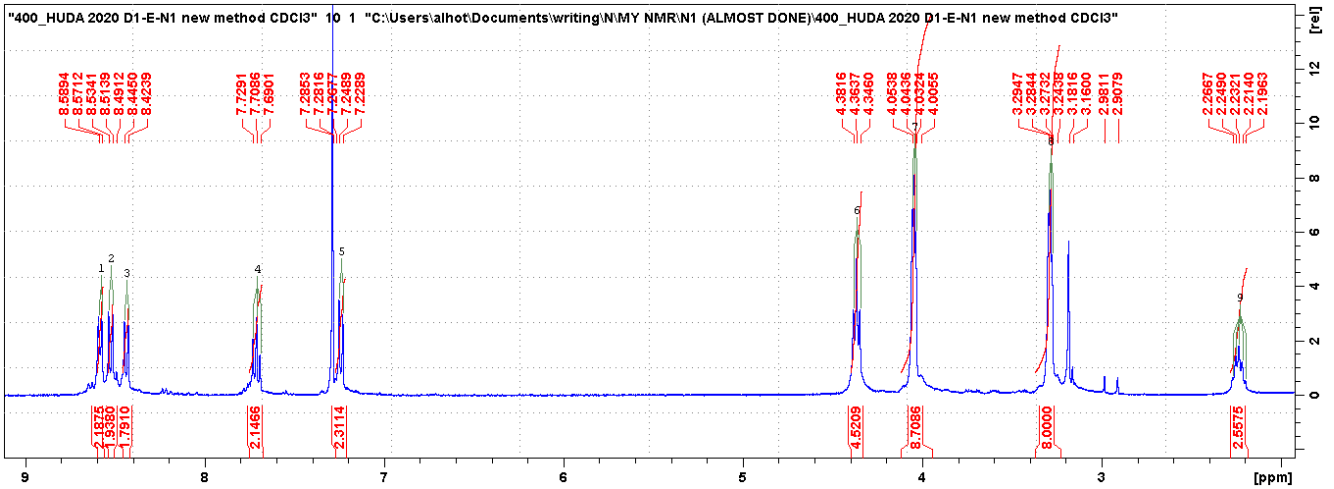

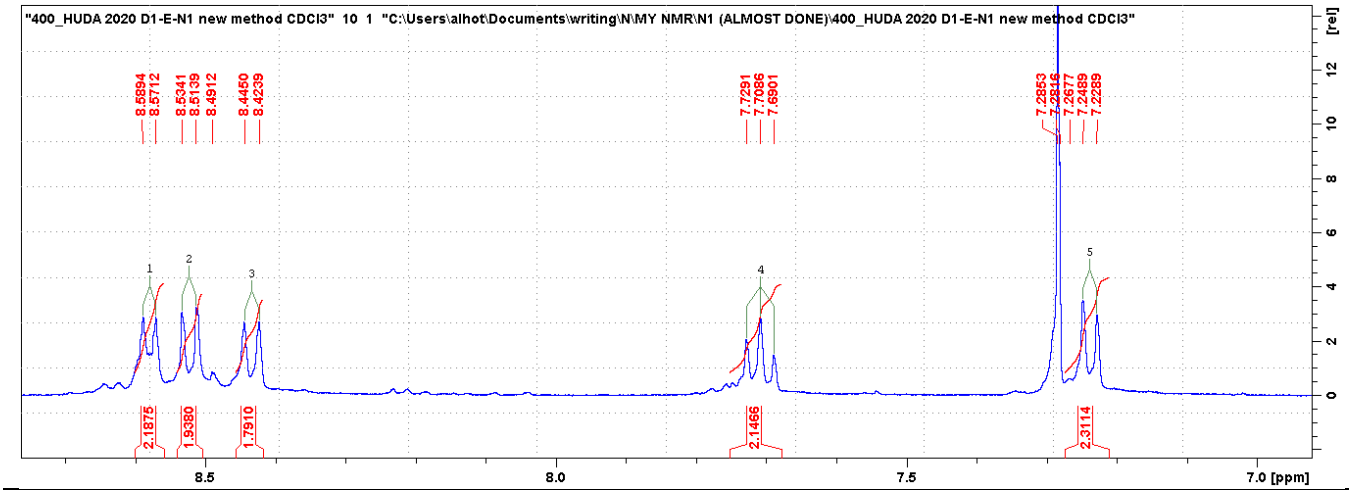

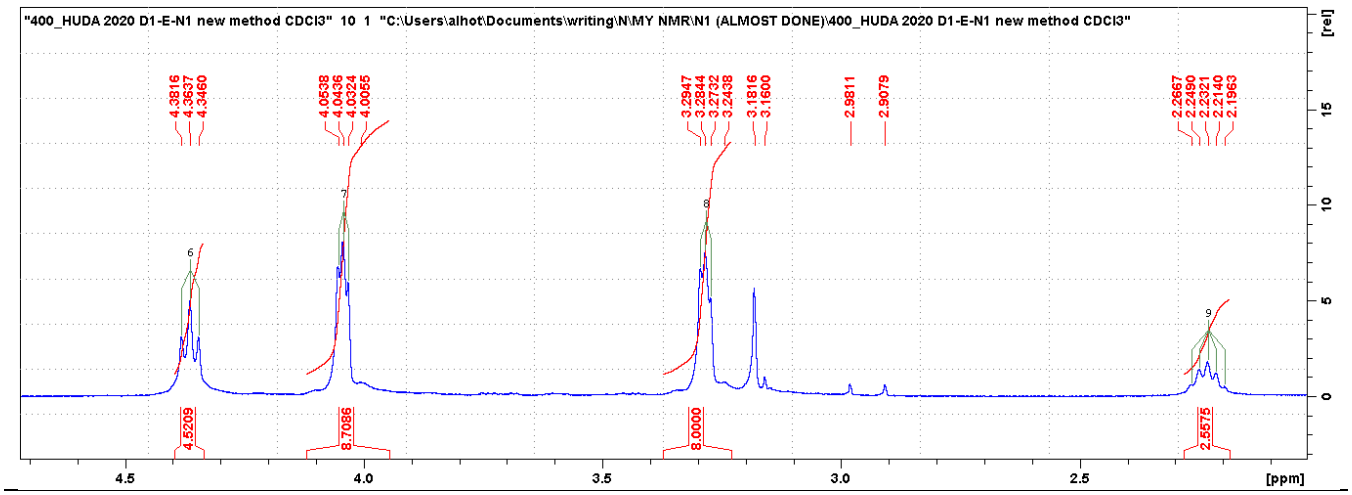

^{1}H NMR (400 MHz, $CDCl_3$): δ(ppm): 8.58 (d,2H, *J* = 7.28, Hz, Ar-CH), 8.52 (d, 2H, *J*=8.08 Hz, Ar-CH), 8.43(d, 2H, *J*=8.44, Ar-CH), 7.70(t, *J*=7.80, 2H, Ar-CH), 7.23 (t, 2H, *J* = 8.00 Hz, Ar-CH), 4.36 (t, J= 7.12, 4H, CH_2), 4.04 (t, 8H, *J*= 4.28, CH_2), 3.28 (t, *J*=4.30 Hz, 8H, CH_2), 2.23 (quint, J=7.04, 2H, CH_2). **HR TOF MS ASAP+** calc for [$C_{35}H_{33}N_4O_6$] 605.2400 found 605.2402.

400_HUDA 2020 D1-F-N1 new method CDCl3

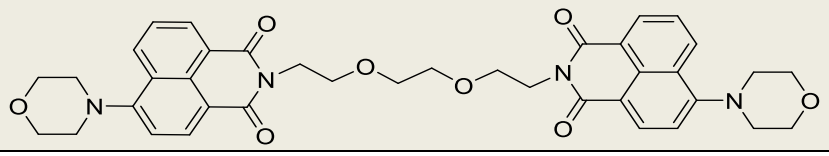

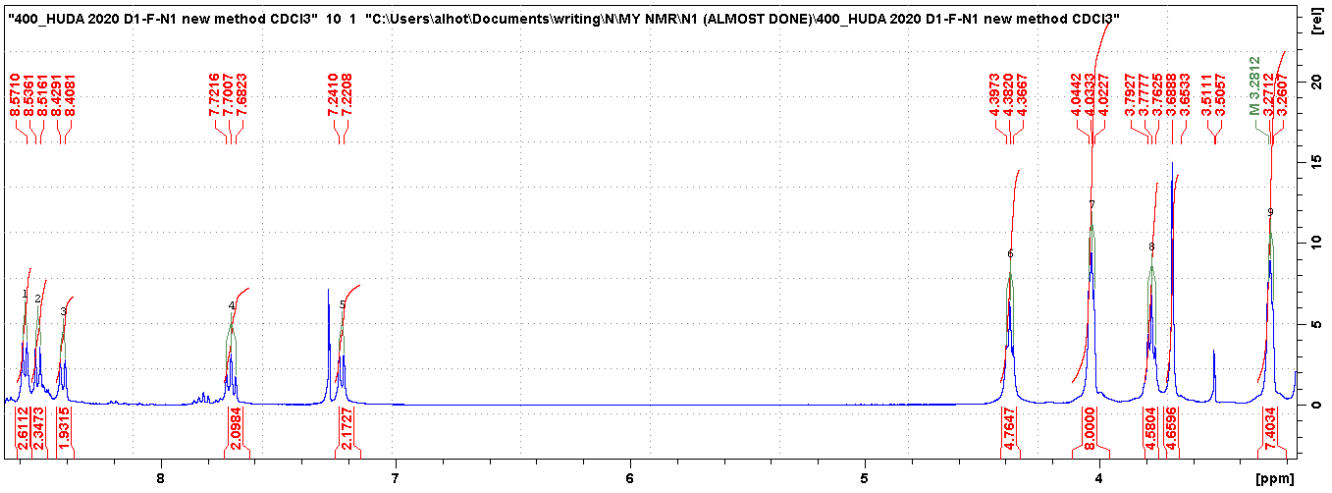

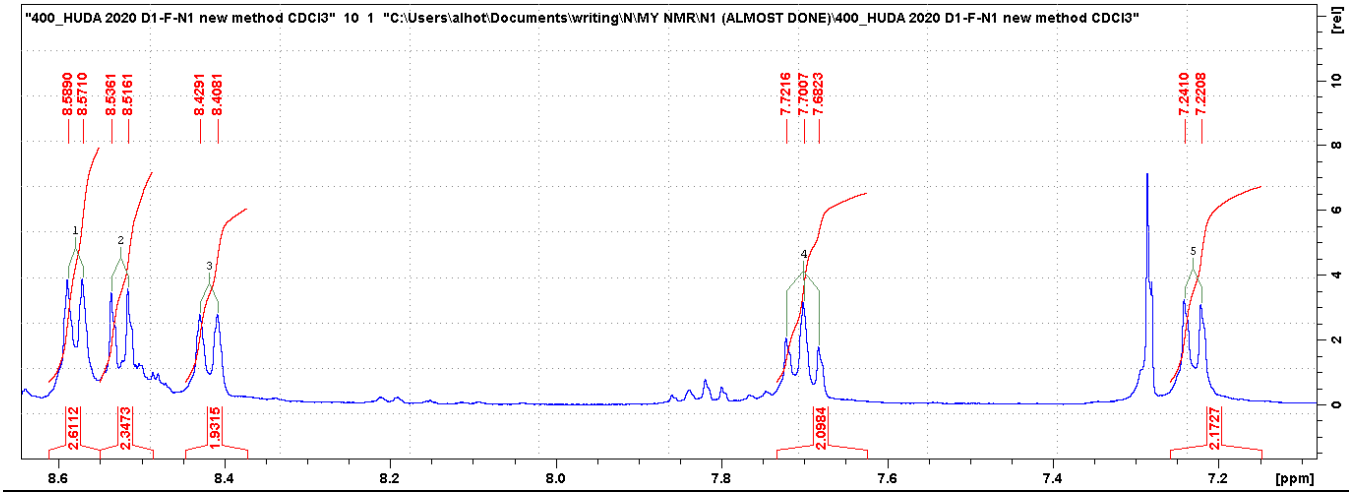

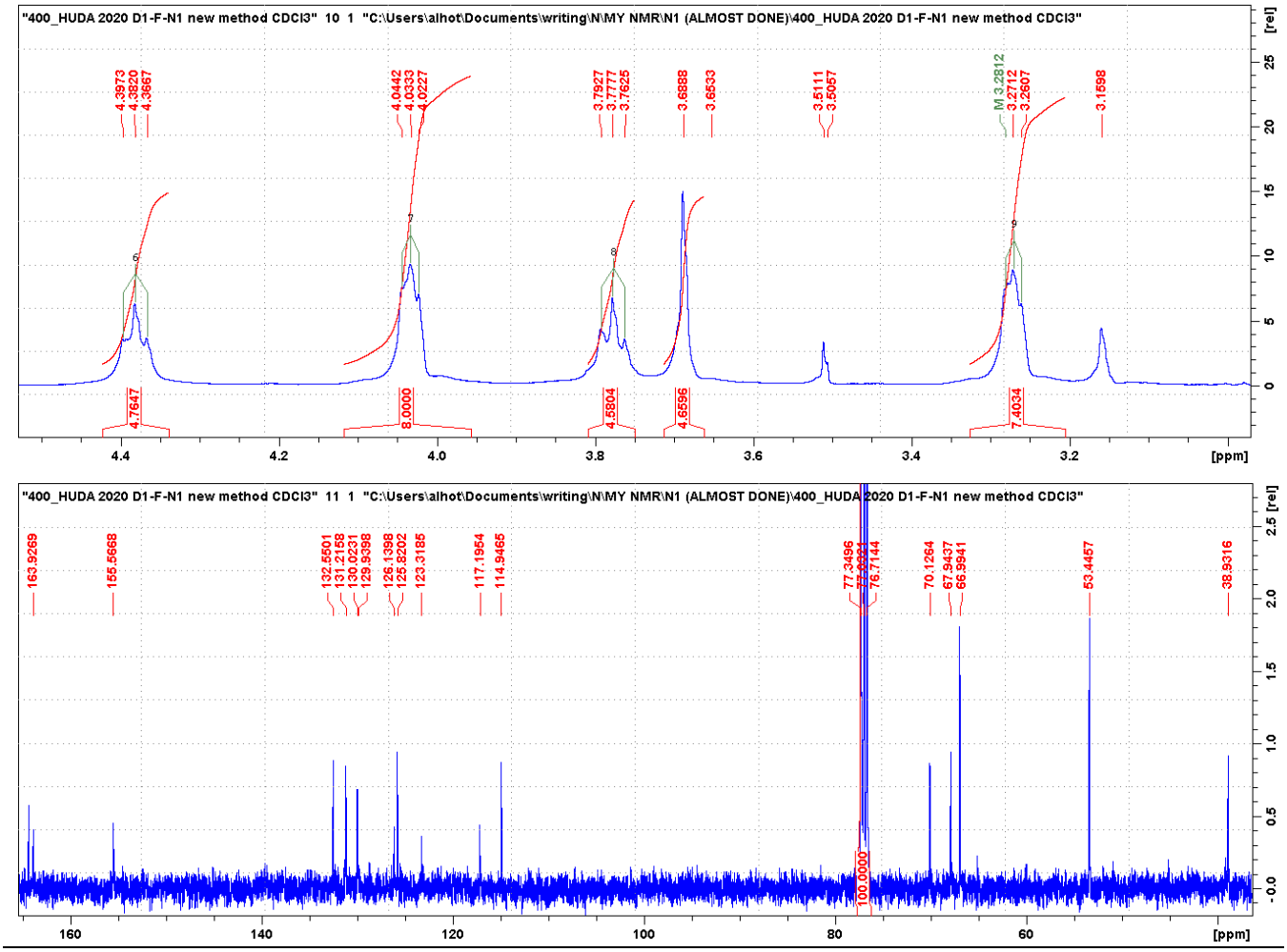

^{1}H NMR (400 MHz, $CDCl_3$): δ(ppm): 8.58 (d, 2H, *J* =7.20 Hz, Ar-CH), 8.52 (d, 2H, *J* = 8.00 Hz, Ar-CH), 8.41 (d, 2H, *J* =8.40 Hz, Ar-CH), 7.70 (t, 2H, *J* = 7.86 Hz, Ar-CH), 7.23 (d, 2H, *J* = 8.08 Hz, Ar-CH), 4.38 (t, 4H, *J*=6.12 Hz, CH_2), 4.03 (t,8H, *J*=4.30 Hz, CH_2), 3.77 (t, 4H, *J*=6.04 Hz, CH_2), 3.68 (s, 4H, CH_2), 3.27 (t, 8H, *J*=4.10 Hz, CH_2). **^{13}C NMR (400 MHz, $CDCl_3$): δ(ppm):** 164.39, 163.92, 155.56, 132.55, 131.21, 130.02, 129.93, 126.13, 125.82, 123.31, 117.19, 114.94, 70.12, 67.94, 66.99, 53.44, 38.93. **HR TOF MS ASAP+** calc for [$C_{38}H_{39}N_4O_8$] 679.2768 found 679.2767.

400_HUDA 2020 M1-N2 new methode DMSO

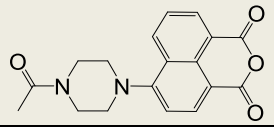

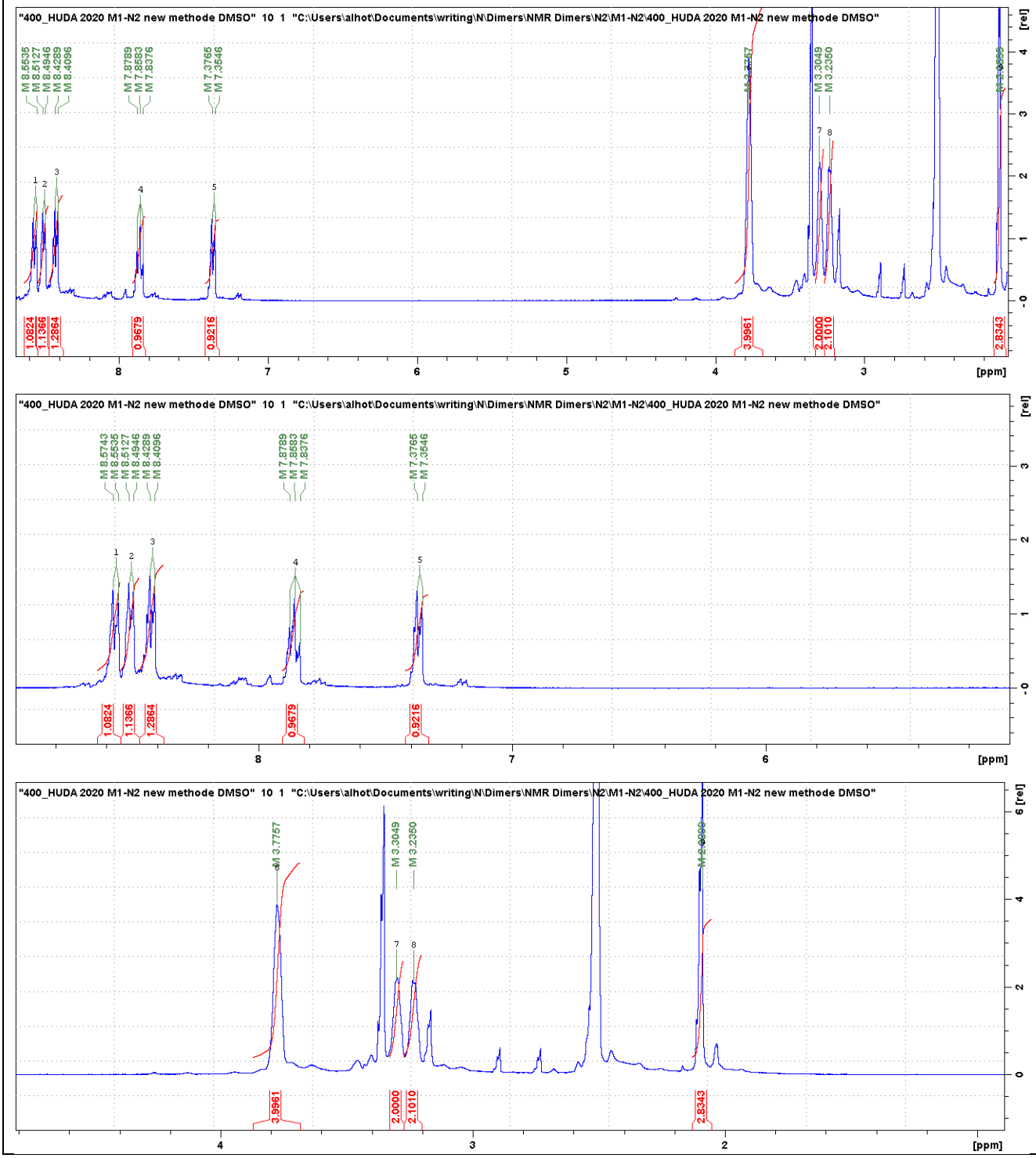

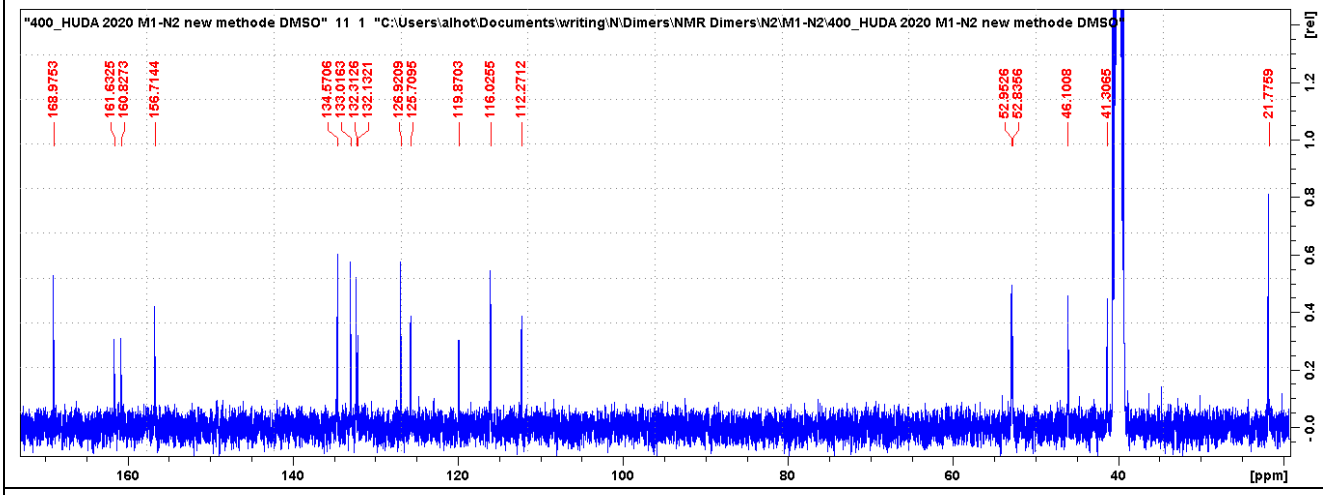

^{1}H NMR (400 MHz, DMSO): δ(ppm): 8.55 (d, 2H, *J* =8.32 Hz, Ar-CH), 8.50 (d, 2H, *J* = 7.24 Hz, Ar-CH), 8.41 (d, 2H, *J* =7.72 Hz, Ar-CH), 7.85 (t, 2H, *J* = 8.26 Hz, Ar-CH), 7.36 (d, 2H, *J* = 8.76 Hz, Ar-CH), 3.77 (br.s, 4H, CH_2), 3.30 (br.s, 2H, CH_2), 3.23 (br.s, 2H, CH_2), 2.08 (s, 3H, CH_3). **^{13}C NMR (400 MHz, DMSO): δ(ppm):** 168.97, 161.63, 160.82, 156.71, 134.57, 133.01, 132.31, 132.13, 126.92, 125.70, 119.87, 116.02, 112.27, 52.95, 52.83, 46.10, 41.30, 21.77. **TOF MS ES+** expected mass 324.11, found 325.12

500_HUDA 2021 D1-E-N2 2nd crude 2nd col col 5-7 CDCl3\ Acetone and DCM were observed

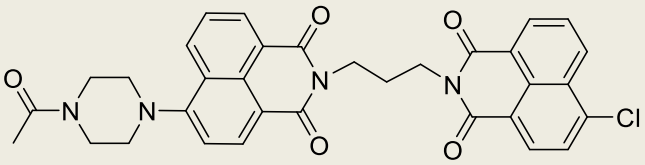

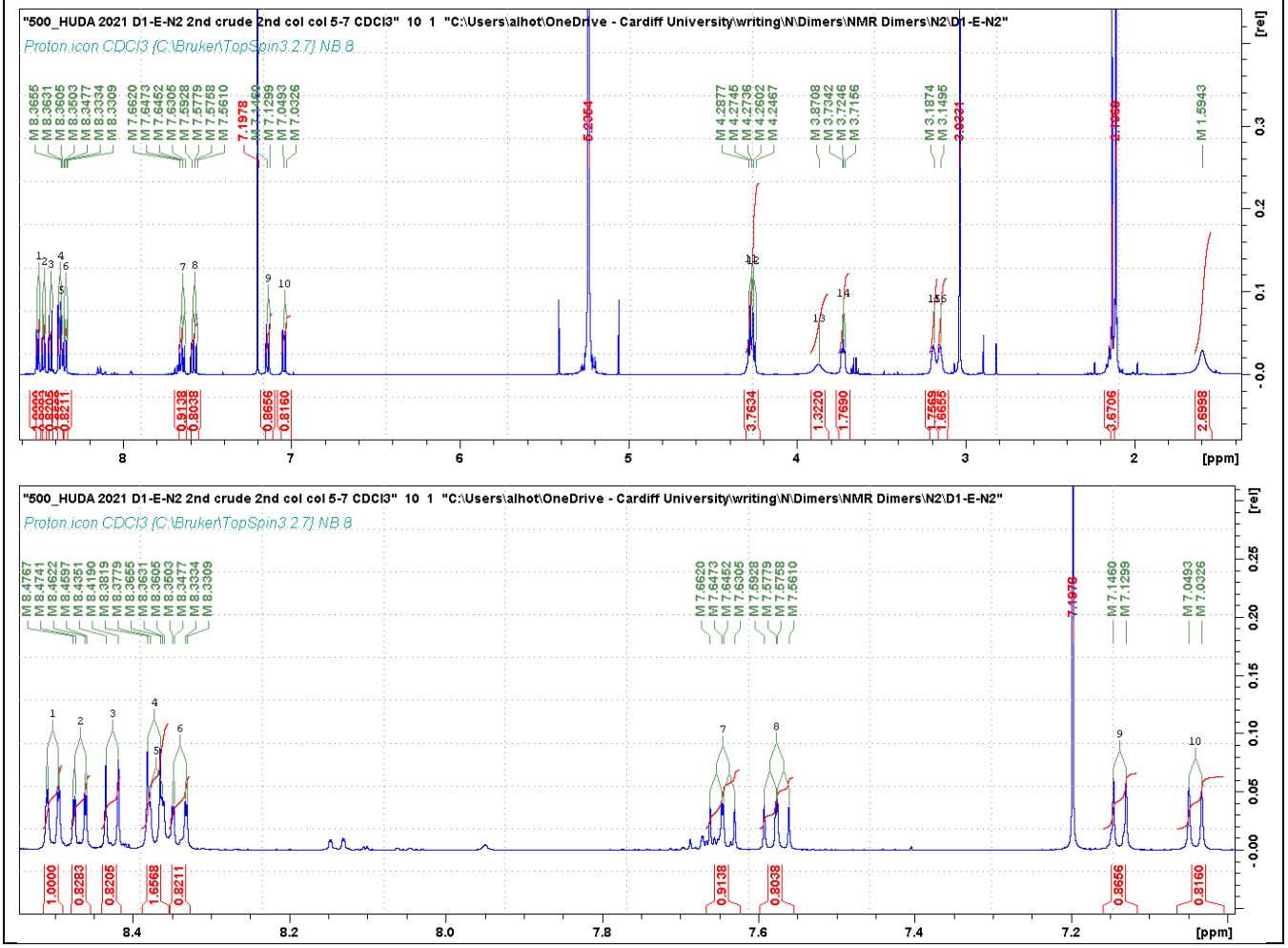

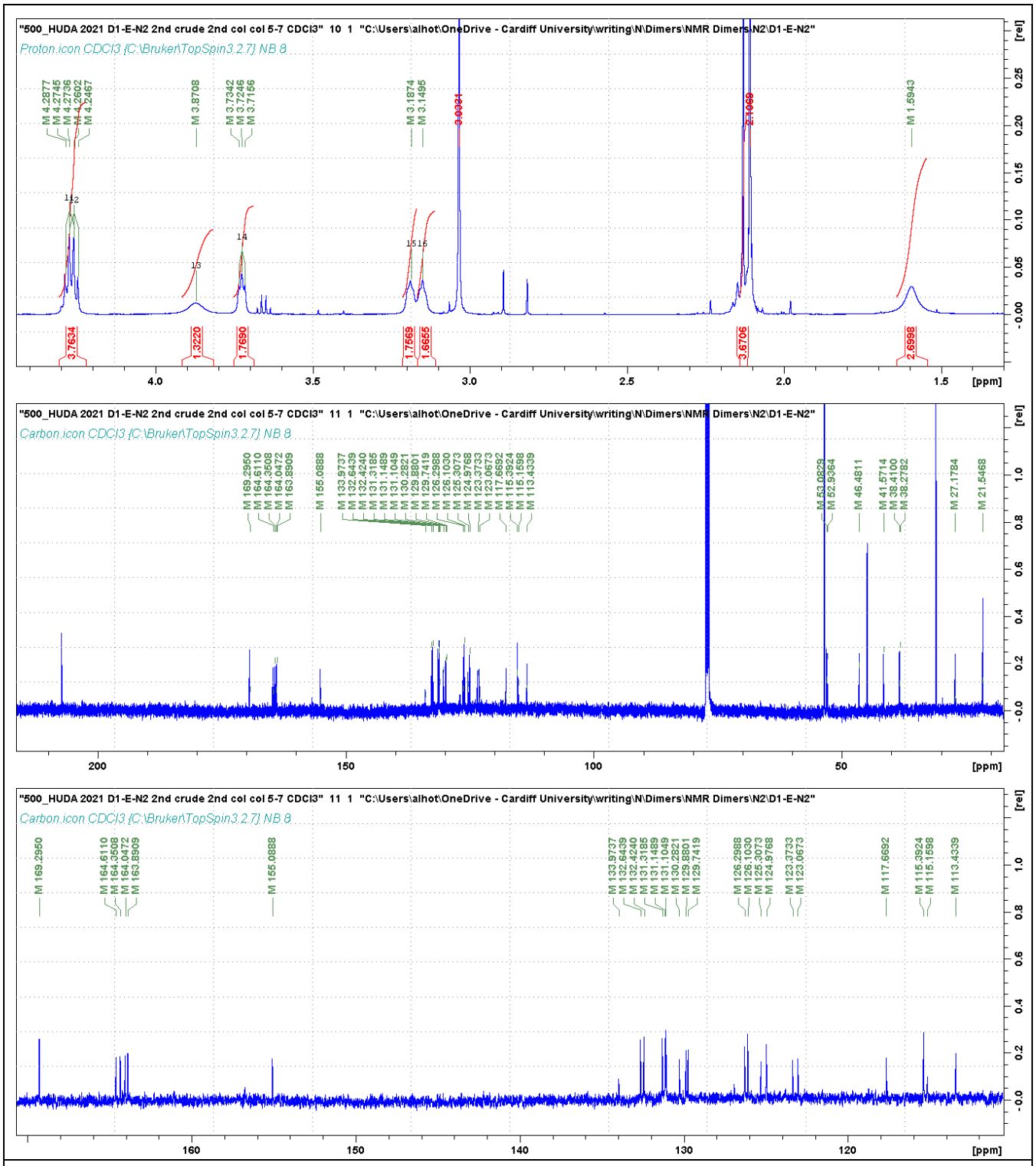

^{1}H NMR (500 MHz, DMSO): δ(ppm): 8.50 (dd, 1H, *J* =7.25 Hz, *J* = 0.95 Hz, Ar-CH), 8.46 (dd, 2H, *J* = 7.22 Hz, *J*=1.27 Hz, Ar-CH),), 8.41 (d, 1H, *J* = 8.05 Hz, Ar-CH), 8.37 (d, 1H, *J* = 8.30 Hz, Ar-CH), 8.37 (d, 1H, *J*=7.40, Ar-CH), 8.34 (dd, 1H, *J* = 8.42 Hz, *J*=1.27 Hz, Ar-CH), 7.64 (dd, 2H, *J* = 8.40, *J*= 7.35 Hz, Ar-CH), 7.57 (dd, 2H, *J* = 8.47 Hz, *J*= 7.42, Ar-CH), 7.13 (d, 1H, *J* = 8.05 Hz, Ar-CH), 7.03 (d, 1H, *J*=8.35, Ar-CH), 4.27 (t, *J*=6.87, 2H, CH_2), 4.26 (d, 2H, J=6.72, CH_2), 3.87 (br.s, 2H, CH_2), 3.72 (t, *J*=4.65, 2H, CH_2), 3.18 (br.s, 2H, CH_2), 3.14 (br.s, 2H, CH_2), 2.12 (s, 3H,

CH_3), 1.59(br.s, 2H, CH_2). **^{13}C NMR (500 MHz, DMSO): δ(ppm):** 169.29, 164.61, 164.35, 164.04, 163.89, 155.08, 133.97, 132.64, 132.42, 131.31, 131.14, 131.10, 130.28, 129.88, 129.74, 126.29, 126.10, 125.30, 124.97, 123.37, 123.06, 117.66, 115.39, 115.15, 113.43, 53.08, 52.93, 46.48, 41.57, 38.41, 38.27, 27.17, 21.54. **HR TOF MS ES+** calc for [$C_{33}H_{29}N_4O_5$] 561.2138 found 561.2129.

500_HUDA 2021 D1-E-N2 2nd crude 2nd col col 30-45 CDCl3\ Ethanol and DCM were observed (eluent)

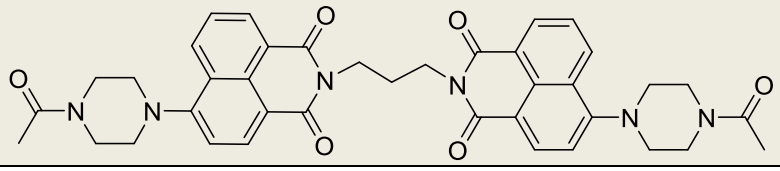

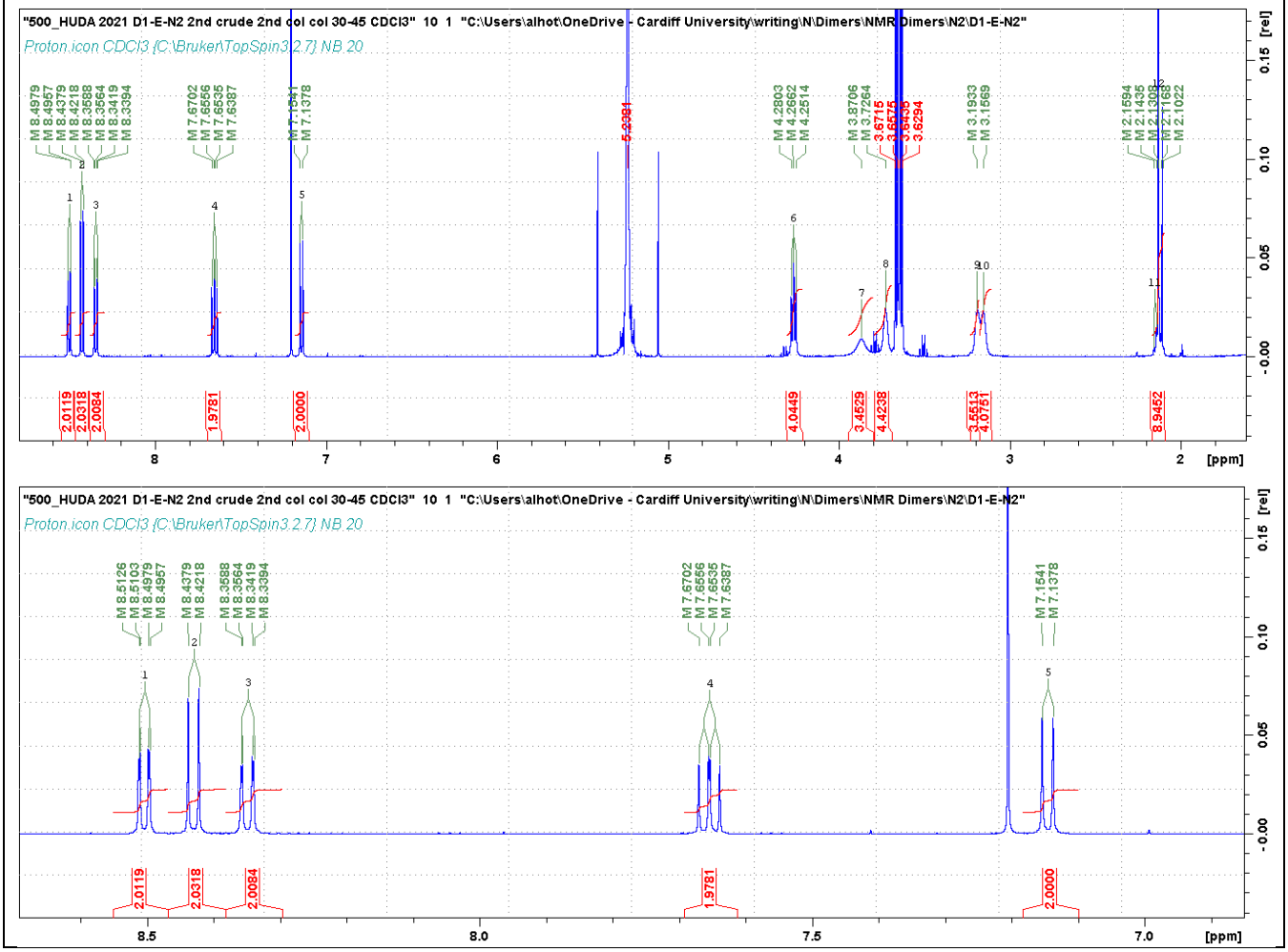

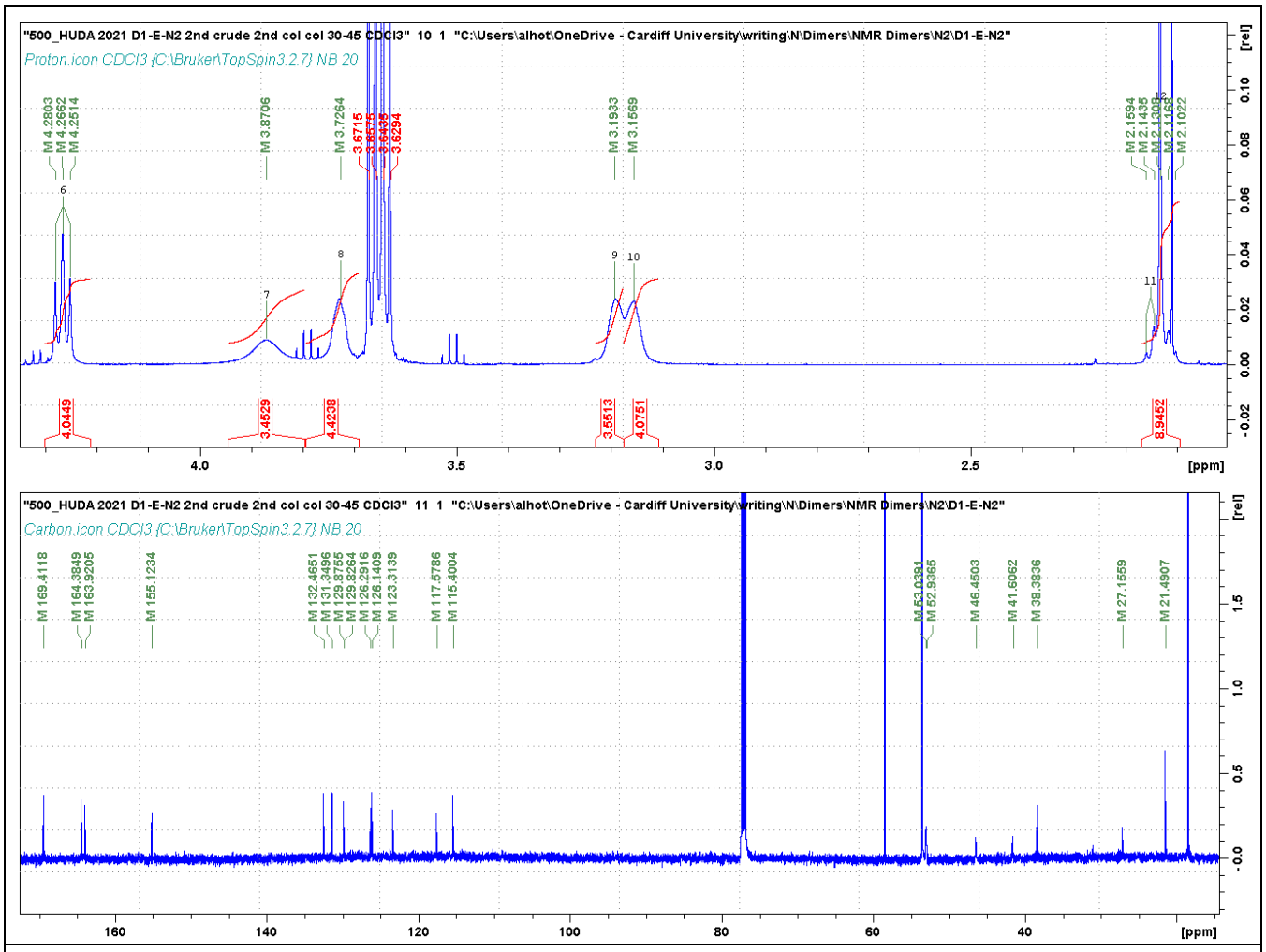

^{1}H NMR (500 MHz, DMSO): δ(ppm): 8.49 (dd, 2H, *J* =7.32 Hz, *J* = 1.12 Hz Ar-CH), 8.43 (d, 2H, *J* = 8.05 Hz, Ar-CH), 8.34 (dd, 2H, *J* = 8.47Hz, *J*=1.22 Hz, Ar-CH), 7.65 (dd, 2H, *J* = 8.40, *J*= 7.35 Hz, Ar-CH), 7.14 (d, 2H, *J* = 8.15 Hz, Ar-CH), 4.26(t, *J*=7.22, 4H, CH_2), 3.87 (br.s, 4H, CH_2), 3.72 (br.s, 4H, CH_2), 3.19 (s, 4H, CH_2), 3.15 (br.s, 4H, CH_2), 2.12 (s, 6H, CH_3), 2.12(quin, 2H, *J*=7.95, CH_2). **^{13}C NMR (500 MHz, DMSO): δ(ppm):** 169.41, 164.38, 163.92, 155.12, 132.46, 131.34, 129.87, 129.82, 126.29, 126.14, 123.31, 117.57, 115.40, 53.03, 52.93, 46.45, 41.60, 38.38, 27.15, 21.49. **HR TOF MS ES+** calc for [$C_{39}H_{39}N_6O_6$] 687.2931 found 687.2960

500_HUDA 2021 D1-F-N2 DMF 72h MeOH col 7-9 CHCl3

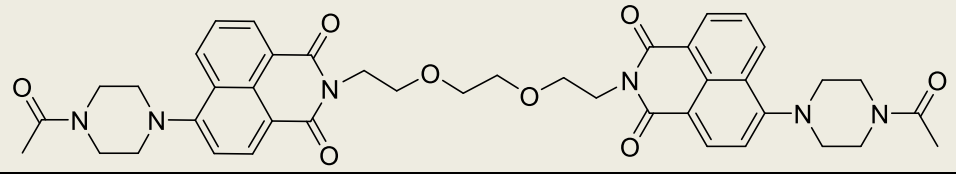

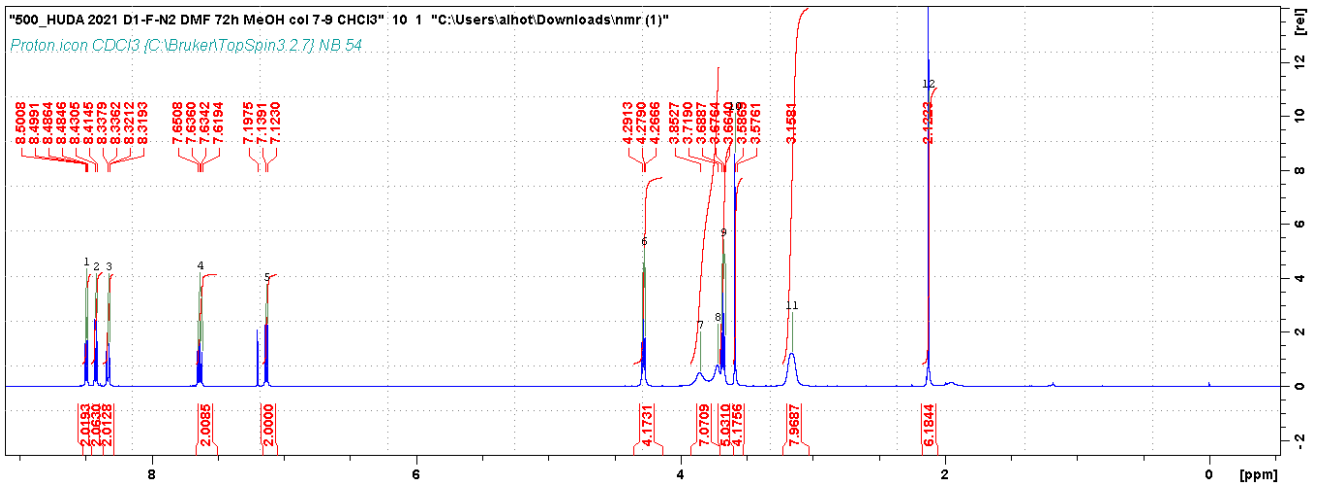

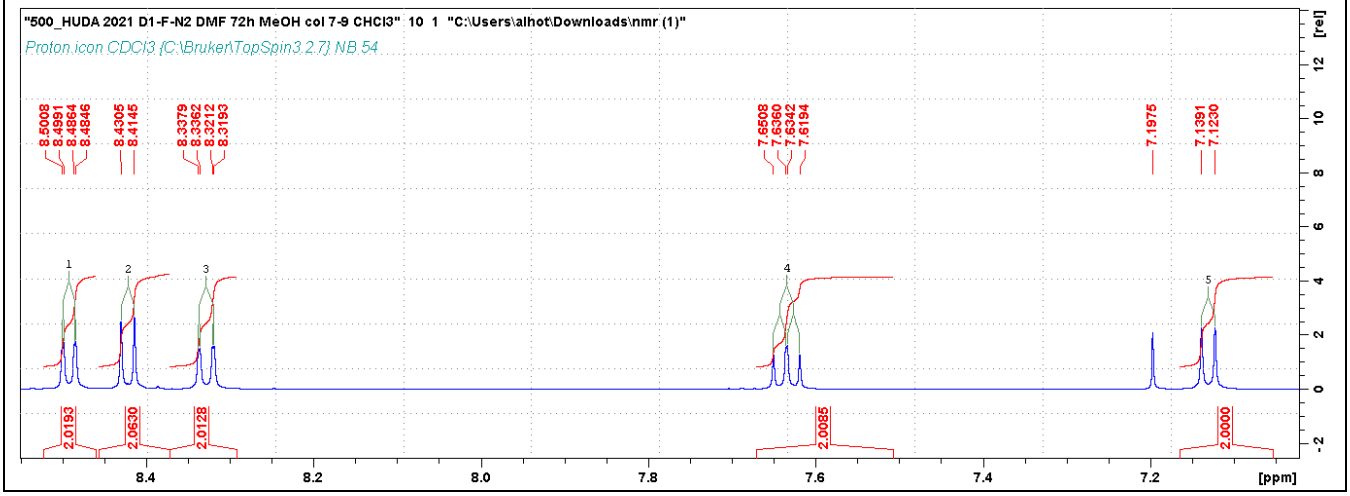

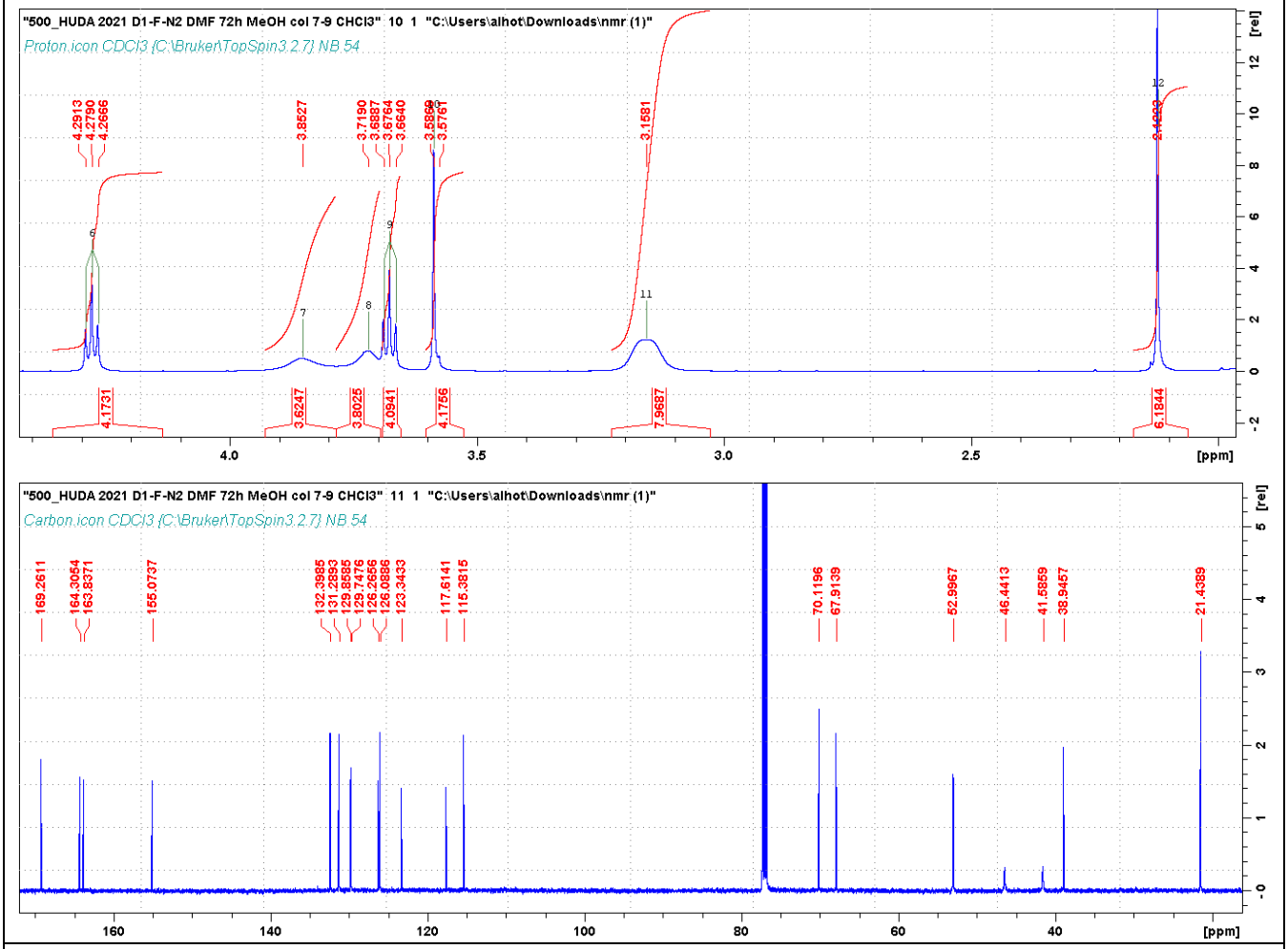

^{1}H NMR (500 MHz, DMSO): δ(ppm): 8.49 (dd, 2H, *J* =7.22 Hz, *J* = 0.87 Hz Ar-CH), 8.42 (d, 2H, *J* = 8.00 Hz, Ar-CH), 8.32 (dd, 2H, *J* = 8.40Hz, *J*=0.90 Hz, Ar-CH), 7.63 (dd, 2H, *J* = 8.30, *J*= 7.40 Hz, Ar-CH), 7.12 (d, 2H, *J* = 8.05 Hz, Ar-CH), 4.27(t, *J*=6.17, 4H, CH_2), 3.85 (br.s, 4H, CH_2), 3.71 (br.s, 4H, CH_2), 3.67(t, *J*=6.17, 4H, CH_2), 3.58 (s, 4H, CH_2), 3.15 (br.s, 8H, CH_2), 2.12 (s, 6H, CH_3). **^{13}C NMR (500 MHz, DMSO): δ(ppm):** 169.26, 164.30, 163.83, 155.07, 132.39, 131.28, 129.85, 129.74, 126.26, 126.08, 123.34, 117.61, 115.38, 70.11, 67.91, 52.99(2C), 46.44, 41.58, 38.94, 21.43. **HR TOF MS ES+** calc for[$C_{42}H_{45}N_6O_8$] 761.3299 found 761.3333.

500_HUDA 2021 D1-F-N2 72h DMF MeOH col 4 CDCl3

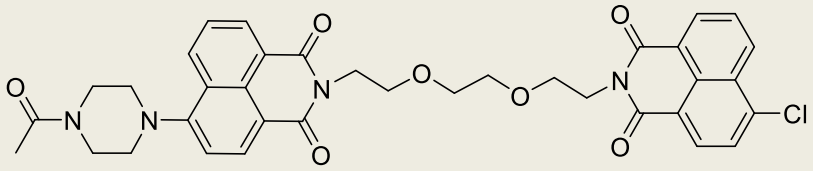

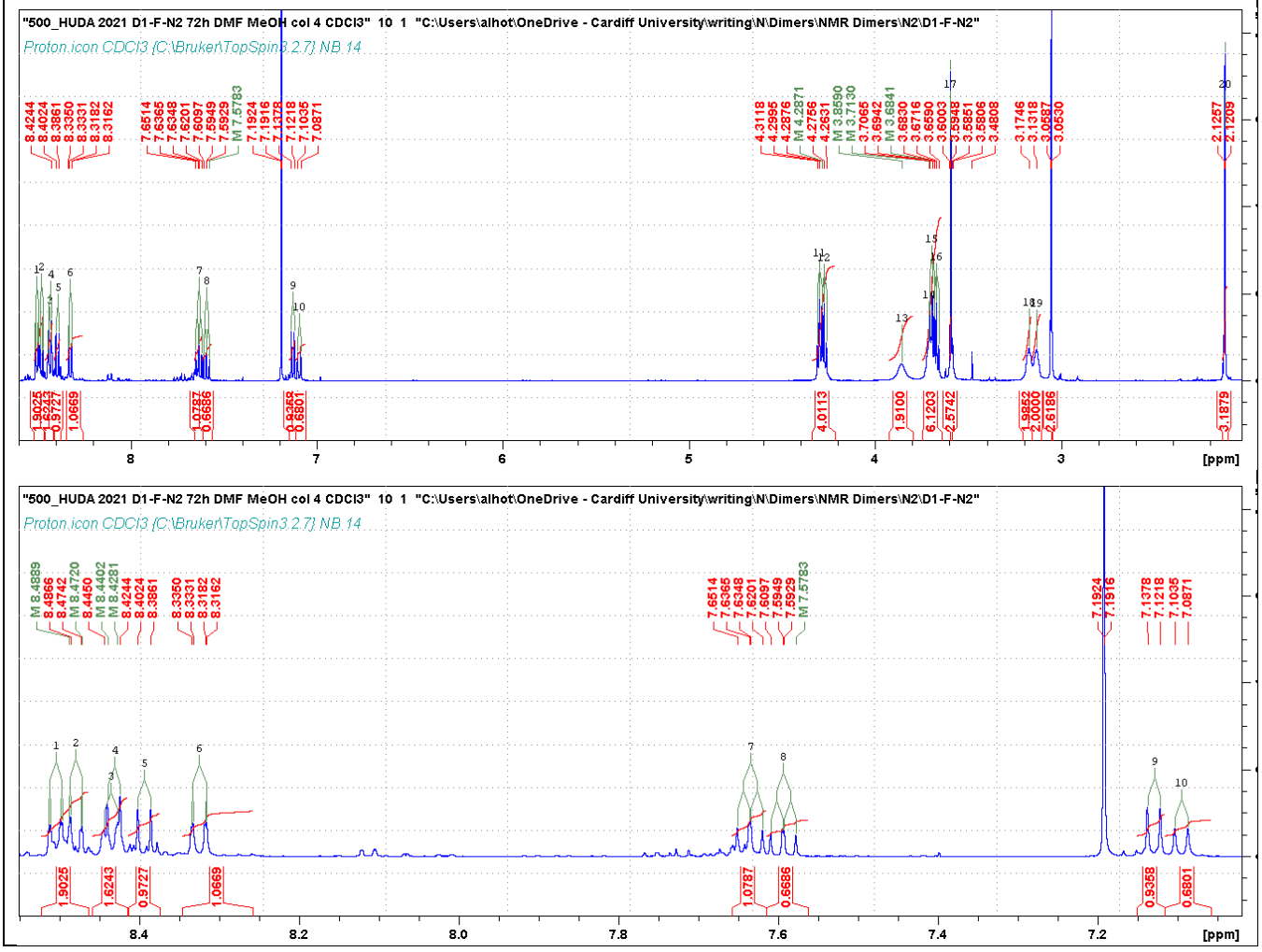

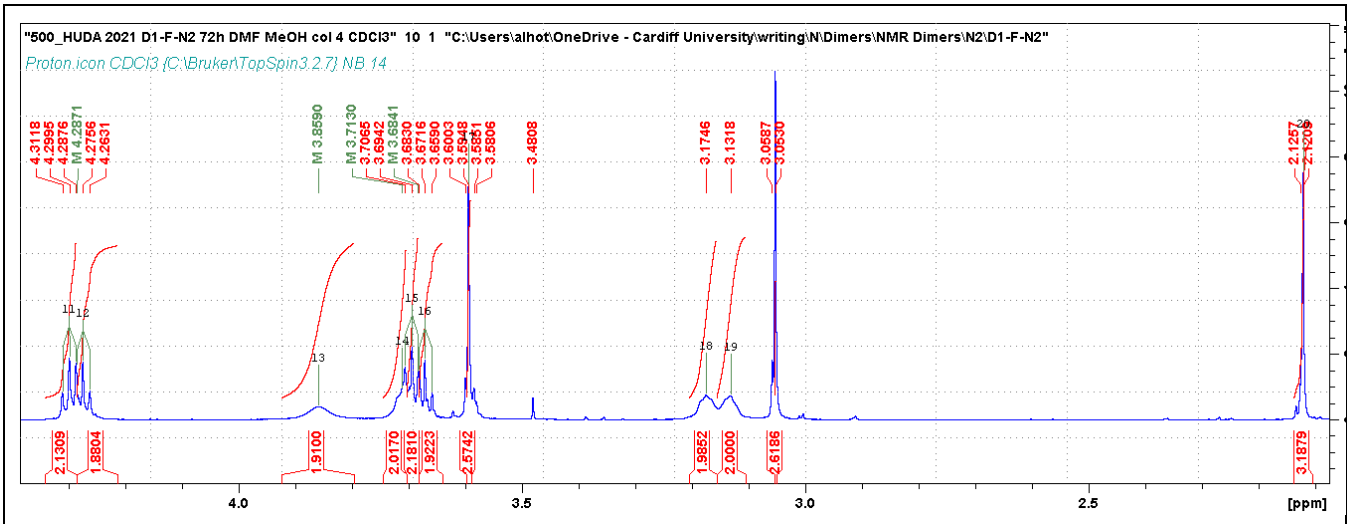

^{1}H NMR (500 MHz, DMSO): δ(ppm): 8.50 (dd, 1H, *J* =7.32 Hz, *J* = 1.12 Hz Ar-CH), 8.48 (dd, 1H, *J* =7.32 Hz, *J* = 1.12 Hz Ar-CH), 8.43 (d, 1H, *J* = 9.00 Hz, Ar-CH), 8.43 (d, 1H, *J* = 7.90 Hz, Ar-CH), 8.39 (d, 1H, *J* = 8.15 Hz, Ar-CH), 8.32 (dd, 1H, *J* = 8.42Hz, *J*=0.97 Hz, Ar-CH), 7.63 (dd, 1H, *J* = 8.25, *J*= 7.40 Hz, Ar-CH), 7.59 (dd, 1H, *J* = 8.35, *J*= 7.35 Hz, Ar-CH), 7.13 (d, 1H, *J* = 8.00 Hz, Ar-CH), 7.09 (d, 1H, *J* = 8.20 Hz, Ar-CH), 4.29 (t, *J*=6.05, 2H, CH_2), 4.27(t, *J*=6.00, 2H, CH_2), 3.85 (br.s, 2H, CH_2), 3.71 (br.s, 2H, CH_2), 3.69(t, *J*=5.60, 2H, CH_2), 3.67 (t, *J*=6.00, 2H, CH_2), 3.59 (s, 2H, CH_2), 3.17 (br.s, 2H, CH_2), 3.13 (br.s, 2H, CH_2), 3.05 (s, 2H, CH_2), 2.12 (s, 3H, CH_3). **HR TOF MS ES+** calc for [$C_{36}H_{34}N_4O_7Cl$] calc 669.2116 found 669.2131

400_HUDA 2020 M1-SU1 NO HCL DMSO

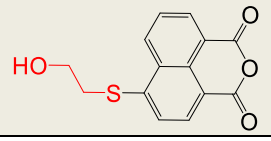

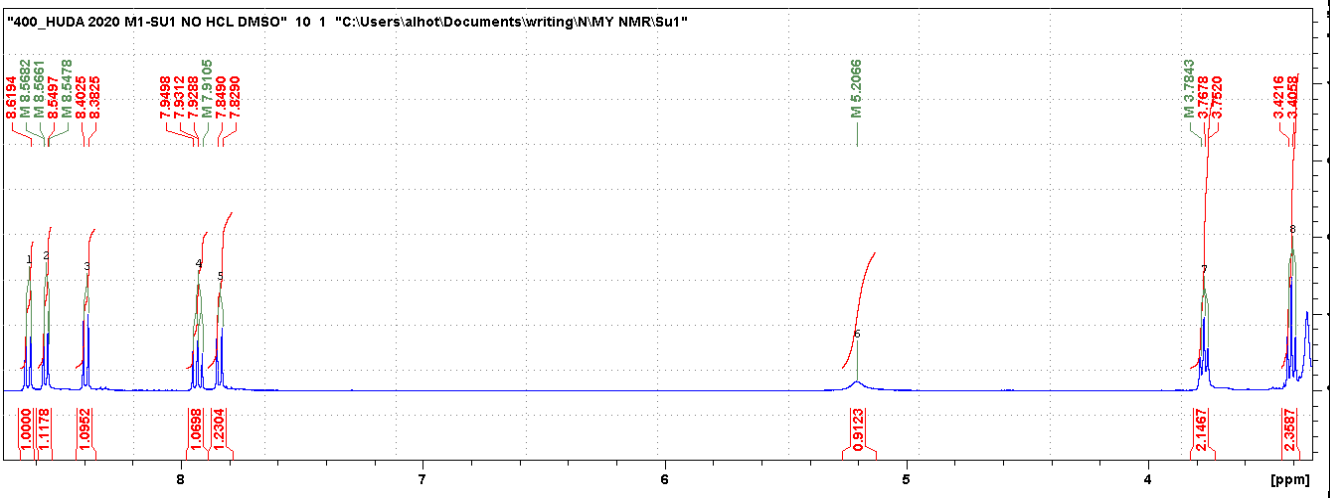

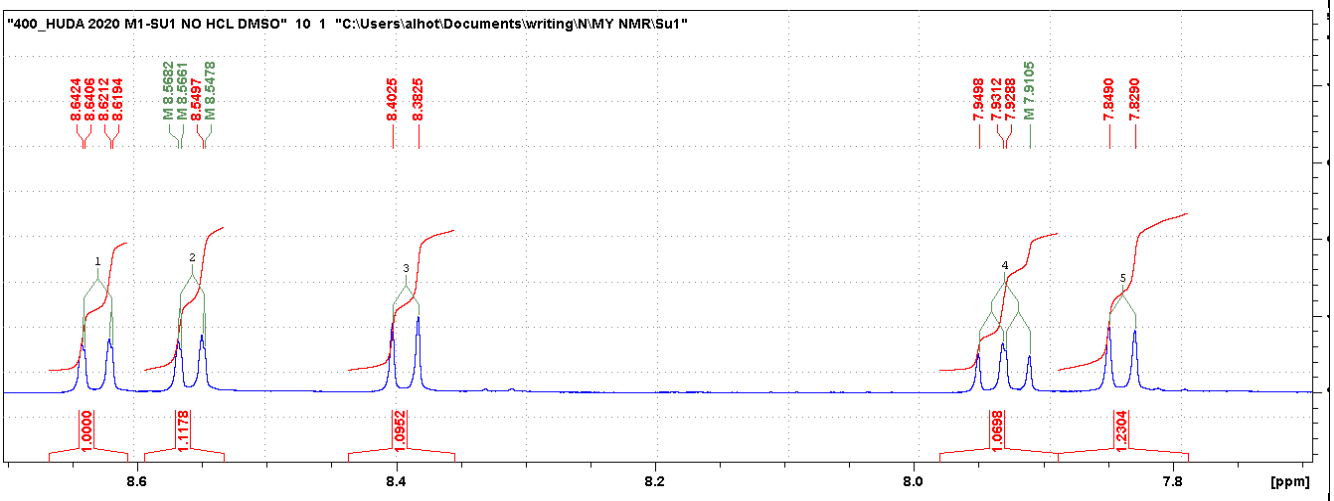

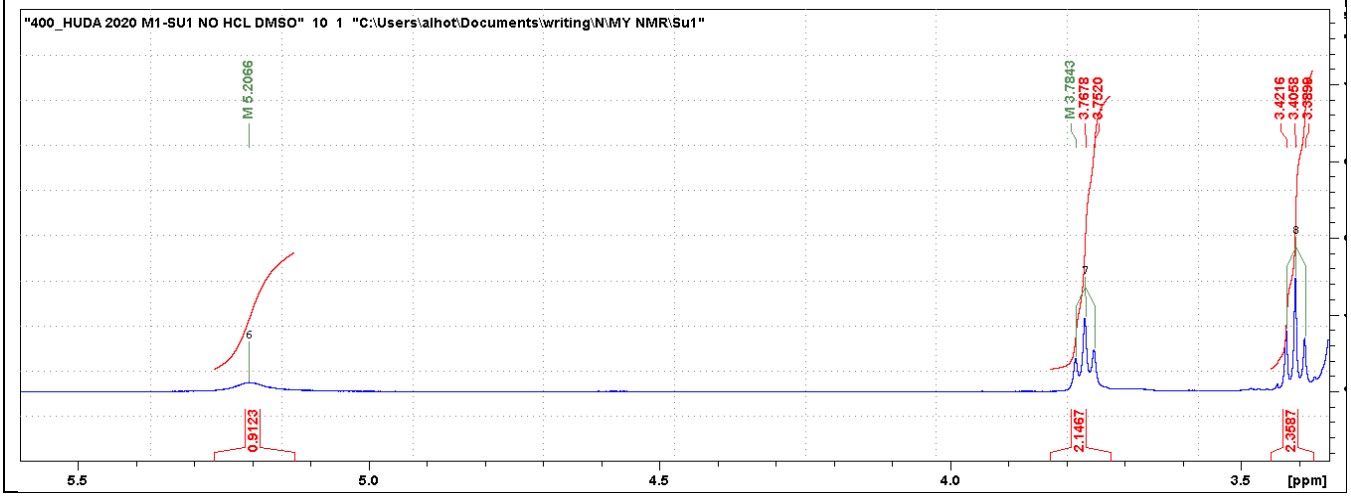

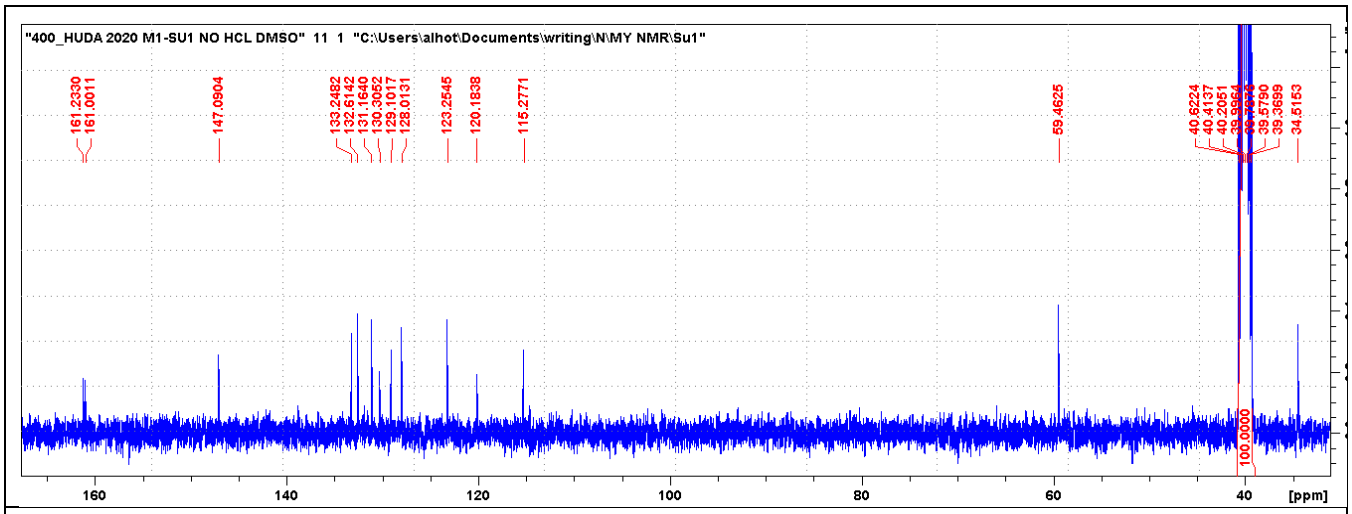

^{1}H NMR (400 MHz, $CDCl_3$): δ(ppm): 8.63 (dd, *J* = 8.48 Hz, *J* = 0.72 Hz, 1H), 8.55 (d, *J* = 7.28 Hz, 1H), 8.39 (d, *J* = 8 Hz, 1H), 7.92 (dd, *J* = 8.4 Hz, *J* = 7.44 Hz, 1H), 7.83 (d, *J* = 8 Hz, 1H), 5.20 (s,1H, OH), 3.76 (t, *J* = 6.32 Hz, 2H, CH_2), 3.40 (t, *J* = 6.32 Hz, 2H, CH_2). **^{13}C NMR (400 MHz, $CDCl_3$): δ(ppm):** 161.23, 161.00, 147.09, 133.24, 132.61, 131.16, 130.30, 129.10, 128.01, 123.25, 120.18, 115.27, 59.46, 34.51. **HR TOF MS ES+** calcd for [$C_{14}H_{11}O_4S$] 275.0378 found 275.0372.

400_HUDA 2020 Conf D1-A-Su1 DMF-H2O DMSO [did not purified]

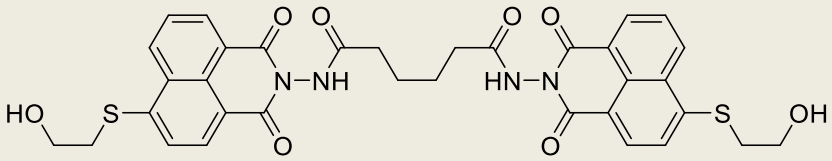

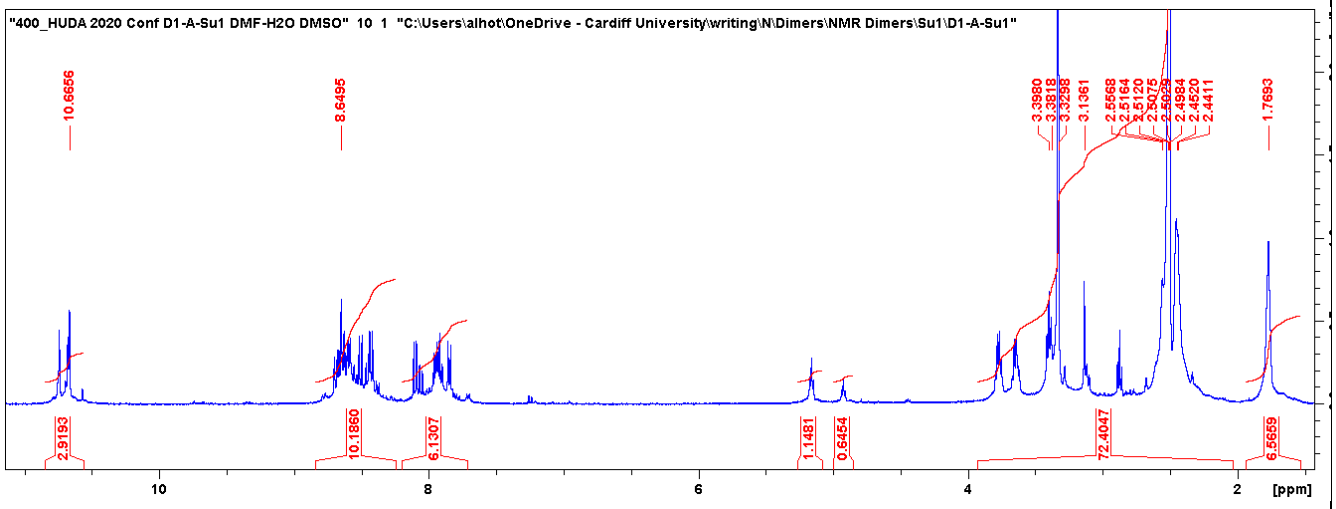

500_HUDA 2021 conf D1-B-Su1 HCl DMSO\ 13C: 500_HUDA 2021 conf D1-B-Su1 mass DMSO

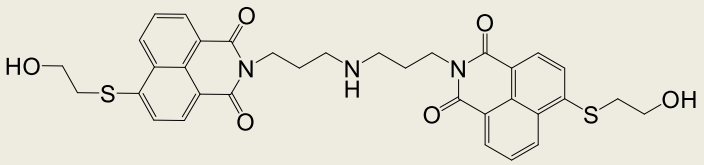

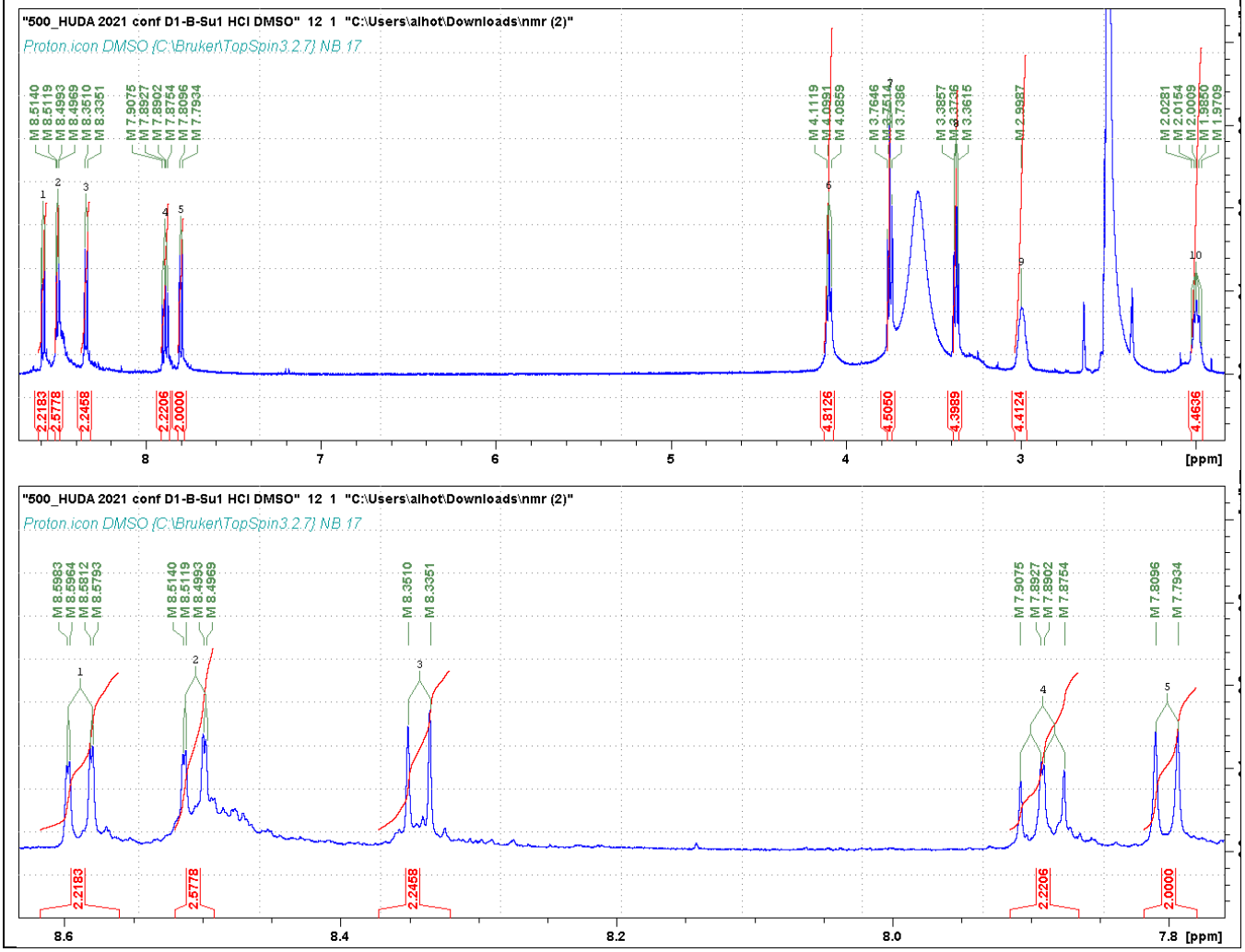

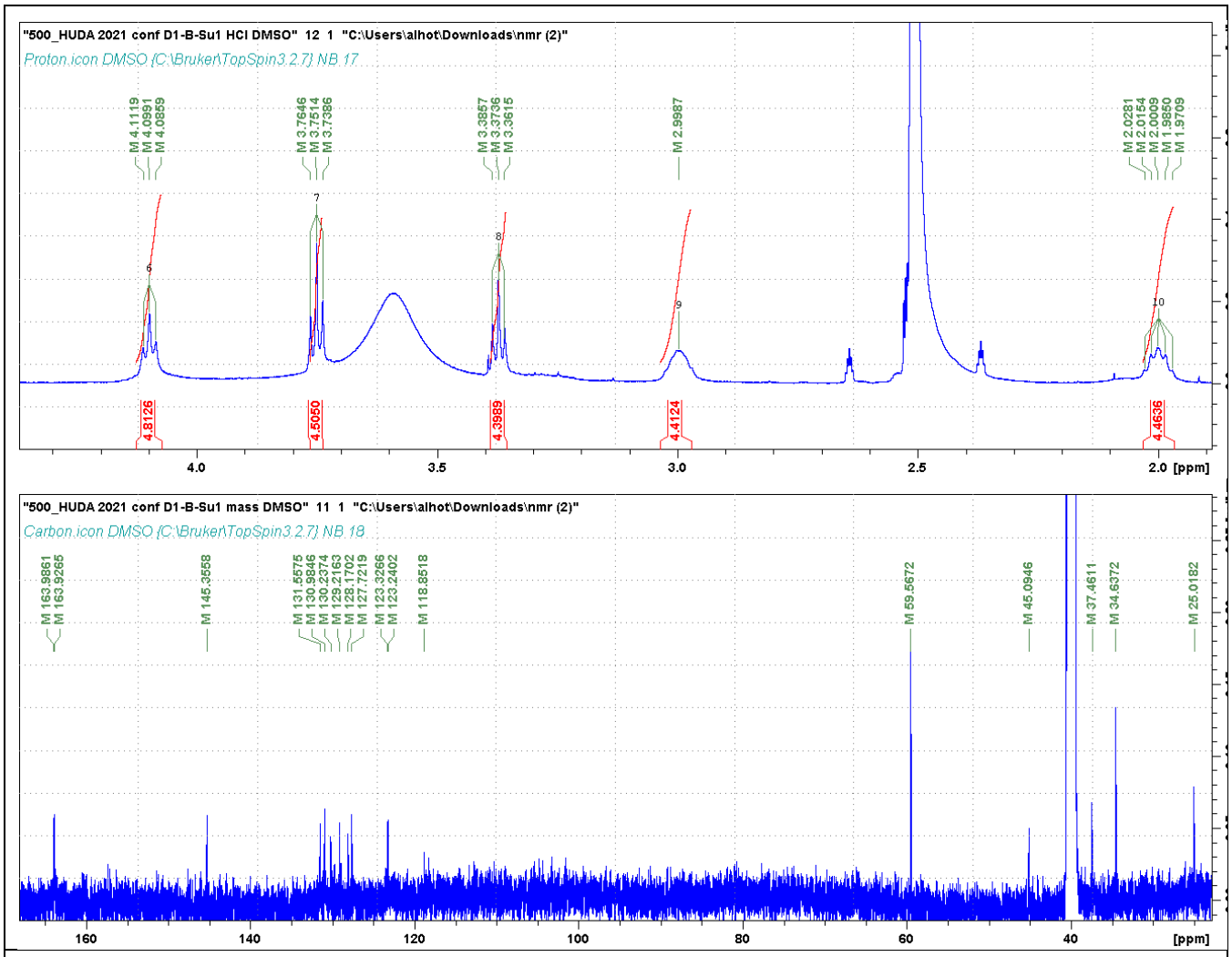

^{1}H NMR (400 MHz, $CDCl_3$): δ(ppm): 8.85 (dd, *J* = 8.55 Hz, *J* = 0.95 Hz, 2H, Ar-CH), 8.50 (dd, *J* = 7.42, *J* = 1.12 Hz, 2H, Ar-CH), 8.34 (d, *J* = 7.95 Hz, 2H, Ar-CH), 7.89 (dd, *J* = 8.65 Hz, *J* = 7.40 Hz, 2H, Ar-CH), 7.80 (d, *J* = 8.10 Hz, 2H, Ar-CH), 4.09 (t, *J* = 6.50 Hz, 4H, CH_2), 3.75 (t, *J* = 6.50 Hz, 4H, CH_2), 3.37 (t, *J* = 6.05 Hz, 4H, CH_2). 2.99 (br signal, 4H, CH_2), 2.00 (quin, *J* = 7.15 Hz, 4H, CH_2).**^{13}C NMR (500 MHz, DMSO): δ(ppm):** 163.98, 163.92, 145.35, 131.55, 130.98, 130.23, 129.21, 128.17, 127.72, 123.32, 123.24, 118.85, 59.56, 45.09, 37.46, 34.63, 25.01.

400_HUDA 2021 D1-C-Su1 DMF 2h HCl DMSO [did not purified]

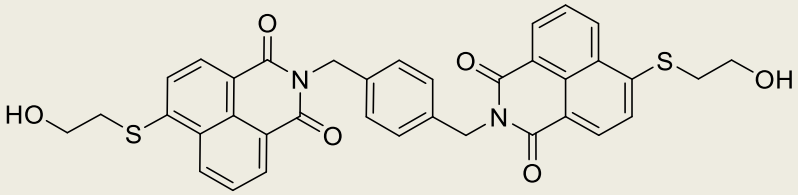

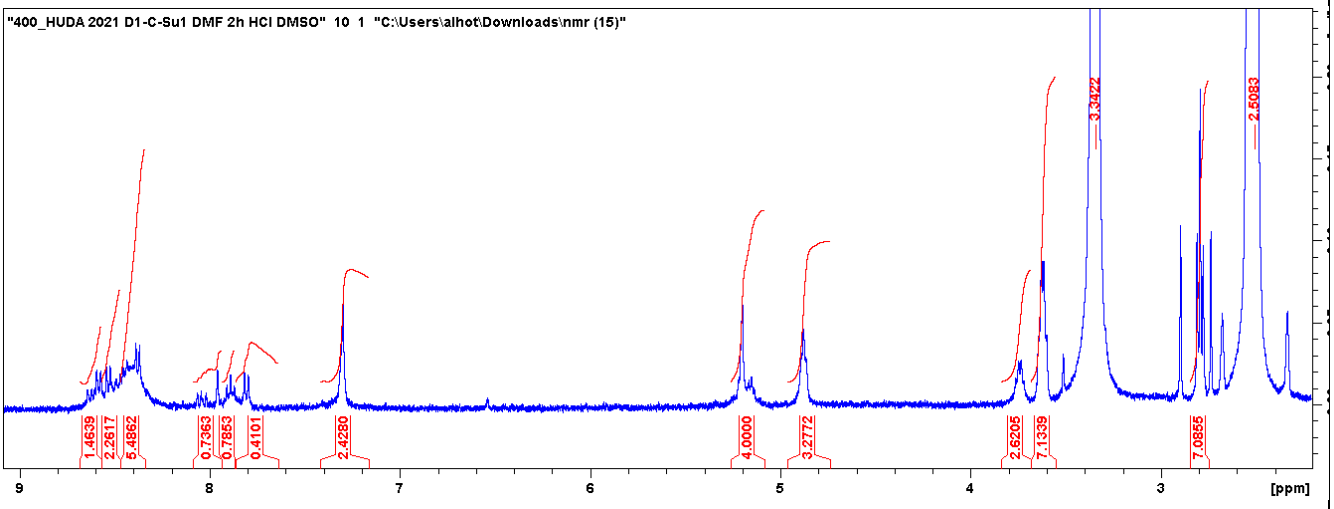

400_HUDA 2020 D1-E-Su1 NO HCl DMSO

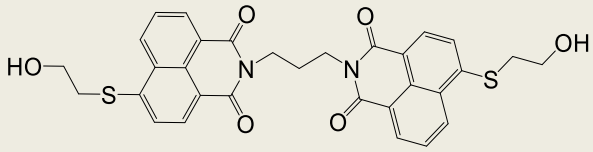

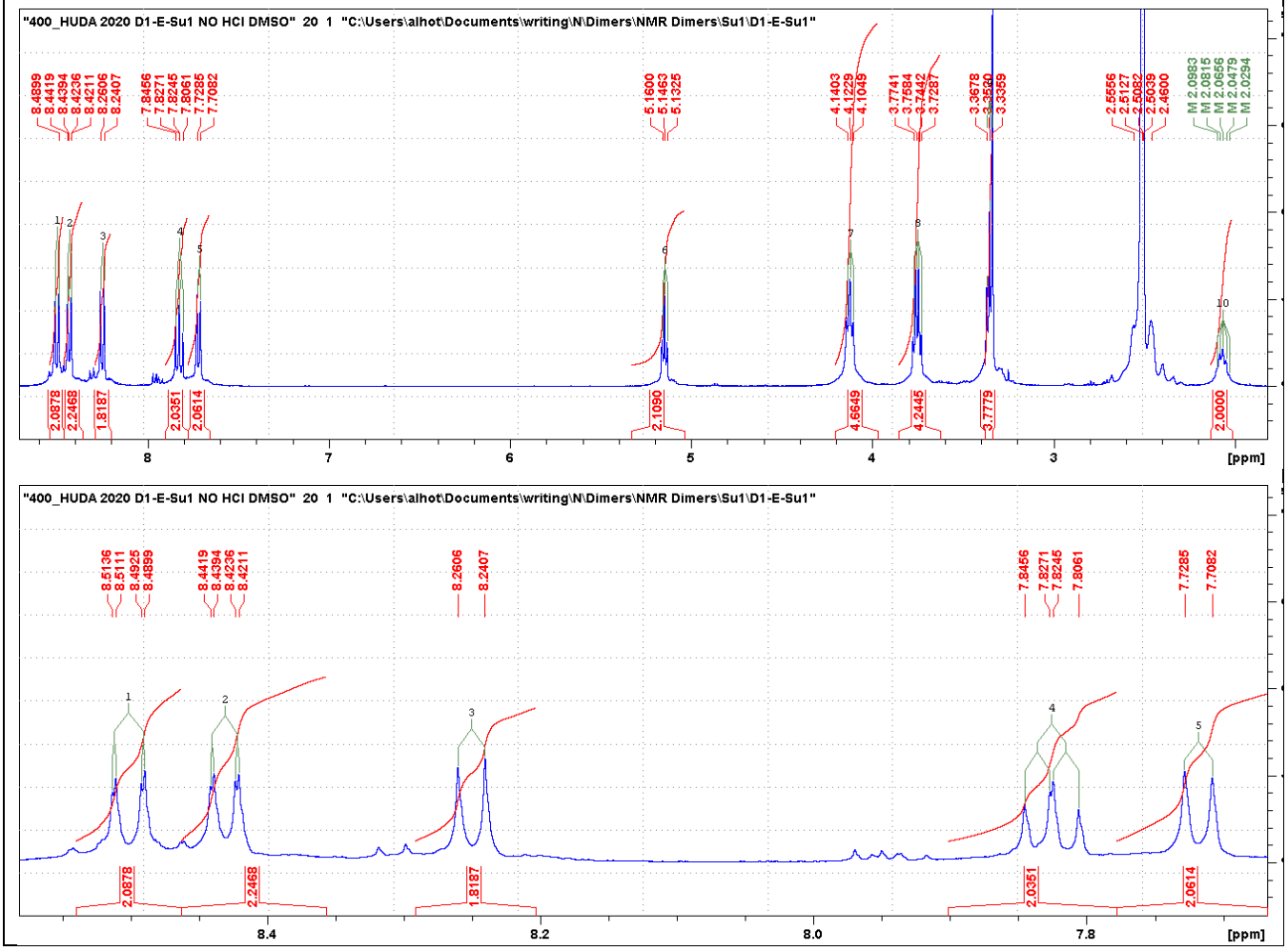

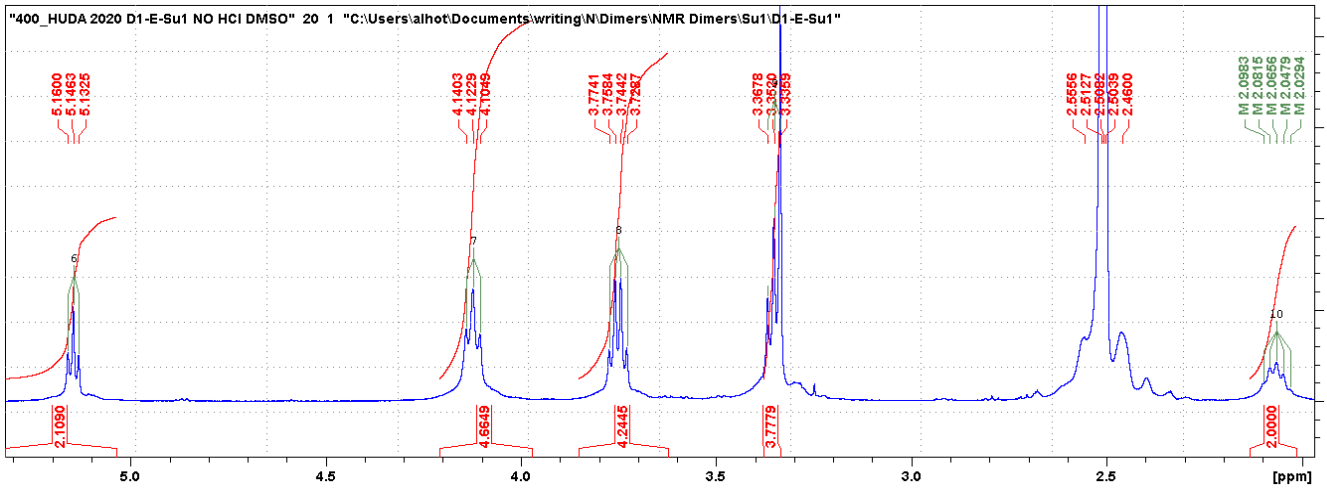

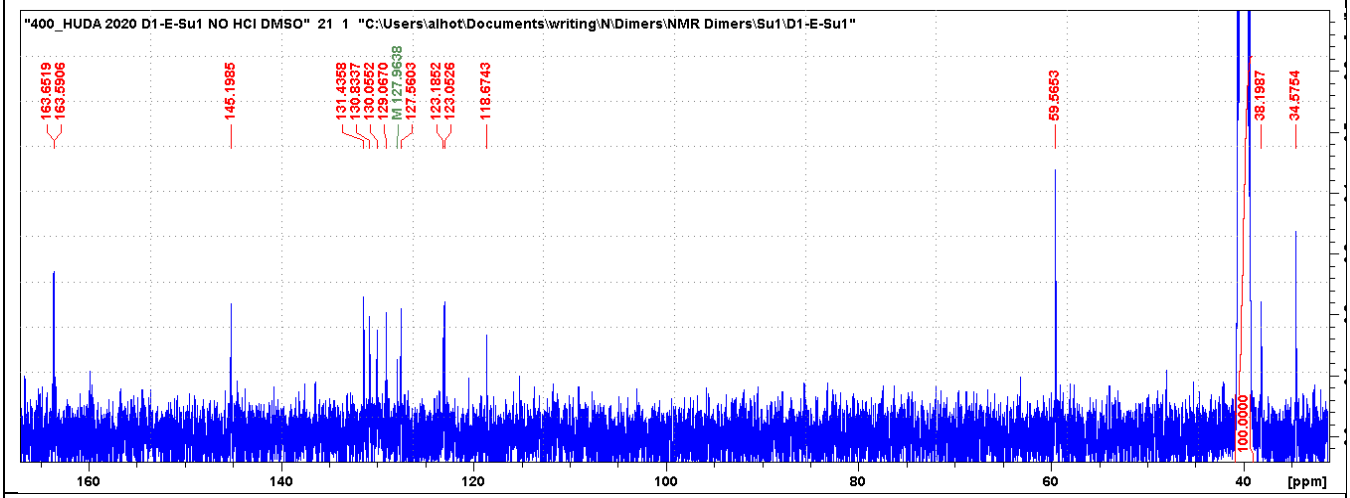

^{1}H NMR (400 MHz, $CDCl_3$): δ(ppm): 8.50 (dd, *J* = 8.46 Hz, *J* = 1.02 Hz, 2H, Ar-CH), 8.42 (dd, *J* = 7.32 Hz, J=1.00 Hz, 2H, Ar-CH), 8.25 (d, *J* = 7.96 Hz, 2H, Ar-CH), 7.82 (dd, *J* = 8.42 Hz, *J* = 7.38 Hz, 2H, Ar-CH), 7.71 (d, *J* = 8.12 Hz, 1H), 5.14 (t, *J*=5.50, 2H, OH), 4.12 (t, *J* = 7.08 Hz, 4H, CH_2), 3.75 (q, *J* = 6.05 Hz, 4H, CH_2), 3.35 (t, *J* = 6.38 Hz, 4H, CH_2), 2.06 (quint, *J* = 6.89 Hz, 2H, CH_2). **^{13}C NMR (400 MHz, $CDCl_3$): δ(ppm):** 163.65, 163.59, 145.19, 131.43, 130.83, 130.05, 129.06, 127.96, 127.56, 123.18, 123.05, 118.67, 59.56, 38.19, 34.57. **HR TOF MS ES+** calc for [$C_{31}H_{27}N_2O_6S_2$] 587.1311 found 587.1320.

400_HUDA 2020 D1-F-Su1-NO HCl DMSO

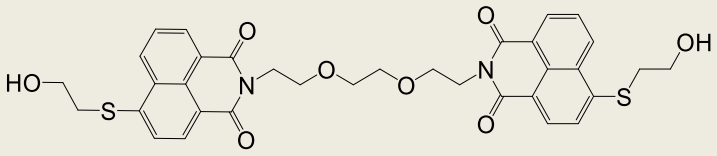

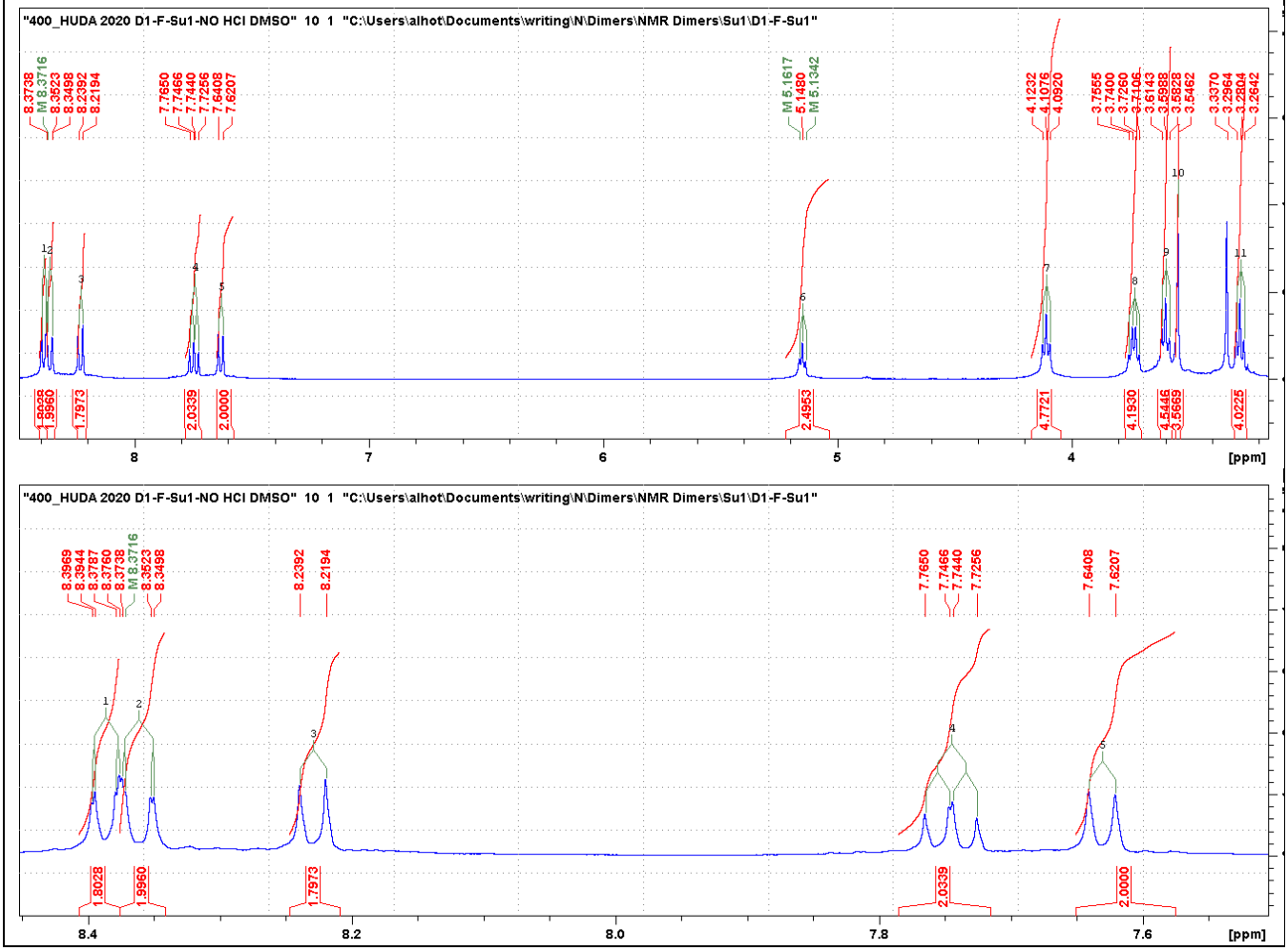

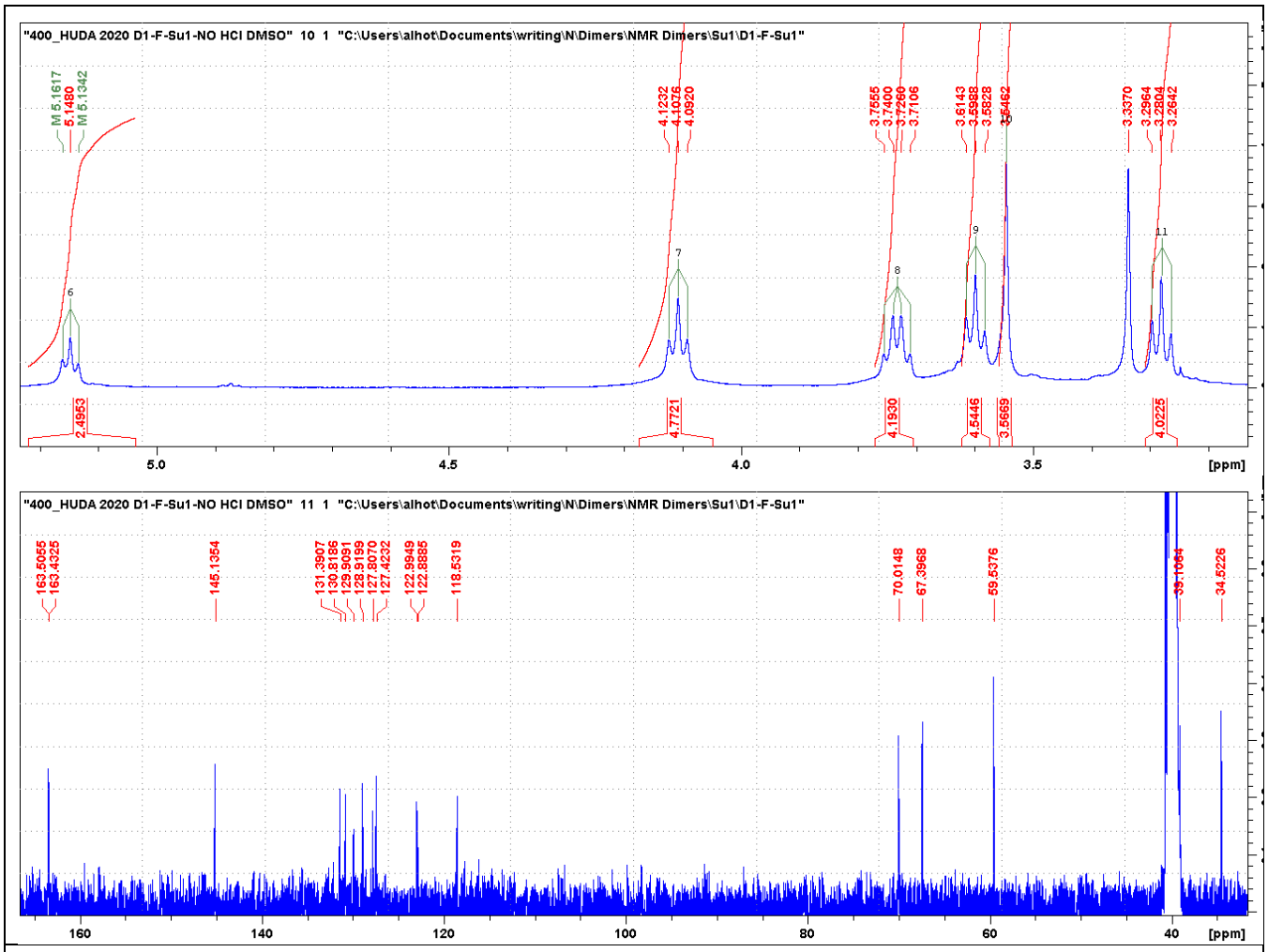

^{1}H NMR (400 MHz, $CDCl_3$): δ(ppm): 8.38 (dd, *J* = 7.32 Hz, *J* = 1.04 Hz, 2H, Ar-CH), 8.36 (dd, *J* = 8.66 Hz, J=0.94 Hz, 2H, Ar-CH), 8.22 (d, *J* = 7.92 Hz, 2H, Ar-CH), 7.74 (dd, *J* = 8.40 Hz, *J* = 7.36 Hz, 2H, Ar-CH), 7.63 (d, *J* = 8.04 Hz, 2H, Ar-CH), 5.14 (t, *J*=5.50, 2H, OH), 4.10 (t, *J* = 6.24 Hz, 4H, CH_2), 3.73 (q, *J* = 5.98 Hz, 4H, CH_2), 3.59 (t, *J* = 6.30 Hz, 4H, CH_2), 3.54 (s, 4H,CH_2), 3.28 (t, *J* = 6.44 Hz, 4H, CH_2). **^{13}C NMR (400 MHz, $CDCl_3$): δ(ppm):** 163.50, 163.43, 145.13, 131.39, 130.81, 129.90, 128.91, 127.80, 127.42, 122.99, 122.88, 118.53, 70.01, 67.39, 59.53, 39.10, 34.52. **HR TOF MS ES+** calc for [$C_{34}H_{33}N_2O_8S_2$] 661.1678 found 661.1691.

400_HUDA 2020 M1-Su4 DMSO

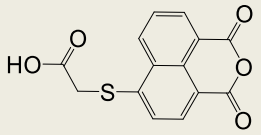

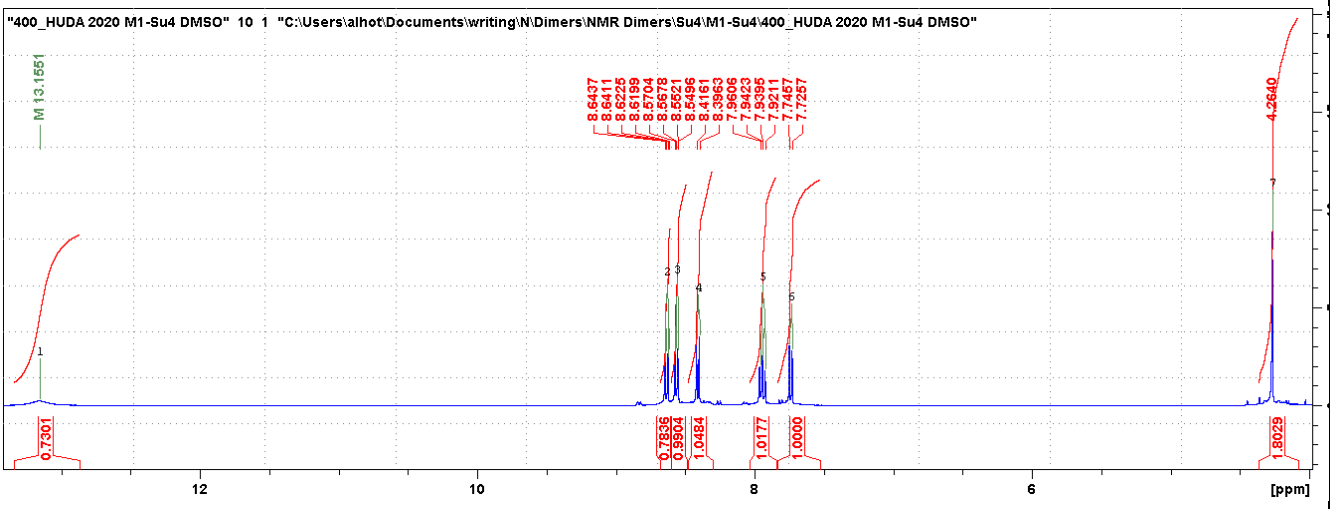

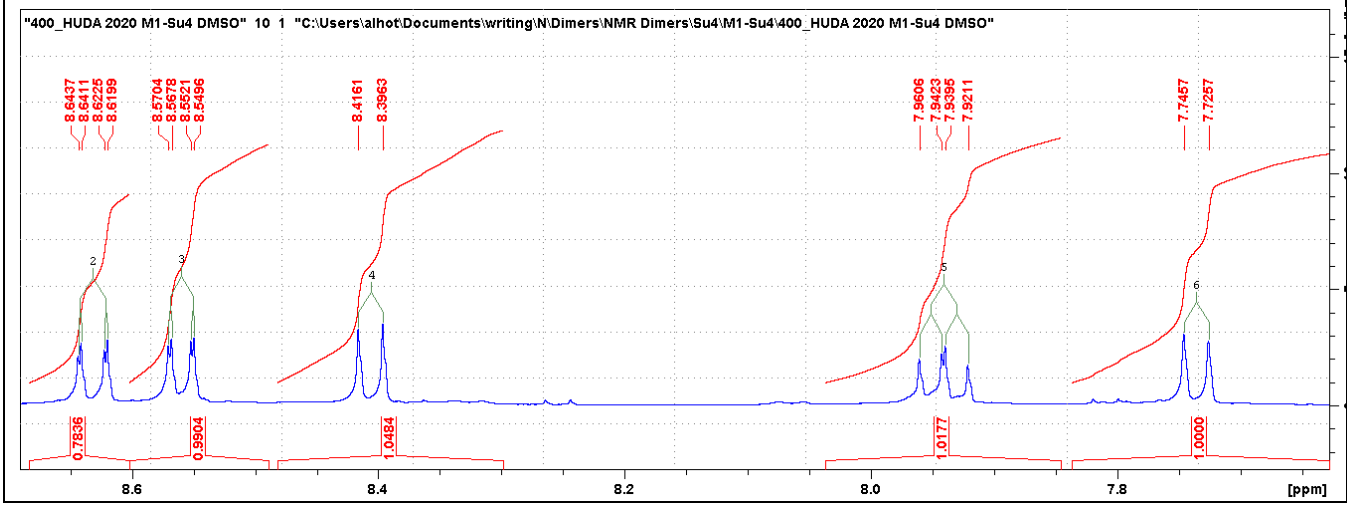

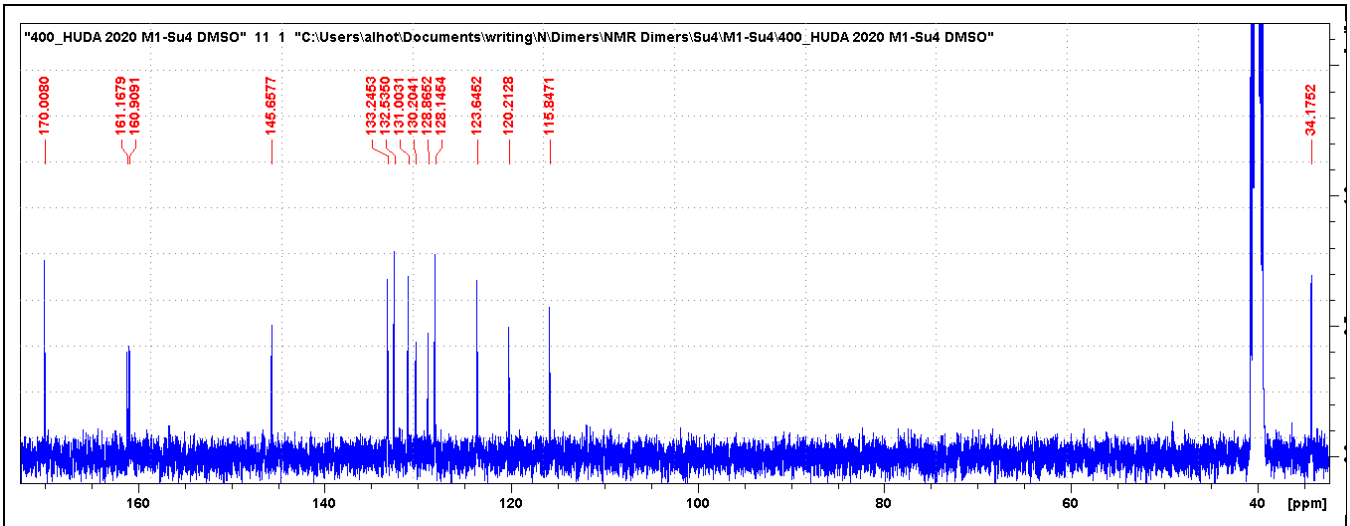

^{1}H NMR (400 MHz, DMSO): δ(ppm): 13.15 (s, 1H, OH), 8.63 (dd, *J* =8.48 Hz, *J* = 1.04 Hz, 1H, Ar-CH), 8.56 (dd, *J* = 7.30 Hz, *J* = 1.02 Hz, 1H, Ar-CH), 8.40 (d, *J* = 7.92 Hz, 1H, Ar-CH), 7.93 (dd, *J* = 8.46 Hz, *J* = 7.34 Hz, 1H, Ar-CH), 7.73 (d, *J* = 8.00 Hz, 1H, Ar-CH), 4.26 (s, 2H, CH_2). **^{13}C NMR (400 MHz, DMSO): δ(ppm):** 170.00, 161.16, 160.90, 145.65, 133.24, 132.53, 131.00, 130.20, 128.86, 128.14, 123.64, 120.21, 115.84, 34.17. **HR TOF MS ES+** calc for [$C_{14}H_9O_5S$] 289.0171 found 289.0161.

400_HUDA 2020 D1-A-Su4 DMSO

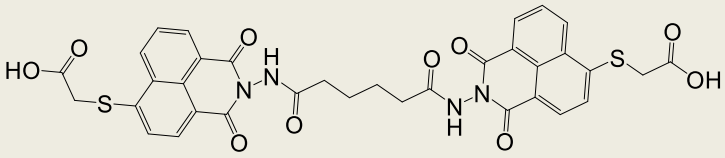

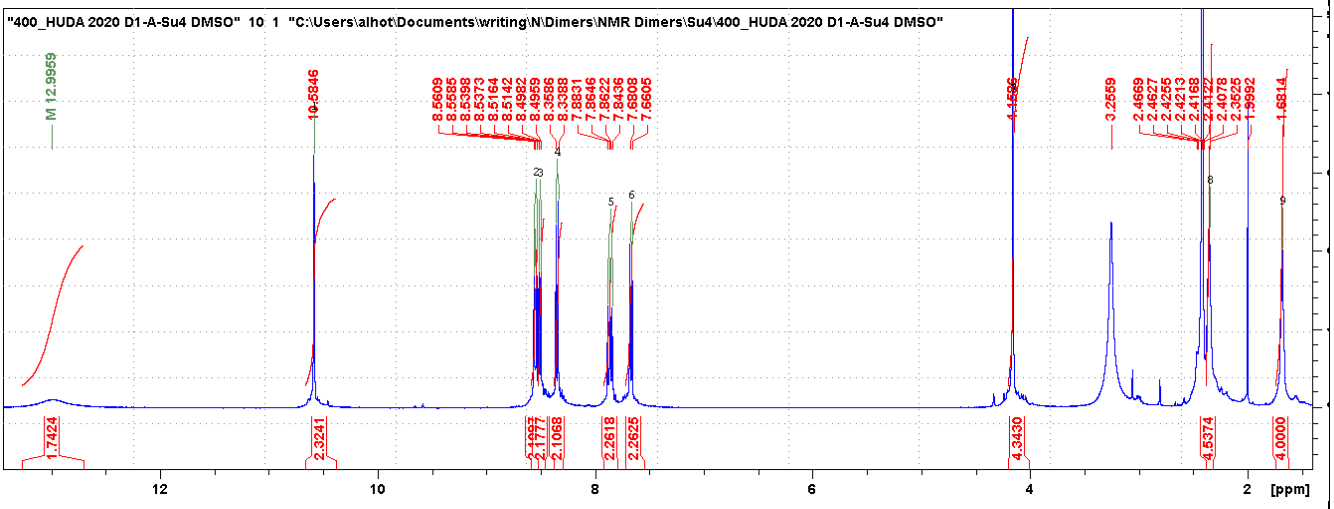

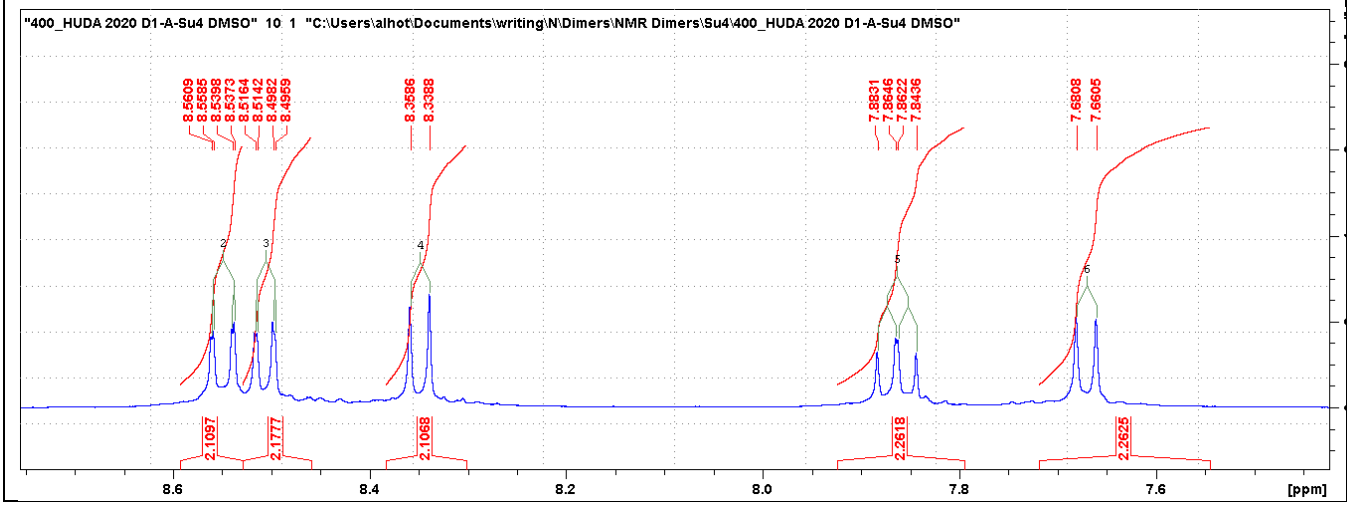

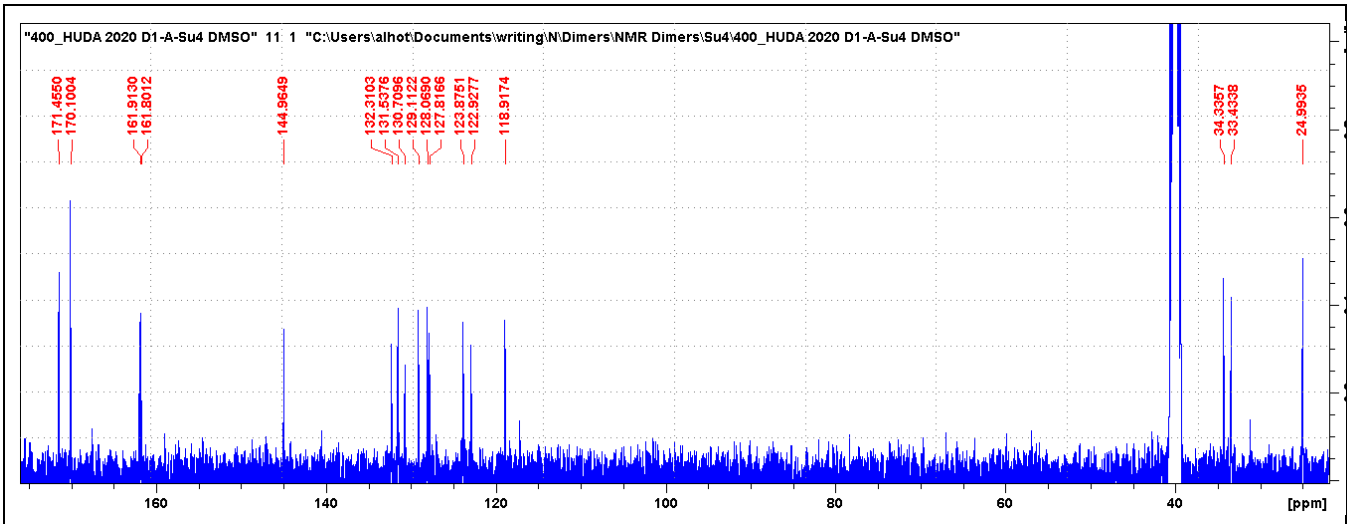

^{1}H NMR (400 MHz, DMSO): δ(ppm): 12.99 (s, 2H, OH), 10.58 (s, 2H, N-H), 8.54 (dd, *J* =8.46 Hz, *J* = 0.98 Hz, 2H, Ar-CH), 8.50 (dd, *J* = 7.30 Hz, *J* = 0.90 Hz, 2H, Ar-CH), 8.34 (d, *J* = 7.92 Hz, 2H, Ar-CH), 7.86 (dd, *J* = 8.37 Hz, *J* = 7.42 Hz, 2H, Ar-CH), 7.67 (d, *J* = 8.12 Hz, 2H, Ar-CH), 4.16 (s, 4H, CH_2), 2.35 (br.s, 4H, CH_2), 1.68 (br.s, 4H, CH_2). **^{13}C NMR (400 MHz, DMSO): δ(ppm):** 171.45, 170.10, 161.91, 161.80, 144.96, 132.31, 131.53, 130.70, 129.11, 128.06, 127.81, 123.87, 122.92, 118.91, 34.33, 33.43, 24.99. **HR TOF MS ES+** calc for [$C_{34}H_{27}N_4O_{10}S_2$] 715.1169 found 715.1181.

500_HUDA 2021 D1-B-Su4 DMF 5h 100 HCl dry DMSO

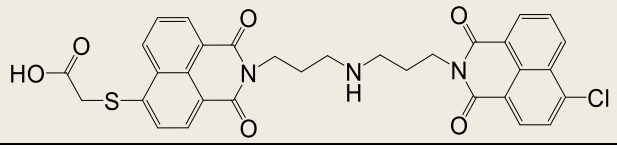

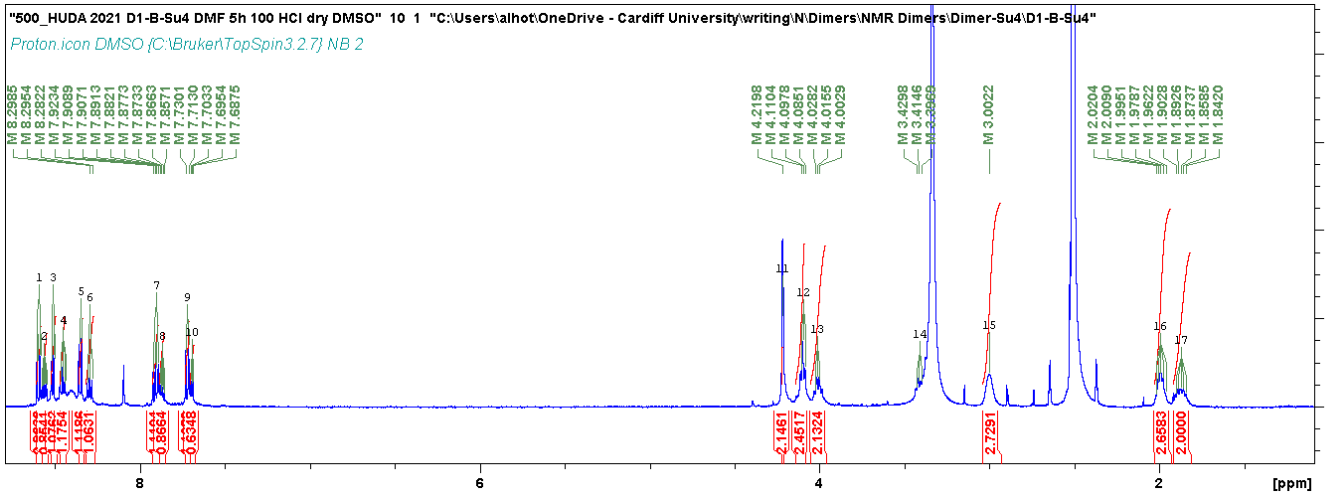

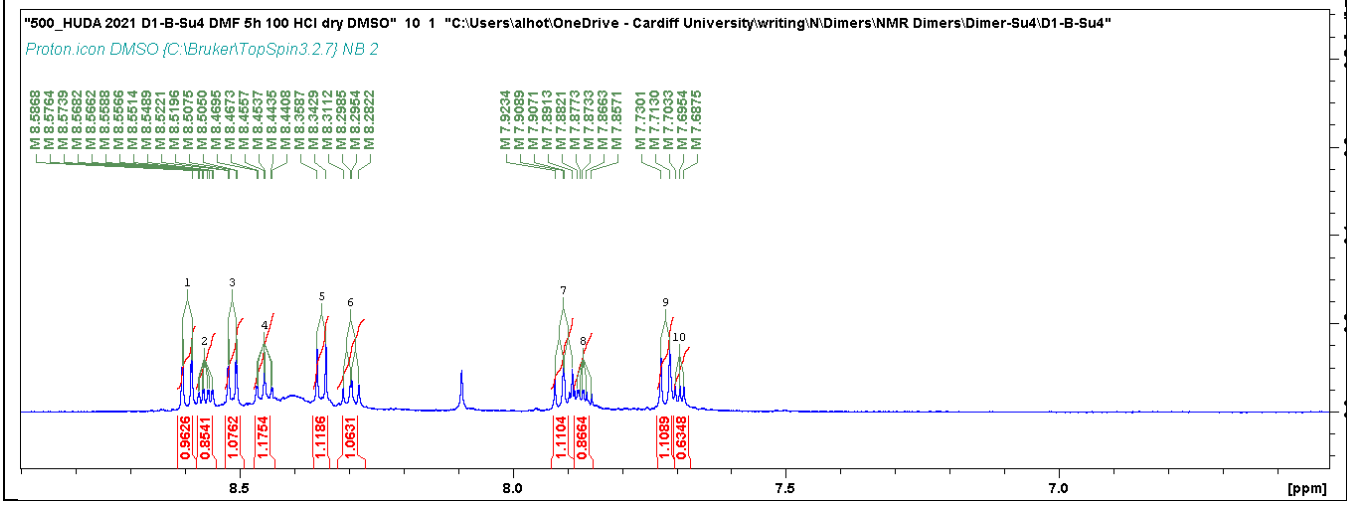

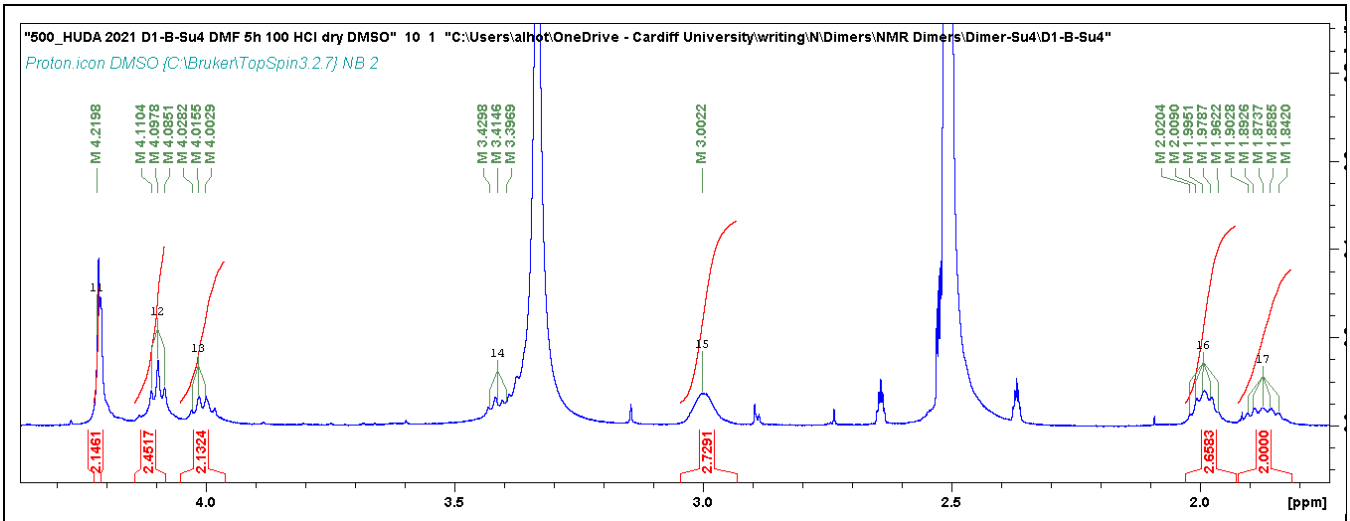

^{1}H NMR (500 MHz, DMSO): δ(ppm): 8.59 (dd, *J* =8.5, *J* =1.0 Hz, 1H, Ar-CH), 8.56 (m, 1H, Ar-CH), 8.51 (dd, *J*=7.30, *J*=1.2 Hz, 1H,Ar-CH), 8.45 (m, 1H, Ar-CH), 8.35 (d, *J* = 7.9 Hz, 2H, Ar-CH), 8.29 (dd, *J* = 8.0, *J* = 7.5 Hz, 1H, Ar-CH), 7.90 (dd, *J* = 8.5, *J* = 7.5 Hz, 1H, Ar-CH), 7.87 (m, 1H, Ar-CH), 7.72 (d, *J* = 8.6 Hz, 1H, Ar-CH), 7.69 (m, 1H, Ar-CH), 4.21 (s, 2H, CH_2), 4.09 (t, *J* = 6.3 Hz, 2H, CH_2), 4.01(m, 2H, CH_2), 3.00 (b. signal, 2H, CH_2), 1.99 (quin, *J* = 7.3 Hz, 2H, CH_2), 1.85 (quin, *J* = 7.6 Hz, 2H, CH_2).

500_HUDA 2021 D1-C-Su4 DMF 5h 100 HCl dry DMSO

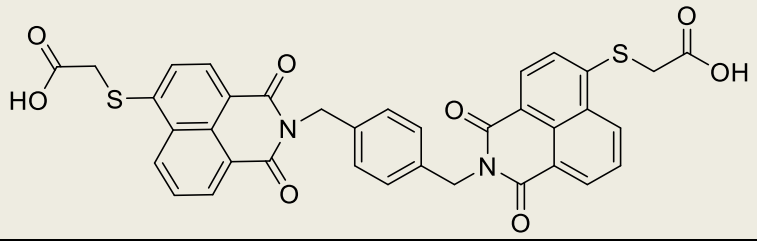

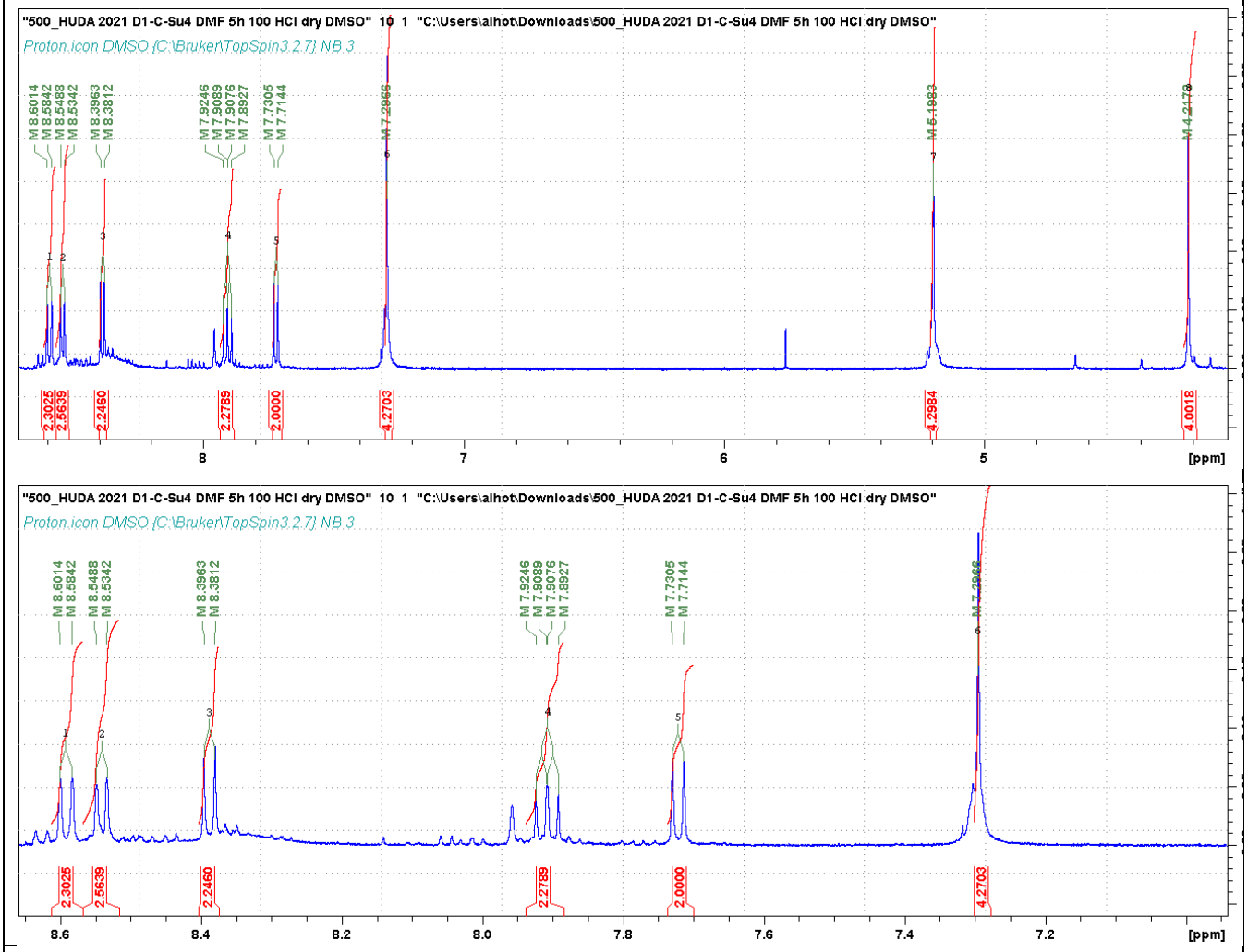

^{1}H NMR (400 MHz, DMSO): δ(ppm): 8.59 (d, *J* =8.60 Hz, 2H, Ar-CH), 8.54 (d, *J* = 7.30 Hz, 2H, Ar-CH), 8.38 (d, *J* = 7.55 Hz, 2H, Ar-CH), 7.90 (dd, *J* = 8.30 Hz, *J* = 7.65 Hz, 2H, Ar-CH), 7.72 (d, *J* = 8.05 Hz, 2H, Ar-CH), 7.29 (s, 4H, Ar-CH), 7.29 (s, 4H, Ar-CH), 5.19 (s, 4H, CH_2), 4.16 (s, 4H, CH_2), 4.21 (s, 4H, CH_2).

400_HUDA 21019 D1-E-SU4-HCL 1h DMSO

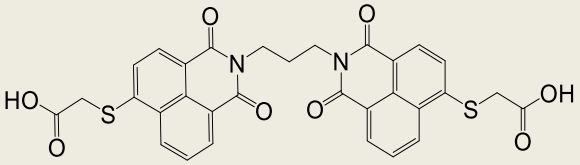

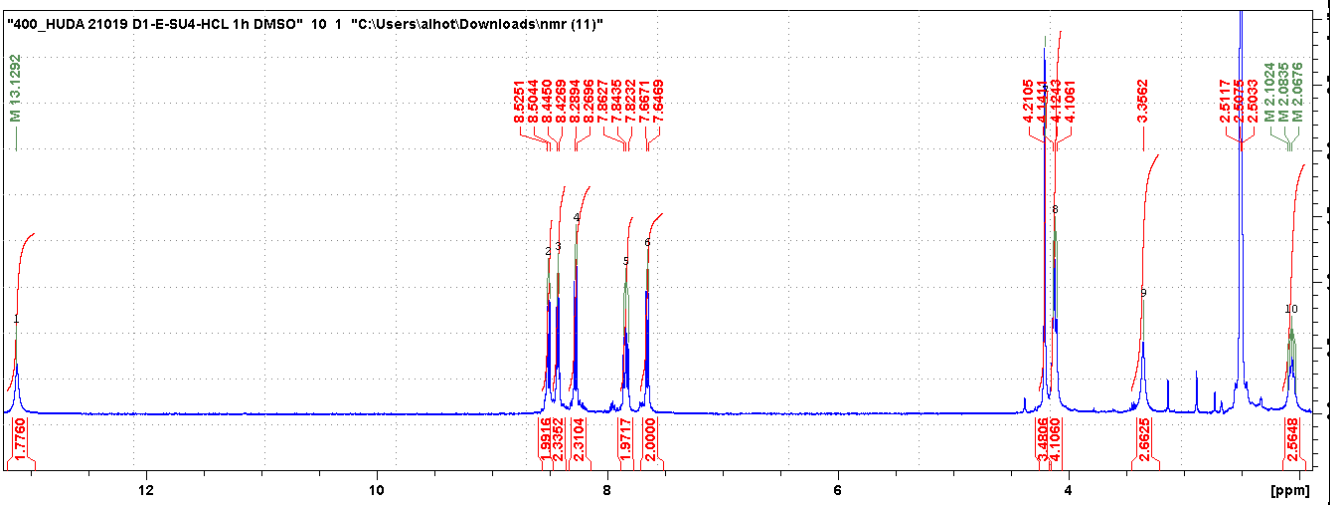

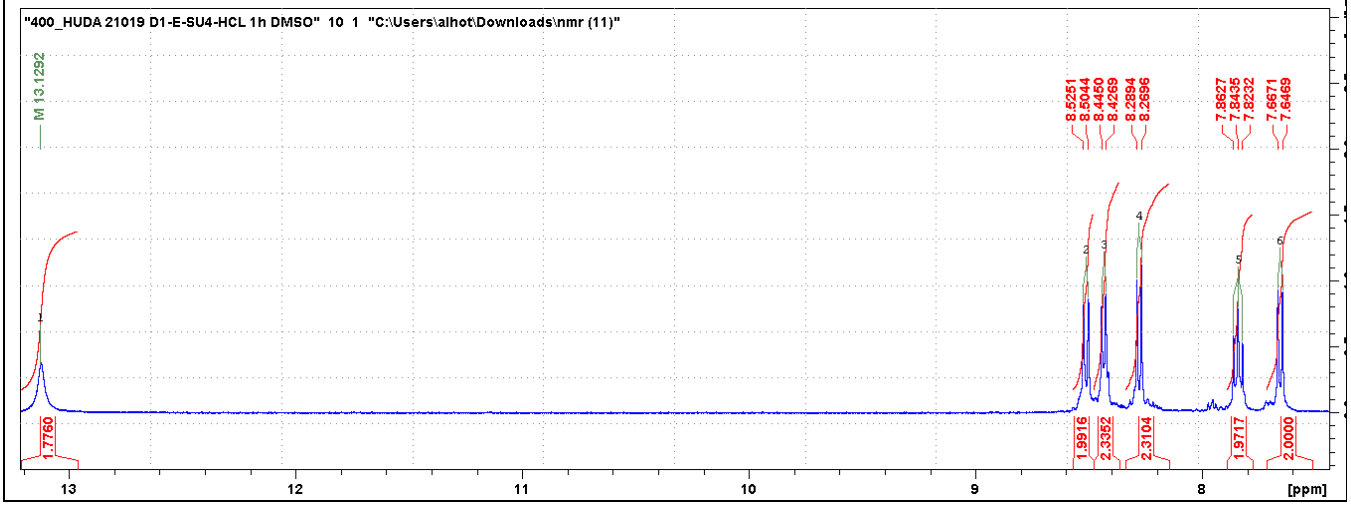

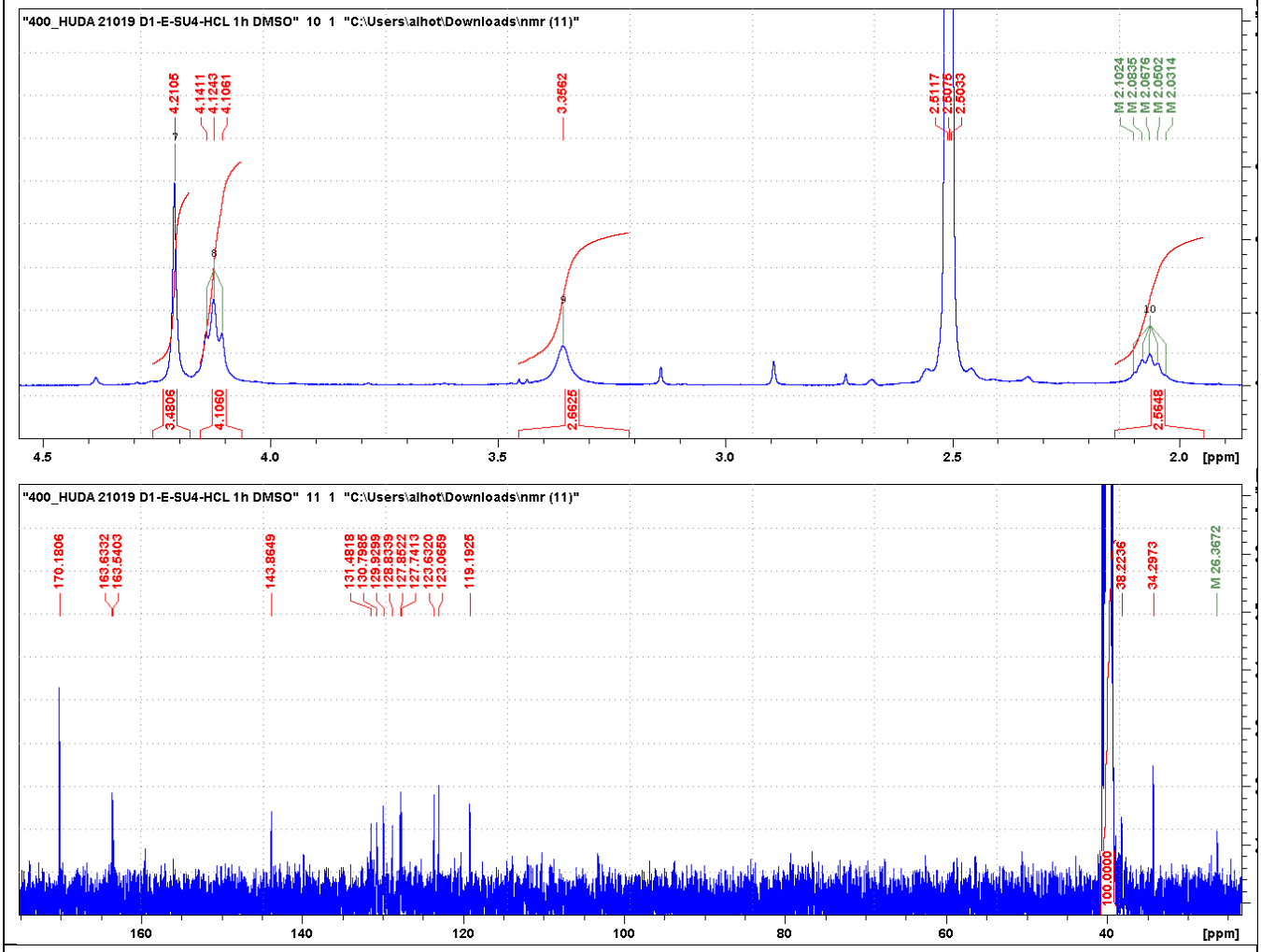

^{1}H NMR (400 MHz, DMSO): δ(ppm): 13.12 (s, 2H, OH), 8.51 (d, *J* =8.28 Hz, 2H, Ar-CH), 8.43 (d, *J* = 7.24 Hz, 2H, Ar-CH), 8.27 (d, *J* = 7.92 Hz, 2H, Ar-CH), 7.84 (t, *J* = 7.90 Hz, 2H, Ar-CH), 7.65 (d, *J* = 8.08 Hz, 2H, Ar-CH), 4.21 (s, 4H, CH_2), 4.12 (t, *J*=7.00 Hz, 4H, CH_2), 2.06 (quin, *J*= 7.10, 2H, CH_2). **^{13}C NMR (400 MHz, DMSO): δ(ppm):** 170.18, 163.63, 163.54, 143.86, 131.48, 130.79, 129.92, 128.83, 127.85, 127.74, 123.63, 123.06, 119.19, 38.22, 34.29, 26.36. **HR TOF MS ES+** calc for [$C_{31}H_{23}N_2O_8S_2$] 615.0896 found 615.0898.

500_HUDA 2021 D1-F-Su4 DMSO

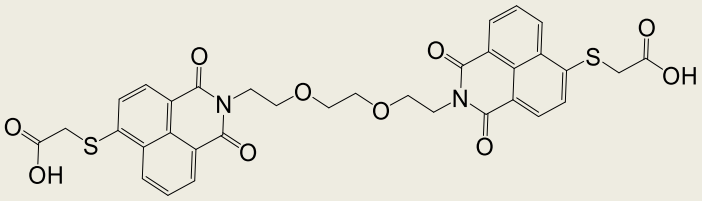

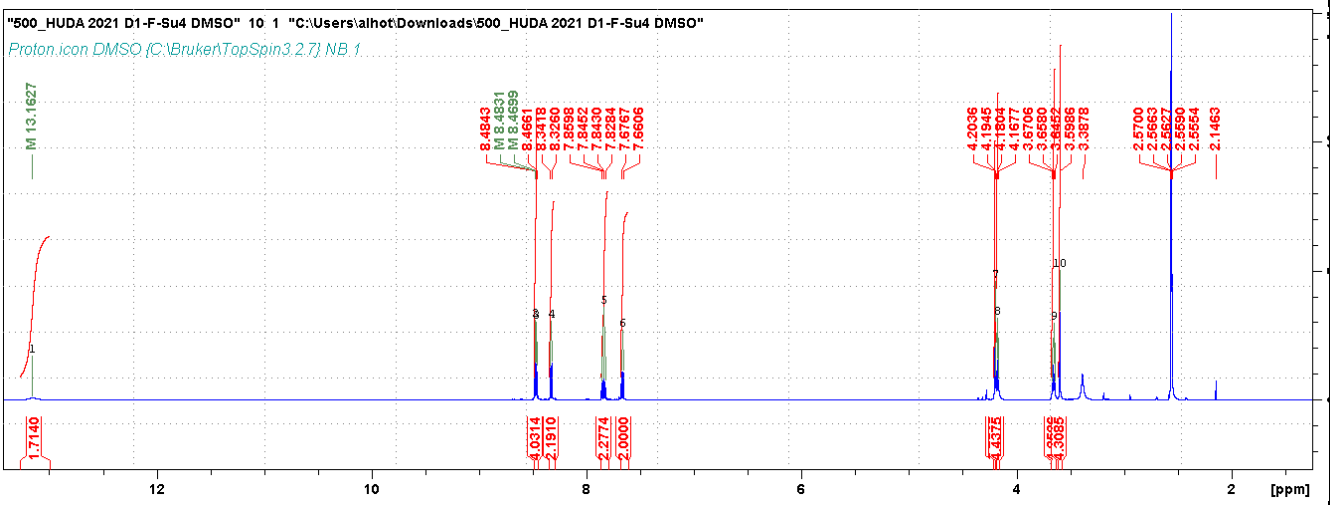

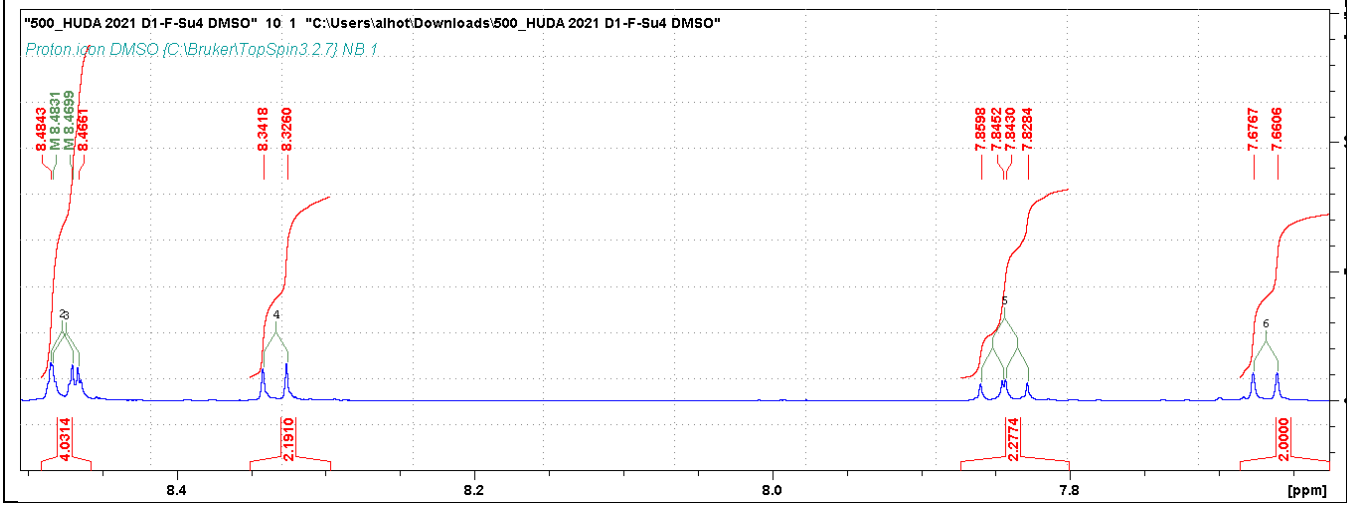

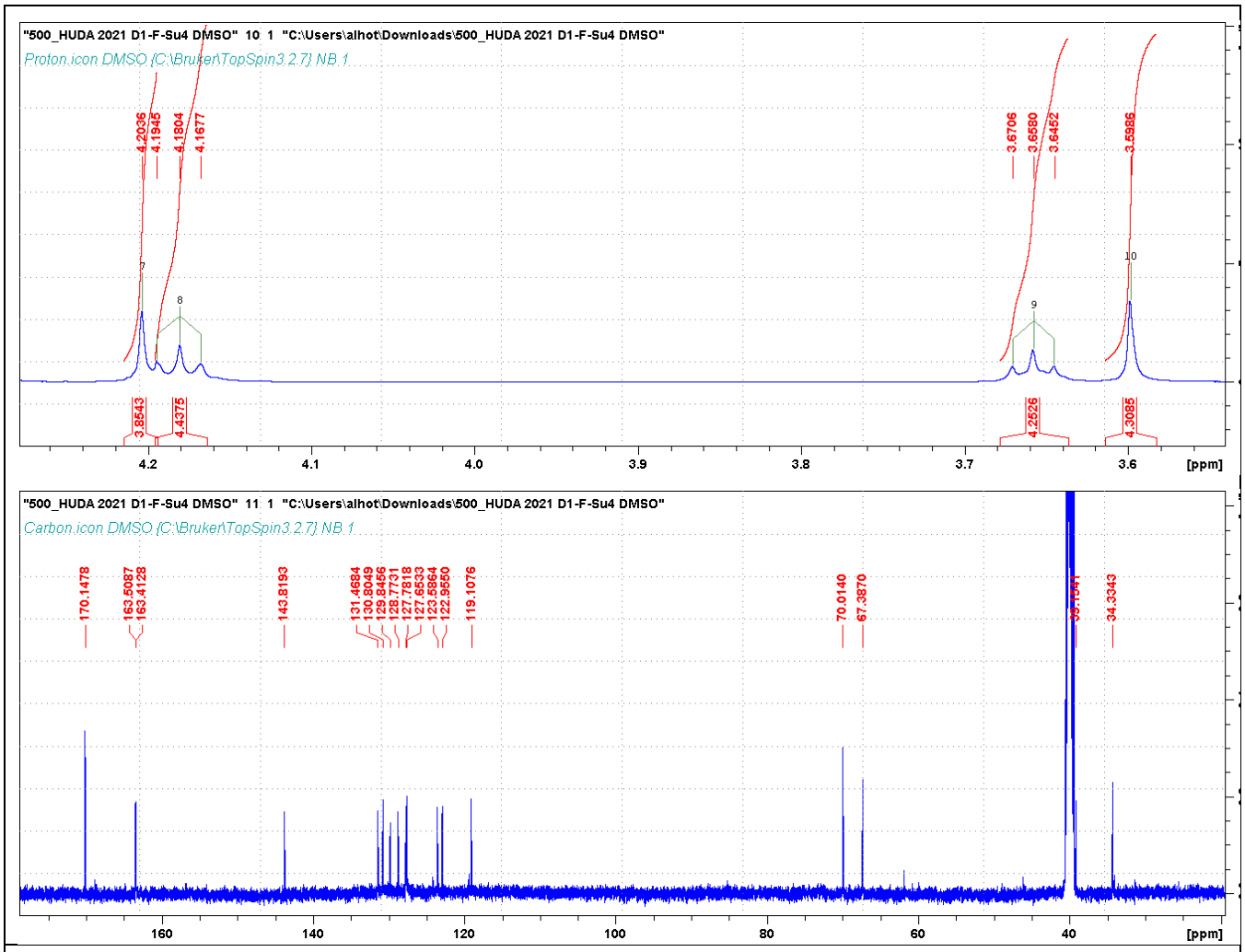

^{1}H NMR (500 MHz, DMSO): δ(ppm): 13.16 (s, 2H, OH), 8.47 (d, *J* =7.20 Hz, 2H, Ar-CH), 8.46 (d, *J* = 8.50 Hz, 2H, Ar-CH), 8.33 (d, *J* = 7.90 Hz, 2H, Ar-CH), 7.84 (dd, *J* = 8.40 Hz, *J*=7.30 2H, Ar-CH), 7.66 (d, *J* = 8.05 Hz, 2H, Ar-CH), 4.20 (s, 4H, CH_2), 4.18 (t, *J*=6.70 Hz, 4H, CH_2), 3.65 (t, *J*= 6.35, 4H, CH_2), 3.59 (s,4H, CH_2). **^{13}C NMR (500 MHz, DMSO): δ(ppm):** 170.14, 163.50, 163.41, 143.81, 131.46, 130.80, 129.84, 128.77, 127.78, 127.65, 123.58, 122.95, 119.10, 70.01, 67.38, 39.15, 34.33. **HR TOF MS ES+** calc for [$C_{34}H_{29}N_2O_{10}S_2$] 689.1264 found 689.1272.

1H NMR: 400_JNM_180320_M1SU4_CHROMO\500_HUDA 2020 M1-Su4-S1 DMSO

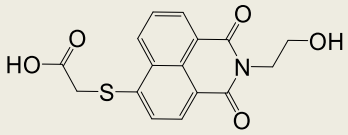

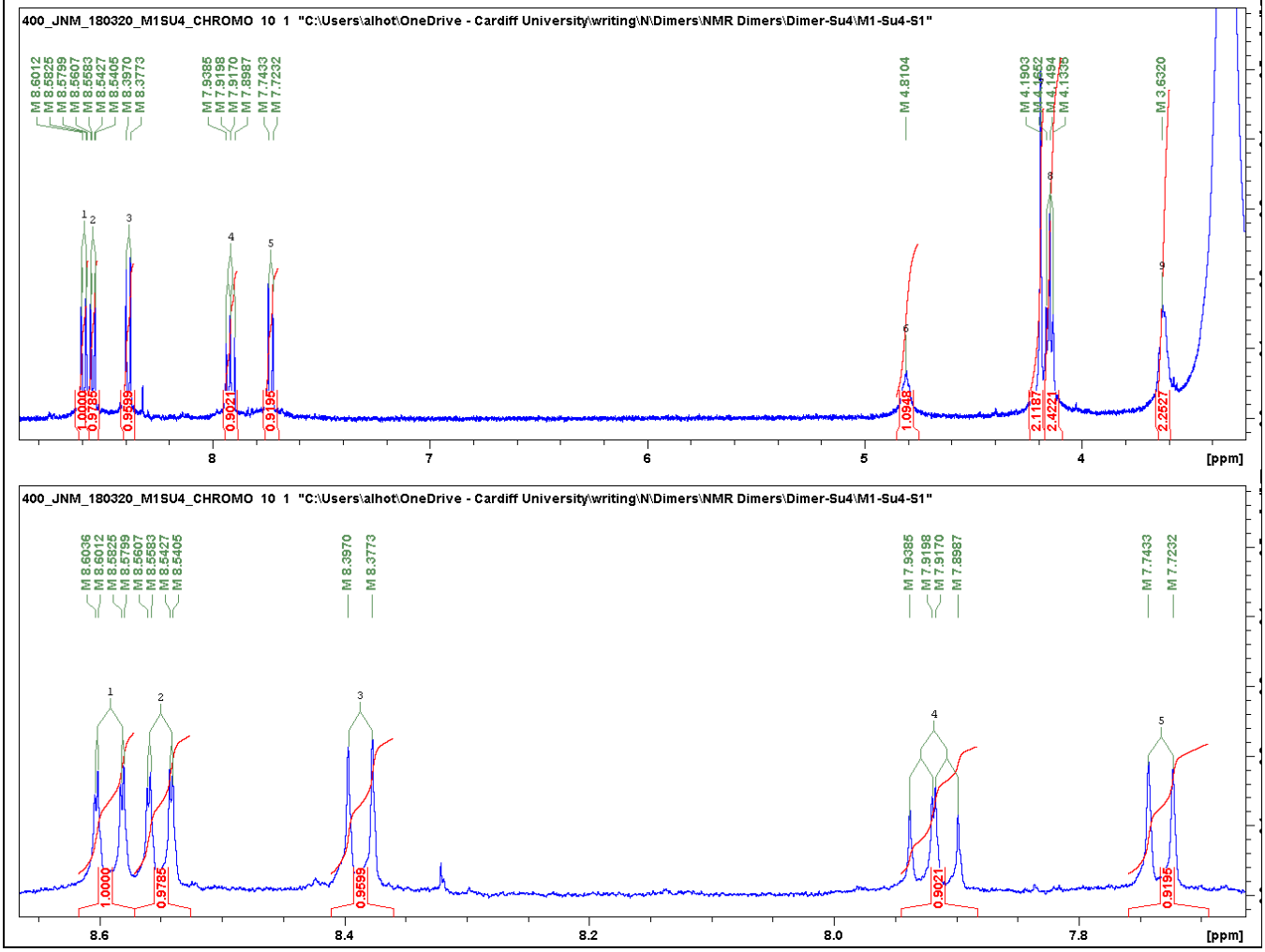

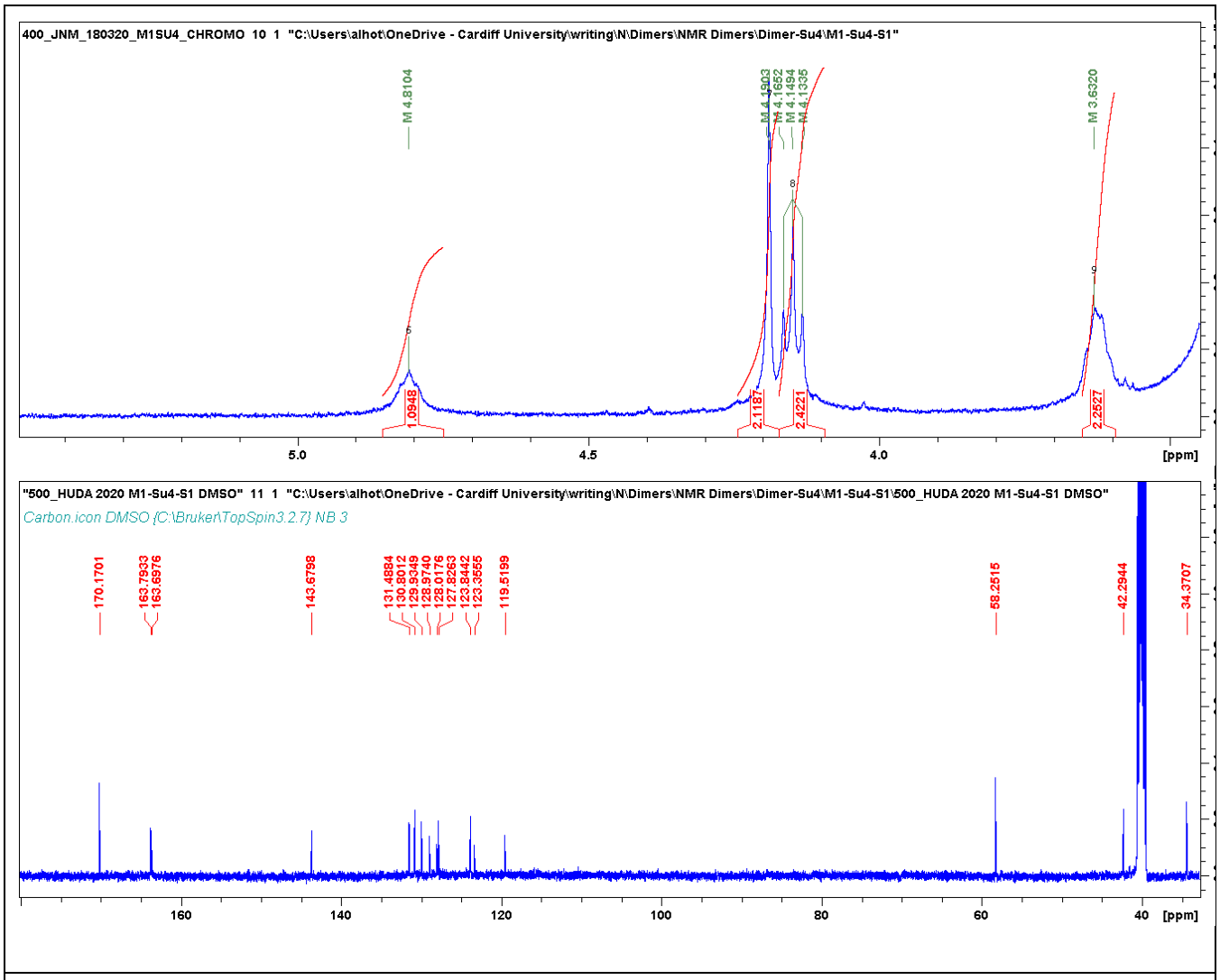

^{1}H NMR (400 MHz, DMSO): δ(ppm): 8.60 (1H, dd, *J*=8.5, *J*=1.0, Ar-CH), 8.55 (1H, dd, *J*= 7.2, 0.9, Ar-CH), 8.38 (1H, d, *J*= 7.9 Hz, Ar-CH), 7.91 (1H, dd, *J*=8.5, *J*=7.4 Hz, Ar-CH), 7.73 (1H, d, *J*= 8.0, Ar-CH), 4.81 (1H, s, OH), 4.19 (2H, s, CH_2), 4.15 (2H, t, *J*= 6.3 Hz, CH_2). 3.63 (2H, br signal, CH_2). **^{13}C NMR (100 MHz, DMSO): δ(ppm):** 170.2, 163.8, 163.7, 143.7, 131.5, 130.8, 129.9, 129.0, 128.0, 127.8, 123.8, 123.4, 119.5, 58.3, 42.3, 34.4.

A3.2 Characterization of compounds using mass spectrometry

Comp.	Mass spectrum code	Comp.	Mass spectrum code	Comp.	Mass spectrum code
3.8a	NB_MS30379_HR_ES	3.9	NB_MS30479_HR_ASAP	3.10a	NB_MS30399_HR_ES
3.8b	NB_MS30378_HR_ES	3.9b	NB_MS35415_HR_ES	3.10b	NB_MS33561_HR_ES
3.8c	NB_MS30376_HR_ES	3.9c	NB_MS30480_LR_ES	3.10c	NB_MS30404_HR_ES
3.8e	NB_MS30377_HR_ES	3.9e	NB_MS30481_HR_ES	3.10e	NB_MS30476_HR_ASAP
3.8d	NB_MS30401_HR_ES	3.9d	NB_MS35563_HR_ES	3.10d	NB_MS30477_HR_ASAP
3.11	NB_MS33587_LR_ES	3.12	NB_MS30402_HR_ES	3.13a	NB_MS33538_HR_ES
3.11dd	Re__MS35499_LR_ES	3.12b	NS	3.13c	NS
3.11d	MS35498_HR_ES	3.12e	NB_MS33562_HR_ES	3.13e	NB_MS33543_HR_ES
3.11ee	MS35497_HR_ES	3.12f	NB_MS33563_HR_ES	3.13d	NB_MS33544_HR_ES
3.11e	MS35496_HR_ES	-	-	-	-
NS: not soluble					

A3.3 UV-vis titration spectra

Comp.	1st titration	2nd titration	3rd titration
3.9	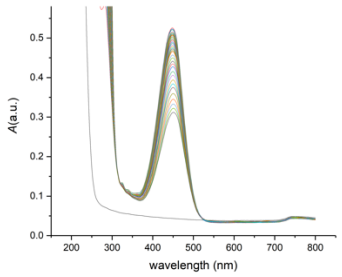	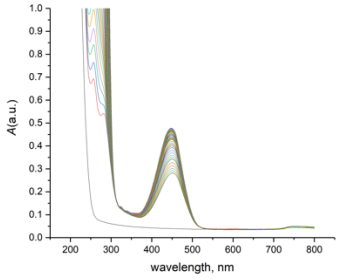	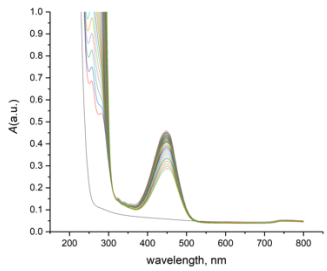
3.9b	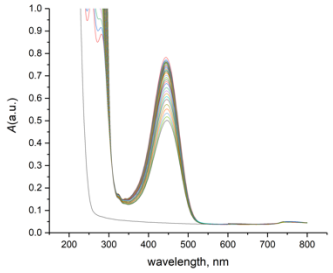	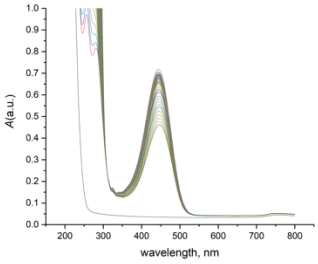	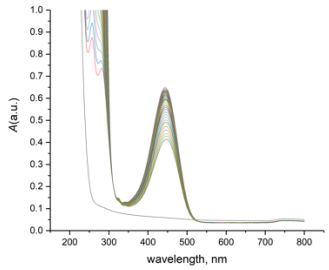
3.9c	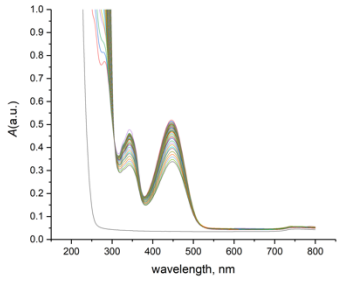	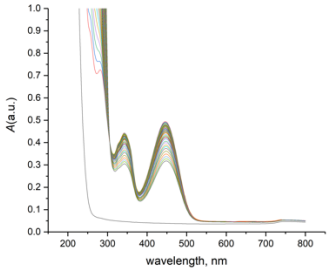	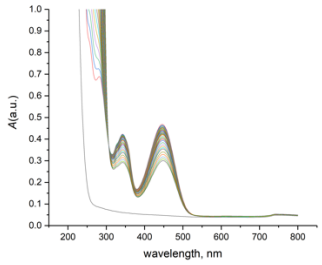
3.9e	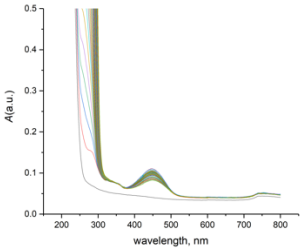	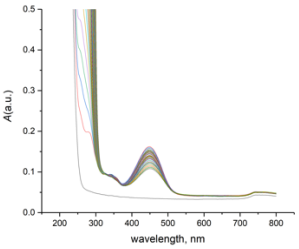	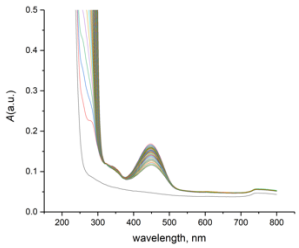

Comp.	1st titration	2nd titration	3rd titration
3.9d	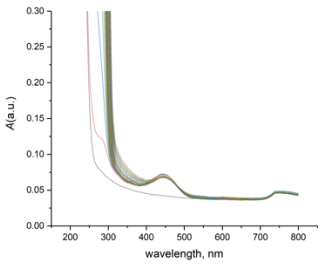	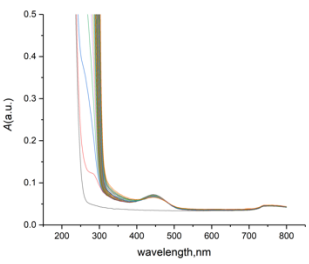	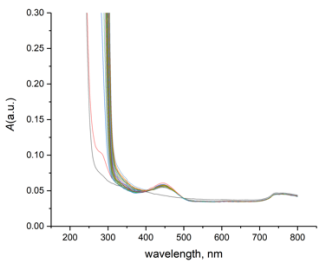
3.10b	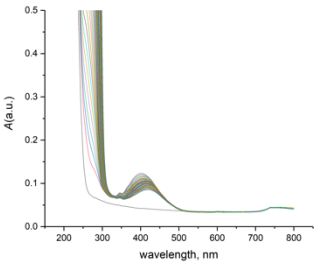	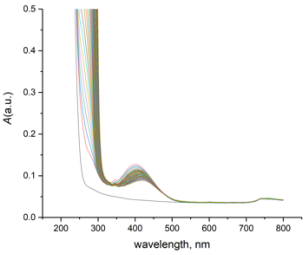	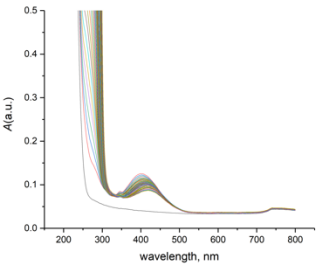
3.11d	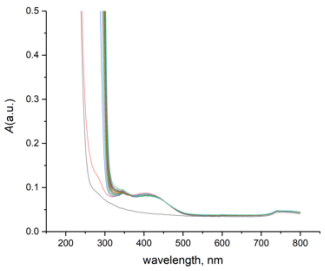	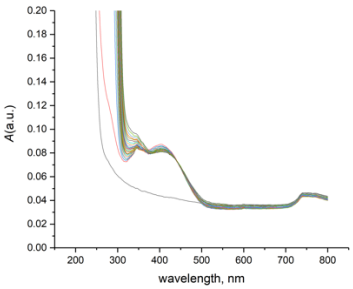	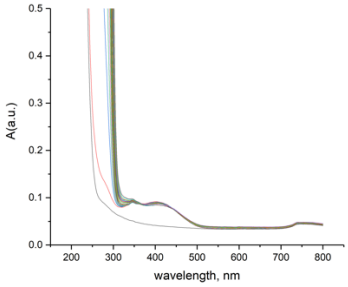
3.12b	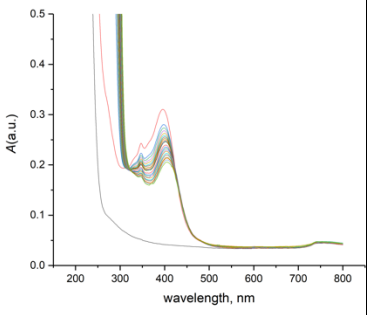	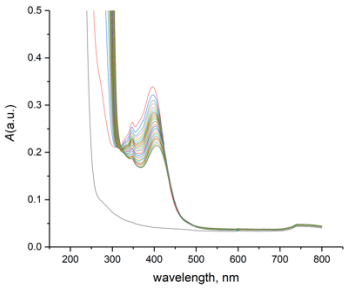	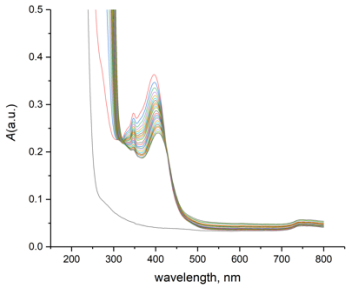

Comp.	1st titration	2nd titration	3rd titration
3.12d	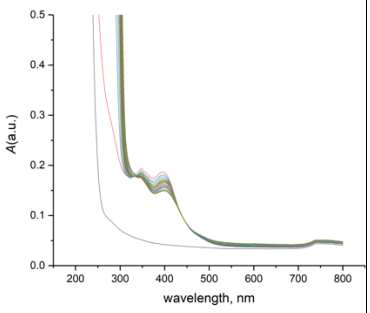	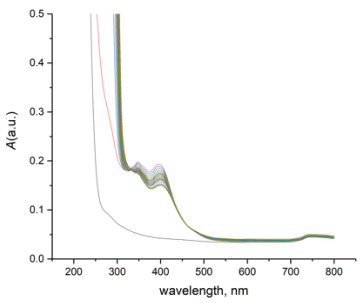	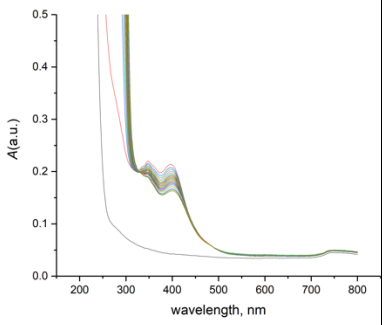
3.13a	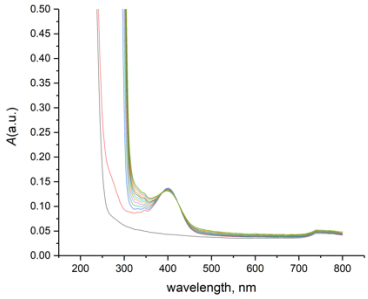	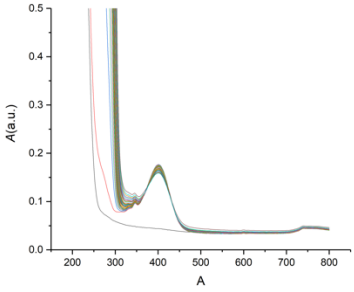	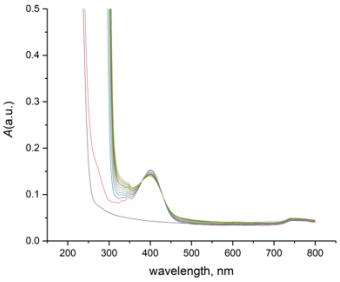
3.13e	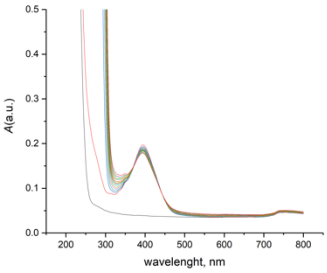	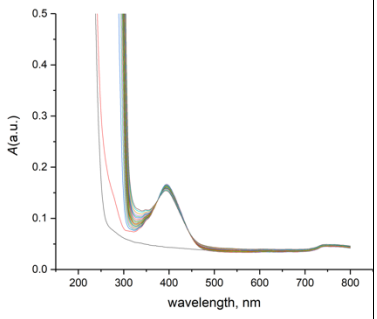	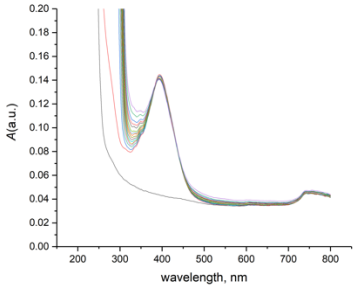
3.13d	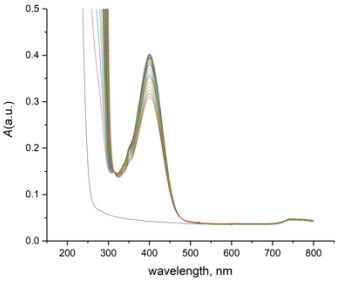	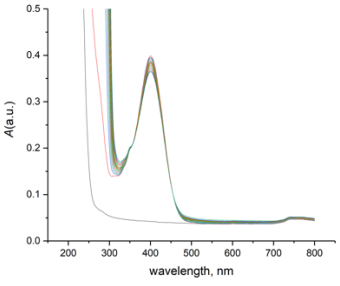	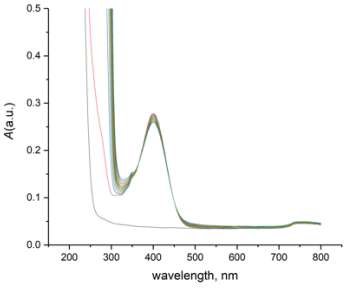

A3.4 Unrestricted preliminary fitting of UV-visible titration data

3.9	**1st titration**	**2nd titration**	**3rd titration**	**Global fit**
***K* / M^{-1}**	(6.78±1.91)×10^4	(13.1±3.6)×10^4	(0.36±1.31)×10^4	(4.03±1.44)×10^4
***n* / basepairs**	8.72±0.49	11.59±0.38	2.43±7.21	8.82±0.86
***K* (*n*=3) / M^{-1}**	5574±481.7	3715±421.4	4546±428.5	4717±384
Bathochromic shift, nm	(448- 451 nm)			
3.9b	**1st titration**	**2nd titration**	**3rd titration**	**Global fit**
***K* / M^{-1}**	(3.7±2.7)×10^5	(6.1±5.5)×10^5	(2.6±1.3)×10^5	(2.5±1.2)×10^5
***n* / basepairs**	15.11±0.92	15.47±1.0	19.44±0.98	16.65±0.85
***K* (n=6) / M^{-1}**	7828±2112	8758±2639	6746±1175	7549±1318
Bathochromic shift, nm	(444- 447 nm)			
3.9c	**1st titration**	**2nd titration**	**3rd titration**	**Global fit**
***K* / M^{-1}**	(8.03±3.97)×10^4	296.9±8.51×10^4	(3.1±2. 4)×10^4	(8.1±3.7)×10^4
***n* / basepairs**	10.86±1.83	0.14±39.83	9.73±4.12	12.70±1.89
***K* (n=6) / M^{-1}**	(2.3±0.3)×10^4	(1.9±0.2)×10^4	(1.4±0.1)×10^4	(1. 9±0.2)×10^4

Bathochromic shift, nm	(447-449)			
3.9d	**1st titration**	**2nd titration**	**3rd titration**	**Global fit**
***K* / M^{-1}**	(1.17±1.85)×10^{7}	4858±1.41×10^{7}	8070±3.13×10^{6}	(8.7±13.1)×10^{6}
***n* / basepairs**	157.1±29.39	0.99±2872	1.01±409.3	100.0±24.16
***K* (n=6) / M^{-1}**	(2.48±0.89)×10^{4}	(3.08±0.6)×10^{4}	(4.62±0.93)×10^{4}	(4.48±1.92)×10^{4}
Bathochromic shift, nm	444-448			
3.9e	**1st titration**	**2nd titration**	**3rd titration**	**Global fit**
***K* / M^{-1}**	2004±5.64×10^{5}	1268±3.99×10^{5}	876±7.51×10^{4}	(1.51±3.08)×10^{4}
***n* / basepairs**	0.14±37.43	0.13±40.75	0.14±12.13	1.70±3.27
***K* (n=6) / M^{-1}**	(9.81±1.62)×10^{4}	(7.38±0.57)×10^{4}	(4.30±0.36)×10^{4}	(6.13±0.43)×10^{4}
Bathochromic shift, nm	448-450			
3.10b	**1st titration**	**2nd titration**	**3rd titration**	**Global fit**
***K* / M^{-1}**	(0.41±5.64)×10^{4}	(2.17±1.01)×10^{5}	(2.64±8.61)×10^{5}	(1.7×±0.7)×10^{5}
***n* / basepairs**	0.13±1.85	3.314±1.12	4.45±0.98	3.36±1.02
***K* (*n*=6) / M^{-1}**	(2.70±0.16)×10^{5}	(5.19±0.51)×10^{5}	(4.18±0.29)×10^{5}	(4.0±0.3)×10^{5}

Bathochromic shift, nm	(401-421 nm)			
3.11d	**1st titration**	**2nd titration**	**3rd titration**	**Global fit**
***K* / M^{-1}**	$1.1\times10^{7}\pm3.8\times10^{7}$	$8.92\times10^{6}\pm1.42\times10^{7}$	$6.70\times10^{29}\pm1.32\times10^{41}$	$2817\pm1.28\times10^{6}$
***n* / basepairs**	93.27±43.74	77.95±19.15	76.05±23.5	0.86±390.4
***K* (*n*=6) / M^{-1}**	$(8.99\pm5.36)\times10^{4}$	$(9.18\pm2.93)\times10^{4}$	$(4.32\pm4.33)\times10^{4}$	$(2.04\pm0.7)\times10^{4}$
Bathochromic shift, nm	403-405			
3.12b	**1st titration**	**2nd titration**	**3rd titration**	**Global fit**
***K* / M^{-1}**	$867.0\pm6.36\times10^{5}$	$(1.00\pm0.58)\times10^{5}$	$(2.56\pm1.37)\times10^{5}$	$(1.36\pm0.59)\times10^{5}$
***n* / basepairs**	0.19±138.9	15.53±5.57	19.69±4.38	16.43±3.98
***K* (*n*=6) / M^{-1}**	$(3.21\pm0.24)\times10^{4}$	$(2.86\pm0.25)\times10^{4}$	$(1.96\pm0.13)\times10^{4}$	$(3.38\pm0.28)\times10^{4}$
Bathochromic shift, nm	396-406			
3.12d	**1st titration**	**2nd titration**	**3rd titration**	**Global fit**
***K* / M^{-1}**	$1611\pm2.65\times10^{6}$	$(1.73\pm1.42)\times10^{5}$	$(3.27\pm1.92)\times10^{5}$	$(2.98\pm2.15)\times10^{5}$
***n* / basepairs**	0.75±1234	42.82±18.11	58.20±11.70	55.84±15.55
***K* (*n*=6) / M^{-1}**	$(1.37\pm0.13)\times10^{4}$	$(1.27\pm0.14)\times10^{4}$	$(1.14\pm0.14)\times10^{4}$	$(1.24\pm0.17)\times10^{4}$
Bathochromic shift, nm	396-400			
3.13a	**1st titration**	**2nd titration**	**3rd titration**	**Global fit**
***K* / M^{-1}**	$3.03\times10^{20}\pm2.77\times10^{31}$	$1.62\times10^{18}\pm1.75\times10^{29}$	$2.74\times10^{6}\pm1.68\times10^{8}$	$4.24\times10^{27}\pm0.0$
***n* / basepairs**	18.20±0.0	$750.9\pm27\times10^{9}$	$750.9\pm27\times10^{9}$	1233±0.0

***K* (*n*=6) / M^{-1}**	$0.32\pm6.23\times10^{10}$	0.47±490.2	0.42±155.8	0.3±272.0
3.13d	**1st titration**	**2nd titration**	**3rd titration**	**Global fit**
***K* / M^{-1}**	$6.75\times10^{38}\pm0.00$	$1.85\times10^{43}\pm6.16\times10^{43}$	$3.06\times10^{42}\pm0.00$	$1.84\times10^{30}\pm6.34\times10^{40}$
***n* / basepairs**	758±0.00	$291.2\pm6.69\times10^{8}$	286.0±0.00	$2848\pm5.20\times10^{9}$
***K* (*n*=6) / M^{-1}**	0.83±2634	0.34±207.7	0.44±133.0	0.40±278.8
3.13e	**1st titration**	**2nd titration**	**3rd titration**	**Global fit**
***K* / M^{-1}**	$1.36\times10^{20}\pm0.00$	$1.20\times10^{26}\pm1.26\times10^{37}$	$6.58\times10^{19}\pm9.62\times10^{30}$	$1.50\times10^{44}\pm1.04\times10^{44}$
***n* / basepairs**	32.38±20.80	523.3±93.88	716.1±42.92	$1303\pm1.66\times10^{9}$
***K* (*n*=6) / M^{-1}**	$0.10\pm1.11\times10^{10}$	0.37±176.8	0.35±80.68	0.31±81.77

Appendix for Chapter 4

A4.1 Characterization of compounds using NMR spectroscopy

400_HUDA 2020 M1-mono DMSO\13C NMR: 500_HUDA 2021 conf M1-mono DMSO

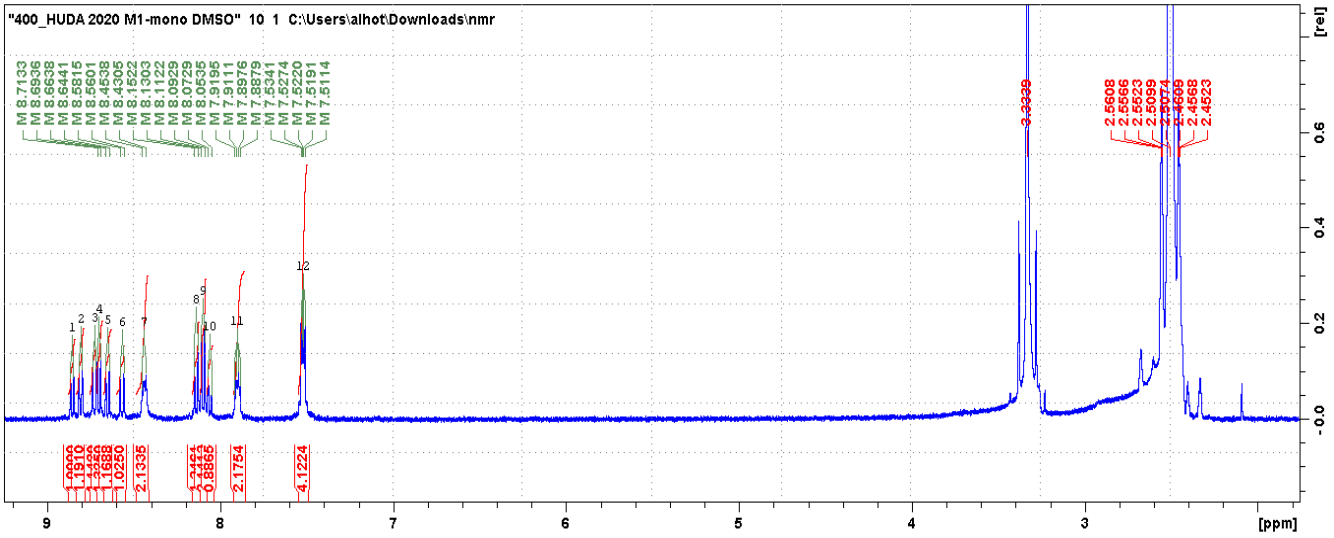

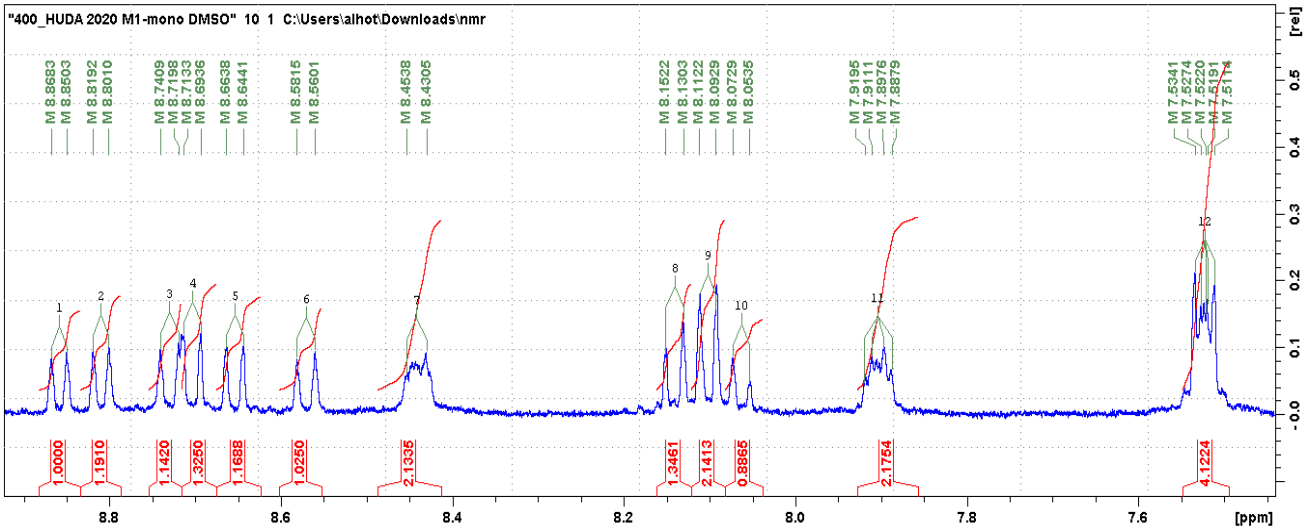

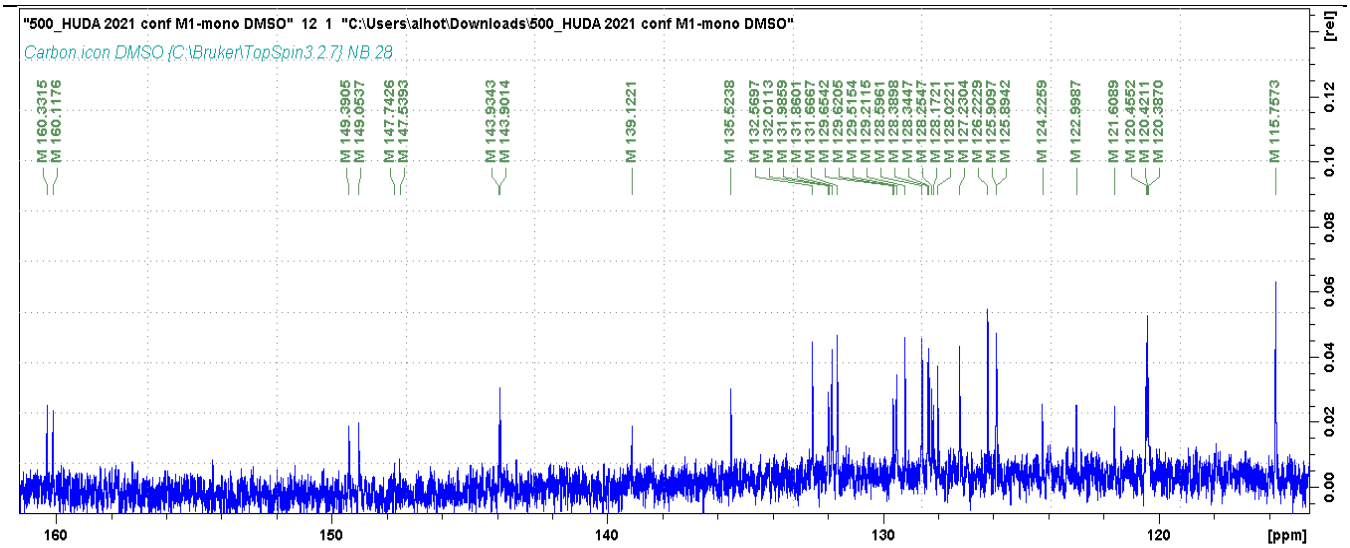

^{1}HNMR (400 MHz, DMSO): δ(ppm) 8.85 (d, *J*= 7.20, 1H, Ar-CH), 8.80 (d, *J*= 7.28, 1H, Ar-CH), 8.73 (d, *J*= 8.44 Hz, 1H, Ar-CH), 8.70 (d, *J*= 7.88 Hz, 1H, Ar-CH), 8.65 (d, *J*= 7.88 Hz, 1H, Ar-CH), 8.57 (d, *J*= 8.56 Hz, 1H, Ar-CH), 8.44 (m, 2H, Ar-CH), 8.14 (d, *J*= 8.76 Hz, 1H, Ar-CH), 8.10 (d, *J*= 7.72 Hz, 2H, Ar-CH), 8.06 (d, *J*= 7.76 Hz, 1H, Ar-CH), 7.90 (m, 2H, Ar-CH), 7.52 (m, 4H, Ar-CH). **^{13}C NMR (500 MHz, DMSO):** 160.33, 160.11, 149.39, 149.05, 147.74, 147.53, 143.93, 143.90, 139.12, 135.52, 132.56, 132.01, 131.98, 131.86, 131.66, 129.65, 129.62, 129.51, 129.21, 128.59, 128.38, 128.34, 128.25, 128.17, 128.02, 127.23, 126.22, 125.90, 125.89, 124.22, 122.99, 121.60, 120.45, 120.421, 120.38, 115.75. **HR FTMS+** calc for [$C_{18}H_{10}N_2OCl$] 305.0482 found 305.0489.

500_HUDA 2021 isomer 1 pure CDCl3

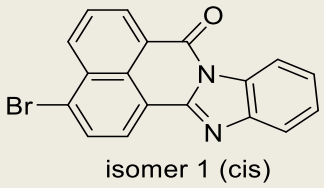

isomer 1 (cis)

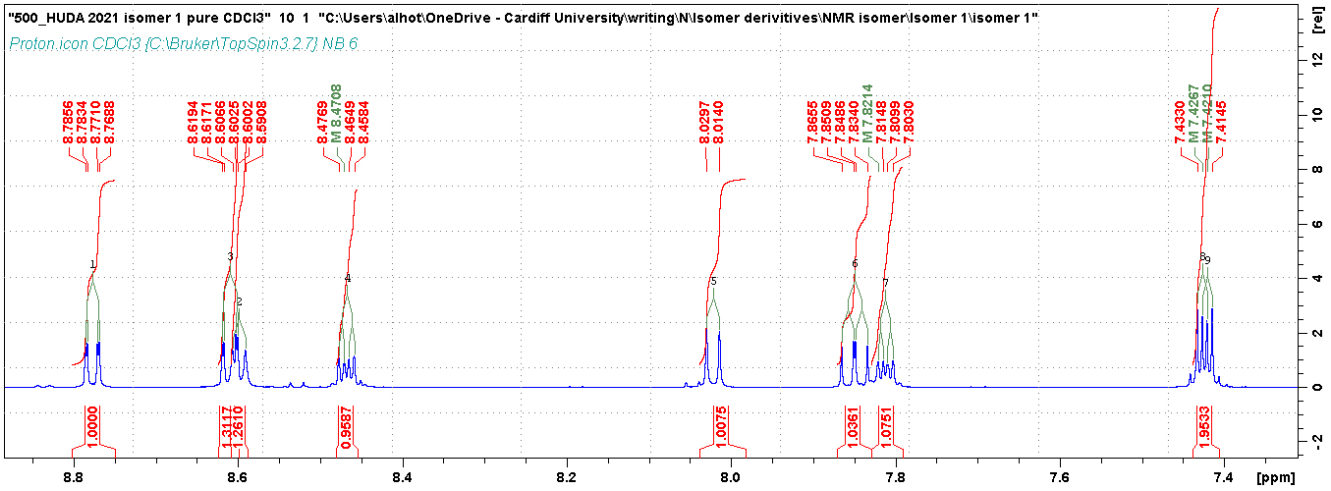

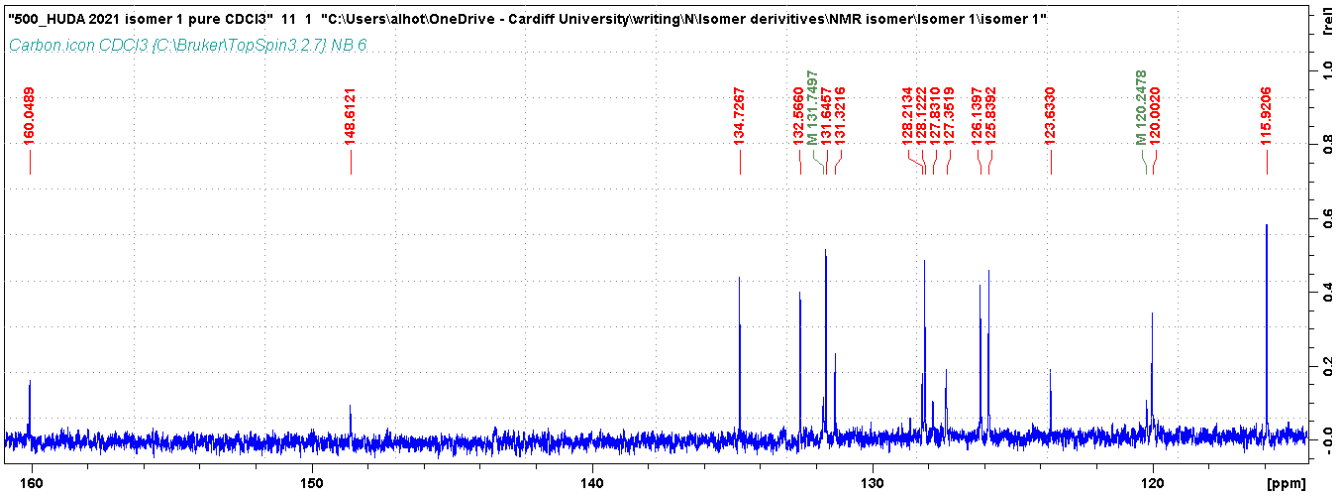

^{1}HNMR (500 MHz, CDCl3): δ(ppm): 8.77 (dd, *J*= 7.30, *J*= 1.10 Hz, 1H, Ar-CH), 8.60 (dd, *J*= 8.45, *J*= 1.15 Hz, 1H, Ar-CH), 8.59 (d, *J*= 7.90 Hz, 1H, Ar-CH), 8.46 (dd, *J*= 6.10, *J*= 3.15 Hz, 1H, Ar-CH), 8.01 (d, *J*= 7.85 Hz, 1H, Ar-CH), 7.84 (dd, *J*= 8.45, *J*= 7.30 Hz, 1H, Ar-CH), 7.80 (dd, *J*= 5.82, *J*= 3.37 Hz, 1H, Ar-CH), 7.42 (d, *J*= 6.05 Hz, 1H, Ar-CH), 7.42 (d, *J*= 6.10 Hz, 1H, Ar-CH). **^{13}C NMR (500 MHz, CDCl3): δ(ppm):** 160.04, 148.61, 134.72, 132.56, 131.74, 131.64, 131.32, 128.21, 128.12, 127.83, 127.35, 126.13, 125.83, 123.63, 120.24, 120.00, 115.92. **HR FTMS+** calc for [$C_{18}H_9N_2Obr$] 347.98928 found 347.9898.

400_HUDA 2021 isomer 1-S1 col 4 dry ACETONE

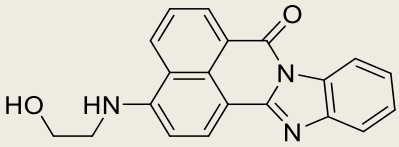

isomer 1 (cis)

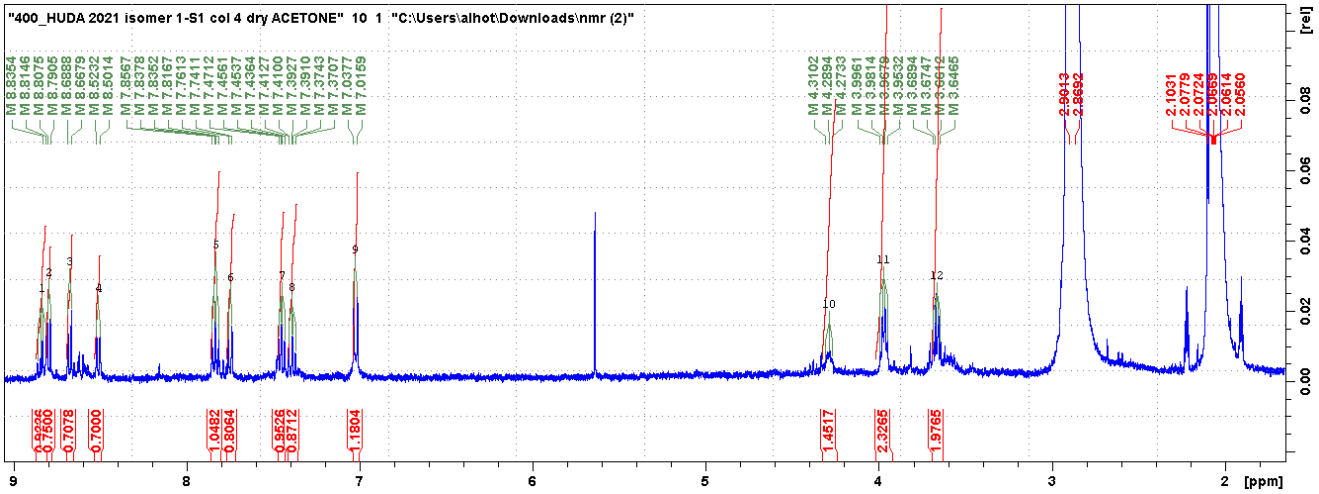

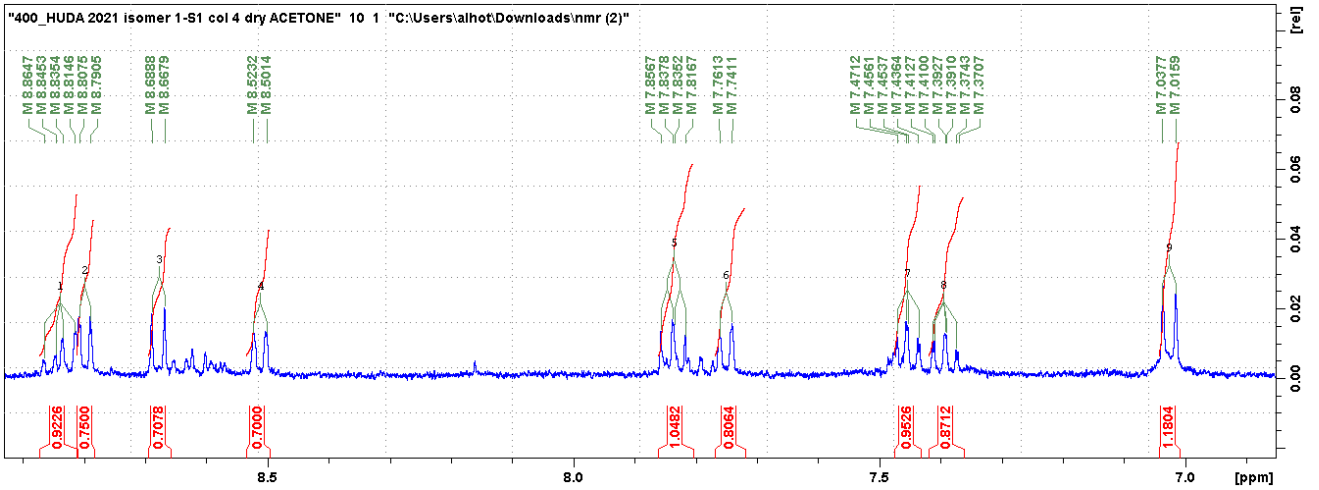

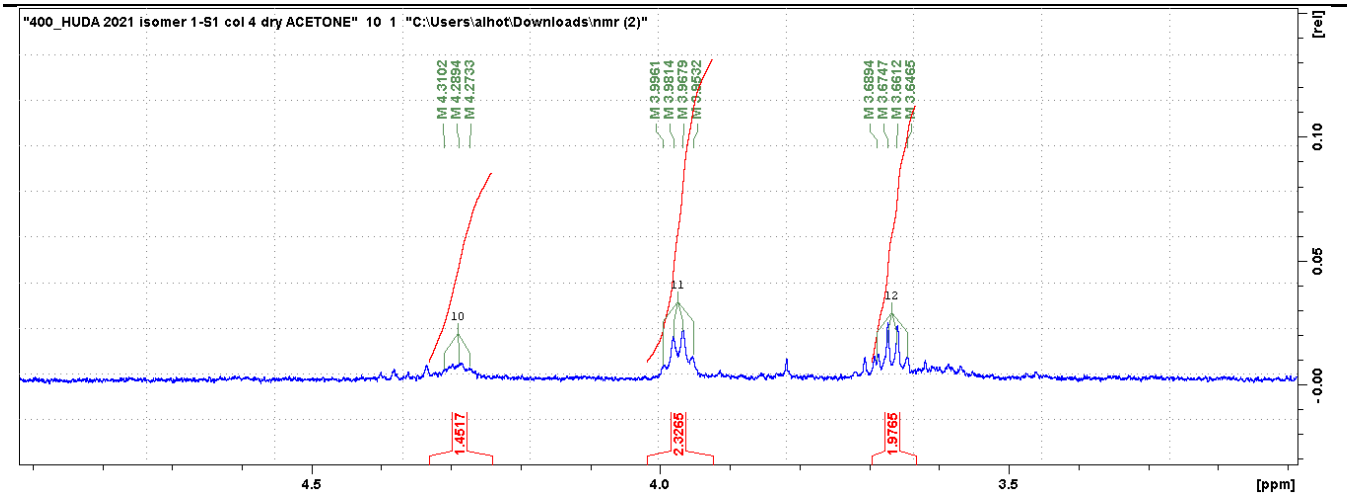

[1]HNMR (400 MHz, ACETONE-d6): δ(ppm): 8.82 (d, *J*= 8.32 Hz, 1H, Ar-CH), 8.79 (d, *J*= 6.80 Hz, 1H, Ar-CH), 8.67 (d, *J*= 8.36 Hz, 1H, Ar-CH), 8.51 (d, *J*= 8.72 Hz, 1H, Ar-CH), 7.83 (dd, *J*= 8.52 Hz, *J*= 7.48 Hz, 1H, Ar-CH), 7.75 (d, *J*= 8.08 Hz, 1H, Ar-CH), 7.45 (m, 1H, Ar-CH), 7.39 (m, 1H, Ar-CH), 7.02 (d, *J*= 8.72 Hz, 1H, Ar-CH), 4.28 (m, 1H, OH), 3.96 (q, *J*= 5.72 Hz, 2H, CH_2), 3.66 (q, *J*= 5.72 Hz, 2H, CH_2).**HR FTMS+** calc for [$C_{20}H_{16}N_3O_2$] 330.1242 found 330.1239.

500_HUDA 2021 isomer1-N1 dry crude ACETONE

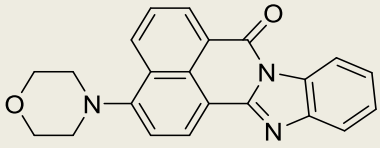

isomer 1 (cis)

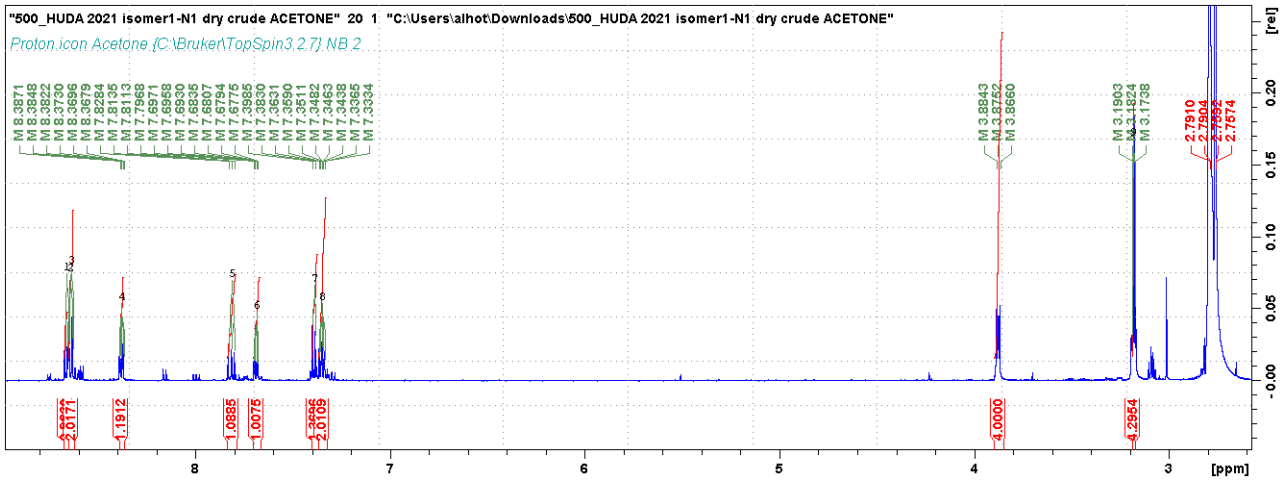

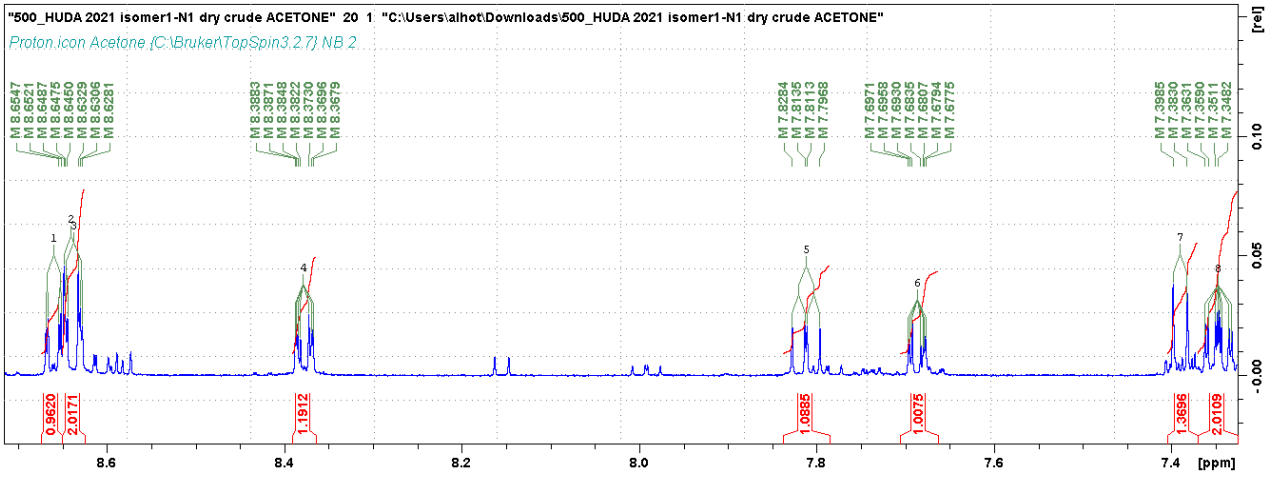

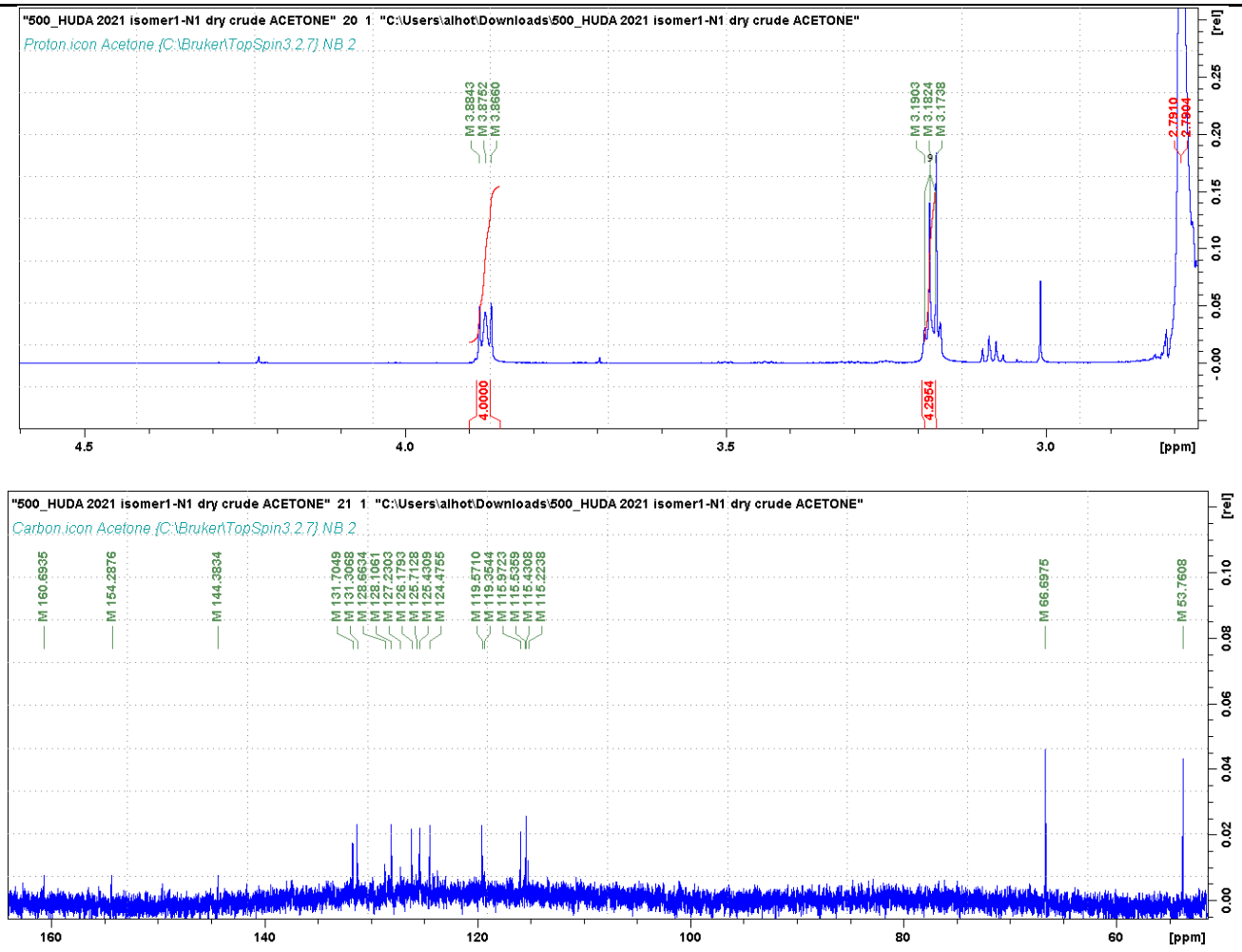

^{1}HNMR (500 MHz, ACETONE-d6): δ(ppm): 8.66 (dd, J= 7.20, J= 1.30 Hz, 1H, Ar-CH), 8.64 (d, J= 7.90, 1H, Ar-CH), 8.63 (dd, J= 8.32, J= 1.22 Hz, 1H, Ar-CH), 8.37 (m, 1H, Ar-CH), 8.81 (dd, J= 8.45, J= 7.35 Hz, 1H, Ar-CH), 7.68 (m, 1H, Ar-CH), 7.39 (d, J= 7.75 Hz, 1H, Ar-CH), 7.34 (m, 2H, Ar-CH), 3.87 (t, J= 4.58 Hz, 4H, CH2), 3.18 (t, J= 4.12 Hz, 4H, CH2). **^{13}C NMR (125 MHz, ACETONE-d6): δ(ppm):** 160.7, 154.3, 144.4, 131.7, 131.3, 128.7, 128.1, 127.2, 126.2, 125.7, 125.4, 124.5, 119.6, 119.4, 116.0, 115.5, 115.4, 115.2, 66.7. **HR FTMS+** calc for [$C_{22}H_{18}N_3O_2$] 356.1399 found 356.1396.

500_HUDA 2021 isomer1-N2 2nd col col 6 ACERONE

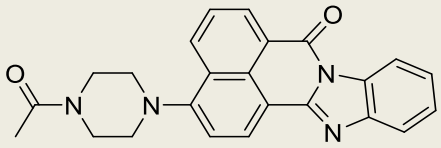

isomer 1 (cis)

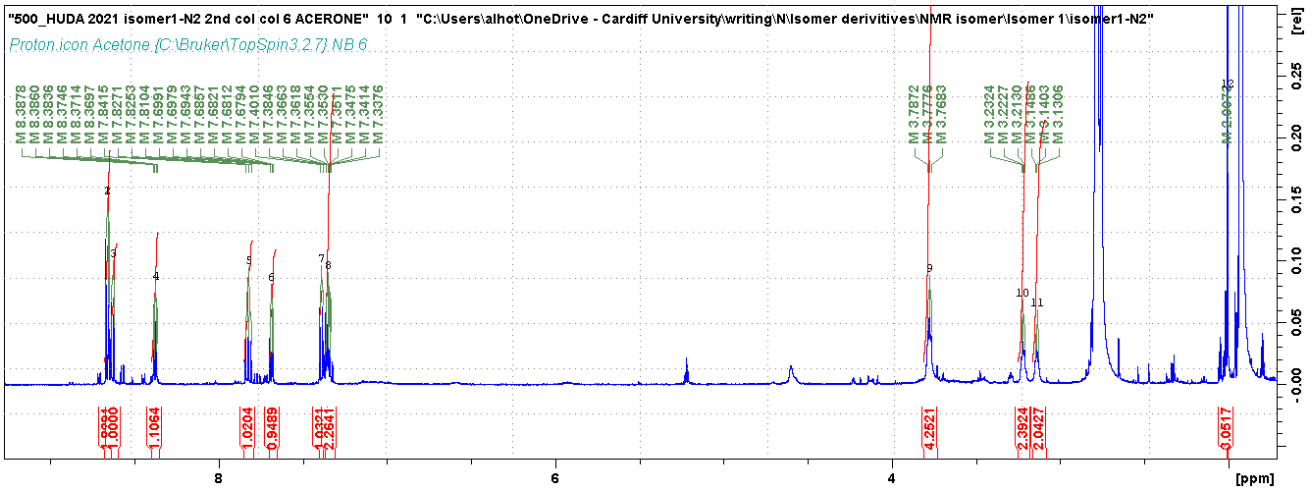

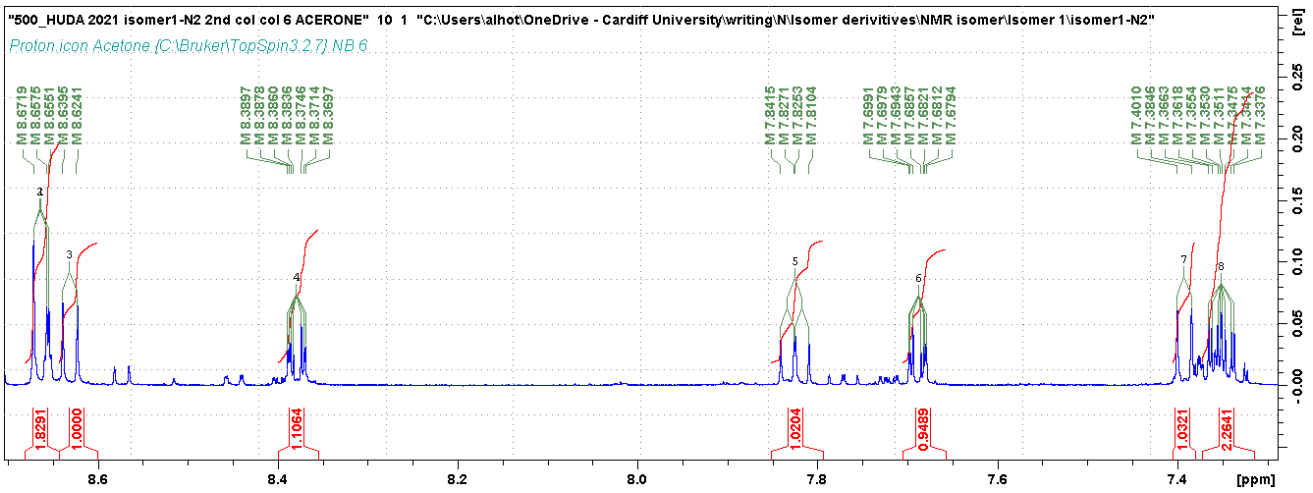

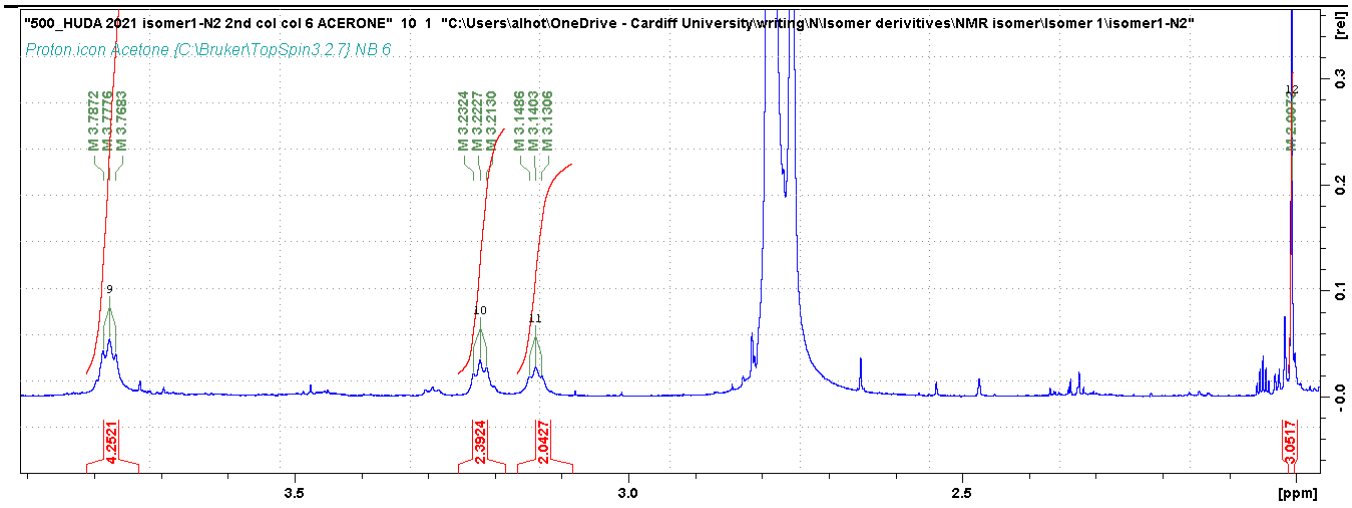

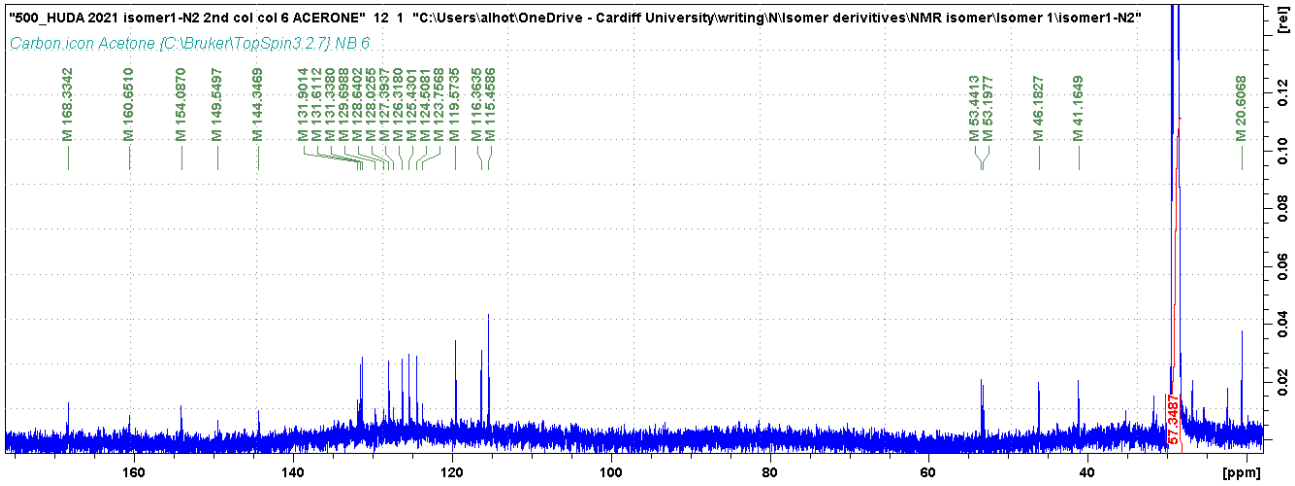

^{1}HNMR (500 MHz, ACETONE-d6): δ(ppm): 8.66 (d, *J*= 7.20 Hz, 1H, Ar-CH), 8.66 (d, *J*= 8.40 Hz, 1H, Ar-CH), 8.63 (d, *J*= 7.70 Hz, 1H, Ar-CH), 8.38 (m, 1H, Ar-CH), 7.82 (dd, *J*= 8.22, *J*= 7.32 Hz, 1H, Ar-CH), 7.68 (m, 1H, Ar-CH), 7.39 (d, *J*= 8.20 Hz, 1H, Ar-CH), 7.35 (m, 2H, Ar-CH), 3.77 (t, *J*= 4.72 Hz, 4H, CH_2), 3.22 (t, *J*= 4.85 Hz, 2H, CH_2), 3.14 (t, *J*= 4.50 Hz, 2H, CH_2), 2.00 (s, 3H, CH_3). **^{13}C NMR (125 MHz, ACETONE-d6): δ(ppm):** 168.3, 160.7, 154.1, 149.5, 144.3, 131.9, 131.6, 131.3, 129.7, 128.6, 128.0, 127.4, 126.3, 125.4, 124.5, 123.8, 119.6, 116.4, 115.5, 53.4, 53.2, 46.2, 41.2, 20.6. **HR TOF MS ES+** calc for [$C_{24}H_{21}N_4O_2$] 397.1674 found 397.1665.

400_HUDA 2021 isomer 1-Su1 col 14 DMSO

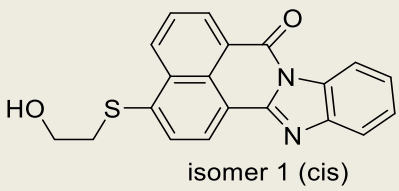

isomer 1 (cis)

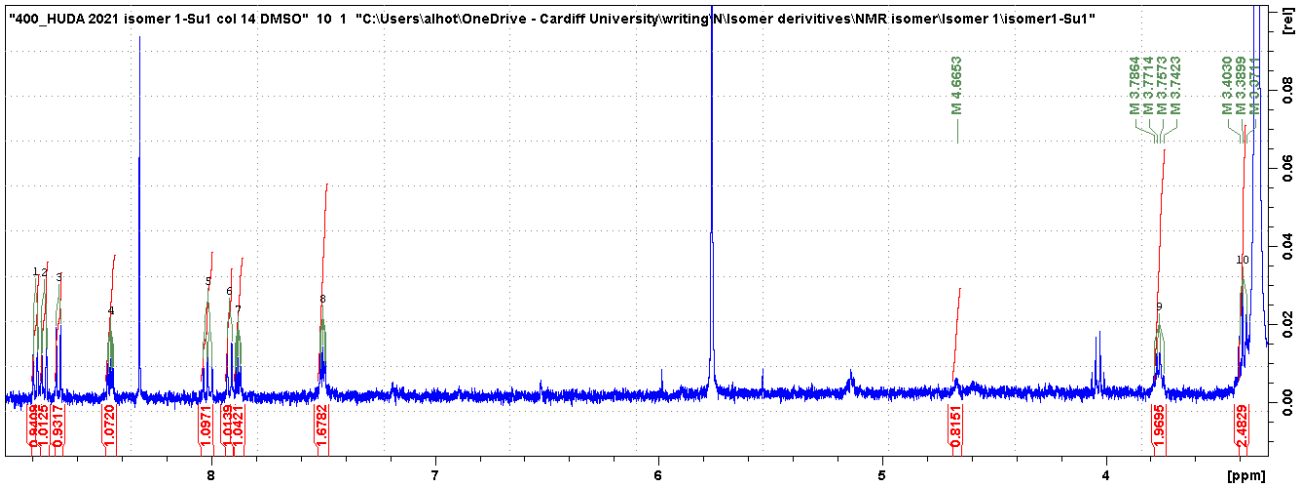

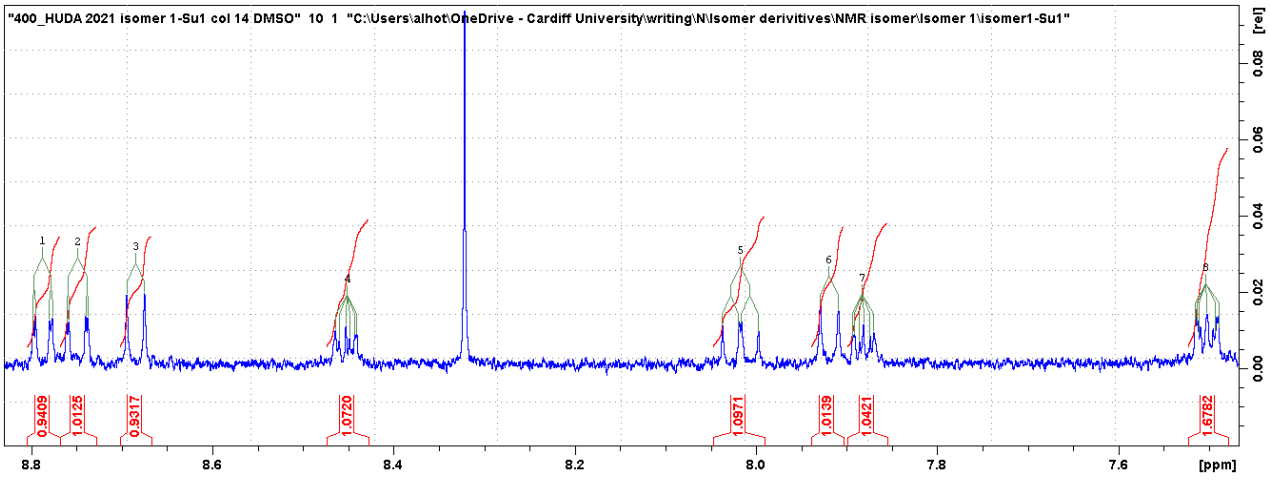

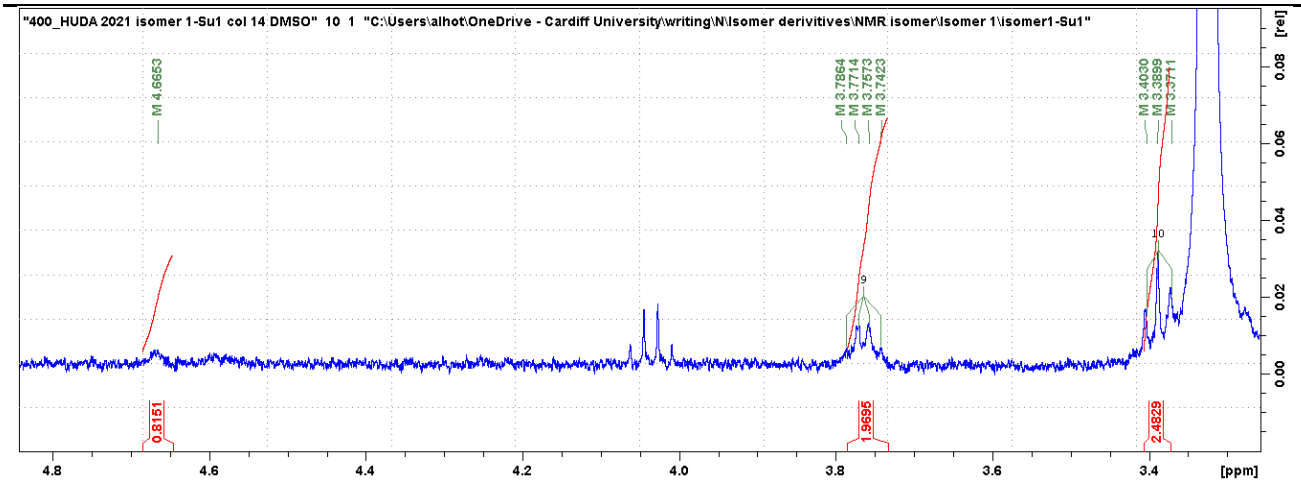

^{1}HNMR (400 MHz, DMSO): δ(ppm): 8.78 (dd, J= 7.44 Hz, J= 1.24 Hz, 1H, Ar-CH), 8.74 (dd, J= 8.46 Hz, J= 0.90 Hz, 1H, Ar-CH), 7.92 (d, J= 7.92 Hz, 1H, Ar-CH), 8.45 (m, 1H, Ar-CH), 8.01 (dd, *J*= 8.52 Hz, *J*= 7.24 Hz, 1H, Ar-CH), 7.92 (d, *J*= 8.04 Hz, 1H, Ar-CH), 7.88 (m, 1H, Ar-CH), 7.50 (m, 2H, Ar-CH), 4.66 (s, 1H, OH), 3.75 (q, *J*= 5.88 Hz, 2H, CH_2), 3.38 (t, *J*= 6.38 Hz, 2H, CH_2). **HR FTMS^{+}** calc for $[C_{20}H_{14}N_2O_2S]$ 346.07705 found 346.0776.

500_HUDA 2021 isomer 2 CDCl3

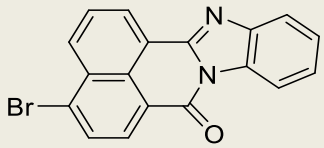

isomer 2 (trans)

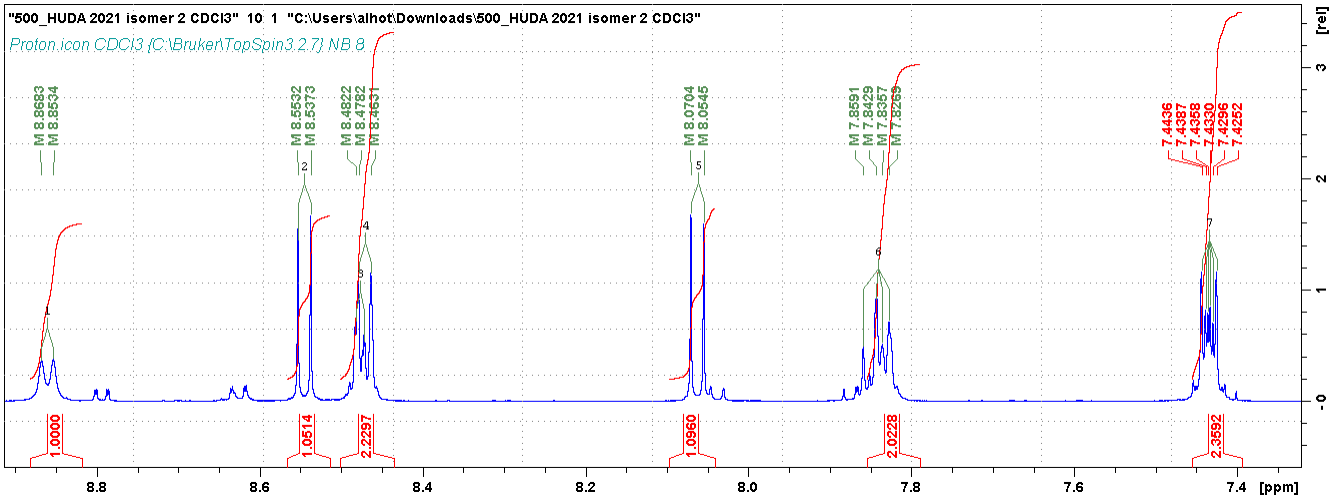

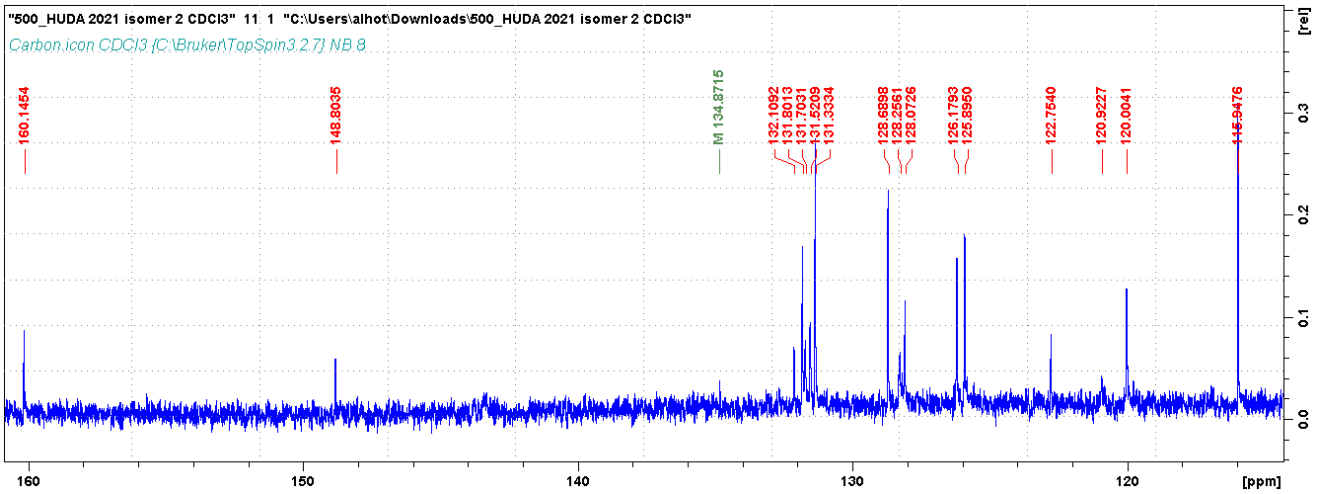

^{1}HNMR (500 MHz, CDCl3): δ(ppm): 8.86 (dd, *J*= 7.45 Hz, 1H, Ar-CH), 8.54 (d, *J*= 7.95 Hz, 1H, Ar-CH), 8.47 (d, *J*= 5.85 Hz, 1H, Ar-CH), 8.47 (d, *J*= 7.55 Hz, 1H, Ar-CH), 8.06 (d, *J*= 7.95 Hz, 1H, Ar-CH), 7.84 (m, 2H, Ar-CH), 7.43 (m, 2H, Ar-CH). **^{13}C NMR (500 MHz, CDCl3): δ(ppm):** 160.14, 148.80, 134.87, 132.10, 131.80, 131.70, 131.52, 131.33, 128.68, 128.25, 128.07, 126.17, 125.89, 122.75, 120.92, 120.00, 115.94. **HR FTMS+** calc for [$C_{18}H_9N_2OBr$] 347.98928 found 347.0805.

400_HUDA 2021 isomer 1-S1 col 4 dry ACETONE (Not consistent with structure)

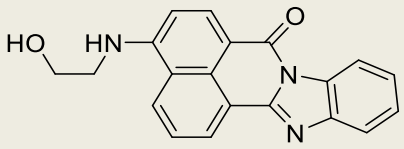

isomer 2-S1 (trans)

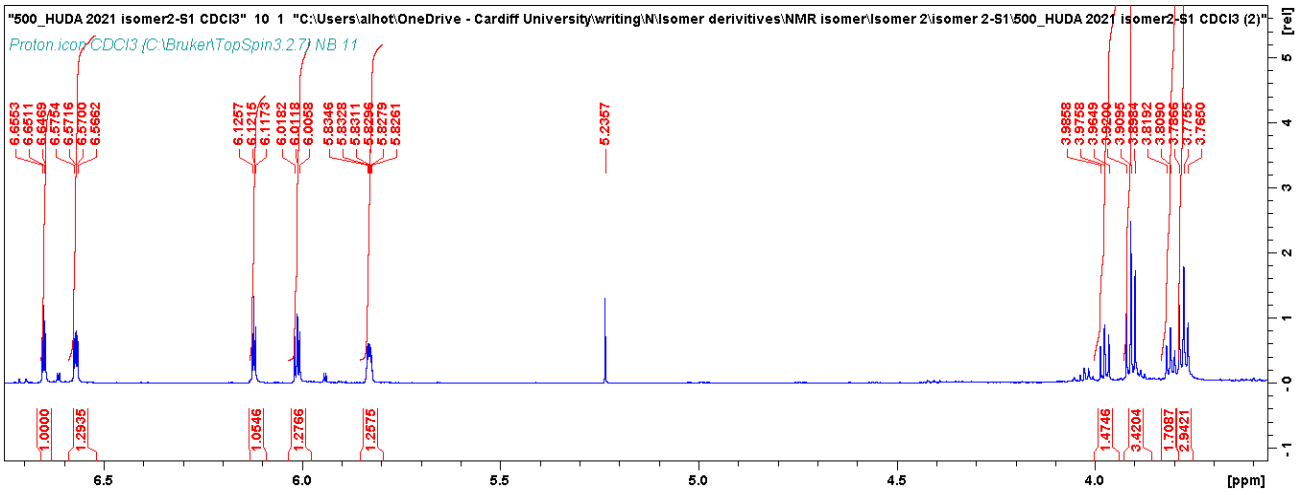

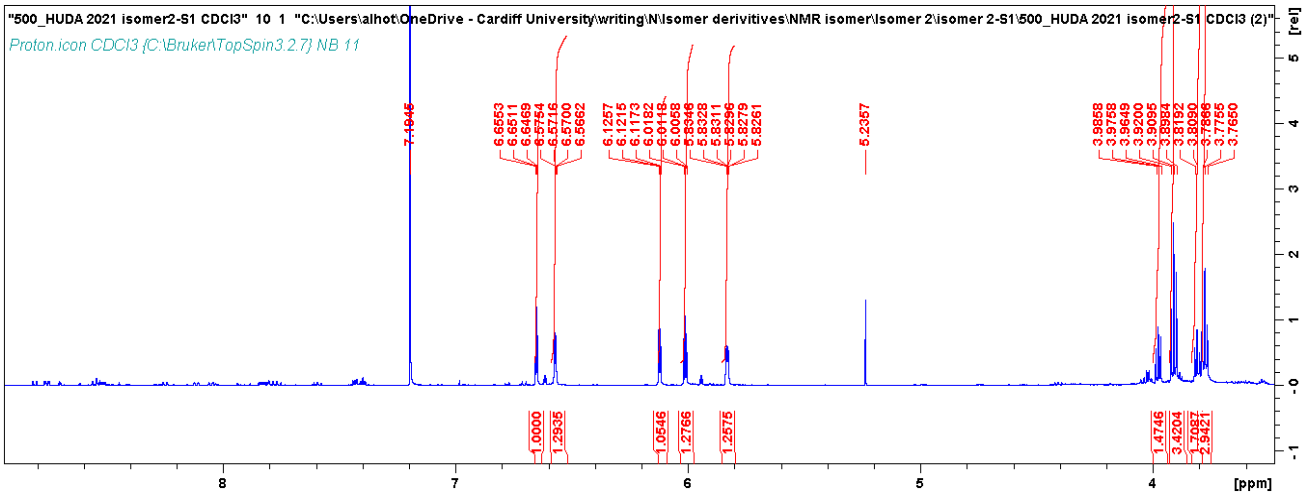

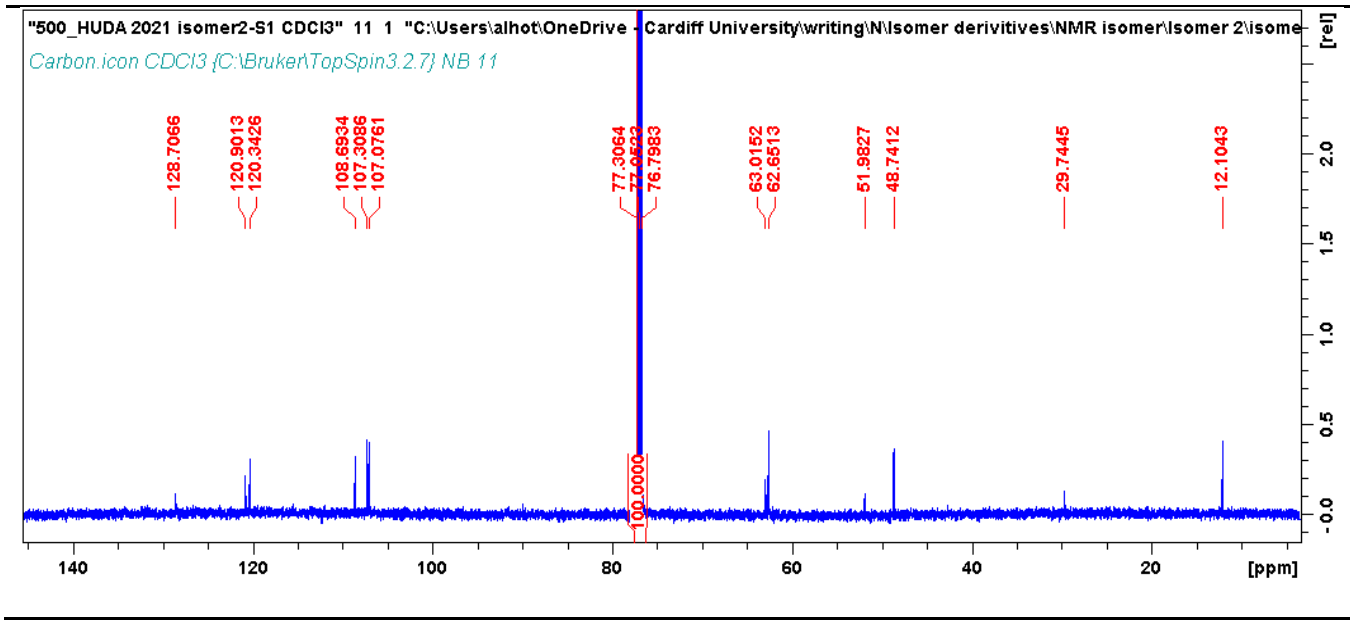
"500_HUDA 2021 isomer2-S1 CDCl3" 11 1 "C:\Users\alhot\OneDrive - Cardiff University\writing\N\Isomer derivitives\NMR isomer\Isomer 2\isome
Carbon.icon CDCl3 {C:\Bruker\TopSpin3.2.7} NB 11
128.7066
120.9013
120.3426
108.6934
107.3086
107.0761
77.3064
77.0522
76.7983
63.0152
62.6513
51.9827
48.7412
29.7445
12.1043
100.0000
[rel]
2.0
1.5
1.0
0.5
-0.0
140
120
100
80
60
40
20
[ppm]

500_HUDA 2021 isomer 2-N1 crude after extraction dry CDCl3

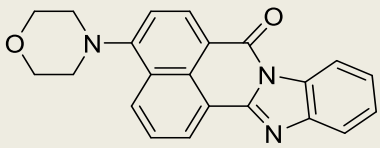

isomer 2 (trans)

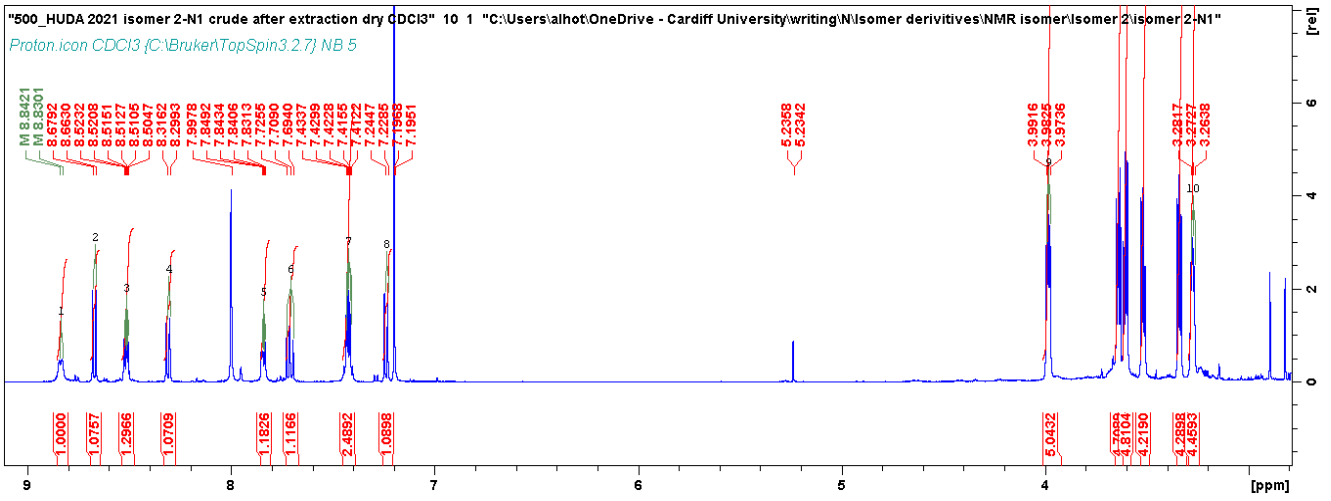

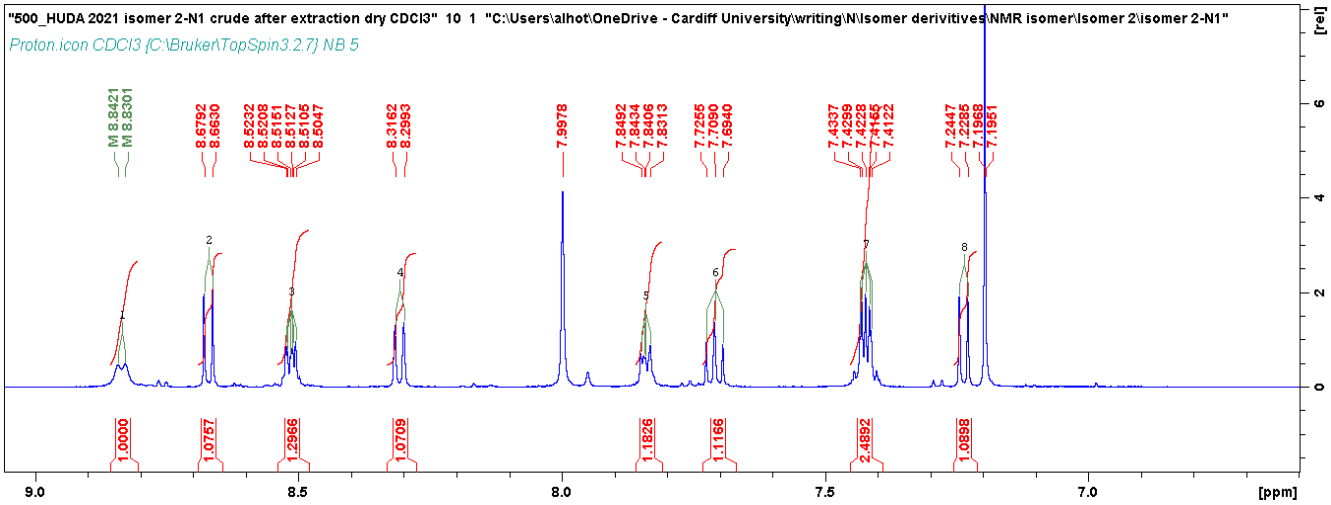

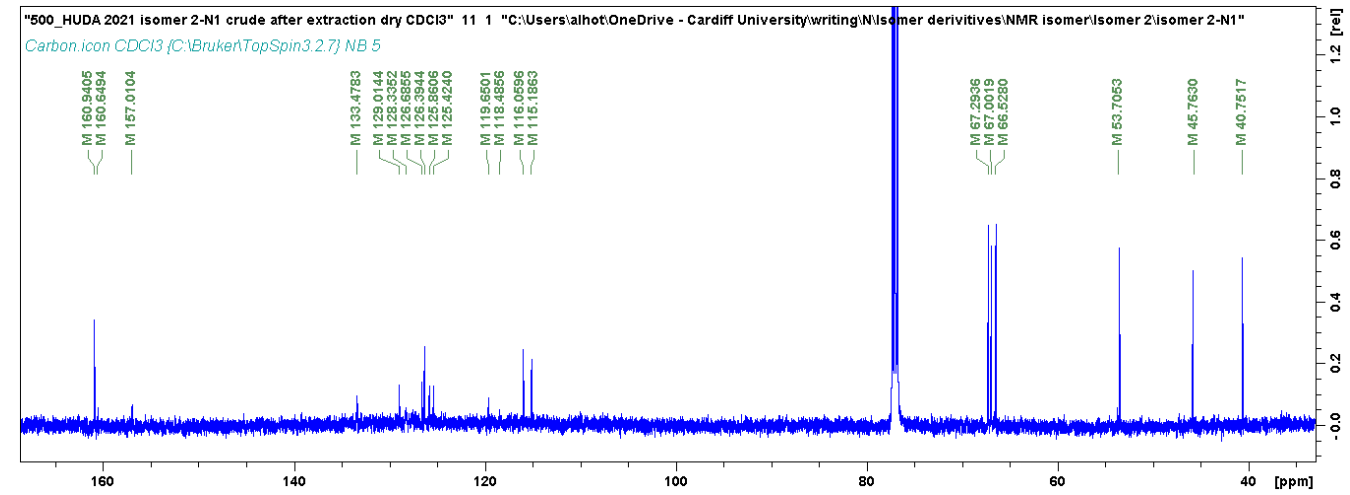
"500_HUDA 2021 isomer 2-N1 crude after extraction dry CDCl3" 11 1 "C:\Users\alhot\OneDrive - Cardiff University\writing\N\Isomer derivitives\NMR isomer\Isomer 2\isomer 2-N1"
Carbon.icon CDCl3 {C:\Bruker\TopSpin3.2.7} NB 5
M 160.9405
M 160.6494
M 157.0104
M 133.4783
M 129.0144
M 128.3352
M 126.5855
M 126.3944
M 125.9606
M 125.4240
M 119.6501
M 118.4856
M 116.0596
M 115.1863
M 67.2936
M 67.0019
M 66.5280
M 53.7053
M 45.7630
M 40.7517
[rel]
[ppm]

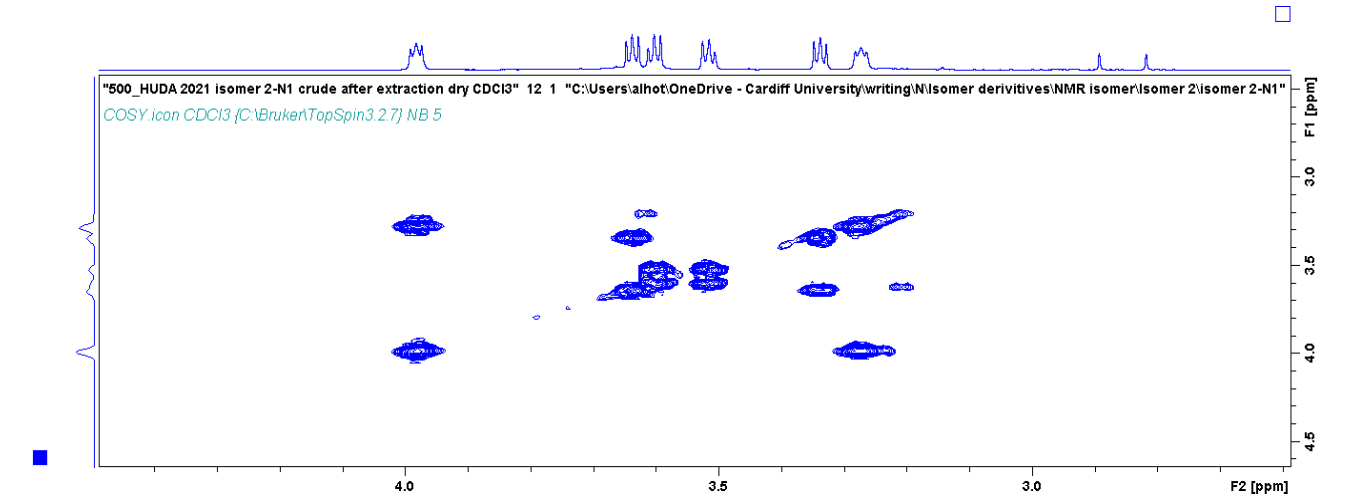
"500_HUDA 2021 isomer 2-N1 crude after extraction dry CDCl3" 12 1 "C:\Users\alhot\OneDrive - Cardiff University\writing\N\Isomer derivitives\NMR isomer\Isomer 2\isomer 2-N1"
COSY.icon CDCl3 {C:\Bruker\TopSpin3.2.7} NB 5
F1 [ppm]
F2 [ppm]

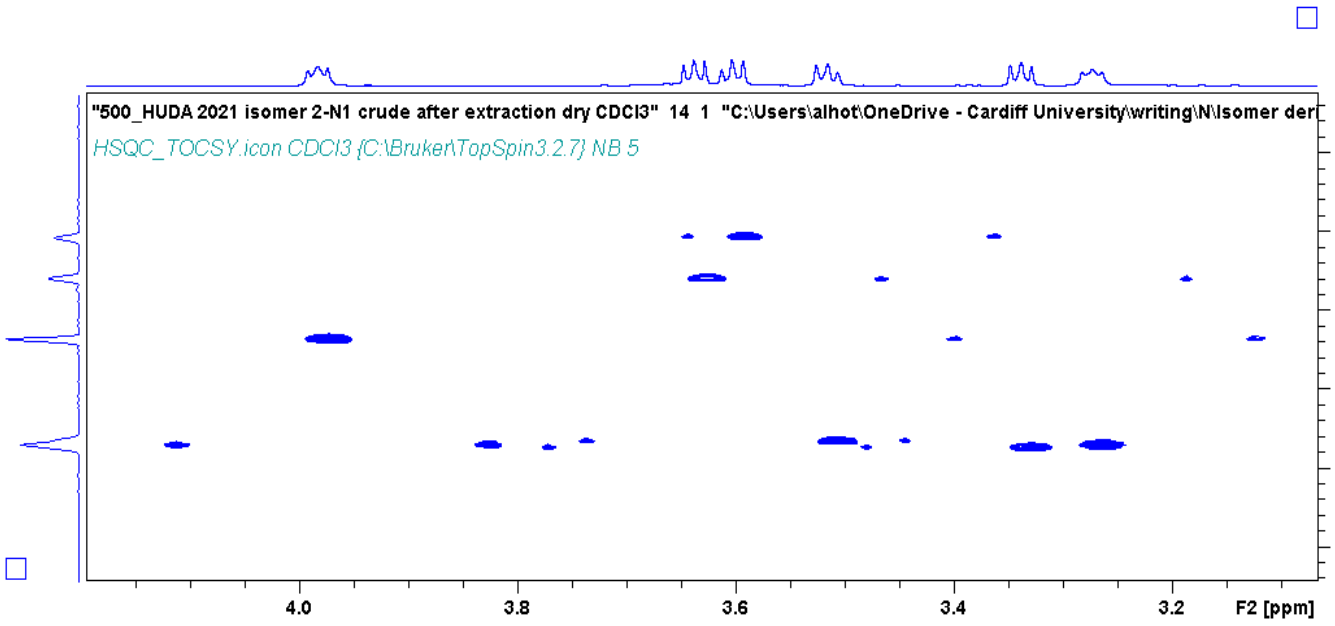

^{1}HNMR (500 MHz, ACETONE-d6): δ(ppm): 8.83 (d, *J*= 6.0, J= 1.30 Hz, 1H, Ar-CH), 8.66 (d, *J*= 8.1, 1H, Ar-CH), 8.51 (m, 1H, Ar-CH), 8.30 (d, *J*=8.5, 1H, Ar-CH), 7.84 (m, 1H, Ar-CH), 7.70 (t, *J*=7.8, 1H, Ar-CH), 7.41 (m, 1H, Ar-CH), 7.22 (d, *J*=8.10, 1H, Ar-CH), 3.98 (t, *J*= 4.50 Hz, 4H, CH_2), 4.47 (t, *J*= 4.5 Hz, 4H, CH_2). **^{13}C NMR (125 MHz, CDCl3): δ (ppm):** 160.9, 160.6, 157.0, 133.5, 129.0, 128.3, 126.7, 126.4, 125.9, 125.4, 119.7, 118.5, 116.1, 115.2, 66.5, 53.7. **HR TOF MS ES+** calc for [$C_{22}H_{18}N_3O_2$] 356.1399 found 356.1399.

500_HUDA 2021 isomer 2-N2 col 5 CDCl3

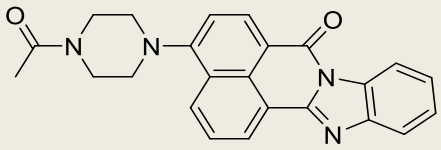

isomer 2 (trans)

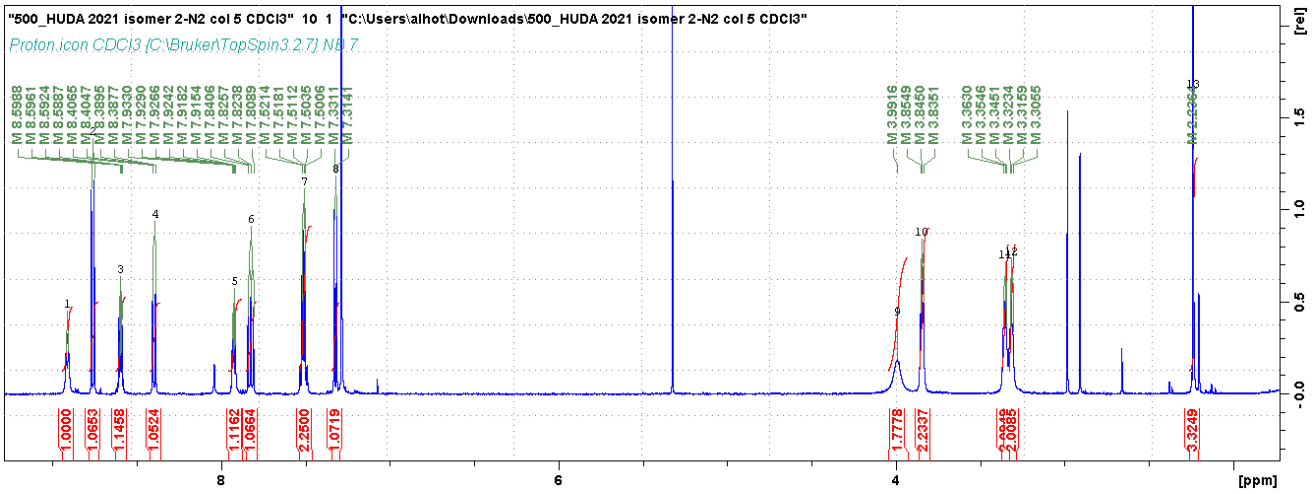

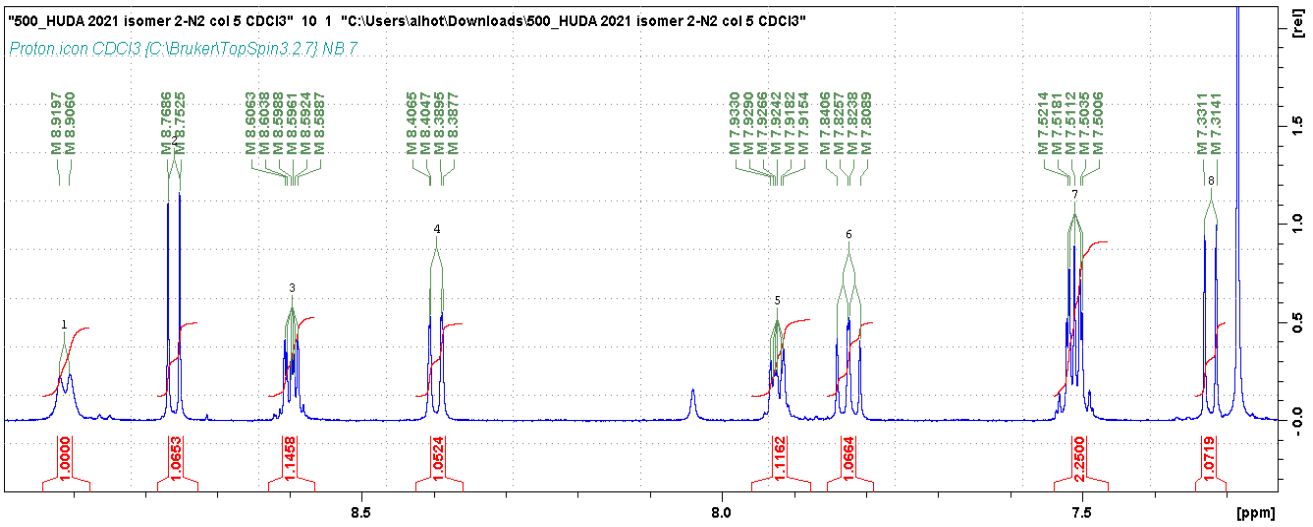

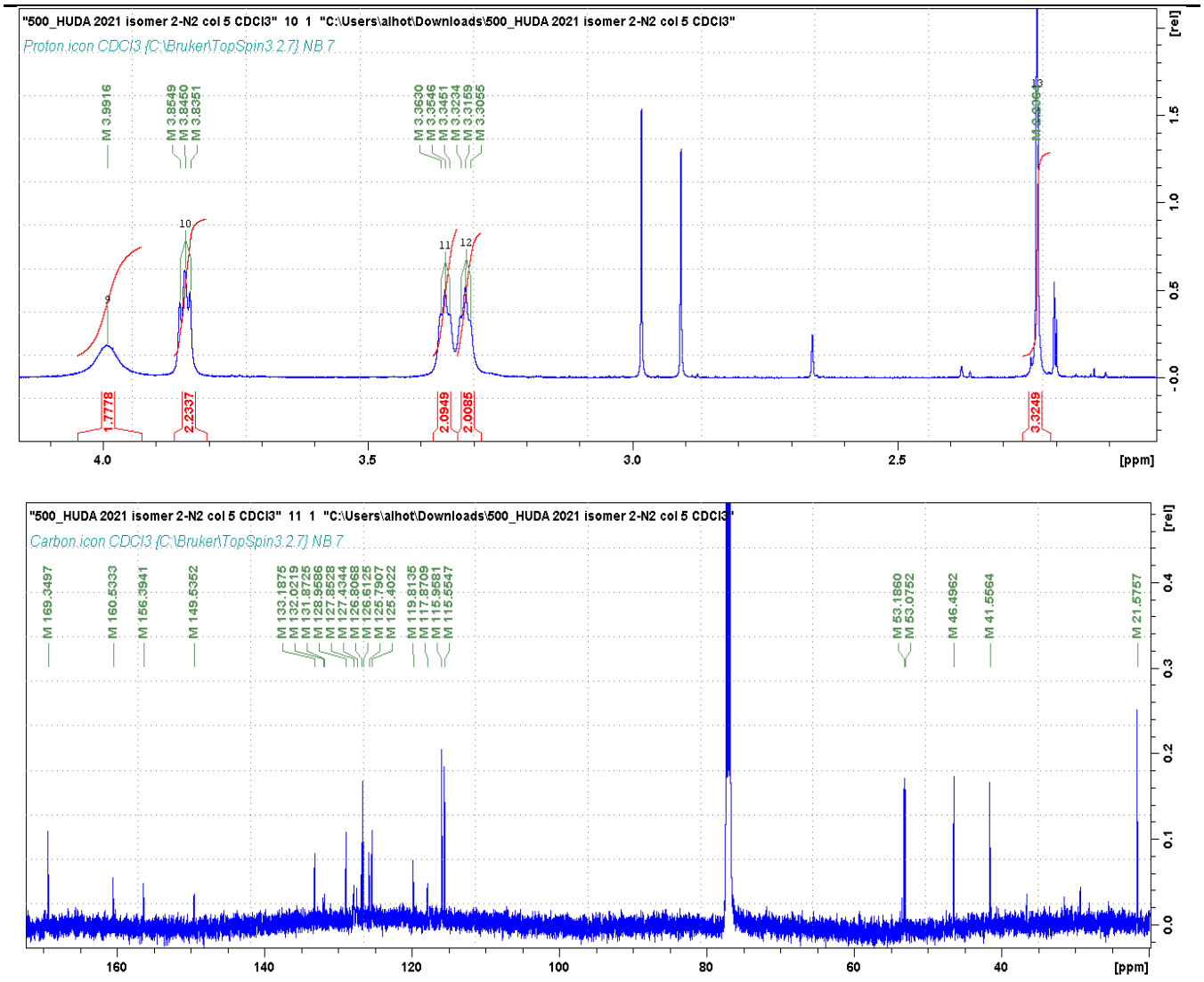

^{1}HNMR (500 MHz, CDCl3): δ(ppm): 8.91 (d, *J*= 6.85 Hz, 1H, Ar-CH), 8.76 (d, *J*= 8.05 Hz, 1H, Ar-CH), 8.59 (m, 1H, Ar-CH), 8.49 (dd, *J*= 8.50 Hz, *J*= 0.90 Hz, 1H, Ar-CH), 7.92 (m, 1H, Ar-CH), 7.82 (dd, *J*= 8.40 Hz, *J*= 7.45 Hz, 1H, Ar-CH), 7.51 (m, 2H, Ar-CH). 7.32 (d, *J*= 8.50 Hz, 1H, Ar-CH), 3.99 (br.signal, 2H, CH_2), 3.84 (t, *J*= 4.95 Hz, 2H,CH_2), 3.35 (t, *J*= 4.47 Hz, 2H,CH_2), 3.31 (t, *J*= 4.47 Hz, 2H,CH_2), 2.23 (s, 3H, CH_3). **^{13}C NMR (500 MHz, CDCl3): δ(ppm):** 169.3, 160.5, 156.4, 149.5, 133.2, 132.0, 131.9, 129.0, 127.9, 127.4, 126.8, 126.6, 125.8, 125.4, 119.8, 117.9, 116.0, 115.6, 53.2, 53.1, 46.5, 41.6, 21.6. **HR TOF MS ES+** calc for [$C_{24}H_{21}N_4O_2$] 397.1665 found 397.1666.

500_HUDA 2021 isomer 2-Su1 col 8 ACETONE

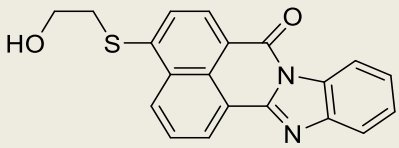

isomer 2 (trans)

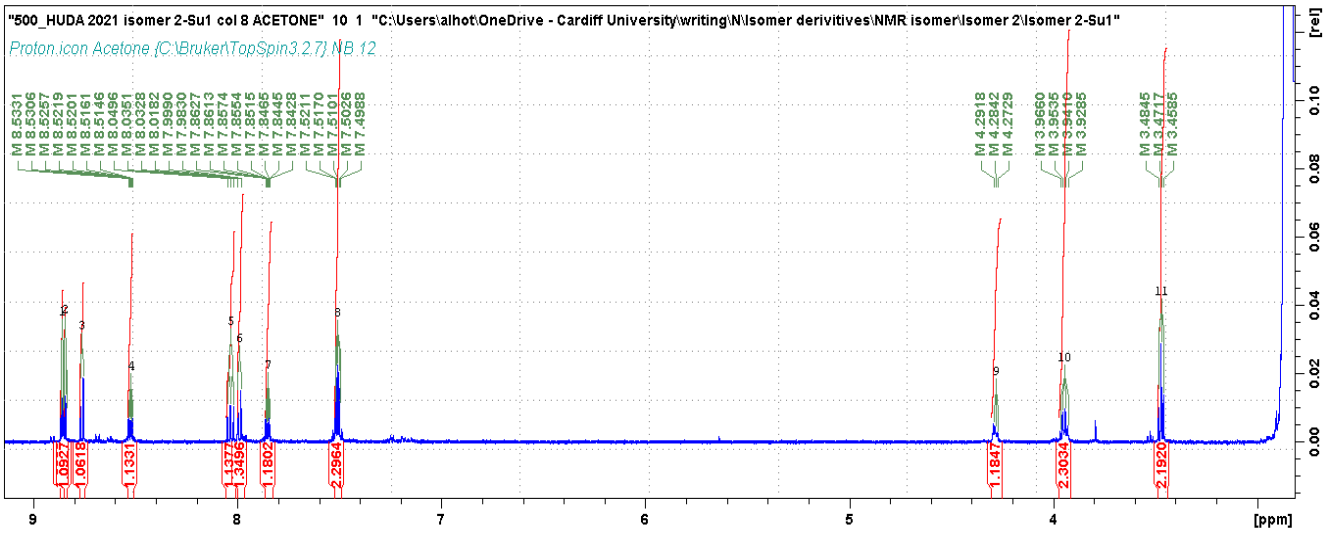

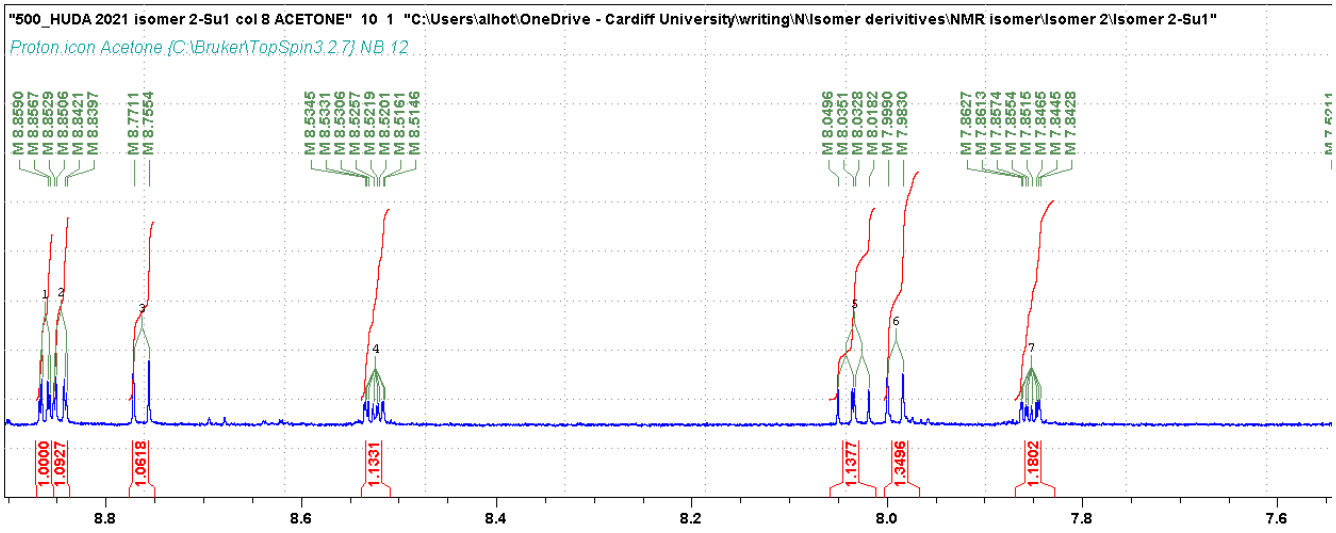

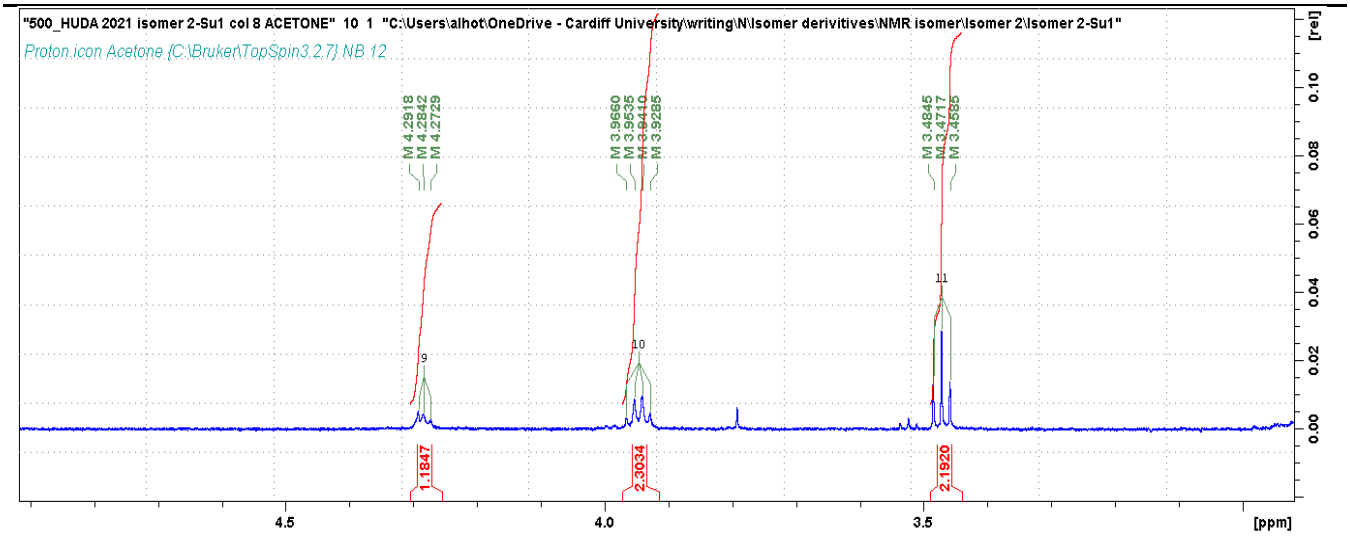

^{1}H-NMR (500 MHz, ACETONE-d_6): δ(ppm): 8.85 (dd, *J*= 7.25, *J*= 1.20 Hz, 1H, Ar-CH), 8.50 (dd, *J*= 8.47, *J*= 1.17 Hz, 1H, Ar-CH), 8.76 (d, *J*= 7.85 Hz, 1H, Ar-CH), 8.52 (m, 1H, Ar-CH), 8.03 (dd, *J*= 8.42, *J*= 7.27 Hz, 1H, Ar-CH), 7.99 (d, *J*= 8.00 Hz, 1H, Ar-CH), 7.85 (m, 1H, Ar-CH), 7.51 (t, *J*= 5.57 Hz, 1H, Ar-CH), 7.51 (d, *J*= 7.30 Hz, 1H, Ar-CH), 4.28 (t, *J*=4.72 Hz, 1H, C-OH), 3.94 (q, *J*= 6.25 Hz, 2H, CH_2), 3.47 (t, *J*= 6.50 Hz, 2H, CH_2).**TOF MS ES+** calc for [$C_{20}H_{15}N_2O_2S$] 347.0854 found 347.0842.

A4.2 Characterization of compounds using mass spectrometry

Comp.	Mass spectrum code	Comp.	Mass spectrum code
4.14\15-Cl	MS35759_HR_ES	4.14d	MS35154_HR_EI
4.14	MS35139_HR_EI	4.15	MS35140_HR_EI
4.14a	MS35582_HR_ES	4.15b	MS35828_HR_ES
4.14b	MS35767_HR_ES	4.15c	MS35843_HR_ES
4.14c	MS35796_HR_ES	4.15d	MS35159_HR_ES

A4.3 UV-vis titration spectra

Compound	1st titration	2nd titration
4.16	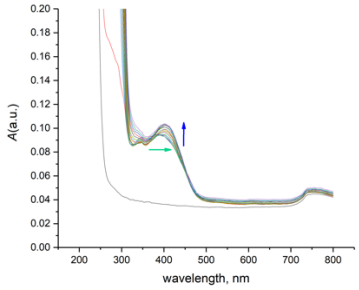	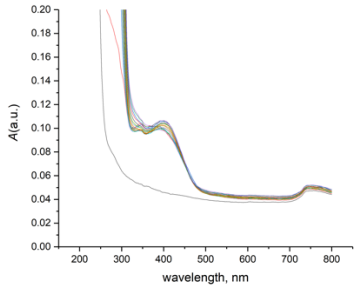
4.16a	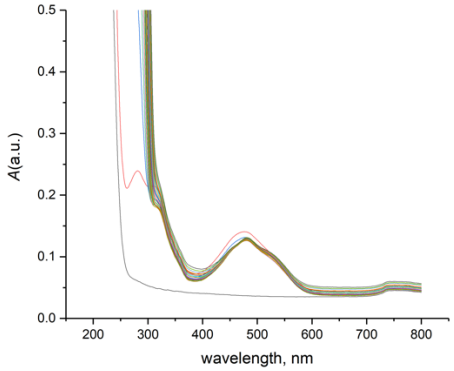	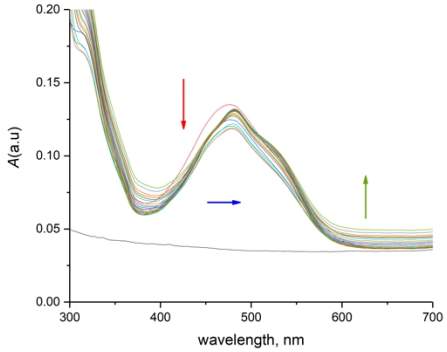
4.16b	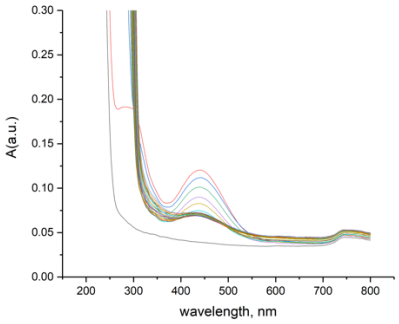	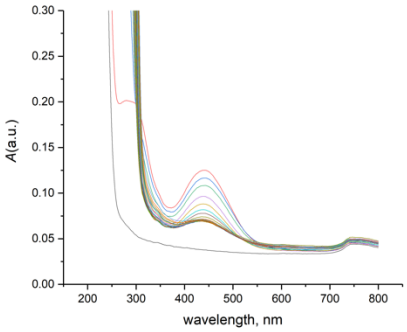

4.16c	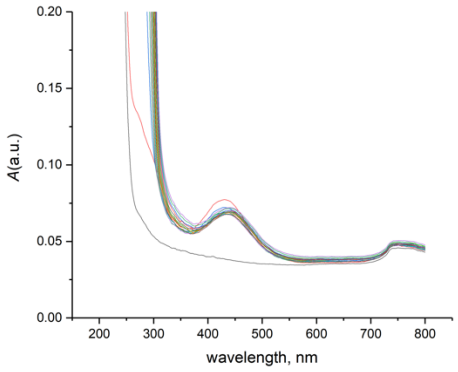	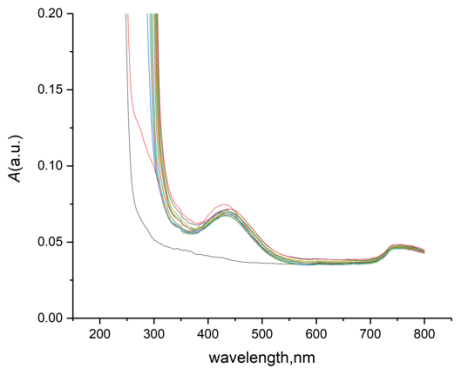
4.16d	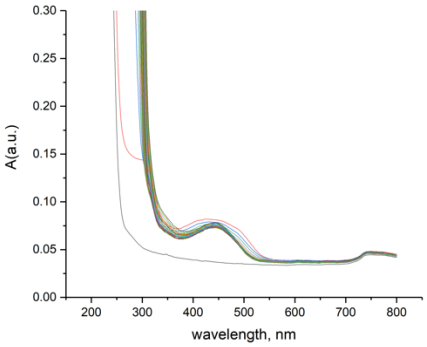	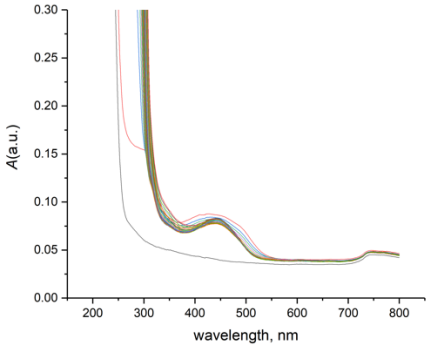
4.17	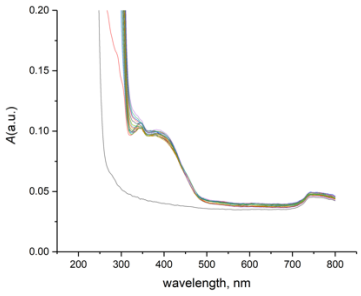	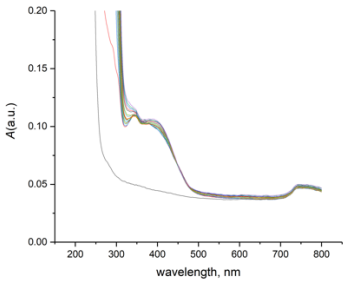
4.17b	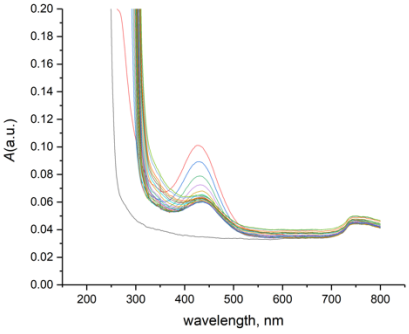	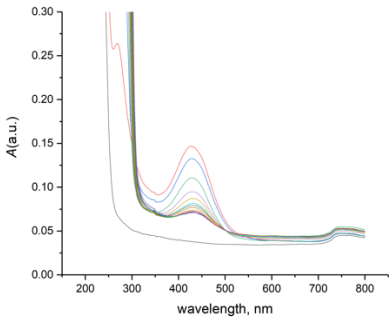

4.17c	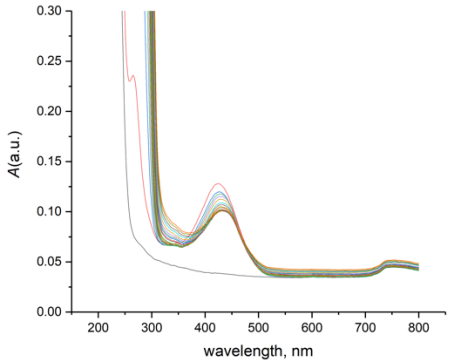 A(a.u.) 0.30 0.25 0.20 0.15 0.10 0.05 0.00 200 300 400 500 600 700 800 wavelength, nm	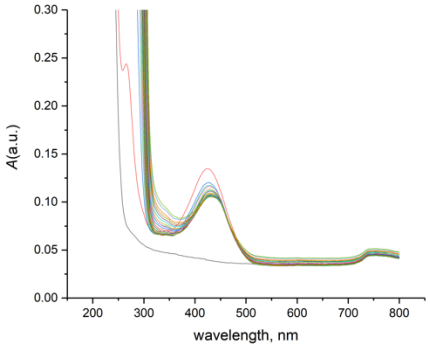 A(a.u.) 0.30 0.25 0.20 0.15 0.10 0.05 0.00 200 300 400 500 600 700 800 wavelength, nm
4.17d	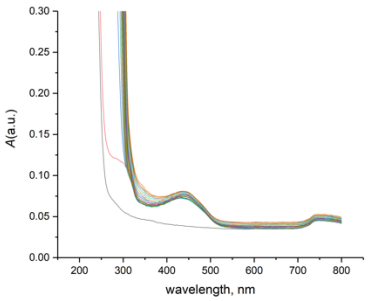 A(a.u.) 0.30 0.25 0.20 0.15 0.10 0.05 0.00 200 300 400 500 600 700 800 wavelength, nm	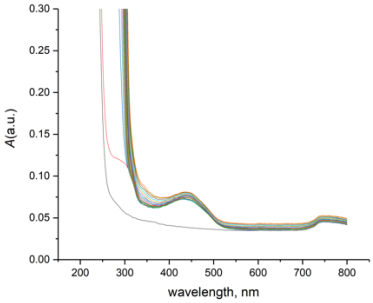 A(a.u.) 0.30 0.25 0.20 0.15 0.10 0.05 0.00 200 300 400 500 600 700 800 wavelength, nm

A4.4 Unrestricted preliminary fitting of UV-visible titration data

4.16	**1st titration**	**2nd titration**	**Global fit**
K **/ M^{-1}**	798.7±1.37×10^{6}	964.2±1.65×10^{6}	5.96±4292
n **/ basepairs**	6.11±1.05×10^{4}	5.33±9133	0.05±36.01
K **(*n*=3) / M^{-1}**	390.6±70.72	540.8±123.9	362.4±144.0
4.17	**1st titration**	**2nd titration**	**Global fit**
K **/ M^{-1}**	1.28×10^{6}±3.75×10^{7}	3.23×10^{6}±2.31×10^{8}	72.74±1.89×10^{5}
n **/ basepairs**	2.25×10^{5}±4.17×10^{8}	3.26×10^{5}±2.02×10^{9}	5333±1.86×10^{7}
K **(*n*=3) / M^{-1}**	0.31±38.64	0.49±107.7	0.31±48.38
4.16a	**1st titration**	**2nd titration**	**Global fit**
K_{app} / M^{-1}	1.26×10^{5}±1.40×10^{6}	(3.67±2.16)×10^{5}	(2.70±2.62)×10^{5}
n **/ basepairs**	25.53±19.66	11.97±4.67	9.37±6.61
K_{app} (*n*=3) / M^{-1}	(1.09±0.21)×10^{4}	(8.55±2.40)×10^{4}	(8.45±3.11)×10^{4}
Bathochromic shift, nm	476-482nm		

4.16b	**1st titration**	**2nd titration**	**Global fit**
K **/ M^{-1}**	(3.69±0.87)×10^{6}	(3.36±0.64)×10^{6}	(1.59±1.19)×10^{7}
n **/ basepairs**	26.34±0.6	27.43±0.49	27.13±0.93
K **(*n*=3) / M^{-1}**	(2.18±0.46)×10^{4}	(3.59±0.89)×10^{4}	(4.01±0.74)×10^{4}
4.17b	**1st titration**	**2nd titration**	**Global fit**
K **/ M^{-1}**	(3.67±2.21)×10^{6}	(1.42±0.46)×10^{5}	(1.70±1.71)×10^{6}
n **/ basepairs**	26.37±2.37	17.38±0.98	16.90±3.12
K **(*n*=3) / M^{-1}**	(5.04±1.09)×10^{4}	(3.29±0.69)×10^{4}	(4.65±1.16)×10^{4}
4.16c	**1st titration**	**2nd titration**	**Global fit**

K_{app} / M^{-1}	$9.34\times10^{5}\pm3.25\times10^{6}$	$1816\pm3.48\times10^{6}$	$(2.98\pm7.81)\times10^{6}$
n **/ basepairs**	182.5±79.09	4.89±9364	148.2±53.27
K_{app} (***n***=3) / M^{-1}	$(0.39\pm0.10)\times10^{4}$	$(0.11\pm0.04)\times10^{4}$	$(4.5\pm3.6)\times10^{3}$
4.17c	**1st titration**	**2nd titration**	**Global fit**
K / M^{-1}	$(1.29\pm1.69)\times10^{7}$	$955.8\pm4.23\times10^{6}$	$(7.97\pm7.78)\times10^{5}$
n **/ basepairs**	39.77±2.59	0.04±180.3	21.30±6.14
K (***n***=3) / M^{-1}	$(2.49\pm0.62)\times10^{4}$	$(8.90\pm2.20)\times10^{4}$	$(4.07\pm0.90)\times10^{4}$
4.16d	**1st titration**	**2nd titration**	**Global fit**
K_{app} / M^{-1}	$(3.22\pm3.23)\times10^{6}$	$1519\pm1.49\times10^{6}$	$2724\pm1.04\times10^{6}$
n **/ basepairs**	272.6±27.09	6.24±6113	4.54±1721
K_{app} (***n***=3) / M^{-1}	$(0.21\pm0.08)\times10^{4}$	$(0.15\pm0.99)\times10^{4}$	$(1.8\pm0.7)\times10^{3}$
4.17d	**1st titration**	**2nd titration**	**Global fit**
K_{app} / M^{-1}	$4.53\times10^{5}\pm1.26\times10^{6}$	$3.11\times10^{5}\pm1.53\times10^{6}$	$7.14\times10^{5}\pm2.82\times10^{6}$
n **/ basepairs**	284.8±337.8	295.8±702.1	367.2±482.9
K_{app} (***n***=3) / M^{-1}	$(2.0\pm0.5)\times10^{3}$	$(1.5\pm0.5)\times10^{3}$	$(2.0\pm0.9)\times10^{3}$

A4.5 X-ray data

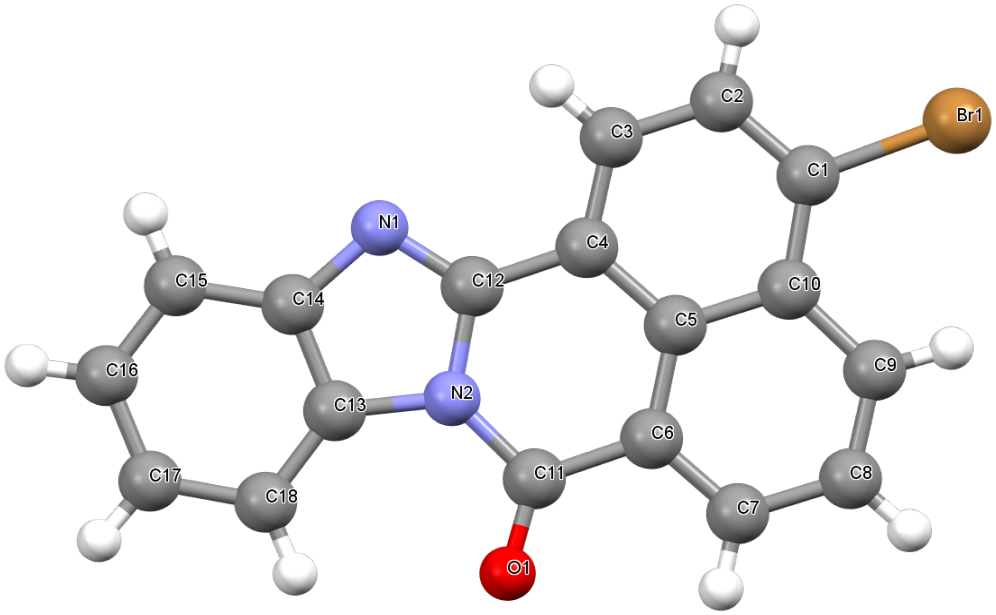

Table 1. Crystal data and structure refinement for njb2001b.

Identification code	njb2001b	
Empirical formula	$C_{18}H_9BrN_2O$, $0.25(CH_2Cl_2)$	
Formula weight	370.41	
Temperature	200(2) K	
Wavelength	1.54184 Å	
Crystal system	Monoclinic	
Space group	P 21/c	
Unit cell dimensions	a = 14.4604(9) Å	α= 90°.
	b = 3.8489(2) Å	β= 96.888(5)°.
	c = 26.7708(14) Å	γ = 90°.
Volume	1479.22(14) $Å^3$	
Z	4	
Density (calculated)	1.663 Mg/m^3	
Absorption coefficient	4.656 mm^{-1}	
F(000)	738	
Crystal size	0.541 x 0.094 x 0.030 mm^3	
Theta range for data collection	4.254 to 76.786°.	
Index ranges	-18<=h<=13, -4<=k<=4, -33<=l<=33	
Reflections collected	11731	
Independent reflections	3081 [R(int) = 0.0517]	
Completeness to theta = 67.684°	99.9 %	
Absorption correction	Gaussian	
Max. and min. transmission	1.000 and 0.273	
Refinement method	Full-matrix least-squares on F^2	
Data / restraints / parameters	3081 / 1162 / 417	
Goodness-of-fit on F^2	1.110	

Final R indices [I>2sigma(I)]	R1 = 0.0764, wR2 = 0.2114
R indices (all data)	R1 = 0.0842, wR2 = 0.2193
Extinction coefficient	n/a
Largest diff. peak and hole	1.322 and -0.621 e.Å^{-3}

Table 2. Atomic coordinates (x 10^4) and equivalent isotropic displacement parameters ($Å^2$x 10^3) for njb2001b. U(eq) is defined as one third of the trace of the orthogonalized U^{ij} tensor.

	x	y	z	U(eq)
C(1)	7026(4)	8094(14)	11133(2)	42(1)
C(2)	6180(4)	8631(15)	10852(2)	44(1)
C(3)	6049(3)	7669(14)	10351(2)	42(1)
C(4)	6769(3)	6207(13)	10125(2)	36(1)
C(5)	7647(3)	5597(13)	10411(2)	35(1)
C(6)	8385(3)	4004(13)	10188(2)	38(1)
C(7)	9235(4)	3423(17)	10467(2)	47(1)
C(8)	9383(4)	4405(17)	10977(2)	52(1)
C(9)	8682(4)	5925(16)	11197(2)	47(1)
C(10)	7787(4)	6562(14)	10928(2)	39(1)
C(11)	8255(3)	2889(14)	9655(2)	39(1)
C(12)	6652(3)	5264(13)	9600(2)	37(1)
C(13)	7073(4)	3084(14)	8886(2)	42(1)
C(14)	6160(4)	4355(15)	8823(2)	44(1)
C(15)	5621(5)	4194(18)	8349(2)	54(1)
C(16)	6033(5)	2754(19)	7960(2)	59(1)
C(17)	6939(5)	1439(19)	8031(2)	58(1)
C(18)	7492(5)	1574(17)	8497(2)	51(1)
N(1)	5911(3)	5721(13)	9272(2)	43(1)
N(2)	7388(3)	3666(11)	9394(2)	38(1)
O(1)	8823(3)	1274(13)	9448(2)	56(1)
Br(1)	7156(1)	9485(2)	11817(1)	61(1)

C(1A)	6675(13)	1710(30)	8458(5)	50(2)
C(2A)	5947(12)	3510(30)	8620(6)	48(2)
C(3A)	6010(14)	4730(30)	9109(7)	42(3)
C(4A)	6802(16)	4180(50)	9445(7)	40(2)
C(5A)	7562(15)	2320(60)	9284(7)	42(3)
C(6A)	8384(18)	1710(90)	9620(9)	41(3)
C(7A)	9121(19)	-100(110)	9464(13)	45(4)
C(8A)	9070(19)	-1360(110)	8969(13)	49(5)
C(9A)	8288(17)	-800(80)	8641(11)	49(4)
C(10A)	7505(14)	1050(60)	8782(7)	45(3)
C(11A)	8470(20)	2980(100)	10145(9)	40(3)
C(12A)	6880(20)	5430(60)	9956(7)	38(2)
C(13A)	7580(30)	6260(80)	10741(8)	40(2)
C(14A)	6690(30)	7730(70)	10668(10)	40(2)
C(15A)	6340(30)	9480(80)	11065(13)	43(3)
C(16A)	6900(40)	9670(100)	11517(12)	44(3)
C(17A)	7790(40)	8190(110)	11583(10)	44(3)
C(18A)	8160(30)	6430(110)	11196(10)	43(3)
N(1A)	6270(20)	7180(60)	10178(10)	39(3)
N(2A)	7700(20)	4770(80)	10277(8)	38(2)
O(1AA)	9150(30)	2560(130)	10454(13)	44(6)
Br(1A)	6553(10)	90(30)	7783(4)	38(4)
Cl(1)	9457(10)	670(70)	7700(7)	320(11)
C(19)	9581(19)	5180(70)	7635(14)	103(12)

Table 3. Bond lengths [Å] and angles [°] for njb2001b.

C(1)-C(2)	1.374(8)
C(1)-C(10)	1.416(7)
C(1)-Br(1)	1.896(5)
C(2)-C(3)	1.380(8)
C(2)-H(2)	0.9500
C(3)-C(4)	1.385(7)
C(3)-H(3)	0.9500
C(4)-C(5)	1.421(7)
C(4)-C(12)	1.442(7)
C(5)-C(6)	1.423(7)
C(5)-C(10)	1.422(7)
C(6)-C(7)	1.378(8)
C(6)-C(11)	1.480(7)
C(7)-C(8)	1.408(9)
C(7)-H(7)	0.9500
C(8)-C(9)	1.363(9)
C(8)-H(8)	0.9500
C(9)-C(10)	1.425(8)
C(9)-H(9)	0.9500
C(11)-O(1)	1.216(6)
C(11)-N(2)	1.393(6)
C(12)-N(1)	1.312(7)
C(12)-N(2)	1.400(6)
C(13)-C(18)	1.393(8)
C(13)-C(14)	1.399(8)

C(13)-N(2)	1.400(7)
C(14)-N(1)	1.399(8)
C(14)-C(15)	1.408(8)
C(15)-C(16)	1.377(10)
C(15)-H(15)	0.9500
C(16)-C(17)	1.396(10)
C(16)-H(16)	0.9500
C(17)-C(18)	1.399(9)
C(17)-H(17)	0.9500
C(18)-H(18)	0.9500
C(1A)-C(2A)	1.374(12)
C(1A)-C(10A)	1.417(12)
C(1A)-Br(1A)	1.899(11)
C(2A)-C(3A)	1.382(12)
C(2A)-H(2A)	0.9500
C(3A)-C(4A)	1.386(11)
C(3A)-H(3A)	0.9500
C(4A)-C(5A)	1.421(11)
C(4A)-C(12A)	1.442(11)
C(5A)-C(6A)	1.422(11)
C(5A)-C(10A)	1.423(12)
C(6A)-C(7A)	1.377(12)
C(6A)-C(11A)	1.479(12)
C(7A)-C(8A)	1.407(14)
C(7A)-H(7A)	0.9500
C(8A)-C(9A)	1.363(13)
C(8A)-H(8A)	0.9500

C(9A)-C(10A)	1.425(12)
C(9A)-H(9A)	0.9500
C(11A)-O(1AA)	1.216(12)
C(11A)-N(2A)	1.392(11)
C(12A)-N(1A)	1.312(12)
C(12A)-N(2A)	1.401(11)
C(13A)-C(18A)	1.393(12)
C(13A)-C(14A)	1.398(12)
C(13A)-N(2A)	1.398(11)
C(14A)-N(1A)	1.399(12)
C(14A)-C(15A)	1.407(12)
C(15A)-C(16A)	1.377(14)
C(15A)-H(15A)	0.9500
C(16A)-C(17A)	1.397(14)
C(16A)-H(16A)	0.9500
C(17A)-C(18A)	1.400(14)
C(17A)-H(17A)	0.9500
C(18A)-H(18A)	0.9500
Cl(1)-C(19)#1	2.130(12)
Cl(1)-C(19)#2	1.752(11)
Cl(1)-C(19)	1.755(11)
C(19)-H(19A)	0.9900
C(19)-H(19B)	0.9900

C(2)-C(1)-C(10)	122.2(5)
C(2)-C(1)-Br(1)	117.7(4)
C(10)-C(1)-Br(1)	120.1(4)

C(1)-C(2)-C(3)	120.0(5)
C(1)-C(2)-H(2)	120.0
C(3)-C(2)-H(2)	120.0
C(2)-C(3)-C(4)	120.7(5)
C(2)-C(3)-H(3)	119.6
C(4)-C(3)-H(3)	119.6
C(3)-C(4)-C(5)	120.1(5)
C(3)-C(4)-C(12)	121.4(5)
C(5)-C(4)-C(12)	118.5(4)
C(4)-C(5)-C(6)	120.7(5)
C(4)-C(5)-C(10)	119.7(4)
C(6)-C(5)-C(10)	119.6(5)
C(7)-C(6)-C(5)	120.6(5)
C(7)-C(6)-C(11)	118.4(5)
C(5)-C(6)-C(11)	121.0(5)
C(6)-C(7)-C(8)	120.2(5)
C(6)-C(7)-H(7)	119.9
C(8)-C(7)-H(7)	119.9
C(9)-C(8)-C(7)	120.0(5)
C(9)-C(8)-H(8)	120.0
C(7)-C(8)-H(8)	120.0
C(8)-C(9)-C(10)	122.1(5)
C(8)-C(9)-H(9)	118.9
C(10)-C(9)-H(9)	118.9
C(1)-C(10)-C(5)	117.3(5)
C(1)-C(10)-C(9)	125.2(5)
C(5)-C(10)-C(9)	117.5(5)

O(1)-C(11)-N(2)	119.8(5)
O(1)-C(11)-C(6)	125.0(5)
N(2)-C(11)-C(6)	115.1(4)
N(1)-C(12)-N(2)	113.2(5)
N(1)-C(12)-C(4)	127.6(5)
N(2)-C(12)-C(4)	119.3(4)
C(18)-C(13)-C(14)	123.0(5)
C(18)-C(13)-N(2)	132.3(5)
C(14)-C(13)-N(2)	104.7(5)
C(13)-C(14)-N(1)	111.4(5)
C(13)-C(14)-C(15)	120.3(6)
N(1)-C(14)-C(15)	128.3(5)
C(16)-C(15)-C(14)	117.2(6)
C(16)-C(15)-H(15)	121.4
C(14)-C(15)-H(15)	121.4
C(15)-C(16)-C(17)	121.8(6)
C(15)-C(16)-H(16)	119.1
C(17)-C(16)-H(16)	119.1
C(18)-C(17)-C(16)	122.4(6)
C(18)-C(17)-H(17)	118.8
C(16)-C(17)-H(17)	118.8
C(13)-C(18)-C(17)	115.3(6)
C(13)-C(18)-H(18)	122.3
C(17)-C(18)-H(18)	122.3
C(12)-N(1)-C(14)	104.6(4)
C(11)-N(2)-C(12)	125.3(4)
C(11)-N(2)-C(13)	128.5(4)

C(12)-N(2)-C(13)	106.2(4)
C(2A)-C(1A)-C(10A)	121.5(11)
C(2A)-C(1A)-Br(1A)	118.6(11)
C(10A)-C(1A)-Br(1A)	119.9(10)
C(1A)-C(2A)-C(3A)	120.3(12)
C(1A)-C(2A)-H(2A)	119.9
C(3A)-C(2A)-H(2A)	119.9
C(2A)-C(3A)-C(4A)	121.2(12)
C(2A)-C(3A)-H(3A)	119.4
C(4A)-C(3A)-H(3A)	119.4
C(3A)-C(4A)-C(5A)	119.2(11)
C(3A)-C(4A)-C(12A)	122.1(12)
C(5A)-C(4A)-C(12A)	118.6(11)
C(6A)-C(5A)-C(4A)	120.6(11)
C(6A)-C(5A)-C(10A)	119.3(11)
C(4A)-C(5A)-C(10A)	120.0(11)
C(7A)-C(6A)-C(5A)	120.7(12)
C(7A)-C(6A)-C(11A)	118.1(12)
C(5A)-C(6A)-C(11A)	121.2(11)
C(6A)-C(7A)-C(8A)	120.3(14)
C(6A)-C(7A)-H(7A)	119.9
C(8A)-C(7A)-H(7A)	119.9
C(9A)-C(8A)-C(7A)	119.9(14)
C(9A)-C(8A)-H(8A)	120.1
C(7A)-C(8A)-H(8A)	120.1
C(8A)-C(9A)-C(10A)	122.2(14)
C(8A)-C(9A)-H(9A)	118.9

C(10A)-C(9A)-H(9A)	118.9
C(1A)-C(10A)-C(5A)	117.7(11)
C(1A)-C(10A)-C(9A)	124.7(12)
C(5A)-C(10A)-C(9A)	117.6(12)
O(1AA)-C(11A)-N(2A)	119.9(16)
O(1AA)-C(11A)-C(6A)	125.1(16)
N(2A)-C(11A)-C(6A)	115.0(11)
N(1A)-C(12A)-N(2A)	112.7(11)
N(1A)-C(12A)-C(4A)	128.1(13)
N(2A)-C(12A)-C(4A)	119.1(11)
C(18A)-C(13A)-C(14A)	123.3(13)
C(18A)-C(13A)-N(2A)	132.2(13)
C(14A)-C(13A)-N(2A)	104.5(10)
C(13A)-C(14A)-N(1A)	111.4(10)
C(13A)-C(14A)-C(15A)	120.1(13)
N(1A)-C(14A)-C(15A)	128.5(13)
C(16A)-C(15A)-C(14A)	117.3(14)
C(16A)-C(15A)-H(15A)	121.4
C(14A)-C(15A)-H(15A)	121.4
C(15A)-C(16A)-C(17A)	121.8(15)
C(15A)-C(16A)-H(16A)	119.1
C(17A)-C(16A)-H(16A)	119.1
C(18A)-C(17A)-C(16A)	122.3(15)
C(18A)-C(17A)-H(17A)	118.8
C(16A)-C(17A)-H(17A)	118.8
C(13A)-C(18A)-C(17A)	115.2(14)
C(13A)-C(18A)-H(18A)	122.4

C(17A)-C(18A)-H(18A)	122.4
C(12A)-N(1A)-C(14A)	104.8(11)
C(11A)-N(2A)-C(13A)	128.0(12)
C(11A)-N(2A)-C(12A)	125.4(12)
C(13A)-N(2A)-C(12A)	106.6(10)
C(19)#1-Cl(1)-C(19)#2	76.8(7)
C(19)#1-Cl(1)-C(19)	164.2(12)
C(19)#2-Cl(1)-C(19)	87.7(6)
Cl(1)#3-C(19)-Cl(1)	104.7(8)
Cl(1)#3-C(19)-H(19A)	110.8
Cl(1)-C(19)-H(19A)	110.8
Cl(1)#3-C(19)-H(19B)	110.8
Cl(1)-C(19)-H(19B)	110.8
H(19A)-C(19)-H(19B)	108.9

Symmetry transformations used to generate equivalent atoms:

#1 x,y-1,z #2 -x+2,y-1/2,-z+3/2 #3 -x+2,y+1/2,-z+3/2

Table 4. Anisotropic displacement parameters ($Å^2$x 10^3)for njb2001b. The anisotropic displacement factor exponent takes the form: $-2\pi^2[h^2a^{*2}U^{11} + ... + 2 h k a^* b^* U^{12}]$

	U^{11}	U^{22}	U^{33}	U^{23}	U^{13}	U^{12}
C(1)	53(2)	32(2)	43(2)	-1(2)	13(2)	0(2)
C(2)	48(2)	38(2)	49(2)	2(2)	16(2)	5(2)
C(3)	39(2)	38(2)	49(2)	5(2)	13(2)	8(2)
C(4)	36(2)	32(2)	40(2)	3(2)	9(2)	5(2)
C(5)	37(2)	32(2)	38(2)	3(2)	8(2)	2(2)
C(6)	36(2)	33(2)	47(2)	3(2)	10(2)	4(2)
C(7)	38(2)	46(3)	57(3)	2(2)	7(2)	5(2)
C(8)	43(2)	55(3)	55(3)	5(2)	-5(2)	2(2)
C(9)	47(2)	47(3)	44(2)	1(2)	-4(2)	-1(2)
C(10)	45(2)	33(2)	40(2)	2(2)	6(2)	0(2)
C(11)	37(2)	36(2)	46(2)	2(2)	10(2)	7(2)
C(12)	36(2)	35(2)	41(2)	5(2)	8(2)	2(2)
C(13)	48(2)	38(2)	41(2)	3(2)	8(2)	-2(2)
C(14)	47(2)	43(2)	41(2)	4(2)	4(2)	-5(2)
C(15)	56(3)	55(3)	48(3)	6(2)	-1(2)	-7(2)
C(16)	73(3)	58(3)	45(3)	0(2)	1(2)	-12(3)
C(17)	79(3)	53(3)	43(3)	-4(3)	9(3)	-6(3)
C(18)	63(3)	45(3)	47(2)	-1(2)	13(2)	-1(2)
N(1)	39(2)	46(2)	44(2)	7(2)	4(2)	3(2)
N(2)	39(2)	34(2)	42(2)	0(2)	8(2)	4(2)
O(1)	47(2)	63(3)	58(2)	-8(2)	11(2)	20(2)
Br(1)	90(1)	50(1)	45(1)	-6(1)	18(1)	0(1)

C(1A)	58(4)	47(4)	44(4)	1(4)	6(4)	-4(4)
C(2A)	51(4)	47(4)	44(4)	3(4)	5(4)	-4(4)
C(3A)	43(4)	41(4)	42(4)	4(4)	6(4)	-1(4)
C(4A)	41(4)	38(4)	42(4)	3(4)	7(4)	1(4)
C(5A)	43(4)	40(4)	44(4)	1(4)	7(4)	2(4)
C(6A)	40(4)	39(4)	45(4)	1(4)	8(4)	4(4)
C(7A)	43(6)	44(6)	47(6)	0(6)	8(6)	4(6)
C(8A)	50(7)	48(7)	50(7)	0(6)	8(6)	3(6)
C(9A)	53(6)	47(6)	48(6)	0(6)	8(6)	0(6)
C(10A)	50(4)	42(4)	45(4)	1(4)	8(4)	0(4)
C(11A)	38(4)	38(4)	45(4)	2(4)	8(4)	3(4)
C(12A)	38(4)	36(4)	42(4)	2(4)	9(4)	3(4)
C(13A)	43(4)	36(4)	41(4)	2(4)	6(4)	1(4)
C(14A)	43(4)	36(4)	43(4)	2(4)	10(4)	3(4)
C(15A)	48(5)	37(5)	45(5)	1(5)	11(5)	1(5)
C(16A)	51(5)	38(5)	45(5)	1(5)	10(5)	1(5)
C(17A)	50(5)	40(5)	44(5)	1(4)	7(4)	0(4)
C(18A)	47(5)	38(5)	43(5)	1(5)	5(5)	0(5)
N(1A)	40(4)	36(4)	43(4)	2(4)	10(4)	3(4)
N(2A)	39(4)	35(4)	41(4)	2(4)	8(4)	2(4)
O(1AA)	39(10)	42(10)	51(10)	3(10)	8(9)	3(9)
Br(1A)	69(7)	27(6)	20(5)	-2(4)	15(5)	-2(5)
Cl(1)	305(13)	354(14)	292(13)	-2(9)	3(9)	2(9)
C(19)	101(14)	110(15)	90(14)	-5(10)	-21(9)	7(10)

Table 5. Hydrogen coordinates (x 10^4) and isotropic displacement parameters ($Å^2$x 10^3) for njb2001b.

	x	y	z	U(eq)
H(2)	5684	9664	11002	53
H(3)	5459	8013	10160	50
H(7)	9724	2357	10314	56
H(8)	9970	4008	11167	62
H(9)	8795	6581	11541	56
H(15)	5000	5043	8300	64
H(16)	5691	2653	7634	71
H(17)	7188	416	7753	70
H(18)	8111	697	8544	61
H(2A)	5398	3919	8396	57
H(3A)	5501	5971	9216	50
H(7A)	9667	-488	9693	54
H(8A)	9580	-2601	8863	59
H(9A)	8264	-1667	8308	59
H(15A)	5734	10485	11023	51
H(16A)	6679	10837	11792	53
H(17A)	8152	8383	11902	53
H(18A)	8767	5429	11240	51
H(19A)	9015	6196	7446	124
H(19B)	9696	6312	7968	124

Appendix for Chapter 5

A5.1 Characterization of compounds using NMR spectroscopy

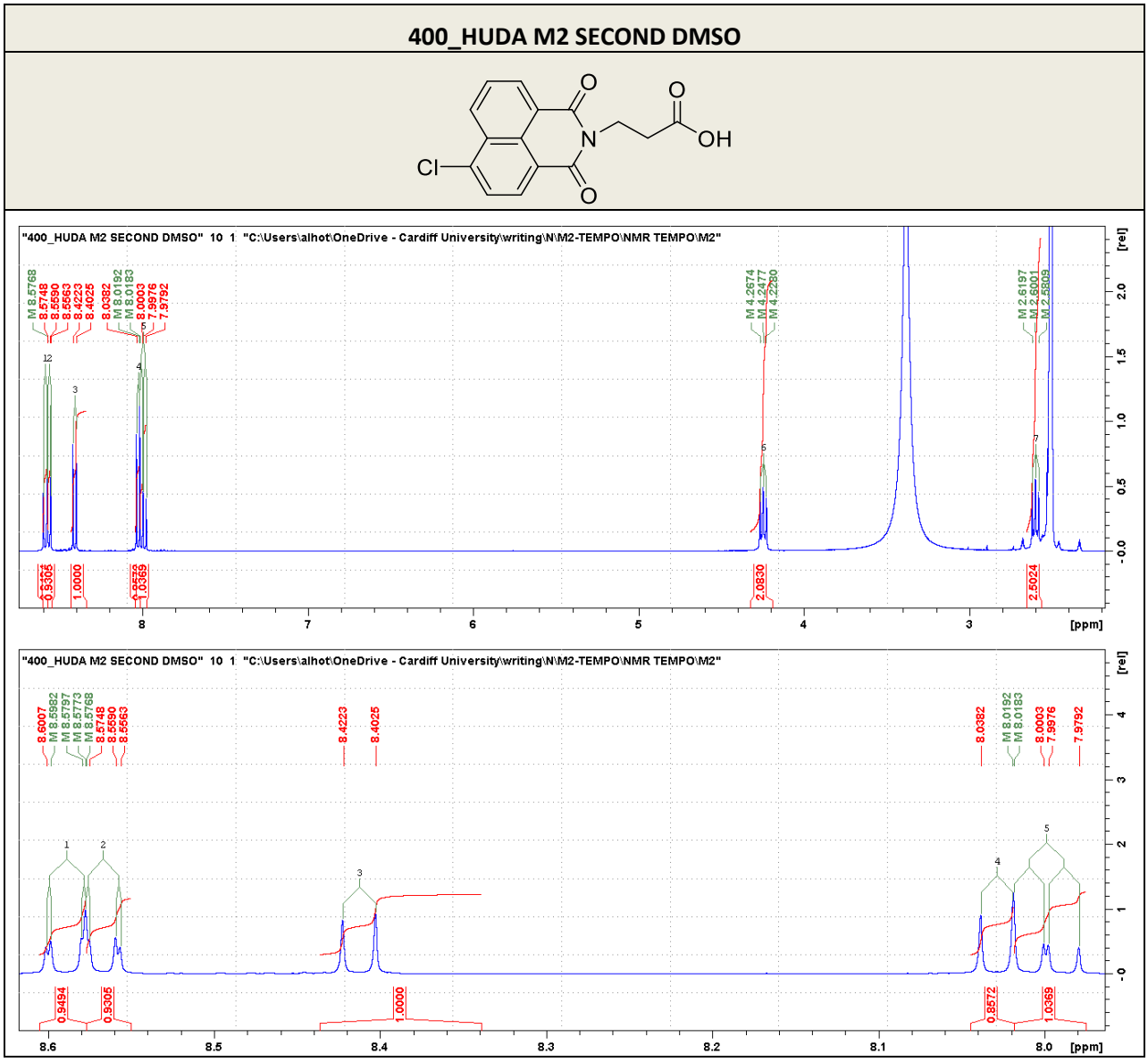

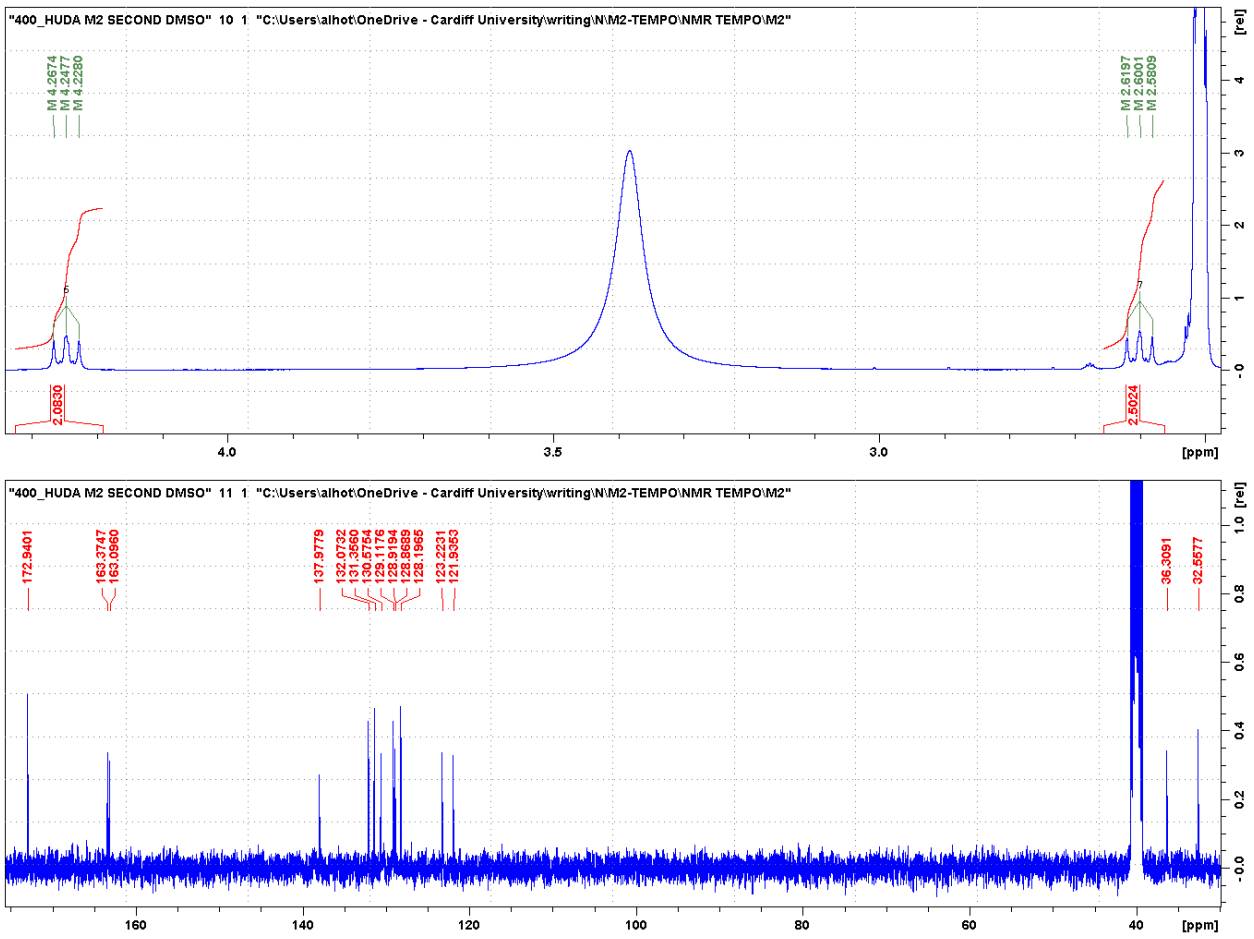

^{1}H NMR (400 MHz, DMSO): δ(ppm): 8.58 (dd, 1H, *J* = 8.38 Hz, *J* = 0.98 Hz, Ar-CH), 8.56 **(**dd, 1H, *J* = 7.36 Hz, *J* = 1.04 Hz, Ar-CH), 8.41 (d, 1H, *J* = 7.92 Hz, Ar-CH), 8.02 (d, 1H, *J* = 7.60 Hz, Ar-CH), 8.00 (dd, 1H, *J* = 8.36 Hz, *J* = 7.28 Hz, Ar-CH), 4.24 (t, 2H, *J* =7.88 Hz, CH_2), 2.60 (t, 2H, *J*=7.76, CH_2); **^{13}C NMR (100 MHz, DMSO): δ(ppm):** 172.94, 163.37, 163.09, 137.97, 132.07, 131.35, 130.57, 129.11, 128.91, 128.86, 128.19, 123.22, 121.93, 36.30, 32.55. **HR TOF MS ES+** calc for [$C_{15}H_{11}NO_4Cl$] 304.0377 found 304.0368.

500_HUDA 2021 M2-N1 2nd protocol DMSO

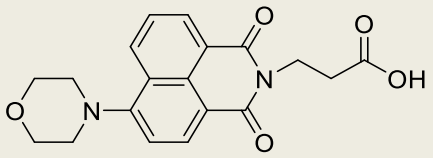

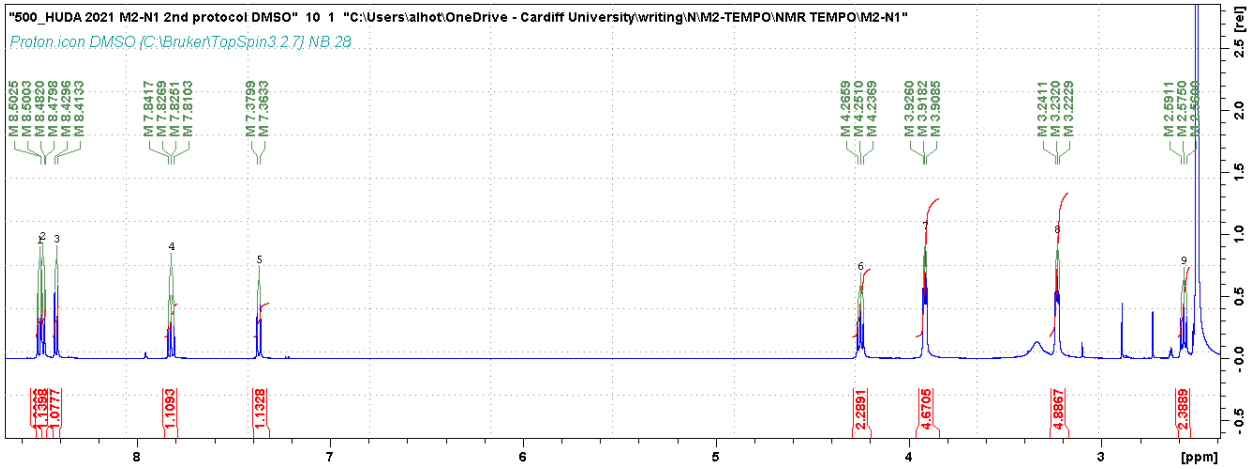

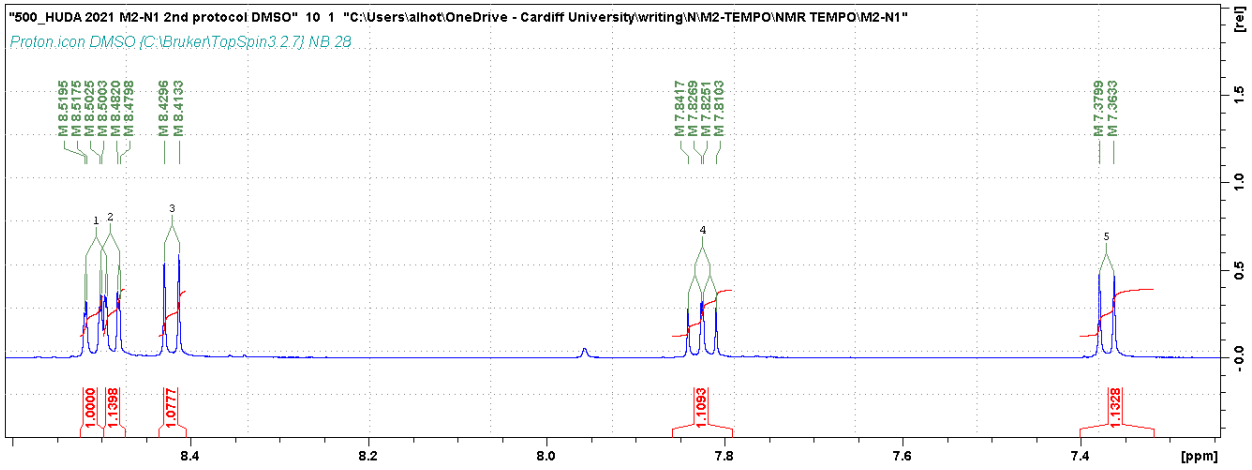

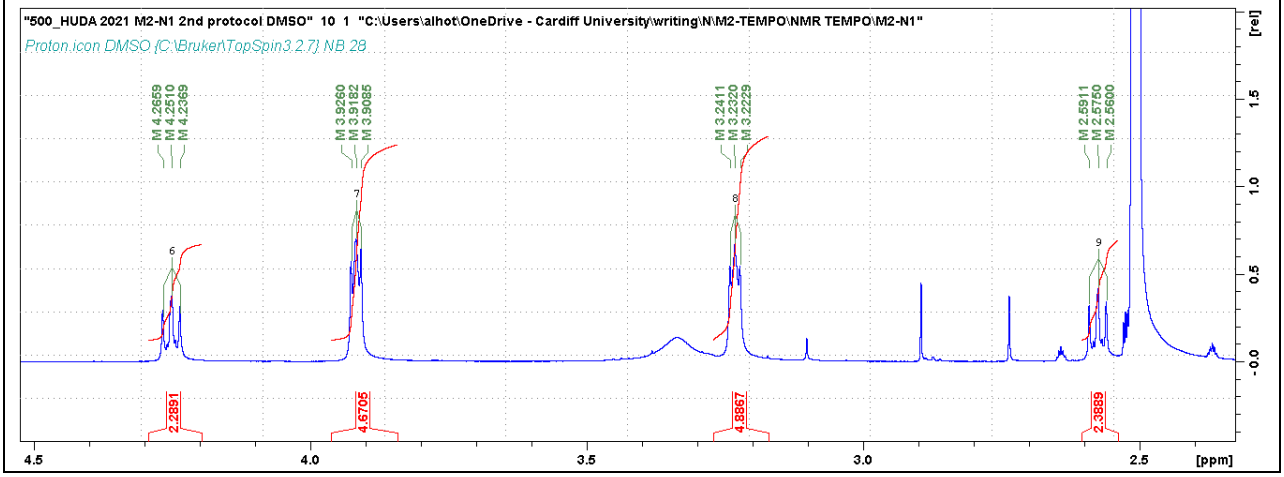

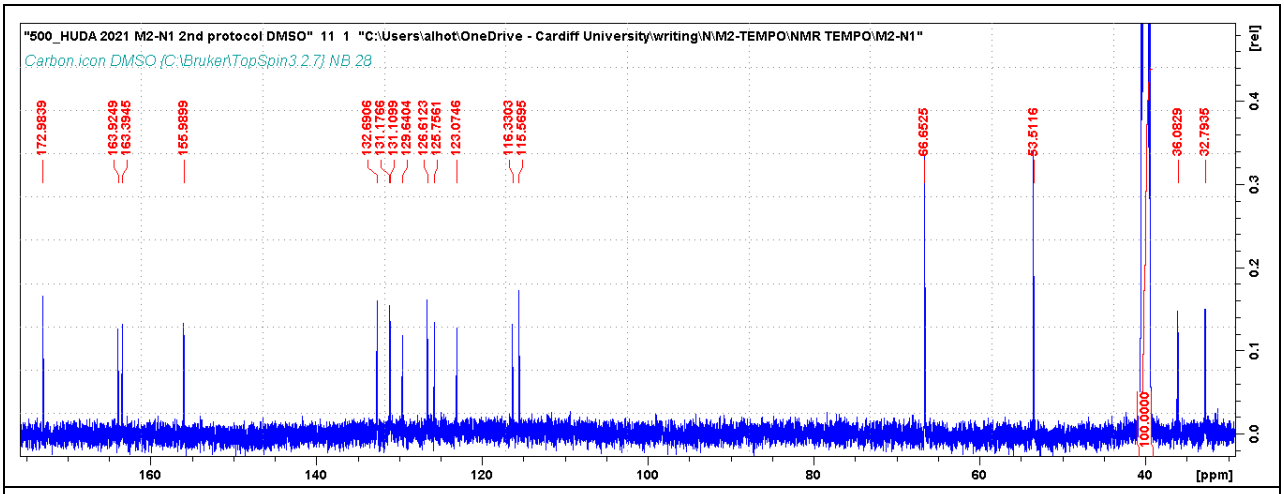

^{1}H NMR (500 MHz, $CDCl_3$): δ(ppm): 8.50 (dd, 1H, *J* =8.55 Hz, *J* =1.05 Hz), 8.48 (dd, 1H, *J* = 7.30 Hz, *J* =1.05 Hz), 8.42 (d, 1H, *J* = 8.15 Hz), 7.82 (dd, 1H, *J* = 8.30 Hz, *J* =7.40 Hz), 7.37 (d, 1H, *J* = 8.30 Hz), 4.25 (t, 2H, *J* =7.25 Hz), 3.91 (t, 4H, *J* =4.37 Hz), 3.23 (t, 4H, *J* =4.55 Hz), 2.57 (t, 2H, *J*=7.77); **^{13}C NMR (125 MHz, DMSO-d_6)** δ 172.98, 163.92, 163.39, 155.98, 132.69, 131.17, 131.10, 129.64, 126.61, 125.75, 123.07, 116.33, 115.56, 66.65, 53.51, 36.08, 32.79. **HR TOF MS ES+** calc for [$C_{19}H_{19}N_2O_5$] 355.1294 found 355.1296.

500_HUDA 2021 M2-N2 col 2 DMSO\ 500_HUDA 2021 M2-N2 2nd protocol DMSO

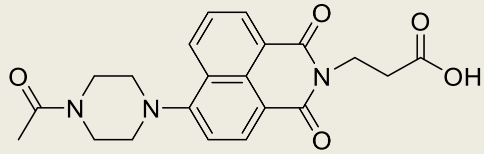

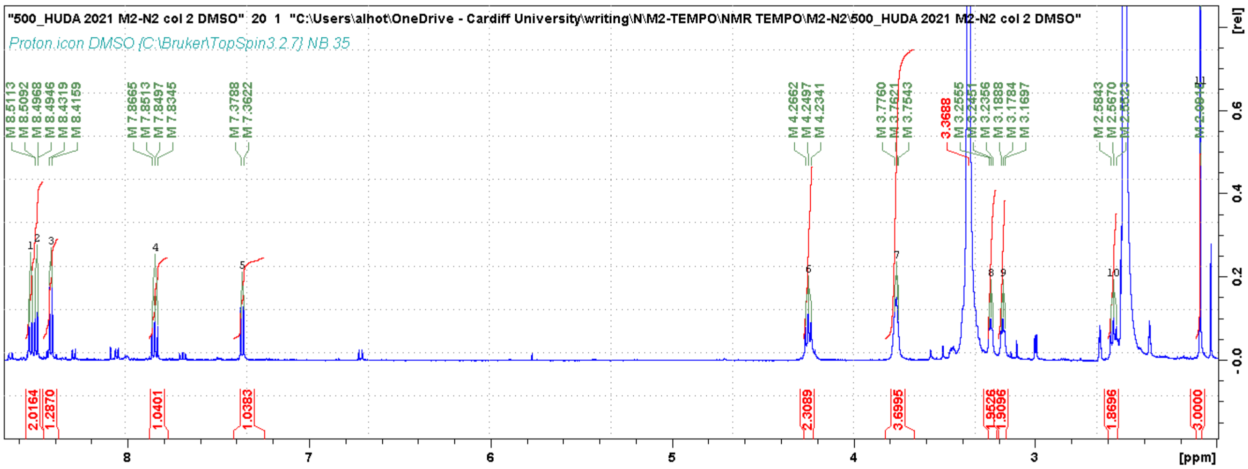

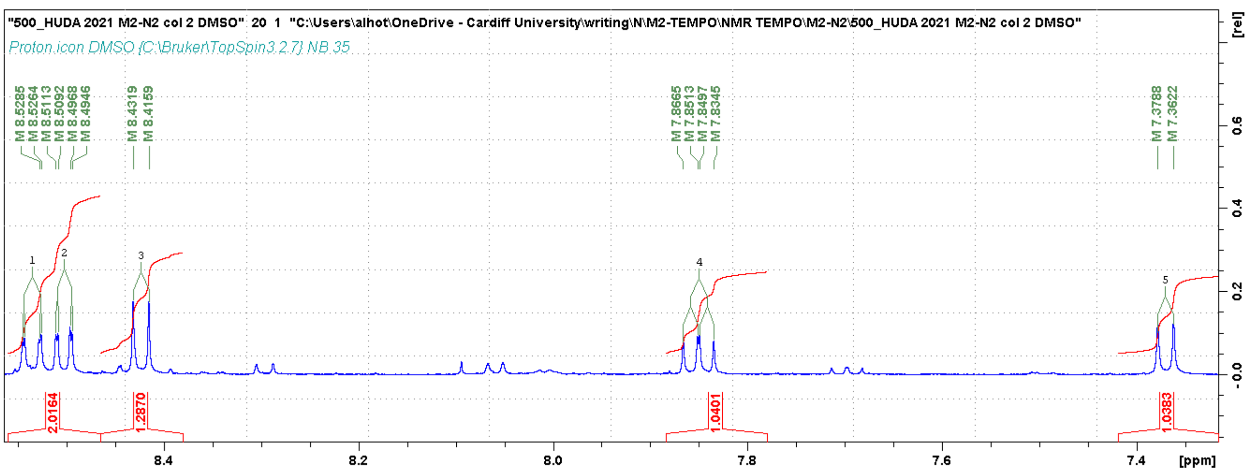

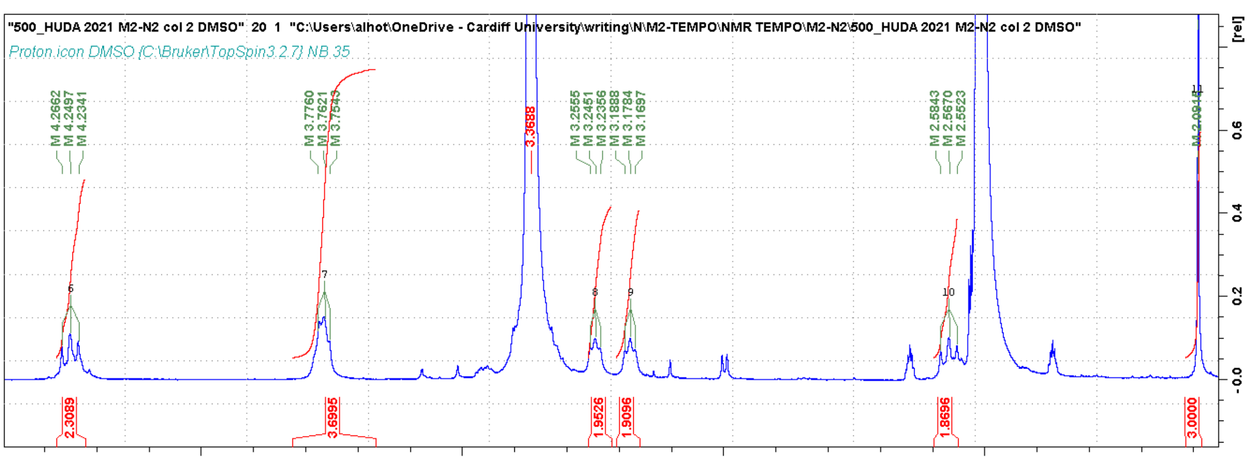

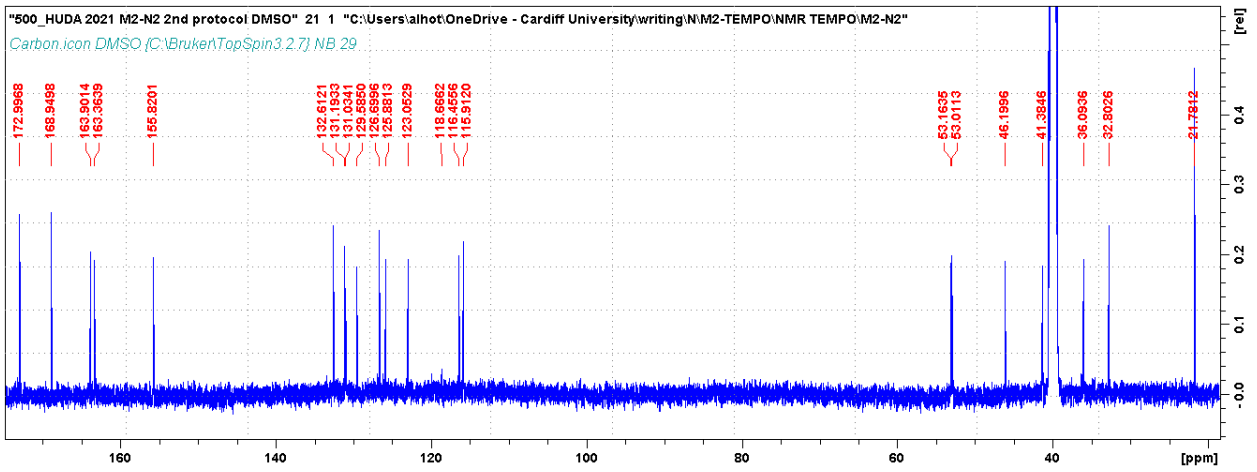

^{1}H NMR (500 MHz, DMSO-d_6): δ(ppm): 8.53 (dd, 1H, *J*= 8.50 Hz, *J*=1.05 Hz, Ar-CH), 8.50 (d, 1H, *J* = 7.27 Hz, *J*=1.07 Hz, Ar-CH), 8.42 (d, 1H, *J* = 8.00 Hz, Ar-CH), 7.85 (dd, 1H, *J* = 8.40 Hz, *J*=7.60 Hz, Ar-CH), 7.37 (d, 1H, *J* = 8.30 Hz, Ar-CH), 4.29 (t, 2H, *J* =8.02 Hz, CH_2), 3.76 (m, 4H, CH_2), 3.24 (t, 2H, *J* =4.97 Hz, CH_2), 3.17 (t, 4H, *J*=4.77, CH_2); 2.56 (t, 4H, *J*=8.00, CH_2); 2.09 (s, 3H, CH_3); **^{13}C NMR (125 MHz, DMSO-d_6) δ** 172.99, 168.94, 163.90, 163.36, 155.82, 132.61, 131.19, 131.03, 129.58, 126.69, 125.88, 123.05, 118.66, 116.45, 115.91, 53.16, 53.01, 46.19, 41.38, 36.09, 32.80, 21.78. **HR TOF MS ES+** calc for [$C_{21}H_{22}N_3O_5$] 396.1559 found 396.1560.

400_HUDA 2020 M2-Su1 crude DMF 24h HCl ether ACETONE

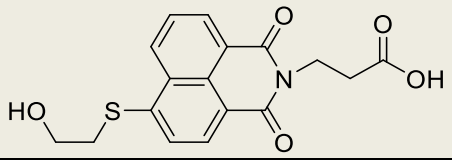

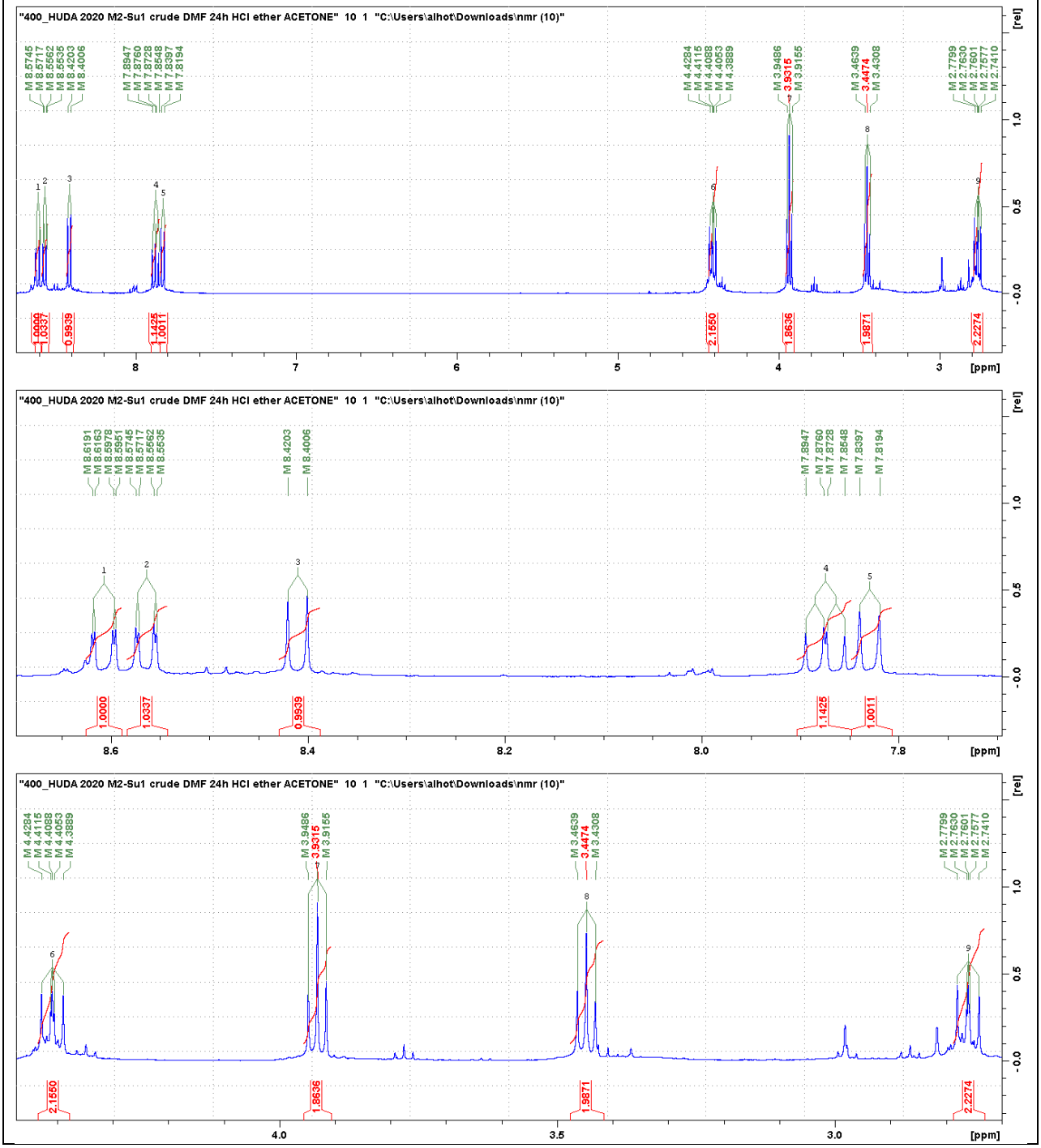

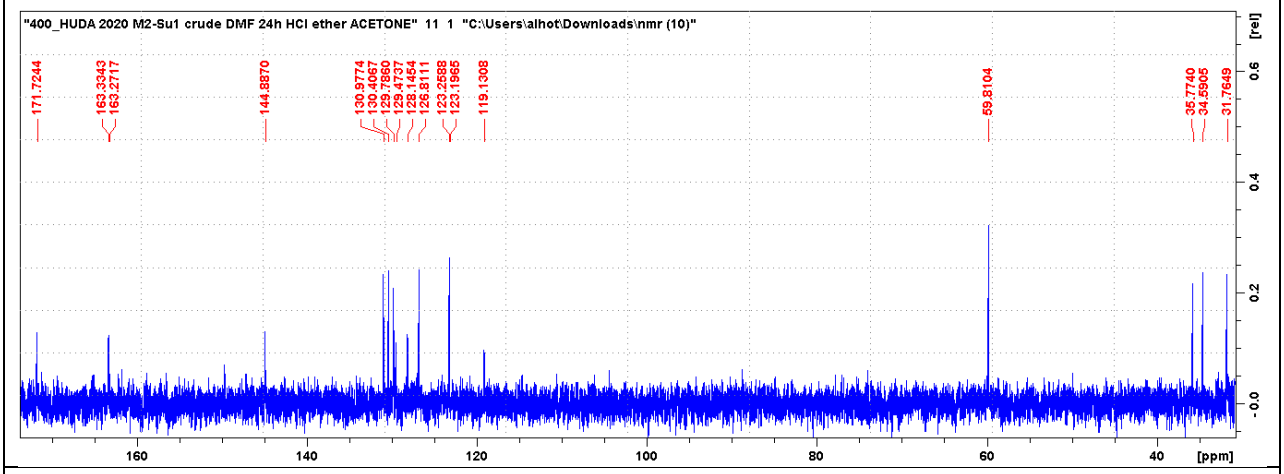

^{1}H NMR (400 MHz, ACETONE): δ(ppm): 8.60 (dd, 1H, J =8.50 Hz, J =1.10 Hz, Ar-CH), 8.56 (dd, 1H, J = 7.30 Hz, J = 1.10 H, Ar-CH), 8.41 (d, 1H, *J* = 7.88 Hz, Ar-CH), 7.87 (dd, 1H, *J* = 8.62 Hz, *J* = 7.34 Hz, Ar-CH), 7.82 (d, 1H, *J*= 8.12 Hz, Ar-CH), 4.40 (m, 2H, CH_2), 3.93 (t, 2H, *J*=6.62 Hz, CH_2), 3.44 (t, 2H, *J* =6.62 Hz, CH_2), 2.76 (m, 2H, CH_2); **^{13}C NMR (100 MHz, ACETONE): δ(ppm):** 171.72, 163.33, 163.27, 144.88, 130.97, 130.40, 129.78, 129.47, 128.14, 126.81, 123.25, 123.19, 119.13, 59.81, 35.77, 34.59, 31.76. **HR TOF MS ES+** calc for [$C_{17}H_{16}NO_5S$] 346.0749 found 346.0745.

500_JHUDA 2021 M2-Su4 DMF 24h HCl DMSO\ DMF observed in the spectrum

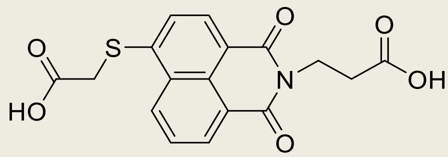

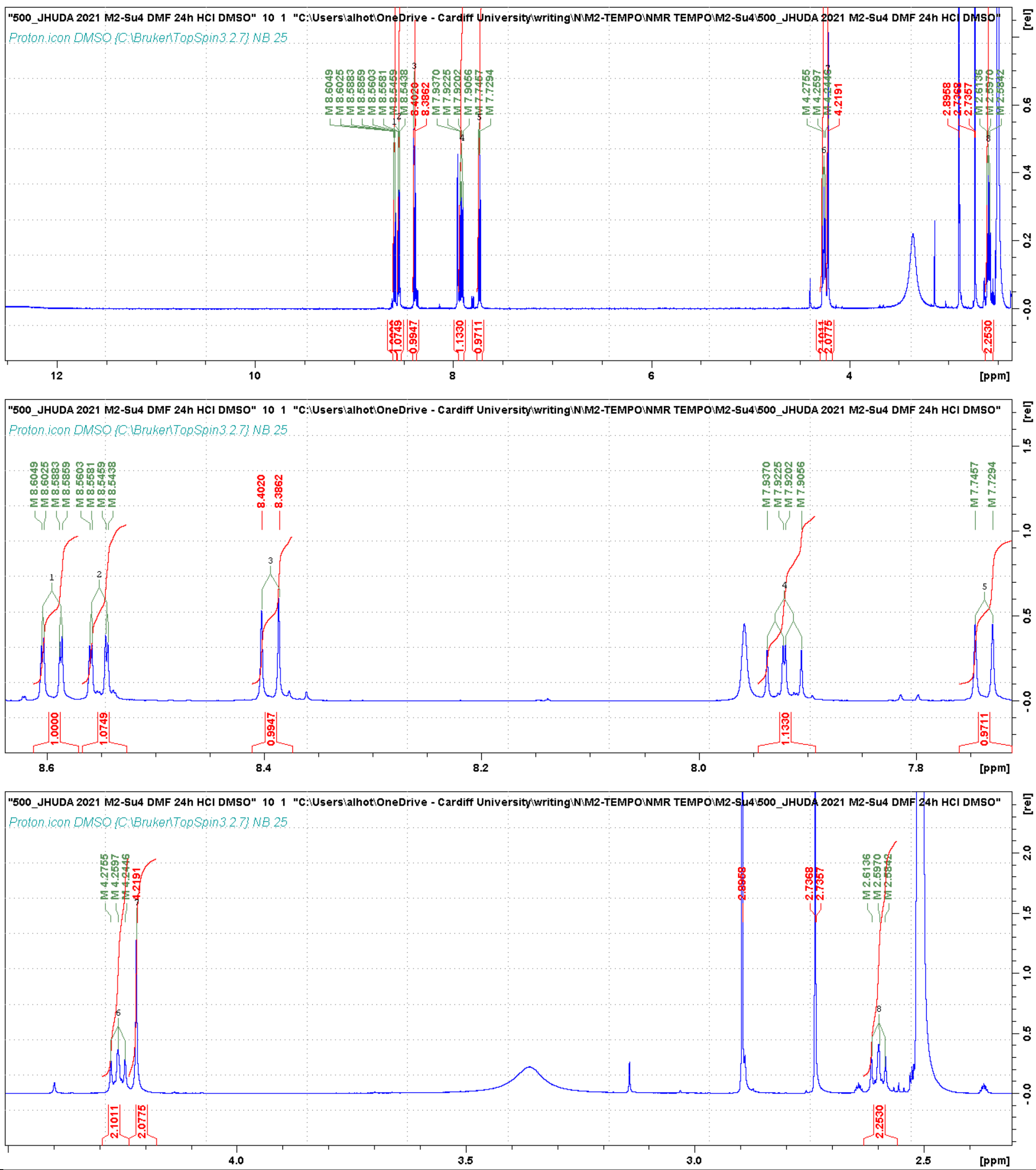

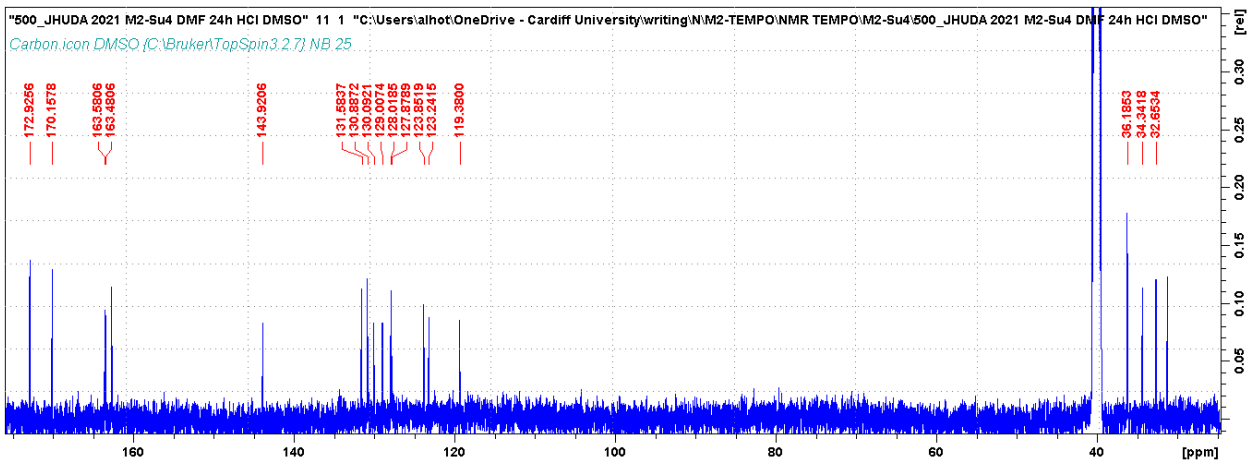

^{1}H NMR (500 MHz, DMSO): δ(ppm): 8.59 (dd, 1H, *J*=8.30 Hz, J =1.20 Hz, Ar-CH), 8.54 (dd, 1H, *J*= 7.17 Hz, *J*= 1.07 H, Ar-CH), 8.39 (d, 1H, *J*= 7.90 Hz, Ar-CH), 7.92 (dd, 1H, *J* = 8.42 Hz, *J* = 7.27 Hz, Ar-CH), 7.73 (d, 1H, *J*= 8.15 Hz, Ar-CH), 4.25 (t, 2H, *J*=7.72 Hz, CH_2), 4.21 (s, 2H, CH_2), 2.59 (t, 2H, *J* =7.35 Hz, CH_2). **^{13}C NMR (125 MHz, DMSO): δ(ppm):** 172.92, 170.15, 163.58, 163.48, 143.92, 131.58, 130.88, 130.09, 129.00, 128.01, 1527.87, 123.85, 123.24, 119.38, 36.18, 34.34, 32.65. **HR TOF MS ES+** calc for [$C_{17}H_{14}NO_6S$] 360.0542 found 360.0539.

A5.2 Characterization of compounds using mass spectrometry

Comp.	Mass spectrum code	Comp.	Mass spectrum code
5.14	NB_MS30391_HR_ES	5.12b	NB_MS36139_HR_ES
5.15b	NB_MS35992_HR_ES	5.12c	NB_MS36140_HR_ES
5.15c	NB_MS35760_HR_ES	5.12d	NB_MS35962_HR_ES
5.15d	NB_MS30390_HR_ES	5.12e	NB_MS36029_HR_ES
5.15e	NB_ MS35761_HR_ES	5.13a	MS35892_HR_ES
5.13e	NB_MS33658_HR_ES	5.13d	NB_MS33680_HR_ES

A5.3 UV-vis titration spectra

	1st titration	2nd titration	3rd titration
5.12 b	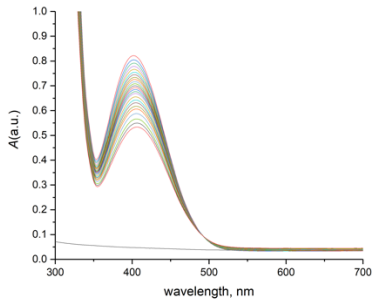	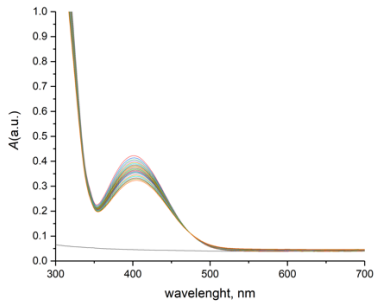	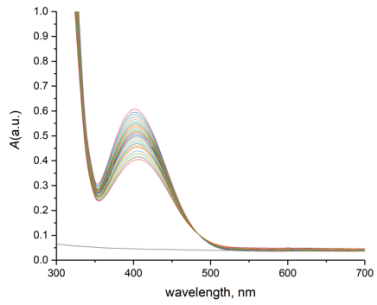
5.12 c	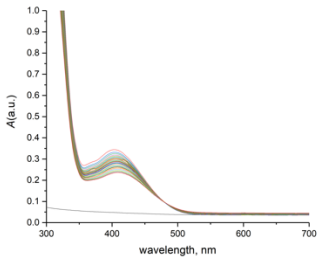	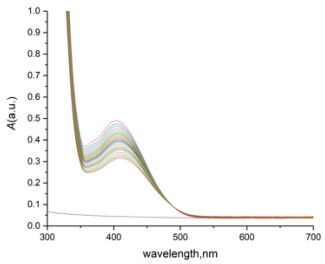	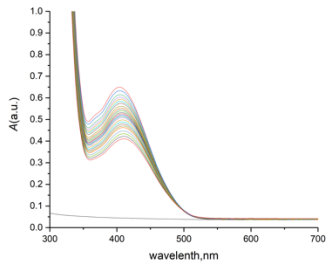
5.12 d	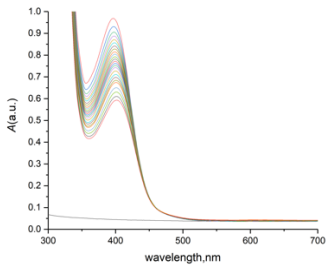	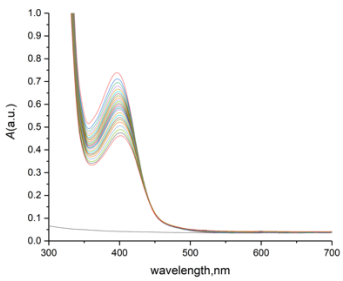	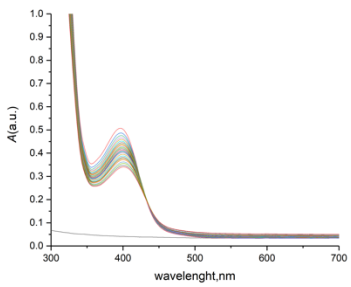
5.12 e	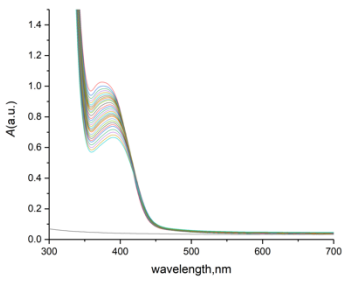	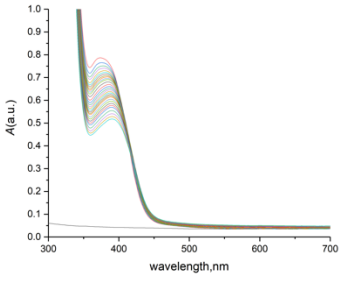	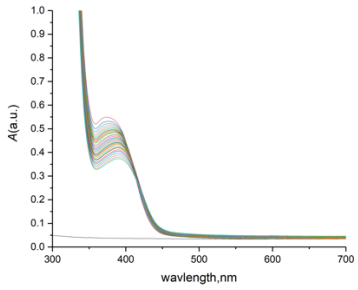

A5.4 Unrestricted preliminary fitting of UV-visible titration data

5.12b	1st titration	2nd titration	3rd titration	Global fit
***K* / M^{-1}**	$1.14\times10^4\pm3863$	$3.26\times10^4\pm2.47\times10^4$	$1.31\times10^5\pm2.49\times10^4$	642.1±1788
***n* / basepairs**	8.05±1.65	14.78±5.48	18.63±0.77	0.73±1.97
***K* (n=3) / M^{-1}**	2643±122.1	3558±376.3	4102±448.3	2998±215.8
Bathochromic shift, nm	401-405			
5.12c	**1st titration**	**2nd titration**	**3rd titration**	**Global fit**
***K* / M^{-1}**	$(8.7\pm5.11)\times10^4$	$(3.0\pm1.0)\times10^4$	$(3.6\pm0.9)\times10^4$	0.01±0.31
***n* / basepairs**	18.69±4.66	13.42±2.23	11.72±1.26	$7.94\times10^{-6}\pm2.51\times10^{-4}$
***K* (*n*=3) / M^{-1}**	6526±817.8	3830±225.9	4295±292.9	4363±324.1
Bathochromic shift, nm	403-409			
5.12d	**1st titration**	**2nd titration**	**3rd titration**	**Global fit**
***K* / M^{-1}**	5576±4678	2972±4373	$1.07\times10^5\pm7.36\times10^4$	0.01±0.24
***n* / basepairs**	3.63±2.36	2.17±2.85	12.36±3.16	$5.03\times10^{-6}\pm1.87\times10^{-4}$
***K* (*n*=3) / M^{-1}**	4402±275.3	4305±214.0	$1.15\times10^4\pm1890$	4725±434.5
Bathochromic shift, nm	396-402			
5.12e	**1st titration**	**2nd titration**	**3rd titration**	**Global fit**
***K* / M^{-1}**	$(4.61\pm1.37)\times10^4$	$(7.75\pm2.70)\times10^4$	$(11.6\pm6.39)\times10^4$	$(3.38\pm0.7385)\times10^4$
***n* / basepairs**	7.67±0.79	9.17±1.01	10.38±1.88	6.50±0.66
***K* (*n*=3) / M^{-1}**	8150±710.6	$1.00\times10^4\pm1032$	$1.39\times10^4\pm1926$	9558±642.2

Bathochromic shift, nm	374-389